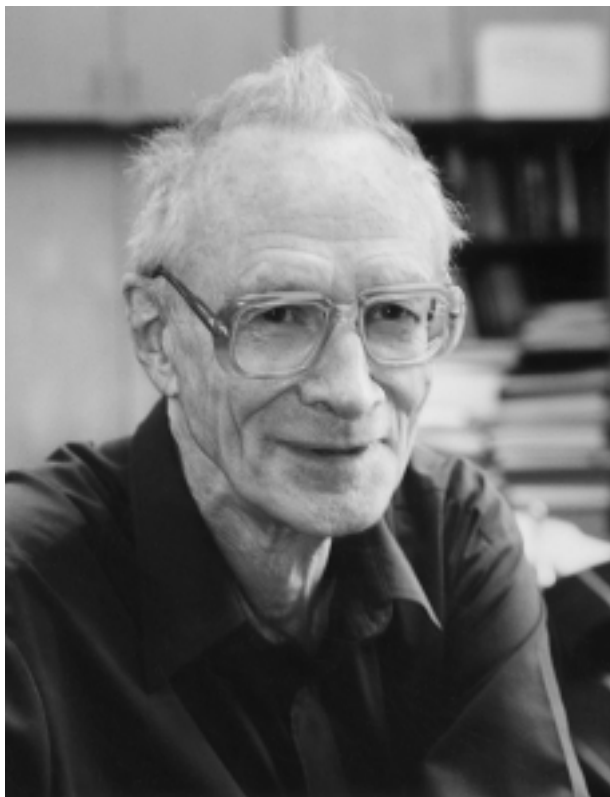


Spartak Timofeevich Belyaev



On October 27, 2003, Spartak Timofeevich Belyaev, a renowned theoretical physicist, an outstanding organizer of science and teacher, will celebrate his 80th birthday.

S.T. Belyaev belongs to the generation of physicists whose first experience of adult life was associated with World War II. In June 1941, immediately after graduating from school, he began working as a lathe operator at a factory, but, as soon as August of the same year, he joined the army in the field as a volunteer. Being demobilized after the end of hostilities, Spartak Timofeevich joined, in 1946, the Faculty of Physics at Moscow State University; after a year, he moved to the Faculty of Physics and Technology (which later evolved into the famous Moscow Institute for Physics and Technology), from which he graduated in 1952 with honors.

The scientific activity of Belyaev began as early as 1947 (when he was still a student) under the supervision of G.I. Budker at A.B. Migdal's theoretical division of the legendary LIPAN (which was

then transformed into the Institute of Atomic Energy, IAE). His first studies were devoted to the kinetics of a dilute ionized gas. There, he was able to give the first consistent derivation of a relativistic kinetic equation and to propose efficient methods for solving this equation. Among important results that Belyaev obtained in this period, those concerning the interesting problem of the multiquantum recombination of an ionized gas, where a nice idea of describing this process in terms of diffusion in energy space was applied, are worthy of special note. The results of those studies were used and further developed in subsequent investigations into plasma physics and the physics of electron beams. They were included in the monograph *Physical Kinetics* that was published as the 10th volume of the *Course of Theoretical Physics* by L.D. Landau and E.M. Lifshitz.

In 1955, Belyaev addressed nuclear-physics problems for the first time. In those years, the problem of studying the spin dependence of nuclear forces became urgent, and it was required for this to create a source of polarized particles. In solving this problem, Belyaev was among the first who proposed employing a strong nonuniform field, in which the hyperfine structure of source atoms is destroyed, whereupon they are separated in the fine-structure components; therefore, the magnetic quantum numbers of the electron shell and of the corresponding nucleus are fixed individually. This idea was successfully implemented first at IAE and then at other research centers. It permitted obtaining intense beams of polarized nuclei for nuclear-physics investigations.

In the late 1950s, Belyaev, together with Migdal and V.M. Galitsky, became one of the founding fathers of a new realm in theoretical physics, the quantum theory of many-body systems. He was the first to use the mathematical technique of Green's functions to describe the properties of a nonideal Bose gas and introduced a so-called anomalous Green's function. This pioneering idea played an important role in the development of the theory of superfluidity and superconductivity, making it possible to determine correctly the spectrum of single-particle excitations of a nonideal Bose gas. Belyaev's studies on the theory of a nonideal Bose gas has long become classic and form an indispensable part of relevant textbooks. Interest in them was rekindled when it became possible

to study the Bose condensation of atomic gases in magnetic traps experimentally.

A new stage of Belyaev's scientific activity began at the end of 1957, when he was sent for a year to the Niels Bohr Institute in Copenhagen. This was the time when the classic studies of J. Bardeen, L.N. Cooper, and J. Schrieffer and, somewhat later on, of N.N. Bogolyubov on the theory of superconductivity had just appeared. There arose the idea—it was first put forth by A. Bohr, B. Mottelson, and D. Pines—that methods used in the theory of superconductivity are applicable to describing the properties of nuclei. This idea was brilliantly realized in Belyaev's article "Effects of Pair Correlations in Nuclear Properties," published in 1959. This study became highly seminal: on a unified basis, it explained a wide range of seemingly unrelated physics phenomena, including the gap in the single-particle spectrum of nonmagic nuclei, a considerable decrease in the moments of inertia of deformed nuclei in relation to the rigid-body value, the stability of a spherical shape for nuclei close to magic ones, and a sharp transition from spherical to deformed nuclei as the nuclear shell is filled with nucleons. The emergence of low-lying collective quadrupole excitations was also explained for the first time, and their role in the phase transition from spherical to deformed nuclei was understood. This article gained Belyaev worldwide recognition and initiated a vigorous development of nuclear theory on the basis of modern many-body methods.

In 1962, Belyaev moved to Novosibirsk, where he soon became head of the theoretical department at the Institute of Nuclear Physics, Siberian Division, USSR Academy of Sciences. Assisted by a group of disciples, he continued there his investigations into nuclear theory. Together with B.A. Romyantsev, Belyaev predicted theoretically new types of collective nuclear vibrations: coherent fluctuations of pairing and spin-orbit vibrations. Among outstanding results of the Novosibirsk period, it is necessary to indicate those that are reported in the article "Anharmonic Effects of Vibrations of Spherical Nuclei," which was written together with V.G. Zelevinsky and which was devoted to describing effects of anharmonicity in quadrupole vibrations. The boson-expansion method proposed by these authors, which is known as the Belyaev-Zelevinsky method, was used in a great number of studies later on and was included in monographs devoted to theoretical nuclear physics. In 1965, the journal *Yadernaya Fizika*, known in the English-speaking world as *Physics of Atomic Nuclei*, began to be published. Its first issue was opened by Belyaev's article devoted to studying the interaction of single-particle and collective degrees of freedom, which is especially important in

nuclei belonging to the transition region. A correct description of the rotational spectra of nuclei is of crucial significance, since the existing simplified approaches cannot be used to construct a unified theory of collective degrees of freedom of the nucleus with allowance for their interactions. The radically new generalized-density-matrix method proposed by Belyaev makes it possible to treat nuclear rotations as an independent branch of the spectrum of collective nuclear excitations in its own right and opens the possibility of constructing a microscopic description of critical phenomena in finite systems.

Belyaev made a great contribution to the development of the Institute of Nuclear Physics in Novosibirsk as an institution of universally recognized authority. A person of theoretical-physics mold, one of the brilliant representatives of Landau's school, he was nevertheless well aware of the experimental situation in various fields of physics. Owing to this, he could take an active part in discussions on the general program of development of the Institute of Nuclear Physics in Novosibirsk and, later on, after his return in 1978 to IAE, be a successful director of the Institute of General and Nuclear Physics there.

The pedagogical and scientific social activity of Belyaev is also widely acclaimed. Being head of Novosibirsk State University and of some scientific departments in various periods of time there and at other educational centers, he greatly contributed to bringing up young scientists. Presently, he is head of the Institute of Natural Sciences and Ecology at the Russian Research Centre Kurchatov Institute. In his teaching activities, Belyaev strictly follows his basic guiding principle: scientific investigations and the preparation of specialists for them must form a unified process. A thoughtful and careful attitude of Belyaev to each problem and to each subordinate has a favorable impact on the work of scientific groups headed by him. He reached the highest academic degrees and was a recipient of government awards. For his outstanding contributions to the development of many lines of research, Belyaev was awarded a Landau medal in 1998.

Dear Spartak Timofeevich, your friends, colleagues, and numerous disciples heartily wish you health, prosperity, and many years of creative activity. These congratulations are shared by the Editorial Board of the *Physics of Atomic Nuclei*, which prepared this issue for your anniversary. The number of scientists who wanted to take part in it was so great that we had to postpone part of the articles until a special issue that is supposed to appear at the beginning of next year.

REVIEWS

Nuclear Pairing: New Perspectives*

V. Zelevinsky¹⁾ and A. Volya²⁾

Received February 24, 2003

Abstract—Nuclear pairing correlations are known to play an important role in various single-particle and collective aspects of nuclear structure. After the first idea by A. Bohr, B. Mottelson, and D. Pines on similarity of nuclear pairing to electron superconductivity, S.T. Belyaev gave a thorough analysis of the manifestations of pairing in complex nuclei. The current revival of interest in nuclear pairing is connected to the shift of modern nuclear physics towards nuclei far from stability; many loosely bound nuclei are particle-stable only due to the pairing. The theoretical methods borrowed from macroscopic superconductivity turn out to be insufficient for finite systems such as nuclei, in particular, for the cases of weak pairing and proximity of continuum states. We suggest a simple numerical procedure of exact solution of the nuclear pairing problem and discuss the physical features of this complete solution. We show also how the continuum states can be naturally included in the consideration bridging the gap between the structure and reactions. The path from coherent pairing to chaos and thermalization and perspectives of new theoretical approaches based on the full solution of pairing are discussed. © 2003 MAIK “Nauka/Interperiodica”.

1. INTRODUCTION

Nuclear pairing is one of the main and long-standing pillars of current understanding of nuclear structure. Pairing provides an important contribution to the odd–even mass difference in the phenomenological mass formulas [1]. As an empirical fact, the pairing was put in the foundation of the shell model by Mayer and Jensen [2] in order to be able to predict ground-state spins and other properties of nonmagic nuclei. In the shell-model framework, the classification of paired states is usually performed with the aid of the seniority scheme [3, 4], where the seniority counts a number of unpaired particles; a similar scheme is used in atomic spectroscopy [5]. The Bardeen–Cooper–Schrieffer (BCS) microscopic theory of superconductivity [6] elucidated the main features of the ground state, excitation spectrum, transition probabilities, and phase transition in a Fermi system governed by the attractive pairing. Immediately after that, Bohr, Mottelson, and Pines pointed out [7] the similarity between the superconducting pairing correlations and observed pairing effects in nuclei. The thorough application of the BCS approach to the nuclear problem was done by Belyaev in his seminal paper [8]. It was quantitatively

demonstrated that the pairing correlations influence nearly all phenomena in low-energy nuclear physics: binding energy, single-particle spectra, transition probabilities, collective vibrational modes, onset of deformation, rotational moment of inertia, level density, and thermal properties.

The BCS theory, as well as its advanced form the Hartree–Fock–Bogolyubov (HFB) method (see [9] and references therein), is formulated in a way fully appropriate for macroscopic quantum systems; in fact, it gives an asymptotically exact solution [10] in the thermodynamic limit. For mesoscopic systems, such as nuclei, atomic clusters, quantum dots, fullerenes, nanotubes, or small metallic grains, this approach, although qualitatively reflecting the main physical features, turns out to be insufficient. The total number N of particles is preserved in this method only on average. Since we have to describe the spectroscopy and reactions for a specific nuclide, we need either to add special projection procedures [11–14] that fix the exact value of N or generalize the formalism by approximately including the matrix elements restoring the particle number conservation [15–18].

Another drawback of the BCS or HFB approaches is a sharp phase transition as a function of parameters or temperature. As pointed out by Belyaev [8], in a system with a discrete single-particle spectrum, the Cooper phenomenon requires, in contrast to a macroscopic Fermi gas, a certain minimum strength of pairing attraction. For a weaker pairing, the mean-field approaches, such as BCS or HFB, give only a trivial normal solution, while in reality the effects of pairing

*This article was submitted by the authors in English.

¹⁾National Superconducting Cyclotron Laboratory, Michigan State University; Department of Physics and Astronomy, Michigan State University, East Lansing, MI, 48824 USA; e-mail: zelevinsky@nscl.msu.edu

²⁾Department of Physics, Florida State University, Tallahassee, FL, 32306, USA; e-mail: volya@martech.fsu.edu

correlations still exist. The pairing correlations in the mean-field framework also vanish immediately after the thermal phase transition. These predictions are incorrect for mesoscopic systems. The exact shell-model calculations show [19] that the pairing correlations do not disappear at the BCS transition point, revealing instead a long tail of “fluctuational superconductivity.”

The main field of interest in nuclear structure is currently shifted to the nuclei far from stability. As we move to loosely bound systems, the influence of the continuum becomes exceedingly important. Along with that, all attractive correlations are to be taken into account properly in order to determine the position of the drip line. The correct treatment of pairing as the main attractive part of the residual interaction is absolutely essential for such problems. Some nuclides, like the notorious ^{11}Li , are bound just due to the pairing correlations between the outermost neutrons, an example of a real Cooper pair [20]. The theory of pairing including both discrete and continuum single-particle levels is still in its infancy [21].

Finally, there is a clear necessity to understand the interplay of pairing with other parts of the residual nuclear interactions going beyond the mean-field approximation of the HFB method. Of course, in the lower part of the nuclear chart (p , sd , and pf shells), there are well-developed modern shell-model methods and reliable effective interactions of the nucleons in the truncated single-particle space (see, for example, [22–25]). With the possibility of incorporating additional stochastic and statistical elements [26–28], the shell-model calculations are able to describe an impressive amount of spectroscopic data. Unfortunately, the qualitative interpretation of results obtained by the large-scale shell-model diagonalization in terms of simple physical models is getting quite difficult as the matrix dimensions approach the limit of current computational strength. In addition, one needs to mention that the continuum problem is not solved in the standard shell-model approach based on the discrete spectrum. Therefore, the gap between the shell model for nuclear structure and the reaction theory is widening.

In this situation, it is alluring to first separate the pairing part of the nuclear interaction and to solve the corresponding many-body problem exactly. As was shown in [29], the exact solution is numerically simple and eliminates all drawbacks related to the BCS approximation. At the same time, it is still close enough to the standard images of nuclear structure. This exact solution can serve as a zero-order step or a background that allows one to look for new approaches and approximations to the full problem,

effects of other interactions, inclusion of the continuum, relation to the reaction cross sections, and so on.

In what follows, we start with sketching the traditional approaches and the exact solution of the pairing problem. We compare the exact results with the BCS approximation, for both the ground and the excited states; demonstrate the possibility of including the continuum physics; and consider chaotic aspects of pairing, a topic practically unexplored in the literature. We complete the paper with a discussion of the perspectives of new approximations based on the exact pairing solution.

2. APPROACHING THE SOLUTION OF THE PAIRING PROBLEM

A. Pairing Hamiltonian

We formulate the pairing problem in the restricted single-particle space of fermionic orbitals assuming the Hamiltonian

$$H_p = \sum_1 \epsilon_1 a_1^\dagger a_1 - \frac{1}{4} \sum_{1,2} G_{12} p_1^\dagger p_2. \quad (1)$$

Here, the subscripts 1, ... run over the complete set of orthogonal single-particle basis states, and we assume the Kramers double-degeneracy of time-conjugate orbitals $|1\rangle$ and $|\bar{1}\rangle$. The pair creation, p_1^\dagger , and annihilation, p_1 , operators are defined as

$$p_1^\dagger = a_1^\dagger a_{\bar{1}}^\dagger, \quad p_1 = a_{\bar{1}} a_1, \quad (2)$$

and the double time-reversal acts as $|\bar{\bar{1}}\rangle = -|1\rangle$. In the important case of spherical symmetry of the mean field that supports degenerate orbitals $|jm\rangle$ with energies ϵ_j , angular momentum j , and projection $j_z = m$, the pairing Hamiltonian can be conveniently written as

$$H_p = \sum_j \epsilon_j \hat{N}_j - \sum_{jj'} G_{jj'} L_j^\dagger L_{j'}, \quad (3)$$

where we use the operator notation

$$\hat{N}_j = \sum_m \hat{n}_{jm} = \sum_m a_{jm}^\dagger a_{jm} \quad (4)$$

for the occupancy operators and $(a_{\bar{1}} \rightarrow a_{j\bar{m}} = (-1)^{j-m} a_{j-m})$

$$L_j = \frac{1}{2} \sum_m (-1)^{j-m} a_{j-m} a_{jm}, \quad (5)$$

$$L_j^\dagger = \frac{1}{2} \sum_m (-1)^{j-m} a_{jm}^\dagger a_{j-m}^\dagger$$

for annihilation and creation operators of pairs in a state with certain quantum numbers of total angular momentum and its projection, $J = M = 0$. Essentially the same Hamiltonian (1) can describe the situation in the deformed mean field.

The pairing interaction is defined in terms of real matrix elements of diagonal pair attraction, $G_{11} > 0$, and off-diagonal ones, $G_{12} = G_{21}$, for pair transfer between the orbitals 1 and 2. We limit ourselves here to the pairing of identical particles (isospin $T = 1$) in states with zero total pair angular momentum; consideration of the $T = 0$ proton–neutron pairing would require a nonzero spin of the pair.

B. BCS Approach

In the BCS theory, the ground state $|0\rangle_{\text{BCS}}$ of the paired system with Hamiltonian (1) is determined by minimizing the ground-state energy with a trial wave function

$$\begin{aligned} |0\rangle_{\text{BCS}} &= \Pi_{1>0}(u_1 - v_1 p_1^\dagger)|0\rangle \quad (6) \\ &= \Pi_{1>0} u_1 \exp\left(-\frac{v_1}{u_1} p_1^\dagger\right) |0\rangle, \end{aligned}$$

where the variational parameters for each pair of time-conjugate orbitals, u_1 and v_1 , can be taken as real numbers subject to the normalization $u_1^2 + v_1^2 = 1$. In our discussion, we denote $|N; s \dots\rangle$ as the lowest in energy N -particle state with quantum numbers s, \dots . We use the notation $|s\rangle_{\text{BCS}}$ for the BCS state with s quasiparticles that has an uncertain particle number; for this reason, N is not shown; however, it is assumed that the state corresponds to an average particle number \bar{N} . The restriction $1 > 0$ means that the time-conjugate orbitals are not counted twice. The exponential form of the variational wave function shows that this state is generated as a coherent state of fermionic pairs; this feature can be put in a foundation of methods going beyond the BCS [30, 31].

The variational solution is given via the occupation amplitudes

$$\begin{aligned} v_1^2 = n_1 &= \frac{1}{2} \left(1 - \frac{\epsilon_1}{e_1}\right), \quad (7) \\ u_1^2 = 1 - n_1 &= \frac{1}{2} \left(1 + \frac{\epsilon_1}{e_1}\right), \end{aligned}$$

where $e_1 = \sqrt{\epsilon_1^2 + \Delta_1^2}$ is the quasiparticle energy and Δ_1 is the BCS energy gap. The gap equation arising from the minimization of energy is

$$\Delta_1 = \frac{1}{2} {}_{\text{BCS}}\langle 0 | \sum_2 G_{12} p_2^\dagger | 0 \rangle_{\text{BCS}} = \sum_2 \frac{G_{12}}{2e_2} \Delta_2. \quad (8)$$

The ground state and low-lying excited states of paired systems can be classified introducing quasi-particle creation operators

$$\alpha_1^\dagger = u_1 a_1^\dagger - v_1 a_{\bar{1}}. \quad (9)$$

This transformation is canonical due to the correct normalization of u and v . The BCS vacuum $|0\rangle_{\text{BCS}}$ in (6) can be defined as $\alpha|0\rangle_{\text{BCS}} = 0$. The Bogolyubov transformation (9) mixes particle and hole states.

One of the problems in the BCS application to small systems is particle-number nonconservation, which follows from the form of the wave function (6). A common practice to fix the number of particles is to introduce a chemical potential μ by the shift of single-particle energies $\epsilon \rightarrow \epsilon - \mu$. The right total particle number is restored on average through the condition

$$\sum_1 n_1(\mu) = \bar{N}. \quad (10)$$

The uncertainty of the total particle number is given by

$$(\Delta N^2) = \overline{N^2} - \bar{N}^2 = \sum_1 n_1(1 - n_1). \quad (11)$$

Practically, this fluctuation is of the order of $\sqrt{(\Delta N^2)} \approx 2$. Given that relative fluctuations go down with increasing N , the BCS solution is asymptotically exact in the thermodynamic limit of macroscopic systems [10]. The contribution to the energy from the fluctuation is quadratic in the number of particles [32] and thus gives an extra correction of the monopole type. Special methods, such as Lipkin–Nogami [11, 12] techniques, were invented in order to suppress the particle-number fluctuations.

The particle-number violation in the BCS is an example of spontaneous symmetry breaking with respect to phase rotations generated by the number operator, $U(\phi) = \exp(-i\phi\hat{N}/2)$. While the pairing Hamiltonian is invariant under this rotation, $[H_p, U(\phi)] = 0$, the trial ground state $|0\rangle_{\text{BCS}}$ has a preferred orientation, with the usual consequences of the appearance of Anderson–Goldstone–Nambu modes, whose properties are influenced by the mesoscopic nature of the nuclear systems [33]. A number of projection techniques have been developed within the framework of the symmetry-violation treatment (see [34] and references therein).

C. Recursive Method with Particle-Number Conservation

Instead of introducing the pair condensate of the pairs with an uncertain particle number, another possibility was explored [15, 17, 35], where the matrix elements of relevant operators explicitly keep memory

of the exact particle number. The gap is defined now as a matrix element of the pair-annihilation operator between the ground states $|N; 0\rangle$ of the neighboring even systems,

$$\Delta_1(N) = \frac{1}{2} \langle N-2; 0 | \sum_2 G_{12} p_2 | N; 0 \rangle. \quad (12)$$

Similarly, the particle-number dependence enters the single-particle transition amplitudes between adjacent even and odd systems,

$$v_1(N) = \langle N-1; \tilde{1} | a_1 | N; 0 \rangle, \quad (13)$$

$$u_1(N) = \langle N+1; 1 | a_1^\dagger | N; 0 \rangle.$$

Here, one needs to consider a sequence of ground states $|N; 0\rangle$ with energies $E(N)$. It is assumed that the spectra of adjacent odd nuclei start with energies $E(N \pm 1; 1)$ of the states $|N \pm 1; 1\rangle$ containing one unpaired nucleon with quantum numbers 1.

The exact operator equations of motion for the single-particle operators a_1 and a_1^\dagger ,

$$[a_1, H] = \epsilon_1 a_1 + \frac{1}{2} \sum_2 G_{12} a_1^\dagger p_2, \quad (14)$$

$$[a_1^\dagger, H] = -\epsilon_1 a_1^\dagger - \frac{1}{2} \sum_2 G_{12} p_2^\dagger a_1, \quad (15)$$

can be used to construct recursive in N equations for the gap (12) and single-particle transition amplitudes (13). The approximation of no condensate disturbance by an extra particle [15, 35],

$$\langle N-1; 1 | \sum_2 G_{12} a_1^\dagger p_2 | N; 0 \rangle \quad (16)$$

$$\approx \langle N-1; 1 | a_1^\dagger | N-2; 0 \rangle$$

$$\times \langle N-2; 0 | \sum_2 G_{12} p_2 | N; 0 \rangle = 2\Delta_1(N) u_1(N-2),$$

leads to the recursion relation connecting adjacent even nuclei,

$$|v_1(N-2)|^2 = 1 - \frac{|\Delta_1(N)|^2}{[e_1(N) - \epsilon'_1(N)]^2} |v_1(N)|^2, \quad (17)$$

where the N -dependent chemical potential is introduced,

$$\mu(N) = \frac{1}{2} (E(N) - E(N-2)), \quad (18)$$

and quasiparticle excitation energy is defined as

$$e_1^2 = \epsilon'_1(N)^2 + |\Delta_1(N)|^2, \quad (19)$$

with shifted single-particle energies

$$\epsilon'_1(N) = \epsilon_1 - \frac{G_{11}}{2} - \mu(N). \quad (20)$$

The analogs of the number-conservation equation and the gap self-consistency condition now read

$$\Omega - N + 2 = \sum_1 \frac{|\Delta_1(N)|^2}{[e_1(N) - \epsilon'_1(N)]^2} |v_1(N)|^2, \quad (21)$$

where Ω is the total capacity of fermionic space, and

$$\Delta_1(N) = \frac{1}{2} \sum_2 G_{12} \frac{\Delta_2(N) |v_2(N)|^2}{e_2(N) - \epsilon'_2(N)}. \quad (22)$$

The pairing problem formulated in this manner allows a recursive solution in both directions, starting from the empty shell or from the completely filled shell. This solution reduces to the BCS under assumption that the gap does not change in the transition from N to $N-2$, the same approximation of particle-number uncertainty that leads to the BCS particle-number fluctuation (11). Based on this feature, the BCS energy can be efficiently corrected by the substitution $\bar{N} \rightarrow \bar{N} - 1$ [36]. Corrections to such iterative methods via inclusion of pair-vibration excitations in the intermediate states of Eq. (16) with further diagonalization are also possible [17], as well as the treatment of the excitations with random phase approximation (RPA) techniques [37, 38].

The particle-conserving treatment does not resolve another problem of the BCS solution, namely, the sudden disappearance of pairing correlations when coupling becomes too weak. The gap equations, (8) and (22), have only trivial $\Delta = 0$ solutions if the pairing strength G is too small compared to the single-particle energy spacings. The point of this phase transition is roughly at the critical coupling strength G_c ,

$$G_c \nu_F = 1, \quad (23)$$

where both the pairing strength and the density of single-particle states ν_F are taken at Fermi energy. Many nuclear systems in the shell-model picture are close to or even below the point of the BCS instability, although the pairing correlations still do exist [29]. As will be discussed later, near the phase transition, in the so-called pair-vibrational regime, the fluctuations drive pair scattering to an almost chaotic level, leading to a sharp increase in the mixing between the states of the same seniority. This randomness makes the approximation (16) or any truncation of states mixed by the pair vibrations inappropriate. Various projection techniques also seriously suffer in the region of weak pairing. More advanced approaches, such as HFB + RPA, break down in the vicinity of the phase transition, though the pairing solution can still be continued into the region beyond the critical point using the RPA based on the Hartree-Fock solution

for a normal state. This treatment drastically improves the prediction for the ground-state energy [18]. The methods of equations of motion [32, 39] and variational techniques can be used to better account for the RPA ground-state correlations [40]. Being applied to superfluid Fermi systems, these methods demonstrated a considerable improvement [40, 41].

3. EXACT SOLUTION OF THE PAIRING PROBLEM

Historically, a few suggestions were put forward for the exact solution of the pairing problem. The Richardson method, described in the series of papers [42, 43], provides a formally exact way for solving the pairing Hamiltonian. This method reduces the large-scale diagonalization of a many-body Hamiltonian matrix in a truncated Hilbert space to a set of coupled equations ($\Omega_j = 2j + 1$)

$$\sum_j \frac{\Omega_j}{2\epsilon_j - z_\lambda} - \sum_{\lambda' \neq \lambda} \frac{4}{z_{\lambda'} - z_\lambda} = \frac{2}{G} \quad (24)$$

for unknown parameters z_λ , their number being equal to that of valence particle pairs. The ground-state energy is then equal to $E(N) = \sum_\lambda^{N/2} z_\lambda$.

Recently, this solution was revived and reinterpreted [44] with the aid of the electrostatic analogy, similar to that used by Dyson in his theory [45] of random level ensembles. Unfortunately, the Richardson solution is only valid for special pairing forces—for example, $G_{jj'} = G = \text{const}$. It also requires serious numerical efforts rapidly growing with the number of particles. Recently, exact solutions have also been approached with sophisticated mathematical tools as infinite-dimensional algebras [46]. Such formally exact solutions have a certain merit from a mathematical point of view and might be useful for developing simple models [47, 48]. However, they are not very promising for practical problems in nuclear physics.

The natural way of solving the pairing problem is related to the direct Fock space diagonalization. For deformed nuclei with doubly degenerate single-particle orbitals, this approach supplemented by the appropriate use of symmetries and truncations was already shown to be quite effective [49, 50]. The diagonalization of the general pairing Hamiltonian (3) is much simpler than that of the full shell-model Hamiltonian due to the possibility of classifying many-body states within the seniority scheme [3, 4, 51], especially in the case of spherical symmetry (3). Long ago, it was shown [51, 52] that this approach is useful not only in the exactly solvable degenerate model but in a realistic shell-model context as well. With a perspective to complement the pairing problem with the subsequent account of other parts of the residual

interaction, we consider this path promising and quite practical.

It is well known that the pair annihilation L_j , pair creation L_j^\dagger , and occupation number operator (shifted to the middle of the j subshell)

$$L_j^\circ = \frac{1}{2}\hat{N}_j - \frac{1}{4}\Omega_j, \quad \Omega_j = 2j + 1, \quad (25)$$

form an $SU(2)$ algebra of “quasispin” for each j subshell,

$$[L_j, L_{j'}^\circ] = \delta_{jj'}L_j, \quad [L_j^\dagger, L_{j'}^\circ] = -\delta_{jj'}L_j^\dagger, \quad (26)$$

$$[L_j, L_{j'}^\dagger] = -2\delta_{jj'}L_j^\circ.$$

Therefore, the pairing Hamiltonian (3) preserves all partial quasispins Λ_j ,

$$\mathbf{L}_j^2 = (L_j^\circ)^2 + \frac{1}{2}(L_j^\dagger L_j + L_j L_j^\dagger) = \Lambda_j(\Lambda_j + 1). \quad (27)$$

The partial seniority quantum numbers,

$$s_j = \Omega/2 - 2\Lambda_j, \quad (28)$$

are also conserved. They express the number of unpaired, and therefore not participating in the pairing interaction (3), particles. The fully paired j level corresponds to the maximum partial quasispin $\Lambda_j = \Omega/4$ and lowest partial seniority $s_j = 0$.

The pair transfer $L_{j'}^\dagger L_j$ between the levels $j \rightarrow j'$ changes the occupancies, i.e., projections L_j° and $L_{j'}^\circ$, keeping intact the lengths of quasispins Λ_j and $\Lambda_{j'}$, and, whence, seniorities s_j and $s_{j'}$. The space is decomposed into sectors with given partial seniorities s_j , and the basis states within each sector can be labeled by the set of occupancies N_j under a constraint $\sum_j N_j = N$, the total valence particle number. The passive (unpaired) particles occupy fixed orbitals and create nonzero seniorities. They influence the dynamics indirectly, through the Pauli blocking. The states with zero total seniority $s = \sum_j s_j$ have the total spin $J = 0$, while for $s \neq 0$ the further decomposition with respect to the rotation group is possible, and some many-body states with different angular momentum coupling but the same seniorities remain degenerate.

Using the states with given values of s_j and various possible occupancies N_j as a basis, it is easy to construct the Hamiltonian matrix that is essentially the matrix with respect to the sets of N_j . The diagonal matrix elements are

$$\langle \{s_j\}, \{N_j\} | H_p | \{s_j\}, \{N_j\} \rangle \quad (29)$$

$$= \sum_j \left[\epsilon_j N_j - \frac{G_{jj}}{4} (N_j - s_j)(\Omega_j - s_j - N_j + 2) \right].$$

Table 1. Single-particle energies and pairing matrix elements $V_0(jj; j'j')$ (in MeV) for the shell-model space from ^{100}Sn to ^{132}Sn (matrix elements are determined from G -matrix calculations)

	$g_{7/2}$	$d_{5/2}$	$d_{3/2}$	$s_{1/2}$	$h_{11/2}$
ϵ_j	-6.121	-5.508	-3.749	-3.891	-3.778
$g_{7/2}$	0.9850	0.5711	0.5184	0.2920	1.1454
$d_{5/2}$		0.7063	0.9056	0.3456	0.9546
$d_{3/2}$			0.4063	0.3515	0.6102
$s_{1/2}$				0.7244	0.4265
$h_{11/2}$					1.0599

Each term in the square brackets gives a full solution for the pairing problem on a degenerate j level. Clearly, as long as seniority is small, $s_j \ll \Omega_j$, each unpaired particle increases energy by $\Delta_j = G_{jj}\Omega_j/4$, and this quantity plays the role analogous to that of the energy gap in the BCS theory. The off-diagonal matrix elements for the pair transfer $j' \rightarrow j$ are

$$H_{j' \rightarrow j} = -\frac{G_{jj'}}{4}[(N_{j'} - s_{j'})(\Omega_{j'} - s_{j'} - N_{j'} + 2) \times (\Omega_j - s_j - N_j)(N_j - s_j + 2)]^{1/2}. \quad (30)$$

The highest matrix dimension is encountered for the lowest possible total seniority, $s = 0$ for an even number of particles and $s = 1$ for an odd number of particles. But, even for heavy nuclei, this dimension does not exceed a few thousand (in modern shell-model computations, one has to deal with dimensions 10^8 and higher in the m scheme). In addition, the Hamiltonian matrix is very sparse. As a result of the numerical diagonalization, we obtain the spectrum of states for a given set of seniorities. For example, for an even system, the condition $s = 0$ selects all zero partial seniorities, $s_j = 0$. All those states correspond to pair condensates that differ by the distribution of the average partial occupancies $\{N_j\}$ among the subshells. In a standard language of the BCS theory supplemented by the RPA, the excited states for $s = 0$ are various pair vibrations. However, here we do not make any assumptions of boson character or harmonic spectrum of excitations. The next section illustrates the typical results of the diagonalization.

4. EXAMPLE: A CHAIN OF EVEN ISOTOPES

The longest known chain of tin isotopes is a subject of extensive experimental and theoretical studies. Even considering the proton subsystem, $Z = 50$, as

an inert core, we have to deal with a neutron model space that is too large for a direct diagonalization. Modern computational techniques that use the Lanczos iteration method allow for exact determination of a few low-lying states in systems with up to 12 valence particles [53]. These results are essential for testing the approximate techniques. It is known that pairing correlations play a major role in forming the ground-state wave functions of tin isotopes.

Unlike in many other nuclear systems, pairing in tin isotopes is quite strong and stable, being sufficiently above the point of the BCS phase transition. There is only a relatively minor weakening in the mass region near ^{114}Sn due to a gap between $d_{5/2}$ and $g_{7/2}$ and the rest of the single-particle orbitals. We specifically would like to explore this region in order to discuss the physics of the BCS phase transition.

For tin isotopes ranging in mass number from $A = 100$ to 132 , we assume a configuration space between the two neutron magic numbers 50 and 82. The valence neutron space contains here five single-particle orbitals, $h_{11/2}$, $d_{3/2}$, $s_{1/2}$, $g_{7/2}$, and $d_{5/2}$. We adopt parameters shown in Table 1, the single-particle energies taken from experimental data and the interaction matrix elements from the G -matrix calculation [53]. The interaction parameters V_0 in Table 1 are related to the pairing strengths $G_{jj'}$ as

$$G_{jj'} = V_0(jj; j'j') \frac{2}{\sqrt{(2j+1)(2j'+1)}}. \quad (31)$$

The shell-model calculations with these parameters reproduce the spectroscopy of tin isotopes in the region $A = 120$ to 130 with a good accuracy. In parallel, we discuss similar effects in calcium isotopes, where we used a well-established FPD6 interaction [24]. The fp neutron valence space covers calcium isotopes from ^{40}Ca to ^{60}Ca . The weakening of pairing in Ca occurs near ^{48}Ca , i.e., for the $f_{7/2}$ subshell closure. Results of the calculation for the ^{114}Sn region are shown in Table 2 and for the ^{48}Ca region in Table 3.

An important consequence of the proximity to the BCS phase transition is a reduction of pairing correlation energy predicted by the BCS but not confirmed by the exact solution. In the tin example, the BCS underpredicts the binding energy by about 0.4 MeV, while for calcium this number reaches 0.6 MeV. A similar difference appears in one-nucleon separation energy $S_j(N) = E(N-1) - E(N)$ (index j here denotes the orbital of the unpaired nucleon in an odd- N system), as can be seen from the comparison of rows (e) and (f) with the corresponding BCS prediction, lines (m) and (n), Tables 2 and 3. As stressed in [29], this discrepancy can be crucial for the nuclei near drip lines. Unfortunately, the BCS can hardly be improved

Table 2. The results of the exact pairing solution (EP) compared to the BCS solution for the ^{114}Sn nucleus (the interaction matrix elements are determined by the G -matrix calculations—see text; the separation energies S_j , quasiparticle energies e_j , and the pairing gaps Δ_j are given in MeV)

		$g_{7/2}$	$d_{5/2}$	$d_{3/2}$	$s_{1/2}$	$h_{11/2}$
EP						
(a)	$N_j(N)$	6.96	4.46	0.627	0.356	1.6
(b)	$n_j(N)$	0.870	0.744	0.157	0.178	0.133
(c)	$u_j^2(N)$	0.128	0.252	0.838	0.817	0.863
(d)	$v_j^2(N)$	0.865	0.736	0.155	0.177	0.131
(e)	$S_j(N+1)$	2.8	3.13	3.14	3.39	3.29
(f)	$S_j(N)$	6.86	6.55	7.25	6.98	7.12
(g)	$ \langle N+2; 0 P_j^\dagger N; 0\rangle $	0.68	0.779	0.617	0.514	1.03
(h)	$ \langle N; 0 P_j N-2; 0\rangle $	0.81	0.93	0.524	0.396	0.845
BCS						
(i)	$N_j(N)$	6.71	4.14	0.726	0.507	1.91
(j)	$n_j(N)$	0.839	0.69	0.181	0.254	0.159
(k)	Δ_j	1.31	1.43	1.43	1.38	1.25
(l)	e_j	1.78	1.55	1.86	1.59	1.71
(m)	$S_j(N+1)$	2.89	3.21	3.11	3.21	3.26
(n)	$S_j(N)$	6.89	6.64	7.2	7.03	7.06
(o)	${}_{\text{BCS}}\langle 0 P_j 0\rangle_{\text{BCS}}$	0.734	0.801	0.545	0.435	0.896

Note: EP: $E(^{114}\text{Sn}) = -86.308$, $E(^{116}\text{Sn}) = -95.942$, $E(^{112}\text{Sn}) = -75.831$. BCS: $E(^{114}\text{Sn}) = -85.938$, $\mu = -5.035$.

with respect to the treatment of weak pairing. Even for the complicated particle-number projection techniques accompanied by variational procedures on a broader set of mean-field states, it remains unclear to what extent it is possible to describe the pairing phase transition, and whether the high-lying pair vibrations are included, the step needed to account for missing correlation energy.

Another related feature is the difference in predicted occupation numbers that can be inferred from comparing rows (a) and (b) with (i) and (j) in Tables 2 and 3. A proper account of this difference can partially help to correct the binding energy. In the presence of additional interactions, the monopole contribution to the energy can be particularly sensitive to the precise occupation numbers. Furthermore, in the use of mean-field methods for paired systems, a good

Table 3. Properties of the weakly paired ^{48}Ca nucleus (the FPD6 interaction was used in these calculations; all energies are given in MeV)

		j	7/2	3/2	5/2	1/2
		ϵ_j	-8.39	-6.5	-1.9	-4.48
EP						
(a)	$N_j(N)$	6.87	0.85	0.173	0.111	
(b)	$n_j(N)$	0.858	0.212	0.0288	0.0557	
(c)	$u_j^2(N)$	0.133	0.779	0.97	0.939	
(d)	$v_j^2(N)$	0.848	0.212	0.0281	0.0555	
(e)	$S_j(N+1)$	4.48	5.78	1.55	4.09	
(f)	$S_j(N)$	9.64	9.75	14.1	11.5	
(g)	$\langle N+2; 0 P_j^\dagger N; 0\rangle$	0.706	0.928	0.289	0.309	
(h)	$\langle N; 0 P_j N-2; 0\rangle$	1.07	0.612	0.288	0.232	
BCS						
(i)	$N_j(N)$	6.5	1.22	0.155	0.124	
(j)	$n_j(N)$	0.813	0.304	0.0258	0.062	
(k)	Δ_j	1.66	1.44	1.73	1.53	
(l)	e_j	2.13	1.56	5.45	3.18	
(m)	$S_j(N+1)$	4.5	5.66	1.64	4.1	
(n)	$S_j(N)$	9.64	9.51	13.8	11.3	
(o)	${}_{\text{BCS}}\langle 0 P_j 0\rangle_{\text{BCS}}$	0.78	0.651	0.275	0.241	

Note: EP: $E(^{48}\text{Ca}) = -71.215$, $E(^{50}\text{Ca}) = -85.149$, $E(^{46}\text{Ca}) = -55.501$. BCS: $E(^{48}\text{Ca}) = -70.591$, $\mu = -7.335$.

reconstruction of the density matrix generated by the pairing is of critical importance.

The exact pairing treatment (EP) becomes increasingly important in considering the reaction amplitudes with paired nuclei. The one-nucleon transition amplitudes defined in the exact solution via Eq. (13) can be compared with the corresponding BCS quantities. Since, similar to the recursive approach, these amplitudes connect different nuclei, the standard BCS relations $v_j^2 = n_j$, $u_j^2 = 1 - n_j$, and $u_j^2 + v_j^2 = 1$ are no longer true. Deviations from these equalities are clearly enhanced in the phase transition region, where adding an extra particle can make a sharp difference. The BCS theory with an uncertain particle number does not account for such effects. The pair emission amplitudes generated by normalized pair transfer operators $P_j = L_j \sqrt{2/(2j+1)}$ exhibit even larger differences. Rows (g) and (h) of Tables 2 and 3 show these amplitudes for adjacent even systems. The numbers are noticeably different

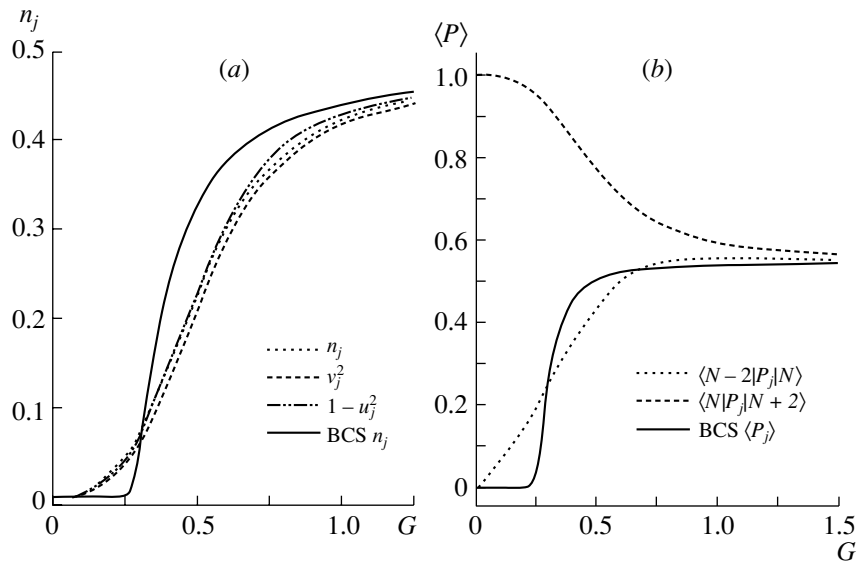


Fig. 1. Comparison of BCS and EP solutions for the ladder system as a function of pairing strength G . The single-particle level spacing sets the unit of energy. (a) Occupation numbers for the sixth level (first level above the Fermi surface) and spectroscopic factors for capture and decay are compared. (b) For the same level, the pair emission and pair absorption amplitudes are compared.

[in the BCS approach, they are replaced with a single set shown in row (o)]. These discrepancies are particularly crucial for weakly bound nuclei, since not only the binding energy is affected by the improved treatment of pairing, but also there are significant corrections to the reaction amplitudes.

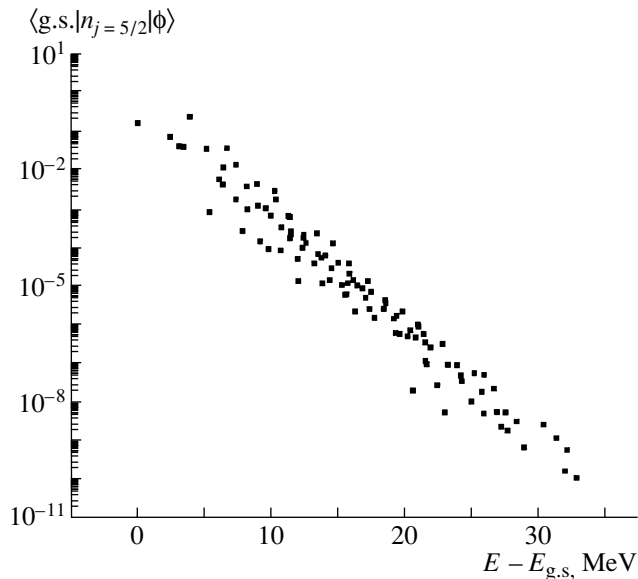


Fig. 2. Matrix elements of the operator n_j for the $d_{5/2}$ level in ^{114}Sn between the ground state and all pair vibrational states ϕ (zero seniority) plotted as a function of excitation energy of the state ϕ .

Further insight into the situation can be gained by varying the coupling strength. For this purpose, we consider a “ladder” model that contains ten doubly degenerate single-particle orbitals equally spaced with the interval of a unit of energy. The valence space is assumed to be half-occupied with $N = 10$ particles. The most interesting region is near the Fermi surface, $\epsilon_F = 5$. For Fig. 1, we consider the first single-particle level above the Fermi energy. As in the previous example, the BCS result deviates significantly from the exact solution near the phase transition, around $G = 0.5$, as seen from Fig. 1a. In the same region, one can observe a slight difference between v_j^2 , $1 - u_j^2$, and n_j in the exact solution. For the pair emission process, the differences between the BCS and exact solution become more pronounced. Here, the particle-number uncertainty is crucial, since the level under consideration is above the Fermi energy for $N = 10$, but below it for $N = 12$.

Contrasting the exact solution with the mean-field picture, we can notice that the occupation-number operators \hat{N}_j in general may have nonzero off-diagonal matrix elements between states of the same seniority. In Figs. 2 (^{114}Sn) and 3 (the ladder model), the matrix elements between the ground state and all $s = 0$ states are shown as a function of excitation energy. In all cases, the off-diagonal matrix elements rapidly fall off. In the case of weak pairing (Fig. 3, circles), one can still see the structure of excited states based on the equidistant single-particle spectrum. For stronger pairing (compared to

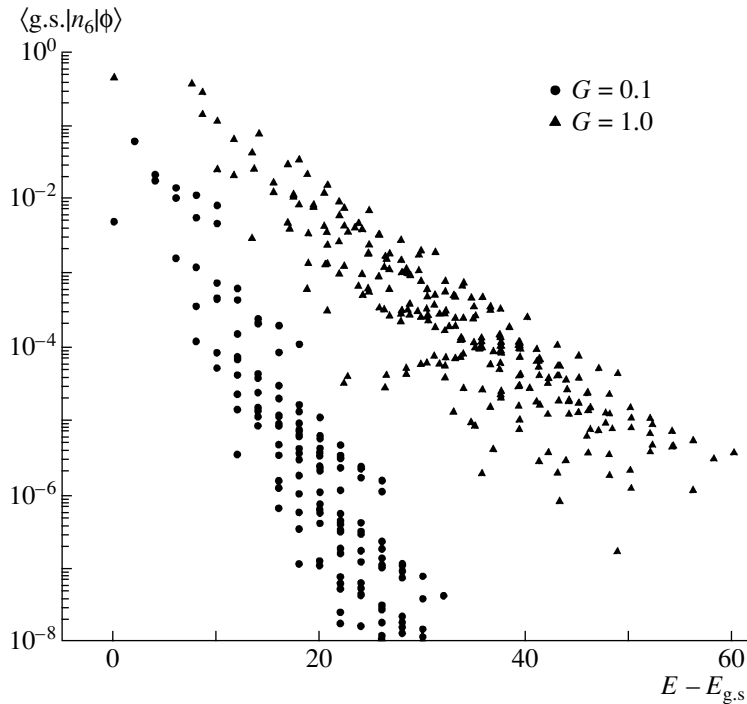


Fig. 3. Matrix elements of n_6 (the sixth single-particle state in the ladder model) between the ground state and excited $s = 0$ states as a function of excitation energy expressed in the units of ladder spacing.

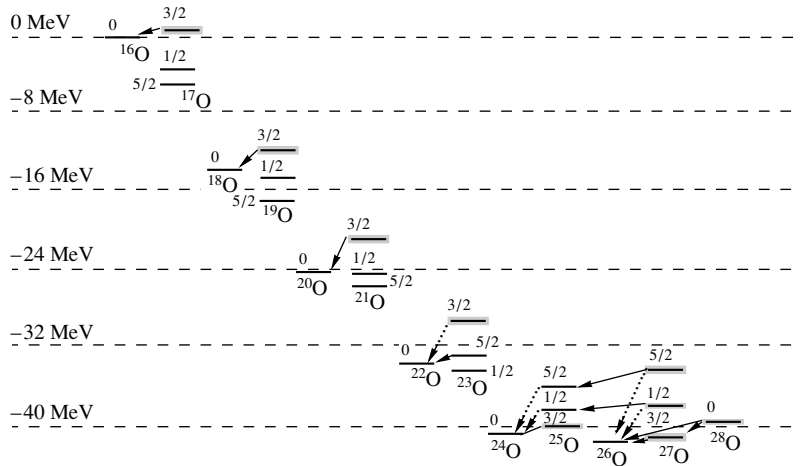


Fig. 4. Schematic picture of lowest seniority states and possible decays in oxygen isotopes. Dotted arrows indicate the decays blocked by seniority conservation.

the single-particle level spacing), Fig. 3, triangles, as well as in the realistic case for spherical symmetry, Fig. 2, the decrease in matrix elements is more uniform and can be approximated on average by an exponential function of excitation energy. This indicates chaotization of motion even in the sector with seniority $s = 0$ [54]. Only a very few states with relatively large matrix elements may carry pair-vibrational features. As follows from the extended shell-model analysis [55], the exponential tails of

the strength functions are typical for many-body quantum chaos [56]. The property of exponential convergence was demonstrated in [28], and the extrapolation based on this property was later used [57–59] as a practical tool for getting reliable quantitative results in shell-model calculations of intractable large dimensions.

Table 4. Seniority $s = 0$ and $s = 1$ states in oxygen isotopes (Energies and neutron decay widths are shown. Results are compared to the known data. Ground-state energies relative to the ^{16}O core are given in bold. The rest of the energies are excitation energies in a given nucleus)

A	J	E , MeV	Γ , keV	E_{exp} , MeV	Γ_{exp} , keV
16	0	-0.00	0	-0.00	0
17	5/2	-3.94	0	-4.14	0
17	1/2	0.78	0	0.87	0
17	3/2	5.59	96	5.08	96
18	0	-12.17	0	-12.19	0
19	5/2	-15.75	0	-16.14	0
19	1/2	1.33	0	1.47	0
19	3/2	5.22	101	6.12	110
20	0	-23.41	0	-23.75	0
21	5/2	-26.67	0	-27.55	0
21	1/2	1.38	0		
21	3/2	4.60	63		
22	0	-33.94	0	-34.40	0
23	1/2	-35.78	0	-37.15	0
23	5/2	2.12	0		
23	3/2	2.57	13		
24	0	-40.54	0	-40.85	0
25	3/2	-39.82	14		
25	1/2	2.37	0		
25	5/2	4.98	0		
26	0	-42.04	0		
27	3/2	-40.29	339		
27	1/2	3.42	59		
27	5/2	6.45	223		
28	0	-41.26	121		

5. CONTINUUM EFFECTS

As the main interest of low-energy nuclear physics is moving to nuclei far from the valley of stability, the continuum effects become exceedingly important for a unified description of the structure of barely stable nuclei and corresponding nuclear reactions. The pairing part of the residual interaction in some cases is the main source of the nuclear binding; spectroscopic factors and reaction amplitudes are also critically dependent on pairing.

As a demonstration of a realistic shell-model calculation combining the discrete spectrum and the continuum, we consider oxygen isotopes in the mass region $A = 16$ to 28. In this study, we use a universal sd -shell model description with semiempirical effective interaction (USD)[25]. The model space includes three single-particle orbitals $1s_{1/2}$, $0d_{5/2}$, and $0d_{3/2}$ with corresponding single-particle energies of -3.16 , -3.95 , and 1.65 MeV. The residual interaction is defined in the most general form with the aid of a set of 63 reduced two-body matrix elements in pair channels with angular momentum L and isospin T , $\langle(j_3\tau_3, j_4\tau_4)LT|V|(j_1\tau_1, j_2\tau_2)LT\rangle$, that scale with nuclear mass as $(A/18)^{-0.3}$.

In the discrete spectrum, the full shell-model treatment is possible for such light systems. Aiming at the study of the continuum effects, which significantly increase the computational load, here we truncate the shell-model space to include only seniority $s = 0$ and $s = 1$ states. This method, “exact pairing + monopole,” is known [29] to work well for shell-model systems involving only one type of nucleons (in the case of the oxygen isotope chain, only neutrons and the interaction matrix elements with isospin $T = 1$ are involved). The two important ingredients of residual nuclear forces are treated by this method exactly: the monopole interaction that governs the binding energy behavior throughout the mass region, and pairing that is responsible for the emergence of the pair condensate, renormalization of single-particle properties, and collective pair vibrations.

In the resulting simplified shell-model description, the set of the original 30 two-body matrix elements in the $T = 1$ channel is reduced to 12 most important linear combinations. Six of these are the two-body matrix elements for pair scattering in the $L = 0$ channel describing pairing, and the other six correspond to the monopole force in the particle–hole channel,

$$\bar{V}_{j,j'} \equiv \sum_{L \neq 0} (2L + 1) \langle(j, j')L1|V|(j, j')L1\rangle, \quad (32)$$

where j and j' refer to one of the three single-particle levels.

We assume here that the $0d_{3/2}$ orbital belongs to the single-particle continuum and, therefore, its energy has an imaginary part. In this model, we account for two possible decay channels $|c\rangle$ for each initial state $|\Phi\rangle$, a one-body channel, $c = 1$, and a two-body channel, $c = 2$. The one-body decay changes the seniority of the $0d_{3/2}$ orbital from 1 to 0 in the decay of an odd- A nucleus and from 0 to 1 for an even- A nucleus. The two-body decay with zero angular momentum of the pair removes two paired particles and does not change the seniority. The two channels

lead to the lowest energy state of allowed seniority in the daughter nucleus; transitions to excited pair-vibrational states are ignored. This results in

$$e_{3/2}(\Phi) = \epsilon_{3/2} - \frac{i}{2}\alpha_{3/2}(E_{\Phi} - E^{(1)})^{5/2} \quad (33)$$

$$- i\alpha_{3/2}(E_{\Phi} - E^{(2)})^{5/2},$$

where we assumed that one- and two-body decay parameters $\gamma_j^{(c)}$ are related as $\gamma_{3/2}^{(1)} = \gamma_{3/2}^{(2)}/2 \equiv \gamma_{3/2}$ and the particles are emitted in the d -wave with $\ell = 2$. The energy dependence of the widths near decay thresholds $E^{(c)}$ is very important; $\alpha_{3/2}$ is the reduced width parameter that differs from $\gamma_{3/2}$ by the absence of the energy factor. Three states with the valence particle at one of the single-particle orbitals can be identified as the $5/2^+$ ground state and $1/2^+$ and $3/2^+$ excited states in the spectrum of ^{17}O . Their energies relative to ^{16}O correspond to the single-particle energies in the USD model. Experimental evidence indicates that the $3/2^+$ state decays via neutron emission with the width $\Gamma(^{17}\text{O}) = 96$ keV. This information allows us to fix our parameter $\alpha_{3/2} = \Gamma(^{17}\text{O})/(\epsilon_{3/2})^{5/2} = 0.028$ (MeV) $^{-3/2}$. The other two states are particle-bound, $\gamma_{1/2} = \gamma_{5/2} = 0$.

With complex single-particle energies, the non-Hermitian effective Hamiltonian for the many-body system is constructed in a regular way [60, 61]. The Hamiltonian includes the Hermitian pairing and monopole terms as well as the energy-dependent non-Hermitian effective interaction through the open decay channels, the structure of which is dictated by unitarity [61]. Energy dependence is determined by the proximity of thresholds [Eq. (33)]. We move along the chain of isotopes starting from ^{16}O . In this way, for each A the properties of the possible daughter systems $A - 1$ and $A - 2$ are known. The chain of isotopes under consideration is shown in Fig. 4, which includes $s = 0$ and $s = 1$ states and indicates possible decays. The decays indicated by the dotted arrows are blocked in our model due to the exact seniority conservation. Nonpairing interactions in the full shell model mix seniorities, making these decays possible. Since the effective Hamiltonian depends on energy and all threshold energies have to be determined self-consistently, we solve this extremely nonlinear problem iteratively. We start from the shell-model energies $E_{s,m}$ corresponding to a nondecaying system. Then, the diagonalization of the Hamiltonian at this energy allows us to determine the next approximation to the complex energies $\mathcal{E} = E - (i/2)\Gamma$ that give the position and the width of a resonance. This cycle is repeated until convergence, which is usually achieved in less than ten iterations.

The results of the calculations and comparison with experimental data for oxygen isotopes are shown in Table 4. Despite numerous oversimplifications related to seniority truncation, limitations on the configuration mixing, and restrictions on possible decay channels and final states, the overall agreement observed in Table 4 is quite good. If experimental data are not available, the results can be considered as predictions. The main merit of this calculation is in demonstrating the power and practicality of the EP method extended to continuum problems. The same calculation also predicts [62] the cross sections of the processes related to the included channels, providing the unified description of the structure and reactions with loosely bound nuclei.

6. THERMAL PROPERTIES

A. BCS Approach

The properties of the dense spectrum of highly excited states are usually described in statistical terms of level density, entropy, and temperature. The shell-model analysis [19, 63] revealed a certain similarity between many-body quantum chaos and thermalization. In particular, the Fermi liquid approach to the complex many-body system modeled as a gas of interacting quasiparticles turns out to be applicable not only in the vicinity of the Fermi surface, but even at high excitation energy.

Here, we consider the thermalization properties of the paired system. Related subjects have been recently discussed in the literature by a number of authors (see [64] and references therein). The BCS operates with the quasiparticle thermal ensemble. The expectation value for an occupancy of a given single-particle state is

$$n = \langle a^\dagger a \rangle = u^2 \langle \alpha^\dagger \alpha \rangle + v^2 \langle \tilde{\alpha} \tilde{\alpha}^\dagger \rangle + uv \langle \alpha^\dagger \tilde{\alpha}^\dagger + \tilde{\alpha} \alpha \rangle. \quad (34)$$

Under the assumption of the thermal-equilibrium quasiparticle distribution, the last term in (34) disappears, while the first and the second terms give

$$\langle \alpha_j^\dagger \alpha_j \rangle = \nu_j, \quad \langle \tilde{\alpha}_j \tilde{\alpha}_j^\dagger \rangle = 1 - \nu_j. \quad (35)$$

The occupation numbers for quasiparticles are defined by the Fermi distribution with zero chemical potential,

$$\nu_j(T) = [1 + \exp(\beta e_j)]^{-1}, \quad \beta = 1/T, \quad (36)$$

and temperature-dependent quasiparticle energies

$$e_j(T) = \sqrt{(\epsilon_j - \mu)^2 + \Delta_j^2(T)}. \quad (37)$$

The thermal evolution of the pairing gap $\Delta(T)$ is determined by the self-consistent BCS equation with the quasiparticle blocking factor included,

$$\Delta_j(T) = \sum_{j'} G_{jj'} \frac{[1 - \nu_{j'}(T) - \nu_{\bar{j}'}(T)] \Delta_{j'}(T)}{2e_{j'}(T)}. \quad (38)$$

The occupation numbers of original particles are given by

$$n_j = u_j^2 \nu_j + v_j^2 (1 - \nu_j), \quad (39)$$

where the coherence factors u and v also depend on temperature via $e_j(T)$. (This discussion is closely related to [65].) As a result, we obtain equations for the gap (38) and chemical potential using Eq. (39) at a given external temperature T that governs the quasiparticle distribution.

B. Statistical Spectroscopy of Pairing

The form of the pairing Hamiltonian allows for a relatively simple calculation of its spectroscopic moments. In this section, we limit our consideration to the zero seniority block of a ladder system of total capacity Ω with doubly degenerate orbitals; the generalization for more realistic cases is straightforward. In the ladder system, the diagonal matrix elements simply renormalize single-particle energies. It is convenient to set the chemical potential to zero and use variables $\varepsilon_1 = \varepsilon_1 - G_{11}/2$ following Eq. (20). We also denote the off-diagonal pairing matrix elements as $G_{12} = (1 - \delta_{12})G_{12}$.

The centroid of the distribution is determined by the single-particle spectrum,

$$\langle\langle E \rangle\rangle = N\bar{\varepsilon}. \quad (40)$$

Here, the double brackets imply averaging over all many-body states, while the overline means averaging over single-particle states according to the definition

$$\overline{\mathcal{G}^k} = \frac{2}{\Omega} \text{tr}(\mathcal{G}^k). \quad (41)$$

The second moment of the distribution, the variance, is a sum in quadratures of the single-particle width and the width due to pairing,

$$\sigma^2 = \langle\langle (E - \langle\langle E \rangle\rangle)^2 \rangle\rangle = \frac{2N(\Omega - N)}{\Omega - 2} \times \left(\overline{(\varepsilon - \bar{\varepsilon})^2} + \frac{1}{4} \overline{\mathcal{G}^2} \right). \quad (42)$$

The third moment, the skewness, indicates deviations from the normal distribution. It is given by

$$\langle\langle (E - \langle\langle E \rangle\rangle)^3 \rangle\rangle = -\frac{N(\Omega - N)(\Omega - N - 2)}{(\Omega - 2)(\Omega - 4)} \overline{\mathcal{G}^3}. \quad (43)$$

All odd central moments are asymmetric in \mathcal{G} and thus vanish for $\mathcal{G} = 0$. The skewness is also a special case since in the ladder system it does not depend on single-particle energies. For attractive pairing, the skewness is always negative, indicating a longer tail of the distribution towards lower energies. This supports the pairing character of the low-lying states that due to their collective nature are pushed further down from the centroid of the distribution.

The density of states $\rho(E)$ allows for a thermodynamical determination of the temperature,

$$\frac{1}{T} = \frac{\partial}{\partial E} \ln(\rho(E)). \quad (44)$$

Despite the presence of higher moments, the density of states of paired systems, as in a more general class of two-body Hamiltonians [19], can be closely approximated by a Gaussian distribution. An actual distribution $\rho(E)$ is shown in Fig. 5. Assuming a Gaussian distribution with the mean value (40) and the width σ , Eq. (42), the temperature as a function of energy can be found [19] using (44),

$$T(E) = \frac{\sigma^2}{\langle\langle E \rangle\rangle - E}. \quad (45)$$

The negative- T branch is an artifact of the finite Hilbert space.

The Gaussian distribution gets distorted when the pairing becomes strong and the low-lying states become very collective. A minor manifestation of this collectivity is seen in Fig. 5b for $G = 1$. As G grows, the deviations from the Gaussian shape become more transparent, clearly revealing the seniority structure, as seen in Fig. 6.

C. Quasiparticle Temperature

As was discussed in detail in [19, 63], there is no unique definition of temperature in a self-sustaining isolated mesoscopic system. Complementary to the thermodynamic (microcanonical) definition of the previous subsection, we can find the effective value of temperature for each individual many-body state by fitting the occupation numbers found in the EP solution to those given by the thermal ensemble [Eq. (39)]. We can refer to this assignment as a measurement with the aid of a quasiparticle thermometer and denote the resulting temperature as \mathcal{T} .

The correspondence between excitation energy and quasiparticle temperature \mathcal{T} for each eigenstate in the 12-level model is presented in Fig. 7. The scattered points clearly display a regular trend to thermalization in agreement with the hyperbolas predicted by Eq. (45). Although the thermodynamic and quasiparticle temperatures are well correlated (Fig. 8)

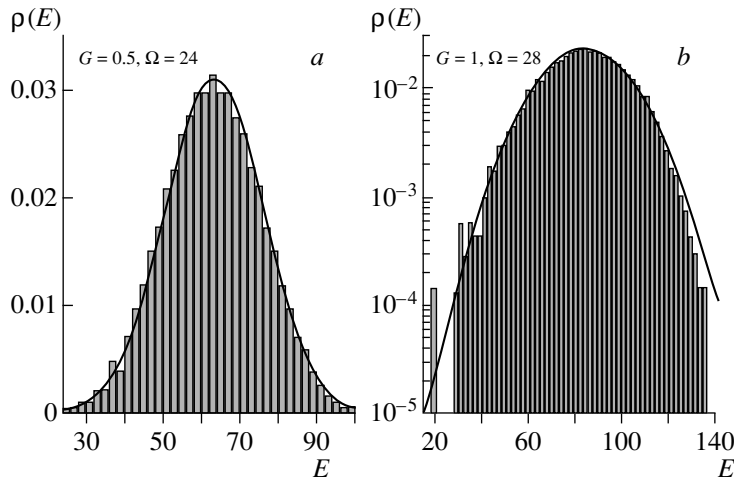


Fig. 5. Density of states as a function of energy is shown by the histogram. The solid curve indicates the Gaussian distribution with the parameters determined by Eqs. (40) and (42). Both panels refer to half-occupied systems. Panel (a) for the 12-level system with $G = 0.5$ displays an overall good Gaussian fit, while the deviations are clearer in panel (b), where the density of states is plotted on a log scale for a 14-level system with stronger pairing, $G = 1$. Here, the effect of negative skewness is visible, as well as the presence of the gap. The unit of energy is set by the single-particle level spacing in the ladder.

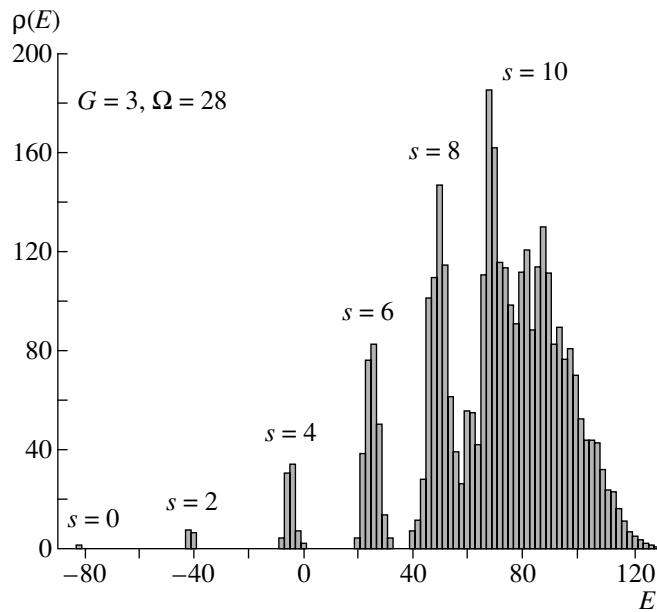


Fig. 6. Density of states in the half-occupied system with $\Omega = 28$ and pairing strength $G = 3$. The strong pairing dominates the single-particle structure, resulting in peaks of the level density that correspond to the quasispin families of the degenerate model. The 14-level equally spaced single-particle ladder structure is assumed with spacing setting the unit of energy.

their numerical scales are different, $T \approx 2.5T$. Furthermore, the concept of quasiparticle thermalization is meaningful only for relatively weak pairing, where large fluctuations due to the proximity of the phase transition are present. The quality of thermalization deteriorates as stronger pairing makes the dynamics more and more regular. The inability of the strongly paired system to fully thermalize the dynamics was demonstrated earlier [54]. The role of nonpairing

interactions is essential for equilibration. But the failure of the single-particle thermometer to reflect correctly the spectral evolution in the limit of very strong interaction is a general feature [19, 63].

D. Pairing Phase Transition

In Fig. 9, the pairing gap is plotted as a function of quasiparticle temperature. The gap was calculated

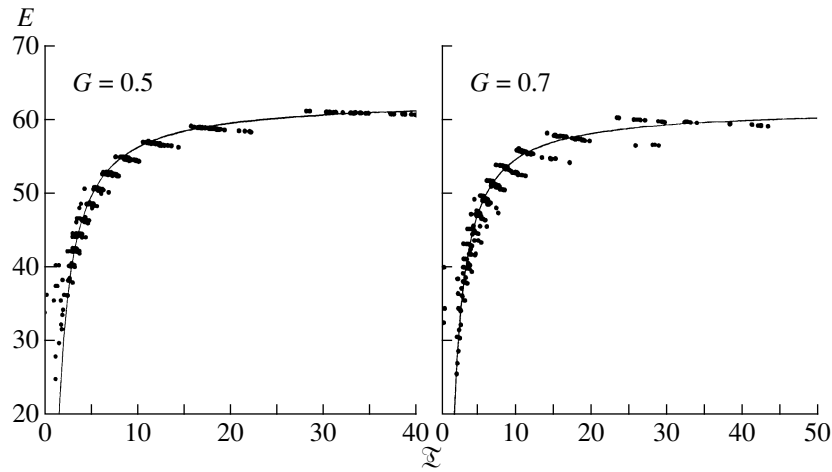


Fig. 7. Excitation energy and quasiparticle temperature T of individual states in the half-occupied, 12-level ladder model. The solid line shows the energy–temperature relation from Eq. (45), assuming scaling $T \approx 2.5T$. All quantities are expressed in the units of energy set by the single-particle ladder spacing.

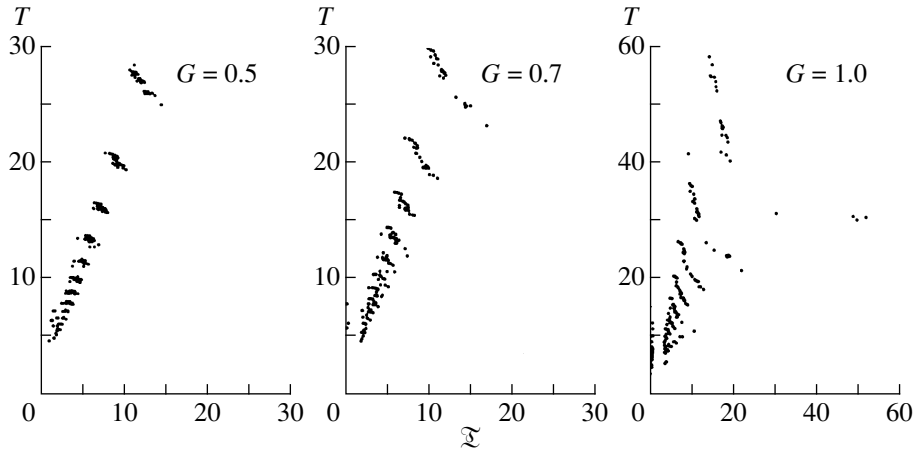


Fig. 8. Comparison of thermodynamic and quasiparticle temperatures for the half-occupied, 12-level ladder model. Three panels correspond to pairing strengths $G = 0.5, 0.7,$ and 1.0 . The unit of energy is set by the ladder spacing. The regular trends in scattered points confirm approximate thermalization with temperature ratio $T \approx 2.5T$. The agreement deteriorates for stronger pairing.

using Eq. (38) with the quasiparticle temperature replacing the BCS external temperature parameter. This makes the consideration consistent with the occupancies given by Eqs. (36) and (39). The half-occupied, 12-level ladder model was again used for this example. The choice of a larger system not only results in the increased number of $s = 0$ states, but, more importantly, reduces the particle-number fluctuations that can disrupt the fitting procedure, especially in the pairing phase transition region.

Figure 9 demonstrates the phase transition from the paired state at lower temperature (or excitation energy) to a normal state at higher temperature. Few low-lying states have a considerable pairing gap, whereas the gap disappears in sufficiently ex-

cited states. The invariant entropy [66] can be an alternative method for visualizing the phase transition [54, 67]. This quantity is basis-independent and reflects the sensitivity of a particular eigenstate to the changes in a parameter of the many-body Hamiltonian, here, the pairing strength G . The peak in the invariant entropy points out the location of the pairing phase transition as a function of G and excitation energy E of a particular state. However, it is important to note that the phase transition pattern is strongly influenced [19, 63] by other parts of residual interaction.

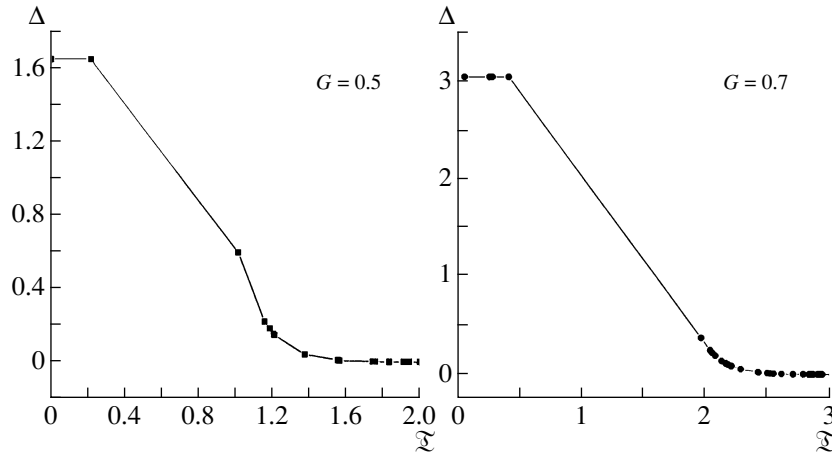


Fig. 9. Pairing gap as a function of quasiparticle temperature in the 12-level model (spacing sets the unit of energy) with pairing strength $G = 0.5$ and 0.7 .

7. NEW THEORETICAL PERSPECTIVES

A. Hartree–Fock Approximation Based on the Exact Pairing Solution

Instead of the normal Fermi occupation picture with a Slater determinant as a trial many-body function for the mean-field approximation, the EP solution with its specific single-particle occupancies provides a new starting point for the consistent consideration of other parts of the residual interaction. In this subsection, we illustrate this point with the help of Belyaev's [68] pairing plus quadrupole ($P + Q$) model Hamiltonian for a single- j level,

$$H = -GL^\dagger L - \frac{\chi}{2} \sum_{\kappa} \mathcal{M}_{2\kappa}^\dagger \mathcal{M}_{2\kappa}, \quad (46)$$

where the multipole operators are defined as

$$\mathcal{M}_{K\kappa} = \sum_{m_1 m_2} (-1)^{j-m_1} \begin{pmatrix} j & K & j \\ -m_1 & \kappa & m_2 \end{pmatrix} a_2^\dagger a_1. \quad (47)$$

Only the ratio χ/G of the strength of quadrupole–quadrupole interaction to the pairing strength is important since the energy scale can be fixed so that $G = 1$.

In the pure pairing limit, $\chi = 0$, the degenerate pairing model is recovered with the ground-state energy ($\Omega = 2j + 1$)

$$E = G \frac{N}{4} (\Omega - N + 2). \quad (48)$$

Pairing correlation energy in the BCS with constant pairing is given by Δ^2/G . For the exact solution, we define the correlation energy as the ground-state expectation value of the pairing part of the Hamiltonian

with the monopole contribution subtracted. In the degenerate case,

$$E_{\text{corr}} = G \frac{N}{4} (\Omega - N). \quad (49)$$

The opposite limit with no pairing can be treated by making a transition to a deformed mean field in the Hartree approximation [69]. For axially symmetric deformation, the expectation value of the quadrupole moment is

$$\langle \mathcal{M}_{20} \rangle = \sum_m \frac{2[3m^2 - j(j+1)]}{\sqrt{\Omega(\Omega^2 - 1)(\Omega^2 - 4)}} n_m \quad (50)$$

in terms of the occupation numbers $n_m = \langle a_m^\dagger a_m \rangle$ in the intrinsic frame with the z axis oriented along the symmetry axis. In this case,

$$\langle \mathcal{M}_{2-2} \rangle = \langle \mathcal{M}_{22} \rangle = 0. \quad (51)$$

The deformed single-particle energies in the body-fixed frame can be obtained via the usual self-consistency requirement,

$$\epsilon_m = -\chi \frac{2[3m^2 - j(j+1)]}{\sqrt{\Omega(\Omega^2 - 1)(\Omega^2 - 2)}} \langle \mathcal{M}_{20} \rangle. \quad (52)$$

The energy minimum for an even- N system corresponds to the Fermi occupation of the $N/2$ lowest pairwise degenerate orbitals $|m| = 1/2, 3/2, \dots, (N-1)/2$ for prolate or $|m| = j, j-1, \dots, j-(N-2)/2$ for oblate shape. The corresponding quadrupole moment is then given by

$$\langle \mathcal{M}_{20} \rangle = -\frac{1}{2} \frac{N(\Omega^2 - N^2)}{\sqrt{\Omega(\Omega^2 - 1)(\Omega^2 - 4)}} \quad (53)$$

for prolate deformation and

$$\langle \mathcal{M}_{20} \rangle = \frac{1}{2} \frac{N(2\Omega - N)(\Omega - N)}{\sqrt{\Omega(\Omega^2 - 1)(\Omega^2 - 4)}} \quad (54)$$

for oblate deformation. Deformation energy is quadratic in $\langle \mathcal{M}_{20} \rangle$, so that the oblate deformation is preferred for $N < \Omega/2$ and the prolate one for $N > \Omega/2$. In the special case of a half-occupied system, the deformation energies corresponding to oblate and prolate shapes become equal.

The full problem is driven by the competition between pairing and deformation. While deformation tends to split the single-particle energies (Nilsson orbitals), Eq. (52), the pairing can resist such a shape transition by creating a particle distribution unfavorable for deformation. In the single- j model, these effects have been discussed by Baranger and Kumar [69] with the help of the BCS and the Hartree approximation. However, as demonstrated earlier, the BCS may be unreliable in the transitional region. The use of the projected HFB and the resulting improvement against traditional HFB for a similar single- j model have recently been discussed in [70]. Our goal here is to supplement the Hartree treatment with the exact pairing solution.

Similar to the Hartree + BCS approach in [69], we look for a self-consistent solution, where the occupation numbers in the deformed basis agree with the exact solution to the pairing problem [71]. Prior to calculations, one can estimate the ratio χ/G corresponding to the BCS phase transition. Assuming for example an oblate shape with $N \leq \Omega/2$, we have the Fermi energy at $m = j - (N - 2)/2$ with the density of single-particle states found approximately as $\nu_F = 2/(\epsilon_{m-1} - \epsilon_m)$, which for a half-occupied system leads to

$$(\chi/G)_{\text{crit}} \approx 3.6\Omega. \quad (55)$$

In Fig. 10, we present the results for a model with $j = 19/2$. The particle number $N = 8$ was selected to avoid an exactly half-occupied shell when particle-hole symmetry and oblate-to-prolate shape change lead to special features that are of no interest for our goal. For this model, the transition from spherical to deformed shape takes place at $\chi/G \approx 70$ [Eq. (55)]. The pairing correlation energy shown in Fig. 10a as a function of χ/G starts near $\chi/G = 0$ with a value prescribed by the degenerate model. As the relative strength of the quadrupole-quadrupole interaction increases, the deformation inhibits pairing. However, in Fig. 10a, we see a key difference between the BCS and exact treatment. Within the BCS, the pairing correlation energy goes to zero quite sharply once the system becomes deformed. In contrast, the exact solution finds that pairing correlations decay very slowly and extend far into the deformed region. In Fig. 10b, the expectation value of $\langle \mathcal{M}_{20} \rangle$ is shown as a function of χ/G . In the pairing limit $\chi/G \rightarrow 0$, the deformation is zero, whereas in the deformed limit the value $\langle \mathcal{M}_{20} \rangle$

is expressed via Eq. (54) or (53). Here again, the exact treatment produces a softened and extended phase transition.

The Hartree approximation ignores another important effect relevant to our consideration, namely, the contribution of the exchange terms to the pairing channel. This contribution is particularly strong in small systems and leads to an additional enhancement of the pairing strength $G \rightarrow G + 2\chi/\Omega^2$ [72]. The results of Hartree-Fock + EP calculations that include this additional term are shown in Fig. 11. Due to the exchange term, pairing correlations never disappear. The presence of pairing correlations in a pure quadrupole-quadrupole Hamiltonian is also confirmed by an exact solution in the full shell-model diagonalization [72]. The BCS treatment, however, fails to reproduce this effect.

B. New Random Phase Approximation

Here we show how the RPA-like approximation can be developed starting from the exact solution of the pairing problem. There are two main types of RPA used in the literature (and a variety of close approaches distinguished by the details of the formalism), the RPA based on the vacuum of noninteracting particles or that of the BCS, or HFB, quasiparticles (the so-called QRPA). We will try to describe collective vibrations generated by the residual interaction on top of the exact ground state of the pairing problem. The formalism of the generalized density matrix [73, 74] seems to be suitable for this purpose.

The generalized density matrix (GDM) is the set of the operators

$$R_{12} = a_2^\dagger a_1 \quad (56)$$

acting in the full Hilbert space of a many-body system; this set at the same time forms a matrix labeled by single-particle subscripts (1, 2). We do not perform any canonical transformation to the quasiparticle operators and therefore work invariably within a system of a certain particle number. The one-body observables as operators in many-body space are traces of the GDM operator over single-particle indices,

$$Q = \sum_a q_a \quad \Rightarrow \quad Q = \sum_{12} q_{12} a_1^\dagger a_2 = \text{tr}(qR). \quad (57)$$

With the Hamiltonian of the system taken as a sum of independent particle energies in the mean field, ϵ_1 , and the general residual two-body interaction $V_{12;34}$, the exact operator equations of motion for the GDM can be symbolically written as

$$[R, H] = [S, R], \quad (58)$$

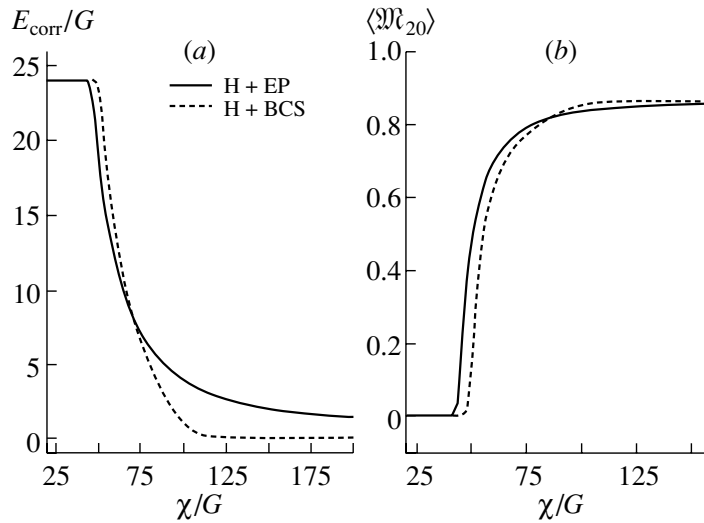


Fig. 10. Comparison of pairing correlation energy (a) and quadrupole deformation (b) for Hartree + BCS and Hartree + EP treatments of the $P + Q$ model for a single- j level, $j = 19/2$, and $N = 8$ particles.

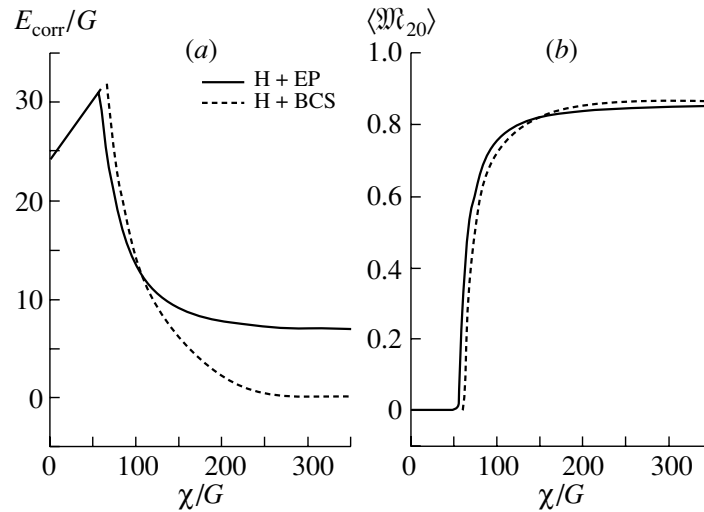


Fig. 11. Comparison of pairing correlation energy and quadrupole deformation; in contrast to Fig. 10, the exchange contribution from the quadrupole–quadrupole interaction to the pairing channel is included.

where S is the generalized self-consistent field operator (a linear functional of the GDM),

$$S = \epsilon + W\{R\}, \quad W_{14}\{R\} = \sum_{23} V_{12;34} R_{32}, \quad (59)$$

and the interaction matrix elements are antisymmetrized.

Now, we assume that the Hamiltonian contains the pairing part (1) as well as other residual interactions, $H = H_p + H'$. Correspondingly, we can set

$$\begin{aligned} R &= R^\circ + R', & W &= W^\circ + W', & (60) \\ W^\circ &= W\{R^\circ\}, & W' &= W\{R'\}. \end{aligned}$$

The assumption of the exact solution of the pairing problem means that we found the occupancies, R° , and the pairing potential, W° , satisfying

$$[R^\circ, H_p] = [\epsilon + W^\circ, R^\circ]. \quad (61)$$

This stage of the solution provides the states $|s, a\rangle$ with seniority s and energy E_{sa} , where a numbers the states within the subset of certain seniority; if needed, we also can explicitly indicate rotational quantum numbers J_a and M_a . The remaining part R' of the GDM should satisfy

$$\begin{aligned} &[R', H_p] + [R^\circ, H'] + [R', H'] & (62) \\ &= [W', R^\circ] + [\epsilon + W^\circ, R'] + [W', R']. \end{aligned}$$

The commutators in such expressions are to be understood as, for example,

$$[W', R']_{12} = \sum_3 (W'_{13} R'_{32} - R'_{13} W'_{32}). \quad (63)$$

This is the point where we can make RPA-like approximations.

For definiteness, we consider the transitions from the paired states $s = 0, J = 0$ to the states with $s = 2, J \neq 0$ in the next sector. We are looking for a collective mode that is related to such excitations. This means that there exist states, in our case coherent combinations of excited states with certain J , that have large off-diagonal matrix elements of excitation by a one-body multipole operator from the ground state. The latter can in turn be renormalized by the collective mode. Let us characterize this branch of the spectrum with the help of collective coordinates α and conjugate momenta π (we omit in this symbolic derivation their quantum numbers of angular momentum and its projection). These variables are Hermitian quantum operators that satisfy the commutation relation $[\alpha, \pi] = i$ so that no procedure of subsequent requantization is needed. The collective Hamiltonian of the mode can be written as

$$H' = \frac{1}{2} C \alpha^2 + \frac{1}{2B} \pi^2 + \dots, \quad (64)$$

where the scalar contraction of the tensor operators is implied and the dots include high-order anharmonic terms important for the soft mode [75, 76].

We are looking for the operator solution of Eq. (62) in the form of an expansion in collective operators α and π ,

$$R'_{12} = r_{12}^{(10)} \alpha + r_{12}^{(01)} \pi + \dots \quad (65)$$

and

$$W'_{12} = w_{12}^{(10)} \alpha + w_{12}^{(01)} \pi + \dots, \quad (66)$$

where the superscripts (n, m) refer to the component containing n collective coordinate and m collective momentum operators. The dots again denote the higher order parts, $n + m > 1$, symmetrized in due way [75, 76]. The collective operators producing the transition in many-body space are written explicitly, whereas the coefficients $r_{12}^{(nm)}$ and $w_{12}^{(nm)}$ are the c numbers to be found as single-particle amplitudes of the coherent superposition that forms a collective mode. The operator expansion (65), (66) does not assume the smallness of anharmonic effects—we merely decompose the problem in various operator structures. In the present context, we limit ourselves to the harmonic part, although it can be used [75, 76] for situations of strong anharmonicity as well.

The operator R , by definition (56), has seniority selection rules $|\Delta s| = 2$. We take in the operator

Eq. (62) matrix elements $\langle 0|c\rangle$ between the ground state $|0\rangle$ and the collective state $|c\rangle$ in the adjacent sector $s = 2$ with angular momentum corresponding to that of collective operators α and π . Now, we evaluate the matrix elements of various terms in Eq. (62) aiming at the segregation of terms linear in α and π . The first term on the left-hand side gives, according to Eq. (65),

$$[R'_{12}, H_p] = (\bar{E}_c^\circ - \bar{E}_0^\circ)(r_{12}^{(10)} \alpha + r_{12}^{(01)} \pi). \quad (67)$$

Here, the barred energies are the centroids of the energy distribution of the actual ground state and the one-phonon state in the sectors $s = 0$ and $s = 2$, respectively. The second term on the left in Eq. (62) does not have the required matrix elements, whereas in the commutator $[R', H']$ we need to perform commutation explicitly using the assumed form of the collective operators (65)–(67),

$$[R'_{12}, H'] = \frac{i}{B} r_{12}^{(10)} \pi - i C r_{12}^{(01)} \alpha. \quad (68)$$

The situation with the terms $[W^\circ, R']$ and $[W', R^\circ]$ is more complicated. Within each sector of given s , the pairing solution GDM R° has not only diagonal but also off-diagonal elements between the eigenstates of H_p . As shown in Figs. 2 and 3, very few pair-vibrational states have significant off-diagonal matrix elements of this type. For our illustrative purposes, here we neglect the off-diagonal terms within a given sector and take into account only diagonal elements of R° and W° . The neglected contributions correspond to the anharmonic admixtures of pair vibrations to multipole modes and can be easily included in the consideration. Because of the specific character of the monopole pairing interaction, the matrix elements of R° and W° are diagonal over single-particle subscripts as well. Higher order structures in the collective Hamiltonian and in the GDM, as well as terms generated by the commutator $[W', R']$, do not contribute to matrix elements linear in α and π and with the selection rule $\Delta s = 2$. But, similar to Eq. (67), the commutators with R° and W° bring in the differences of the single-particle occupancies and pairing potentials averaged over the states contributing to the collective mode.

As a result, we come to the coupled equations for the coordinate and momentum RPA amplitudes (these contributions can be distinguished by their behavior under time-reversal operation in the sector with $J \neq 0$):

$$r_{12}^{(10)} \Omega_{12} - i C r_{12}^{(01)} = [\bar{n}_2(c) - \bar{n}_1(0)] w_{12}^{(10)}, \quad (69)$$

$$r_{12}^{(01)} \Omega_{12} + \frac{i}{B} r_{12}^{(10)} = [\bar{n}_2(c) - \bar{n}_1(0)] w_{12}^{(01)}. \quad (70)$$

Here, the generalized frequencies are introduced,

$$\Omega_{12} = \bar{E}_c^\circ - \bar{E}_0^\circ + \epsilon_2 - \epsilon_1 + \bar{W}_c^\circ - \bar{W}_0^\circ. \quad (71)$$

This set of equations leads to a formal solution, analogous to that in the conventional RPA,

$$r_{12}^{(10)} = \frac{[\bar{n}_2(c) - \bar{n}_1(0)]}{\Omega_{12}^2 - \omega^2} (\Omega_{12} w_{12}^{(10)} + iC w_{12}^{(01)}), \quad (72)$$

$$r_{12}^{(01)} = \frac{[\bar{n}_2(c) - \bar{n}_1(0)]}{\Omega_{12}^2 - \omega^2} (\Omega_{12} w_{12}^{(01)} - \frac{i}{B} w_{12}^{(10)}), \quad (73)$$

where the unknown collective frequency is $\omega = (C/B)^{1/2}$.

The collective elements of the GDM are to be found from the integral Eqs. (72) and (73) with the specific choice of the residual interaction self-consistently generating the field W' [Eq. (60)]. This can be done explicitly in the case of the factorizable multipole–multipole force; the frequency ω and correct normalization of the mode are also obtained in this process similar to the standard procedure in terms of the barred quantities. Having at our disposal the phonon amplitudes $r_{12}^{(10)}$ and $r_{12}^{(01)}$, we can self-consistently find the barred quantities averaged over the collective wave functions. This procedure, which reminds one of the thermal RPA built on the equilibrium density matrix but with occupation numbers and mean-field corrections defined by the interaction rather than by an external heat bath, can be performed in an iterative manner. The cranking description for the deformed nucleus can also be reformulated in the same spirit; it is interesting to note that the pure EP solution predicts [54] an yrast-line with the moment of inertia close to the rigid-body value.

8. CONCLUSION

The pioneering work by Belyaev [8] carried out a detailed analysis of pairing phenomena in nuclei. Applying the BCS techniques in the nuclear shell-model environment, he demonstrated the effects of pairing on various nuclear properties, including the ground-state structure, single-particle transitions, collective vibrations, onset of deformations, and rotations. It was shown that the Cooper phenomenon in systems with a discrete single-particle spectrum does require, in contrast to large systems, a certain strength of the pairing interaction. The drawbacks of the BCS approximation, related to the particle-number violation and the sharp disappearance of pairing correlations at the phase transition point, were also pointed out.

The development started with Belyaev's work and, supported by similar studies [77, 78], was continued throughout the next forty years. Now, the pairing problem is alive and well, being one of the main

chapters of modern nuclear physics and mesoscopic physics in general. The interest in pairing is constantly revived by the accumulation of data and especially by the advances towards nuclei from stability, where the pairing is a key tool that determines the binding of a system and its response to the excitation. At this point, it becomes increasingly important to get rid of the shortcomings of the BCS approximation and unify the description of the structure and reactions.

We presented a way of solving the pairing problem essentially along the lines similar to that of Belyaev's paper, replacing the BCS approximation by the exact solution simplified by the seniority symmetry. As a magnifying glass, this solution reveals and fixes the weak points of the standard approach. We saw the importance of the exact treatment for the ground state, low-lying excitations, coupling through the continuum, and spectroscopic factors associated with single-particle removal and pair emission (transfer) reactions. We could also discuss on the new basis the global properties of the spectrum, thermalization, and the phase transition region. In many cases, this exact treatment of pairing is in practice simpler than solving the BCS equations with necessary corrections.

Certainly, the pairing problem is only a part of the physics of strongly interacting self-sustaining systems. Other interactions, with their own coherent and chaotic features, should be included in the consideration. We gave preliminary answers to the questions of further approximations necessary for the cases when the full problem does not allow for a complete solution. New generalizations of the mean-field approach and random-phase approximations can be developed on the background of the exactly found paired state. The interplay of pairing and other residual interactions can be an exciting and practically important topic of future studies.

The inspiring influence of Belyaev's ideas is gratefully acknowledged by the authors, who belong to the first and third generation of his pupils.

ACKNOWLEDGMENTS

We are grateful to B.A. Brown for collaboration and numerous discussions.

This work was supported by the NSF, grant nos. PHY-0070911 and PHY-0244453, and by the US Department of Energy, Nuclear Physics Division, contract no. W-31-109-ENG-38.

REFERENCES

1. A. Bohr and B. R. Mottelson, *Nuclear Structure*, Vol. 1: *Single-Particle Motion* (Benjamin, New York, 1969).
2. M. G. Mayer and J. H. D. Jensen, *Elementary Theory of Nuclear Shell Structure* (Wiley, New York, 1955).
3. G. Racah, Phys. Rev. **63**, 367 (1943).
4. G. Racah and I. Talmi, Phys. Rev. **89**, 913 (1953).
5. B. R. Judd, *Operator Techniques in Atomic Spectroscopy* (Princeton University Press, Princeton, 1998).
6. J. Bardeen, L. N. Cooper, and J. R. Schrieffer, Phys. Rev. **106**, 162 (1957); Phys. Rev. **108**, 1175 (1957).
7. A. Bohr, B. R. Mottelson, and D. Pines, Phys. Rev. **110**, 936 (1958).
8. S. T. Belyaev, K. Dan. Vidensk. Selsk. Mat. Fys. Medd. **31** (11) (1959).
9. A. L. Goodman, Adv. Nucl. Phys. **11**, 263 (1979).
10. N. N. Bogoliubov, Zh. Éksp. Teor. Fiz. **34**, 58 (1958); Physica **26**, 1 (1960).
11. H. J. Lipkin, Ann. Phys. (N.Y.) **9**, 272 (1960).
12. Y. Nogami, Phys. Rev. **134**, B313 (1964); Y. Nogami and I. J. Zucker, Nucl. Phys. **60**, 203 (1964).
13. W. Satula and R. Wyss, Nucl. Phys. A **676**, 120 (2000).
14. J. A. Sheikh and P. Ring, Nucl. Phys. A **665**, 71 (2000).
15. G. Do Dang and A. Klein, Phys. Rev. **143**, 735 (1966); Phys. Rev. **147**, 689 (1966).
16. J. Bang and J. Krumlinde, Nucl. Phys. A **141**, 18 (1970).
17. F. Andreozzi, A. Covello, A. Gargano, *et al.*, Phys. Rev. C **21**, 1094 (1980); Phys. Rev. C **32**, 293 (1985).
18. K. Hagino and G. F. Bertsch, Nucl. Phys. A **679**, 163 (2000).
19. V. Zelevinsky, B. A. Brown, N. Frazier, and M. Horoi, Phys. Rep. **276**, 85 (1996).
20. N. Giovanardi, F. Barranco, R. A. Broglia, and E. Vigezzi, Phys. Rev. C **65**, 041304 (2002).
21. K. Bennaceur, J. Dobaczewski, and M. Ploszajczak, Phys. Rev. C **60**, 034308 (1999).
22. A. Poves and A. P. Zuker, Phys. Rep. **70**, 235 (1981).
23. B. A. Brown and B. H. Wildenthal, Annu. Rev. Nucl. Part. Sci. **38**, 29 (1988).
24. W. A. Richter, M. G. van der Merwe, R. E. Julies, and B. A. Brown, Nucl. Phys. A **523**, 325 (1991).
25. B. Wildenthal, Prog. Part. Nucl. Phys. **11**, 5 (1984).
26. Y. Alhassid, D. J. Dean, S. E. Koonin, *et al.*, Phys. Rev. Lett. **72**, 613 (1994).
27. M. Honma, T. Mizusaki, and T. Otsuka, Phys. Rev. Lett. **77**, 3315 (1996).
28. M. Horoi, A. Volya, and V. Zelevinsky, Phys. Rev. Lett. **82**, 2064 (1999).
29. A. Volya, B. A. Brown, and V. Zelevinsky, Phys. Lett. B **509**, 37 (2001).
30. H. Chen, T. Song, and D. J. Rowe, Nucl. Phys. A **582**, 181 (1995).
31. Yang Yi and Xu Gong-ou, Phys. Rev. C **43**, 1225 (1991).
32. D. J. Rowe, *Nuclear Collective Motion, Models, and Theory* (Methuen and Co., London, 1970).
33. R. A. Broglia, J. Terasaki, and N. Giovanardi, Phys. Rep. **335**, 1 (2000).
34. P. Ring and P. Schuck, *The Nuclear Many-Body Problem* (Springer-Verlag, New York, 1980).
35. G. Do Dang, R. M. Dreizler, A. Klein, and C. Wu, Phys. Rev. **172**, 1022 (1968).
36. A. Volya and V. Zelevinsky, Preprint MSUCL-1144 (1999).
37. J. Högaasen-Feldman, Nucl. Phys. **28**, 258 (1961).
38. O. Johns, Nucl. Phys. A **154**, 65 (1970).
39. D. J. Rowe, Rev. Mod. Phys. **40**, 153 (1968).
40. J. Dukelsky and P. Schuck, Nucl. Phys. A **512**, 466 (1990); Phys. Lett. B **387**, 233 (1996).
41. F. Krmpotic, E. J. V. de Passos, D. S. Delion, *et al.*, Nucl. Phys. A **637**, 295 (1998).
42. R. W. Richardson, Phys. Lett. **3**, 277 (1963); Phys. Lett. **5**, 82 (1963); Phys. Lett. **14**, 325 (1965); J. Math. Phys. (N.Y.) **6**, 1034 (1965); J. Math. Phys. (N.Y.) **18**, 1802 (1977); Phys. Rev. **141**, 949 (1966); Phys. Rev. **144**, 874 (1966); Phys. Rev. **159**, 792 (1967).
43. R. W. Richardson and N. Sherman, Nucl. Phys. **52**, 221 (1964).
44. J. Dukelsky, C. Esebbag, and S. Pittel, Phys. Rev. Lett. **88**, 062501 (2002).
45. F. J. Dyson, J. Math. Phys. (N.Y.) **3**, 166 (1962).
46. Feng Pan, J. P. Draayer, and W. E. Ormand, Phys. Lett. B **422**, 1 (1998).
47. Feng Pan, J. P. Draayer, and Lu Guo, J. Phys. A **33**, 1597 (2000).
48. J. Dukelsky and P. Schuck, Phys. Rev. Lett. **86**, 4207 (2001).
49. O. Burglin and N. Rowley, Nucl. Phys. A **602**, 21 (1996).
50. H. Molière and J. Dudek, Phys. Rev. C **56**, 1795 (1997).
51. A. K. Kerman, R. D. Lawson, and M. H. Macfarlane, Phys. Rev. **124**, 162 (1961).
52. N. Auerbach, Nucl. Phys. **76**, 321 (1966).
53. A. Holt, T. Engeland, M. Hjorth-Jensen, and E. Osnes, Nucl. Phys. A **634**, 41 (1998).
54. A. Volya, V. Zelevinsky, and B. A. Brown, Phys. Rev. C **65**, 054312 (2002).
55. N. Frazier, B. A. Brown, and V. Zelevinsky, Phys. Rev. C **54**, 1665 (1996).
56. V. G. Zelevinsky, Yad. Fiz. **65**, 1220 (2002) [Phys. At. Nucl. **65**, 1188 (2002)].
57. M. Horoi, B. A. Brown, and V. Zelevinsky, Phys. Rev. C **65**, 027303 (2002).
58. V. Zelevinsky and A. Volya, in *Challenges of Nuclear Structure*, Ed. by A. Covello (World Sci., Singapore, 2002), p. 261.
59. M. Horoi, B. A. Brown, and V. Zelevinsky, Phys. Rev. C **67**, 034303 (2003).
60. C. Mahaux and H. A. Weidenmüller, *Shell-Model Approach to Nuclear Reactions* (North-Holland, Amsterdam, 1969).
61. V. V. Sokolov and V. G. Zelevinsky, Nucl. Phys. A **504**, 562 (1989).

62. A. Volya and V. Zelevinsky, Phys. Rev. C **67**, 054322 (2003).
63. V. Zelevinsky, Annu. Rev. Nucl. Part. Sci. **46**, 237 (1996).
64. M. Guttormsen, M. Hjorth-Jensen, E. Melby, *et al.*, Phys. Rev. C **64**, 034319 (2001).
65. N. Dinh Dang and V. Zelevinsky, Phys. Rev. C **64**, 064319 (2001).
66. V. V. Sokolov, B. A. Brown, and V. Zelevinsky, Phys. Rev. E **58**, 56 (1998).
67. P. Cejnar, V. Zelevinsky, and V. V. Sokolov, Phys. Rev. E **63**, 036127 (2001).
68. S. T. Belyaev, Zh. Éksp. Teor. Fiz. **39**, 1387 (1961) [Sov. Phys. JETP **12**, 968 (1961)].
69. M. Baranger and K. Kumar, Nucl. Phys. **62**, 113 (1965).
70. J. A. Sheikh, P. Ring, E. Lopes, and R. Rossignoli, Phys. Rev. C **66**, 044318 (2002).
71. A. Volya, B. A. Brown, and V. Zelevinsky, Prog. Theor. Phys. Suppl. **146**, 636 (2002).
72. A. Volya, Phys. Rev. C **65**, 044311 (2002).
73. S. T. Belyaev and V. G. Zelevinsky, Yad. Fiz. **16**, 1195 (1972) [Sov. J. Nucl. Phys. **16**, 657 (1972)].
74. V. G. Zelevinsky, Prog. Theor. Phys. Suppl. **74–75**, 251 (1983).
75. V. Zelevinsky and A. Volya, in *Perspectives of Nuclear Structure and Nuclear Reactions* (Dubna, 2002), p. 101.
76. V. Zelevinsky, AIP Conf. Proc. **638**, 155 (2002).
77. V. G. Soloviev, Nucl. Phys. **9**, 655 (1958/1959); K. Dan. Vidensk. Selsk. Mat. Fys. Medd. **1** (11) (1961).
78. A. B. Migdal, Nucl. Phys. **13**, 655 (1959).

From the Bose–Einstein to Fermion Condensation*

M. Ya. Amusia^{1),2)}, A. Z. Msezane³⁾, and V. R. Shaginyan^{3),4)}**

Received January 27, 2003

Abstract—The appearance of the fermion condensation, which can be compared to the Bose–Einstein condensation, in different Fermi liquids is considered; its properties are discussed; and a large amount of experimental evidence in favor of the existence of the fermion condensate (FC) is presented. We show that the appearance of FC is a signature of the fermion condensation quantum phase transition (FCQPT), which separates the regions of normal and strongly correlated liquids. Beyond the FCQPT point, the quasiparticle system is divided into two subsystems, one containing normal quasiparticles and the other, FC, localized at the Fermi level. In the superconducting state, the quasiparticle dispersion in systems with FC can be represented by two straight lines, characterized by effective masses M_{FC}^* and M_{L}^* and intersecting near the binding energy E_0 , which is of the order of the superconducting gap. The same quasiparticle picture and the energy scale E_0 persist in the normal state. We demonstrate that fermion systems with FC have features of a “quantum protectorate” and show that strongly correlated systems with FC, which exhibit large deviations from the Landau Fermi liquid behavior, can be driven into the Landau Fermi liquid by applying a small magnetic field B at low temperatures. Thus, the essence of strongly correlated electron liquids can be controlled by weak magnetic fields. A reentrance into the strongly correlated regime is observed if the magnetic field B decreases to zero, while the effective mass M^* diverges as $M^* \propto 1/\sqrt{B}$. The regime is restored at some temperature $T^* \propto \sqrt{B}$. The behavior of Fermi systems that approach FCQPT from the disordered phase is considered. This behavior can be viewed as a highly correlated one, because the effective mass is large and strongly depends on the density. We expect that FCQPT takes place in trapped Fermi gases and in low-density neutron matter, leading to stabilization of the matter by lowering its ground-state energy. When the system recedes from FCQPT, the effective mass becomes density independent and the system is suited perfectly to be conventional Landau Fermi liquid.

© 2003 MAIK “Nauka/Interperiodica”.

1. INTRODUCTION

This paper is dedicated to the eightieth birthday of S.T. Belyaev, whose contribution to modern theoretical physics is enormous indeed. His interest in and deep understanding of different domains of physics, including the experimental one, is very impressive. Always on the front line of scientific research, he is a source of inspiration for mature physicists and an excellent role model for the beginners. We sincerely wish Belyaev long healthy years to come.

Experimental and theoretical explorations of Bose systems below the temperatures of Bose–Einstein

condensation have entailed great difficulties. Among the pioneers of the theoretical studies is Belyaev, in whose papers a solid base for taking into account the interaction among bosons at low temperatures has been established [1, 2].

In a system of interacting bosons at temperatures lower than the temperature of Bose–Einstein condensation, a finite number of particles are concentrated in the lowest level. In the case of a noninteracting Bose gas at zero temperature, $T = 0$, this number is simply equal to the total number of particles in the system. In a homogeneous system of noninteracting bosons, the lowest level is the state with zero momentum, and the ground-state energy is equal to zero. For a noninteracting Fermi system, such a state is impossible, and its ground-state energy $E_{\text{g.s}}$ reduces to the kinetic energy and is proportional to the total number of particles. Imagine an interacting system of fermions with a pure repulsive interaction. Let us increase its interaction strength. As soon as it becomes sufficiently large and the potential energy starts to prevail over the kinetic energy, we can expect the system to undergo a phase transition when a finite number of the Cooper-like pairs with an infinitely

*This article was submitted by the authors in English.

¹⁾Racah Institute of Physics, Hebrew University, Jerusalem, Israel.

²⁾Ioffe Physicotechnical Institute, Russian Academy of Sciences, Politekhnicheskaya ul. 26, St. Petersburg, 194021 Russia.

³⁾CTSPS, Clark Atlanta University, Atlanta, GA, 30314 USA.

⁴⁾Petersburg Nuclear Physics Institute, Russian Academy of Sciences, Gatchina, 188350 Russia.

** e-mail: vrshag@thd.pnpi.spb.ru

small binding energy can condense at the Fermi level. Such a state resembles the Bose–Einstein condensation and can be viewed as fermion condensation. This phase transition leads to the onset of the fermion condensate (FC) and separates a strongly interacting Fermi liquid from a strongly correlated one. Lowering the potential energy, the fermion condensation decreases the total energy. Unlike the Bose–Einstein condensation, which occurs even in a system of noninteracting bosons, the fermion condensation can take place if the coupling constant of the interaction is large or the corresponding Landau amplitudes are large and repulsive.

One of the most challenging problems of modern physics is the structure and properties of systems with large coupling constants. It is well known that the theory of liquids with strong interaction is close to the problem of systems with a large coupling constant. The first solution to this problem was offered by the Landau theory of Fermi liquids, later called “normal,” by introducing the notion of quasiparticles and parameters that characterize the effective interaction among them [3]. The Landau theory can be viewed as the low-energy effective theory in which high-energy degrees of freedom are removed at the cost of introducing the effective interaction parameters. Usually, it is assumed that the stability of the ground state of a Landau liquid is determined by the Pomeranchuk stability conditions: the stability is violated when even one of the Landau effective interaction parameters is negative and reaches a critical value. Note that the new phase, new ground state, at which the stability conditions are restored, can in principle again be described within the framework of the same theory.

It has been demonstrated, however, rather recently [4] that the Pomeranchuk conditions cover not all possible instabilities: one of them is missed. It corresponds to the situation when, at the temperature $T = 0$, the effective mass, the most important characteristic of Landau quasiparticles, can become infinitely large. Such a situation, leading to profound consequences, can take place when the corresponding Landau amplitude being repulsive reaches some critical value. This leads to a completely new class of strongly correlated Fermi liquids with FC [4, 5], which is separated from that of a normal Fermi liquid by the fermion condensation quantum phase transition (FCQPT) [6].

In the FCQPT case, we are dealing with the strong coupling limit, where an absolutely reliable answer cannot be given on the bases of a pure theoretical first-principles foundation. Therefore, the only way to verify that FC occurs is to consider experimental facts that can be interpreted as confirming the existence of such a state. We believe that

these facts are seen in some features of those two-dimensional (2D) systems with interacting electrons or holes which can be represented by doped quantum wells and high- T_c superconductors. Considering the heavy-fermion metals, the 2D systems of ^3He , the trapped neutrons, and Fermi gases, we will show that FC can also exist in these systems.

The goal of our paper is to describe the behavior of Fermi systems with FC and to show that the existing data on strongly correlated liquids can be well understood within the theory of Fermi liquids with FC. In Section 2, we review the general features of Fermi liquids with FC in their normal state. Section 3 is devoted to consideration of the superconductivity in the presence of FC. We show that the superconducting state is totally transformed by the presence of FC. For instance, the maximum value Δ_1 of the superconducting gap can be as large as $\Delta_1 \sim 0.1\varepsilon_F$, while for normal superconductors one has $\Delta_1 \sim 10^{-3}\varepsilon_F$. Here, ε_F is the Fermi level. In Section 4, we describe the quasiparticle’s dispersion and its line shape and show that they strongly deviate from the case of normal Landau liquids. In Section 5, we apply our theory to explain the main properties of heavy-fermion metals. We demonstrate that it is possible to control the main properties, or even the essence, of strongly correlated electron liquids by weak magnetic fields. Section 6 deals with the possibility of FCQPT in different Fermi systems, such as 2D systems of electrons and 2D ^3He liquids, neutron matter at low density, and trapped Fermi gases. In Section 7, we describe the behavior of Fermi systems which approach FCQPT from the disordered phase. In the vicinity of FCQPT, this behavior can be viewed as a highly correlated one, because the effective mass is large and strongly depends on the density. Finally, in Section 8, we summarize our main results.

2. NORMAL STATE OF FERMION LIQUIDS WITH FC

Let us start by explaining the important points of the FC theory, which is a special solution of the Fermi liquid theory equations [3] for the quasiparticle occupation numbers $n(p, T)$,

$$\begin{aligned} \frac{\delta(F - \mu N)}{\delta n(p, T)} &= \varepsilon(p, T) - \mu(T) \\ -T \ln \frac{1 - n(p, T)}{n(p, T)} &= 0, \end{aligned} \quad (1)$$

which depends on the momentum p and temperature T . Here, $F = E - TS$ is the free energy, S is the entropy, and μ is the chemical potential, while

$$\varepsilon(p, T) = \frac{\delta E[n(p, T)]}{\delta n(p, T)} \quad (2)$$

is the quasiparticle energy. This energy is a functional of $n(p, T)$, just like the total energy $E[n(p, T)]$, entropy $S[n(p, T)]$, and other thermodynamic functions. The entropy $S[n(p, T)]$ is given by the familiar expression

$$S[n(p, T)] = - \sum_p [n(p, T) \ln n(p, T) + (1 - n(p, T)) \ln(1 - n(p, T))],$$

which stems from purely combinatorial considerations. Equation (1) is usually presented as the Fermi–Dirac distribution

$$n(p, T) = \left\{ 1 + \exp \left[\frac{\varepsilon(p, T) - \mu}{T} \right] \right\}^{-1}. \quad (3)$$

At $T \rightarrow 0$, one gets from Eqs. (1) and (3) the standard solution $n_F(p, T \rightarrow 0) \rightarrow \theta(p_F - p)$, with $\varepsilon(p \simeq p_F) - \mu = p_F(p - p_F)/M_L^*$, where p_F is the Fermi momentum and M_L^* is the Landau effective mass [3]:

$$\frac{1}{M_L^*} = \frac{1}{p} \frac{d\varepsilon(p, T=0)}{dp} \Big|_{p=p_F}. \quad (4)$$

It is implied that M_L^* is positive and finite at the Fermi momentum p_F . As a result, the T -dependent corrections to M_L^* , to the quasiparticle energy $\varepsilon(p)$, and to other quantities start with T^2 terms. But this solution is not the only one possible. There exist also “anomalous” solutions to Eq. (1) associated with the so-called fermion condensation [4, 7]. Being continuous and satisfying the inequality $0 < n(p) < 1$ within some region in p , such solutions $n(p)$ admit a finite value for the logarithm in Eq. (1) at $T \rightarrow 0$, yielding

$$\varepsilon(p) = \frac{\delta E[n(p)]}{\delta n(p)} = \mu; \quad p_i \leq p \leq p_f. \quad (5)$$

At $T = 0$, Eq. (5) determines the FCQPT, possessing solutions at some density $x = x_{FC}$ as soon as the effective interfermion interaction becomes sufficiently strong [7, 8]. For instance, in an ordinary electron liquid, the effective interelectron interaction is proportional to the dimensionless average interparticle distance $r_s = r_0/a_B$, with $r_0 \sim 1/p_F$ being the average distance and a_B the Bohr radius. When fermion condensation can take place at $r_s > 1$, it is considered to be in a low-density electron liquid [8].

Equation (5) leads to the minimum value of E , as a functional of $n(p)$, when a strong rearrangement of the single-particle spectra can take place in the system under consideration. We see from Eq. (5) that the occupation numbers $n(p)$ become variational parameters: the FC solution appears if the energy E can be lowered by alteration of the occupation numbers $n(p)$. Thus, within the region $p_i < p < p_f$, the solution $n(p) = n_F(p) + \delta n(p)$ deviates from the

Fermi step function $n_F(p)$ in such a way that the energy $\varepsilon(p)$ stays constant, while outside this region $n(p)$ coincides with $n_F(p)$. It is essential to note that the general consideration presented above has been verified by inspecting some simple models. As a result, it was shown that the onset of the FC does lead to lowering of the free energy [7, 9].

It follows from the above consideration that the superconductivity order parameter $\kappa(\mathbf{p}) = \sqrt{n(\mathbf{p})(1 - n(\mathbf{p}))}$ has a nonzero value over the region occupied by FC. The superconducting gap $\Delta(\mathbf{p})$, being linear in the coupling constant of the particle–particle interaction $V(\mathbf{p}_1, \mathbf{p}_2)$, increases the value of T_c because one has $2T_c \simeq \Delta_1$ [9] within the standard Bardeen–Cooper–Schrieffer (BCS) theory [10]. As shown in Section 3, if the superconducting gap is nonzero, $\Delta_1 \neq 0$, the FC quasiparticle effective mass becomes finite. Consequently, the density of states at the Fermi level becomes finite and the quasiparticles involved are delocalized. On the other hand, even at $T = 0$, Δ_1 can vanish, provided the interparticle interaction $V(\mathbf{p}_1, \mathbf{p}_2)$ is either repulsive or absent. Then, as seen from Eq. (5), the Landau quasiparticle system becomes separated into two subsystems. The first contains the Landau quasiparticles, while the second, related to FC, is localized at the Fermi surface and is formed by dispersionless quasiparticles. As a result, beyond the point of the FC phase transition, the standard Kohn–Sham scheme for the single-particle equations is no longer valid [11]. Such a behavior of systems with FC is clearly different from what one expects from the well-known local-density approach. Therefore, this is generally a very powerful method is hardly applicable to the description of systems with FC. It is also seen from Eq. (5) that a system with FC has a well-defined Fermi surface.

Let us assume that, with the decrease in the density or growth of the interaction strength, FC has just taken place. It means that $p_i \rightarrow p_f \rightarrow p_F$, and the deviation $\delta n(p)$ is small. Expanding the functional $E[n(p)]$ in a Taylor series with respect to $\delta n(p)$ and retaining the leading terms, one obtains from Eq. (5) the following relation:

$$\mu = \varepsilon(\mathbf{p}) = \varepsilon_0(\mathbf{p}) + \int F_L(\mathbf{p}, \mathbf{p}_1) \delta n(\mathbf{p}_1) \frac{d\mathbf{p}_1}{(2\pi)^2}; \quad (6)$$

$$p_i \leq p \leq p_f,$$

where $F_L(\mathbf{p}, \mathbf{p}_1) = \delta^2 E / \delta n(\mathbf{p}) \delta n(\mathbf{p}_1)$ is the Landau effective interaction. Both quantities, the interaction and the single-particle energy $\varepsilon_0(p)$, are calculated at $n(p) = n_F(p)$. Equation (6) acquires nontrivial solutions at some density $x = x_{FC}$, and FCQPT takes place if the Landau amplitudes depending on the density are positive and sufficiently large so that the potential energy is greater than the kinetic energy. Then,

the transformation of the Fermi step function $n(p) = \theta(p_F - p)$ into the smooth function defined by Eq. (5) becomes possible [4, 7]. It is seen from Eq. (5) that the FC quasiparticles form a collective state, since their energies are defined by the macroscopic number of quasiparticles within the momentum region $p_i - p_f$. The shape of the excitation spectra related to FC is not affected by the Landau interaction, which, generally speaking, depends on the system's properties, including the collective states, impurities, etc. The only thing determined by the interaction is the width of the FC region $p_i - p_f$, provided the interaction is sufficiently strong to produce the FC phase transition at all. Thus, we can conclude that the spectra related to FC are of a universal form, being dependent, as we will see below, mainly on temperature T if $T > T_c$ or on the superconducting gap at $T < T_c$.

According to Eq. (1), the single-particle excitations $\varepsilon(p, T)$ within the interval $p_i - p_f$ at $T_c \leq T \ll T_f$ are linear in T , which can be simplified at the Fermi level [12]. One obtains by expanding $\ln(\dots)$ in terms of $n(p)$

$$\begin{aligned} \varepsilon(p, T) - \mu(T) &= T \ln \frac{1 - n(p)}{n(p)} \\ &\simeq T \frac{1 - 2n(p)}{n(p)} \Big|_{p \simeq p_F}. \end{aligned} \quad (7)$$

Here, T_f is the temperature above which FC effects become insignificant [9],

$$\frac{T_f}{\varepsilon_F} \sim \frac{p_f^2 - p_i^2}{2M\varepsilon_F} \sim \frac{\Omega_{FC}}{\Omega_F}. \quad (8)$$

In this formula, M denotes the bare electron mass, Ω_{FC} is the FC volume, ε_F is the Fermi energy, and Ω_F is the volume of the Fermi sphere. We note that, at $T_c \leq T \ll T_f$, the occupation numbers $n(p)$ are approximately independent of T , being given by Eq. (5). According to Eq. (1), the dispersionless plateau $\varepsilon(p) = \mu$ is slightly turned counterclockwise about μ . As a result, the plateau is just a little tilted and rounded off at the end points. According to Eq. (7), the effective mass M_{FC}^* related to FC is given by

$$M_{FC}^* \simeq p_F \frac{p_f - p_i}{4T}. \quad (9)$$

To obtain Eq. (9), an approximation for the derivative $dn(p)/dp \simeq -1/(p_f - p_i)$ was used.

Having in mind that $(p_f - p_i) \ll p_F$ and using Eqs. (8) and (9), we obtain the following estimates for the effective mass M_{FC}^* :

$$\frac{M_{FC}^*}{M} \sim \frac{N(0)}{N_0(0)} \sim \frac{T_f}{T}. \quad (10)$$

Equations (9) and (10) show the temperature dependence of M_{FC}^* . In Eq. (10), $N_0(0)$ is the density of states of noninteracting electron gas and $N(0)$ is the density of states at the Fermi level. Multiplying both sides of Eq. (9) by $(p_f - p_i)$, we obtain the energy scale E_0 separating the slowly dispersing low-energy part related to the effective mass M_{FC}^* from the faster dispersing relatively high energy part defined by the effective mass M_L^* [6, 13]:

$$E_0 \simeq 4T. \quad (11)$$

It is seen from Eq. (11) that the scale E_0 does not depend on the condensate volume. The single-particle excitations are defined according to Eq. (9), by the temperature and by $(p_f - p_i)$, given by Eq. (5). Thus, we conclude that the one-electron spectrum is negligibly disturbed by thermal excitations, impurities, etc., which are the features of the “quantum protectorate” [14, 15].

It is pertinent to note that, outside the FC region, the single-particle spectrum is not affected by the temperature, being defined by M_L^* . Thus, we come to the conclusion that a system with FC is characterized by two effective masses: M_{FC}^* , which is related to the single-particle spectrum at a lower energy scale, and M_L^* , describing the spectrum at a higher energy scale. The existence of two effective masses is manifested by a break (or kink) in the quasiparticle dispersion, which can be approximated by two straight lines intersecting at the energy E_0 . This break takes place at temperatures $T_c \leq T \ll T_f$, in accord with the experimental data [16], and, as we will see, at $T \leq T_c$, which is also in accord with the experimental facts [16, 17]. The quasiparticle formalism is applicable to this problem, since the width γ of single-particle excitations is not large compared to their energy, being proportional to the temperature, $\gamma \sim T$, at $T > T_c$ [9]. The line shape can be approximated by a simple Lorentzian [13], consistent with experimental data obtained from scans at a constant binding energy [18] (see Section 4).

It is seen from Eqs. (5) and (10) that, at the point of FC phase transition $p_f \rightarrow p_i \rightarrow p_F$, M_{FC}^* and the density of states tend to infinity. One can conclude that, at $T = 0$ and as soon as $x \rightarrow x_{FC}$, FCQPT takes place, being connected to the absolute growth of M_L^* .

It is essential to have in mind that the onset of the charge-density-wave instability in a many-electron system, such as an electron liquid, which takes place as soon as the effective interelectron constant reaches its critical value $r_s = r_{cdw}$, is preceded by unlimited growth of the effective mass (see Section 4). Therefore, the FC occurs before the onset of the charge-density wave. Hence, at $T = 0$, when r_s reaches its critical value r_{FC} corresponding to x_{FC} , $r_{FC} < r_{cdw}$,

FCQPT inevitably takes place [8]. It is pertinent to note that this growth of the effective mass with decreasing electron density was observed experimentally in a metallic 2D electron system in silicon at $r_s \simeq 7.5$ [19]. Therefore, we can take $r_{FC} \sim 7.5$. On the other hand, there exist charge density waves or strong fluctuations of charge ordering in underdoped high- T_c superconductors [20]. Thus, the formation of FC in high- T_c compounds can be thought of as a general property of an electron liquid of low density that is embedded in these solids rather than an uncommon and anomalous solution to Eq. (1) [8]. Beyond the point of FCQPT, the condensate volume is proportional to $(r_s - r_{FC})$, as well as $T_f/\varepsilon_F \sim (r_s - r_{FC})/r_{FC}$, at least when $(r_s - r_{FC})/r_{FC} \ll 1$, and we obtain

$$\frac{r_s - r_{FC}}{r_{FC}} \sim \frac{p_f - p_i}{p_F} \sim \frac{x_{FC} - x}{x_{FC}}. \quad (12)$$

FC serves as a stimulator that creates new phase transitions, which lift the degeneration of the spectrum. For example, FC can generate spin-density waves or an antiferromagnetic phase transition, thus leading to a whole variety of new properties of the system under consideration. Then, the onset of the charge-density-wave is preceded by FCQPT, and both of these phases can coexist at a sufficiently low density, when $r_s \geq r_{cdw}$.

We have demonstrated above that superconductivity is strongly aided by FC, because both of the phases are characterized by the same order parameter. As a result, the superconductivity, removing the spectrum degeneration, “wins” the competition with the other phase transitions up to the critical temperature T_c . We now turn to the consideration of the superconducting state and quasiparticle dispersions at $T \leq T_c$.

3. THE SUPERCONDUCTING STATE

At $T = 0$, the ground-state energy $E_{g.s}[\kappa(\mathbf{p}), n(\mathbf{p})]$ of a 2D electron liquid is a functional of the order parameter of the superconducting state $\kappa(\mathbf{p})$ and of the quasiparticle occupation numbers $n(\mathbf{p})$. This energy is determined by the known equation of the weak-coupling theory of superconductivity (see, e.g., [21])

$$E_{g.s} = E[n(\mathbf{p})] + \int \lambda_0 V(\mathbf{p}_1, \mathbf{p}_2) \kappa(\mathbf{p}_1) \times \kappa^*(\mathbf{p}_2) \frac{d\mathbf{p}_1 d\mathbf{p}_2}{(2\pi)^4}. \quad (13)$$

Here, $E[n(\mathbf{p})]$ is the ground-state energy of a normal Fermi liquid, $n(\mathbf{p}) = v^2(\mathbf{p})$, and $\kappa(\mathbf{p}) =$

$v(\mathbf{p})\sqrt{1 - v^2(\mathbf{p})}$. It is assumed that the pairing interaction $\lambda_0 V(\mathbf{p}_1, \mathbf{p}_2)$ is weak. Minimizing $E_{g.s}$ with respect to $\kappa(\mathbf{p})$, we obtain the equation connecting the single-particle energy $\varepsilon(\mathbf{p})$ to $\Delta(\mathbf{p})$,

$$\varepsilon(\mathbf{p}) - \mu = \Delta(\mathbf{p}) \frac{1 - 2v^2(\mathbf{p})}{2\kappa(\mathbf{p})}, \quad (14)$$

where the single-particle energy $\varepsilon(\mathbf{p})$ is determined by the Landau Eq. (2). The equation for the superconducting gap $\Delta(\mathbf{p})$ takes the form

$$\Delta(\mathbf{p}) = - \int \lambda_0 V(\mathbf{p}, \mathbf{p}_1) \kappa(\mathbf{p}_1) \frac{d\mathbf{p}_1}{4\pi^2} \quad (15)$$

$$= - \frac{1}{2} \int \lambda_0 V(\mathbf{p}, \mathbf{p}_1) \frac{\Delta(\mathbf{p}_1)}{\sqrt{(\varepsilon(\mathbf{p}_1) - \mu)^2 + \Delta^2(\mathbf{p}_1)}} \frac{d\mathbf{p}_1}{4\pi^2}.$$

If $\lambda_0 \rightarrow 0$, then the maximum value $\Delta_1 \rightarrow 0$ and Eq. (14) reduces to Eq. (5) [4]:

$$\varepsilon(\mathbf{p}) - \mu = 0, \text{ if } 0 < n(\mathbf{p}) < 1; \quad p_i \leq p \leq p_f. \quad (16)$$

Now, we can study the relationships between the state defined by Eq. (16), or by Eq. (5), and the superconductivity. At $T = 0$, Eq. (16) defines a particular state of a Fermi liquid with FC for which the modulus of the order parameter $|\kappa(\mathbf{p})|$ has finite values in the L_{FC} range of momenta $p_i \leq p \leq p_f$, and $\Delta_1 \rightarrow 0$ in the L_{FC} . Such a state can be considered as superconducting, with an infinitely small value of Δ_1 , so that the entropy of this state is equal to zero. It is obvious that this state, being driven by the quantum phase transition, disappears at $T > 0$ [6]. Any quantum phase transition that takes place at temperature $T = 0$ is determined by a control parameter other than temperature, for instance, by pressure, by magnetic field, or by the density of mobile charge carriers $x \sim 1/r_s^2$. The quantum phase transition occurs at the quantum critical point. In a common case, this point is the end of a line of continuous transitions at $T = 0$.

As any phase transition, the quantum phase transition is related to the order parameter, which induces a broken symmetry. In our case, as we show in Section 2, the control parameter is the density of a system, which determines the strength of the Landau effective interaction, and the order parameter is $\kappa(\mathbf{p})$. As we point out in Section 5, the existence of such a state can be revealed experimentally. Since the order parameter $\kappa(\mathbf{p})$ is suppressed by a magnetic field B , when $B^2 \sim \Delta_1^2$, a weak magnetic field B will destroy the state with FC, converting the strongly correlated Fermi liquid into a normal Landau Fermi liquid. In this case, the magnetic field plays the role of the control parameter.

When $p_i \rightarrow p_F \rightarrow p_f$, Eq. (16) determines the critical point r_{FC} at which FCQPT takes place. It follows from Eq. (16) that the system becomes divided into two quasiparticle subsystems: the first subsystem in the L_{FC} range is characterized by quasiparticles with effective mass $M_{FC}^* \propto 1/\Delta_1$, while the second one is occupied by quasiparticles with finite mass M_L^* and momenta $p < p_i$. The density of states near the Fermi level tends to infinity, $N(0) \sim M_{FC}^* \sim 1/\Delta_1$. The quasiparticles with M_{FC}^* occupy the same energy level and form pairs with binding energy of the order of Δ_1 and with average momentum $p_0, p_0/p_F \sim (p_f - p_i)/p_F \ll 1$. Therefore, this state strongly resembles Bose–Einstein condensation when quasiparticles occupy the same energy level. But these have to be spread over the range L_{FC} in momentum space due to the exclusion principle. In contrast to Bose–Einstein condensation, the fermion condensation temperature is $T_c = 0$. And in contrast to ordinary superconductivity, fermion condensation is driven by Landau repulsive interaction rather than by relatively weak attractive quasiparticle–quasiparticle interaction $\lambda_0 V(\mathbf{p}_1, \mathbf{p}_2)$.

If $\lambda_0 \neq 0$, Δ_1 becomes finite, leading to a finite value of the effective mass M_{FC}^* in L_{FC} , which can be obtained from Eq. (14) [6, 13]:

$$M_{FC}^* \simeq p_F \frac{p_f - p_i}{2\Delta_1}. \quad (17)$$

As to the energy scale, it is determined by the parameter E_0 :

$$E_0 = \varepsilon(\mathbf{p}_f) - \varepsilon(\mathbf{p}_i) \simeq 2 \frac{(p_f - p_F)p_F}{M_{FC}^*} \simeq 2\Delta_1. \quad (18)$$

It is natural to assume that we have returned back to the Landau Fermi liquid theory, eliminating high-energy degrees of freedom and introducing the quasiparticles. The only difference between the Landau Fermi liquid and Fermi liquid after FCQPT is that we have to expand the number of relevant low-energy degrees of freedom by introducing a new type of quasiparticles with effective mass M_{FC}^* given by Eq. (17) and energy scale E_0 given by Eq. (18). Properties of these new quasiparticles are closely related to the properties of the superconducting state, as follows from Eqs. (14), (17), and (18). We may say that the quasiparticle system in the range L_{FC} becomes very “soft” and is to be considered as a strongly correlated liquid. On the other hand, the system’s properties and dynamics are dominated by a strong collective effect having its origin in FCQPT and determined by the macroscopic number of quasiparticles in the range L_{FC} . Such a system cannot be disturbed by the scattering of individual quasiparticles and has features of a “quantum protectorate” [6, 14, 15].

We assume that the range L_{FC} is small, $(p_f - p_F)/p_F \ll 1$, and $2\Delta_1 \ll T_f$, so that the order parameter $\kappa(\mathbf{p})$ is governed mainly by FC [6, 26]. To solve Eq. (15) analytically, we take the BCS approximation for the interaction [10]: $\lambda_0 V(\mathbf{p}, \mathbf{p}_1) = -\lambda_0$ if $|\varepsilon(\mathbf{p}) - \mu| \leq \omega_D$, i.e., the interaction is zero outside this region, with ω_D being the characteristic phonon energy. As a result, the gap becomes dependent only on the temperature, $\Delta(\mathbf{p}) = \Delta_1(T)$, being independent of the momentum, and Eq. (15) takes the form

$$1 = N_{FC} \lambda_0 \int_0^{E_0/2} \frac{d\xi}{\sqrt{\xi^2 + \Delta_1^2(0)}} + N_L \lambda_0 \int_{E_0/2}^{\omega_D} \frac{d\xi}{\sqrt{\xi^2 + \Delta_1^2(0)}}. \quad (19)$$

Here, we set $\xi = \varepsilon(\mathbf{p}) - \mu$ and introduce the density of states N_{FC} in the L_{FC} , or E_0 , range. It follows from Eq. (17) that $N_{FC} = (p_f - p_F)p_F/2\pi\Delta_1(0)$. The density of states N_L in the range $(\omega_D - E_0/2)$ has the standard form $N_L = M_L^*/2\pi$. If the energy scale $E_0 \rightarrow 0$, Eq. (19) reduces to the BCS equation. On the other hand, assuming that $E_0 \leq 2\omega_D$ and omitting the second integral on the right-hand side of Eq. (19), we obtain

$$\begin{aligned} \Delta_1(0) &= \frac{\lambda_0 p_F (p_f - p_F)}{2\pi} \ln(1 + \sqrt{2}) \\ &= 2\beta \varepsilon_F \frac{p_f - p_F}{p_F} \ln(1 + \sqrt{2}), \end{aligned} \quad (20)$$

where the Fermi energy $\varepsilon_F = p_F^2/2M_L^*$, and the dimensionless coupling constant β is given by the relation $\beta = \lambda_0 M_L^*/2\pi$. Taking the usual values of β as $\beta \simeq 0.3$ and assuming $(p_f - p_F)/p_F \simeq 0.2$, we get from Eq. (20) a large value of $\Delta_1(0) \sim 0.1\varepsilon_F$, while for normal metals one has $\Delta_1(0) \sim 10^{-3}\varepsilon_F$. Taking into account the omitted integral, we obtain

$$\begin{aligned} \Delta_1(0) &\simeq 2\beta \varepsilon_F \frac{p_f - p_F}{p_F} \ln(1 + \sqrt{2}) \\ &\quad \times \left(1 + \beta \ln \frac{2\omega_D}{E_0}\right). \end{aligned} \quad (21)$$

It is seen from Eq. (21) that the correction due to the second integral is small, provided $E_0 \simeq 2\omega_D$. Below, we show that $2T_c \simeq \Delta_1(0)$, which leads to the conclusion that there is no isotope effect since Δ_1 is independent of ω_D . But this effect is restored as $E_0 \rightarrow 0$. Assuming $E_0 \sim \omega_D$ and $E_0 > \omega_D$, we see that Eq. (21) has no standard solutions $\Delta(p) = \Delta_1(T = 0)$, because $\omega_D < \varepsilon(p \simeq p_f) - \mu$ and the interaction vanishes at these momenta. The only

way to obtain solutions is to restore the condition $E_0 < \omega_D$. For instance, we can define such a momentum $p_D < p_f$ that

$$\Delta_1(0) = 2\beta\varepsilon_F \frac{p_D - p_F}{p_F} \ln(1 + \sqrt{2}) = \omega_D, \quad (22)$$

while the other part in the L_{FC} range can be occupied by a gap Δ_2 of different sign, $\Delta_1/\Delta_2 < 0$. It follows from Eq. (22) that the isotope effect is preserved, while both gaps can have s -wave symmetry.

At $T \simeq T_c$, Eqs. (17) and (18) are replaced by the equation, which is valid also at $T_c \leq T \ll T_f$ in accordance with Eq. (9) [6],

$$M_{FC}^* \simeq p_F \frac{p_f - p_i}{4T_c}, \quad E_0 \simeq 4T_c; \quad (23)$$

$$\text{if } T_c \leq T \text{ and } M_{FC}^* \simeq p_F \frac{p_f - p_i}{4T}, \quad E_0 \simeq 4T.$$

Equation (19) is replaced by its conventional finite-temperature generalization

$$1 = N_{FC}\lambda_0 \quad (24)$$

$$\times \int_0^{E_0/2} \frac{d\xi}{\sqrt{\xi^2 + \Delta_1^2(T)}} \tanh \frac{\sqrt{\xi^2 + \Delta_1^2(T)}}{2T}$$

$$+ N_L\lambda_0 \int_{E_0/2}^{\omega_D} \frac{d\xi}{\sqrt{\xi^2 + \Delta_1^2(T)}} \tanh \frac{\sqrt{\xi^2 + \Delta_1^2(T)}}{2T}.$$

Setting $\Delta_1(T \rightarrow T_c) \rightarrow 0$, we obtain from Eq. (24)

$$2T_c \simeq \Delta_1(0), \quad (25)$$

with $\Delta_1(T=0)$ being given by Eq. (20). Comparing Eqs. (17), (23), and (25), we see that M_{FC}^* and E_0 are almost temperature independent at $T \leq T_c$.

Now let us comment on some special features of the superconducting state with FC. One can define T_c as the temperature when $\Delta_1(T_c) \equiv 0$. At $T \geq T_c$, Eq. (24) has only the trivial solution $\Delta_1 \equiv 0$. On the other hand, T_c can be defined as a temperature at which the superconductivity disappears. Thus, we have two different definitions, which can lead to two different temperatures T_c and T^* in the case of the d -wave symmetry of the gap. It was shown [13, 22] that, in the case of the d -wave superconductivity in the presence of FC, there is a nontrivial solution to Eq. (24) at $T_c \leq T \leq T^*$ corresponding to the pseudogap state. It happens when the gap occupies only such a part of the Fermi surface, which shrinks as the temperature increases. Here, T^* defines the temperature at which $\Delta_1(T^*) \equiv 0$ and the pseudogap state vanishes. The superconductivity is destroyed at T_c , and the ratio $2\Delta_1/T_c$ can vary in a wide range and strongly depends upon the material's properties, as follows from considerations given in [13, 22, 23].

Therefore, if a pseudogap exists above T_c , then T_c is to be replaced by T^* and Eq. (25) takes the form

$$2T^* \simeq \Delta_1(0). \quad (26)$$

The ratio $2\Delta_1/T_c$ can reach very high values. For instance, in the case of $\text{Bi}_2\text{Sr}_2\text{CaCu}_2\text{O}_{6+\delta}$, where the superconductivity and the pseudogap are considered to be of common origin, $2\Delta_1/T_c$ is about 28, while the ratio $2\Delta_1/T^* \simeq 4$, which is in agreement with the experimental data for various cuprates [24]. Note that Eq. (20) also gives a good description of the maximum gap Δ_1 in the case of d -wave superconductivity, because the different regions with the maximum absolute value of Δ_1 and the maximal density of states can be considered as disconnected [25]. Therefore, the gap in this region is formed by attractive phonon interaction, which is approximately independent of the momenta.

Consider now two possible types of the superconducting gap $\Delta(\mathbf{p})$ given by Eq. (15) and defined by the interaction $\lambda_0 V(\mathbf{p}, \mathbf{p}_1)$. If this interaction is dominated by a phonon-mediated attraction, the even solution of Eq. (15) with the s wave or the $s+d$ mixed waves will have the lowest energy. Provided the pairing interaction $\lambda_0 V(\mathbf{p}_1, \mathbf{p}_2)$ is the combination of both attractive interaction and sufficiently strong repulsive interaction, the d -wave odd superconductivity can take place (see, e.g., [25]). But both the s -wave even symmetry and the d -wave odd one lead to approximately the same value of the gap Δ_1 in Eq. (21) [26]. Therefore, the nonuniversal pairing symmetries in high- T_c superconductivity are likely the result of the pairing interaction and the d -wave pairing symmetry is not essential. This point of view is supported by the data [27–31]. If only the d -wave pairing existed, the transition from superconducting gap to pseudogap could take place, so that the superconductivity would be destroyed at T_c , with the superconducting gap being smoothly transformed into the pseudogap, which closes at some temperature $T^* > T_c$ [22, 23]. In the case of the s -wave pairing, we can expect the absence of the pseudogap phenomenon in accordance with the experimental observation (see [31] and references therein).

We now turn to a consideration of the maximum value of the superconducting gap Δ_1 as a function of the density x of the mobile charge carriers. Rewriting in terms of $x \sim r_s^2$ and $x_{FC} \sim r_{FC}^2$, which are related to the variables p_i and p_f by Eq. (12), Eq. (21) becomes

$$\Delta_1 \propto \beta(x_{FC} - x)x. \quad (27)$$

Here, we take into account that the Fermi level $\varepsilon_F \propto p_F^2$, the density $x \propto p_F^2$, and thus, $\varepsilon_F \propto x$. We can reliably assume that $T_c \propto \Delta_1$, because the empirically obtained simple bell-shaped curve of $T_c(x)$

in the high temperature superconductors [32] should have only a smooth dependence. Then, $T_c(x)$ in accordance with the data has the form [33]

$$T_c(x) \propto \beta(x_{FC} - x)x. \quad (28)$$

As an example of the implementation of the previous analysis, let us consider the main features of a room-temperature superconductor. The superconductor has to be a quasi-2D structure like cuprates. From Eq. (21), it follows that $\Delta_1 \sim \beta\varepsilon_F \propto \beta/r_s^2$. Noting that FCQPT in 3D systems takes place at $r_s \sim 20$ and in 2D systems at $r_s \sim 8$ [8], we can expect that Δ_1 of 3D systems comprises 10% of the corresponding maximum value of the 2D superconducting gap, reaching a value as high as 60 meV for underdoped crystals with $T_c = 70$ K [34]. On the other hand, it is seen from Eq. (21) that Δ_1 can even be large, $\Delta_1 \sim 75$ meV, and one can expect $T_c \sim 300$ K in the case of s -wave pairing, as follows from the simple relation $2T_c \simeq \Delta_1$. In fact, we can safely take $\varepsilon_F \sim 300$ meV, $\beta \sim 0.5$, and $(p_f - p_i)/p_F \sim 0.5$. Thus, a possible room-temperature superconductor has to be the s -wave superconductor in order to get rid of the pseudogap phenomena, which tremendously reduces the transition temperature. The density x of the mobile charge carriers must satisfy the condition $x \leq x_{FC}$ and be flexible to reach the optimal doping level $x_{opt} \simeq x_{FC}/2$.

Now we turn to the calculations of the gap and the specific heat at the temperatures $T \rightarrow T_c$. It is worth noting that this consideration is valid provided $T^* = T_c$, otherwise the discontinuity considered below is smoothed out over the temperature range $T^* - T_c$. For the sake of simplicity, we calculate the main contribution to the gap and the specific heat coming from the FC. The function $\Delta_1(T \rightarrow T_c)$ is found from Eq. (24) by expanding the right-hand side of the first integral in powers of Δ_1 and omitting the contribution from the second integral on the right-hand side of Eq. (24). This procedure leads to the following equation [26]:

$$\Delta_1(T) \simeq 3.4T_c \sqrt{1 - \frac{T}{T_c}}. \quad (29)$$

Thus, the gap in the spectrum of the single-particle excitations has the usual behavior. To calculate the specific heat, the conventional expression for the entropy S [10] can be used:

$$S = -2 \int [f(\mathbf{p}) \ln f(\mathbf{p}) + (1 - f(\mathbf{p})) \times \ln(1 - f(\mathbf{p}))] \frac{d\mathbf{p}}{(2\pi)^2}, \quad (30)$$

where

$$f(\mathbf{p}) = \frac{1}{1 + \exp[E(\mathbf{p})/T]}; \quad (31)$$

$$E(\mathbf{p}) = \sqrt{(\varepsilon(\mathbf{p}) - \mu)^2 + \Delta_1^2(T)}.$$

The specific heat C is determined by the equation

$$C = T \frac{dS}{dT} \simeq 4 \frac{N_{FC}}{T^2} \int_0^{E_0} f(E)(1 - f(E)) \times \left[E^2 + T\Delta_1(T) \frac{d\Delta_1(T)}{dT} \right] d\xi + 4 \frac{N_L}{T^2} \times \int_{E_0}^{\omega_D} f(E)(1 - f(E)) \left[E^2 + T\Delta_1(T) \frac{d\Delta_1(T)}{dT} \right] d\xi. \quad (32)$$

In deriving Eq. (32), we again used the variable ξ and the densities of states N_{FC} and N_L , just as before in connection with Eq. (19), and employed the notation $E = \sqrt{\xi^2 + \Delta_1^2(T)}$. Equation (32) predicts the conventional discontinuity δC in the specific heat C at T_c because of the last term in the square brackets of Eq. (32). Using Eq. (29) to calculate this term and omitting the second integral on the right-hand side of Eq. (32), we obtain

$$\delta C \simeq \frac{3}{2\pi} (p_f - p_i) p_F. \quad (33)$$

This is in contrast to the conventional result, where the discontinuity is a linear function of T_c . δC is independent of the critical temperature T_c , because, as seen from Eq. (17), the density of states varies inversely with T_c . Note that, in deriving Eq. (33), we took into account the main contribution coming from the FC. This term vanishes as soon as $E_0 \rightarrow 0$, and the second integral of Eq. (32) gives the conventional result.

4. THE LINE SHAPE OF THE SINGLE-PARTICLE SPECTRA

The line shape $L(q, \omega)$ of the single-particle spectrum is a function of two variables. Measurements carried out at a fixed binding energy $\omega = \omega_0$, with ω_0 being the energy of a single-particle excitation, determine the line shape $L(q, \omega = \omega_0)$ as a function of the momentum q . We have shown above that M_{FC}^* is finite and constant at $T \leq T_c$. Therefore, at excitation energies $\omega \leq E_0$, the system behaves like an ordinary superconducting Fermi liquid with the effective mass given by Eq. (17) [6, 13]. At $T_c \leq T$, the low-energy effective mass M_{FC}^* is finite and is given by Eq. (9). Once again, at energies $\omega < E_0$, the system behaves as a Fermi liquid, the single-particle spectrum is well defined, and the width of single-particle excitations is of the order of T [6, 9]. This behavior was observed in experiments measuring the line shape at a fixed energy [18, 35].

The line shape can also be determined as a function $L(q = q_0, \omega)$ at a fixed $q = q_0$. At small ω , the line shape resembles the one considered above, and $L(q = q_0, \omega)$ has the characteristic maximum and width. At energies $\omega \geq E_0$, the quasiparticles with the mass M_L^* become important, leading to the increase in $L(q = q_0, \omega)$. As a result, the function $L(q = q_0, \omega)$ possesses the known peak–dip–hump structure [36] directly defined by the existence of the two effective masses M_{FC}^* and M_L^* [6, 13]. We can conclude that, in contrast to the Landau quasiparticles, these quasiparticles have a more complicated line shape.

To develop deeper quantitative and analytical insight into the problem, we use the Kramers–Krönig transformation to construct the imaginary part $\text{Im}\Sigma(\mathbf{p}, \varepsilon)$ of the self-energy $\Sigma(\mathbf{p}, \varepsilon)$ starting with the real one $\text{Re}\Sigma(\mathbf{p}, \varepsilon)$, which defines the effective mass [37]

$$\frac{1}{M^*} = \left(\frac{1}{M} + \frac{1}{p_F} \frac{\partial \text{Re}\Sigma}{\partial p} \right) / \left(1 - \frac{\partial \text{Re}\Sigma}{\partial \varepsilon} \right). \quad (34)$$

Here, M is the bare mass, while the relevant momenta p and energies ε obey the following strong inequalities: $|p - p_F|/p_F \ll 1$ and $\varepsilon/\varepsilon_F \ll 1$. We take $\text{Re}\Sigma(\mathbf{p}, \varepsilon)$ in the simplest form that accounts for the change in the effective mass at the energy scale E_0 :

$$\begin{aligned} \text{Re}\Sigma(\mathbf{p}, \varepsilon) = & -\varepsilon \frac{M_{FC}^*}{M} + \left(\varepsilon - \frac{E_0}{2} \right) \frac{M_{FC}^* - M_L^*}{M} \\ & \times \left[\theta \left(\varepsilon - \frac{E_0}{2} \right) + \theta \left(-\varepsilon - \frac{E_0}{2} \right) \right]. \end{aligned} \quad (35)$$

Here, $\theta(\varepsilon)$ is a step function. Note that, in order to ensure a smooth transition from the single-particle spectrum characterized by M_{FC}^* to the spectrum defined by M_L^* , the step function must be replaced by some smooth function. Upon inserting Eq. (35) into Eq. (34), we can check that, inside the interval $(-E_0/2, E_0/2)$, the effective mass $M^* \simeq M_{FC}^*$, and outside the interval $M^* \simeq M_L^*$. By applying the Kramers–Krönig transformation to $\text{Re}\Sigma(\mathbf{p}, \varepsilon)$, we obtain the imaginary part of the self-energy [26]

$$\begin{aligned} \text{Im}\Sigma(\mathbf{p}, \varepsilon) \sim & \varepsilon^2 \frac{M_{FC}^*}{\varepsilon_F M} + \frac{M_{FC}^* - M_L^*}{M} \\ & \times \left(\varepsilon \ln \left| \frac{\varepsilon + E_0/2}{\varepsilon - E_0/2} \right| + \frac{E_0}{2} \ln \left| \frac{\varepsilon^2 - E_0^2/4}{E_0^2/4} \right| \right). \end{aligned} \quad (36)$$

We see from Eq. (36) that, at $\varepsilon/E_0 \ll 1$, the imaginary part is proportional to ε^2 ; at $2\varepsilon/E_0 \simeq 1$, $\text{Im}\Sigma \sim \varepsilon$; and at $E_0/\varepsilon \ll 1$, the main contribution to the imaginary part is approximately constant. This is the behavior that gives rise to the known peak–dip–hump structure. It is seen from Eq. (36) that, when

$E_0 \rightarrow 0$, the second term on the right-hand side tends to zero and the single-particle excitations become better defined, resembling the situation in a normal Fermi liquid, and the peak–dip–hump structure eventually vanishes. On the other hand, the quasiparticle amplitude $a(\mathbf{p})$ is given by [37]

$$\frac{1}{a(\mathbf{p})} = 1 - \frac{\partial \text{Re}\Sigma(\mathbf{p}, \varepsilon)}{\partial \varepsilon}. \quad (37)$$

It follows from Eq. (34) that the quasiparticle amplitude $a(\mathbf{p})$ rises as the effective mass M_{FC}^* decreases. Since, as follows from Eq. (12), $M_{FC}^* \sim (p_f - p_i)/p_F \sim (x_{FC} - x)/x_{FC}$, we have to conclude that the amplitude $a(\mathbf{p})$ rises as the level of doping increases. Thus, the single-particle excitations become better defined in highly overdoped samples. It is worth noting that such a behavior was observed experimentally in highly overdoped Bi-2212, where the gap size is about 10 meV [38]. Such a small size of the gap verifies that the region occupied by the FC is small since $E_0/2 \simeq \Delta_1$.

5. HEAVY-FERMION METALS

Now, we consider the behavior of a many-electron system with FC in magnetic fields, assuming that the coupling constant $\lambda_0 \neq 0$ is infinitely small. As we have seen in Section 3, at $T = 0$ the superconducting order parameter $\kappa(\mathbf{p})$ is finite in the FC range, while the maximum value of the superconducting gap $\Delta_1 \propto \lambda_0$ is infinitely small. Therefore, any small magnetic field $B \neq 0$ can be considered as a critical field and will destroy the coherence of $\kappa(\mathbf{p})$ and thus FC itself. To define the type of FC rearrangement, simple energy arguments are sufficient. On one hand, the energy gain ΔE_B due to the magnetic field B is $\Delta E_B \propto B^2$ and tends to zero with $B \rightarrow 0$. On the other hand, occupying the finite-range L_{FC} in the momentum space, the formation of FC leads to a finite gain in the ground-state energy [4]. Thus, a new ground state replacing FC should have almost the same energy as the former one. Such a state is given by the multiconnected Fermi spheres resembling an onion, where the smooth quasiparticle distribution function $n(\mathbf{p})$ in the L_{FC} range is replaced by a multiconnected distribution $\nu(\mathbf{p})$ [39]:

$$\nu(\mathbf{p}) = \sum_{k=1}^n \theta(p - p_{2k-1}) \theta(p_{2k} - p). \quad (38)$$

Here, the parameters $p_i \leq p_1 < p_2 < \dots < p_{2n} \leq p_f$ are adjusted to obey the normalization condition

$$\int_{p_{2k}}^{p_{2k+3}} \nu(\mathbf{p}) \frac{d\mathbf{p}}{(2\pi)^3} = \int_{p_{2k}}^{p_{2k+3}} n(\mathbf{p}) \frac{d\mathbf{p}}{(2\pi)^3}. \quad (39)$$

For definiteness, let us consider the most interesting case of a 3D system, while the consideration of a 2D system also goes along the same line. We note that the idea of multiconnected Fermi spheres, with production of new, interior segments of the Fermi surface, has been considered already [40, 41]. Let us assume that the thickness of each interior block is approximately the same, $p_{2k+1} - p_{2k} \simeq \delta p$, and δp is defined by B . Then, the single-particle energy in the region L_{FC} can be fitted by

$$\varepsilon(\mathbf{p}) - \mu \sim \mu \frac{\delta p}{p_F} \left[\sin \left(\frac{p}{\delta p} \right) + b(p) \right]. \quad (40)$$

The blocks are formed, since all the single-particle states around the minimum values of the fast sine function are occupied and those around its maximum values are empty, the average occupation being controlled by a slow function $b(\mathbf{p}) \approx \cos[\pi n(\mathbf{p})]$. It follows from Eq. (40) that the effective mass m^* at each internal Fermi surface is of the order of the bare mass M , $m^* \sim M$. Upon replacing $n(\mathbf{p})$ in Eq. (5) by $\nu(\mathbf{p})$, defined by Eqs. (38) and (39), and using Simpson's rule, we find that the minimum loss in the ground-state energy due to formation of the blocks is about $(\delta p)^4$. This result can be understood by considering that the continuous FC function $n(\mathbf{p})$ delivers the minimum value to the energy functional $E[n(\mathbf{p})]$, while the approximation of $\nu(\mathbf{p})$ by steps of size δp produces the minimum error of the order of $(\delta p)^4$. On the other hand, this loss must be compensated by the energy gain due to the magnetic field. Thus, we come to the following relation:

$$\delta p \propto \sqrt{B}. \quad (41)$$

When the Zeeman splitting is taken into account in the dispersion law, Eq. (40), each of the blocks is polarized, since their outer areas are occupied only by polarized spin-up quasiparticles. The width of each area in the momentum space δp_0 is given by

$$\frac{p_F \delta p_0}{m^*} \sim B \mu_{\text{eff}}, \quad (42)$$

where $\mu_{\text{eff}} \sim \mu_B$ is the effective magnetic moment of an electron. We can consider such a polarization without altering the previous estimates, since it follows from Eq. (41) that $\delta p_0/\delta p \ll 1$. The total polarization ΔP is obtained by multiplying δp_0 by the number of blocks N , which is proportional to $1/\delta p$, $N \sim (p_f - p_i)/\delta p$. Taking into account Eq. (41), we obtain

$$\Delta P \sim m^* \frac{p_f - p_i}{\delta p} B \mu_{\text{eff}} \propto \sqrt{B}, \quad (43)$$

which prevails over the contribution $\sim B$ obtained within the Landau Fermi liquid theory. On the other

hand, this quantity can be expressed as

$$\Delta P \propto M^* B, \quad (44)$$

where M^* is the “average” effective mass related to the finite density of states at the Fermi level,

$$M^* \sim N m^* \propto \frac{1}{\delta p}. \quad (45)$$

We can also conclude that M^* defines the specific heat.

Equation (41) can be discussed differently, starting with a different assumption, namely, that a multiconnected Fermi sphere can be approximated by a single block. Let us set $\lambda_0 = 0$. Then, the energy gain due to the magnetic field is given by $\Delta E_B \sim B^2 M^*$. The energy loss ΔE_{FC} due to rearrangement of the FC state can be estimated using the Landau formula [3]

$$\Delta E_{FC} = \int (\varepsilon(\mathbf{p}) - \mu) \delta n(\mathbf{p}) \frac{d\mathbf{p}^3}{(2\pi)^3}. \quad (46)$$

As we have seen above, the region occupied by the variation $\delta n(\mathbf{p})$ has the length δp , while $(\varepsilon(\mathbf{p}) - \mu) \sim (p - p_F) p_F / M^*$. As a result, we have $\Delta E_{FC} = (\delta p)^2 / M^*$. Equating ΔE_B and ΔE_{FC} and taking into account Eq. (45), we arrive at the relation

$$\frac{(\delta p)^2}{M^*} \propto (\delta p)^3 \propto \frac{B^2}{\delta p}, \quad (47)$$

which coincides with Eq. (41). It follows from Eqs. (43) and (44) that the effective mass M^* diverges as

$$M^* \propto \frac{1}{\sqrt{B}}. \quad (48)$$

Equation (48) shows that, by applying a magnetic field B , the system can be driven back into the Landau Fermi liquid with the effective mass $M^*(B)$ dependent on the magnetic field. This means that the coefficients $A(B)$, $\gamma_0(B)$, and $\chi_0(B)$ in the resistivity, $\rho(T) = \rho_0 + \Delta\rho$ with $\Delta\rho = A(B)T^2$ and $A(B) \propto (M^*)^2$; specific heat, $C/T = \gamma_0(B)$; and magnetic susceptibility depend on the effective mass in accordance with the Landau Fermi liquid theory. It was demonstrated that the constancy of the well-known Kadowaki–Woods ratio, $A/\gamma_0^2 \simeq \text{const}$ [42], is obeyed by systems in the highly correlated regime when the effective mass is sufficiently large [43]. Therefore, we are led to the conclusion that, by applying magnetic fields, the system is driven back into the Landau Fermi liquid, where the constancy of the Kadowaki–Woods ratio is obeyed. Since the resistivity is given by $\Delta\rho \propto (M^*)^2$ [43], we obtain from Eq. (48)

$$A(B) \propto \frac{1}{B}. \quad (49)$$

At finite temperatures, the system remains in the Landau Fermi liquid, but there exists a temperature $T^*(B)$ at which the polarized state is destroyed. To calculate the function $T^*(B)$, we observe that the effective mass M^* characterizing the single-particle spectrum cannot be changed at $T^*(B)$. In other words, at the crossover point, we have to compare the effective mass $M^*(T)$ defined by $T^*(B)$, Eq. (9), and $M^*(B)$ defined by the magnetic field B , Eq. (48), $M^*(T) \sim M^*(B)$,

$$\frac{1}{M^*} \propto T^*(B) \propto \sqrt{B}. \quad (50)$$

As a result, we obtain

$$T^*(B) \propto \sqrt{B}. \quad (51)$$

At temperatures $T \geq T^*(B)$, the system comes back into the state with M^* defined by Eq. (9), and we do not observe the Landau Fermi liquid behavior. We can conclude that Eq. (51) determines the line in the B - T phase diagram which separates the region of the B -dependent effective mass from the region of the T -dependent effective mass (see also Section 7). At the temperature $T^*(B)$, there occurs a crossover from the T^2 dependence of the resistivity to the T dependence. It follows from Eq. (51) that a heavy-fermion system at some temperature T can be driven back into the Landau Fermi liquid by applying a strong enough magnetic field $B \geq B_{\text{cr}} \propto (T^*(B))^2$. We can also conclude that, at finite temperature T , the effective mass of a heavy-fermion system is relatively field-independent at magnetic fields $B \leq B_{\text{cr}}$ and shows a more pronounced metallic behavior at $B > B_{\text{cr}}$, since the effective mass decreases [see Eq. (48)]. The same behavior of the effective mass can be observed in the Shubnikov–de Haas oscillation measurements. We note that our consideration is valid for temperatures $T \ll T_f$. From Eqs. (50) and (51), we obtain a unique possibility to control the essence of the strongly correlated liquid by weak magnetic fields that induce the change of the non-Fermi liquid behavior to Landau Fermi liquid behavior.

Now, we can consider the nature of the field-induced quantum critical point in YbRh_2Si_2 . The properties of this antiferromagnetic (AF) heavy-fermion metal with the ordering Néel temperature $T_N = 70$ mK were recently investigated in [44, 45]. In the AF state, this metal shows Landau Fermi liquid behavior. As soon as the weak AF order is suppressed either by a tiny volume expansion or by temperature, pronounced deviations from the Landau Fermi liquid behavior are observed. The experimental facts show that the spin-density wave picture failed when considering the data obtained [44–46]. We assume that the electron density in YbRh_2Si_2 is close to the critical value $(x_{\text{FC}} - x)/x_{\text{FC}} \ll 1$ [47], so that

the state with FC can be easily suppressed by weak magnetic fields or by the AF state. In the AF state, the effective mass is finite and the electron system of YbRh_2Si_2 possesses the Landau Fermi liquid behavior. When the AF state is suppressed at $T > T_N$, the system comes back into a non-Fermi liquid. By tuning $T_N \rightarrow 0$ at a critical field $B = B_{c0}$, the itinerant AF order is suppressed and replaced by spin fluctuations [45]. Thus, we can expect the absence of any long-ranged magnetic order in this state, and the situation corresponds to a paramagnetic system with strong correlations without the field, $B = 0$. As a result, the FC state is restored and we can observe non-Fermi-liquid behavior at any temperatures in accordance with experimental facts [44]. As soon as an excessive magnetic field $B > B_{c0}$ is applied, the system is driven back into the Landau Fermi liquid. To describe the behavior of the effective mass, we can use Eq. (48) replacing B by $B - B_{c0}$:

$$M^* \propto \frac{1}{\sqrt{B - B_{c0}}}. \quad (52)$$

Equation (52) demonstrates the $1/\sqrt{B - B_{c0}}$ divergence of the effective mass, and therefore the coefficients $\gamma_0(B)$ and $\chi_0(B)$ should have the same behavior. Meanwhile, the coefficient $A(B)$ diverges as $1/(B - B_{c0})$, being proportional to $(M^*)^2$ [43] and thus preserving the Kadowaki–Woods ratio, in agreement with the experimental finding [44]. To construct a B - T phase diagram for YbRh_2Si_2 , we use the same replacement $B \rightarrow B - B_{c0}$ in Eq. (51), so that

$$T^*(B) \simeq c\sqrt{B - B_{c0}}, \quad (53)$$

where c is a constant.

The phase diagram given by Eq. (53) is in good quantitative agreement with the experimental data [44]. We note that our consideration is valid at temperatures $T \ll T_f$. The experimental phase diagram shows that the behavior $T^* \propto \sqrt{B - B_{c0}}$ is observed up to 150 mK [44] and allows us to estimate the magnitude of T_f , which can reach at least 1 K in this system. We can conclude that a new type of quantum critical point observed in a heavy-fermion metal YbRh_2Si_2 can be identified as FCQPT with the order parameter $\kappa(\mathbf{p})$ and with the gap Δ_1 being infinitely small [47, 48]. Recent measurements on the heavy-metal compound CeRu_2Si_2 carried out at microkelvin temperatures down to 170 μK show that the critical field B_{c0} can be as small as 0.02 mT [49]. Note that it follows directly from our consideration that a similar B - T phase diagram given by Eq. (53) can be observed at least in the case of strongly overdoped high-temperature compounds. This is correct, except very close to the small values of both B and T , because at $T \leq T_c$ the magnetic

field has to be $B > B_c$, where B_c is the critical field suppressing the superconductivity. We assume that this behavior was observed in overdoped Tl-2201 compounds at millikelvin temperatures [50, 51].

6. APPEARANCE OF FCQPT IN DIFFERENT FERMION LIQUIDS

It is widely believed that unusual properties of the strongly correlated liquids observed in high-temperature superconductors, heavy-fermion metals, 2D ^3He , etc., are determined by quantum phase transitions. Therefore, immediate experimental studies of relevant quantum phase transitions and of their quantum critical points are of crucial importance for understanding the physics of high-temperature superconductivity and strongly correlated systems. In case of high-temperature superconductors, these studies are difficult to carry out, because all the corresponding area is occupied by the superconductivity. On the other hand, recent experimental data on different Fermi liquids in the highly correlated regime at the critical point and above the point can help to illuminate both the nature of this point and the control parameter by which this point is driven. Experimental facts on strongly interacting high-density 2D ^3He [52, 53] show that the effective mass diverges when the density at which 2D ^3He liquid begins to solidify is approached [53]. Then, a sharp increase in the effective mass is observed when in a metallic 2D electron system the density tends to the critical density of the metal–insulator transition point, which occurs at sufficiently low densities [19]. Note that there is no ferromagnetic instability in both Fermi systems and the relevant Landau amplitude $F_0^a > -1$ [19, 53], in accordance with the almost-localized fermion model [54].

Now, we consider the divergence of the effective mass in 2D and 3D Fermi liquids at $T = 0$, when the density x approaches FCQPT from the side of normal Landau Fermi liquid. First, we calculate the divergence of M^* as a function of the difference $(x_{\text{FC}} - x)$ in the case of 2D ^3He . For this purpose, we use the equation for M^* obtained in [8], where the divergence of the effective mass M^* due to the onset of FC in different Fermi liquids, including ^3He , was predicted:

$$\frac{1}{M^*} = \frac{1}{M} + \frac{1}{4\pi^2} \quad (54)$$

$$\times \int_{-1}^1 \int_0^{g_0} \frac{v(q(y))}{[1 - R(q(y), \omega = 0, g)\chi_0(q(y), \omega = 0)]^2} \times \frac{ydydg}{\sqrt{1 - y^2}}.$$

Here, we adopt the notation $p_F\sqrt{2(1 - y)} = q(y)$ with $q(y)$ being the transferred momentum, M is the bare mass, ω is the frequency, $v(q)$ is the bare interaction, and the integral is taken over the coupling constant g from zero to its real value g_0 . In Eq. (54), both $\chi_0(q, \omega)$ and $R(q, \omega, g)$, being the linear response function of a noninteracting Fermi liquid and the effective interaction, respectively, define the linear response function of the system in question:

$$\chi(q, \omega, g) = \frac{\chi_0(q, \omega)}{1 - R(q, \omega, g)\chi_0(q, \omega)}. \quad (55)$$

In the vicinity of the charge-density wave instability, occurring at the density x_{cdw} , the singular part of the function χ^{-1} on the disordered side is of the well-known form (see, e.g., [32])

$$\chi^{-1}(q, \omega, g) \propto (x_{\text{cdw}} - x) + (q - q_c)^2 + (g_0 - g), \quad (56)$$

where $q_c \sim 2p_F$ is the wave number of the charge-density wave order. Upon substituting Eq. (56) into Eq. (54) and integrating, the equation for the effective mass M^* can be cast into the form

$$\frac{1}{M^*} = \frac{1}{M} - \frac{C}{\sqrt{x_{\text{cdw}} - x}}, \quad (57)$$

with C being some positive constant. It is seen from Eq. (57) that M^* diverges at some point x_{FC} referred to as the critical point, at which FCQPT occurs, as a function of the difference $(x_{\text{FC}} - x)$ [47]:

$$M^* \propto \frac{1}{x_{\text{FC}} - x}. \quad (58)$$

It follows from the derivation of Eqs. (57) and (58) that their forms are independent of the bare interaction $v(q)$. Therefore, both of these equations are also applicable to 2D electron liquid or to another Fermi liquid. It is also seen from Eqs. (57) and (58) that FCQPT precedes the formation of charge-density waves. As a consequence of this, the effective mass diverges at high densities in the case of 2D ^3He and at low densities in case of 2D electron systems, in accordance with experimental facts [19, 53]. Note that, in both cases, the difference $(x_{\text{FC}} - x)$ has to be positive, because x_{FC} represents the solution to Eq. (57). Thus, in considering the many-electron systems, we have to replace $(x_{\text{FC}} - x)$ by $(x - x_{\text{FC}})$. In case of a 3D system, the effective mass is given by [8]

$$\frac{1}{M^*} = \frac{1}{M} + \frac{p_F}{4\pi^2} \quad (59)$$

$$\times \int_{-1}^1 \int_0^{g_0} \frac{v(q(y))ydydg}{[1 - R(q(y), \omega = 0, g)\chi_0(q(y), \omega = 0)]^2}.$$

A comparison of Eqs. (54) and (59) shows that there is no fundamental difference between these equations, and in the same way we again arrive at Eqs. (57) and (58). The only difference between 2D electron systems and 3D ones is that in the latter FCQPT occurs at densities which are well below those corresponding to 2D systems. For bulk ${}^3\text{He}$, FCQPT probably cannot take place since it is absorbed by the first-order solidification [53].

Now, we address the problem of the fermion condensation in dilute Fermi gases and in low-density neutron matter. We consider an infinitely extended system composed of Fermi particles, or atoms, interacting by an artificially constructed potential with the desirable scattering length a . These objects may be viewed as trapped Fermi gases, which are systems composed of Fermi atoms interacting by a potential with almost any desirable scattering length, similarly to that done for trapped Bose gases (see, e.g., [55]). If a is negative, the system becomes unstable at densities $x \sim |a|^{-3}$, provided the scattering length is the dominant parameter of the problem. That means that $|a|$ is much bigger than the radius of the interaction or any other relevant parameter of the system. The compressibility $K(x)$ vanishes at the density $x_{c1} \sim |a|^{-3}$, making the system completely unstable [56]. Expressing the linear response function in terms of the compressibility [57],

$$\chi(q \rightarrow 0, i\omega \rightarrow 0) = - \left(\frac{d^2 E}{dx^2} \right)^{-1}, \quad (60)$$

we find that the linear response function has a pole at the origin of coordinates, $q \simeq 0$, $\omega \simeq 0$, at the same point x_{c1} . To find the behavior of the effective mass M^* as a function of the density, we substitute Eq. (56) into Eq. (59) taking into account that $x_{cdw} = x_{c1}$ and $q_c/p_F \ll 1$ due to Eq. (60). At low momenta $q/p_F \sim 1$, the potential $v(q)$ is attractive, because the scattering length is the dominant parameter and negative. Therefore, the integral on the right-hand side of Eq. (59) is negative and diverges at $x \rightarrow x_{c1}$. The above considerations can also be applied to the clarification of the fact that the effective mass M^* is again given by Eq. (58) with $x_{FC} < x_{c1}$. Note that the superfluid correlation cannot stop the system from squeezing, since its contribution to the ground-state energy is negative. After all, the superfluid correlations can be considered as additional degrees of freedom, which can therefore only decrease the energy. We conclude that FCQPT can be observed in traps by measuring the density of states at the Fermi level, which becomes extremely large as $x \rightarrow x_{FC}$. Note that, at these densities, the system remains stable because $x_{FC} < x_{c1}$. It seems quite probable that the neutron–neutron scattering length ($a \simeq -20$ fm) is

sufficiently large to be the dominant parameter and to permit the neutron matter to have an equilibrium energy, density, and the singular point x_{c1} , at which the compressibility vanishes [58]. Therefore, we can expect that FCQPT takes place in low-density neutron matter, leading to stabilization of the matter by lowering its ground-state energy. A more detailed analysis of this possibility will be published elsewhere.

A few remarks are in order. We have seen that, above the critical point x_{FC} , the effective mass M^* is finite and, therefore, the system exhibits the Landau Fermi liquid behavior. If $|x - x_{FC}|/x_{FC} \ll 1$, the behavior can be viewed as a highly correlated one, because the effective mass, given by Eq. (58), strongly depends on the density and is very large (see Section 7). Beyond this region, the effective mass is approximately constant and the system becomes a normal Landau Fermi liquid. We can expect to observe such a highly correlated electron (or hole) liquid in heavily overdoped high- T_c compounds, which are located beyond the superconducting dome. We recall that, beyond the FCQPT point, the superconducting gap Δ_1 can be very small or even absent [see Eq. (27)]. Indeed, recent experimental data have shown that this liquid does exist in heavily overdoped nonsuperconducting $\text{La}_{1.7}\text{Sr}_{0.3}\text{CuO}_4$ [59].

7. BEHAVIOR OF HIGHLY CORRELATED LIQUID

As we have seen in Section 6, when a Fermi system approaches FCQPT from the disordered phase, it remains the Landau Fermi liquid with the effective mass M^* strongly depending on the density $x_{FC} - x$, temperature, and magnetic field B , provided that $|x_{FC} - x|/x_{FC} \ll 1$ and $T \geq T^*(x)$ [47]. This state of the system, with M^* strongly depending on T , x , and B , resembles a strongly correlated liquid. In contrast to a strongly correlated liquid, there is no energy scale E_0 and the system under consideration is the Landau Fermi liquid at sufficiently low temperatures with the effective mass $M^* \simeq \text{const}$. Therefore, this liquid can be called a highly correlated liquid. Obviously, a highly correlated liquid must have uncommon properties.

In this section, we study the behavior of a highly correlated electron liquid in magnetic fields. We show that, at $T \geq T^*(x)$, the effective mass starts to depend on the temperature, $M^* \propto T^{-1/2}$. This $T^{-1/2}$ dependence of the effective mass at elevated temperatures leads to the non-Fermi liquid behavior of the resistivity, $\rho(T) \sim \rho_0 + aT + bT^{3/2}$. The application of magnetic field B restores the common T^2 behavior of the resistivity, $\rho \simeq \rho_0 + AT^2$, with $A \propto (M^*)^2$. Both the effective mass and coefficient A depend on

the magnetic field, $M^*(B) \propto B^{-2/3}$ and $A \propto B^{-4/3}$ being approximately independent of the temperature at $T \leq T^*(B) \propto B^{4/3}$. At $T > T^*(B)$, the $T^{-1/2}$ dependence of the effective mass is reestablished. We demonstrate that this B – T phase diagram has a strong impact on the magnetoresistance (MR) of the highly correlated electron liquid. The MR as a function of the temperature exhibits a transition from negative values of MR at $T \rightarrow 0$ to positive values at $T \propto B^{4/3}$. Thus, at $T \geq T^*(B)$, MR as a function of the temperature possesses a node at $T \propto B^{4/3}$. Such a behavior is of general form and takes place in both 3D highly correlated systems and 2D ones.

It follows from Eq. (58) that effective mass is finite, provided that $|x - x_{\text{FC}}| \equiv \Delta x > 0$. Therefore, the system represents the Landau Fermi liquid. In case of electronic systems, the Wiedemann–Franz law holds at $T \rightarrow 0$, and the Kadowaki–Woods ratio is preserved. Beyond the region $|x - x_{\text{FC}}|/x_{\text{FC}} \ll 1$, the effective mass is approximately constant and the system becomes a conventional Landau Fermi liquid. On the other hand, M^* diverges as the density x tends to the critical point of FCQPT. As a result, the effective mass strongly depends on such quantities as the temperature, pressure, magnetic field, given that they exceed their critical values. For example, when T exceeds some temperature $T^*(x)$, Eq. (58) is no longer valid, and M^* depends on the temperature as well. To evaluate this dependence, we calculate the deviation $\Delta x(T)$ generated by T . The temperature smoothing out the Fermi function $\theta(p_{\text{F}} - p)$ at p_{F} induces the variation $p_{\text{F}}\Delta p/M^*(x) \sim T$ and $\Delta x(T)/x_{\text{FC}} \sim M^*(x)T/p_{\text{F}}^2$, where p_{F} is the Fermi momentum and M is the bare electron mass. The deviation Δx can be expressed in terms of $M^*(x)$ using Eq. (58), $\Delta x/x_{\text{FC}} \sim M/M^*(x)$. Comparing these deviations, we find that, at $T \geq T^*(x)$, the effective mass depends noticeably on the temperature, and the equation for $T^*(x)$ becomes

$$T^*(x) \sim p_{\text{F}}^2 \frac{M}{(M^*(x))^2} \sim \varepsilon_{\text{F}}(x) \left(\frac{M}{M^*(x)} \right)^2. \quad (61)$$

Here, $\varepsilon_{\text{F}}(x)$ is the Fermi energy of noninteracting electrons with mass M . It follows from Eq. (61) that M^* is always finite at temperatures $T > 0$. We can consider $T^*(x)$ as the energy scale $e_0(x) \simeq T^*(x)$. This scale defines the area $(\mu - e_0(x))$ in the single-particle spectrum, where M^* is approximately constant, being given by $M^* = d\varepsilon(p)/dp$ [3]. According to Eqs. (58) and (61), it is easily verified that $e_0(x)$ can be written in the form

$$e_0(x) \sim \varepsilon_{\text{F}} \left(\frac{x - x_{\text{FC}}}{x_{\text{FC}}} \right)^2. \quad (62)$$

At $T \ll e_0(x)$ and above the critical point, the effective mass $M^*(x)$ is finite, the energy scale E_0 given by Eq. (18) vanishes, and the system exhibits the Landau Fermi liquid behavior. At temperatures $T \geq e_0(x)$, the effective mass M^* starts to depend on the temperature and the non-Fermi liquid behavior is observed. Thus, at $|x - x_{\text{FC}}|/x_{\text{FC}} \ll 1$, the system can be considered as a highly correlated one: at $T \ll e_0(x)$, the system is a Landau Fermi liquid, while at temperatures $T \geq e_0(x)$ the system possesses the non-Fermi liquid behavior.

At $T \geq T^*(x)$, the main contribution to Δx comes from the temperature; therefore,

$$M^* \sim M \frac{x_{\text{FC}}}{\Delta x(T)} \sim M \frac{\varepsilon_{\text{F}}}{M^* T}. \quad (63)$$

As a result, we obtain

$$M^*(T) \sim M \left(\frac{\varepsilon_{\text{F}}}{T} \right)^{1/2}. \quad (64)$$

Equation (64) allows us to evaluate the resistivity as a function of T . There are two terms contributing to the resistivity. Taking into account that $A \sim (M^*)^2$ and Eq. (64), we obtain the first term $\rho_1(T) \sim T$. The second term $\rho_2(T)$ is related to the quasiparticle width γ . When $M/M^* \ll 1$, the width $\gamma \propto (M^*)^3 T^2 / \epsilon(M^*) \propto T^{3/2}$, where $\epsilon(M^*) \propto (M^*)^2$ is the dielectric constant [13, 43]. Combining both of the contributions, we find that the resistivity is given by

$$\rho(T) - \rho_0 \sim aT + bT^{3/2}. \quad (65)$$

Here, a and b are constants. Thus, it turns out that, at low temperatures, $T < T^*(x)$, the resistivity $\rho(T) - \rho_0 \sim AT^2$. At higher temperatures, the effective mass depends on the temperature and the main contribution comes from the first term on the right-hand side of Eq. (65), while $\rho(T) - \rho_0$ follows the $T^{3/2}$ dependence at elevated temperatures.

In the same way as Eq. (64) was derived, we can obtain the equation determining $M^*(B)$ [47]. The application of magnetic field B leads to a weakly polarized state, or Zeeman splitting, when some levels at the Fermi level are occupied by spin-up polarized quasiparticles. The width $\delta p = p_{\text{F}1} - p_{\text{F}2}$ of the area in momentum space occupied by these quasiparticles is of the order

$$\frac{p_{\text{F}}\delta p}{M^*} \sim B\mu_{\text{eff}}.$$

Here, $\mu_{\text{eff}} \sim \mu_{\text{B}}$ is the electron magnetic effective moment, $p_{\text{F}1}$ is the Fermi momentum of the spin-up electrons, and $p_{\text{F}2}$ is the Fermi momentum of the

spin-down electrons. As a result, the Zeeman splitting leads to the change Δx in the density x :

$$\frac{\Delta x}{x_{\text{FC}}} \sim \frac{\delta p^2}{p_{\text{F}}^2}.$$

We assume that $\Delta x/x_{\text{FC}} \ll 1$. Now, it follows that

$$M^*(B) \sim M \left(\frac{\varepsilon_{\text{F}}}{B\mu_{\text{eff}}} \right)^{2/3}. \quad (66)$$

We note that M^* is determined by Eq. (66) as long as $M^*(B) \leq M^*(x)$, otherwise we have to use Eq. (58). It follows from Eq. (66) that the application of a magnetic field reduces the effective mass. Note that, if there exists an itinerant magnetic order in the system which is suppressed by magnetic field $B = B_{c0}$, Eq. (66) has to be replaced by the equation [48] (see also Section 5)

$$M^*(B) \propto \left(\frac{1}{B - B_{c0}} \right)^{2/3}. \quad (67)$$

The coefficient $A(B) \propto (M^*(B))^2$ diverges as

$$A(B) \propto \left(\frac{1}{B - B_{c0}} \right)^{4/3}. \quad (68)$$

At elevated temperature, there is a temperature $T^*(B)$ at which $M^*(B) \simeq M^*(T)$. Comparing Eq. (64) and Eq. (67), we see that $T^*(B)$ is given by

$$T^*(B) \propto (B - B_{c0})^{4/3}. \quad (69)$$

At $T \geq T^*(x)$, Eq. (69) determines the line in the B - T phase diagram that separates the region of the B -dependent effective mass from the region of the T -dependent effective mass. At the temperature $T^*(B)$, a crossover from the T^2 dependence of the resistivity to the T dependence occurs: at $T < T^*(B)$, the effective mass is given by Eq. (67), and at $T > T^*(B)$, M^* is given by Eq. (64).

Using the B - T phase diagram just presented, we consider the behavior of MR,

$$\rho_{\text{MR}}(B, T) = \frac{\rho(B, T) - \rho(0, T)}{\rho(0, T)}, \quad (70)$$

as a function of magnetic field B and T . Here, $\rho(B, T)$ is the resistivity measured at the magnetic field B and temperature T . We assume that the contribution $\Delta\rho_{\text{MR}}(B)$ coming from the magnetic field B can be treated within the low-field approximation and given by the well-known Kohler's rule,

$$\Delta\rho_{\text{MR}}(B) \sim B^2\rho(0, \Theta_{\text{D}})/\rho(0, T), \quad (71)$$

where Θ_{D} is the Debye temperature. Note that the low-field approximation implies that $\Delta\rho_{\text{MR}}(B) \ll$

$\rho(0, T) \equiv \rho(T)$. Substituting Eq. (71) into Eq. (70), we find that

$$\begin{aligned} & \rho_{\text{MR}}(B, T) \quad (72) \\ & \sim \frac{c(M^*(B, T))^2 T^2 + \Delta\rho_{\text{MR}}(B) - c(M^*(0, T))^2 T^2}{\rho(0, T)}. \end{aligned}$$

Here, $M^*(B, T)$ denotes the effective mass M^* which now depends on both the magnetic field and the temperature, and c is a constant.

Consider MR given by Eq. (72) as a function of B at some temperature $T = T_0$. At low temperatures $T_0 \leq T^*(x)$, the system behaves as a common Landau Fermi liquid, and MR is an increasing function of B . When the temperature T_0 is sufficiently high, $T^*(B) < T_0$, and the magnetic field is small, $M^*(B, T)$ is given by Eq. (64). Therefore, the difference $\Delta M^* = |M^*(B, T) - M^*(0, T)|$ is small and the main contribution is given by $\Delta\rho_{\text{MR}}(B)$. As a result, MR is an increasing function of B . At elevated B , the difference ΔM^* becomes a decreasing function of B , and MR as a function of B reaches its maximum value at $T^*(B) \sim T_0$. In accordance with Eq. (69), $T^*(B)$ determines the crossover from the T^2 dependence of the resistivity to the T dependence. Differentiating the function $\rho_{\text{MR}}(B, T)$ given by Eq. (72) with respect to B , one can verify that the derivative is negative at sufficiently large values of the magnetic field when $T^*(B) \simeq T_0$. Thus, we are led to the conclusion that the crossover manifests itself as the maximum of MR as a function of B .

We now consider MR as a function of T at some B_0 . At $T < T^*(x)$, we have a normal Landau Fermi liquid. At low temperatures $T^*(x) \leq T \ll T^*(B_0)$, it follows from Eqs. (64) and (67) that $M^*(B_0)/M^*(T) \ll 1$, and MR is determined by the resistivity $\rho(0, T)$. Note that B_0 has to be comparatively high to ensure the inequality $T^*(x) \leq T \ll T^*(B_0)$. As a result, MR tends to -1 , $\rho_{\text{MR}}(B_0, T \rightarrow 0) \simeq -1$. Differentiating the function $\rho_{\text{MR}}(B_0, T)$ with respect to B_0 , we can check that its slope becomes steeper as B_0 is decreased, being proportional to $(B_0 - B_{c0})^{-7/3}$. At $T = T_1 \sim T^*(B_0)$, MR possesses a node, because at this point the effective mass $M^*(B_0) \simeq M^*(T)$ and $\rho(B_0, T) \simeq \rho(0, T)$. Again, we can conclude that the crossover from the T^2 dependence of the resistivity to the T dependence of the resistivity, which occurs at $T \sim T^*(B_0)$, manifests itself in the transition from negative MR to positive MR. At $T > T^*(B_0)$, the main contribution to MR comes from $\Delta\rho_{\text{MR}}(B_0)$, and MR reaches its maximum value. Upon using Eq. (71) and taking into account that, at this point, T has to be determined by Eq. (69), $T \propto (B_0 - B_{c0})^{4/3}$, we find that the maximum value $\rho_{\text{MR}}^m(B_0)$ of MR

is $\rho_{\text{MR}}^m(B_0) \propto (B_0 - B_{c0})^{-2/3}$. Thus, the maximum value is a decreasing function of B_0 . At $T^*(B_0) \ll T$, MR is a decreasing function of the temperature, and at elevated temperatures MR eventually vanishes since $\Delta\rho_{\text{MR}}(B_0)/\rho(T) \ll 1$.

The recent paper [60] reports on measurements of the resistivity of CeCoIn₅ in a magnetic field. With increasing field, the resistivity evolves from the T temperature dependence to the T^2 dependence, while the field dependence of $A(B) \sim (M^*(B))^2$ displays the critical behavior best fitted by the function $A(B) \propto (B - B_{c0})^{-\alpha}$, with $\alpha \simeq 1.37$ [60]. All these facts are in good agreement with the B – T phase diagram given by Eq. (69). The critical behavior displaying $\alpha = 4/3$ [47] and described by Eq. (68) is also in good agreement with the data. A transition from negative MR to positive MR with increasing T was also observed [60]. We believe that an additional analysis of the data [60] can reveal that the crossover from the T^2 dependence of the resistivity to the T dependence occurs at $T \propto (B - B_{c0})^{4/3}$. As well, this analysis could reveal supplementary peculiarities of MR. The behavior of the heavy-fermion metal CeCoIn₅ in magnetic fields displayed in [60] can be identified as the highly correlated behavior of a Landau Fermi liquid approaching FCQPT from the disordered phase [47].

8. SUMMARY AND CONCLUSION

We have discussed the appearance of the fermion condensation, which can be compared to the Bose–Einstein condensation. A number of pieces of experimental evidence have been presented that are supportive to the idea of the existence of FC in different liquids. We have demonstrated also that experimental facts collected in different materials, belonging to high- T_c superconductors, heavy-fermion metals, and strongly correlated 2D structures, can be explained within the framework of the theory based on FCQPT.

We have shown that the appearance of FC is a quantum phase transition that separates the regions of normal and strongly correlated liquids. Beyond the fermion condensation point, the quasiparticle system is divided into two subsystems, one containing normal quasiparticles, the other being occupied by fermion condensate localized at the Fermi level. In the superconducting state, the quasiparticle dispersion in systems with FC can be represented by two straight lines, characterized by effective masses M_{FC}^* and M_{L}^* and intersecting near the binding energy E_0 , which is of the order of the superconducting gap. The same quasiparticle picture and the energy scale E_0 persist in the normal state. We have demonstrated that fermion systems with FC have features of a “quantum protectorate” and shown that the theory

of high-temperature superconductivity, based on the fermion condensation quantum phase transition and on the conventional theory of superconductivity, permits the description of high values of T_c and of the maximum value of the gap Δ_1 , which may be as big as $\Delta_1 \sim 0.1\varepsilon_{\text{F}}$ or even larger. We have also traced the transition from conventional superconductors to high- T_c ones. We have shown by a simple, although self-consistent, analysis that the general features of the shape of the critical temperature $T_c(x)$ as a function of the density x of the mobile carriers in the high- T_c compounds can be understood within the framework of the theory.

We have demonstrated that strongly correlated many-electron systems with FC, which exhibit strong deviations from the Landau Fermi liquid behavior, can be driven into the Landau Fermi liquid by applying a small magnetic field B at low temperatures. A reentrance into the strongly correlated regime is observed if the magnetic field B decreases to zero, while the effective mass M^* diverges as $M^* \propto 1/\sqrt{B}$. The regime is restored at some temperature $T^* \propto \sqrt{B}$. This behavior is of a general form, takes place in both 3D and 2D strongly correlated systems, and demonstrates the possibility to control the essence of strongly correlated electron liquids by weak magnetic fields.

The appearance of FCQPT in 2D strongly correlated structures, in trapped Fermi gases, and in low-density neutron matter has been considered. We have provided an explanation of the experimental data on the divergence of the effective mass in a 2D electron liquid and in 2D ³He, as well as shown that, above the critical point, the system exhibits the Landau Fermi liquid behavior. We expect that FCQPT takes place in trapped Fermi gases and in low-density neutron matter, leading to stabilization of the matter by lowering its ground-state energy. If $|x - x_{\text{FC}}|/x_{\text{FC}} \ll 1$, the behavior can be viewed as a highly correlated one, because the effective mass is very large and strongly depends on the density. Beyond this region, the effective mass is approximately constant and the system becomes a normal Landau Fermi liquid.

The behavior in magnetic fields of a highly correlated electron liquid approaching FCQPT from the disordered phase has been considered. We have shown that, at sufficiently high temperatures, the effective mass starts to depend on T , $M^* \propto T^{-1/2}$. This $T^{-1/2}$ dependence of the effective mass at elevated temperatures leads to the non-Fermi liquid behavior of the resistivity. The application of a magnetic field B restores the common T^2 behavior of the resistivity. We have demonstrated that this B – T phase diagram has a strong impact on the magnetoresistance of the highly correlated electron liquid. The MR as a

function of the temperature exhibits a transition from negative values of MR at $T \rightarrow 0$ to positive values at $T \propto B^{4/3}$.

We conclude that FCQPT can be viewed as a universal cause of the non-Fermi liquid behavior observed in different metals and liquids.

ACKNOWLEDGMENTS

One of us (V.R.S.) expresses his gratitude to CT-SPS for the hospitality during his stay in Atlanta and for financial support that made this stay possible. M.Y.A. is grateful to the Hebrew University Intramural fund of the Hebrew University for financial support. A.Z.M. acknowledges support from the US Department of Energy, Division of Chemical Sciences, Office of Basic Energy Sciences, Office of Energy Research.

This work was supported in part by the Russian Foundation for Basic Research, project no. 01-02-17189.

REFERENCES

- S. T. Belyaev, Zh. Éksp. Teor. Fiz. **34**, 417 (1958) [Sov. Phys. JETP **7**, 289 (1958)].
- S. T. Belyaev, Zh. Éksp. Teor. Fiz. **34**, 433 (1958) [Sov. Phys. JETP **7**, 299 (1958)].
- L. D. Landau, Zh. Éksp. Teor. Fiz. **30**, 1058 (1956) [Sov. Phys. JETP **3**, 920 (1956)].
- V. A. Khodel and V. R. Shaginyan, Pis'ma Zh. Éksp. Teor. Fiz. **51**, 488 (1990) [JETP Lett. **51**, 553 (1990)].
- G. E. Volovik, Pis'ma Zh. Éksp. Teor. Fiz. **53**, 208 (1991) [JETP Lett. **53**, 222 (1991)].
- M. Ya. Amusia and V. R. Shaginyan, Pis'ma Zh. Éksp. Teor. Fiz. **73**, 268 (2001) [JETP Lett. **73**, 232 (2001)]; Phys. Rev. B **63**, 224507 (2001); V. R. Shaginyan, Physica B **312–313**, 413 (2002).
- V. A. Khodel, V. R. Shaginyan, and V. V. Khodel, Phys. Rep. **249**, 1 (1994).
- V. A. Khodel, V. R. Shaginyan, and M. V. Zverev, Pis'ma Zh. Éksp. Teor. Fiz. **65**, 242 (1997) [JETP Lett. **65**, 253 (1997)].
- J. Dukelsky, V. A. Khodel, P. Schuck, and V. R. Shaginyan, Z. Phys. B **102**, 245 (1997); V. A. Khodel and V. R. Shaginyan, Condens. Matter Theor. **12**, 222 (1997).
- J. Bardeen, L. N. Cooper, and J. R. Schrieffer, Phys. Rev. **108**, 1175 (1957).
- V. R. Shaginyan, Phys. Lett. A **249**, 237 (1998).
- V. A. Khodel, J. W. Clark, and V. R. Shaginyan, Solid State Commun. **96**, 353 (1995).
- S. A. Artamonov and V. R. Shaginyan, Zh. Éksp. Teor. Fiz. **119**, 331 (2001) [JETP **92**, 287 (2001)].
- R. B. Laughlin and D. Pines, Proc. Natl. Acad. Sci. U.S.A. **97**, 28 (2000).
- P. W. Anderson, cond-mat/0007185; cond-mat/0007287.
- P. V. Bogdanov *et al.*, Phys. Rev. Lett. **85**, 2581 (2000).
- A. Kaminski *et al.*, Phys. Rev. Lett. **86**, 1070 (2001).
- T. Valla *et al.*, Science **285**, 2110 (1999); T. Valla *et al.*, Phys. Rev. Lett. **85**, 828 (2000).
- A. A. Shashkin, S. V. Kravchenko, V. T. Dolgoplov, and T. M. Klapwijk, Phys. Rev. B **66**, 073303 (2002).
- G. Grüner, *Density Waves in Solids* (Addison-Wesley, Reading, 1994).
- D. R. Tilley and J. Tilley, *Superfluidity and Superconductivity* (Bristol, Hilger, 1985).
- V. R. Shaginyan, Pis'ma Zh. Éksp. Teor. Fiz. **68**, 491 (1998).
- M. Ya. Amusia and V. R. Shaginyan, Phys. Lett. A **298**, 193 (2002).
- M. Kugler *et al.*, Phys. Rev. Lett. **86**, 4911 (2001).
- A. A. Abrikosov, Phys. Rev. B **52**, R15738 (1995); cond-mat/9912394.
- M. Ya. Amusia, S. A. Artamonov, and V. R. Shaginyan, Pis'ma Zh. Éksp. Teor. Fiz. **74**, 396 (2001).
- N.-C. Yeh *et al.*, Phys. Rev. Lett. **87**, 087003 (2001).
- A. Biswas *et al.*, Phys. Rev. Lett. **88**, 207004 (2002).
- J. A. Skinta *et al.*, Phys. Rev. Lett. **88**, 207005 (2002).
- J. A. Skinta *et al.*, Phys. Rev. Lett. **88**, 207003 (2002).
- C.-T. Chen *et al.*, Phys. Rev. Lett. **88**, 227002 (2002).
- C. M. Varma, Z. Nussinov, and W. Wim van Saarloos, Phys. Rep. **361**, 267 (2002).
- M. Ya. Amusia and V. R. Shaginyan, Pis'ma Zh. Éksp. Teor. Fiz. **76**, 774 (2002).
- N. Miyakawa *et al.*, Phys. Rev. Lett. **83**, 1018 (1999).
- D. L. Feng *et al.*, cond-mat/0107073.
- D. S. Dessau *et al.*, Phys. Rev. Lett. **66**, 2160 (1991).
- A. B. Migdal, *Theory of Finite Fermi Systems and Applications to Atomic Nuclei* (Benjamin, Reading, 1977).
- Z. Yusof *et al.*, Phys. Rev. Lett. **88**, 167006 (2002); cond-mat/0104367.
- S. A. Artamonov, V. R. Shaginyan, and Yu. G. Pogorelov, JETP Lett. **68**, 942 (1998).
- M. de Llano and J. P. Vary, Phys. Rev. C **19**, 1083 (1979); M. de Llano, A. Plastino, and J. G. Zabolitsky, Phys. Rev. C **20**, 2418 (1979).
- M. V. Zverev and M. Baldo, cond-mat/9807324.
- K. Kadowaki and S. B. Woods, Solid State Commun. **58**, 507 (1986).
- V. A. Khodel and P. Schuck, Z. Phys. B **104**, 505 (1997).
- P. Gegenwart *et al.*, Phys. Rev. Lett. **89**, 056402 (2002); cond-mat/0207570.
- K. Ishida *et al.*, Phys. Rev. Lett. **89**, 107202 (2002).
- P. Coleman *et al.*, J. Phys.: Condens. Matter **13**, R723 (2001); P. Coleman, cond-mat/0206003.
- V. R. Shaginyan, cond-mat/0208568; cond-mat/0212624; cond-mat/0301019; Pis'ma Zh. Éksp. Teor. Fiz. **77**, 104 (2003); Pis'ma Zh. Éksp. Teor. Fiz. (in press).

48. Yu. G. Pogorelov and V. R. Shaginyan, *Pis'ma Zh. Éksp. Teor. Fiz.* **76**, 614 (2002).
49. T. Takahashi *et al.*, cond-mat/0212238.
50. C. Proust *et al.*, *Phys. Rev. Lett.* **89**, 147003 (2002).
51. A. P. Mackenzie *et al.*, *Phys. Rev. B* **53**, 5848 (1996).
52. K.-D. Morhard *et al.*, *Phys. Rev. B* **53**, 2658 (1996).
53. A. Casey *et al.*, *J. Low Temp. Phys.* **113**, 293 (1998).
54. M. Pfitzner and P. Wölfe, *Phys. Rev. B* **33**, 2003 (1986).
55. S. Inouye *et al.*, *Nature* **392**, 151 (1998).
56. M. Ya. Amusia, A. Z. Msezane, and V. R. Shaginyan, *Phys. Lett. A* **293**, 205 (2002).
57. L. D. Landau and E. M. Lifshitz, *Statistical Physics* (Addison–Wesley, Reading, 1970), Part 1.
58. M. Ya. Amusia and V. R. Shaginyan, *Eur. Phys. J. A* **8**, 77 (2000).
59. S. Nakamae *et al.*, cond-mat/0212283.
60. J. Paglione *et al.*, cond-mat/0212502.

NUCLEI
Experiment

Storage of Ultracold Neutrons in Vessels Whose Walls Are Made from Graphite, Fluorine Polymer Oil, or Heavy-Water Ice

S. S. Arzumanov, L. N. Bondarenko*, V. I. Morozov, Yu. N. Panin, and P. Geltenbort¹⁾

Russian Research Centre Kurchatov Institute, pl. Kurchatova 1, Moscow, 123182 Russia

Received March 20, 2002; in final form, April 17, 2003

Abstract—The possibility of attaining the calculated probabilities of the losses of ultracold neutrons (UCN) stored in vessels whose walls are made from graphite, fluorine polymer oil, or heavy-water ice is tested experimentally. It is found that UCN hitting the walls of a graphite vessel undergo additional inelastic scattering not predicted by the theory. It is shown that this scattering may be due to the presence of surface hydrogen that provides a channel of UCN leakage slightly varying with temperature. For vessels whose walls are coated with fluorine polymer oil, additional inelastic UCN scattering is also observed and is found to be efficiently suppressed with decreasing temperature. The experimentally observed and calculated values of the probabilities of UCN losses are shown to be in good agreement for vessels whose walls are made from heavy-water ice. © 2003 MAIK “Nauka/Interperiodica”.

INTRODUCTION

If ultracold neutrons (UCN) are stored in vessels, the probability of their losses per unit time is $\lambda_{\text{tot}} = \lambda_{\beta} + \lambda_l$, where $\lambda_{\beta} = 113 \times 10^{-5} \text{ s}^{-1}$ is the probability of the neutron beta decay and λ_l is the probability of UCN losses caused by the capture and inelastic scattering of neutrons undergoing collisions with the vessel walls. In accordance with the current theory of UCN storage, $\lambda_l = \eta\gamma(v)$, where η is the ratio of the imaginary and real parts of the potential used to describe neutron interaction with matter and $\gamma(v)$ is a geometric factor that is calculated for a specific experiment with allowance for gravity and which is dependent on the neutron speed v and on the size and shape of the vessel. The quantity η is determined as

$$\eta = \eta_c + \eta_{\text{in}} = \frac{mv[\sigma_c(v) + \sigma_{\text{in}}(v, T)]}{4\pi b\hbar}, \quad (1)$$

where m is the neutron mass; T is temperature; b is the scattering length for coherent interaction; and σ_c and σ_{in} are, respectively, the capture and the inelastic-scattering cross section. The calculation of η is usually based on experimental cross sections in the cold-neutron region, where the cross sections for inelastic processes obey the $\sigma \sim v^{-1}$ law. Experiments devoted to measuring the neutron lifetime by the UCN storage method required designing vessels with $\lambda_l \ll \lambda_{\beta}$; for many years, experimentalists have therefore focused their attention on the use of vessels manufactured from materials characterized by small cross sections

for capture and inelastic scattering. In the case where inelastic UCN scattering was suppressed at low temperatures to such an extent that capture remained the main channel of UCN losses, the theoretically expected values of η were 10^{-7} – 10^{-6} for a number of materials (beryllium, graphite, oxygen, and so on). The expected probabilities λ_l were 10^{-6} – 10^{-5} s^{-1} for $\gamma(v)$ values on the order of 5 – 10 s^{-1} , which correspond to the 0.5- to 1-m vessels typically used for UCN storage in practice. However, numerous investigations of UCN storage revealed that, for almost all materials, values obtained for η are substantially higher than their calculated counterparts over a wide range of temperatures. This discrepancy generated a great number of experimental and theoretical studies, the earliest of them being surveyed in [1–3]. As a result, it was found that, to a considerable extent, the excess of the experimental values of η over the calculated ones is due to additional inelastic UCN scattering into the thermal energy region [4]. A possible explanation of this effect by a surface contamination with hydrogen was indirectly suggested both by the theoretical estimations in [5, 6] and by data that the method of nuclear reactions yields for the hydrogen concentration at the surface of some materials [7, 8]. However, a direct correlation between the observed additional inelastic scattering and the surface contamination with hydrogen was established owing to the development of the technique of neutron-radiation analysis of γ rays originating from UCN interaction with the surface [9–12]. In this way, it was found that there is a hydrogen-containing layer at the surface of all materials used for UCN storage and that

¹⁾Laue-Langevin Institute, Grenoble, France

* e-mail: bond@foton.polyn.kiae.su

this layer causes the inelastic scattering and capture of UCN. The hydrogen concentration in the surface layer depends on the material used and on the method of initial surface purification (washing, chemical etching, electropolishing, and so on) and can be as great as 10^{17} atom/cm². In this case, the effective value of the parameter η can reach a value on the order of 10^{-3} because of additional inelastic scattering on hydrogen. A feature peculiar to these layers was that, for all materials subjected to a relevant study, the ratio of the cross sections for inelastic scattering and capture on hydrogen in a layer—that is, $\sigma_{\text{in}}^H/\sigma_c^H$ —depended only slightly on the type of material, varying within the range of 15–20 at room temperature [12]. This suggests that an identical hydrogen-containing film of thickness up to 50 Å remains at the surface of all materials after initial purification. (We note that $\sigma_{\text{in}}^H/\sigma_c^H \sim 12\text{--}16$ for hydrogen-containing materials at $T = 300$ K.)

Secondary, more thorough, purification was performed by means of either high-temperature annealing in a vacuum or a gas discharge. Investigations of UCN by the method of (n, γ) analysis revealed that the main fraction of the hydrogen-containing layer desorbed from the surface after high-temperature annealing. This was confirmed by the decrease in the probability of the inelastic scattering and capture of UCN on hydrogen in direct proportion to the annealing time and temperature. Even after prolonged annealing (for tens of hours) at 700–800 K, however, additional inelastic UCN scattering remains, providing an excessive value of the parameter η at a level of $(3\text{--}10) \times 10^{-5}$. In this case, the surface concentration of hydrogen falls to a level at which the accuracy of the (n, γ) analysis only allows one to set an upper limit on the concentration of residual surface hydrogen. Here, it is possible that residual inelastic scattering is caused by hydrogen that cannot be removed by ordinary methods of surface purification. If, on the other hand, there is no hydrogen at the surface, excessive inelastic scattering is due to other physical reasons not predicted by the existing theory. This possibility was indirectly suggested by the results of the experiments reported in [13, 14] and devoted to studying the temperature dependence of the time of UCN storage in vessels made from stainless steel and aluminum coated with a sputtered beryllium layer. In both cases, even an intense cooling down to 6–10 K led to a decrease in the probability of additional losses only by a factor of 1.5 to 2 with respect to the probability of such losses at $T = 300$ K. It seemed that UCN reflected from the surface experienced some unknown interaction that depended on temperature only slightly or was independent of temperature and which could be formally characterized by a cross section of

$\sigma_x = 0.9$ b at a speed of $v_{\text{th}} = 2200$ m/s [14]. Since the cross section for inelastic scattering on hydrogen dissolved in a metal must be greatly dependent on temperature, a slight temperature dependence of the probability of additional losses rendered the “hydrogen” origin of the effect questionable. It was just this contradiction that brought about the term “anomalous” UCN losses, which became generally accepted in the literature, and various hypotheses aimed at explaining this phenomenon.

This article reports on an investigation into the process of UCN storage in vessels whose walls are coated with graphite, a hydrogen-free fluorine polymer oil, and heavy-water ice. In just the same way as beryllium, these materials are characterized by small cross sections for capture and inelastic scattering; therefore, they must be promising for manufacturing low-temperature vessels with $\lambda_l \ll \lambda_\beta$. The main objective of this study was to find out whether it is possible to attain the calculated losses for these materials and to clarify the physical mechanism of processes hindering this.

The investigation was performed along a few lines. In order to calculate the theoretical values of the parameter η , we first measured the total cross sections for cold-neutron interaction with fluorine polymer oils and heavy water. The inelastic scattering and capture of UCN on a graphite surface were studied by the method of (n, γ) analysis. The experimental values η_{expt} for graphite and fluorine polymer oil were determined in direct experiments studying UCN storage. Also, the data of earlier studies were used for heavy-water ice and fluorine polymer oil.

1. TOTAL CROSS SECTIONS FOR COLD-NEUTRON INTERACTION WITH HEAVY WATER, FLUORINE POLYMER OIL, AND GRAPHITE

For neutrons of energy below the Bragg jump, the total cross section $\sigma_{\text{tot}} = \sigma_e^{\text{inc}} + \sigma_{\text{in}} + \sigma_c$, where σ_e^{inc} is the incoherent-elastic-scattering cross section, which does not exceed a few barn for the majority of materials, with the exception of hydrogen. As the speed decreases, the cross sections σ_{in} and σ_c increase in inverse proportion to the neutron speed in matter, $v = \sqrt{v_0^2 - v_{\text{lim}}^2}$, where v_0 is the speed of neutrons in a vacuum and v_{lim} is the limiting speed. For very cold neutrons, the cross section is $\sigma_{\text{tot}} \approx \sigma_c + \sigma_{\text{in}}$ at a speed of about 10 m/s; therefore, measurement of the total cross section in this region would make it possible to assess the calculated value of η .

Figure 1 shows the results obtained by measuring the temperature dependences of σ_{tot} (per atom) for heavy water D₂O and for the fluorine polymer

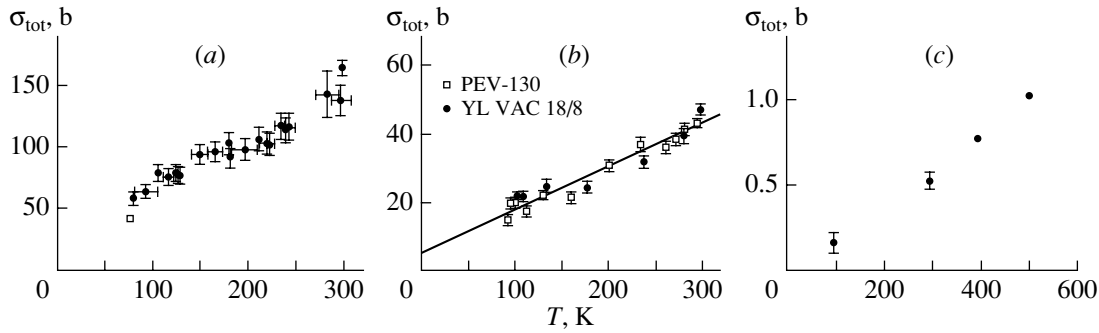


Fig. 1. Total cross section σ_{tot} as a function of temperature T (a) for heavy water, (b) for fluorine polymer oils, and (c) for graphite.

oils PEV-130 ($\text{OCFCF}_3\text{CF}_2$) $_n$, which was made in Russia, and YL VAC 18/8 ($\text{F}_3\text{CCF}_2\text{OCF}_2\text{CF}_5$) $_n$, which was made in Italy. The procedure of measurements performed by passing a vertical neutron beam through samples at a speed of $v_0 = 9.0(4)$ m/s is described in [15].

Figure 1a shows the dependence $\sigma_{\text{tot}}(T)$ for D_2O containing an admixture of H_2O whose amount does not exceed 0.15%. The density of D_2O at 4°C is 1.1 g/cm³, which corresponds to $v_{\text{lim}} = 5.3$ m/s and the neutron speed of $v = 7.3(5)$ m/s in the sample. It can be seen from the figure that σ_{tot} decreases with decreasing temperature, because the inelastic cross section is suppressed. The contribution of the capture cross section is 0.12 b, and the contribution of the cross section for incoherent elastic scattering is about 1.5 b. A sample 3.1 cm thick and 3 cm in diameter was used in the measurements. When cooled, this sample transformed from a liquid to a solid state, forming an optically transparent and homogeneous crystal that retained these properties to 180 K. Below 180 K, the crystal cracked, forming an inhomogeneous structure, which could have caused an additional elastic scattering of neutrons on inhomogeneities of the density. In this case, the angular divergence of the passing beam and the effective path of neutrons in the sample could have increased, with the result that the cross sections measured in the temperature region below 180 K could have been overestimated. In order to estimate this effect, we used data from [16], where σ_{tot} for D_2O ice was measured in the energy range $(0.2\text{--}0.8)\times 10^{-3}$ eV at 77 K. It was found that, in this energy range, the inhomogeneity of the sample has virtually no effect on the results of the measurements. The cross section σ_{in} rescaled for a speed of 7.3(5) m/s from data given in [16] is 42(3) b, and the total cross section is 43.6(30) b (it is represented by the open box in Fig. 1a). According to our data, the total cross section is 57.8(40) b at 80 K. This discrepancy may be associated with elastic scattering on

inhomogeneities that leads to a 15 to 25% increase in the measured total cross section. For the subsequent analysis of the experimental data on UCN storage at 80 K in a vessel whose walls are made from D_2O ice, the total cross section $\sigma_{\text{in}} + \sigma_c$ was taken to be 42.1(30) b at $v = 7.3(5)$ m/s.

Figure 1b shows $\sigma_{\text{tot}}(T)$ measured for the fluorine polymer oils PEV-1 and YL VAC 18/8. At 20°C, the limiting speed for the oils is $v_{\text{lim}} = 4.55$ m/s, which corresponds to the neutron speed of $v = 7.8(5)$ m/s in the sample. At this speed value, the capture cross section is 2.2 b for YL VAC 18/8 and 1.9 b for PEV-1. The cross section for incoherent elastic scattering does not exceed 1 b. It can be seen from Fig. 1b that, for the two types of oil, the total cross sections are close in magnitude and decrease with decreasing temperature because of a decrease in the cross section for inelastic scattering. It should be noted that the values obtained for the cross sections can be used to determine $\sigma_{\text{in}} + \sigma_c$ only for temperatures above 200 to 220 K. Below these temperatures, the samples cracked, which was observed visually and which could have resulted in elastic scattering on inhomogeneities. In the subsequent analysis, the results obtained by measuring $\sigma_{\text{tot}}(T)$ below 200 to 220 K were therefore only used to set an upper limit on $\sigma_{\text{in}} + \sigma_c$.

Elastic scattering on inhomogeneities of the graphite density appeared to be so intense that it was impossible to measure σ_{tot} as a function of T at a neutron speed of $v_0 = 9.0(4)$ m/s directly. In view of this, the experimental results from [17] for $\sigma_{\text{tot}}(T)$ at the neutron speed of 530 m/s, which are presented in Fig. 1c, were used to calculate η . In this case, the contribution of capture processes to the total cross section was 1.6×10^{-3} b. The cross section for incoherent elastic scattering was smaller than 0.01 b.

2. STORAGE OF UCN IN A VESSEL FROM PYROLYTIC GRAPHITE

2.1. Experimental Procedure

Neutrons were accumulated in a 7-l cylindrical vessel 40 cm in length manufactured from pyrolytic graphite characterized by the limiting energy of $E_{\text{lim}} = 170$ neV (Fig. 2a). The inlet hole of the vessel was closed with a flat graphite shutter. The vessel was placed within an intermediate vacuum chamber 106 cm in length and 27 cm in diameter, which was manufactured from stainless steel; a vertical neutron guide with an inlet window from 100- μm Al foil was connected to the chamber bottom. The heating elements and the guides of liquid-nitrogen supply were arranged at the outer surface of the chamber. The chamber had an independent system of oil-free evacuation providing a vacuum at a pressure of 10^{-6} torr.

The chamber temperature was varied in the range 80–700 K. The temperature of the graphite vessel varied within this range as well owing to radiant heat transfer between its walls and the chamber surface. The intermediate chamber was placed in the vacuum housing that involved an independent system of evacuation to 10^{-5} torr. The system of double evacuation eliminated the transfer of possible hydrogen-containing impurities from a residual gas of the setup to the surface of the vessel on its cooling almost completely. After the evacuation of the intermediate chamber and the closing of the evacuation valve, the chamber became a hermetic volume containing a residual gas at a pressure of $p = 10^{-6}$ torr and occurring in a 10^{-5} -torr vacuum. This ruled out the penetration of a gas into the chamber from the environment through microleaks in welded connections. In principle, molecules containing hydrogen—those of water, for example—could condense at the surface of the vessel and the inner surface of the sealed chamber on its cooling, but their number could not exceed the number of molecules of the residual gas in the chamber, $N = n\Omega p/p_0 = 2.8 \times 10^{15}$, where $n = 2.7 \times 10^{19} \text{ cm}^{-3}$ is the Loschmidt number, $\Omega = 80$ l is the chamber volume, and $p_0 = 760$ torr. Since the area of the inner surface of the graphite vessel was $2 \times 10^3 \text{ cm}^2$, the surface density of condensed-water molecules was obviously below $1.4 \times 10^{12} \text{ cm}^{-2}$ —that is, 10^{-3} – 10^{-4} of monolayer.

The transfer of UCN from the TGV source (Laue-Langevin Institute, Grenoble) to the intermediate chamber containing a vessel was accomplished with the aid of a horizontal guide from stainless steel with $E_{\text{lim}} = 180$ neV and a vertical neutron guide with two inlet shutters. The spectrum of neutrons that filled the chamber and the vessel featured virtually no UCN

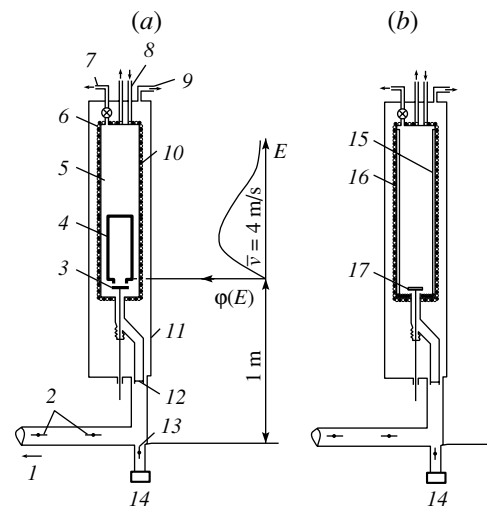


Fig. 2. Schematic of experiments aimed at studying UCN storage in (a) a graphite vessel and (b) an intermediate vessel: (1) guide to the UCN source, (2) UCN shutters, (3) UCN graphite shutter, (4) graphite vessel, (5) intermediate chamber, (6) guides of the cooling system, (7) high-vacuum evacuation of the vessel, (8) guides of the liquid nitrogen supply, (9) high-vacuum evacuation of the intermediate chamber, (10) line of the heater, (11) vacuum housing, (12) Al foil, (13) shutter of the UCN detector area, (14) UCN detector, (15) layer of fluorine polymer oil, (16) chamber of UCN storage, and (17) shutter of the chamber of UCN storage.

able to reach altitudes above 2 m in the gravitational field. The vessel bottom was located at 1-m height with respect to the UCN source axis; therefore, the endpoint of the UCN spectrum in the vessel did not exceed 100 neV.

The UCN storage time τ_{st} as a function of temperature T was measured in the experiment. The measurements were performed after storing UCN in a closed graphite vessel for a time interval sufficient for a complete purification of the intermediate chamber from UCN accumulated in it. During purification, the shutter of the UCN detector, to which neutrons accumulated in the chamber flowed, was open. After the purification of the chamber, the vessel shutter was opened, and the number of neutrons, $N(t) = N(0) \exp(-t/\tau_{\text{st}})$, that remained in the vessel was measured as a function of time t . The τ_{st} value determined the total probability λ_{tot} of neutron disappearance from the vessel per unit time,

$$1/\tau_{\text{st}} = \lambda_{\text{tot}} = \lambda_{\beta} + \lambda_{\text{leak}} + \lambda_{\text{wh}} + \lambda_t, \quad (2)$$

where λ_{leak} is the probability of UCN leakage through the slot between the shutter and the closed inlet hole of the vessel and λ_{wh} is the probability of UCN leakage as the result of slight heating caused by neutron interaction with the moving shutter or by quasielastic reflections from the vessel walls.

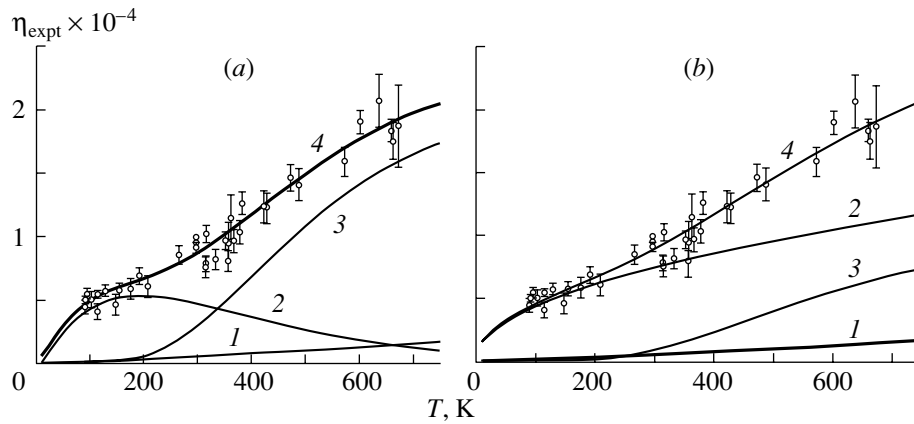


Fig. 3. Parameter η_{expt} as a function of temperature for a graphite vessel and results of experimental-data interpolation on the basis of (a) the two-oscillator model and (b) the model employing one oscillator and assuming the presence of a hydrogen gas at the surface. Individual model contributions to η_{expt} are illustrated by the curves: (1) contribution of the inelastic scattering of UCN and their capture by graphite in both panels, (2) contribution of the low-temperature oscillator in Fig. 3a or contribution of two-dimensional hydrogen gas in Fig. 3b, (3) contribution of the high-temperature oscillator in Fig. 3a or contribution of hydrogen dissolved in graphite in Fig. 3b, and (4) summary dependence of η_{expt} on temperature in both panels.

The probability λ_{leak} was determined experimentally by counting the number of UCN escaping from the closed vessel. The probability λ_{wh} due to mechanical heating was negligible, since the shutter moved at a speed of 1 cm/s and since it took 1 s to close the vessel. A rare process of weak UCN heating caused by quasielastic reflections from the storage-vessel walls could not have led to a noticeable leakage since the endpoint of the spectrum was substantially less than the graphite limiting energy and since the probability of this process was rather small for graphite (below 0.3×10^{-7} [18]).

The λ_l value was determined from relation (2) with the measured λ_{tot} probability. The γ value was

calculated with allowance for gravitation at a mean UCN speed assessed by the characteristic time of their escape from the vessel. The experimental value was $\eta_{\text{expt}} = \lambda_l/\gamma$.

2.2. Results of the Measurement of η_{expt}

Figure 3 shows the experimentally measured parameter η_{expt} for a graphite vessel at various temperatures. Curve 1 corresponds to the dependence $\eta(T)$ calculated by formula (1) with the cross sections $\sigma_{\text{in}} + \sigma_c$ obtained from the data presented in Fig. 1c. Prior to the measurements, the first annealing of the vessel was performed at $T = 680$ K for 24 hours. For a few hours, the annealing procedure was accompanied by the intense desorption of surface and volume impurities from graphite. The $\eta_{\text{expt}} (T = 300$ K) value measured after the annealing was 9.4×10^{-5} , which was considerably above the value calculated for this temperature. In view of this, the second, long-term, annealing of the vessel was performed at $T = 680$ K for 150 h. After that, oxygen was supplied to the vessel (at a pressure of 20 mbar), and the third, additional, annealing was performed for 24 h. The test measurement of $\eta_{\text{expt}} (T = 300$ K) showed that this value remained 9.4×10^{-5} —that is, a further purification of the surface by annealing yielded no result.

The vessel temperature was raised to 680 K to perform the main measurements. After that, the vessel was cooled slowly to 90 K, and the vessel temperature was fixed for a period needed for measuring η_{expt} . At 90 K, we measured η_{expt} a few times within 2 days and found no substantial variation of η_{expt} that could have been caused by an increase in the amount of

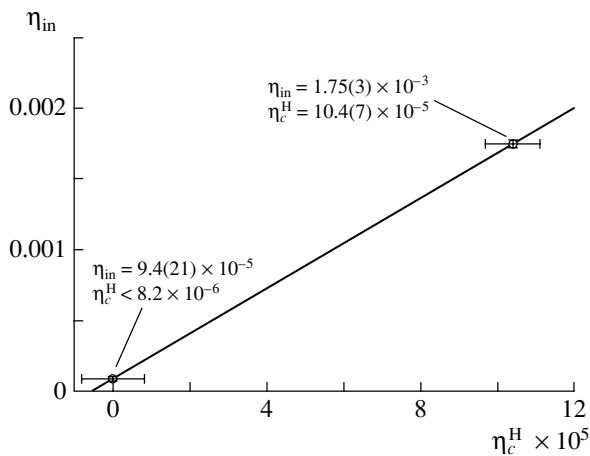


Fig. 4. Partial parameter η_{in} associated with the channel of inelastic UCN scattering as a function of the partial parameter η_c^{H} associated with the channel of UCN capture by hydrogen for pyrolytic graphite.

hydrogen-containing impurities at the vessel surface. In the course of a slow heating of the vessel from 90 K to 300 K, the initial η_{expt} value of $9.45(45) \times 10^{-5}$ was restored at 300 K.

A comparison of the experimental dependence $\eta_{\text{expt}}(T)$ with the calculated one $\eta(T)$ suggests an unpredicted additional UCN interaction with the graphite surface. Since this interaction features a temperature dependence—albeit a rather slight one—the interaction must be caused by inelastic UCN scattering to some extent.

In order to test this assumption, the graphite surface was studied by the method of (n, γ) analysis by using UCN. The measurement procedure [10–12] involved irradiating the vessel graphite with neutrons and analyzing the product gamma radiation with a germanium detector. The capture of UCN at the surface by various isotopes was identified by the typical spectrum of gamma radiation in (n, γ) reactions. The capture of UCN by surface hydrogen was identified by 2.23-MeV gamma rays from the reaction $n(p, d)\gamma$. A converter from ^{10}B was used to identify inelastic UCN scattering. When UCN heated to a thermal energy at the graphite surface entered the converter, the germanium detector recorded 477-keV gamma rays from the reaction $n + ^{10}\text{B} \rightarrow ^7\text{Li} + \alpha + \gamma$ (477 keV). The procedure used allowed us to determine the partial values of the parameter η for inelastic UCN scattering at $T = 300$ K (η_{in}), as well as the partial values $\eta_{\text{c}}^{\text{H}}$ and $\eta_{\text{c}}^{\text{C}}$ associated with capture by surface hydrogen and carbon, respectively. The measurements were performed prior to high-vacuum annealing of graphite at $T = 680$ K and after it.

As might have been expected, UCN capture by carbon appeared to be negligible ($\eta_{\text{c}}^{\text{C}} < 2 \times 10^{-6}$). Figure 4 shows two experimental values obtained in the measurements of η_{in} and $\eta_{\text{c}}^{\text{H}}$. A lot of hydrogen was adsorbed at the graphite surface before annealing, leading to additional inelastic scattering of UCN and their capture (right circle in the figure). After annealing (left circle), the amount of hydrogen decreased to such an extent that we could only estimate an upper limit on the corresponding capture value, $\eta_{\text{c}}^{\text{H}} < 8.2 \times 10^{-6}$. At the same time, inelastic UCN scattering that yields $\eta_{\text{in}} = 9.4(21) \times 10^{-5}$ remained after annealing. We would like to note that, within the errors, the sum $\eta_{\text{in}} + \eta_{\text{c}}^{\text{H}} + \eta_{\text{c}}^{\text{C}} = 9.4(23) \times 10^{-5}$ is in agreement with the value of $\eta_{\text{expt}} = 9.45(45) \times 10^{-5}$, which was obtained in studying UCN storage in a graphite vessel at $T = 300$ K. Thus, we can conclude that not less than 75% of the additional interaction observed in UCN storage is inelastic scattering (at a 67% C.L.). However, there is only an estimate of the

upper limit on UCN capture by hydrogen; therefore, the observed inelastic scattering may be of a hydrogen origin, but it also may be of some other physical origin. Since the hydrogen hypothesis is more realistic, it is of interest to find out whether the observed temperature dependence of η_{expt} can be explained within this hypothesis.

2.3. Analysis of the Temperature Dependence of η_{expt}

If atoms of hydrogen dissolved in the surface layer of matter form a simple Bravais cubic lattice [5, 6, 19], the double-differential cross section for inelastic scattering accompanied by phonon absorption is given by

$$\frac{d^2\sigma_{\text{in}}}{d\Omega d\varepsilon} = \frac{k\hbar b_{\text{inc}}^2}{k_0\varepsilon} \left(\frac{q^2}{6MN} \right) \exp(-2W) \frac{g(\varepsilon/\hbar)}{\exp(\varepsilon/\hbar) - 1}, \quad (3)$$

where $\hbar k_0$ and $\hbar k$ are the momenta of, respectively, the incident and the scattered neutron; $\hbar q = \hbar(k_0 - k)$ is the momentum transfer in scattering; b_{inc} is the incoherent scattering amplitude; $M = m$ is the mass of a lattice nucleus; N is the number of hydrogen atoms in the sample; ε is the energy transfer to the neutron in scattering; $g(\omega)$ is the density of phonon states; $\omega = \varepsilon/\hbar$; and $\exp(-2W)$ is the Debye–Waller factor. Since $\hbar k_0 \ll \hbar k$ for UCN, the expression for Debye–Waller factor in the Einstein model with $g(\omega) = 3N(\omega - \omega_0)$ takes the form

$$\begin{aligned} & \exp(-2W) \quad (4) \\ & = \exp\left(-\frac{\hbar q^2}{6MN} \int_0^{\omega_{\text{max}}} g(\omega) \coth\left(\frac{\hbar\omega}{2kT}\right) \frac{d\omega}{\omega}\right) \\ & = \exp\left(-\coth\left(\frac{\hbar\omega_0}{2kT}\right)\right), \end{aligned}$$

where ω_0 is the frequency of hydrogen oscillations. In this case, the integrated scattering cross section is

$$\sigma_{\text{in}} \propto \sqrt{\hbar\omega_0} \frac{\exp\left(-\coth\left(\frac{\hbar\omega_0}{2kT}\right)\right)}{\exp\left(\frac{\hbar\omega_0}{kT}\right) - 1}. \quad (5)$$

In studying vibrational spectra of metal hydrides [20], one treats relation (3) as the definition of the effective density of states, assuming that $M = m$ for the optical branch of the spectrum $g(\omega)$ and that, for the acoustic branch, M is determined by the mass of nuclei of the substance in which hydrogen is dissolved. Further, we assume that hydrogen dissolved in the surface layer of graphite can be represented as a system formed by two oscillators of low (ω_1) and high (ω_2) frequency, so that $g(\omega) =$

$3N(p\delta(\omega - \omega_1) + (1 - p)\delta(\omega - \omega_2))$, where p is the relative fraction of the frequency ω_1 . In this case, the effective mass is set to the carbon mass $M = 12$ for the frequency ω_1 and to the proton mass for the frequency ω_2 . The integrated cross section then takes the form

$$\sigma_{\text{in}} \propto \frac{p}{12} \sqrt{\hbar\omega_1} \frac{\exp\left(-\frac{1}{12} \coth\left(\frac{\hbar\omega_1}{2kT}\right)\right)}{\exp\left(\frac{\hbar\omega_1}{kT}\right) - 1} + (1 - p) \sqrt{\hbar\omega_2} \frac{\exp\left(-\coth\left(\frac{\hbar\omega_2}{2kT}\right)\right)}{\exp\left(\frac{\hbar\omega_2}{kT}\right) - 1}. \quad (6)$$

Adjusting the frequencies ω_1 and ω_2 and their relative fraction p , we can fit the theoretical dependence (6) to the experimental data displayed in Fig. 4. For this purpose, we represent the experimental value of the parameter in question as

$$\eta_{\text{expt}} = \eta_{\text{in}}^{\text{C}} + \eta^{\text{H}}, \quad (7)$$

where $\eta_{\text{in}}^{\text{C}}$ is the contribution that arises from inelastic UCN scattering on graphite and which is taken into account by the theory and $\eta^{\text{H}} = \eta_{\text{in}}^{\text{H}} + \eta_c^{\text{H}}$ is the contribution caused by the inelastic scattering and capture of UCN on hydrogen. For substances containing hydrogen, the ratio of the cross section for inelastic scattering on hydrogen to that for capture by hydrogen is about 16 at room temperature. Using this value, we obtain

$$\eta^{\text{H}} = \eta_c^{\text{H}} \left(1 + \frac{16}{A} \left(\frac{p\sqrt{T_1} \exp\left(-\frac{1}{12} \coth\left(\frac{T_1}{2T}\right)\right)}{\exp\left(\frac{T_1}{T}\right) - 1} + (1 - p) \sqrt{T_2} \frac{\exp\left(-\coth\left(\frac{T_2}{2T}\right)\right)}{\exp\left(\frac{T_2}{T}\right) - 1} \right) \right), \quad (8)$$

where $T_1 = \hbar\omega_1/k$, $T_2 = \hbar\omega_2/k$, and

$$A = \frac{p\sqrt{T_1}}{12} \frac{\exp\left(-\frac{1}{12} \coth\left(\frac{T_1}{600}\right)\right)}{\exp\left(\frac{T_1}{300}\right) - 1} + (1 - p) \sqrt{T_2} \frac{\exp\left(-\coth\left(\frac{T_2}{600}\right)\right)}{\exp\left(\frac{T_2}{300}\right) - 1}.$$

The quantities η_c^{H} , T_1 , T_2 , and p are adjustable parameters subjected to the conditions $\eta_c^{\text{H}} < 8.2 \times 10^{-6}$ and $T_2 \approx 1000$ – 2000 K. The latter condition follows from the energy scale of optical vibrations in metal hydrides [20]. In this case, a satisfactory fit is obtained at a low-frequency-oscillator temperature T_1 in the range 20–60 K. By way of example, Fig. 3a shows this fit at $T_1 = 30$ K, $T_2 = 1050$ K, and $p = 0.4$. We note that the model being considered disregards the contribution of multiphonon processes, which become significant when the Debye–Waller factor differs noticeably from unity.

The experimental dependence of η_{expt} can be explained within the model of a two-dimensional hydrogen gas at the surface [5]. This model assumes that hydrogen is strongly coupled to the surface, but that it moves freely along it. In this case, $\sigma_{\text{in}} = \sigma_0 \bar{v}/v \propto \sqrt{T}$, where $\sigma_0 = 20$ b is the cross section for scattering on a free proton and \bar{v} is the mean speed of hydrogen at the surface. Taken individually, this model is unable to explain the temperature dependence of the observed inelastic scattering. If, however, we assume that a fraction of surface hydrogen is dissolved in the crystal lattice and that the remaining fraction of it resides at the surface in the form of a free two-dimensional gas, then this combined model can explain the above results.

In the combined model, the parameter η_{expt} can be represented as

$$\eta_{\text{expt}} = \eta_{\text{in}}^{\text{C}} + \eta^{\text{H-solved}} + \eta^{\text{H-gas}}, \quad (9)$$

where $\eta^{\text{H-gas}}$ is the contribution of hydrogen as the surface gas and $\eta^{\text{H-solved}}$ is the contribution of dissolved hydrogen, whose oscillations can be described by an oscillator at a characteristic temperature T_2 .

The last two terms in (9) can be written as

$$\eta^{\text{H-solved}} = \eta_c^{\text{H-solved}} \times \left[1 + 16 \frac{\left(\exp\left(\frac{T_2}{300}\right) - 1\right) \exp\left(-\coth\left(\frac{T_2}{2T}\right)\right)}{\exp\left(-\coth\left(\frac{T_2}{600}\right)\right) \left(\exp\left(\frac{T_2}{T}\right) - 1\right)} \right], \quad (10)$$

$$\eta^{\text{H-gas}} = \eta_c^{\text{H-gas}} \left(1 + 60 \sqrt{\frac{T}{300}} \right), \quad (11)$$

where $\eta^{\text{H-solved}}$ and $\eta^{\text{H-gas}}$ are the respective contributions of UCN capture by hydrogen. The fact that $\sigma_{\text{in}}/\sigma_c \approx 60$ for a gas of free protons at 300 K is used in (11). Adjusting the temperature T_2 and the parameters $\eta_c^{\text{H-solved}}$ and $\eta_c^{\text{H-gas}}$ under the condition that their sum must be below 8.2×10^{-6} , we can fit relation (9) to the experimental dependence $\eta_{\text{expt}}(T)$.

Figure 3*b* displays the resulting fit. The best fit was obtained at $\eta^{\text{H-gas}} = 1.22 \times 10^{-6}$, $\eta^{\text{H-solved}} = 0.54 \times 10^{-6}$, and $T_2 = 1200$ K. These values correspond to a dissolved-hydrogen concentration in graphite between 2 and 3 at. % and to its surface density of about 10^{16} atom/cm².

It is obvious that the above satisfactory fits on the basis of the models being considered cannot be viewed as compelling physical proof of the hydrogen nature of the observed effect. The purpose of our discussion was to attract the attention of researchers to the fact that hydrogen in surface layers can have highly peculiar forms of coupling to matter and to indicate that the corresponding vibrational spectra may be radically different from those in the bulk of a substance. In order to explain the observed hydrogen effect, it is obviously necessary to assume the existence of a pronounced acoustic mode of vibrations that is characterized by a very low energy of 1.5–5.0 meV or to adopt quite an exotic model of two-dimensional hydrogen gas. However, the abandonment of the hydrogen hypothesis requires accepting the fact that, in graphite, there is theoretically unpredicted inelastic scattering that is weakly dependent on temperature and which manifests itself only in the subbarrier reflection of UCN, its cross section rescaled for $v_{\text{th}} = 2200$ m/s being about 1–1.5 b.

3. UCN STORAGE IN VESSELS WITH WALLS COATED WITH FLUORINE POLYMER OIL

3.1. Experimental Procedure

The fluorine-polymer oil YL VAC 18/8 is a viscous liquid at room temperature; it wets well and covers any solid surface. After a prolonged evacuation in a vacuum (for a few days), the oil releases atmospheric air dissolved in the bulk of it and contains virtually no hydrogen or water. Owing to these properties, fluorine polymer oils could be used to shield surface hydrogen when applied as a coating to the inner surface of storage vessels. However, oils lose the properties of a liquid gradually with decreasing temperature and increasing viscosity and crack at 220 K, forming a structure similar to a polycrystalline one. Our investigations revealed that, if the oil is applied to the surface of a metallic vessel made from copper, stainless steel, or aluminum, its layer cracks and separates from the surface when the temperature is reduced to 220 K. Pyrolytic graphite proved to be the only material that retains an oil coating at its surface in the temperature region down to 80 K. When the graphite temperature fell to 220 K, oil layers 10–50 μm thick cracked and became nontransparent, but they did not separate from the surface.

To study UCN storage in a vessel coated with fluorine-polymer oil, we used the same setup as in the experiments with a graphite vessel (Fig. 2). There were two versions of this experiment.

In the first version, UCN were stored in a pyrolytic-graphite vessel (Fig. 2*a*) whose walls were coated with a fluorine-polymer-oil layer 20 μm thick. The temperature range under study was 80–350 K.

In the second version, UCN were stored in an intermediate chamber (Fig. 2*b*) whose surface was coated with a thick (about 0.2–0.3 mm) fluorine-polymer-oil layer. Ultracold neutrons were supplied to the chamber through a hole made in the bottom and equipped with a flat shutter that could close it. To ensure the isotropy of the UCN flux, the chamber bottom was covered with shot 3 mm in diameter, which was also coated with oil. The temperature range studied in that case was 220–310 K. Some of the results of these measurements were published in [21].

In just the same way as in the experiments with a graphite vessel, λ_l was determined from the measured probabilities λ_{tot} and λ_{leak} by using relation (2). We calculated γ for the mean speed of UCN accumulated in the vessel, taking gravity into account. The mean speed was assessed from the characteristic time of the escape of UCN from the chamber or the vessel. The experimental value of the parameter η_{expt} was determined as $\eta_{\text{expt}} = \lambda_l/\gamma$.

3.2. Measurements of η_{expt}

Figure 5 displays the measured values of η_{expt} . Also shown in this figure (diamonds) are values calculated for $\eta(T)$ by using the experimental cross sections ($\sigma_c + \sigma_{\text{in}}$) from the data in Fig. 1*a*. As was mentioned above, the values of $\eta(T)$ in the region $T < 220$ K can be treated only as an upper limit on this quantity.

If UCN were stored in a graphite vessel coated with fluorine polymer oil (boxes in Fig. 5), the values of η_{expt} were 3–5 times greater than the calculated ones over the entire temperature range studied here. In the case of UCN storage in a chamber coated with fluorine polymer oil (closed circles), $\eta_{\text{expt}} = 2.42(21) \times 10^{-5}$ is three times as great as the calculated value at $T = 300$ K. The discrepancy decreases markedly with decreasing temperature. At 218 K (which is close to the temperature of cracking), $\eta_{\text{expt}} = 7.25(81) \times 10^{-6}$, and the value of $\eta = 4.5(3) \times 10^{-6}$ is obtained by means of a linear interpolation on the basis of three points measured for $T > 220$ K. Thus, the contribution of additional inelastic scattering to η_{expt} decreases to $2.75(86) \times 10^{-6}$.

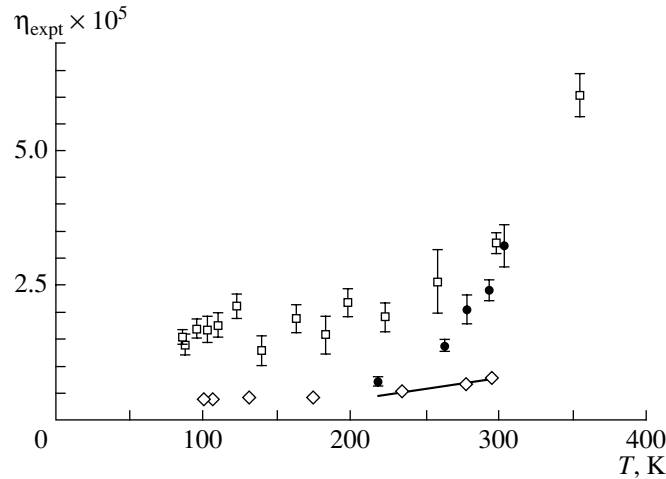


Fig. 5. Results obtained by measuring η_{expt} for vessels coated with the fluorine polymer oil YL VAC 18/8: (open boxes) data obtained for graphite surfaces coated with oil and (closed circles) data for stainless-steel vessels coated with oil. Diamonds represent the calculated dependence $\eta(T)$.

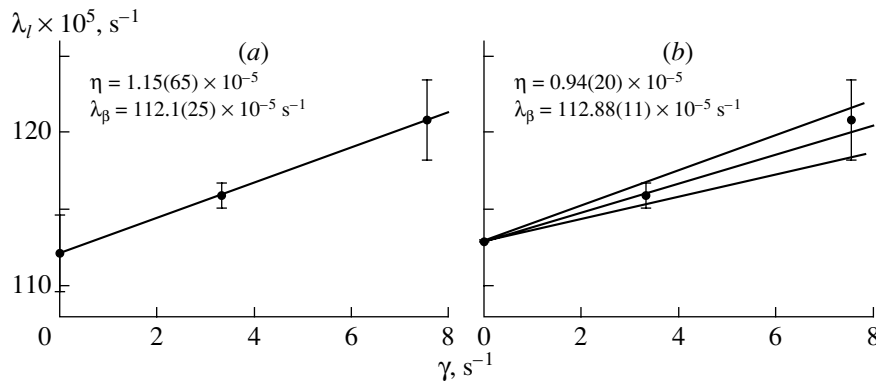


Fig. 6. Probability λ_l of UCN losses in a vessel with heavy-ice walls as a function of the geometric factor of the experiment (γ): (a) linear extrapolation performed according to data from [23] and (b) linear extrapolation with the fixed world-average value of λ_β .

Analyzing both experiments, we can assume that the complete shielding of the graphite surface is not achieved when UCN are stored in a graphite vessel whose walls are coated with a 20- μm layer of the fluorine polymer oil. Microcracks seem to appear in the oil layer with decreasing temperature and can cause a considerable increase in η_{expt} for a number of reasons, such as direct UCN penetration into the graphite, an increase in the layer roughness, and a splitting-induced increase in the inner surface of the vessel. The second experiment demonstrates that UCN undergo theoretically unpredicted additional inelastic scattering when they interact with the surface of the fluorine polymer oil. The difference $\eta_{\text{expt}} - \eta$ caused by this process is 1.6×10^{-5} at $T = 300$ K. Here, it should be noted that, according to various estimates [18, 22], the probability of a weak heating of UCN at this temperature per one interaction event is 0.2–

0.5×10^{-5} . Therefore, we cannot rule out the contribution of a weak heating of UCN to the observed effect at a level of 15–30%. Since there is no reliable information about hydrogen at the fluorine-polymer-oil surface, we cannot rule out the contribution of inelastic scattering due to hydrogen either. Finally, the observed additional scattering may be associated with phenomena occurring at the liquid surface. It is of fundamental importance that the additional inelastic scattering is efficiently suppressed as temperature decreases to 220 K, whereupon the observed losses approach the calculated level. Upon rescaling to the thermal speed, the additional inelastic scattering at $T = 300$ K corresponds to a cross section of 0.3 b; at $T = 218$ K, this cross section is 0.050(15) b.

4. UCN STORAGE IN A VESSEL WITH WALLS MADE FROM HEAVY-WATER ICE

In one of the pioneering studies devoted to measuring the free-neutron lifetime [23], UCN were stored in a vertical vessel where heavy-water ice 3000 Å thick was deposited onto its walls by means of low-temperature condensation at 80 K. The experiment was performed for two geometric conditions. At first, UCN were stored in an empty vessel, in which case γ was minimal (3.33 s^{-1}). The storage time obtained in this way was 863(6) s, which corresponded to the loss probability of $\lambda_l = 115.87(80) \times 10^{-5} \text{ s}^{-1}$. In the second case, additional plates covered with ice were inserted into the vessel, with the result that γ increased to 7.55 s^{-1} , whereupon λ_l became $120.8(26) \times 10^{-5} \text{ s}^{-1}$.

For two values of γ , Fig. 6a shows the results obtained by measuring λ_l , which were then used to determine the neutron-decay probability of $\lambda_\beta = 112.1(25) \times 10^{-5} \text{ s}^{-1}$ by means of a linear extrapolation of γ to zero, this probability corresponding to the lifetime of 892(20) s. The formation of an ice layer in a hermetic vacuum vessel was a feature that was peculiar to that experiment and which eliminated the possibility of contamination with hydrogen from the residual gas of the vessel volume. On the other hand, the diffuse penetration of hydrogen into the ice layer from the aluminum walls of the vessel was negligible, since the coefficients of hydrogen diffusion decrease sharply in all materials with decreasing temperature. This gives grounds to believe that, in the experiment reported in [23], UCN were stored in a vessel whose walls coated with heavy-water ice contained no hydrogen contamination. Therefore, a comparison of η_{expt} obtained in that experiment with the theoretical value of η for heavy-water ice at 80 K is of interest for testing the hypothesis of the hydrogen origin of the additional UCN losses.

The accuracy of the value $\eta_{\text{expt}} = 1.15(65) \times 10^{-5}$ obtained in [23] was not high, because both η_{expt} and the neutron lifetime were determined in the same experiment, but the latter was known at that time with an error of about 10 s. Since the world-average weighted value of the lifetime is currently known to a high precision, $\tau_\beta = 885.9(9) \text{ s}$, the results from [23] can be improved by setting $\lambda_\beta = 112.88(115) \times 10^{-5} \text{ s}^{-1}$. This enables us to determine, by using the same data, the value of $\eta_{\text{expt}} = 0.94(20) \times 10^{-5} \text{ s}$ more accurately (Fig. 6b).

From the data in Fig. 1a, we obtain $\sigma_c + \sigma_{\text{in}} = 42.1(30) \text{ b}$ at a neutron speed of $7.3(5) \text{ m/s}$ in ice, whence it follows that $\eta = 0.65(5) \times 10^{-5}$. Thus, the discrepancy between the experimental and theoretical

values of η for heavy-water ice at 80 K, if any, is within a factor of 1.5–2. In any case, the effective cross section estimated at a neutron speed of 2200 m/s for other possible processes that could cause additional UCN losses does not exceed 0.1 b at a 67% C.L. On the other hand, this discrepancy can be reasonably explained by the roughness of the ice surface at the vessel walls [2].

5. CONCLUSION

The possibility of attaining the calculated probabilities of the losses of UCN stored in graphite vessels and in vessels coated with fluorine polymer oil and heavy-water ice has been tested experimentally. The existence of theoretically unpredicted inelastic UCN scattering in UCN collisions with the walls has been established for graphite vessels. It has been shown that additional scattering may be associated with the presence of hydrogen at the surface, this providing a UCN leakage channel characterized by a slight temperature dependence. This hypothesis requires either the existence of a pronounced acoustic vibrational mode of extremely low characteristic energies (1.5–5.0 meV) in the frequency spectrum of dissolved hydrogen or the use of quite an exotic model featuring two-dimensional hydrogen gas at the surface. At the moment, it is therefore impossible to draw a definitive conclusion that the additional inelastic scattering is of a completely hydrogen origin. This issue will remain open until the accuracy in determining the probability of UCN capture by hydrogen at the graphite surface by means of the (n, γ) method is improved considerably.

Additional UCN scattering has also been established for vessels whose walls are coated with fluorine polymer oil. In contrast to the case of graphite, the probability of this scattering is suppressed efficiently with decreasing temperature, with the result that losses at a level close to the calculated one can be attained even at 220 K. The probabilities of the experimental and calculated losses have been shown to be in good agreement for vessels whose walls were coated with heavy-water ice at 80 K, in which case a possible surface contamination with hydrogen was minimized. On one hand, the results obtained here favor the hydrogen hypothesis of anomalous UCN losses at the graphite surface; on the other hand, they indicate that the process of anomalous interaction is not universal for different materials, since the cross section may take different values for them.

ACKNOWLEDGMENTS

We are grateful to S.T. Belyaev for his help in the organization of our studies and for enlightening discussions on the results that we obtained.

Numerous discussions with R. Golub, V.V. Nesvizhevsky, A.V. Strelkov, A.P. Serebrov, V.K. Ignatovich, and E.I. Korobkina on the problems considered in our article are gratefully acknowledged.

This work was supported by the Russian Foundation for Basic Research (project no. 00-02-17865).

REFERENCES

1. F. L. Shapiro, Report of Joint Inst. Nucl. Res. No. R3-7135 (Dubna, 1973).
2. V. K. Ignatovich, *The Physics of Ultracold Neutrons* (Nauka, Moscow, 1986; Oxford Univ. Press, Oxford, 1990).
3. V. I. Morozov, *Storage of Ultracold Neutrons in Closed Vessels* (Dimitrovgrad, 1982).
4. A. V. Strelkov and M. Heltzer, Preprint No. R3-10815 (Joint Inst. Nucl. Res., Dubna, 1977).
5. V. K. Ignatovich and L. M. Satarov, Preprint No. 2820 (Inst. At. Energy, Moscow, 1977).
6. D. I. Blokhintsev and N. M. Plakida, Report of Joint Inst. Nucl. Res. No. R4-10381 (Dubna, 1977).
7. W. A. Lanford and B. Golub, Phys. Rev. Lett. **39**, 1509 (1977).
8. P. H. La Marche *et al.*, Nucl. Instrum. Methods **189**, 533 (1981).
9. S. V. Zhukov, V. L. Kuznetsov, V. I. Morozov, *et al.*, Pis'ma Zh. Éksp. Teor. Fiz. **57**, 446 (1993) [JETP Lett. **57**, 464 (1993)].
10. S. S. Arzumanov *et al.*, Preprint No. 6010-2 (Inst. At. Energy, Moscow, 1996).
11. S. S. Arzumanov *et al.*, Nucl. Instrum. Methods Phys. Res. A **440**, 690 (2000).
12. V. I. Morozov, *Mini-Workshop ILL* (2000).
13. P. Ageron *et al.*, Z. Phys. B **59**, 261 (1985).
14. V. P. Al'fimenkov *et al.*, Pis'ma Zh. Éksp. Teor. Fiz. **55**, 92 (1992) [JETP Lett. **55**, 84 (1992)].
15. L. N. Bondarenko *et al.*, *ISINN-10* (Dubna, 2002).
16. Von Wolfram Gissler, Z. Kristallogr. **118**, 149 (1963).
17. V. F. Turchin, *Slow Neutrons* (Atomizdat, Moscow, 1963; Israel Program for Scientific Translations, Jerusalem, 1965).
18. A. P. Serebrov, *Mini-Workshop ILL* (2000).
19. I. I. Gurevich and L. V. Tarasov, *Low-Energy Neutron Physics* (Nauka, Moscow, 1965; North-Holland, Amsterdam, 1968).
20. T. Schwinger, in *Hydrogen in Metals*, Ed. by G. Alefeld and J. Volkl (Springer, Heidelberg, 1978; Mir, Moscow, 1981), Vol. 1.
21. L. N. Bondarenko *et al.*, Yad. Fiz. **65**, 13 (2002) [Phys. At. Nucl. **65**, 11 (2002)].
22. V. Mampe *et al.*, Pis'ma Zh. Éksp. Teor. Fiz. **57**, 77 (1993) [JETP Lett. **57**, 82 (1993)].
23. V. I. Morozov, Nucl. Instrum. Methods Phys. Res. A **284**, 108 (1989).

Translated by E. Kozlovskii

Neutron Optics of Strongly Absorbing Media and Interaction of Long-Wave Neutrons with Gadolinium Films

A. I. Frank*, V. I. Bodnarchuk, P. Geltenbort¹⁾, I. L. Karpikhin²⁾, G. V. Kulin, and O. V. Kulina

Joint Institute for Nuclear Research, Dubna, Moscow oblast, 141980 Russia

Received March 6, 2003

Abstract—The modern state of neutron optics of absorbing media is briefly surveyed. In all probability, there are no physics arguments that would constrain, in the case of strong absorption, the applicability of the commonly accepted Fermi–Foldy dispersion law for neutron waves. In accord with previously known results, it is found that the coefficient of reflection of neutrons from the boundary of a strongly absorbing medium tends to unity with decreasing velocity of neutrons incident on this medium. At low neutron energies peculiar to the case of ultracold neutrons, the complex scattering length for neutron–nucleus interaction proves to be constant, whence it follows that the cross section for neutron capture by a free nucleus obeys the $1/v$ law. The cross section for the analogous process on nuclei within a medium is described by the $1/v'$ law, where $v' = \hbar k'/m$, with k' being the real part of the neutron wave number in the medium. As the incident-neutron velocity v decreases, the velocity v' in a medium tends to some limiting value. From the coefficient of reflection of cold neutrons that is measured as a function of the wavelength and the angle of incidence, a refined value is found for the real part of the scattering length for neutron interaction with gadolinium nuclei. An experiment was performed where ultracold neutrons were transmitted through thin samples containing natural gadolinium. In analyzing the results of this experiment, use was made of the value found here for the real part of the neutron–nucleus scattering length. The experiment indicates that the imaginary part of the scattering length is a constant or, what is the same, that, for neutron velocities ranging from 4 to about 120 m/s, the $1/v$ law for the cross section for neutron capture by a free nucleus is valid to within 6%. © 2003 MAIK “Nauka/Interperiodica”.

1. INTRODUCTION

It is well known that the neutron-optics properties of a medium are completely determined by the complex scattering length for the coherent interaction of neutrons with nuclei of atoms forming this medium. For the majority of nuclei, the real part of the scattering length exceeds its imaginary part by a few orders of magnitude. In this case, processes induced by radiative neutron capture by nuclei of the medium lead to the attenuation of a wave over distances considerably exceeding the relevant wavelength, the real part of the wave number in the medium and, accordingly, the index of refraction for neutrons being dependent only slightly on the absorption cross section. A similarly weak dependence on the capture cross section is peculiar to the coefficient of reflection from the medium boundary as well.

There are, however, a number of substances whose nuclei possess a very large cross section for the capture of thermal neutrons. In the majority of cases,

this is due to the presence of resonances in the cross section for radiative capture in the region of thermal energies. The imaginary part of the scattering length can then be commensurate with its real part or even exceed it. For such substances, all optical characteristics of the medium are strongly dependent on the cross section for neutron capture by individual nuclei.

Interest in neutron optics of absorbing media has quickened considerably in recent years. This was motivated by a wide application of absorbing substances in neutron polarizers, especially in view of the fact that requirements on the quality of such polarizers have become ever more stringent. Moreover, the experimental results reported in [1], which are quite unexpected, attracted closer attention to the problem. On the other hand, this realm of neutron optics has not yet received adequate experimental study because of difficulties in performing relevant experiments.

Theoretical investigations into the problem being discussed were performed in [2–7]. In 1961, Gurevich and Nemirovsky [3] showed that, as the velocity of neutrons incident on an absorbing medium tends to zero, the effective capture cross section approaches a finite limit instead of going to infinity. It should be emphasized that one implies here an effective cross

¹⁾Laue–Langevin Institute, Grenoble, France.

²⁾Institute of Theoretical and Experimental Physics, Bol'shaya Cheremushkinskaya ul. 25, Moscow, 117259 Russia.

* e-mail: frank@nf.jinr.ru

section for nuclei in a dense medium rather than the cross section for a free nucleus. In the same article of those authors, it was indicated that the absorption of a wave is always accompanied by its reflection. Among other things, they presented an estimate for the coefficient of reflection of ultracold neutrons from the surface of gadolinium, which possesses a giant cross section.

Treating the dispersion of neutron waves on the basis of classic theory pioneered by Foldy [8] and Lax [9], I. Frank [4] derived general expressions for the complex index of refraction of neutron waves in an absorbing medium. Only the very fact that the effective scattering length for neutron–nucleus interaction is complex-valued is of importance in this approach, the questions concerning the origin of its imaginary part being set apart. It does not seem that there are constraints on the applicability of this theory in the case of very strong absorption. Some of the results reported in [4] will be given below.

In contrast to [4], the theoretical analysis of Gurevich and Lomonosov in [5, 7] relied on the fact that, in strongly absorbing media, the disappearance of a neutron is due to radiative capture. Those authors arrived at the conclusion that, at very low neutron energies, the dependence $\sigma \propto 1/v$ for the neutron-capture cross section gives way to the dependence $\sigma \propto v$. This means that the capture cross section tends to zero as the neutron velocity decreases indefinitely. But as before, this concerns the effective cross section for a nucleus occurring in a dense medium (of a thin film in the case being discussed).

We would also like to mention the studies of Rubio and Kumar [10] and Jayannavar [11], who revisited the reflective properties of an absorbing potential. Those authors analyzed some corollaries of the well-known circumstance that, in the case of interaction with a complex-valued potential having sharp boundaries, a strong absorption of a wave is always accompanied by its reflection (see, for example, [3]).

2. ELEMENTARY THEORY

2.1. Infinitely Thin Absorbing Plane

In order to illustrate some general features of phenomena that arise in the interaction of a neutron wave with an absorbing sample, we will consider the model of an infinitely thin plane, disregarding correlations between the positions of scatterers (such correlations are insignificant in the present case). The sample in question can then be fully characterized by the complex-valued scattering length for interaction with an individual nucleus, b , and by the number of scatterers per unit area, ρ_2 . The problem reduces to calculating the amplitude for scattering on a delta-function potential. This problem is well known in

quantum mechanics (see, for example, [12]) and was repeatedly discussed in connection with various problems in neutron optics [10, 11, 13–15]. A solution can be represented in the form

$$\begin{aligned} r &= \frac{-iS}{1+iS}, & t &= \frac{1}{1+iS}, \\ S &= \frac{2\pi\rho_2 b}{k_0}, & b &= b' - ib'', \end{aligned} \quad (1)$$

where r and t are the amplitudes of, respectively, the reflected and the transmitted wave and k_0 is the wave number, the incident flux being normalized to unity. Evaluating the flux that remains within the substance of the sample,

$$\Sigma = 1 - |r|^2 - |t|^2, \quad (2)$$

we obtain the following expression for the effective cross section $\sigma = \Sigma/\rho_2$ for neutron absorption on an individual nucleus in the sample:

$$\sigma = \frac{4\pi b''}{k_0} \frac{1}{1 + \frac{4\pi\rho_2 b''}{k_0} + \frac{4\pi^2\rho_2^2}{k_0^2} |b|^2}. \quad (3)$$

For an indefinitely dilute two-dimensional medium, in which case $\rho_2 \rightarrow 0$, the following relation holds in accordance with the optical theorem:

$$\sigma \rightarrow \sigma_0 = \frac{4\pi}{k_0} b''. \quad (4)$$

In the case where the density of scatterers, ρ_2 , is finite, the effective cross section for nuclei lying in a plane is smaller than the cross section for a free nucleus. If the wave number is not overly small, we can disregard the third term in the denominator on the right-hand side of (3). We then have

$$\sigma \cong \frac{\sigma_0}{1 + \sigma_0\rho_2}, \quad \sigma_0\rho_2 \ll 1. \quad (5)$$

From (4) and (5), it can be seen that the effective cross section in a medium grows with decreasing wave number, along with the cross section, σ_0 , $\sigma_0 \propto 1/k_0$. However, this growth is moderated by the increasing factor $\sigma_0\rho_2$.

The limiting case of ultraslow neutrons [15] corresponds to fulfillment of the inequality $\frac{\rho_2 |b|}{k_0} \gg 1$ and to the dominance of the third term in the denominator on the right-hand side of (3); we then have

$$\sigma \cong \frac{1}{\pi\rho_2^2} \frac{b''}{|b|^2} k_0, \quad \sigma_0\rho_2 \gg 1. \quad (6)$$

Thus, we see that, at very low neutron velocities, the effective cross section for nuclei in a thin sample proves to be proportional to the incident-neutron

velocity, in quantitative agreement with the results obtained in [7]. As the neutron velocity decreases indefinitely, this cross section tends to zero.

This result has a simple qualitative explanation. As was indicated previously in [14, 15] and as can be immediately seen from (1), the amplitude of the wave that is reflected from a plane has a pronounced resonance character. If absorption is negligible ($b'' \ll b'$), the coefficient of reflection, $R = |r|^2$, is given by the resonance Wigner formula

$$R = \frac{\nu^2}{\nu^2 + k_0^2}, \quad \nu = 2\pi\rho_2 |b|, \quad (7)$$

which corresponds to scattering on a level at a negative energy for $b' < 0$ or on a virtual level for $b' > 0$. But in the general case, it follows from (1) that

$$R = \frac{4\pi^2 \rho^2 |b|^2}{k_0^2} \left(1 + \frac{4\pi\rho_2 b''}{k_0} + \frac{4\pi^2 \rho_2^2}{k_0^2} |b|^2 \right)^{-1}. \quad (8)$$

For ultraslow neutrons, in which case $k_0 \ll \rho_2 |b|$, expression (8) reduces to expression (7), which was obtained for a perfectly transparent medium. In the limit of $k_0 \rightarrow 0$, it leads to the following result: $R \rightarrow 1$. Thus, an effective decrease in the capture cross section with decreasing neutron energy is due to an ever increasing and eventually dominant role of reflection.

2.2. Case of Absorbing Medium

In the above case of a thin sample, the problem being considered involved only one value of the wave number, k_0 . It is obvious that, in the case of an extended sample, which, in the limiting case, goes over to a semi-infinite medium, it is necessary to introduce, in addition, the wave number k that characterizes the wave within the sample. The relation between these wave numbers is given by the dispersion law $k(k_0^2)$. For waves of any origin, we have the relation [9]

$$k^2 = k_0^2 + 4\pi\rho f(0), \quad (9)$$

where $f(0)$ is the amplitude of the wave scattered at zero angle and ρ is the number of scatterers per unit volume. By virtue of the optical theorem

$$\sigma_{\text{tot}} = \frac{4\pi}{k_0} \text{Im}[f(0)], \quad (10)$$

which relates the total cross section σ_{tot} to the amplitude for forward scattering, this amplitude is always complex-valued. Accordingly, the wave number in the medium, k —it is determined by the dispersion relation (9)—is also complex-valued. For very slow neutrons, it is common practice to use, instead of the amplitude, the scattering length b [16], where $b =$

$-\lim[f(0)]$ for $k_0 \rightarrow 0$. In this case, the formulation of the optical theorem in Eq. (10) (with the substitution of $-b$ for f) remains valid, but it involves, instead of the total cross section, the cross section σ_{eff} for all processes leading to the withdrawal of neutrons from the coherent state and including capture (see, for example, [13]). In the majority of cases, the scattering length b is constant. From the invariability of its imaginary part, it follows that the quantity $\sigma_{\text{eff}}(k)k$ is constant, which corresponds to the $1/v$ law for the cross section σ_{eff} . Obviously, the dispersion relation then has the form

$$k^2 = k_0^2 - 4\pi\rho b, \quad k = k' + ik'', \quad b = b' - ib''. \quad (11)$$

In the case of normal incidence of a wave on substance,³⁾ the corresponding neutron wave function in a medium has the form of an attenuated wave; that is,

$$\psi(x) = t \exp [(ik' - k'')x], \quad (12)$$

where t is the amplitude of the wave at the boundary of the medium. Evaluating the flux density at a given point in the substance by means of a standard procedure, we obtain

$$j = |\psi(x)|^2 \frac{\hbar k'}{m}, \quad |\psi(x)|^2 = t^2 \exp(-2k''x). \quad (13)$$

Thus, we see that, in the expression for the flux, the quantity $v' = \hbar k'/m$ plays the role of the velocity in the medium [4] and that the attenuation of the wave is determined by the imaginary part of the wave vector k'' . In just the same way as k' , k'' depends both on the real and on the imaginary part of the scattering length b .

Following [4], we will derive explicit expressions for both parts of the wave vector in a medium. Recasting formulas (11) into the form of two equations,

$$k'^2 - k''^2 = k_0^2 - 4\pi\rho b', \quad k'k'' = 2\pi\rho b'', \quad (14)$$

we obtain

$$k' = \sqrt{\frac{k_0^2 - 4\pi\rho b'}{2} + \sqrt{\frac{(k_0^2 - 4\pi\rho b')^2}{4} + (2\pi\rho b'')^2}}, \quad (15)$$

$$k'' = \sqrt{\frac{4\pi\rho b'' - k_0^2}{2} + \sqrt{\frac{(k_0^2 - 4\pi\rho b')^2}{4} + (2\pi\rho b'')^2}}, \quad (16)$$

³⁾We note that, in the case of an arbitrary angle of incidence, the components of the complex wave vector in a medium are not parallel to each other. In this case, the imaginary part of k is orthogonal to the boundary of the substance. Here, we will not analyze interesting corollaries from this circumstance, restricting our consideration to the case of normal incidence of a wave on the boundary of a medium.

where one implies the arithmetic (positive) values of the square roots.

Equations (14)–(16) completely determine the neutron wave function in a medium; in order to solve the problem of reflection from and transmission through an arbitrary sample, it only remains to write the corresponding continuity conditions at the interfaces.

Implying that, in the ensuing analysis, we will be dealing only with rather slow neutrons and following the generally accepted terminology [4], we will distinguish between ultracold and very cold neutrons by the sign of the quantity $C = k_0^2 - 4\pi\rho b'$. For very cold neutrons in the case of substances characterized by not very strong absorption and of energies not very close to the threshold,

$$(4\pi\rho b'')^2 \ll (k_0^2 - 4\pi\rho b')^2, \quad (17)$$

we obtain

$$k' \cong \sqrt{k_0^2 - 4\pi\rho b'}, \quad k'' = \frac{2\pi\rho b''}{k'} \cong \frac{2\pi\rho b''}{\sqrt{k_0^2 - 4\pi\rho b'}}. \quad (18)$$

Substituting these expressions into (13) and making the substitution

$$b'' = \sigma_{\text{eff}}(k_0)k_0/4\pi, \quad (19)$$

we arrive at

$$|\psi(x)|^2 = t^2 \exp\left(-\frac{\rho\sigma_{\text{eff}}(k_0)k_0}{k'}x\right). \quad (20)$$

Thus, both the quantum-mechanical flux (13) and its attenuation (20), which is caused by absorption in the case of very cold neutrons, are determined by the effective velocity of neutrons in matter,

$$v' = \frac{\hbar}{m}k'. \quad (21)$$

Let us now consider the case of ultracold neutrons ($C < 0$). Under the same conditions (17), we similarly obtain

$$k' \cong \frac{2\pi\rho b''}{\sqrt{4\pi\rho b' - k_0^2}}, \quad k'' \cong \sqrt{4\pi\rho b' - k_0^2}. \quad (22)$$

From the condition in (17), which is assumed to be valid here, it follows that $k'' \gg k'$. The wave is attenuated in matter efficiently, but, now, this is due to almost complete external reflection rather than to absorption. Nonetheless, the real part of k is not equal exactly to zero—it is obviously related to the absorptive properties of matter. The flux that is associated with it and which is directed toward the interior of matter [see Eq. (13)] owes its existence to neutron absorption in matter [4].

Let us now remove the condition in (17) and return to the general case of an absorbing medium.

From (15), it immediately follows that, as the velocity of neutrons incident on a medium tends to zero, the real part of the wave number, along with the effective velocity in matter, reaches some limiting value, instead of approaching zero; that is,

$$k'_{\text{min}} = \sqrt{2\pi\rho b' \left[\sqrt{1 + \left(\frac{b''}{b'}\right)^2} - 1 \right]}, \quad (23)$$

$$v'_{\text{min}} = \frac{\hbar}{m}k'_{\text{min}}.$$

As a result, the increase in the cross section for neutron absorption is restricted from above by the quantity

$$\sigma_{\text{max}} = \frac{\sigma(k_0)k_0}{k'_{\text{min}}}. \quad (24)$$

Thus, we see that, in the case of ultracold neutrons, the effective cross section for neutron absorption increases in proportion to $1/v'$ with decreasing neutron velocity. But the effective velocity v' itself cannot be arbitrary small—it is bounded from below by the limiting value in (23). As was predicted in [3], this is precisely the physical reason behind the saturation of the cross section. In the case of a very strong absorption, $b'' \gg b'$, we have

$$k'_{\text{min}} = \sqrt{2\pi\rho b''}, \quad \sigma_{\text{max}} = 2\sqrt{2\pi b''/\rho}, \quad (25)$$

which is in accord with [3].

By no means does this conclusion contradict the results presented in the preceding section. In the absence of a medium, we determined the cross section on the basis of the ratio of the flux captured by the sample to the flux incident on it. But in the present section, we determine the cross section on the basis of the attenuation of that part of the flux which has already entered the medium, the magnitude of the coefficient of reflection from the interface not being discussed. At the same time, the role of reflection becomes more pronounced with decreasing neutron velocity in this case as well. For an infinitely extended medium, the amplitude of the reflected wave is given by the well-known expression

$$r = \frac{k_0 - k}{k_0 + k}. \quad (26)$$

Obviously, the entire flux that entered a semi-infinite medium is absorbed in it. At very low neutron velocities, we obtain the following expression for the fraction of absorbed neutrons:

$$\alpha = 1 - |r|^2 = \frac{2k'k_0}{4\pi\rho|b|}, \quad k_0 \rightarrow 0. \quad (27)$$

From this expression, we can see that, in accord with the aforesaid, α decreases in proportion to the neutron velocity in this case as well.

3. SCATTERING LENGTH FOR THE COHERENT INTERACTION OF SLOW NEUTRONS WITH GADOLINIUM NUCLEI

Among known substances that absorb neutrons, gadolinium is one of the strongest absorbers. This is the reason why it is extensively used in neutron physics. Moreover, investigation of the propagation and absorption of neutron waves in this substance makes it possible to test, under limiting conditions, fundamentals of the theoretical neutron optics of absorbing media. In order to meet the requirements of applied neutron optics and to perform a comparison of experimental data on ultracold-neutron transmission through thin gadolinium samples (see Section 4 below) with the results of calculations, we address here data on the scattering length for coherent neutron interaction with gadolinium nuclei.

3.1. Complex-Valued Scattering Length for Neutron Interaction with Gadolinium Nuclei

Two gadolinium isotopes, ^{155}Gd and ^{157}Gd , have resonances in the cross section for radiative neutron capture near the thermal region, and this is the reason why the cross section for neutron capture in natural gadolinium is so large. It is well known that, in this case, the energy dependence of the scattering length is described by the Breit–Wigner formula (see, for example, [17])

$$a_{\text{coh}} = r_0 + \sum_j \frac{2\lambda_j \Gamma_{n,j} (E - E_j)}{4(E - E_j)^2 + \Gamma_j^2} + i \sum_j \frac{\lambda_j \Gamma_{n,j} \Gamma_j}{4(E - E_j)^2 + \Gamma_j^2}, \quad (28)$$

where a_{coh} is the scattering length for the interaction with a free nucleus, r_0 is the potential-scattering length, $\Gamma_{n,j}$ is the neutron width of the j resonance, Γ_j is its total width, and E is the neutron energy. The scattering length for a bound nucleus is $b = a_{\text{coh}}(A + 1)/A$, where A is the mass number. For gadolinium, $A \approx 155$, in which case a and b differ by less than one percent; in view of this, we will disregard this distinction below. As can be seen from (28), both the real and the imaginary part of the scattering length change sharply in the vicinity of resonances. In Fig. 1, the resonance contribution $b(E)$ to the real part of the scattering length for natural gadolinium is shown as a function of energy. This graph was calculated on the basis of the Breit–Wigner formula with allowance for the parameters of closely lying resonances. Here, we employed the representation $\text{Re}(b) = b_0 + b(E)$, in which the constant term b_0 takes into account both the real part of the potential-scattering length, r_0 , and the contributions of all far

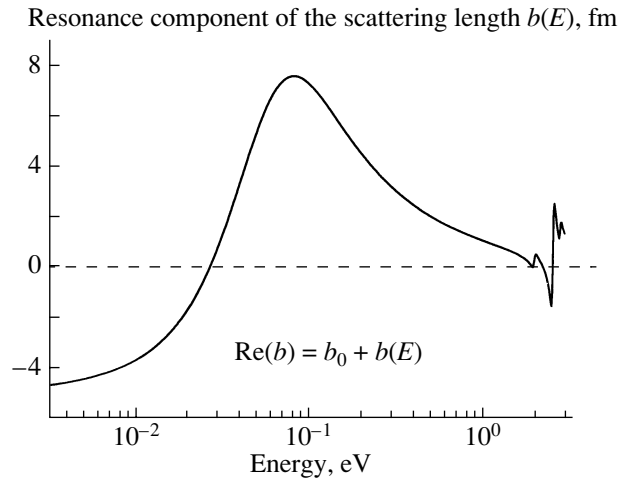


Fig. 1. Real part of the scattering length for natural gadolinium as a function of energy (results of the calculation). The constant component b_0 is taken here for the reference point.

resonances. From Fig. 1, it can be seen that, in the energy range from zero to 1 eV, the real part of the scattering length changes by more than 12 fm.

For neutrons of energy much less than the resonance value, the denominator in the Breit–Wigner formula reduces to a constant. Since the quantity $\lambda \Gamma_n$, which appears in the numerator of this formula, is also a constant for s -wave resonances, the complex scattering length for ultracold neutrons is equal to the constant $b = b_0 + b(0)$.

For the majority of practical calculations, it is necessary to know the complex value of b precisely, which, with the exception of the particular case of ultracold neutrons, is always strongly dependent on energy. The imaginary part of b can easily be calculated either by formula (28) with the known resonance parameters from [17] or by means of the optical theorem on the basis of the known cross section. In the case being considered, the total cross section is nearly coincident with the dominant radiative-capture cross section, $\sigma_{\text{eff}} \cong \sigma_\gamma$, which is well known [18].

The situation around the real part of b is more complicated. A few experimental values are given

Table 1

Re(b), fm	Method, λ	Year, references
9.5 ± 0.2	Diffraction, Epithermal neutrons	1975 [20, 21]
6.2	Compilation, 1.8 Å	1984 [17]
5.1 ± 0.4	Interferometry, 1.86 Å	1985 [22]
10	Reflectometry, 1–5 Å	1992 [23]

for this quantity in the tables of coherent scattering lengths in [19], the experimental result having the smallest declared error [20] being indicated there for the recommended value. These data, supplemented with those from [21, 23] (references to the earlier studies of the quoted authors are omitted here), are presented in Table 1.

The measurements reported in [20, 21] were performed by the neutron-diffraction method with epithermal neutrons over a wide energy range. The authors of those studies state that the results obtained by measuring the quantity b are indicative of its invariability in the energy range from 0.2 to approximately 2 eV, where there is a resonance. This conclusion, which contradicts the Breit–Wigner formula (see Fig. 1), seems dubious.

The experiment with a neutron interferometer in [22] was devoted to directly measuring the phase shift caused by the real part of the index of refraction,

$$\Delta\Phi = k_0(n' - 1)d, \quad n' = k'/k_0, \quad (29)$$

where d is the sample thickness. In the case of thermal neutrons, the imaginary part of the scattering length makes a negligible contribution to n' ; that is,

$$n' \cong 1 - \frac{2\pi\rho b'}{k_0^2} \left[1 + \left(\frac{2\pi\rho b''}{k_0^2} \right)^2 \right], \quad k_0^2 \gg \rho b', \rho b''. \quad (30)$$

The measurements were performed at the wavelength of $\lambda = 1.86 \text{ \AA}$, and the value quoted in Table 1 is the experimental result extracted from the measured phase shift at this wavelength value. For the real part of b at the thermal point, the value obtained by rescaling this result on the basis of the Breit–Wigner formula with allowance for two main resonances in gadolinium is $5.7 \pm 0.4 \text{ fm}$, which is close to the value quoted in [17].

Korneev *et al.* [23] measured the coefficient of neutron reflection, $R(\lambda)$, from a gadolinium layer deposited on the surface of a flat substrate. The measurements were performed by the time-of-flight method in the wavelength range $\lambda = 1\text{--}5 \text{ \AA}$. The coefficient of reflection, $R(\lambda)$, depends on the complex-valued quantity $b(\lambda)$, which was calculated on the basis of Eq. (28). The result displayed in the table concerns the constant component b_0 . The experiment reported in [23] was devoted to measuring the reflective properties of gadolinium rather than the scattering length proper; in view of this, the error in this quantity was not presented there.

Thus, we can see that available data are controversial and that the results of the most precise experiment are questionable. All of this furnishes a sufficient motivation for undertaking a new measurement of

the scattering length for coherent neutron interaction with gadolinium nuclei.

3.2. Measurement of the Scattering Length for Gadolinium by the Method of Reflection from a Mirror

Upon the reflection of a neutron wave from the boundary of a medium, the wave-number component parallel to the medium surface must remain unchanged. For this requirement to be satisfied, it is sufficient that the medium be homogeneous along its boundary. Therefore, the dispersion relation (11) is also valid for the wave-number components orthogonal to the surface of the medium [4, 14]; that is,

$$k_{\perp}^2 = k_{0\perp}^2 - 4\pi\rho b(k_0^2), \quad k_{\perp} = k'_{\perp} + ik''_{\perp}, \quad (31)$$

where it has been considered that the proximity of resonances, which is typical of strongly absorbing media, leads to an energy dependence in the scattering length. With allowance for this circumstance, formulas (15) and (16) remain valid if the wave numbers k_0 and k are replaced there by their normal components. For the coefficient of reflection from the boundary of the medium, we must use, instead of (26), the expression

$$r(k_0, k_0^2) = \frac{k_{0\perp} - k_{\perp}(k_{0\perp}, k_0^2)}{k_{0\perp} + k_{\perp}(k_{0\perp}, k_0^2)}, \quad R = |r|^2. \quad (32)$$

Figure 2 shows the calculated coefficient of reflection from the surface of a gadolinium mirror at a glancing angle of 5 mrad. The imaginary part of the scattering length, $\text{Im}(b)$, and the contribution to the real part of the scattering length $b(E)$ from the closest resonances were calculated by the Breit–Wigner formula. The constant part of the scattering length, b_0 , was a variable parameter. It can be seen that by no means is the coefficient of cold-neutron reflection from a gadolinium surface small and that it depends on the parameter b_0 rather strongly, and these were the circumstances that were used in [23]. Our experiment is also based on measuring the coefficient of neutron reflection from a gadolinium mirror [24].

The measurements were conducted by using the REFLEX neutron reflectometer installed at the IBR-2 reactor of the I.M. Frank Laboratory for Neutron Physics at the Joint Institute for Nuclear Research (Dubna, Russia)[25]. The sample used was manufactured by means of the magnetron sputtering of natural gadolinium onto a glass substrate of dimensions $5 \times 8 \text{ cm}^2$. The thickness of the gadolinium layer was about 1000 \AA . In order to prevent gadolinium from oxidation, it was covered with a thin (50 \AA) titanium layer. There is every reason to believe that the titanium layer was completely oxidized.

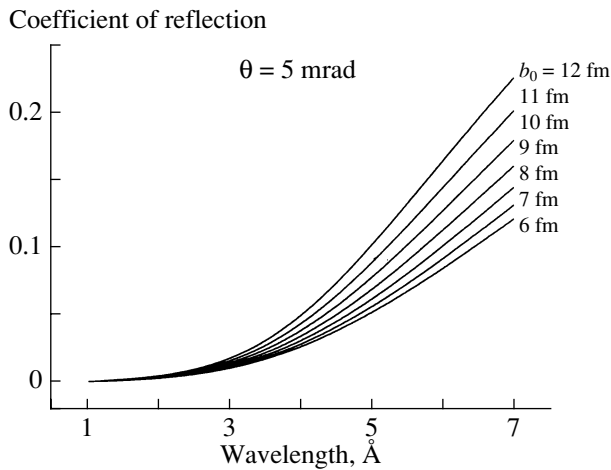


Fig. 2. Coefficient of neutron reflection from the surface of a gadolinium mirror versus the neutron wavelength according to calculations at various values of the constant part b_0 of the scattering length.

The measurements were performed by the time-of-flight method in the wavelength range 3.5–8 Å at glancing angles of 3.78 and 4.88 mrad. In those cases, the angular resolution of the instrument assumed values of 5.5 and 4.3%, respectively. The coefficient of reflection was determined in a natural way, as the ratio of the intensities of the reflected and incident beams, a normalization with allowance for the time of measurements and the monitoring of the reactor power being performed. The length of the mirror was insufficient for completely covering the incident beam, and this was taken into account by introducing yet another normalization factor. The corresponding geometric factor $x = N_1/N_2$, where N_1 and N_2 the intensities of the beam, respectively, without and with the mirror in the operating position, was measured as a function of the wavelength. It proved to be constant to a fairly high precision, and this indicates that the mirror is not transparent to neutrons in the wavelength range used.

The results of the measurements are given in Fig. 3. The theoretical curves calculated by formulas (15), (16), and (32) were fitted to our experimental data obtained at two glancing angles. In constructing these curves, the imaginary part of the scattering length, $\text{Im}(b)$, and the contribution of the closest resonances to the real part of the scattering length $b(E)$ were calculated by the Breit–Wigner formula. The constant part of the scattering length, b_0 , was the only varied parameter, which was common to both measurements. In the calculations, we took into account the presence of a protecting layer, setting the density of the scattering length for coherent interaction to $\rho b = 2.61 \times 10^{10} \text{ cm}^{-2}$, which corresponds to titanium dioxide (TiO_2).

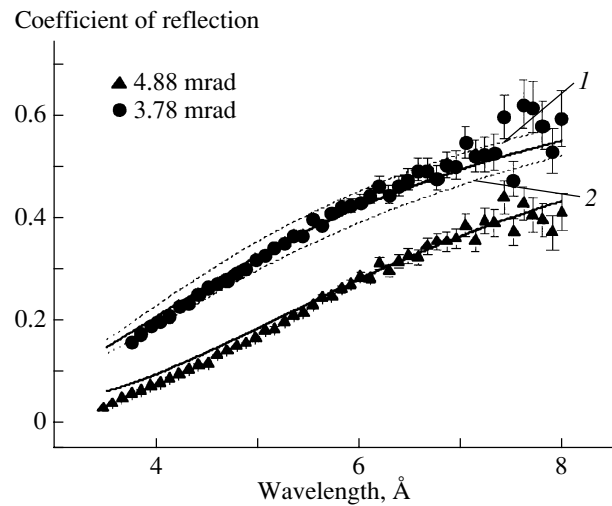


Fig. 3. Experimental data on the coefficient of reflection from a gadolinium mirror at two glancing angles, along with the results of the calculations at $b_0 = 11.5$ fm (solid curves) and the theoretical results for an angle of 3.78 mrad at $b_0 = 12.5$ and 10.5 fm (dashed curves 1 and 2, respectively).

Although the theoretical curves reproduce experimental data quite satisfactorily, their agreement with experimental data is not perfect. In all probability, there are moderate methodological errors or unknown factors that were disregarded in the calculations. The most probable reason behind these discrepancies is associated with an incomplete knowledge of the properties of the sample—in particular, of the surface distribution of oxygen in the sample oxidized in air.

Nevertheless, the experiment proved to be rather sensitive to the value of b_0 , as is demonstrated by a comparison of the results of the measurements at an angle of 3.78 mrad with the results of the calculations that were performed for three values of b_0 (see Fig. 3). For the constant contribution to the real part of the scattering length for gadolinium, our eventual estimate is $b_0 = 11.5 \pm 0.7$ fm.

3.3. Scattering Length for the Interaction of Ultracold Neutrons with Gadolinium Nuclei

On the basis of the result quoted above for b_0 , we can easily evaluate the scattering length for the case of ultracold neutrons. Upon taking into account the resonance contribution $b = b_0 + b(0)$ according to the Breit–Wigner formula, we obtain $\text{Re}(b)_{UCN} = 5.8 \pm 0.7$ fm. The imaginary part of the scattering length can easily be derived by using the optical theorem, $\text{Im}(b) = k\sigma_{\text{tot}}/4\pi$. In the case being considered, the total cross section is nearly coincident with the cross section for radiative capture, $\sigma_{\text{tot}} \cong \sigma_\gamma$. On the basis of data from [18] on the cross section for capture in

gadolinium isotopes that make a dominant contribution to the cross section, we find that, for the natural isotopic composition of gadolinium, $\sigma_\gamma = 5.9 \times 10^5$ b at an energy of $E = 10^{-4}$ eV. This leads to the value of $\text{Im}(b) = 10.4$ fm.

We also note that, from the invariability of the real and imaginary parts of the scattering length for ultracold neutrons, it follows that, when necessary, one can make use of the concept of a complex-valued effective potential that correctly describes the interaction of ultracold neutrons with gadolinium,

$$U = \frac{2\pi\hbar^2}{m}\rho b = V - iW, \quad (33)$$

the imaginary part of this potential ($W \cong 82$ neV) exceeding significantly its real part ($V \cong 45$ neV).

4. MEASUREMENT OF ULTRACOLD-NEUTRON TRANSMISSION THROUGH THIN GADOLINIUM FILMS

Until recently, the neutron optics of strongly absorbing media was not well studied experimentally. An attempt at experimentally observing the reflection of ultracold neutrons from strongly absorbing substances was made in [26]. Later on, this effect was reliably demonstrated in the experimental studies reported in [27]. Only in 1999 did H. Rauch and his collaborators [1] launch an experiment aimed at measuring the cross section for ultracold-neutron capture by gadolinium samples.

In accordance with the aforesaid, the scattering length for ultracold-neutron interaction with gadolinium nuclei must be a complex-valued constant, whence it follows that the $1/v'$ law must be valid for the cross section characterizing the capture of ultracold neutrons by gadolinium nuclei. According to Rauch *et al.* [1], however, their experimental results furnish strong evidence of a deviation from the $1/v$ law for the ultracold-neutron-capture cross section (see also [28]). We undertook a new experiment to study the transmission of ultracold neutrons through thin films of natural gadolinium. It was performed by using the cold-neutron source of the Laue–Langevin Institute (Grenoble, France) [29].

4.1. Experimental Facility, Experimental Conditions, and Procedure of Measurements

1. Layout of the facility. As a basic element, our experimental facility employed a gravitational spectrometer of ultracold neutrons that was equipped with interference filters [30–32] and which was somewhat modified to meet special demands of the present experiment. The layout of the spectrometer is displayed

in Fig. 4. Ultracold neutrons from the source used entered the chamber intended for a preliminary purification of the spectrum. After a few reflections from the chamber walls, some of these neutrons found their way to the annular corridor leading to the main chamber. The outer and the inner diameter of the corridor were 130 and 110 mm, respectively. The sample being studied, which was manufactured in the form of a thin-film structure deposited onto a silicon substrate 150 mm in diameter and 0.6 mm in thickness, was fastened at the outlet of corridor. The sample was arranged in such a way that it completely covered the cross section of the corridor. In order to prevent the penetration of ultracold neutrons into the main volume of the spectrometer through the gaps of the structure, the fastening workpieces were covered with a polyethylene film, which was virtually “black” for ultracold neutrons.

Neutrons that went out of the corridor and which traversed the sample entered the neutron guide formed by six glass mirrors with vertical walls. A filter that played the role of an energy analyzer was placed within the neutron guide. The position of the analyzer in altitude could be changed with aid of a high-precision gear driven by a step engine. Neutrons that traversed the analyzer were recorded by a proportional He^3 detector.

In order to prevent the possible multiple reflection of ultracold neutrons between the sample and the analyzer, a polyethylene disk of diameter about 100 mm (not shown in the figure), which played the role of an absorber, was arranged immediately beneath the sample.

A neutron interference filter [33] was the main spectroscopic element of the instrument. In order to analyze the energy of neutrons, we employed a five-layer filter formed by alternating layers of a nickel–vanadium alloy and titanium, these layers being deposited by the method of magnetron sputtering onto a silicon substrate. A 7% addition of vanadium to nickel reduced the temperature of the phase transition to a ferromagnetic state. The widths of the layers were 270, 166, 530, 166, and 270 Å. Three NiV layers (two outer layers and the central one) are characterized by a higher scattering-length density ρb and a greater effective potential, $U = (2\pi\hbar^2/m)\rho b \cong 230$ neV, whereas the effective potential of titanium is negative.

Thus, the potential relief of the filter had the form of three potential barriers separated by two identical wells. The widths of the potential wells (thicknesses of the titanium films) were chosen in such a way that the system had a quasibound-state level. The inevitable splitting of the level due to the presence of two wells did not have a strong effect on the properties

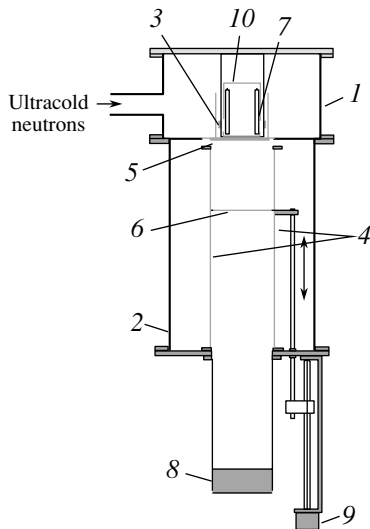


Fig. 4. Layout of our experimental facility for measuring the transmission of ultracold neutrons through gadolinium samples: (1) preliminary-purification chamber, (2) main vacuum chamber, (3) annular corridor equipped with a polyethylene convertor heating ultracold neutrons, (4) glass neutron guide, (5) sample, (6) analyzer, (7) monitoring detectors of heated neutrons, (8) detector of ultracold neutrons, (9) step engine, and (10) casing of the monitor.

of the filter, since the spacing between the levels was commensurate with their natural width. As a result, the neutron-transmission function was characterized by a narrow resonance (of width about 4 neV) at an energy of 107 neV, which is much lower than the barrier height. For this filter, the calculated transmission curve is shown in Fig. 5. Rich experience gained in using interference filters [30–32]—in particular, the filter that is described above—gives every ground to state that the calculated position of the peak agrees with the actual one to within 1 neV.

Obviously, the filter transmits well neutrons whose energy is above the barrier. They traverse the filter freely and generate a background. In order to reduce this component of the background, we employed a dedicated device that consisted of 120 alternating Ni(N) and Ti/Zr layers and which included an interference mirror (so-called supermirror) reflecting neutrons of energy in the region below some 700 neV. A specially calculated antireflecting structure was deposited onto the supermirror. This filter has a transmission window in the region of ultracold-neutron energy, but it efficiently reflects very cold neutrons, which are faster [30, 32]. In the following, this device, whose transmissivity is displayed in Fig. 6, will be referred to as a window.

The two devices forming the analyzer were fastened together in a movable holder within the neutron guide. The transmissivity of the analyzer is described

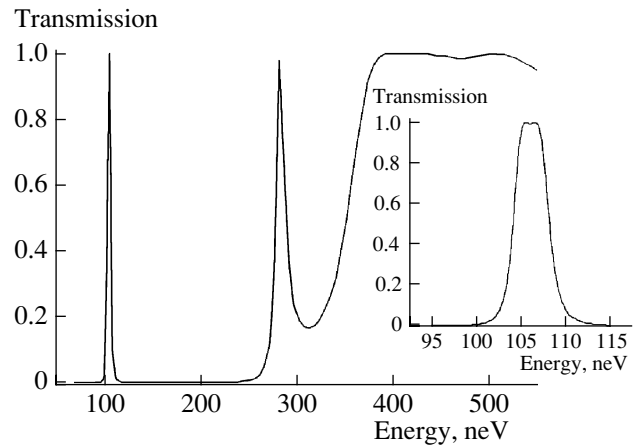


Fig. 5. Transmissivity of the interference filter used in the analyzer. The inset shows the resonance-tunneling peak.

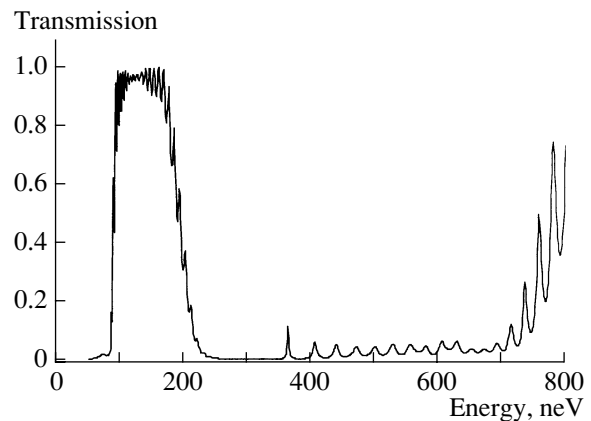


Fig. 6. Transmissivity of the filter used as a window to reduce the background of very cold neutrons.

by the product of the transmission functions of the two devices. Below 250 neV, there is only one transmission peak at $E_a = 107$ neV; in the range between 250 and 700 neV, the transmissivity of the analyzer is as low as a few percent. Thus, the analyzer transmitted those ultracold neutrons to the detector whose energy at the point of its location was E_r . However, the neutrons were accelerated in the gravitational field of the Earth on their path from the sample to the analyzer, so that their energy was lower when they traversed the sample. The change in energy per 1 cm of altitude is $mg = 1.025$ neV/cm. By changing the distance between the sample and the analyzer, we were able to perform scanning in the energy of neutrons traversing the sample.

Since the experiment was aimed at measuring the absolute value of the transmissivity of the samples, it was necessary to monitor the flux of ultracold neutrons in the immediate vicinity of a sample—that is, within the corridor along which the neutrons were

Table 2

Sample no. 1		Sample no. 3	
substance of the layer	measured layer thickness, Å	substance of the layer	measured layer thickness, Å
TiO ₂	50	SiO ₂	15
Ti	15	Si	29
Gd	235	Gd	255
Ti	50	SiO ₂	22
Si	Substrate	Si	Substrate

supplied. For this purpose, four pieces of a polyethylene film (β in Fig. 4) were fastened within the corridor at its inner wall. The total area of the film was about 5 cm². Polyethylene has a very large cross section for noncoherent inelastic scattering ($\sigma_{ne} \approx 3.5 \times 10^4$ b); therefore, it heats ultracold neutrons efficiently. The detector of heated neutrons was positioned in the central nonevacuated volume. It was designed as an assembly of 13 proportional He³ detectors of diameter 12 mm connected in parallel. The entire assembly was surrounded by a cadmium screen (10) that shielded it from the external background and the background of heated neutrons that were produced in the preliminary-purification chamber. At the level of the polyethylene converter, this screen had an annular slit of height about 1.5 cm. Under the conditions of the present experiment, the monitor counting rate was about 20 count/s; of these, about 2.5 count/s were due to background. The absorption of ultracold neutrons in the converter led to about a 10% loss of instrument counts.

2. Samples. We had four gadolinium-containing samples at our disposal. Of these, three were in the form of a natural-gadolinium film deposited by the method of magnetron sputtering onto a silicon substrate. In two cases, an additional thin film (sublayer) from titanium was deposited between the substrate and the gadolinium film for some technological reasons. In order to protect gadolinium from oxidation, it was covered with a thin layer of titanium or silicon. For three samples, we know the results of measurements with an x-ray reflectometer. For two of them, these data are quoted in Table 2.

Sample no. 2 was similar to sample no. 1, but it had the gadolinium-film thickness reduced to 150 Å. There are no data from x-ray measurements for this

sample. The fourth sample was a multilayer structure formed by 15 pairs of gadolinium and silicon films. The thickness of each layer was about 10 Å, which is much less than the wavelength of ultracold neutrons. In addition, the interlayer surfaces separating the films were not perfect, but they had roughness whose dimensions were commensurate with the thickness of the layers. Physically, this sample was therefore gadolinium diluted with silicon. It was covered with a 50-Å layer of silicon.

A silicon plate was taken for the fifth, reference, sample in testing the procedure for measuring the transmission of neutron.

3. Procedure of measurements and analysis of the background. The objective of the present measurements was to determine the experimental value of the transmissivity of a sample—that is, the ratio of the flux that traversed the sample to the incident flux. Instead of the flux incident on a sample, we measured, in this experiment, the flux in the absence of a sample. It is obvious that, in addition to accurately monitoring the flux, it is necessary, in using this method, to take correctly into account the backgrounds of the facility.

Since an interference filter is the spectrometric element of the instrument, all detector counts whose origin is not associated with a tunnel penetration through the filter at the resonance must be treated as background counts. Listed immediately below are possible sources of the background:

- (i) intrinsic detector background (background of the experimental hall);
- (ii) background of heated neutrons originating from inelastic scattering in the inlet chamber of the spectrometer;
- (iii) background of very cold neutrons that traversed the sample and the analyzer;
- (iv) background of heated neutrons generated by ultracold neutrons that traversed the sample and which then suffered inelastic scattering on the internal elements of the spectrometer;
- (v) background of ultracold neutrons that traversed the sample, but which bypassed the analyzer in finding their way to the detector upon undergoing a few reflections in the spectrometer chamber.

The first two components of the background do not change upon the replacement of a sample. The remaining three are associated with neutrons that traversed the spectrometer through the supplying corridor and a sample if it is mounted at the outlet of the corridor. Obviously, this background changes upon the replacement of a sample.

In order to measure the background, it is necessary to eliminate the tunnel passage of ultracold neutrons through the analyzer without changing other

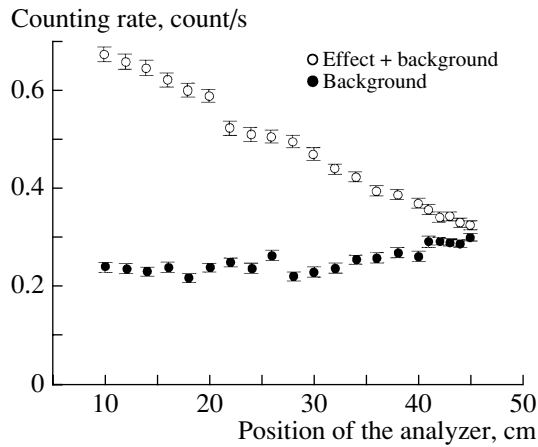


Fig. 7. Total counting rate and that for background in the transmission of ultracold neutrons through sample no. 3.

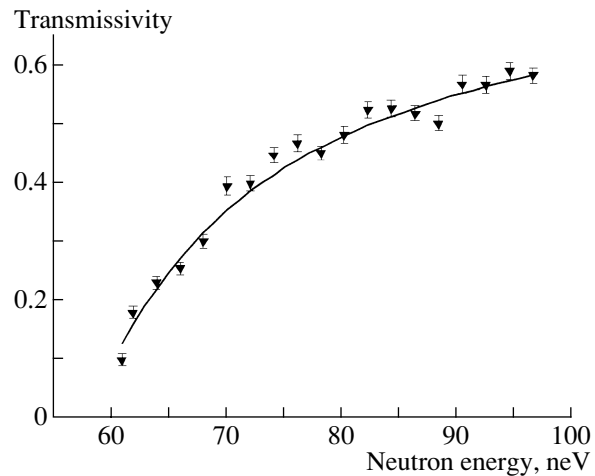


Fig. 8. Transmissivity of a silicon plate: (solid curve) results of the calculation and (points) experimental data.

conditions of the experiment. The replacement of the analyzing filter deposited onto a silicon substrate by a thin nickel film on the identical substrate would be a procedure that conforms most closely to this requirement.

For each of the samples and for the case of the open corridor, the measurements were performed two times. In measuring the total counting rate (effect plus background) the interference filter on a silicon substrate and the window filter were in the holder of the analyzer, while, in measuring the background, a Ni(N) film of thickness 1370 Å on the identical silicon substrate and the window filter were placed in that holder. In either case, we measured the detector counting rate as a function of the position of the analyzer holder. The possible uncontrollable changes in the external background and in the parameters of the measuring equipment within the time interval separating the two measurements in question inevitably plagued this procedure. Yet, the external background (about 0.05 count/s) constituted a relatively small fraction of the total background. For one of the samples, Fig. 7 displays the results obtained by measuring the total counting rate and that which is associated with the background. The position of the analyzer was measured with respect to the sample.

4.2. Calculation of Transmission through the Samples

1. Calculation of transmission through a silicon plate. In rigorously calculating the coefficient of transmission through a planar sample, it is necessary to take into account the interference between the waves that are multiply reflected from its boundaries. In actual cases, however, where the spectrum has a finite width, the inclusion of this interference is physically meaningful only if the so-called coherence

length $L_c = \lambda^2/\Delta\lambda$ is commensurate with the thickness of the plate (in the expression for the coherence length, $\Delta\lambda$ is the width of the spectrum).

In our experiment, 0.6-mm-thick plates from a silicon single crystal were used as substrates. Such a plate was also chosen as a separate sample for testing correctness of the procedure used in our measurements. The relative wavelength spread $\Delta\lambda/\lambda$ was about 0.02 at a wavelength value of $\lambda \approx 10^{-5}$ cm. Thus, the sample thickness was two orders of magnitude larger than the coherence length $L_c \approx 5 \times 10^{-4}$ cm, so that coherence effects could not be observed in our experiment.

In our calculation of transmission through a silicon sample, we therefore invoked considerations inspired by the wave facet of the problem only in determining the coefficient of reflection from the vacuum–silicon boundary, $R = |r|^2$, according to Eqs. (11) and (26), b being treated here as a real-valued quantity. However, the calculation of the transmission proper was of course performed with allowance for absorption and multiple reflection from the boundaries, the latter being taken into account according to the formulas

$$T = \frac{(1 - R)^2 \xi}{1 - (R\xi)^2}, \quad \xi = \exp\left(-\rho \frac{\sigma_t k_t}{k'} d\right) \quad (34)$$

(see, for example, [34]), where T is the transmissivity of the plate, σ_t is the sum of the cross section for the capture of thermal neutrons in silicon and the cross section for their inelastic scattering there, k_t is the thermal-neutron wave number, and d is the plate thickness. Formulas (34) take fully into account the effective increase in the length of the neutron path in matter due to multiple reflection. Since these formulas involve the coefficient of reflection rather than the

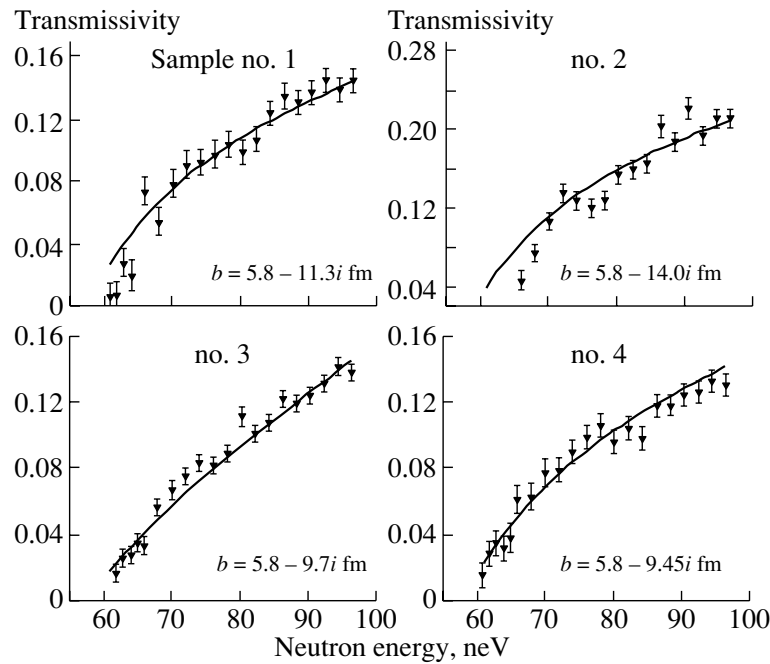


Fig. 9. Measured transmissivity of samples containing gadolinium (points). The solid curves represent the results of the calculations with the parameter values corresponding to the best fit to data.

relevant amplitude, they disregard the relationships between the phases of the waves completely. Thereby, interference effects are eliminated from the consideration. It should also be noted that the distinction between the wave number of ultracold neutrons in matter and its vacuum value is taken into account in the second equation in (34). Moreover, it is assumed that the $1/v'$ law is valid for the cross section describing losses. We took the value of $\sigma_t = 0.18$ b for this cross section at the thermal point.

2. Calculation of transmission through multilayer samples. Since all samples, with the exception of the aforementioned silicon plate, had a multilayered structure, the calculation of transmission was performed by the matrix method that is usually applied to such objects.⁴⁾ The presence of oxide films at the external surface of the sample and at the surface of the silicon substrate was taken into account here. The calculation was based on the formulas

$$T = |t|^2, \quad t = 2 \frac{\alpha M_{1,1} + i\beta M_{1,2}}{\alpha + \beta}, \quad (35)$$

$$\alpha = M_{1,2} + iM_{2,2}, \quad \beta = iM_{1,1} - M_{2,1},$$

where T is the transmissivity of the sample and M is the characteristic matrix of the system. This matrix is

⁴⁾A.I. Frank is grateful to B.P. Toperverg, who taught him how to use this straightforward and nice method.

obtained by multiplying the matrices S_i of dimension 2×2 that describe each layer. Specifically, we have

$$M = \prod_i S_i, \quad (36)$$

$$S_i = \begin{pmatrix} \cos(k_i \ell_i) & \frac{k_0}{k_i} \sin(k_i \ell_i) \\ -\frac{k_0}{k_i'} \sin(k_i \ell_i) & -\cos(k_i \ell_i) \end{pmatrix},$$

$$k_i^2 = k_0^2 - 4\pi(\rho b)_i,$$

where k_i is the complex-valued wave number of neutrons in the substance of the i th layer [it is given by formulas (14)–(16)], $(\rho b)_i$ is the scattering-length density there, and ℓ_i is the thickness of this layer. Complex-valued scattering lengths were used to describe gadolinium layers and the thick silicon substrate. In calculating the above matrices for the thin layers of titanium, silicon, and oxide layers, we disregarded the imaginary part of the scattering length.

In the calculation of transmission through samples, the thick silicon substrate is a part inherent in the multilayered structure being considered. Under these conditions, the elimination of the aforementioned unphysical interference effects from the consideration presents a nontrivial problem. In this case, it is not correct to eliminate, from the calculation, the complex-valued amplitude of the reflected wave, since the calculation of the wave field in the finely layered

part of the sample is impossible without information about the phase of the reflected wave.

A correct result can be obtained if calculations performed without resorting to simplifying assumptions employ some specific set of parameters $(k\ell)_i$. In this case, one can vary, within rather narrow ranges, the wavelength or the sample thickness. The eventual result must then be averaged, $T = \langle T_j \rangle$. In practical calculations, this trick, which is physically substantiated, involves difficulties because of unwieldiness of the required manipulations. Moreover, it is difficult to incorporate it into the fitting procedure, in which case repeated calculations with the variable parameter in question are required. In view of this, we only employed this trick to test a different computational procedure that is simpler, but which, in general, is not quite correct. The latter consists in setting the real part of the argument to zero from the very beginning in the calculation of the sines and cosines in the matrix for silicon, S_{Si} , whereby we eliminated the oscillating term $\text{Re}(k\ell)$. Upon making sure that the two methods yield close results, we then took the simplest of these for a basic one.

4.3. Experimental Results

For each of the six pairs of measurements of the effect and background—an open corridor, silicon, and four measurements with gadolinium samples—we constructed a difference curve. The curves obtained upon background subtraction were rescaled to neutron energies at the point of escape from a sample with allowance for the known position of the transmission line of the analyzer (107 neV) and the value of mg . The ratio of the counting rate for ultracold neutrons transmitted through a sample to the counting rate for the open corridor determined the transmissivity of the sample. In all of the cases, we introduced a correction for the monitor counting rate. The relative magnitude of this correction ranged between 10 and 12%. This was due to the actual change in the density of neutrons in the corridor, whose outlet was covered

with the sample—reflecting neutrons, the sample returns part of the ultracold neutrons to the corridor, whereby their density is increased.

The results obtained by measuring the transmissivity of the 620- μm silicon plate are shown in Fig. 8, along with the results of our calculations. In fitting our theoretical curves to the experimental results for samples containing gadolinium, we fixed the real part of the scattering length and employed its imaginary part as an adjustable parameter. It was precisely the quantity whose value we extracted from our experimental data. The results of data processing are given in Fig. 9 and in Table 3.

The error quoted in this table includes the error in the measurement of the real part of the coherent-scattering length. It can be seen that the results for the imaginary part of the scattering length that were extracted from data on the transmissivity of four samples agree fairly well with each other. Only the results for sample no. 2, for which there are no data of x-ray measurements, stand somewhat apart. Upon performing averaging over all four results, we arrive at a value of $\text{Im}(b)_{UCN} = 10.6 \pm 0.6$ fm, to be compared with the value of $\text{Im}(b)_{VCN} = 10.4$ fm, which was obtained from the (n, γ) cross section for cold neutrons.

5. CONCLUSION

We have considered the present-day state of the theoretical optics of absorbing media. We have found no physical arguments that would constrain the validity of the dispersion relation $k^2(k_0^2) = k_0^2 - 4\pi\rho b(k_0^2)$ in the case of arbitrarily strong absorption. In specific calculations, it is only necessary to take into account the energy dependence of the complex-valued coherent-scattering length. In this case, the problem of the reflection, transmission, and absorption of waves incident on a known sample can be solved within traditional approaches by imposing the continuity condition on the wave function and its derivative at the boundary of matter. In the case of ultracold neutrons, the complex-valued scattering length must be treated as a constant, although its value may differ significantly from that at the thermal point.

From the results obtained by measuring the coefficient of neutron reflection over a broad range of wavelength values, we have found a refined value for the constant component of the real part of the scattering length for neutron interaction with gadolinium nuclei. Upon taking into account the resonance contribution, which is determined by the Breit–Wigner formula, one can find the scattering length proper at any wavelength value.

Table 3

Sample	Measured quantity $\text{Im}(b)$, fm
1	11.3 ± 1
2	14.0 ± 1.6
3	9.7 ± 1
4	9.5 ± 1

We have performed an experiment aimed at studying the transmission of ultracold neutrons through samples containing natural gadolinium. In analyzing data from this experiment, we have employed the value found here for the real part of the scattering length. Our experimental data suggest that, to within 6%, the imaginary part of the scattering length is constant for neutron velocities ranging from 4 to about 120 m/s. This means that, within this range, the $1/v$ law is valid for the cross section describing neutron capture by a free nucleus. Simultaneously, we have verified the validity of the commonly accepted dispersion relation for neutron waves in matter where absorption is extremely strong.

In a sense, the physical conditions of the experiment are unique. The velocity of neutrons in matter, $\hbar k'/m$, was about 3.6 m/s, the corresponding cross section for neutron capture being as large as 23 Mb. The absorption range was about 300 Å at an effective wavelength of about 1100 Å. Although any deviations from the predictions of the theory outlined above could hardly be expected even under these, extreme, conditions, the very fact of their validity, which was verified in a direct experiment for the first time, seems not quite trivial.

ACKNOWLEDGMENTS

We are grateful E.I. Kats, V.V. Lomonosov, V.G. Nosov, L.B. Pikel'ner, H. Rauch, and E.I. Sharapov for stimulating discussions. We are also indebted to N. Watanabe for kindly sending us the text of the article quoted in [21]. The assistance of A.V. Androsov in preparing the experiment and of I. Anderson, V.I. Ul'yanov, and P. Hoghoi, who manufactured the gadolinium-containing samples that we used, is gratefully acknowledged. Special thanks are due to the Aspect enterprise and, personally, to V.I. Lushchikov for placing at our disposal detectors of thermal neutrons that were fabricated by this enterprise.

This work supported by INTAS (project no. 00-00043).

REFERENCES

1. H. Rauch, M. Zawisky, Ch. Stellmach, and P. Geltenbort, *Phys. Rev. Lett.* **83**, 4955 (1999).
2. M. L. Goldberger and F. Seitz, *Phys. Rev.* **71**, 294 (1947).
3. I. I. Gurevich and P. É. Nemirovskii, *Zh. Éksp. Teor. Fiz.* **41**, 1175 (1961); I. I. Gurevich and L. V. Tarasov, *The Low Energy Neutrons Physics* (Nauka, Moscow, 1965; North-Holland, Amsterdam, 1968).
4. I. M. Frank, in *Proceedings of the II International School on Neutron Physics*, D3-7991 (Joint Inst. Nucl. Res., 1974); *Usp. Fiz. Nauk* **161** (11), 109 (1991).
5. A. I. Gurevich and V. V. Lomonosov, *Yad. Fiz.* **60**, 589 (1997) [*Phys. At. Nucl.* **60**, 510 (1997)].
6. T. Y. Tudorovsky and A. L. Barabanov, in *Proceedings of the IX International Seminar on Interaction of Neutrons with Nuclei, ISINN-9* (Dubna, 2001), p. 425.
7. V. V. Lomonosov and A. I. Gurevich, *Zh. Éksp. Teor. Fiz.* **122**, 928 (2002) [*JETP* **95**, 800 (2002)].
8. L. L. Foldy, *Phys. Rev.* **67**, 107 (1945).
9. M. Lax, *Rev. Mod. Phys.* **23**, 287 (1951); *Phys. Rev.* **85**, 621 (1952).
10. F. Rubio and N. Kumar, *Phys. Rev. B* **47**, 2420 (1993).
11. A. M. Jayannavar, *Phys. Rev. B* **49**, 14718 (1994).
12. V. M. Galitskii, B. M. Karnaukhov, and V. I. Kogan, *Problems in Quantum Mechanics* (Nauka, Moscow, 1981), p. 24.
13. V. K. Ignatovich, *Physics of Ultra Cold Neutrons* (Nauka, Moscow, 1986).
14. A. I. Frank and V. G. Nosov, *Yad. Fiz.* **58**, 453 (1995) [*Phys. At. Nucl.* **58**, 402 (1995)].
15. V. G. Nosov and A. I. Frank, *Phys. Rev. A* **55**, 1129 (1997).
16. A. L. Barabanov and S. T. Belyaev, *Yad. Fiz.* **62**, 824 (1999) [*Phys. At. Nucl.* **62**, 769 (1999)].
17. S. F. Mughabghab, *Neutron Cross Section* (Academic Press, London, 1984).
18. International Atomic Energy Agency, Vienna, *NGATLAS Nuclear Data Collection*, <http://www-nds.iaea.org/ngatlas/>.
19. http://www.ati.ac.at/neutropt/scattering/Scattering_lengths_table_20010419.pdf.
20. N. Watanabe, Y. Ishikawa, K. Takei, and H. Suzuki, *Kakuriken Kenkyu Hokoku* **8/9**, 302 (1975); <http://inisdb.iaea.org>
21. N. Watanabe, Y. Ishikawa, K. Takei, and H. Suzuki, in *Proceedings of Neutron Scattering Conference (Petten 1975)*, p. 360.
22. H. Rauch and D. Tuppinger, *Z. Phys. A* **322**, 427 (1985).
23. D. A. Korneev, V. V. Pasyuk, A. V. Petrenko, and H. Lankovski, *Nucl. Instrum. Methods Phys. Res. B* **63**, 328 (1992).
24. A. I. Frank, V. I. Bondarchuk, G. V. Kulin, and O. V. Kulina, Report of Joint Inst. Nucl. Res. No. R3-2002-288 (Dubna, 2002).
25. V. L. Aksenov, D. A. Korneev, and L. P. Chernenko, *Proc. SPIE* **1738**, 335 (1992).
26. V. V. Golikov, E. N. Kulagin, and Yu. V. Nikitenko, *Kratk. Soobshch. OIYaI*, Nos. 9–85, 26 (1985).
27. V. I. Morozov, M. I. Novopol'tsev, Yu. N. Panin, *et al.*, *Pis'ma Zh. Éksp. Teor. Fiz.* **46**, 301 (1987) [*JETP Lett.* **46**, 377 (1987)]; M. I. Novopol'tsev and Yu. N. Pokotolovskii, Report of Joint Inst. Nucl. Res. No. P3-87-408 (Dubna, 1987).

28. J. Felber, R. Gähler, and R. Golub, Phys. Rev. Lett. **85**, 5667 (2000); H. Rauch, M. Zawisky, Ch. Stellmach, and P. Geltenbort, Phys. Rev. Lett. **85**, 5668 (2000).
29. A. Steyerl, H. Nagel, F. Schriber, *et al.*, Phys. Lett. A **116**, 347 (1986); <http://whisky.ill.fr/Yellow-Book/PF2/>.
30. I. V. Bondarenko, V. I. Bodnarchuk, S. N. Balashov, *et al.*, Yad. Fiz. **62**, 775 (1999) [Phys. At. Nucl. **62**, 721 (1999)].
31. I. V. Bondarenko, A. I. Frank, S. N. Balashov, *et al.*, Nucl. Instrum. Methods Phys. Res. A **440**, 591 (2000).
32. A. I. Frank, S. V. Balashov, V. I. Bodnarchuk, *et al.*, Proc. SPIE **3767**, 360 (1999).
33. A. Steyerl, W. Drexel, S. S. Malik, and E. Gudsmiedl, Physica B **151**, 36 (1988).
34. V. I. Ignatovich, Yad. Fiz. **62**, 792 (1999) [Phys. At. Nucl. **62**, 738 (1999)].

Translated by A. Isaakyan

T-Odd Asymmetries in the Angular Distributions of Fragments Originating from the Ternary Fission of Nuclei

V. E. Bunakov¹⁾ and S. G. Kadmsky²⁾*

Received February 10, 2003

Abstract—A version of a theoretical explanation is proposed for the recently discovered effect of *T*-odd correlation in ternary nuclear fission induced by polarized neutrons. It is shown that the inclusion of the Coriolis interaction between a third particle and the fissile-nucleus spin within the quantum theory of fission makes it possible to explain the experimental features of the effect and provides a correct estimate of its magnitude. © 2003 MAIK “Nauka/Interperiodica”.

1. INTRODUCTION

In studying the differential cross sections for (n, f) reactions in which unpolarized target nuclei irradiated with longitudinally polarized cold neutrons undergo ternary fission, Jesinger *et al.* [1] revealed triplet correlations of the form

$$\sigma[\mathbf{e}_{\text{LF}} \times \mathbf{e}_3], \quad (1)$$

where σ , \mathbf{e}_{LF} , and \mathbf{e}_3 are unit vectors whose directions coincide with the directions of, respectively, the neutron-polarization vector, light-fragment emission, and third-particle emission. The geometry of the experiment was chosen in such a way that the vectors \mathbf{e}_{LF} and σ were parallel to, respectively, the z and the y axis of the laboratory frame, while the vector \mathbf{e}_3 lay in the (x, z) plane. In this case, formula (1) can be represented as

$$\begin{aligned} \sigma[\mathbf{e}_{\text{LF}} \times \mathbf{e}_3] &= \sigma_y(\mathbf{e}_{\text{LF}})_z \cdot (\mathbf{e}_3)_x \\ &= (\sigma)_y(\mathbf{e}_{\text{LF}})_z \cos \varphi_3 \sin \theta_3, \end{aligned} \quad (2)$$

where the angles θ_3 and φ_3 specify the direction of third-particle emission in the laboratory frame. From this expression, it can be seen that the triplet correlation (1) has a maximum value at $\varphi_3 = 0$ and $\theta_3 = \pi/2$; if the vector \mathbf{e}_3 lies in the (x, z) plane, in which case $\varphi_3 = 0$, this correlation is weakly dependent on the angle θ_3 in the region $60^\circ \leq \theta_3 \leq 120^\circ$, where $\sin \theta_3$ changes from 0.87 to 1.

The experiment in question resulted in finding values of the asymmetry coefficient D defined as

$$D = \frac{\sigma_+ - \sigma_-}{\sigma_+ + \sigma_-}, \quad (3)$$

where σ_+ and σ_- are the differential cross sections for the reaction being studied at, respectively, a positive and a negative helicity of the incident neutron beam.

Values found for the asymmetry coefficient D in the case of two types of third particles (alpha particles and tritons) were virtually independent of the angle θ_3 of third-particle emission with respect to the direction of light-fragment emission. It will be shown below that the sum of the differential cross sections that appears in the denominator on the right-hand side of Eq. (3) ($\sigma_+ + \sigma_-$) coincides with the double-differential cross section for the corresponding reaction (n, f) with unpolarized neutrons and that it depends on the angle θ_3 rather strongly [2]. In view of this, only if the numerator on the right-hand side of Eq. (3) (that is, the cross-section difference $\sigma_+ - \sigma_-$) features a significant θ_3 dependence similar to the corresponding dependence of the cross-section sum ($\sigma_+ + \sigma_-$) can the asymmetry coefficient D (3) be weakly dependent on the angle θ_3 . It follows that the θ_3 dependence of the cross sections σ_+ and σ_- differs from the aforementioned weak dependence of the *T*-odd correlation on the angle θ_3 in Eqs. (1) and (2). This means that the cross sections σ_+ and σ_- involve a *T*-odd correlation whose structure is more complicated than that in (1). At the same time, the correlation in Eq. (1) reflects correctly the properties of the cross sections σ_+ and σ_- with respect to the space reflection of the vectors σ , \mathbf{e}_{LF} , and \mathbf{e}_3 and with respect to their change under time inversion.

The experimental investigations reported in [1] revealed that the coefficients D increased with increasing kinetic energy E_3 of a third particle. The values found for the asymmetry coefficient $\langle D \rangle$ averaged over the energy E_3 proved to be rather close for alpha particles and tritons; specifically, they are [1]

$$\langle D_\alpha \rangle = -(2.52 \pm 0.14) \times 10^{-3};$$

¹⁾Petersburg Nuclear Physics Institute, Russian Academy of Sciences, Gatchina, 188350 Russia.

²⁾Voronezh State University, Universitetskaya pl. 1, Voronezh, 394693 Russia.

* e-mail: kadmsky@phys.vsu.ru

$$\langle D_t \rangle = -(1.99 \pm 0.63) \times 10^{-3}$$

for ^{233}U target nuclei and

$$\langle D_\alpha \rangle = +(0.83 \pm 0.11) \times 10^{-3}; \quad (4)$$

$$\langle D_t \rangle = +(0.60 \pm 0.41) \times 10^{-3}$$

for ^{235}U target nuclei.

The correlation specified by Eq. (1) is a T -odd one since it changes sign under time inversion. At the same time, it is a P -even one since it does not change sign under the spatial inversion of the vectors \mathbf{e}_3 and \mathbf{e}_{LF} (or the third-particle and light-fragment momenta), which are associated with the properties of the fissile nucleus being considered. It does not involve the unit vector \mathbf{e}_n aligned with the incident-neutron momentum. In this respect, it differs from the P -even correlations $\sigma[\mathbf{e}_n \times \mathbf{e}_{\text{LF}}]$ and $\sigma[\mathbf{e}_n \times \mathbf{e}_3]$, which are responsible for the emergence of right-left asymmetry, which were previously investigated in [3–6] for the case of nuclear fission induced by transversely polarized neutrons, and which are generated by the interference between the fission amplitudes for s - and p -wave neutron resonances of the compound nucleus. This means that the emergence of correlations of the type in (1) is due to a similar interference between fission amplitudes for neutron resonances of the same parity. Since cold neutrons generate s -wave neutron resonances with the highest probabilities, we can restrict our investigation of the correlation in (1) to considering only s -wave neutron resonances.

In [3, 4], the physical origin of T -odd effects was attributed to the dependence of the probability of ternary fission on the projection of the orbital angular momentum of a third particle onto the spin of the partly polarized rotating compound nucleus that is formed upon the absorption of a polarized neutron by the target nucleus and which emits this particle. The structure of the Hamiltonian that takes into account the coupling of the orbital angular momentum of a third particle to the spin of the compound nucleus coincides with the structure of the Hamiltonian that describes the Coriolis interaction between a third particle and the rotation of the compound nucleus. Owing to Coriolis forces, a third particle is more easily emitted in the direction of the rotation of the system being considered than against this direction, and it is precisely the circumstance that explains the emergence of the asymmetry specified by Eq. (3). Semiclassical estimates of this phenomenon within the statistical model made it possible to assess correctly the order of magnitude and the sign of values obtained experimentally for $\langle D \rangle$. By using phenomenological values for the excitation energies of fission fragments and the experimental fact that these energies anticorrelate with the third-particle energies E_3 (see, for example, [2]), the experimental dependence of the effect

on E_3 was explained quite satisfactorily. Despite fairly good agreement with experimental data and despite quite clear physics behind the model in question, it is rather rough, however. The use of the semiclassical (and classical as well) approach in this model at low values of angular momenta does not seem well justified. Moreover, almost all angular correlations in nuclear reactions result from quantum interference effects, which cannot be described within the statistical model.

In [5], a theoretical scheme was developed that makes it possible, in principle, to calculate the asymmetry coefficient in ternary fission for alpha particles—that is, the coefficient D_α in Eq. (3). This scheme was based on introducing a nuclear spin-orbit alpha-particle interaction with fission fragments that is proportional to $(\mathbf{l} \cdot \mathbf{J}_0)$, where \mathbf{l} is the orbital angular momentum of the alpha particle involved and \mathbf{J}_0 is the total spin of fission fragments that includes their relative orbital angular momentum \mathbf{L} . In addition, it was assumed in [5] that the spin \mathbf{J}_0 can be replaced by the total spin of the nucleus undergoing fission, \mathbf{J} , and this made it possible to obtain an analytic expression for the coefficient D_α . As will be shown below, the spin-orbit alpha-particle interaction with fission fragments, which preserves the total spin J of the system undergoing fission and its projection K onto the symmetry axis of this system, leads to zero effect for T -odd correlations of the form in Eq. (1), which are considered here. That the result obtained in [5] for the coefficient D_α was nonzero stemmed from the use of the aforementioned assumption there, which from the point of view of symmetry resulted in the replacement of the spin-orbit interaction between the alpha particle and fission fragments by its Coriolis interaction with the system undergoing fission.

A quantum-mechanical theory of the fission process was developed in [6, 7], and this theory made it possible to substantiate [8] the origin of the mechanisms of binary and ternary spontaneous and low-energy induced fission of nuclei and to explain the experimentally observed emergence of high values of fission-fragment spins. Methods of this theory enabled one to analyze P -odd and P -even asymmetries (see [9] and [10], respectively) in the binary fission of nuclei and to make predictions for values of the coefficients of these asymmetries in the ternary fission of the same nuclei.

The objective of the present study is to analyze the T -odd-asymmetry coefficients (3) for the case of alpha particles in the ternary fission of nuclei on the basis of methods developed in [7–10]. In this analysis, it is assumed that the Coriolis interaction between the

alpha particle and the fissile system under consideration as a discrete unit plays a dominant role in the formation of T -odd correlations of the form (1).

2. ANGULAR DISTRIBUTIONS OF PRODUCTS ORIGINATING FROM THE TERNARY FISSION OF NUCLEI IN (n, f) REACTIONS

Let us consider (n, f) reactions in which an unpolarized target nucleus having a spin I , its projection M_I onto the z axis of the laboratory frame, and a parity π undergoes ternary fission induced by longitudinally polarized cold neutrons. We assume that the reactions being considered proceed through the formation of s -wave neutron resonances of a compound nucleus that, at equilibrium values of the deformation parameters of the axisymmetric compound nucleus, are described by the wave functions $\Psi_s^{J_s \pi M}$, where J_s is their spin; M is its projection onto the z axis of the laboratory frame; π is their parity; and s stands for other quantum numbers, including the atomic weight A and the charge Z of the compound nucleus.

For a further investigation, we will make use of the conventions adopted in [8–10] and the results presented in those articles, where the mechanisms of binary and ternary nuclear fission were explored within the quantum-mechanical theory of the fission process [6, 7].

Let us consider the effective wave function $A_{m_s}^{I \pi M_I}$ that is defined as a superposition of the wave functions for neutron resonances excited in the reaction (n, f) being studied and which is normalized in such a way as to take into account the properties of the entrance neutron channel; that is,

$$A_{m_s}^{I \pi M_I} = \sum_{s J_s} h_s^{J_s} C_{I \frac{1}{2} M_I m_s}^{J_s M} \Psi_s^{J_s \pi M}, \quad (5)$$

where

$$h_s^{J_s} = \frac{\sqrt{\Gamma_{sn}^{J_s}}}{E - E_s^{J_s} + i\Gamma_s^{J_s}/2}. \quad (6)$$

Here, $\sqrt{\Gamma_{sn}^{J_s}}$ is the amplitude of the neutron width with respect to the decay of the s -wave neutron resonance; E is the total c.m. energy of the system undergoing fission; and $E_s^{J_s}$ and $\Gamma_s^{J_s}$ are, respectively, the energy and the total width of the s -wave neutron resonance. In expression (6), we have taken into account the smallness of neutron potential phase shifts for cold neutrons. By using the results obtained in [9, 10], the asymptotic behavior of the neutron-resonance wave function $\Psi_s^{J_s \pi M}$ in the vicinity of

the point of compound-nucleus scission into ternary-fission fragments can be represented in the form

$$\Psi_s^{J_s \pi M} \rightarrow \sum_{K_s t q} a_{K_s}^{J_s} b_{ts K_s}^{J_s \pi} c_{qt K_s}^{J_s \pi} \Psi_{q K_s}^{J_s \pi M}, \quad (7)$$

where $a_{K_s}^{J_s}$ is the amplitude of the Coriolis interaction-induced mixing [12, 13] of the projections K_s of the spin J_s onto the symmetry axis of the axisymmetric nucleus undergoing fission, this symmetry axis being coincident with the z' axis of the intrinsic coordinate frame of this nucleus. This amplitude has an absolute value equal to $(2J_s + 1)^{-1/2}$ and a random sign. In expression (7), $b_{ts K_s}^{J_s \pi}$ is the amplitude for the transition of a neutron-resonance state in the course of fissile-nucleus evolution associated with variations in nuclear deformation parameters to the transition fission state t described by the wave function $\Psi_{t K_s}^{J_s \pi M}$ and defined at the saddle point of the deformation potential [11]. The amplitude $b_{ts K_s}^{J_s \pi}$ is of random character, its expectation value being equal to N_s^{-1} , where N_s is the number of multi-nucleon shell functions forming the basis of random Wigner matrices [11]. The quantity $c_{qt K_s}^{J_s \pi}$ controls the dynamical amplitude for the transition from the transition fission state whose wave function is $\Psi_{t K_s}^{J_s \pi M}$ to a fission-mode state whose wave function $\Psi_{q K_s}^{J_s \pi M}$ describes the prescission configuration of the nucleus undergoing fission. For the case of ternary fission that is asymmetric with respect to the charges Z_i and the masses A_i of nascent fragments ($i = 1, 2$, $A_1 < A_2$, $Z_1 < Z_2$), the $J_s \pi q K_s$ fission mode is associated with an axisymmetric pearlike shape of the nucleus undergoing fission at finite values of static octupole-deformation parameters [14], in which case the wave function $\Psi_{q K_s}^{J_s \pi M}$ for the fission mode can be represented in the form [11]

$$\begin{aligned} \Psi_{q K_s}^{J_s \pi M} = & \sqrt{\frac{2J_s + 1}{16\pi^2}} [(1 - \delta_{K_s, 0}) \\ & \times \{ D_{M K_s}^{J_s}(\omega) \chi_{q K_s}^{\pi}(\xi) + (-1)^{J_s + K_s} \\ & \times D_{M - K_s}^{J_s}(\omega) \chi_{q K_s}^{\pi}(\xi) \} + \delta_{K_s, 0} \sqrt{2} D_{M 0}^{J_s}(\omega) \chi_{qn}^{\pi}(\xi)], \end{aligned} \quad (8)$$

where $D_{M K_s}^{J_s}(\omega)$ is a generalized spherical harmonic dependent on the Euler angles $(\alpha, \beta, \gamma) \equiv \omega$ characterizing the orientation of the intrinsic axes of a fissile nucleus with respect to the axes of the laboratory frame. The intrinsic wave functions for a fissile nucleus, $\chi_{qn}^{\pi}(\xi)$ at $K_s = 0$ and $\chi_{q K_s}^{\pi}(\xi)$ at $K_s > 0$, which are dependent on the internal coordinates ξ of

the nucleus, have the form [11]

$$\begin{aligned} \chi_{qn}^\pi(\xi) &= \frac{i(1-\pi)}{2\sqrt{2}}(\psi_{qn}(\xi) + \pi\hat{P}\psi_{qn}(\xi)); \quad (9) \\ \chi_{qK_s}^\pi(\xi) &= \frac{i(1-\pi)}{2\sqrt{2}}(\psi_{qK_s}(\xi) + \pi\hat{P}\psi_{qK_s}(\xi)), \end{aligned}$$

where \hat{P} is the operator of reflections of spatial coordinates, while the functions $\psi_{qn}(\xi)$ and $\psi_{qK_s}(\xi)$ are not pure in parity and correspond to a pearlike shape of the nucleus undergoing fission. We also have $\chi_{qK_s}^\pi(\xi) = T\chi_{qK_s}^\pi(\xi)$, where T is the time-inversion operator; the function $\chi_{qn}^\pi(\xi)$ is the eigenfunction of the operator T for the eigenvalue $n = (-1)^{J_s}$. After the scission of the nucleus undergoing fission into ternary-fission fragments, the fission-mode wave function $\Psi_{qK_s}^{J_s\pi M}$ goes over to the function $(\Psi_{qK_s}^{J_s\pi M})_{as}$, which, with allowance for a three-body character of ternary-fission channels [15, 16], can be represented as [7, 8]

$$(\Psi_{qK_s}^{J_s\pi M})_{as} = \sum_{\alpha} U_{\alpha}^{J_s\pi M} \frac{e^{i(k_c\rho - L_0\pi/2)}}{\rho^{5/2}} \sqrt{\frac{\Gamma_{qK_s\alpha}^{J_s\pi}}{\hbar v_c}}, \quad (10)$$

where $U_{\alpha}^{J_s\pi M}$ is a channel function that has the form

$$\begin{aligned} U_{\alpha}^{J_s\pi M} &= \{ \Psi_{\sigma_1 K_1}^{J_1\pi_1 M_1}(\omega, \xi_1) \{ \Psi_{\sigma_2 K_2}^{J_2\pi_2 M_2}(\omega, \xi_2) \\ &\times i^L Y_{LM_L}(\Omega_{\mathbf{R}}) \}_{j m_j} \}_{JM} Y_{l_0}(\theta_{\mathbf{r}, \mathbf{R}}) \frac{Y_{Ll\lambda}(\varepsilon)}{\sin \varepsilon \cos \varepsilon} \psi_3(\xi_3). \end{aligned} \quad (11)$$

In expression (11), the radius vectors \mathbf{r} and \mathbf{R} are defined as $\mathbf{R} = \mathbf{R}_1 - \mathbf{R}_2$ and $\mathbf{r} = \mathbf{R}_3 - (\mathbf{R}_1 A_1 + \mathbf{R}_2 A_2)/(A_1 + A_2)$, with \mathbf{R}_i and \mathbf{R}_3 being the coordinates of, respectively, the center of mass of the i th fission fragment and a third particle; $\psi_3(\xi_3)$ is the intrinsic wave function describing a third particle, for which we will take an alpha particle; the solid angle $\Omega_{\mathbf{R}}$ specifies the direction of the radius vector \mathbf{R} in the laboratory frame; and $\theta_{\mathbf{r}, \mathbf{R}}$ is the angle between the vectors \mathbf{r} and \mathbf{R} . The indices α, c , and β are defined as $\alpha = c\beta L l \lambda$, $c = \sigma_1 \pi_1 K_1 \sigma_2 \pi_2 K_2$, and $\beta = j J_1 J_2$. The functions $Y_{Ll\lambda}(\varepsilon)$ are expressed in terms of Jacobi polynomials [15, 16] and are used as a full basis in the space of angles ε ($0 \leq \varepsilon \leq \pi/2$). The angle ε and the radius ρ are related to the absolute values of the radius vectors \mathbf{r} and \mathbf{R} by the equations [15, 16]

$$R = \sqrt{\frac{M}{M_a}} \rho \sin \varepsilon; \quad r = \sqrt{\frac{M}{M_b}} \rho \cos \varepsilon, \quad (12)$$

where

$$\begin{aligned} M_a &= m \frac{A_1 A_2}{A_1 + A_2}, \quad M_b = \frac{(A_1 + A_2) A_3}{A} m, \\ M &= \sqrt{M_a M_b}. \end{aligned}$$

The angle ε specifies the asymptotic energy of the third particle (see [15, 16]), E_3 ; that is,

$$\varepsilon = \arccos \sqrt{x}, \quad (13)$$

where $x = E_3/E_3^m$. Here, E_3^m is the maximum energy of the third particle, $E_3^m = Q_c(A_1 + A_2)/A$, with Q_c being the total energy of the relative motion of ternary-fission fragments in the channel c . In expression (11), $\Psi_{\sigma_i K_i}^{J_i \pi_i M_i}(\omega, \xi_i)$ is the wave function for the i th axisymmetric fission fragment that does not have odd static deformation—in particular, octupole deformations—and which has a symmetry axis aligned with the symmetry axis of the nucleus undergoing fission. This function can be represented [11] in the form (8) upon replacing the indices $J_s q \pi K_s$ by the indices $J_i \sigma_i \pi_i K_i \xi_i$ and the intrinsic wave functions $\chi_{qK_s}^\pi$, $\chi_{qK_s}^\pi$, and χ_{qn}^π by the corresponding intrinsic wave functions $\chi_{\sigma_i K_i}^{\pi_i}$, $\chi_{\sigma_i K_i}^{\pi_i}$, and $\chi_{\sigma_i n_i}^{\pi_i}$ for fission fragments. Expression (10) involves the quantities $L_0 = L + l + 2\lambda + 3/2$, $k_c = \sqrt{2MQ_c}/\hbar$, and $v_c = \hbar k_c/M$; the amplitude of the partial width with respect ternary fission through the channel α has the form [8]

$$\sqrt{\Gamma_{qK_s\alpha}^{J_s\pi}} = \sqrt{2\pi} \sum_{\alpha'} \left\langle \frac{f_{\alpha'\alpha}^{J_s\pi-}(\rho)}{\rho^{5/2}} U_{\alpha'}^{J_s\pi M} |H| \Psi_{qK_s}^{J_s\pi M} \right\rangle, \quad (14)$$

where the radial function $f_{\alpha'\alpha}^{J_s\pi-}(\rho)$ is determined by solving a set of coupled radial equations with the boundary conditions introduced in [8]. By applying the Wigner transformation [11] in order to go over, in the function $Y_{LM_L}(\Omega_{\mathbf{R}})$, to the intrinsic coordinate frame of the fissile nucleus and taking into account the normalization of the channel function (11) to unity, we can recast (11) into an alternative form; that is,

$$\begin{aligned} U_{\alpha}^{J_s\pi M} &= \sqrt{\frac{(2J_1 + 1)(2J_2 + 1)}{16\pi^2(2j_1 + 1)}} \quad (15) \\ &\times \sum_{KK_j K_L} i^L \Psi_3(\xi_3) Y_{LK_L}(\Omega'_{\mathbf{R}}) Y_{l_0}(\theta_{\mathbf{r}, \mathbf{R}}) \left\{ D_{MK}^{J_s}(\omega) \right. \\ &\times \chi_{\sigma_1 K_1}^{\pi_1}(\xi_1) \chi_{\sigma_2 K_2}^{\pi_2}(\xi_2) C_{J_1 j K_1 K_j}^{J_s K} C_{J_2 L K_2 K_L}^{j K_j} \\ &+ (-1)^{J_1 + J_2 + K_1 + K_2} D_{M-K}^{J_s}(\omega) \chi_{\sigma_1 K_1}^{\pi_1}(\xi_1) \\ &\left. \times \chi_{\sigma_2 K_2}^{\pi_2}(\xi_2) C_{J_1 j - K_1 - K_j}^{J_s - K} C_{J_2 L - K_2 K_L}^{j - K_j} \right\} \frac{Y_{Ll\lambda}(\varepsilon)}{\sin \varepsilon \cos \varepsilon}, \end{aligned}$$

where $K, K_1, K_2 \geq 0$ and where the solid angle $\Omega'_{\mathbf{R}}$ specifies the direction of the radius vector \mathbf{R} in the intrinsic coordinate frame of a fissile nucleus. In expression (15), we have retained only one of the two possible terms [6, 7] for the case of $K = K_1 + K_2$.

For the $K_s > 0$ $J_s \pi q K_s$ fission mode associated with a pearlike shape of the nucleus undergoing fission, we further represent the intrinsic wave function $\chi_{qK_s}^\pi(\xi)$ (9) as an expansion of the form

$$\begin{aligned} \chi_{qK_s}^\pi(\xi) &= \sum_{cLl\lambda} \chi_{\sigma_1 K_1}^{\pi_1}(\xi_1) \chi_{\sigma_2 K_2}^{\pi_2}(\xi_2) \quad (16) \\ &\times Y_{l0}(\theta_{\mathbf{r}\mathbf{R}}) Y_{L0}(\Omega'_{\mathbf{R}}) \left(\frac{1 + \pi(-1)^L}{2} \right) \frac{1 + \pi_1 \pi_2}{2} \\ &\times \frac{Y_{Ll\lambda}(\varepsilon) a_{cLl\lambda}(\rho)}{\sin \varepsilon \cos \varepsilon \rho^{5/2}}, \end{aligned}$$

where it has been considered that, since the radius vector \mathbf{R} is directed, to a high degree of precision, along or against the symmetry axis of the nucleus undergoing fission [7, 8], the relative orbital angular momentum L of fission fragments is orthogonal to the symmetry axis of the nucleus, so that its projection K_L onto this axis is obviously equal to zero. In constructing formula (16), as well as in constructing formula (11), use was made of the fact that, because of the effect of superfluid nucleon–nucleon correlations, the most probable state of the alpha particle formed in the nucleus is that in which $l_i = 0$ ($K_{l_i} = 0$). Nonzero values of the orbital angular momentum l appear in expression (16) only owing to the effect of nonspherical terms in the potential V_α describing alpha-particle interaction with fission fragments. At small values of r , which are characteristic of the internal region of the fissile nucleus in the vicinity of its neck, where the alpha particle is formed, the angular dependence of these nonspherical terms involves only the angles $\theta_{\mathbf{r}\mathbf{R}}$ [8].

By employing the channel function (15), formula (8) with allowance for expansion (16), and the results presented in [8] on the angular distributions of fission fragments due to the mechanism of orientation of the spins and relative orbital angular momenta of fragments, we can represent the partial-fission-width amplitude (14) in the form

$$\begin{aligned} \sqrt{\Gamma_{qK_s\alpha}^{J_s\pi}} &= \sqrt{\frac{(2J_1 + 1)(2J_2 + 1)}{(2J_s + 1)(2j + 1)}} \quad (17) \\ &\times \delta_{K_s, K_1 + K_2} C_{J_1 j K_1 K_2}^{J_s K_s} C_{J_2 L K_2 0}^{j K_2} e^{i\delta_{qcl\lambda}} \sqrt{\Gamma_{qK_s c} b_L} \\ &\times \left(\frac{1 + (-1)^L \pi}{2} \right) \left(\frac{1 + \pi_1 \pi_2}{2} \right) d_{qcl\lambda}, \end{aligned}$$

where $\delta_{qcl\lambda}$ is the potential phase shift arising in the wave function that describes the scattering of fission products on each other; $\Gamma_{qK_s c}$ is a partial fission width that is independent of either the spin J_s or the parity π of the nucleus undergoing fission and which is defined as $\Gamma_{qK_s c} = \sum_{\beta l L \lambda} \Gamma_{qK_s c \beta l L \lambda}^{J_s \pi}$; $b_L = ((2L + 1)/\gamma)((L + 0.5)^4/\gamma^2) \exp[-(L + 0.5)^2/\gamma]$ with

$\gamma = 200$ [8], the relation $\sum_L b_L^2 = 1$ being satisfied; and $d_{qcl\lambda}$ are coefficients that appear in the angular-energy distribution of alpha particles and which satisfy the condition $\sum_{l\lambda} |d_{qcl\lambda}|^2 = 1$.

Substituting the amplitude in the form (17) and the channel function (15) into expression (10), using relation (13), and performing summation over the indices β with allowance for the adiabatic approximation (which is valid in the asymptotic region of the nucleus undergoing fission [6, 7]), we can reduce the function $(\Psi_{qK_s}^{J_s \pi M})_{as}$ (10) to the form

$$\begin{aligned} (\Psi_{qK_s}^{J_s \pi M})_{as} &= \sqrt{\frac{2J + 1}{16\pi^2}} \sum_c [D_{MK_s}^J(\omega) \quad (18) \\ &\times \chi_{\sigma_1 K_1}^{\pi_1}(\xi_1) \chi_{\sigma_2 K_2}^{\pi_2}(\xi_2) + (-1)^{J_s + K_s} D_{M-K_s}^J(\omega) \\ &\times \chi_{\sigma_1 K_1}^{\pi_1}(\xi_1) \chi_{\sigma_2 K_2}^{\pi_2}(\xi_2)] \psi_3(\xi_3) f(\Omega'_{\mathbf{R}}) Q_{qc}(\theta_{\mathbf{r}\mathbf{R}}, x) \\ &\times \sqrt{\Gamma_{qK_s c}} \frac{e^{ik_c \rho}}{\rho^{5/2} \sqrt{x(1-x)}}, \end{aligned}$$

where

$$f(\Omega'_{\mathbf{R}}) = \sum_L Y_{L0}(\Omega'_{\mathbf{R}}) b_L \left(\frac{1 + (-1)^L \pi}{2} \right); \quad (19)$$

$$\begin{aligned} Q_{qc}(\theta_{\mathbf{r}\mathbf{R}}, x) &= \sum_{l\lambda} d_{qcl\lambda} (-1)^\lambda Y_{l0}(\theta_{\mathbf{r}\mathbf{R}}) \quad (20) \\ &\times Y_{l\lambda}(\arccos \sqrt{x}) e^{i\delta_{qcl\lambda}}. \end{aligned}$$

Substituting expressions (7) and (18) into (5), we can calculate the asymptotic behavior of the effective wave function $A_{m_s}^{I\pi M_I}$. Introducing the multidimensional particle-flux-density operator \mathbf{j}_ρ in the direction of the radius vector ρ [15, 16] and integrating it with respect to the intrinsic coordinates ξ_1 , ξ_2 , and ξ_3 of ternary-fission products and with respect to the Euler angles ω , we can obtain the quantity $B^0(\Omega_{\mathbf{R}}, \Omega_{\mathbf{r}}, x)$ that is related to the triple-differential cross section $d^3\sigma/d\Omega_{\mathbf{R}} d\Omega_{\mathbf{r}} dx$ for (n, f) reactions induced by incident neutrons of wave vector k_n by the equation

$$\frac{d^3\sigma}{d\Omega_{\mathbf{R}} d\Omega_{\mathbf{r}} dx} = \frac{4\pi B^0(\Omega_{\mathbf{R}}, \Omega_{\mathbf{r}}, x)}{k_n^2 \sqrt{x(1-x)}} \quad (21)$$

and which is defined as

$$\begin{aligned} B^0(\Omega_{\mathbf{R}}, \Omega_{\mathbf{r}}, x) & \quad (22) \\ &= \sum_{s s' J_s J_s' q K_s} H_{qK_s}^{s J_s s' J_s'} B_{qK_s}^{s J_s s' J_s'}(\Omega_{\mathbf{R}}, \Omega_{\mathbf{r}}, x), \end{aligned}$$

where

$$H_{qK_s}^{s J_s s' J_s'} = \sum_t a_{K_s}^J a_{K_s}^{J'} b_{ts K_s}^{J_s \pi} b_{ts' K_s}^{J_s' \pi} c_{qt K_s}^{J_s \pi} c_{qt K_s}^{J_s' \pi}, \quad (23)$$

$$B_{qK_s}^{sJ_s s'J_{s'}}(\Omega_{\mathbf{R}}, \Omega_{\mathbf{r}}, x) \quad (24)$$

$$= \int d\omega D_{K_s}^{J_s J_{s'}}(\omega) \frac{\sqrt{(2J_s + 1)(2J_{s'} + 1)}}{16\pi^2}$$

$$\times |h_s^{J_s}||h_{s'}^{J_{s'}}| f^2(\Omega'_{\mathbf{R}}) \sum_c \Gamma_{qK_s c} f_{qc}^{sJ_s s'J_{s'}}(\theta_{\mathbf{r}, \mathbf{R}}, x),$$

$$D_{K_s}^{J_s J_{s'}}(\omega) = \sum_{M, M'} \rho^{J_s J_{s'}}(M, M') \quad (25)$$

$$\times [D_{MK_s}^{*J_s}(\omega) D_{M'K_s}^{J_{s'}}(\omega) + (-1)^{J_s + J_{s'} + 2K_s}$$

$$\times D_{M-K_s}^{*J_s}(\omega) D_{M'-K_s}^{J_{s'}}(\omega)],$$

$$f_{qc}^{sJ_s s'J_{s'}}(\theta_{\mathbf{r}, \mathbf{R}}, x) \quad (26)$$

$$= \sum_{\lambda \lambda' \lambda''} d_{qcl\lambda} d_{qc\lambda' \lambda''} (-1)^{\lambda + \lambda''} Y_{l0}(\theta_{\mathbf{r}, \mathbf{R}}) Y_{l'0}(\theta_{\mathbf{r}, \mathbf{R}})$$

$$\times Y_{l\lambda}(\arccos \sqrt{x}) Y_{l'\lambda'}(\arccos \sqrt{x})$$

$$\times \cos(\delta_{qcl\lambda} - \delta_{qc\lambda' \lambda''} + \delta_{sJ_s s'J_{s'}}),$$

with the phase shift $\delta_{sJ_s s'J_{s'}}$ being given by

$$(h_s^{J_s})^* h_{s'}^{J_{s'}} = |h_s^{J_s}||h_{s'}^{J_{s'}}| e^{i\delta_{sJ_s s'J_{s'}}}. \quad (27)$$

In performing integration with respect to ω in (24), one can make use of the phase-space element $d\omega$ in the form $d\omega = d\alpha d\xi_\beta d\gamma$, where $\xi_\beta = \cos \beta$, with the variables α , ξ_β , and γ changing within the intervals $0 \leq \alpha \leq 2\pi$, $-1 \leq \xi_\beta \leq 1$, and $0 \leq \gamma \leq 2\pi$, respectively. Expression (25) involves the spin density matrix $\rho^{J_s J_{s'}}(M, M')$ describing the nucleus undergoing fission and having, in general, off-diagonal elements in J_s and $J_{s'}$. It can be written in the form of the sum over the projections M_I, M'_I, m , and m' as

$$\rho^{J_s J_{s'}}(M, M') \quad (28)$$

$$= \sum_{M_I, M'_I, m, m'} C_{I\frac{1}{2}M_I m}^{J_s M} C_{I\frac{1}{2}M'_I m'}^{J_{s'} M'} \rho_{I\frac{1}{2}}(M_I, M'_I, m, m'),$$

where the spin density matrix $\rho_{I\frac{1}{2}}(M_I, M'_I, m, m')$ is the product of the spin density matrix for the unpolarized target nucleus and the spin density matrix for a polarized neutron whose polarization vector \mathbf{p}_n is aligned with the y axis:

$$\rho_{I\frac{1}{2}}(M_I, M'_I, m, m') \quad (29)$$

$$= \frac{1}{2(2I + 1)} \delta_{M_I, M'_I} [\delta_{m, m'} + p_n(\sigma_y)_{m, m'}].$$

The nuclear spin density matrix (28) can be recast into the form

$$\rho^{J_s J_{s'}}(M, M') = \frac{1}{2(2I + 1)} \delta_{M, M'} \delta_{J_s, J_{s'}} \quad (30)$$

$$+ \rho_\sigma^{J_s J_{s'}}(M, M'),$$

where the component $\rho_\sigma^{J_s J_{s'}}(M, M')$ associated with the polarization of the neutron is given by

$$\rho_\sigma^{J_s J_{s'}}(M, M') = \frac{ip_n}{2(2I + 1)} \quad (31)$$

$$\times \sqrt{\frac{(2J_{s'} + 1)}{3}} A(J_s, J_{s'}) (C_{J_s J_{s'} - MM'}^{11}$$

$$+ C_{J_s J_{s'} - MM'}^{1-1}) (-1)^{2J_s + J_{s'} - M - 1},$$

$$A(J_s, J_{s'}) = \delta_{J_s, J_{s'}} \quad (32)$$

$$\times \left(-\sqrt{\frac{J_s}{J_s + 1}} \delta_{J_s, J_{s'} <} + \sqrt{\frac{J_s + 1}{J_s}} \delta_{J_s, J_{s'} >} \right)$$

$$- \sqrt{\frac{2J_s + 1}{J_s}} \delta_{J_s, J_{s'} + 1} + \sqrt{\frac{2J_s + 1}{J_s}} \delta_{J_s, J_{s'} - 1}$$

with $J_{>} = I + 1/2$, $J_{<} = I - 1/2$. We choose the z axis of the laboratory frame to be aligned with the direction of the radius vector \mathbf{R} . Since the square of the function $f(\Omega'_{\mathbf{R}})$ defined in (19) is close to the Bohr limit because the quantity γ appearing in the definition of the coefficient b_L is large [8], it can be approximated, to a high degree of precision, by the sum of two delta functions as

$$f^2(\Omega'_{\mathbf{R}}) = \frac{1}{2} [\delta(\xi_\beta - 1) + \delta(\xi_\beta + 1)]. \quad (33)$$

In substituting expression (25) into (24) and in performing integration with respect to ξ_β with allowance for the properties of Wigner functions [11],

$$D_{MK}^J(\alpha, \beta, \gamma)|_{\beta=0} = D_{-MK}^J \quad (34)$$

$$\times (\alpha, \pi - \beta, \gamma)|_{\beta=0} (-1)^{J+M} = e^{iM\alpha} e^{iM\gamma} \delta_{M, K},$$

the bracketed term on the right-hand side of (25) reduces to a form that is diagonal in M and M' . But in this case, the spin nuclear-density-matrix component $\rho_\sigma^{J_s J_{s'}}(M, M')$ (31), which depends on the polarization of the neutron and which involves only elements that are off diagonal in the indices M and M' , makes no contribution to the the quantity in (25) and, hence, to the differential cross section (21) for (n, f) reactions. This cross section is then determined by the first term of the nuclear spin density matrix (30), this term being coincident with the nuclear spin density matrix for the case of unpolarized neutrons, and is given by

$$\frac{d^3\sigma_0}{d\Omega_{\mathbf{R}} d\Omega_{\mathbf{r}} dx} = \frac{4\pi B^0(\Omega_{\mathbf{R}}, \Omega_{\mathbf{r}}, x)}{k_n^2 \sqrt{x(1-x)}} \quad (35)$$

$$\times \frac{1}{k_n^2 \sqrt{x(1-x)}} \sum_{s s' J_s q K_s} H_{qK_s}^{sJ_s s'J_{s'}} |h_s^{J_s}||h_{s'}^{J_{s'}}|$$

$$\times \frac{(2J_s + 1)}{2(2I + 1)} \sum_c \Gamma_{qK_s c} f_{qc}^{sJ_s s'J_{s'}}(\theta_{\mathbf{r}}, x).$$

Experimental investigations of differential cross sections for the ternary fission of nuclei in reactions induced by unpolarized neutrons revealed [2] that the angular distributions of alpha particles undergo virtually no changes in response to variations in the alpha-particle energy E_α and depend on the ternary-fission-channel indices c only through the charge and mass asymmetry of fission fragments. At the same time, the energy distributions of alpha particles are virtually independent of either the channel index c or the type of low-energy ternary fission of nuclei. This means that the quantity $d_{qcl\lambda}$ in expression (20) can be approximated as $d_{qcl\lambda} = \bar{d}_{qcl}\bar{d}_{q\lambda}$ and that the potential phase shift $\delta_{qcl\lambda}$ can be treated as a quantity independent of λ . Under the condition that the vector \mathbf{R} is directed along the z axis of the laboratory frame, the quantity $Q_{qc}(\theta_{\mathbf{r}}, x)$ (20) can then be represented in the form

$$Q_{qc}(\theta_{\mathbf{r}}, x) = \tilde{Q}_{qc}(\theta_{\mathbf{r}})\bar{Q}_q(x), \quad (36)$$

where

$$\tilde{Q}_{qc}(\theta_{\mathbf{r}}) = \sum_l \bar{d}_{qcl} Y_{l0}(\theta_{\mathbf{r}}) e^{i\delta_{qcl}}; \quad (37)$$

$$\bar{Q}_q(x) = \sum_\lambda \bar{d}_{q\lambda} Y_\lambda(\arccos \sqrt{x}).$$

In this case, formula (35) for the differential cross section describing (n, f) reactions can be simplified considerably. If we assume that only one fission mode q takes part in the ternary-fission process strongly asymmetric in the masses and charges of fragments and disregard the interference between $s' \neq s$ resonances, integration of the differential cross section in (35) with respect to x yields the angular distribution $f_q(\theta_{\mathbf{r}})$ of alpha particles in the form

$$f_q(\theta_{\mathbf{r}}) \sim \sum_c \Gamma_{qK_s c} \left| \tilde{Q}_{qc}(\theta_{\mathbf{r}}) \right|^2 \equiv \sum_c \Gamma_{qK_s c} f_{qc}(\theta_{\mathbf{r}}). \quad (38)$$

In [7], the experimental angular distribution of alpha particles that was normalized to unity [2] was expanded in a series in spherical harmonics $Y_{L0}(\theta_{\mathbf{r}})$; as a result, the L -dependent coefficients in this expansion were found there and were then used in calculating the coefficients of P -odd and P -even asymmetries (see [9] and [10], respectively) in the ternary fission of nuclei. If one assumes that the potential phase shifts δ_{qcl} are almost completely determined by the potential of alpha-particle interaction with fission fragments and that they are independent of the orbital angular momentum l of the alpha particle, the coefficients \bar{d}_{qcl} can be reconstructed on the basis of the experimental angular distribution of alpha particles in the ternary fission of nuclei [2] and can further be

used to find the distribution of alpha particles with respect to the orbital angular momenta l [7]. In [17], it was found that the signs and the amplitudes of the coefficients \bar{d}_{qcl} found in [7] correlate with the properties of the dipole and the quadrupole component of the nonspherical Coulomb potential of alpha-particle interaction with ternary-fission fragments. The presence of these correlations seems to suggest that the phase shifts δ_{qcl} are independent of the orbital angular momentum l of the alpha particle involved.

In [5], Barabanov proposed employing nuclear spin-orbit interaction between alpha particles and ternary-fission fragments in order to explain the appearance of T -odd correlations of the form (1). Since spin-orbit interactions do not change the total spin J of the fissile system or its projections M and K onto, respectively, the z axis of the laboratory frame and the z' axis of the intrinsic coordinate frame, the property that the functions $D_{MK_s}^{*J_s}(\omega)D_{M'K_s}^{J_{s'}}(\omega)$ and $D_{M-K_s}^{*J_s}(\omega)D_{M'-K_s}^{J_{s'}}(\omega)$ appearing in (25) are diagonal in the indices M and M' immediately indicates, if the z axis is chosen to be aligned with the direction of light-fission-fragment emission and if relation (33) is used, that the spin-dependent component (31) of the nuclear spin density matrix—this component is nondiagonal in the indices M and M' —again makes no contribution to the cross section for (n, f) reactions induced by polarized neutrons. In view of this, a nonzero result for the T -odd correlation (2) in the ternary fission of nuclei cannot be obtained by taking into account spin-orbit forces.

3. CORIOLIS INTERACTION OF AN ALPHA PARTICLE WITH A FISSILE NUCLEUS: T -ODD CORRELATIONS IN CROSS SECTIONS FOR (n, f) REACTIONS

On the basis of an analysis of the mechanisms of ternary nuclear fission and of the structure of potentials used to describe the interaction of products originating from ternary nuclear fission, it was shown in [8] that the motion of the alpha particle in a system undergoing fission can be described as its motion in the field of an extending axisymmetric dumbbell formed by fission fragments whose symmetry axes are aligned, the entire fissile system rotating as a discrete unit. In order to describe a system whose fission is accompanied by the emission of an alpha particle, one can therefore employ the *particle plus rotor* model and introduce the Hamiltonian H_{Cor} describing the Coriolis interaction of the alpha particle with the fissile system. The specific form of this Hamiltonian is [11]

$$H_{\text{Cor}} = -\frac{\hbar^2}{2\mathcal{J}_0} (\hat{J}_+ \hat{I}_- + \hat{J}_- \hat{I}_+), \quad (39)$$

where the operators \hat{J}_\pm and \hat{l}_\pm are defined in the intrinsic coordinate frame of the fissile nucleus as

$$J_\pm = J_{x'} \pm iJ_{y'}; \quad \hat{l}_\pm = \hat{l}_{x'} \pm i\hat{l}_{y'},$$

their action on the function $D_{MK}^J(\omega)$ and the spherical harmonic $Y_{lK_l}(\Omega'_r)$ being given by the formulas

$$\hat{J}_\pm D_{MK}^J(\omega) \quad (40)$$

$$= [(J \pm K)(J \mp K + 1)]^{1/2} D_{M(K \mp 1)}^J(\omega);$$

$$\hat{l}_\pm Y_{lK_l}(\Omega'_r) = [(l \mp K_l)(l \pm K_l + 1)]^{1/2} Y_{l(K_l \pm 1)}(\Omega'_r).$$

As fission fragments move apart, the moment of inertia \mathcal{J}_0 of the system undergoing fission changes from the moment of inertia of the fissile nucleus in the precission configuration to the value $M_c R^2$ for $R \rightarrow \infty$, where M_c is the reduced mass of ternary-fission fragments in the channel c .

Since Coriolis interaction is rather weak, it can be taken into account in the first order of perturbation theory. To do this, it is necessary to replace the fissile nucleus Hamiltonian H by the operator H_{Cor} (39) in expression (14) for the partial-fission-width amplitude, which, in this case, is denoted by $\sqrt{(\Gamma_{qK_s\bar{\alpha}}^{J_s\pi})^{\text{Cor}}}$. Choosing the direction of the z axis in the laboratory frame to be aligned with the direction of light-fragment emission and using relations (33) and (34), we recast the function $Y_{l0}(\theta_{\mathbf{r},\mathbf{R}})$ appearing in expansion (16) into the form

$$Y_{l0}(\theta_{\mathbf{r},\mathbf{R}}) = \sqrt{\frac{4\pi}{2l+1}} \sum_{K_l} Y_{lK_l}(\Omega'_r) Y_{lK_l}^*(\Omega'_R) \quad (41)$$

$$= \sqrt{\frac{4\pi}{2l+1}} \sum_{K_l m_l} Y_{lK_l}(\Omega'_r) D_{m_l K_l}^l(\omega) Y_{l m_l}^*(\Omega_{\mathbf{R}})$$

$$= \sum_{K_l} Y_{lK_l}(\Omega'_r) D_{0K_l}^l(\omega) = Y_{l0}(\Omega'_r) D_{00}^l(\omega).$$

The quantity $\hbar^2/2\mathcal{J}_0$, which appears in the definition of the Hamiltonian H_{Cor} , changes only slightly in the vicinity of the point of scission into fission fragments. Taking into account the expansion in (16) and using relation (40), we can show that the application of the operator H_{Cor} (39) to the unperturbed fission-mode wave function $\Psi_{qK_s}^{J_s\pi M}$ (8) leads to the replacement of the functions $D_{M\pm K_s}^J(\omega) Y_{l0}(\Omega'_r)$ appearing in the definition of the function $\Psi_{qK_s}^{J_s\pi M}$ (8) by functions of the form

$$D_{M(\pm K_s+1)}^{J_s}(\omega) Y_{l1}(\Omega'_r) \quad (42)$$

$$\times \sqrt{l(l+1)(J_s \mp K_s)(J_s \pm K_s + 1)}$$

$$+ D_{M(\pm K_s-1)}^{J_s}(\omega) \times Y_{l-1}(\Omega'_r)$$

$$\sqrt{l(l+1)(J_s \pm K_s)(J_s \mp K_s + 1)}.$$

From the structure of formula (42), it follows that the application of the operator H_{Cor} (39) to the function $\Psi_{qK_s}^{J_s\pi M}$ (8) changes it significantly. In this function, the leading term corresponding to $l = 0$ disappears, while $l \neq 0$ terms become dominant.

If the Coriolis Hamiltonian (39) is used instead of H in expression (14) in order to obtain the partial-fission-width amplitude $\sqrt{(\Gamma_{qK_s\bar{\alpha}}^{J_s\pi})^{\text{Cor}}}$, the channel functions $U_{\alpha}^{J_s\pi M}$ (15) must be replaced by the new channel functions $U_{\bar{\alpha}}^{J_s\pi M}$. The functions $U_{\bar{\alpha}}^{J_s\pi M}$ take into account relation (41) and the character of the action of the Hamiltonian H_{Cor} on the fission-mode wave function $\Psi_{qK_s}^{J_s\pi M}$ [see Eq. (42)] and have the form (15) with the substitution of the index $\bar{\alpha} = \alpha m$, where $m = \pm 1$, for the index α and the functions $D_{M(\pm K+m)}^J(\omega) Y_{lm}(\Omega'_r) D_{00}^l(\omega)$ for the functions $D_{M(\pm K)}^J(\omega) Y_{l0}(\theta_{\mathbf{r},\mathbf{R}})$. Substituting the channel functions $U_{\bar{\alpha}}^{J_s\pi M}$ introduced in this way into formula (14) with the substitution of H_{Cor} (39) for H and taking into account the properties of the functions $(H_{\text{Cor}} \Psi_{qK_s}^{J_s\pi M})$ and relations of the form (33) and of the form (34), we can recast the partial-fission-width amplitude $\sqrt{(\Gamma_{qK_s\bar{\alpha}}^{J_s\pi})^{\text{Cor}}}$ into the form

$$\sqrt{(\Gamma_{qK_s\bar{\alpha}}^{J_s\pi})^{\text{Cor}}} = \sqrt{\frac{(2J_1+1)(2J_2+1)}{(2J_s+1)(2j+1)}} \quad (43)$$

$$\times \sqrt{\Gamma_{qK_s c}} \delta_{K_s, K_1+K_2} b_L \left(\frac{1+(-1)^L \pi}{2} \right)$$

$$\times \left(\frac{1+\pi\pi_1\pi_1}{2} \right) \bar{d}_{qcl}^{\text{Cor}} \bar{d}_{q\lambda}^{\text{Cor}} \sqrt{l(l+1)} e^{i\delta_{qcl}^{\text{Cor}}}$$

$$\times \{ (b_1(J_s, K_s) \delta_{m,1} + b_{-1}(J_s, K_s) \delta_{m,-1})$$

$$\times C_{J_1 j K_1 K_2}^{J_s K_s} C_{J_2 L K_2 0}^{j K_2} + (b_{-1}(J_s, K_s) \delta_{m,1}$$

$$+ b_1(J_s, K_s) \delta_{m,-1}) C_{J_1 j -K_1 -K_2}^{J_s -K_s} C_{J_2 L -K_2 0}^{j -K_2} \},$$

where

$$b_{\pm 1}(J_s, K_s) = \sqrt{(J_s \mp K_s)(J_s \pm K_s + 1)}; \quad (44)$$

$$\sum_{\lambda} (\bar{d}_{q\lambda}^{\text{Cor}})^2 = 1$$

and where the smallness associated with the Coriolis interaction is absorbed in the coefficient $\bar{d}_{qcl}^{\text{Cor}}$. Substituting the partial-width amplitude (43) and the channel function $U_{\bar{\alpha}}^{J_s\pi M}$ into expression (10) and performing summation over the indices β and m , we reduce

the asymptotic function $(\Psi_{qK_s}^{J_s\pi M})_{as}^{Cor}$ to the form

$$\begin{aligned}
 (\Psi_{qK_s}^{J_s\pi M})_{as}^{Cor} &= \sum_{cl} \sqrt{\frac{2J_s+1}{16\pi^2}} \delta_{K_s, K_1+K_2} \quad (45) \\
 &\times D_{00}^l(\omega) e^{i\delta_{qcl}^{Cor}} \sqrt{l(l+1)} \tilde{d}_{qcl}^{Cor} \{ \chi_{\sigma_1 K_1}^{\pi_1}(\xi_1) \chi_{\sigma_2 K_2}^{\pi_2}(\xi_2) \\
 &\quad \times (D_{M(K_s+1)}^{J_s}(\omega) Y_{l1}(\Omega'_{\mathbf{r}}) b_1(J_s, K_s) \\
 &\quad + D_{M(K_s-1)}^{J_s}(\omega) Y_{l-1}(\Omega'_{\mathbf{r}}) b_{-1}(J_s, K_s)) \\
 &\quad + (-1)^{J_s+K_s} \chi_{\sigma_1 K_1}^{\pi_1}(\xi_1) \chi_{\sigma_2 K_2}^{\pi_2}(\xi_2) (D_{M(-K_s+1)}^{J_s}(\omega) \\
 &\quad \times Y_{l1}(\Omega'_{\mathbf{r}}) b_{-1}(J_s, K_s) + D_{M(-K_s-1)}^{J_s}(\omega) Y_{l-1}(\Omega'_{\mathbf{r}}) \\
 &\quad \times b_1(J_s, K_s)) \} \psi_3(\xi_3) f(\Omega'_{\mathbf{R}}) \sqrt{\Gamma_{qK_sc}} \\
 &\quad \times \frac{e^{ik_c\rho}}{\rho^{5/2} \sqrt{x(1-x)}} \bar{Q}_q^{Cor}(x),
 \end{aligned}$$

where the quantity $\bar{Q}_q^{Cor}(x)$ is given by expression (37) with the substitution of $\bar{d}_{q\lambda}^{Cor}$ for $\bar{d}_{q\lambda}$. Adding the asymptotic function $(\Psi_{qK_s}^{J_s\pi M})_{as}^{Cor}$ (45) to the unperturbed asymptotic function $(\Psi_{qK_s}^{J_s\pi M})_{as}$ (18) (which was calculated previously), evaluating the multidimensional particle-flux density in the direction of the radius ρ [15, 16], and integrating this flux with respect to the variables ξ_1, ξ_2, ξ_3 , and ω , we can find the first-order correction in the Coriolis interaction to the differential cross section (21) for (n, f) reactions. This correction is given by the same formula, but, there, the quantity $B^0(\Omega_{\mathbf{R}}, \Omega_{\mathbf{r}}, x)$ must be replaced by the quantity $B^{Cor}(\Omega_{\mathbf{R}}, \Omega_{\mathbf{r}}, x)$ given by (22) when the quantity $B_{qK_s}^{sJ_s s' J'_s}(\Omega_{\mathbf{R}}, \Omega_{\mathbf{r}}, x)$ (24) is replaced by the quantity $(B_{qK_s}^{sJ_s s' J'_s}(\Omega_{\mathbf{R}}, \Omega_{\mathbf{r}}, x))^{Cor}$ having the form

$$\begin{aligned}
 &(B_{qK_s}^{sJ_s s' J'_s}(\Omega_{\mathbf{R}}, \Omega_{\mathbf{r}}, x))^{Cor} \quad (46) \\
 &= \int d\omega \frac{\sqrt{(2J_s+1)(2J_{s'}+1)}}{16\pi^2} \sum_{cl} \Gamma_{qK_sc} f^2(\Omega'_{\mathbf{R}}) \\
 &\times \bar{Q}_q(x) \bar{Q}_q^{Cor}(x) [e^{i\delta_{qcl}^{Cor}} \tilde{Q}_{qc}^*(\theta_{\mathbf{r}}) \tilde{D}_{K_sl}^{sJ_s s' J'_s}(\omega, \Omega'_{\mathbf{r}}) \\
 &\quad + e^{-i\delta_{qcl}^{Cor}} \tilde{Q}_{qc}(\theta_{\mathbf{r}}) \tilde{D}_{K_sl}^{(+sJ_s s' J'_s)}(\omega, \Omega'_{\mathbf{r}})],
 \end{aligned}$$

where

$$\begin{aligned}
 \tilde{D}_{K_sl}^{sJ_s s' J'_s}(\omega, \Omega'_{\mathbf{r}}) &= \sum_{MM'} \rho^{sJ_s s'}(M, M') \quad (47) \\
 &\times D_{00}^l(\omega) \sqrt{l(l+1)} \left\{ (h_{J_s}^{J_s})^* h_{J_{s'}}^{J_{s'}} \left[D_{MK_s}^{*J_s}(\omega) \right. \right. \\
 &\quad \times (D_{M'K_s+1}^{J_{s'}}(\omega) Y_{l1}(\Omega'_{\mathbf{r}}) b_1(J_{s'}, K_s) \\
 &\quad + D_{M'K_s-1}^{J_{s'}}(\omega) Y_{l-1}(\Omega'_{\mathbf{r}}) b_{-1}(J_{s'}, K_s)) \\
 &\quad \left. \left. + (-1)^{J_s+J_{s'}+2K_s} D_{M-K_s}^{*J_s}(\omega) (D_{M'(-K_s+1)}^{J_{s'}}(\omega) \right. \right.
 \end{aligned}$$

$$\begin{aligned}
 &\times Y_{l1}(\Omega'_{\mathbf{r}}) b_{-1}(J_{s'}, K_s) + D_{M'(-K_s+1)}^{J_{s'}}(\omega) \\
 &\quad \left. \left. \times Y_{l-1}(\Omega'_{\mathbf{r}}) b_1(J_{s'}, K_s) \right) \right\}.
 \end{aligned}$$

The function $D_{lK_s}^{(+sJ_s s' J'_s)}(\omega, \Omega'_{\mathbf{r}})$ is obtained from the function in (47) by taking the complex conjugate of the braced expression on the right-hand side of (47) and by interchanging the indices J_s and $J_{s'}$ (M and M') appearing in this expression. By using the theorem of multiplication of generalized spherical harmonics [11] and the representation of the spin component of the nuclear density matrix in the form (31) and performing summation over the indices M and M' , we can recast expression (47) into the form

$$\begin{aligned}
 \tilde{D}_{K_sl}^{sJ_s s' J'_s}(\omega, \Omega'_{\mathbf{r}}) &= ip_n \sqrt{\frac{2J_{s'}+1}{3}} \frac{\sqrt{l(l+1)}}{2(2I+1)} \quad (48) \\
 &\times A(J_s, J_{s'}) (-1)^{2J_s+J_{s'}-1-K_s} D_{00}^l(\omega) \left\{ [(D_{11}^1(\omega) \right. \\
 &\quad + D_{-11}^1(\omega)) C_{J_s J_{s'} - K_s (K_s+1)}^{11} b_1(J_{s'}, K_s) Y_{l1}(\Omega'_{\mathbf{r}}) \\
 &\quad + (D_{1-1}^1(\omega) + D_{-1-1}^1(\omega)) C_{J_s J_{s'} - K_s (K_s-1)}^{1-1} b_{-1} \\
 &\quad \times (J_{s'}, K_s) Y_{l-1}(\Omega'_{\mathbf{r}})] + (-1)^{J_s+J_{s'}+4K_s} [(D_{11}^1(\omega) \\
 &\quad + D_{-11}^1(\omega)) C_{J_s J_{s'} K_s (-K_s+1)}^{11} b_{-1}(J_{s'}, K_s) Y_{l1}(\Omega'_{\mathbf{r}}) \\
 &\quad + (D_{1-1}^1(\omega) + D_{-1-1}^1(\omega)) C_{J_s J_{s'} K_s (-K_s-1)}^{1-1} \\
 &\quad \left. \left. \times b_1(J_{s'}, K_s) Y_{l-1}(\Omega'_{\mathbf{r}}) \right] \right\}.
 \end{aligned}$$

Upon representing the Clebsch–Gordan coefficients appearing in (48) in the form [11]

$$C_{J_s J_{s'} K_s (-K_s \pm 1)}^{1 \pm 1} = C_{J_s J_{s'} - K_s (K_s \mp 1)}^{1 \mp 1} (-1)^{J_s+J_{s'}-1},$$

the phase factor $(-1)^{J_s+J_{s'}+4K_s}$ in front of the second term in the braced expression on the right-hand side of (48) reduces to the phase factor $(-1)^{2J_s+2J_{s'}+4K_s-1} \equiv -1$. We further replace, in (48), the spherical harmonic $Y_{l\pm 1}(\Omega'_{\mathbf{r}})$ by its representation that arises in the laboratory frame owing to the Wigner transformation [11]. Substituting, into (46), the formula obtained in this case for $\tilde{D}_{K_sl}^{sJ_s s' J'_s}(\omega, \Omega'_{\mathbf{r}})$ and the analogous formula for $\tilde{D}_{K_sl}^{(+sJ_s s' J'_s)}(\omega, \Omega'_{\mathbf{r}})$; performing integration with respect to ω for the case where the z axis of the laboratory frame is chosen to be aligned with the vector \mathbf{R} ; and taking into account the structure of the function $f^2(\Omega'_{\mathbf{R}})$ (33) and of relation (34), we can recast the function $B^{Cor}(\Omega_{\mathbf{R}}, \Omega_{\mathbf{r}}, x)$ into the form

$$B^{Cor}(\Omega_{\mathbf{R}}, \Omega_{\mathbf{r}}, x) = \frac{pn\sqrt{3/2\pi}}{4\pi(2I+1)} \quad (49)$$

$$\times \sum_{sJ_s s' J'_s qK_sc} \Gamma_{qK_sc} H_{qK_s}^{sJ_s s' J'_s} f_{qK_sc}^{sJ_s s' J'_s}(\Omega_{\mathbf{r}}, x),$$

where, for the function $f_{qK_s c}^{sJ_s s'J_{s'}}(\Omega_{\mathbf{r}}, x)$, we have

$$f_{qK_s c}^{sJ_s s'J_{s'}}(\Omega_{\mathbf{r}}, x) = \sqrt{(2J_s + 1)(2J_{s'} + 1)} \quad (50)$$

$$\times |h_{s'}^{J_{s'}}| |h_{s'}^{J_{s'}}| F_{K_s}^{J_s J_{s'}}(x) \tilde{f}_{qc}^{sJ_s s'J_{s'}}(\theta_{\mathbf{r}}) \bar{Q}_q(x) \bar{Q}_q^{\text{Cor}}(x),$$

with

$$\tilde{f}_{qc}^{sJ_s s'J_{s'}}(\theta_{\mathbf{r}}) = \sum_{l'} \tilde{d}_{qcl} \tilde{d}_{qcl'}^{\text{Cor}} Y_{l0}(\theta_{\mathbf{r}}) \quad (51)$$

$$\times \sqrt{l'(l'+1)} [Y_{l'-1}(\theta_{\mathbf{r}}) - Y_{l'+1}(\theta_{\mathbf{r}})]$$

$$\times \sin(\delta_{qcl'}^{\text{Cor}} - \delta_{qcl} + \delta_{sJ_s s'J_{s'}});$$

$$F_{K_s}^{J_s J_{s'}} = \sqrt{\frac{2J_{s'} + 1}{3}} A(J_s, J_{s'}) \quad (52)$$

$$\times [C_{J_s J_{s'} - K_s (K_s - 1)}^{1-1} b_{-1}(J_{s'}, K_s)$$

$$- C_{J_s J_{s'} - K_s (K_s + 1)}^{11} b_1(J_{s'}, K_s)] (-1)^{J_{s'} + K_s - 1}.$$

Formula (52) is valid in the case of $K_s > 0$. At $K_s = 0$, the fission widths of the $J_s = I + 1/2$ and

$J_{s'} = I - 1/2$ neutron resonances that are pure in parity π do not interfere since the intrinsic fission-mode wave functions $\chi_{q_n}^{\pi}$ (8) differing in eigenvalue $n = (-1)^{J_s}$ correspond to them. At $K_s = 0$, the function $F_{K_s}^{J_s J_{s'}}$ (52) is therefore replaced by the function $\bar{F}_0^{J_s J_{s'}}$ having the form

$$\bar{F}_0^{J_s J_{s'}} = \delta_{J_s, J_{s'}} \sqrt{\frac{2J_s + 1}{3}} A(J_s, J_s) \quad (53)$$

$$\times \sqrt{J_s(J_s + 1)} (-1)^{J_s - 1} C_{J_s J_s 0 - 1}^{1-1}.$$

At $J_s = 0$, the function $\bar{F}_0^{J_s J_{s'}}$ vanishes, so that neutron resonances of spin $J_s = 0$ do not contribute to the function $B^{\text{Cor}}(\Omega_{\mathbf{R}}, \Omega_{\mathbf{r}}, x)$ (49) and, hence, to the T -odd asymmetry coefficient (3), which can be represented as

$$D_{\alpha}(\Omega_{\mathbf{R}}, x) = \frac{B^{\text{Cor}(+)}(\Omega_{\mathbf{R}}, \Omega_{\mathbf{r}}, x) - B^{\text{Cor}(-)}(\Omega_{\mathbf{R}}, \Omega_{\mathbf{r}}, x)}{2B^0(\Omega_{\mathbf{R}}, \Omega_{\mathbf{r}}, x)} \Big|_{\theta_{\mathbf{R}} = \varphi_{\mathbf{R}} = 0}, \quad (54)$$

where the quantities $B^{\text{Cor}(\pm)}(\Omega_{\mathbf{R}}, \Omega_{\mathbf{r}}, x)$ are given by expression (49), in which the $J_s = J_{s'} = 0$ terms are eliminated from the sums over J_s and $J_{s'}$, these two quantities differing by the inversion of the neutron-polarization vector \mathbf{p}_n , whereupon the sign of the coefficient of the neutron polarization p_n is reversed; the quantity $B^0(\Omega_{\mathbf{R}}, \Omega_{\mathbf{r}}, x)$ is defined by Eq. (35). If we now use, for spherical harmonics, the formula [18]

$$Y_{l-1}(\Omega_{\mathbf{r}}) - Y_{l+1}(\Omega_{\mathbf{r}}) = \frac{\cos \varphi_{\mathbf{r}}}{\sin \theta_{\mathbf{r}}}$$

$$\times \sqrt{\frac{l(l+1)}{\pi(2l+1)}} (P_{l-1}(\cos \theta_{\mathbf{r}}) - P_{l+1}(\cos \theta_{\mathbf{r}})),$$

where $P_{l\pm 1}(\cos \theta_{\mathbf{r}})$ are Legendre polynomials, the functions $\tilde{f}_{qc}^{sJ_s s'J_{s'}}(\theta_{\mathbf{r}})$ (51) can be represented in the form

$$\tilde{f}_{qc}^{sJ_s s'J_{s'}}(\theta_{\mathbf{r}}) = \cos \varphi_{\mathbf{r}} \sum_{l'} \tilde{d}_{qcl} \tilde{d}_{qcl'}^{\text{Cor}} Y_{l0}(\theta_{\mathbf{r}}) \quad (55)$$

$$\times \frac{\sqrt{l'(l'+1)}}{\sin \theta_{\mathbf{r}}} (P_{l'-1}(\cos \theta_{\mathbf{r}}) - P_{l'+1}(\cos \theta_{\mathbf{r}}))$$

$$\times \sqrt{\frac{l'(l'+1)}{\pi(2l'+1)}} \sin(\delta_{qcl'}^{\text{Cor}} - \delta_{qcl} + \delta_{sJ_s s'J_{s'}}).$$

The quantity $B^{\text{Cor}}(\Omega_{\mathbf{R}}, \Omega_{\mathbf{r}}, x)$ (49), which appears in the definition of the T -odd-asymmetry coeffi-

cient (54), possesses properties that are consistent with the symmetry properties of the experimentally investigated correlation given by Eqs. (1) and (2). Indeed, the quantity in (49), as well as the correlation specified in Eqs. (1) and (2), changes sign upon the inversion of the neutron-polarization vector. In just the same way as the correlation in (2), the quantity in (49) is proportional to $\cos \varphi_{\mathbf{r}}$ —that is, it is maximal in absolute value when the unit vector $\mathbf{e}_3 = \mathbf{r}/r$ specifying the direction of alpha-particle emission lies in the (x, z) plane at $\varphi_{\mathbf{r}} = 0$ and vanishes at $\varphi_{\mathbf{r}} = \pi/2$, in which case the vector \mathbf{e}_3 is parallel to the neutron-polarization vector. If alpha particles are recorded in the direction of the x axis, in which case $\varphi_{\mathbf{r}} = 0$ and $\theta_{\mathbf{r}} = \pi/2$, the spherical harmonic $Y_{l0}(\theta_{\mathbf{r}})$ and the Legendre polynomial differences $[P_{l-1}(\cos \theta_{\mathbf{r}}) - P_{l+1}(\cos \theta_{\mathbf{r}})]$, which appear in expression (55), do not vanish, in this case, only at, respectively, even and odd values of the orbital angular momentum l of alpha particles. If the direction of light-fragment emission is reversed, in which case the unit vector $\mathbf{e}_{\text{LF}} = \mathbf{R}/R$ becomes antiparallel to the z axis of the laboratory frame, there arises, in expression (41), the additional factor $(-1)^l$, which leads to the emergence of corresponding factors in the sums over l and l' in (26) and (55). It follows that, upon the inversion of the vector \mathbf{e}_{LF} , the function in (26), which includes even values of l , does not change sign, while the function

in (55), which includes odd values of l , changes sign, with the result that the quantity $B^{\text{Cor}}(\Omega_{\mathbf{R}}, \Omega_{\mathbf{r}}, x)$ (49) also changes sign, and so does the T -odd-asymmetry coefficient (54) together with it, in accordance with the properties of the correlation coefficient specified by Eqs. (1) and (2).

In order to estimate the T -odd-asymmetry coefficient (54), it is necessary to compare the partial-fission-width amplitude $\sqrt{(\Gamma_{qK_s\bar{\alpha}}^{J_s\pi})^{\text{Cor}}}$ (43), which is perturbed by Coriolis interaction, with the unperturbed fission-width-amplitude $\sqrt{\Gamma_{qK_s\alpha}^{J_s\pi}}$ (17). As follows from (14), these amplitudes differ by the substitution of the Coriolis interaction Hamiltonian H_{Cor} (39) for the total fissile-nucleus Hamiltonian H and by the use of the corresponding channel functions. The modulus of the wave function $\Psi_{qK_s}^{J_s\pi M}$ (8) for the fission mode corresponding to a compact shape of a fissile nucleus whose radius depends on angles decreases exponentially beyond this radius [6, 7]. The modulus of the wave function for the potential scattering of fission fragments on each other, this wave function being orthogonal to shell wave functions that form a basis for constructing wave functions describing prescission configurations, begins to decrease exponentially as one moves to the internal region of the fissile nucleus. Therefore, the main contribution to the partial-fission-width amplitude (14) comes from R and r values in the vicinity of the region where the fissile nucleus breaks up into fission fragments [6, 7]—that is, at $R \approx R_m$ and $r \approx r_0$. The quantity R_m was estimated in [8] for an $A \approx 240$ compound nucleus as $R_m \approx 17$ fm, while the value of $r_0 \approx 2$ fm corresponds to the radius of the neck of the prescission configuration of the fissile nucleus. In this region, the quantity $\hbar^2/2\mathcal{J}_0$, which appears in the definition (39) of the Coriolis interaction Hamiltonian, can be estimated at 10^{-3} MeV if, for the moment of inertia \mathcal{J}_0 of the fissile nucleus, use is made of the formula $\mathcal{J}_0 \approx M_c R_m^2 \approx 60mR_m^2$, where M_c is the reduced mass of fragments originating from the fission of an $A \approx 240$ nucleus.

If Coriolis interaction is not taken into account, the angular distribution of alpha particles in the ternary fission of nuclei is determined by the potential that describes the interaction of alpha particles with fission fragments and which enters into the total fissile-nucleus Hamiltonian H appearing in expression (14). This potential makes a dominant contribution to the partial-width amplitude (14) through its values in the region where the Coulomb barrier for the emitted alpha particle is formed and where the nuclear potential of alpha-particle interaction with fission fragments is already negligible.

In order to determine the total potential describing alpha-particle interaction with fission fragments and determining the partial-width amplitude (17), one can therefore use formula for the Coulomb potential V_α^{C} of alpha-particle interaction with fission fragments in the region of Coulomb barrier formation, where $r \ll R$. In this region, the Coulomb potential V_α^{C} was investigated in [8, 15] and can be represented in the form

$$V_\alpha^{\text{C}} = \frac{2(Z-2)e^2}{R} + \frac{8(Z-2)e^2}{R} \left(\frac{r}{R}\right) \quad (56)$$

$$\times \left(\frac{\Delta Z}{Z-2} + \frac{2\Delta A}{A-4}\right) P_1(\cos \theta_{\mathbf{r}, \mathbf{R}})$$

$$+ \frac{16e^2(Z-2)}{R} \left(\frac{r}{R}\right)^2 P_2(\cos \theta_{\mathbf{r}, \mathbf{R}}),$$

where $\Delta Z = Z_1 - Z_2$ and $\Delta A = A_1 - A_2$ are, respectively, the charge and the mass asymmetry of fission fragments. The first term in the potential (56) is independent of the coordinate r and has no effect on the motion of the alpha particle. At the same time, the second and the third term in the potential (56) act on the alpha particle emitted in ternary fission as focusing potentials. The third, quadrupole, term forms the angular distribution of alpha particles that is characterized by a maximum at an angle of 90° with respect to the direction of fission-fragment emission and by a half-width of about 10° . As soon as there appear noticeable charge and mass asymmetries of fission fragments, the second (dipole) term of the potential (56) comes into play, deflecting, against the background of the third term, the maximum of the angular distribution of alpha particles toward an angle of 83° with respect to the direction of light-fragment emission in the (n, f) reaction on a ^{233}U target nucleus. In order to assess the scale of the effect of Coriolis interaction, it is therefore natural to compare $\hbar^2/2\mathcal{J}_0$ with the second and the third term of the Coulomb potential (56) in the region where the Coulomb potential for the alpha particle is formed. Using the value of 92 for Z , the estimate according to which $\Delta Z/Z$ and $\Delta A/A$ do not exceed ≤ 0.2 , and the values r_0 and R_m for r and R and replacing the Legendre polynomials $P_1(\cos \theta_{\mathbf{r}, \mathbf{R}})$ and $P_2(\cos \theta_{\mathbf{r}, \mathbf{R}})$ in (56) by their maximum values of (± 1) , one can estimate the absolute values of the second and the third term in the potential (56) as ≤ 4 and ≤ 1.7 MeV, whence it follows that the dipole term in the potential (56) considerably exceeds the quadrupole term in absolute value. Under the effect of the dipole term, the $l = 1$ harmonic will be predominantly added, in the internal region of a fissile nucleus, to the leading ($l = 0$) harmonic of the α -particle wave function. If it is considered that the matrix element $\langle Y_{10} | P_1 | Y_{00} \rangle$,

which corresponds to the transition of the alpha particle from the $l = 0$ state to the $l = 1$ state, is equal to $1/\sqrt{3}$, the value of $1/\sqrt{3}$ can be used to estimate the averaged Legendre polynomial $P_1(\cos \theta_{\mathbf{r}, \mathbf{R}})$ in the dipole term of the potential (56). In this case, the absolute value of the dipole term in the potential (56) can be estimated at a value not greater than 2.3 MeV. For the ratio of the quantity $\hbar^2/2\mathcal{J}_0$ to the dipole term in the potential (56), we then obtain an estimate not falling below 0.5×10^{-3} , and this is in qualitative agreement with the scale of the experimental values of the asymmetry coefficients in (4).

As can be seen from expression (55), two cases are possible for the source of a T -odd correlation of the type in Eqs. (1) and (2) and for the dependence of the T -odd asymmetry coefficient (3) on the alpha-particle emission angle $\theta_{\mathbf{r}}$.

The first case is realized if the potential phase shifts δ_{qcl} and $\delta_{qcl}^{\text{Cor}}$ change noticeably in response to variations in the orbital angular momentum l of the alpha particle, with the result that the phase-shift differences $(\delta_{qcl} - \delta_{qcl}^{\text{Cor}})$ are not small in relation to unity for some values of l and l' . The angular distribution $\tilde{f}_{qc}^{sJ_s s'J_{s'}}(\theta_{\mathbf{r}})$ (55) of alpha particles will then be significantly different from zero even in the case where only the $s' = s$ and $J_{s'} = J_s$ terms, for which the phase shift $\delta_{sJ_s s'J_{s'}}$ vanishes, are taken into account in the sum over $sJ_s s'J_{s'}$ in (49). This means that the emergence of a T -odd asymmetry in the angular distributions of ternary-fission fragments is possible if only one s -wave neutron resonance characterized by a specific spin value J_s plays a dominant role in some region of energy of neutrons inducing (n, f) reactions. In this case, however, there arises the problem of describing the structure of the $\theta_{\mathbf{r}}$ dependence of the asymmetry coefficient $D_{\alpha}(\Omega_{\mathbf{r}}, x)$ (54). Indeed, the angular distribution (55) at $\varphi_{\mathbf{r}} = 0$ —it controls the $\theta_{\mathbf{r}}$ dependence of the numerator on the right-hand side of (54)—is formed by the interference between the amplitude of the angular distribution of alpha particles that is unperturbed by Coriolis interaction and the amplitude for the analogous distribution perturbed by this interaction. At the same

time, the angular distribution $f_q(\theta_{\mathbf{r}})$ (38) of alpha particles from (n, f) reactions induced by unpolarized neutrons, which determines the $\theta_{\mathbf{r}}$ dependence of the denominator on the right-hand side of (54), can be reduced, upon taking into account the interference of $s \neq s'$ resonances, to the form

$$f_{qc}^{sJ_s s'J_{s'}}(\theta_{\mathbf{r}}) = \sum_{ll'} \tilde{d}_{qcl} \tilde{d}_{qcl'} Y_{l0}(\theta_{\mathbf{r}}) Y_{l'0}(\theta_{\mathbf{r}'}) \times \cos(\delta_{qcl} - \delta_{qcl'} + \delta_{sJ_s s'J_{s'}}). \quad (57)$$

As follows from experimental data reported in [1], the $\theta_{\mathbf{r}}$ dependence of the coefficient D_{α} (3) is rather weak. This means that the angular dependences of the functions in (55) and (57) must be close. But at first glance, this result seems improbable because the functions in (55) and (57) are strongly different in view of the dependence on the phase shifts and on the orbital angular momenta.

The second case corresponds to the situation where the potential phase shifts δ_{qcl} and $\delta_{qcl}^{\text{Cor}}$ are determined primarily by the Coulomb potential and are weakly dependent on the orbital angular momentum l of the alpha particle: $\delta_{qcl} = \delta_{qc}$; $\delta_{qcl}^{\text{Cor}} = \delta_{qc}^{\text{Cor}}$. The investigation that was performed in [17] furnishes some indications of the occurrence of such a situation in the ternary fission of nuclei. In this case, the functions in (55) and (57) can be represented in the form

$$\begin{aligned} \tilde{f}_{qc}^{sJ_s s'J_{s'}}(\theta_{\mathbf{r}}) &= \cos \varphi_{\mathbf{r}} \sin(\delta_{qc}^{\text{Cor}} - \delta_{qc}) + \delta_{sJ_s s'J_{s'}} \sum_l \tilde{d}_{qcl} Y_{l0}(\theta_{\mathbf{r}}) \sum_l \tilde{d}_{qcl}^{\text{Cor}} \\ &\times \frac{1}{\sin \theta_{\mathbf{r}}} (P_{l-1}(\cos \theta_{\mathbf{r}}) - P_{l+1}(\cos \theta_{\mathbf{r}})) \frac{l(l+1)}{\sqrt{\pi(2l+1)}}; \\ f_{qc}^{sJ_s s'J_{s'}}(\theta_{\mathbf{r}}) &= \cos(\delta_{sJ_s s'J_{s'}}) \left(\sum_l \tilde{d}_{qcl} Y_{l0}(\theta_{\mathbf{r}}) \right)^2. \end{aligned} \quad (58)$$

At $\varphi_{\mathbf{r}} = 0$, the angular dependence of the asymmetry coefficient (54) then assumes the form

$$D_{\alpha}(\theta_{\mathbf{r}}) \sim \frac{\sum_l \tilde{d}_{qcl}^{\text{Cor}} (P_{l-1}(\cos \theta_{\mathbf{r}}) - P_{l+1}(\cos \theta_{\mathbf{r}})) l(l+1) / (\sqrt{\pi(2l+1)} \sin \theta_{\mathbf{r}})}{\sum_l \tilde{d}_{qcl} P_l(\cos \theta_{\mathbf{r}}) \sqrt{2l+1} / 4\pi}. \quad (60)$$

Since the phase shifts δ_{qc} and δ_{qc}^{Cor} , which are independent of the orbital angular momentum of the alpha particle, are related to the wave functions describing the potential scattering of alpha particles on

fission fragments and appearing in the partial-width amplitude (14) and are determined primarily by the Coulomb potential of alpha-particle interaction with fission fragments, we can expect that these phase

shifts have rather close values. But it then follows from expression (58) that T -odd correlations of the type in Eqs. (1) and (2) can arise only because of the interference between the fission amplitudes for s -wave neutron resonances differing by their energies and total widths and, in general, by their spin values. This situation is similar to the situation around P -even right–left correlations in binary and ternary fission of nuclei [10, 14]; since these correlations are T -odd, their emergence may only be due to the interference between the fission amplitudes for s - and p -wave neutron resonances.

It was indicated above that, if alpha particles are recorded in the direction of the x axis (at $\varphi_{\mathbf{r}} = 0$ and $\theta_{\mathbf{r}} = \pi/2$), the only nonzero terms in the numerator and the denominator of the expression on the right-hand side of (60) are characterized by, respectively, odd l [because of the properties of the spherical harmonics $Y_{l\pm 1}(\Omega_{\mathbf{r}})$] and even l [because of the properties of the spherical harmonics $Y_{l0}(\Omega_{\mathbf{r}})$]. This result is due, on one hand, to the fact that, in the region of the neck of the prescission configuration of the fissile nucleus, where the product alpha particle is formed, the leading orbital angular momenta of the alpha particle are, as was indicated above, $l = 0$ (in the absence of Coriolis interaction) and $l = 1$ (in the case where Coriolis interaction is taken into account). On the other hand, the nonspherical Coulomb potential (56), which determines predominantly the structure of the function describing the potential scattering of fission fragments, adds, to the orbital angular momenta $l = 0$ and $l = 1$ of the alpha particle, which are leading in the internal region of the fissile nucleus, even orbital angular momenta owing to the quadrupole term in the potential (56) and odd orbital angular momenta owing to the dipole term there. In the semiclassical approximation, which underlies calculations based on the method of trajectories [2], the above effect of the nonspherical Coulomb potential reduces to focusing alpha particles emitted in ternary fission, the direction of this focusing being approximately orthogonal to the direction along which fission fragments move apart, with a slight shift toward a light fragment because of the effect of the dipole term in the potential (56). Focusing of this type is present in the corresponding quantum-mechanical pattern as well. Since the physical origin of this focusing remains unchanged upon going over from the unperturbed alpha-particle wave function in the prescission configuration of a fissile nucleus to that perturbed by Coriolis interaction, one can expect that the amplitude of the angular distribution of alpha particles in the numerator of the expression on the right-hand side of (60) will have features similar to those of the analogous amplitude that is unperturbed by Coriolis interaction and which appears in the denominator of the same expression.

The T -odd-asymmetry coefficient (60) will then be weakly dependent on the angle $\theta_{\mathbf{r}}$, and this is consistent with its experimental properties [1].

As was indicated above, the emergence of odd orbital angular momenta l of the alpha particle in the numerator of the expression on the right-hand side of (60) is entirely due to the dipole term that, because of the charge and mass asymmetry of ternary-fission fragments, appears in the Coulomb potential (56) of alpha-particle interaction with these fragments. The T -odd-asymmetry coefficient (60) will therefore tend to zero upon going over to symmetric fission modes. This means that the T -odd asymmetries (60), as well as P -odd and P -even asymmetries previously investigated in [9, 10] for alpha particles in the ternary fission of nuclei, are entirely due to the presence of charge and mass asymmetries of fission fragments.

For the coefficient defined as in (3), experimental investigations of the T -odd asymmetry for ^{239}Pu target nuclei led to a value [1] that is much less than the analogous coefficients in (4) for ^{233}U and ^{235}U target nuclei and which is insignificant against statistical errors. The following circumstance can be responsible for the smaller value of the coefficient D_{α} (3) for ^{239}Pu . Since the spin I of a ^{239}Pu target is equal to $1/2$, the s -wave neutron resonances of the compound nucleus that are excited upon the capture of a cold neutron can have spin values of both $J_s = 0$ and $J_s = 1$. It was indicated above that neutron resonances of spin $J_s = 0$ do not contribute to the coefficient D_{α} (60) and that the formation of this coefficient is due exclusively to the interference between the fission amplitudes for neutron resonances s and s' of identical spins $J_s = J_{s'} = 1$. In this respect, the case of ^{239}Pu differs from the cases of ^{233}U ($I = 5/2$) and ^{235}U ($I = 7/2$) target nuclei, for which the set of neutron resonances s and s' involved in the formation of the coefficient in (60) is much wider—specifically, these are resonances of spin $J_s = J_{s'} = I + 1/2 \neq 0$ and $J_s = J_{s'} = I - 1/2 \neq 0$ for $J_s \neq J_{s'}$.

According to expressions (49) and (50), the dependence of the T -odd-asymmetry coefficient (60) on the asymptotic energy E_{α} of the alpha particle emitted in ternary fission is given by

$$D_{\alpha}(x) \sim \frac{\bar{Q}_q^{\text{Cor}}(x)}{\bar{Q}_q(x)}, \quad (61)$$

where the functions $\bar{Q}_q^{\text{Cor}}(x)$ and $\bar{Q}_q(x)$ (37) specify the amplitudes of the energy distributions of alpha particles for, respectively, the case of ternary fission perturbed by Coriolis interaction and the case of unperturbed ternary fission. From experimental data reported in [2], it follows that, in the case of nuclear fission induced by unpolarized neutrons, the

square of the amplitude of the energy distribution of alpha particles, $[\bar{Q}_q(x)]^2$, has a broad maximum at an alpha-particle energy of $E_\alpha^0 \approx 16$ MeV, the width of this maximum being $\Delta E_\alpha^0 \approx 10$ MeV. An experimental investigation of the energy dependence of the asymmetry coefficient $D_\alpha(x)$ (3) revealed [1] that this coefficient grows considerably with increasing E_α . This means that the amplitude $\bar{Q}_q^{\text{Cor}}(x)$ of the energy distribution perturbed by Coriolis interaction reproduces the amplitude $\bar{Q}_q(x)$ of the unperturbed angular distribution involving a broad maximum at $E_\alpha^0 \approx 16$ MeV, the former differing from the latter by a coefficient that grows with increasing alpha-particle energy.

For a first approximation, the origin of the dependence of the T -odd-asymmetry coefficient $D_\alpha(E_\alpha)$ (60) on the alpha-particle energy E_α can be related to the features of the dipole term that is present in the Coulomb potential (56) and which is responsible for the emergence of odd orbital angular momenta of the alpha particle, which specify the structure of the numerator of the expression on the right-hand side of (60). The experimental energy distribution of alpha particles in the ternary fission of nuclei [2] indicates that the characteristic energies E_α are much less than the maximum possible energy E_α^m , which is close [see expression (13) and the text that follows it] to the total energy Q_c of the motion of fission fragments in the channel c (about 140 MeV). This means that typical values of $x = E_\alpha/E_\alpha^m$ are so small that the characteristic angles ε in (13) do not deviate from $\pi/2$ strongly. In this case, the quantity R in (12) is proportional to the product $\rho \sin \varepsilon$, which changes only slightly over the entire range of experimentally observed α -particle energies; therefore, it can be replaced by ρ . As to the quantity r in (12), it is proportional to the quantity $\rho \cos \varepsilon$, which is equal to $\rho \sqrt{x}$ [see Eq. (13)]. The dipole term that appears in the potential (56) and which is proportional to r/R^2 will then grow as $\sqrt{x}/\rho \sim \sqrt{E_\alpha}$ with increasing alpha-particle energy. If we assume that the coefficient $D_\alpha(E_\alpha)$ (60) is proportional to the dipole term in the potential (56), this coefficient will vary with alpha-particle energy in proportion to $\sqrt{E_\alpha}$. Thus, even a preliminary rough estimation correctly reflects the experimental trend toward the growth of the effect with increasing E_α .

The theory developed in the present study makes it possible to calculate the energy distributions of alpha particles both for the case of an unperturbed ternary fission of nuclei and for the case of the ternary-fission process perturbed by Coriolis interaction. This problem will be addressed in our future investigations.

4. CONCLUSION

This article reports on a continuation of a large series of studies [6–10, 17] devoted to developing the quantum theory of reactions involving binary or ternary fission of nuclei and to describing the angular distributions of reaction products, as well as various P -odd and P -even correlations in reactions induced by polarized neutrons. In the present study, it has been shown that T -odd asymmetry recently discovered in ternary fission processes induced by polarized neutrons can also be described in principle on the basis of this theory.

In order to explain the T -odd effect, we have introduced, in just the same way as in the model proposed in [3, 4], the Coriolis interaction of the product alpha particle with the spin of the nucleus undergoing fission. In contrast to [3, 4], however, the entire analysis has been performed at the quantum-mechanical level with allowance for the dynamics of the ternary-fission process, a T -odd correlation arising as the result of the interference between T -even and T -odd amplitudes (associated with Coriolis interaction), as in the case of P -odd correlations [10]. This approach has enabled us to describe correctly the scale of the effect, its symmetry with respect to the inversion of the neutron spin and of the direction of light-fragment emission, and the character of the angular and energy dependences for the effect in question. The proof of the fact that T -odd correlations in the ternary fission of nuclei arise only in fission modes that are asymmetric in fragment charges and masses is an important result of the present study.

It has been shown that, in contrast to what occurs in the case of P -even and P -odd correlations, the effect being considered receives contributions from the interference between only s -wave resonances of compound nuclei. Various limiting cases have been explored—in particular, the case where the T -odd asymmetry is due exclusively to the interference of different s -wave neutron resonances (for example, resonances characterized by different values of the spin J_s). In this connection, the possible reason behind the smallness of the effect for ^{239}Pu target nuclei has been indicated.

It has also been proven that spin-orbit interaction, which was considered in [5] and which conserves the projections of the total spin of a fissile system onto the z axis and the symmetry axis, does not contribute to the T -odd effect.

ACKNOWLEDGMENTS

We are grateful to G.A. Petrov, A.L. Barabanov, and W.I. Furman for stimulating discussions.

This work was supported by INTAS (project no. 99-0229) and the Russian Foundation for Basic Research (project no. 03-02-17469).

REFERENCES

1. P. Jesinger *et al.*, Nucl. Instrum. Methods Phys. Res. A **440**, 618 (2000).
2. M. Mutterer and J. P. Theobald, in *Nuclear Decay Modes*, Ed. by D. Poenaru (IOP Publ., Bristol, 1996), Chap. 12.
3. V. E. Bunakov, Yad. Fiz. **65**, 648 (2002) [Phys. At. Nucl. **65**, 616 (2002)].
4. V. E. Bunakov and F. Goennenwein, Yad. Fiz. **65**, 2096 (2002) [Phys. At. Nucl. **65**, 2036 (2002)].
5. A. L. Barabanov, in *Proceedings of ISINN-9* (Dubna, Russia, 2001), p. 93.
6. S. G. Kadmsky, Yad. Fiz. **65**, 1424 (2002) [Phys. At. Nucl. **65**, 1390 (2002)].
7. S. G. Kadmsky, Yad. Fiz. **65**, 1833 (2002) [Phys. At. Nucl. **65**, 1785 (2002)].
8. S. G. Kadmsky, Yad. Fiz. **66** (12) (2003) [Phys. At. Nucl. **66** (12) (2003)].
9. S. G. Kadmsky, Yad. Fiz. **66**, 1739 (2003) [Phys. At. Nucl. **66**, 1691 (2003)].
10. S. G. Kadmsky, Yad. Fiz. **66**, 1038 (2003) [Phys. At. Nucl. **66**, 1005 (2003)].
11. A. Bohr and B. R. Mottelson, *Nuclear Structure* (Benjamin, New York, 1969, 1975; Mir, Moscow, 1971, 1977), Vols. 1, 2.
12. S. G. Kadmskiĭ, V. P. Markushev, and V. I. Furman, Yad. Fiz. **31**, 1175 (1980) [Sov. J. Nucl. Phys. **31**, 607 (1980)].
13. W. I. Furman and I. Kliman, in *Proceedings of the International Symposium on Nuclear Physics, Gaussing, 1987*, p. 86.
14. O. P. Sushkov and V. V. Flambaum, Usp. Fiz. Nauk **136**, 3 (1982).
15. L. M. Delves, Nucl. Phys. **20**, 275 (1960).
16. N. F. Mott and H. S. W. Massey, *The Theory of Atomic Collisions* (Clarendon Press, Oxford, 1965; Mir, Moscow, 1969).
17. S. G. Kadmsky and L. V. Rodionova, Izv. Akad. Nauk, Ser. Fiz. **66**, 613 (2003).
18. D. A. Varshalovich, A. N. Moskalev, and V. K. Khersonskii, *Quantum Theory of Angular Momentum* (Nauka, Leningrad, 1975; World Sci., Singapore, 1988).

Translated by A. Isaakyan

Boson–Fermion Holstein–Primakoff Mapping at Nonzero Temperatures for the Example of the Lipkin Model

A. I. Vdovin*, A. A. Dzhioev**, and A. N. Storozhenko***

Joint Institute for Nuclear Research, Dubna, Moscow oblast, 141980 Russia

Received February 7, 2003

Abstract—Within the formalism of thermo field dynamics, the boson–fermion Holstein–Primakoff transformation is constructed for the case of nonzero temperatures. For the example of the Lipkin model, the transformation in question is used to construct a thermal Hamiltonian in the form of an expansion in the parameter $1/\sqrt{N}$, where N is the number of particles in the system. The temperature dependence of quasiparticle (fermion) and collective-excitation (boson) energies is calculated to terms of order $1/N$.

© 2003 MAIK “Nauka/Interperiodica”.

1. INTRODUCTION

The boson-expansion method was introduced in the theory of the nucleus forty years ago in the studies of Belyaev and Zelevinsky [1] and Marumori, Yamamura, and Tokunaga [2]. The boson-expansion method played an extremely important role in the creation of the microscopic theory of low-energy vibrations of atomic nuclei. This method formed a basis of the so-called algebraic approach in the theory of the nucleus and its most popular phenomenological realization—namely, the interacting-boson model [3]. To a considerable extent, it was owing to the boson-expansion method that internal relationship between “natural” nucleon and phenomenological collective variables was understood (see, for example, [4]).

Some versions of the boson-expansion method were used in studying elementary excitations and their interactions in heated systems formed by a finite number of fermions [5–8]. In constructing boson expansions, there arises, however, an interesting problem that was first noticed by Hatsuda [5]. This problem becomes more comprehensible if one considers it within thermo field dynamics [9]. In discussing the application of the thermo field approach in the theory of the nucleus, Hatsuda revealed that, if one performs the bosonization of the nuclear Hamiltonian prior to heating the system, its statistical properties (within thermo field dynamics, they are determined by the thermal Hamiltonian and the thermal vacuum) will depend on Bose–Einstein occupation numbers, but this is quite strange for a fermion system. Moreover, it was shown, by considering the example of the Lipkin

model, that, in the leading order, this approach (that is, *bosonization prior to heating*) leads to glaringly incorrect results—for example, the approach cannot reproduce the results of the thermal random-phase approximation (RPA). Of course, no problems of this kind arise if one first “heats” the system (that is, constructs a thermal Hamiltonian in doubled Fock space, etc.) and only then performs bosonization [5, 6]. But in this case, the problem at hand becomes technically more involved since the number of boson types that is necessary to map the full space of fermion variables of a heated system increases. By way of example, we indicate that, while the original symmetry of the Lipkin model is $SU(2)$, the symmetry of its thermal Hamiltonian is as high as $SU(4)$ [6]. Moreover, there occur situations where the *mapping prior to heating* approach appears to be more convenient since it enables one to develop a consistent computational scheme not violating original symmetry (for more details, see [10, 11]).

As an alternative to “full bosonization,” it was proposed in [11] to use, as a mapping procedure, an extended, or boson–fermion, Holstein–Primakoff transformation. It turned out that, owing to preserving fermion degrees of freedom, the *mapping prior to heating* approach leads to correct results in this case. First, the thermal behavior of the system is determined by Fermi–Dirac occupation numbers. Second, in the leading order, thermal quasiparticles satisfy the thermal Hartree approximation, while bosons (or phonons) satisfy the thermal RPA.

The present article reports on a continuation of the investigation initiated in [11]. We will construct and diagonalize the thermal Hamiltonian of the Lipkin model in the next-to-leading order of the expansion in $1/\sqrt{N}$, where N is the number of particles in

* e-mail: vdovin@thsun1.jinr.ru

** e-mail: dzhioev@thsun1.jinr.ru

*** e-mail: astorozh@thsun1.jinr.ru

the system being considered. The ensuing exposition is organized as follows. For the sake of convenience, the diagonalization scheme for the Hamiltonian constructed for the Lipkin model in the $1/N$ order and subjected to boson–fermion mapping is outlined in Section 2 for a cold system. A generalization to nonzero temperatures is given in Section 3. The conclusions drawn from the present analysis are briefly summarized in Section 4.

2. BOSON–FERMION HOLSTEIN–PRIMAKOFF MAPPING AND $1/\sqrt{N}$ EXPANSION

The Lipkin model [12] is a system of N fermions that can occur in two degenerate states of energy $-\varepsilon/2$ and $+\varepsilon/2$. The degeneracy multiplicity of each state is $\Omega = N$. It follows that, at zero temperature and in the absence of interaction, the lower state is fully occupied, while the upper state is free. A few versions of the model Hamiltonian were considered in the literature. Here, we use the so-called second version of the Lipkin model, where the Hamiltonian has the form

$$H = \varepsilon J_z - \frac{1}{2} V (J_+ + J_-)^2. \quad (1)$$

The parameter V characterizes the strength of fermion–fermion interaction. The operator-valued expressions for the components of the quasispin J (J_z , J_+ , J_-) are

$$J_z = -\frac{1}{2} N + \frac{1}{2} \sum_{p=1}^N (c_{2p}^+ c_{2p} + c_{1p}^+ c_{1p}), \quad (2)$$

$$J_+ = \sum_{p=1}^N c_{2p}^+ c_{1p}^+ = (J_-)^+,$$

where the operator c_{2p}^+ creates a particle in the higher state, while the operator c_{1p}^+ creates a hole in the lower state. The particle–hole vacuum is defined as

$$c_{2p}|0\rangle = c_{1p}|0\rangle = 0. \quad (3)$$

The quasispin-projection operators obey the commutation relations

$$[J_+, J_-] = 2J_z, \quad [J_z, J_{\pm}] = \pm J_{\pm} \quad (4)$$

and form an $SU(2)$ algebra. By using the commutation relations (4), we can recast the Hamiltonian in (1) into the form

$$H = \varepsilon J_z - \frac{1}{2} V (J_+^2 + J_-^2 + 2J_+ J_- - 2J_z). \quad (5)$$

In a system of interacting fermions, there can arise collective excitations, which are conveniently described in terms of boson operators. In order to

introduce boson degrees of freedom consistently, use is made of the boson-expansion method. In just the same way as in [11], we want to preserve, along with boson degrees of freedom, fermion ones; therefore, we employ the boson–fermion Holstein–Primakoff mapping [13, 14]. According to this type of mapping, the original fermion operators c_{1p} and c_{2p} and the quasispin operators are expressed in terms of the commuting ideal-fermion (quasiparticle) and ideal-boson operators (a_{ip} and B_0^+ , respectively) as

$$c_{1p} = \sqrt{1 - \frac{B_0^+ B_0}{N}} a_{1p} - \frac{B_0}{\sqrt{N}} a_{2p}^+, \quad (6)$$

$$c_{2p} = \sqrt{1 - \frac{B_0^+ B_0}{N}} a_{2p} + \frac{B_0}{\sqrt{N}} a_{1p}^+,$$

$$(J_z)_I = -\frac{1}{2} (N - n^a) + B_0^+ B_0,$$

$$(J_+)_I = \sqrt{N} B_0^+ \sqrt{1 - \frac{B_0^+ B_0 + n^a}{N}} = (J_-)_I^+,$$

$$n^a = \sum_{p=1}^N (a_{2p}^+ a_{2p} + a_{1p}^+ a_{1p}) = \sum_{i,p} a_{ip}^+ a_{ip}, \quad (7)$$

where n^a is the quasiparticle-number operator. By substituting the above expressions for quasispins into (5), we obtain the fermion–boson transform H_I of the original model Hamiltonian.

It is well known that, in the mean-field approximation, the Lipkin model can be either in the so-called normal phase or in a deformed phase, depending on the strength of fermion–fermion interaction. The deformed phase is characterized by the emergence of a boson condensate. In order to take this fact into account, one introduces a boson operator B that differs from the operator B_0 by an appropriately normalized shift; that is,

$$B = B_0 - d\sqrt{N}, \quad B^+ = B_0^+ - d\sqrt{N}.$$

By expressing the quasispin operators (6) in terms of B and B^+ and expanding the square roots in a Taylor series, we now obtain the expansion of the Hamiltonian in (5) written in terms of the ideal-fermion and ideal-boson operators in powers of \sqrt{N} . To terms of order $1/N$ inclusive, we have

$$H_I = N H_0 + N^{1/2} H_1 + N^0 H_2 + N^{-1/2} H_3 \quad (8)$$

$$+ N^{-1} H_4 = N \varepsilon \left(-\frac{1}{2} + d^2 - 2\chi_0 d^2 + 2\chi_0 d^4 \right)$$

$$+ \sqrt{N} \varepsilon d (1 - 2\chi_0 + 4\chi_0 d^2) [B + B^+]$$

$$+ \varepsilon \left(\frac{1}{2} + 2\chi_0 d^2 \right) n^a + \varepsilon (1 + 7\chi_0 d^2 - \chi_0) B^+ B$$

$$\begin{aligned}
 & -\frac{\epsilon\chi_0}{2}(1-5d^2)[B^+B^+ + BB] + \frac{\epsilon\chi_0}{2}(3d^2-1) \\
 & + \frac{\epsilon\chi_0 d}{2\sqrt{N}}\left([4n^a+3][B+B^+] + B^{+3} + B^{+3}\right. \\
 & \left. + 7B^+B^+B + 7B^+BB\right) + \frac{\epsilon\chi_0}{2N}\left(n^a[B^+ + B]^2\right. \\
 & \quad \left. + B^{+3}B + B^+B^{+3} + 2B^+BB^+B\right. \\
 & \quad \left. + \frac{1}{2}[B^+B^+ + BB] + \frac{d^2}{4(1-d^2)}\right).
 \end{aligned}$$

The quantity $\chi_0 = VN/\epsilon$, which appeared above, plays the role of an effective coupling constant. The quantity H_0 —the coefficient of N in the first term of the expansion in (8)—is the ground-state energy of the Lipkin system in the Hartree approximation. By minimizing this energy, we determine d . Two values of d are possible: (i) for $\chi_0 < 1/2$, $d = 0$, which corresponds to the normal phase (n.p.); (ii) for $\chi_0 > 1/2$, $d^2 = (2\chi_0 - 1)/4\chi_0$, which corresponds to a deformed phase (d.p.).

The second term in (8), H_1 —it is linear in the boson operators—vanishes at the above values of d , which correspond to the minima of H_0 .

The next term (of order N^0) corresponds to the RPA and describes independent phonon and quasiparticle excitations in the system. This term is diagonal in the quasiparticle operators. In order to diagonalize it in the boson operators, we make the linear canonical transformation

$$B^+ = uC^+ + vC, \quad B = uC + vC^+, \quad (9)$$

where

$$u^2 - v^2 = \cosh^2 \varphi - \sinh^2 \varphi = 1.$$

From the fact that the term H_2 is diagonal in phonons C , we obtain the following expressions for the transformation coefficients u and v and for the energy ω of a new boson excitation (RPA phonon):

$$\begin{pmatrix} \cosh^2 \varphi \\ \sinh^2 \varphi \end{pmatrix} = \frac{1}{2} \left[\frac{\epsilon(1 + 7\chi_0 d^2 - \chi_0)}{\omega} \pm 1 \right], \quad (10)$$

$$2uv = \sinh 2\varphi = \frac{\epsilon\chi_0(1 - 5d^2)}{\omega},$$

$$\begin{aligned}
 \omega & = \epsilon \left[(1 + 7\chi_0 d^2 - \chi_0)^2 - \chi_0^2 (1 - 5d^2)^2 \right]^{1/2} \quad (11) \\
 & = \begin{cases} \epsilon\sqrt{1 - 2\chi_0} & \text{(n.p.)} \\ \epsilon\sqrt{4\chi_0^2 - 1} & \text{(d.p.)} \end{cases}
 \end{aligned}$$

The term H_2 now takes the form

$$H_2 = W_{\text{RPA}} + E \sum_{i,p} a_{ip}^+ a_{ip} + \omega C^+ C$$

$$= W_{\text{RPA}} + H_{\text{RPA}},$$

where the C number W_{RPA} is the RPA correction to the ground-state energy of the system,

$$\begin{aligned}
 W_{\text{RPA}} & = \frac{\omega - \epsilon(1 + 4\chi_0 d^2)}{2} \\
 & = \begin{cases} (\omega - \epsilon)/2 & \text{(n.p.)} \\ (\omega - 2\epsilon\chi_0)/2 & \text{(d.p.)} \end{cases}
 \end{aligned}$$

and E is the quasiparticle energy in the Hartree approximation,

$$E = \epsilon \left(\frac{1}{2} + 2\chi_0 d^2 \right) = \begin{cases} \epsilon/2 & \text{(n.p.)} \\ \epsilon\chi_0 & \text{(d.p.)} \end{cases}$$

Thus, we see that, to order N^0 , our original system of interacting fermions reduces to the system of noninteracting quasiparticles in the Hartree approximation and noninteracting RPA phonons.

We will perform a further diagonalization of the Hamiltonian in (8), following [14–16] and employing the RPA phonon as one of the basis vectors. The inclusion of higher order terms leads to a renormalization of the phonon and quasiparticle energies and to anharmonic corrections associated with the interaction between different degrees of freedom. Moreover, the expressions for H_2 and H_4 involve constants. These are higher order corrections to the Hartree ground-state energy (consistently implementing the algorithm of perturbation theory, we will disregard, however, their effect on the boson-field shift d). It is worth noting that, in the normal phase, where $d = 0$, the term H_3 also vanishes.

Further, it is necessary to express the remaining quantities H_3 and H_4 in terms of the RPA-phonon operator. By arranging the creation and annihilation operators in a normal order, we obtain

$$\begin{aligned}
 H_3 & = \frac{\epsilon\chi_0 d}{2} (\cosh \varphi + \sinh \varphi) \{ 4n^a [C^+ + C] \\
 & \quad + (\cosh 2\varphi + 3\sinh 2\varphi) [C^+ + C]^3 \\
 & \quad + 4(\cosh 2\varphi - \sinh 2\varphi) \\
 & \quad \times [C^+ C^+ C + C^+ C C] + 4(\cosh 2\varphi - \sinh 2\varphi - 1) \\
 & \quad \times [C^+ + C] \} = H_3^{\text{bf}} + H_3^b,
 \end{aligned} \quad (12)$$

$$\begin{aligned}
 H_4 & = \frac{\epsilon\chi_0}{2} \left\{ (\cosh 2\varphi + \sinh 2\varphi) n^a [2C^+ C + 1] \right. \\
 & \quad \left. + \frac{1}{2} (3 \cosh 4\varphi + 3 \sinh 4\varphi \right. \\
 & \quad \left. + 1) C^+ C^+ C C + (3 \cosh 4\varphi \right. \\
 & \quad \left. + 3 \sinh 4\varphi - 2 \cosh 2\varphi - 2 \sinh 2\varphi + 1) C^+ C \right\} \quad (13)
 \end{aligned}$$

$$\begin{aligned}
 & + \frac{1}{4} \left(3 \cosh 4\varphi + 3 \sinh 4\varphi - 4 \cosh 2\varphi - 4 \sinh 2\varphi \right. \\
 & \quad \left. + \frac{1}{1-d^2} \right) \Big\} + \text{off-diagonal} = H_4^{bf} + H_4^b \\
 & + \frac{\varepsilon\chi_0}{2} (\cosh 2\varphi + \sinh 2\varphi) n^a + \frac{\varepsilon\chi_0}{8} \left(3 \cosh 4\varphi \right. \\
 & \quad \left. + 3 \sinh 4\varphi - 4 \cosh 2\varphi - 4 \sinh 2\varphi + \frac{1}{1-d^2} \right) \\
 & \quad + \text{off-diagonal}.
 \end{aligned}$$

Here, the superscripts *b* and *bf* label, respectively, the purely boson and boson–fermion parts of the terms $H_{3,4}$. In the expression for H_4 , we have included only those operators that have nonvanishing diagonal matrix elements of order $1/N$. Corrections due to off-diagonal terms are of a higher order of smallness ($1/N^2$), since they do not vanish only in the second order of perturbation theory. It would be necessary to take them into account in considering the $O(1/N^{3/2})$ and $O(1/N^2)$ terms of the expansion of H_I , but this is beyond the scope of the present study. The third and the fourth terms in expression (13) are corrections to the quasiparticle energy and to the ground-state energy, respectively.

As was mentioned above, the term $H_3 = H_3^{bf} + H_3^b$ vanishes in the normal phase. With the aid of the relation

$$\cosh 2\varphi + \sinh 2\varphi = \frac{\varepsilon}{\omega}, \tag{14}$$

the Hamiltonian of the Lipkin model in the normal phase to terms of order $1/N$ can therefore be reduced to the form

$$\begin{aligned}
 H_I^{n,p} = & W_0^{n,p} + E^{n,p} \sum_{i,p} a_{ip}^+ a_{ip} + \omega C^+ C \tag{15} \\
 & + \mu^{n,p} n^a C^+ C + \frac{\theta^{n,p}}{2} C^+ C^+ C C,
 \end{aligned}$$

where

$$W^{n,p} = -\frac{N\varepsilon}{2} + \frac{\omega - \varepsilon}{2} + \frac{\varepsilon\chi_0}{8N} \left[\frac{3\varepsilon^2}{\omega^2} - \frac{4\varepsilon}{\omega} + 1 \right], \tag{16}$$

$$\begin{aligned}
 E^{n,p} &= \frac{\varepsilon}{2} \left[1 + \frac{\varepsilon\chi_0}{N\omega} \right], \\
 \omega^{n,p} &= \omega + \frac{\varepsilon\chi_0}{2N} \left[\frac{3\varepsilon^2}{\omega^2} - \frac{2\varepsilon}{\omega} + 1 \right], \\
 \mu^{n,p} &= \frac{\varepsilon^2\chi_0}{N\omega}, \quad \theta^{n,p} = \frac{\varepsilon\chi_0}{2N} \left[\frac{3\varepsilon^2}{\omega^2} + 1 \right].
 \end{aligned}$$

The terms involving the coefficients $\mu^{n,p}$ and $\theta^{n,p}$ are corrections associated with phonon–fermion and

phonon–phonon interactions. We note that the value of $\theta^{n,p}$ coincides with that which was obtained in [17] within the theory of nuclear fields.

Let us now consider the deformed phase where the term H_3 differs from zero. The operators H_3^{bf} and H_3^b include only odd powers of the boson operators—that is, they have zero matrix elements in the RPA-phonon basis. Therefore, the term H_3 must be taken into account simultaneously with the diagonal terms in the operators H_4^{bf} and H_4^b , since they contribute in the same order ($1/N$).

The term $H_3 +$ diagonal part of H_4 can be diagonalized [15, 16] with the aid of new quasiparticle and phonon operators (in the following, they will be referred to as the diagonalizing ones), C_d^+ and $(a_{ip}^+)_d$, respectively, that are related to the original ideal operators by the unitary canonical transformation

$$\begin{aligned}
 C_d^+ &= e^{iS/\sqrt{N}} C^+ e^{-iS/\sqrt{N}}, \tag{17} \\
 (a_{ip}^+)_d &= e^{iS/\sqrt{N}} a_{ip}^+ e^{-iS/\sqrt{N}}.
 \end{aligned}$$

The operator S is chosen in such a way as to diagonalize the Hamiltonian in order $1/\sqrt{N}$. In the deformed phase, the Hamiltonian H_I in (8) in terms of C_d^+ and $(a_{ip}^+)_d$ to order $1/N$ inclusive has the form

$$\begin{aligned}
 H_I &= e^{-iS_d/\sqrt{N}} (H_I)_d e^{iS_d/\sqrt{N}} = (H_I)_d \tag{18} \\
 & + \frac{1}{\sqrt{N}} [(H_I)_d, iS_d] + \frac{1}{2N} [[(H_I)_d, iS_d], iS_d] + \dots \\
 & = W_0 + (H_{\text{RPA}})_d + \frac{1}{\sqrt{N}} \left\{ [(H_{\text{RPA}})_d, iS_d] \right. \\
 & \quad \left. + (H_3^b + H_3^{bf})_d \right\} + \frac{1}{2N} \left\{ [[(H_{\text{RPA}})_d, iS_d], iS_d] \right. \\
 & \quad \left. + 2[(H_3^b + H_3^{bf})_d, iS_d] + 2(H_4^b + H_4^{bf})_d \right\} + \dots
 \end{aligned}$$

Here, we have considered that, for any operator F depending on O and O^+ , F_d is obtained by means of the substitutions $O \rightarrow O_d$ and $O^+ \rightarrow O_d^+$ since $F_d = e^{iS} F e^{-iS}$. Of course, we have $e^{iS} = e^{iS_d}$. For the product of the diagonalizing operators, we will hereafter use the notation $a_d b_d \dots z_d \equiv (a b \dots z)_d$.

The condition that the $O(1/\sqrt{N})$ off-diagonal part of the Hamiltonian in (18) vanishes can be written as

$$[(H_{\text{RPA}})_d, iS_d] = \omega [C_d^+ C_d, iS_d] = -(H_3^b + H_3^{bf})_d. \tag{19}$$

The operator satisfying this equation has the form

$$\begin{aligned}
 iS_d &= iS_d^b + iS_d^{bf}, \\
 iS_d^b &= \left(\alpha C_d^{+3} + \beta C_d^+ C_d^+ C_d + \gamma C_d^+ \right) - (\text{h.c.}),
 \end{aligned}$$

$$iS_d^{bf} = \lambda n_d^a (C_d^+ - C_d), \quad +5 \sinh 2\varphi - 4)n_d^a \Big\}$$

where the coefficients are

$$\begin{aligned} \alpha &= -\frac{\varepsilon\chi_0 d}{6\omega} (\cosh \varphi + \sinh \varphi) \quad (20) \\ &\times (\cosh 2\varphi + 3 \sinh 2\varphi), \\ \beta &= -\frac{\varepsilon\chi_0 d}{2\omega} (\cosh \varphi + \sinh \varphi) \\ &\times (7 \cosh 2\varphi + 5 \sinh 2\varphi), \\ \gamma &= -\frac{\varepsilon\chi_0 d}{2\omega} (\cosh \varphi + \sinh \varphi) \\ &\times (7 \cosh 2\varphi + 5 \sinh 2\varphi - 4), \\ \lambda &= -\frac{2\varepsilon\chi_0 d}{\omega} (\cosh \varphi + \sinh \varphi). \end{aligned}$$

Taking into account the condition in (19), we can recast the Hamiltonian in (18) into the form

$$\begin{aligned} H_I &= W_0 + (H'_{\text{RPA}})_d \quad (21) \\ &+ \frac{1}{2N} \left\{ [(H_3^b + H_3^{bf})_d, iS_d^b + iS_d^{bf}] \right. \\ &\quad \left. + 2(H_4^b + H_4^{bf})_d \right\} + \dots \end{aligned}$$

We have included, in H'_{RPA} , the correction to the quasiparticle energy due to (13) and, in W_0 , the corrections associated with (13) and with the term W_{RPA} . It should be emphasized that, along with the diagonal terms, the braced expression on the right-hand side of (21) involves terms whose diagonal matrix elements are zero and whose contribution is of order $1/N^2$. Following the same line of reasoning as in the case considered above, we can subject the Hamiltonian to an additional unitary transformation that will annihilate all off-diagonal operators in the order $1/N$ and lead to the emergence of extra terms in higher orders. Since, in the order being considered, this transformation will introduce no changes in the Hamiltonian H_I , the off-diagonal terms in (21) can be discarded.

For the commutators in (21), we have

$$\begin{aligned} [(H_3^b)_d, iS_d^b] &= -\frac{\varepsilon\chi_0}{16} \left\{ 6(21 \cosh 4\varphi \right. \\ &+ 19 \sinh 4\varphi) C_d^+ C_d^+ C_d C_d + [12(21 \cosh 4\varphi \\ &\quad + 19 \sinh 4\varphi) - 16(7 \cosh 2\varphi \\ &\quad \quad + 5 \sinh 2\varphi) + 48] C_d^+ C_d \\ &+ [(47 \cosh 4\varphi + 41 \sinh 4\varphi) - (56 \cosh 2\varphi \\ &\quad \quad + 40 \sinh 2\varphi) + 20] \Big\} + \text{off-diagonal,} \\ [(H_3^{bf})_d, iS_d^{bf}] &= -\frac{\varepsilon\chi_0}{4} \left\{ 2(7 \cosh 2\varphi \right. \\ &\quad \left. + 5 \sinh 2\varphi) n_d^a C_d^+ C_d + (7 \cosh 2\varphi \right. \end{aligned}$$

$$\begin{aligned} &+ 5 \sinh 2\varphi - 4)n_d^a \Big\} \\ &+ \text{off-diagonal,} \\ [(H_3^b)_d, iS_d^{bf}] &= -\frac{\varepsilon\chi_0}{4} \left\{ 2(7 \cosh 2\varphi \right. \\ &\quad \left. + 5 \sinh 2\varphi) n_d^a C_d^+ C_d + (7 \cosh 2\varphi \right. \\ &\quad \left. + 5 \sinh 2\varphi - 4)n_d^a \Big\} \\ &+ \text{off-diagonal,} \\ [(H_3^{bf})_d, iS_d^{bf}] &= -\varepsilon\chi_0 (n_d^a)^2 \\ &= -\varepsilon\chi_0 \left\{ n_d^a + \sum_{ip \neq i'p'} (a_{ip}^+ a_{i'p'}^+ a_{i'p'} a_{ip})_d \right\}. \end{aligned}$$

In the calculations, we have employed the following relations for the deformed phase:

$$\begin{aligned} (\cosh 2\varphi + \sinh 2\varphi) &= \frac{\varepsilon(2\chi_0 + 1)}{2\omega}, \\ \frac{\varepsilon\chi_0 d^2}{\omega} (\cosh 2\varphi + \sinh 2\varphi) &= \frac{1}{8}. \end{aligned}$$

Substituting the results obtained for the commutators in (21), we arrive at the Hamiltonian for the Lipkin model in the deformed phase to terms of order $1/N$ inclusive. The result is

$$\begin{aligned} H^{\text{d.p}} &= W_0^{\text{d.p}} + E^{\text{d.p}} n_d^a + \omega^{\text{d.p}} C_d^+ C_d \quad (22) \\ &+ \mu^{\text{d.p}} (n^a C^+ C)_d + \frac{\theta^{\text{d.p}}}{2} (C^+ C^+ C C)_d \\ &+ \tau^{\text{d.p}} \sum_{ip \neq i'p'} (a_{ip}^+ a_{i'p'}^+ a_{i'p'} a_{ip})_d, \end{aligned}$$

where

$$\begin{aligned} W_0^{\text{d.p}} &= -N\varepsilon \frac{4\chi_0^2 + 1}{8\chi_0} + \frac{\omega - 2\varepsilon\chi_0}{2} \quad (23) \\ &- \frac{\varepsilon\chi_0}{N} \left[\frac{\varepsilon^2}{\omega^2} - \frac{2\varepsilon\chi_0}{\omega} + 1 \right], \\ E^{\text{d.p}} &= \varepsilon\chi_0 - \frac{\varepsilon\chi_0}{2N} \left[\frac{4\varepsilon\chi_0}{\omega} - 1 \right], \\ \omega^{\text{d.p}} &= \omega - \frac{2\varepsilon\chi_0}{N} \left[\frac{3\varepsilon^2}{\omega^2} - \frac{2\varepsilon\chi_0}{\omega} + 2 \right], \\ \mu^{\text{d.p}} &= -\frac{4\varepsilon^2\chi_0^2}{N\omega}, \quad \theta^{\text{d.p}} = -\frac{2\varepsilon\chi_0}{N} \left[\frac{3\varepsilon^2}{\omega^2} + 2 \right], \\ \tau^{\text{d.p}} &= -\frac{\varepsilon\chi_0}{2N}. \end{aligned}$$

Thus, the Hamiltonian for the Lipkin model in the deformed phase to terms of order $1/N$ [see Eq. (22)] differs from the corresponding Hamiltonian in the normal phase [see Eq. (15)] not only by the values

of the coefficients of terms having the same structure but also by an additional term that is proportional to $\tau^{d,p}$ and which describes the direct interaction between the diagonalizing quasiparticles.

3. BOSON–FERMION HOLSTEIN–PRIMAKOFF MAPPING FOR A THERMAL SYSTEM

The approach outlined in the preceding section will be generalized here to the case of a heated system by using the methods of thermo field dynamics [9], whose formalism is convenient in dealing with various operator relations.

Within the formalism of thermo field dynamics, the dynamics of a heated system is determined by the thermal Hamiltonian \mathcal{H} and the wave function for the thermal vacuum $|0(T)\rangle$, which is the eigenvector of \mathcal{H} for zero eigenvalue. In order to construct the thermal Hamiltonian, we first formally double the number of the degrees of freedom of the system—that is, we construct the so-called tilde-labeled system having the same structure (in other words, the same Hamiltonian, the same basis vectors, the same observables, and so on) as the original system. In the following, all variables and operators associated with this fictitious system are labeled with a tilde symbol. By way of example, we indicate that, if, for the original system, we have $H|n\rangle = E_n|n\rangle$, then, for the tilde-labeled system, we write $\tilde{H}|\tilde{n}\rangle = E_n|\tilde{n}\rangle$. The full Hilbert space of the heated system is constructed as the direct product of the relevant spaces of the original and the tilde-labeled system. Rules that specify various operations involving ordinary and tilde-labeled operators are formulated within thermo field dynamics [9]. The thermal Hamiltonian of the system is defined as $\mathcal{H} = H - \tilde{H}$, because it is precisely this operator that executes translations along the time axis in a heated system. Thus, the excitation spectrum of the system is obtained by diagonalizing the Hamiltonian \mathcal{H} . The role of the thermal vacuum $|0(T)\rangle$ consists in the following: the expectation value calculated over it for any observable coincides with the statistical expectation value of this variable over the grand canonical ensemble. It should also be noted that the calculation of the statistical expectation value of an observable involves only the relevant operator defined in the space of original rather than tilde-labeled variables. The method for constructing the thermal vacuum will become clear in the course of the ensuing exposition.

In the present study, we follow the strategies adopted in [11] and employ, for the original Hamiltonian, not that in Eq. (1) or Eq. (5) but the Hamiltonian in (8), which was obtained upon the boson–fermion

Holstein–Primakoff mapping and a subsequent expansion in powers of $1/\sqrt{N}$. Moreover, we assume, in introducing temperature, that only ideal fermions, which are images of original physical particles, are heated, while bosons remain, on the contrary, cold, since the role of boson degrees of freedom is auxiliary (we treat them as extra or additional degrees of freedom).

In order to construct the wave function for the thermal vacuum—that is, to heat our system—we perform the thermal Bogolyubov canonical transformation

$$\begin{aligned} a_{ip}^+ &= x_i \beta_{ip}^+ + y_i \tilde{\beta}_{ip}, \\ \tilde{a}_{ip}^+ &= x_i \tilde{\beta}_{ip}^+ - y_i \beta_{ip}, \end{aligned} \quad (24)$$

where the coefficients x_i and y_i depend on temperature and satisfy the condition $x_i^2 + y_i^2 = 1$. After that, we rewrite the Hamiltonian in (8) in terms of the new thermal quasiparticles β_{ip}^+ and $\tilde{\beta}_{ip}^+$. We first do this for the quasiparticle-number operator n^a . The result is

$$n^a = n^\beta + D + N(y_2^2 + y_1^2), \quad (25)$$

where the thermal-quasiparticle-number operator n^β and the operator D are given by

$$\begin{aligned} n^\beta &= \sum_{p=1}^N (\beta_{2p}^+ \beta_{2p} + \beta_{1p}^+ \beta_{1p}) = \sum_{i,p} \beta_{ip}^+ \beta_{ip}, \\ D &= \sum_{i,p} x_i y_i (\beta_{ip}^+ \tilde{\beta}_{ip}^+ + \tilde{\beta}_{ip} \beta_{ip}) \\ &\quad - \sum_{i,p} y_i^2 (\beta_{ip}^+ \beta_{ip} + \tilde{\beta}_{ip}^+ \tilde{\beta}_{ip}). \end{aligned} \quad (26)$$

The operator D satisfies the relation $D = \tilde{D} = D^+$. Taking this relation into account, we have $n^a - \tilde{n}^a = [n^\beta + D] - [\tilde{n}^\beta + D] = n^\beta - \tilde{n}^\beta$; the terms H_0 , H_1 , and H_2 of the Hamiltonian in (8) then assume the form

$$\begin{aligned} H_0 &= \varepsilon \left(-\frac{z}{2} + d^2 - 2\chi_0 z d^2 + 2\chi_0 d^4 \right), \\ H_1 &= \varepsilon d (1 - 2\chi_0 z + 4\chi_0 d^2) [B + B^+], \\ H_2 &= \varepsilon \left(\frac{1}{2} + 2\chi_0 d^2 \right) [n^\beta + D] + \varepsilon (1 + 7\chi_0 d^2 \\ &\quad - \chi_0 z) B^+ B - \frac{\varepsilon \chi_0}{2} (z - 5d^2) [B^+ B^+ + B B] \\ &\quad + \frac{\varepsilon \chi_0}{2} (3d^2 - z), \end{aligned} \quad (27)$$

where $z = 1 - (y_1^2 + y_2^2)$.

In the thermal system, the boson-field shift d depends on T . Its value can be found, along with the values of the coefficients x_i and y_i in the thermal

Bogolyubov transformation, by minimizing the free energy F of the system,

$$F = \langle 0(T) | H_I | 0(T) \rangle - TS - \mu \langle 0(T) | \hat{N} | 0(T) \rangle,$$

where S is the entropy of ideal quasiparticles,

$$S = -N \sum_{i=1,2} [y_i^2 \ln(y_i^2) + x_i^2 \ln(x_i^2)],$$

and \hat{N} is the particle-number operator. The expectation values of H_I and \hat{N} are calculated for the state $|0(T)\rangle$, which is defined as the vacuum with respect to thermal quasiparticles and the boson B . The form of the thermal vacuum is

$$|0(T)\rangle = \exp \left[\sum_{i,p} \frac{y_i(T)}{x_i(T)} a_{ip}^+ \tilde{a}_{ip}^+ + d (B_0^+ + \tilde{B}_0^+) \right] |0\rangle_a |\tilde{0}\rangle_a |0\rangle_B |\tilde{0}\rangle_B,$$

where $a|0\rangle_a = B|0\rangle_B = 0$ and $\tilde{a}|\tilde{0}\rangle_a = \tilde{B}|\tilde{0}\rangle_B = 0$.

The mean energy $\langle 0(T) | H_I | 0(T) \rangle$ is obtained by replacing, in (6), the boson operators by the operator d and the operator n^a by $N(y_1^2 + y_2^2)$. The chemical potential μ is equal to zero because of the symmetry of the system. For $T \neq 0$, the temperature-dependent quantity $\chi_0 z$ plays the role of the effective coupling constant. Depending on it, the minimum value of F is reached at different values of d ,

$$d^2 = \begin{cases} 0, & \chi_0 z < 1/2 \text{ (n.p.)} \\ (2\chi_0 z - 1)/4\chi_0, & \chi_0 z > 1/2 \text{ (d.p.)} \end{cases} \quad (28)$$

Simultaneously, we have $y_i^2 \equiv n_i$, where n_i are the thermal Fermi-Dirac occupation numbers,

$$n_i = n(T) = \frac{1}{1 + \exp(E/T)} \quad (29)$$

with E being the energy of the thermal quasiparticle $\beta_{ip}^+ |0(T)\rangle$,

$$E = \begin{cases} \varepsilon/2 & \text{(n.p.)} \\ \varepsilon\chi_0 z & \text{(d.p.)} \end{cases} \quad (30)$$

It follows from (30) that, in the normal phase, the quasiparticle energy is independent of temperature. The phase-transition temperature T_c is determined by the condition $\chi_0 z = 1/2$. We then have

$$T_c = \frac{\varepsilon}{2} \left[\ln \frac{2\chi_0 + 1}{2\chi_0 - 1} \right]^{-1}. \quad (31)$$

We now rewrite the thermal Hamiltonian $\mathcal{H}_I = H_I - \tilde{H}_I$ in terms of thermal quasiparticles, whereupon we

can diagonalize it in the same way as at $T = 0$ —that is, in two steps. Since $[n^\beta + D] - [\tilde{n}^\beta + \tilde{D}] = n^\beta - \tilde{n}^\beta$, the fermion part is already diagonal. The boson terms H_2 and \tilde{H}_2 can be diagonalized individually because ordinary boson operators are not mixed with tilde-labeled boson operators. We further introduce the RPA phonons C and \tilde{C} as

$$B^+ = uC^+ + vC, \quad \tilde{B}^+ = u\tilde{C}^+ + v\tilde{C}.$$

Requiring that H_2 and \tilde{H}_2 be diagonal in the phonon operators and tilde-labeled phonon operators, respectively, we obtain the amplitudes u and v in the form

$$\begin{aligned} \begin{pmatrix} u^2 \\ v^2 \end{pmatrix} &= \begin{pmatrix} \cosh^2 \varphi \\ \sinh^2 \varphi \end{pmatrix} \\ &= \frac{1}{2} \left[\frac{\varepsilon(1 + 7\chi_0 d^2 - \chi_0 z)}{\omega} \pm 1 \right], \\ \sinh 2\varphi &= \frac{\varepsilon\chi_0(z - 5d^2)}{\omega}, \end{aligned} \quad (32)$$

and the RPA-phonon energy in the form

$$\begin{aligned} \omega &= \varepsilon [(1 + 7\chi_0 d^2 - \chi_0 z)^2 - \chi_0^2(z - 5d^2)^2]^{1/2} \\ &= \begin{cases} \varepsilon\sqrt{1 - 2\chi_0 z} & \text{(n.p.)} \\ \varepsilon\sqrt{4\chi_0^2 z^2 - 1} & \text{(d.p.)} \end{cases} \end{aligned} \quad (33)$$

Thus, the term $H_2 - \tilde{H}_2$ in the thermal Hamiltonian now reduces to

$$\begin{aligned} \mathcal{H}_2 &= H_{\text{RPA}} - \tilde{H}_{\text{RPA}} = E[n^\beta + D] + \omega C^+ C \\ &- \text{t.c.} = E \sum_{i,p} \beta_{ip}^+ \beta_{ip} + \omega C^+ C - \text{t.c.}, \end{aligned}$$

where t.c. stands for the tilde-conjugate counterpart of the expression written explicitly.

Thus, we see that, in the leading order, our heated system of fermions reduces to the system formed by noninteracting thermal quasiparticles in the Hartree approximation and a phonon whose energy depends on T and obeys the thermal RPA equation. The latter circumstance seems nontrivial since we heated only quasiparticles while keeping phonons as if cold (the corresponding thermal Bogolyubov transformation was not performed). This result was obtained earlier in [11] by using a different version of the Hamiltonian for the Lipkin model.

In order to diagonalize the terms \mathcal{H}_3 and \mathcal{H}_4 , we also express them in terms of the operators C and \tilde{C} . Upon arranging the operators in the normal order, we have

$$\mathcal{H}_3 = H_3^b + H_3^{bf} - \text{t.c.}, \quad (34)$$

$$\mathcal{H}_4 = H_4^b + H_4^{bf} + \frac{\varepsilon\chi_0}{2}(\cosh 2\varphi + \sinh 2\varphi)n^\beta - \text{t.c.},$$

where $H_{3(4)}^b$ and $H_{3(4)}^{bf}$ is obtained from (12) and (13) upon the substitution of the operator $[n^\beta + D]$ for the operator n^a . After that, the Hamiltonian \mathcal{H}_I takes the form

$$\mathcal{H}_I = H'_{\text{RPA}} + N^{-1/2}(H_3^b + H_3^{bf}) \quad (35)$$

$$+ N^{-1}(H_4^b + H_4^{bf}) - \text{t.c.}$$

In H'_{RPA} , we have taken into account, as was done in the case of $T = 0$, the renormalization of the quasiparticle energy by virtue of (34).

In the normal phase, the term \mathcal{H}_3 vanishes. Discarding the off-diagonal terms in H_4^b and H_4^{bf} —these terms contribute only in the second order of perturbation theory—and using relation (14), which is valid for $T \neq 0$ as well, we therefore obtain the thermal Hamiltonian for the Lipkin model in the normal phase; that is,

$$H_I^{\text{n.p.}} = E^{\text{n.p.}}n^\beta + \omega^{\text{n.p.}}C^+C \quad (36)$$

$$+ (\mu_1^{\text{n.p.}}n^\beta + \mu_2^{\text{n.p.}}\tilde{n}^\beta)C^+C + \frac{\theta^{\text{n.p.}}}{2}C^+C^+CC - \text{t.c.}$$

The coefficients in (36) are given by

$$E^{\text{n.p.}} = \frac{\varepsilon}{2} \left[1 + \frac{\varepsilon\chi_0}{N\omega} \right], \quad (37)$$

$$\omega^{\text{n.p.}} = \omega + \frac{\varepsilon\chi_0}{2N} \left[\frac{3\varepsilon^2}{\omega^2} - \frac{2\varepsilon}{\omega} + 1 \right],$$

$$\mu_1^{\text{n.p.}} = \frac{\varepsilon^2\chi_0}{2N\omega}(1+z), \quad \mu_2^{\text{n.p.}} = -\frac{\varepsilon^2\chi_0}{2N\omega}(1-z),$$

$$\theta^{\text{n.p.}} = \frac{\varepsilon\chi_0}{2N} \left[\frac{3\varepsilon^2}{\omega^2} + 1 \right].$$

Formally, the expressions for $E^{\text{n.p.}}$, $\omega^{\text{n.p.}}$, and $\theta^{\text{n.p.}}$ have the same form as at $T = 0$. However, they are now dependent on temperature since the RPA-phonon energy ω is temperature-dependent. Thus, corrections of order $1/N$ lead to the emergence of the temperature dependence of the quasiparticle energy in the normal phase. For $T \neq 0$, the Hamiltonian additionally develops a term that is proportional to μ_2 and which describes the interaction between tilde-labeled thermal fermions and the phonon. If $T \rightarrow 0$, then $\mu_2 \rightarrow 0$, in which case expressions (16) are restored. The following circumstance is of interest: although $\chi_0 z \rightarrow 0$ for $T \rightarrow \infty$, neither corrections of order $1/N$ to the quasiparticle energies and to the phonon energy nor anharmonic corrections vanish in this limit. Since $\omega \rightarrow \varepsilon$ for $T \rightarrow \infty$, then

$$E^{\text{n.p.}} \rightarrow \frac{\varepsilon}{2} \left(1 + \frac{\chi_0}{N} \right), \quad (38)$$

$$\omega^{\text{n.p.}} \rightarrow \varepsilon \left(1 + \frac{\chi_0}{N} \right) = 2E^{\text{n.p.}}$$

For the quantities $E^{\text{n.p.}}$ and $\omega^{\text{n.p.}}$, this result can be understood on the basis of an alternative form of the original Hamiltonian of the model in (5): the term $VJ_z/2$ merely leads to a renormalization of the bare energies of the mean-field levels, and relations (38) reflect this fact.

Further, we will diagonalize the thermal Hamiltonian \mathcal{H}_I in the deformed phase. We will seek the generator of the corresponding unitary transformation in the form

$$i\mathcal{S}_d = iS_d + i\tilde{S}_d,$$

where the operators S_d and \tilde{S}_d must satisfy the condition

$$\left[(H_I)_d, i\tilde{S}_d \right] = \left[(\tilde{H}_I)_d, S_d \right] = 0. \quad (39)$$

The condition under which the off-diagonal terms in the thermal Hamiltonian vanish in the order $1/\sqrt{N}$ —it is similar to that in (19)—can be written in the form

$$\left[H'_{\text{RPA}}, iS_d^b + iS_d^{bf} \right] = \omega \left[C_d^+ C_d, iS_d^b + iS_d^{bf} \right]$$

$$= -(H_3^b + H_3^{bf}),$$

$$\left[\tilde{H}'_{\text{RPA}}, \widetilde{iS_d^b + iS_d^{bf}} \right] = \omega \left[\tilde{C}_d^+ \tilde{C}_d, \widetilde{iS_d^b + iS_d^{bf}} \right]$$

$$= -(\widetilde{H_3^b + H_3^{bf}}).$$

Taking into account the relations $[C_d, \tilde{C}_d] = 0$ and $[(n^\beta + D)_d, (\widetilde{n^\beta + D})_d] = 0$, we can easily obtain the expression for S_d ; that is,

$$iS_d = iS_d^b + iS_d^{bf},$$

$$iS_d^b = \left(\alpha C_d^{+3} + \beta C_d^+ C_d^+ C_d + \gamma C_d^+ \right) - (\text{h.c.}),$$

$$iS_d^{bf} = \lambda [n^\beta + D]_d (C_d^+ - C_d),$$

where the coefficients α , β , γ , and λ are given by (20). These coefficients are now dependent on T , since d and ω , as well as $\cosh \varphi$ and $\sinh \varphi$, depend on T .

In terms of the “digonalizing” quasiparticles and a phonon, the expression for the thermal Hamiltonian in the deformed phase to terms of order $1/N$ has the form

$$\mathcal{H}_I = (H'_{\text{RPA}})_d + \frac{1}{2N} \left\{ \left[(H_3^b + H_3^{bf})_d, iS_d^b + iS_d^{bf} \right] \right.$$

$$\left. + 2(H_4^b + H_4^{bf})_d \right\} - \text{t.c.} \quad (40)$$

In just the same way as at $T = 0$, the braced expression in (40) involves operators whose diagonal matrix elements are equal to zero and whose contribution

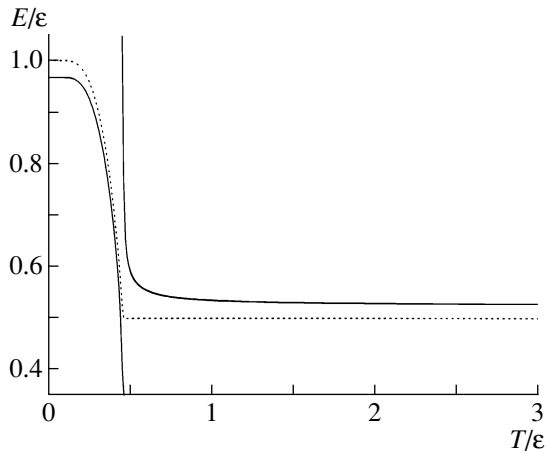


Fig. 1. Quasiparticle energy as a function of temperature T at $\chi_0 = 1.0$ and $N = 20$: (solid curve) result of the calculation in the order $1/N$ and (dotted curve) result in the thermal Hartree approximation (leading order of the expansion, $\sim N^0$).

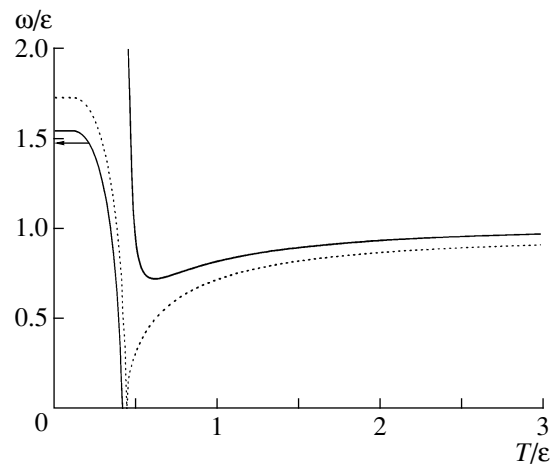


Fig. 2. Phonon energy as a function of temperature T at $\chi_0 = 1.0$ and $N = 20$: (solid curve) result of the calculation in the order $1/N$ and (dotted curve) result in the thermal RPA approximation (leading order of the expansion, $\sim N^0$). The arrow indicates the exact value of the collective-excitation energy at $T = 0$.

does not vanish only in the order $1/N^2$. Following the same line of reasoning as before, we therefore find that the Hamiltonian of the Lipkin model in the deformed phase can be reduced to the form

$$\begin{aligned} \mathcal{H}_I^{\text{d.p.}} = & E^{\text{d.p.}} n_d^\beta + \omega^{\text{d.p.}} C_d^+ C_d \\ & + (\mu_1^{\text{d.p.}} n_d^\beta + \mu_2^{\text{d.p.}} \tilde{n}_d^\beta) C_d^+ C_d + \frac{\theta^{\text{d.p.}}}{2} (C^+ C^+ C C)_d \\ & + \tau^{\text{d.p.}} \sum_{ip \neq i'p'} (\beta_{ip}^+ \beta_{i'p'}^+ \beta_{i'p'} \beta_{ip})_d - \text{t.c.}, \end{aligned}$$

where

$$\begin{aligned} E^{\text{d.p.}} = & \varepsilon \chi_0 z - \frac{\varepsilon \chi_0}{2N} \left[\frac{4\varepsilon \chi_0 z}{\omega} - 2 + z \right], \quad (41) \\ \omega^{\text{d.p.}} = & \omega - \frac{2\varepsilon \chi_0}{N} \left[\frac{3\varepsilon^2}{\omega^2} - \frac{2\varepsilon \chi_0 z}{\omega} + 2 \right], \\ \mu_1^{\text{d.p.}} = & -\frac{2\varepsilon^2 \chi_0^2 z}{N\omega} (1+z), \quad \mu_2^{\text{d.p.}} = \frac{2\varepsilon^2 \chi_0^2 z}{N\omega} (z-1), \\ \theta^{\text{d.p.}} = & -\frac{2\varepsilon \chi_0}{N} \left[\frac{3\varepsilon^2}{\omega^2} + 2 \right], \quad \tau^{\text{d.p.}} = -\frac{\varepsilon \chi_0 z}{2N}. \end{aligned}$$

For the sake of illustration, we have calculated the temperature dependence of the quasiparticle and phonon energies in the Lipkin model at the following parameter values: the number of particles is $N = 20$ and the effective coupling constant at zero temperature is $\chi_0 = 1.0$ (in ε units). The results are given in Figs. 1 and 2, respectively. At the value chosen for χ_0 , the cold system is in the deformed phase. We note that the value calculated for $\omega^{\text{d.p.}}$ with allowance for corrections is in much better agreement at $T = 0$ with the exact result from [18] than the

RPA result (see Fig. 2). With increasing T , the interaction becomes effectively weaker, and the system goes over to the normal phase at $\chi_0 z \approx 0.5$. Since the RPA phonon, whose energy ω vanishes at the phase-transition point, was chosen for a basis state and since corrections depend on inverse powers of ω , perturbation theory becomes invalid in the vicinity of the phase transition, the quantities $\omega(T)$ and $E(T)$ undergoing discontinuity. In the region $T > T_c$, $\omega(T)$ and $E(T)$ tend to their limiting values in (38) for $T \rightarrow \infty$, these values differing from the asymptotic values of the quasiparticle and phonon energies as calculated in the leading order in N —that is, in the Hartree approximation and in the RPA, respectively.

4. CONCLUSION

We have considered the problem of constructing boson expansions that are consistent with the obvious requirements of statistics at nonzero temperatures. The behavior of a heated system of fermions (Lipkin model) has been investigated with the aid of the thermal boson-fermion Holstein-Primakoff expansion constructed within thermo field dynamics. Although the thermalization of the system was performed after mapping, its thermal behavior is determined by Fermi-Dirac statistics owing to the preservation of fermion degrees of freedom. At the same time, the application of a purely boson expansion either leads to contradictions [5] or requires performing mapping upon the thermalization of the system [5, 6], in which case the problem becomes more involved.

On constructing the boson-fermion expansion of the Hamiltonian of the Lipkin model in the parameter

$1/\sqrt{N}$, we have diagonalized the thermal Hamiltonian in the order $1/N$ and calculated the temperature dependence of the quasiparticle and collective-excitation energies.

ACKNOWLEDGMENTS

We are grateful to Z. Aouissat and J. Wambach for stimulating discussions.

REFERENCES

1. S. T. Belyaev and V. G. Zelevinskiĭ, Zh. Éksp. Teor. Fiz. **42**, 1590 (1962) [Sov. Phys. JETP **42**, 1590 (1962)]; S. T. Belyaev and V. G. Zelevinsky, Nucl. Phys. **39**, 582 (1962).
2. T. Marumori, M. Yamamura, and A. Tokunaga, Prog. Theor. Phys. **31**, 1009 (1964).
3. F. Iachello and A. Arima, *The Interacting Boson Model* (Cambridge University Press, Cambridge, 1987).
4. P. Ring and P. Schuck, *The Nuclear Many-Body Problem* (Springer-Verlag, Heidelberg, 1981).
5. T. Hatsuda, Nucl. Phys. A **492**, 187 (1989).
6. N. R. Walet and A. Klein, Nucl. Phys. A **510**, 261 (1990).
7. A. Kuriyama, M. Yamamura, J. da Providência, and C. Providência, Phys. Rev. C **45**, 2196 (1992).
8. O. Civitarese and M. Reboiro, Phys. Rev. C **60**, 034302 (1999).
9. Y. Takahashi and H. Umezawa, Collect. Phenom. **2**, 55 (1975); H. Umezawa, H. Matsumoto, and M. Tachiki, *Thermo Field Dynamics and Condensed States* (North-Holland, Amsterdam, 1982; Mir, Moscow, 1985).
10. Z. Aouissat, P. Schuck, and J. Wambach, Nucl. Phys. A **618**, 402 (1997).
11. Z. Aouissat, A. Storozhenko, A. Vdovin, and J. Wambach, Phys. Rev. C **64**, 015201 (2001).
12. H. J. Lipkin, N. Meshkov, and A. J. Glick, Nucl. Phys. **62**, 188 (1965).
13. E. R. Marshalek, Phys. Lett. B **44B**, 5 (1973).
14. E. R. Marshalek, Nucl. Phys. A **224**, 221 (1974).
15. E. R. Marshalek, Ann. Phys. (N.Y.) **143**, 191 (1982).
16. A. Klein and E. R. Marshalek, Rev. Mod. Phys. **63**, 375 (1991).
17. G. F. Bertsch, P. F. Bortignon, and K. Hagino, Nucl. Phys. A **657**, 59 (1999).
18. S. E. Koonin, *Computational Physics* (Addison-Wesley, Reading, 1986).

Translated by A. Isaakyan

Spin Degrees of Freedom and Flattening of the Spectra of Single-Particle Excitations in Strongly Correlated Fermi Systems*

V. A. Khodel^{1)**}, P. Schuck²⁾, and M. V. Zverev^{1)***}

Received March 31, 2003

Abstract—The impact of long-range spin–spin correlations on the structure of a flat portion in single-particle spectra $\xi(p)$, which emerges beyond the point where the Landau state loses its stability, is studied. We supplement the well-known Nozieres model of a Fermi system with limited scalar long-range forces by a similar long-range spin-dependent term and calculate the spectra versus its strength g . It is found that Nozieres’ results hold as long as $g > 0$. However, with g changing its sign, the spontaneous magnetization is shown to arise at any nonzero g . The increase in the strength $|g|$ is demonstrated to result in shrinkage of the domain in momentum space, occupied by the flat portion of $\xi(p)$, and, eventually, in its vanishing.

© 2003 MAIK “Nauka/Interperiodica”.

The investigation of flattening of single-particle (sp) spectra of Fermi liquids dates back to [1], where long-range correlations, enhanced in the vicinity of an impending ferromagnetic phase transition, were shown to result in the divergence of the effective mass M^* at the transition point. Later, in [2], an idea of the so-called fermion condensation, i.e., a rearrangement of the Landau state, occurring beyond a critical point in strongly correlated Fermi systems with long-range effective interactions, was suggested. A striking feature of this rearrangement is “swelling” of the Fermi surface (FS), i.e., the occurrence of a completely flat portion $\xi(\mathbf{p}) = 0$, called the fermion condensate (FC), in the spectrum $\xi(\mathbf{p})$ measured from the FS.

To gain insight into the problem of fermion condensation, let us turn to the Dyson equation, rewriting it in the form

$$\xi(\mathbf{p}) = \xi_{\mathbf{p}}^0 + \Sigma(\mathbf{p}, \xi(\mathbf{p})) \quad (1)$$

appropriate for finding the FC solutions $\xi(\mathbf{p}) = 0$. The sp mass operator Σ is usually determined by the formula

$$\Sigma(\mathbf{p}, \varepsilon) = \int W(\mathbf{p}, \varepsilon, \mathbf{p}_1, \varepsilon_1) G(\mathbf{p}_1, \varepsilon_1) \frac{d^4 p_1}{(2\pi)^4 i}, \quad (2)$$

where W is an effective interaction between particles and G is the sp Green’s function. It is worth noting

that the imaginary part of $\Sigma(p, \varepsilon)$ vanishes at $\varepsilon = 0$. Therefore, in searching for the FC solutions, only the real part of Σ is relevant.

For a long time, it was reckoned that, in homogeneous Fermi systems, there exists a one-to-one correspondence between the momentum p and the sp energy ξ , at least, close to the FS; i.e., the derivative $(d\xi/dp)_F$ is always positive, a postulate that is virtually being a cornerstone of the Landau theory of Fermi liquid [3]. However, in systems with long-range forces, it might be incorrect. Compelling evidence for that is provided by a phenomenological model suggested by Nozières [4], where W is taken as a constant in the coordinate space. Thus, in this model, Eq. (1) takes the form

$$\xi - \xi_{\mathbf{p}}^0 = f n(\xi), \quad (3)$$

where f is an effective coupling constant, the value of which is taken to be positive, while $n(\xi)$ is the Landau quasiparticle momentum distribution, being 0 at positive ξ and 1 at negative ξ . This equation is easily solved, but we concentrate on its graphical solution (see Fig. 1). Let us draw both the right-hand side and the left-hand side of Eq. (3) as functions of ξ , taking p as an input parameter. The left-hand side of (3), depicted at different p , provides a set of parallel straight lines, while the right-hand side forms a kink, the vertical segment of which is located at $\xi = 0$, no matter what the input is. Crossing points yield the sp spectrum $\xi(p)$. If they lie on any of the two horizontal pieces of the kink, $\xi(p)$ does coincide with the sp spectrum of ideal Fermi gas. An unconventional situation occurs when straight lines cross the steep section of the kink. In this case, the intersection point remains 0 in a finite momentum

*This article was submitted by the authors in English.

¹⁾Russian Research Centre Kurchatov Institute, pl. Kurchatova 1, Moscow, 123182 Russia

²⁾Groupe de Physique Théorique, Institut de Physique Nucléaire Orsay, France; e-mail: schuck@ipno.in2p3.fr

** e-mail: vak@wuphys.wustl.edu

*** e-mail: zverev@mbslab.kiae.ru

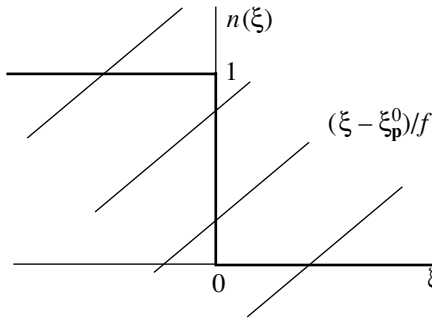


Fig. 1. Graphical illustration of the solution to Eq. (3).

interval $[p_i, p_f]$. This plateau $\xi(p) = 0$, lying exactly at the FS, does form the fermion condensate. Since $\xi(p) = 0$ in the finite volume of momentum space, the density of states $\rho(\varepsilon)$ acquires a singular term $\rho(\varepsilon) \sim \delta(\varepsilon)$. Another salient feature of the fermion condensation phenomenon is that, in the FC domain, the quasiparticle momentum distribution $n_0(p)$ differs from the Landau one. Indeed, upon setting $\xi = 0$ in Eq. (3), one finds

$$n_0(p) = -\xi_{\mathbf{p}}^0/f, \quad p_i < p < p_f, \quad (4)$$

in contrast to the conventional step function $n_F(p) = \theta(p_F - p)$. Thus, the FS does swell, whereas the basic assertion of Landau theory fails.

In dealing with the FC problem, attention is usually paid to the spin-independent part of the effective interaction W (see, e.g., [2, 4–8]). Here, we investigate effects associated with long-range spin–spin components of W , which involve the spin-up quasiparticle distribution $n_+(p)$ and the spin-down one $n_-(p)$. It is instructive to start such an analysis with a generalization of the Nozieres model [4], supplementing it by long-range spin–spin terms. As a result, one obtains two equations,

$$\begin{aligned} \xi_+(p) &= \xi_{\mathbf{p}}^0 + \frac{1}{2}f(n_+(p) + n_-(p)) \\ &\quad + \frac{1}{2}g(n_+(p) - n_-(p)), \\ \xi_-(p) &= \xi_{\mathbf{p}}^0 + \frac{1}{2}f(n_+(p) + n_-(p)) \\ &\quad - \frac{1}{2}g(n_+(p) - n_-(p)) \end{aligned} \quad (5)$$

with a new constant g specifying the long-range spin–spin component of the model effective interaction W . It is worth noting that, in the case of spin fluctuations with nonzero critical momentum $q_c \ll p_F$, presumably relevant to two-dimensional liquid ^3He , the constants in Eq. (5) are related to each other: $g = -f/3$.

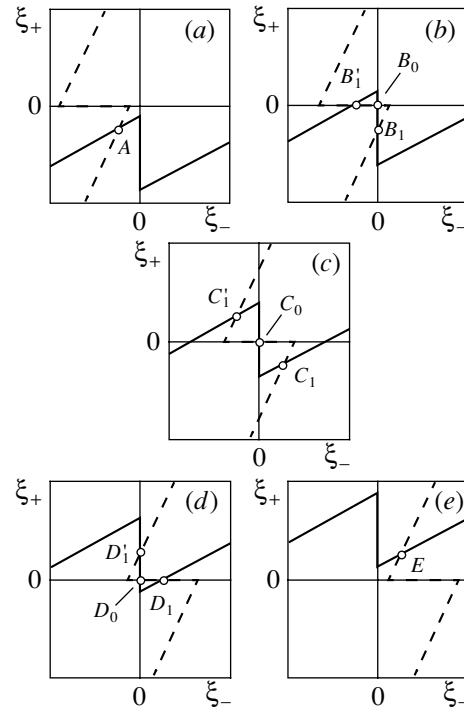


Fig. 2. Graphical illustration of the dynamics of solutions of the set (6) with increasing $\xi_{\mathbf{p}}^0$ in the case of $|g| < f$.

In conventional Fermi liquids, the spontaneous spin S arises only if strength of the spin–spin interaction obeys the Pomeranchuk condition $|G|\rho(0) > 1$, where $\rho(0) = p_F M^*/\pi^2$ is the density of states at the FS in the Landau theory. In the case at issue, the density of states is infinite, so that one can expect the emergence of spontaneous magnetization at any $g < 0$.

To facilitate the solution of the problem, we recast the system (5) into the form

$$\begin{aligned} \xi_+ &= \left(1 - \frac{a}{b}\right)\xi_{\mathbf{p}}^0 + \frac{a}{b}\xi_- + \left(b - \frac{a^2}{b}\right)n_-, \\ \xi_- &= \left(1 - \frac{a}{b}\right)\xi_{\mathbf{p}}^0 + \frac{a}{b}\xi_+ + \left(b - \frac{a^2}{b}\right)n_+, \end{aligned} \quad (6)$$

where $a = (f + g)/2$ and $b = (f - g)/2$. Let us now draw the plot $\xi_+(\xi_-)$, proceeding from the first of Eqs. (6) and treating p as an input parameter. At $\xi_- > 0$ the function $\xi_+(\xi_-)$ is given by the straight line $\xi_+ = (1 - a/b)\xi_{\mathbf{p}}^0 + a\xi_-/b$, while at $\xi_- < 0$ this straight line is slightly shifted: $\xi_+ = (1 - a/b)\xi_{\mathbf{p}}^0 + (b^2 - a^2)/b + a\xi_-/b$. The drawing of its counterpart ξ_- from the second of Eqs. (6) yields another couple of straight lines: $\xi_- = (1 - a/b)\xi_{\mathbf{p}}^0 + a\xi_+/b$ at $\xi_+ > 0$ and $\xi_- = (1 - a/b)\xi_{\mathbf{p}}^0 - (b^2 - a^2)/b + a\xi_-/b$ at $\xi_+ < 0$. As we shall see, both of these curves cross

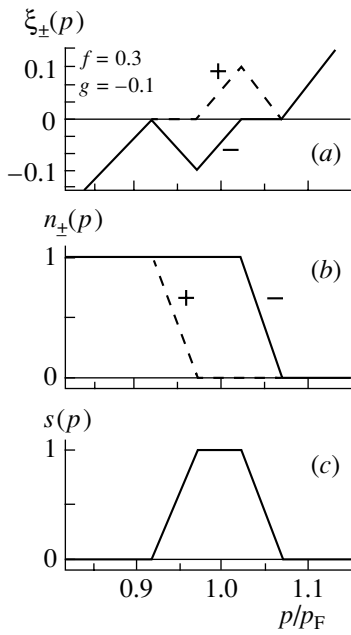


Fig. 3. Single-particle spectra $\xi_{\pm}(p)$ in units of $\varepsilon_F^0 = p_F^2/2M$ (a), occupation numbers $n_{\pm}(p)$ (b), and spontaneous spin $s(p) = n_-(p) - n_+(p)$ (c), calculated for $f = 0.3, g = -0.1$ in units of ε_F^0 .

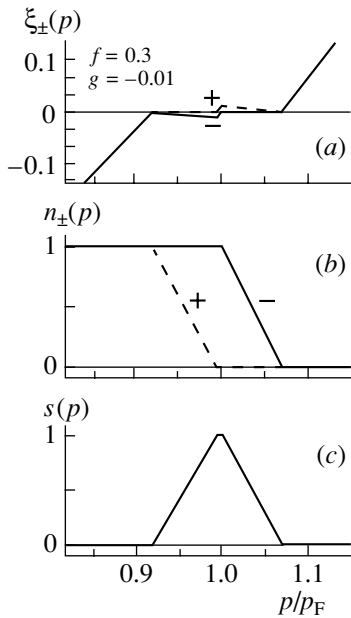


Fig. 4. The same as in Fig. 3 for $f = 0.3, g = -0.01$.

each other either at one or at three points, providing several solutions for the spectra $\xi_{\pm}(p)$.

Some elucidation of the procedure is ensured by Fig. 2, where the evolution of solutions of the set (6) versus the input parameter ξ_p^0 is shown. The solid line corresponds to the dependence $\xi_+(\xi_-)$, given by

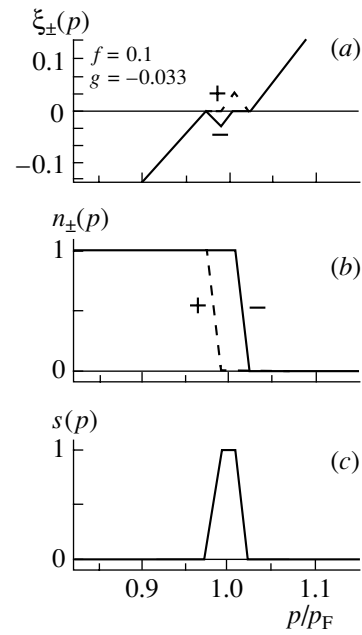


Fig. 5. The same as in Fig. 3 for $f = 0.1, g = -0.033$.

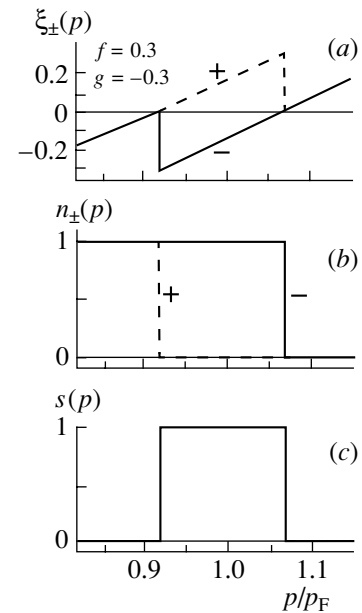


Fig. 6. The same as in Fig. 3 for $f = 0.3, g = -0.3$.

the first equation of the set (6), while the dashed line shows the same dependence resulting from the second equation of the set. The intersection points are indicated by letters. Five panels of Fig. 2 show five different cases referring to different ξ_p^0 . In the first case (Fig. 2a), two zigzag lines have one intersection point A, corresponding to the single solution where both $\xi_+(p)$ and $\xi_-(p)$ are negative. With increasing ξ_p^0 , the intersection point moves to the origin. At a

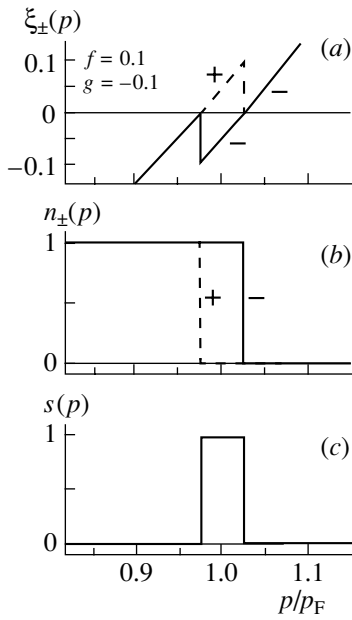


Fig. 7. The same as in Fig. 3 for $f = 0.1, g = -0.1$.

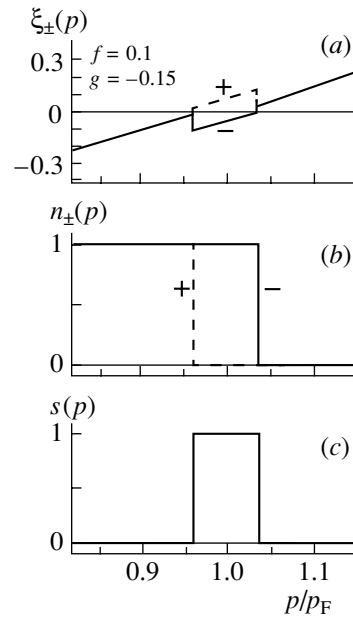


Fig. 9. The same as in Fig. 3 for $f = 0.1, g = -0.15$.

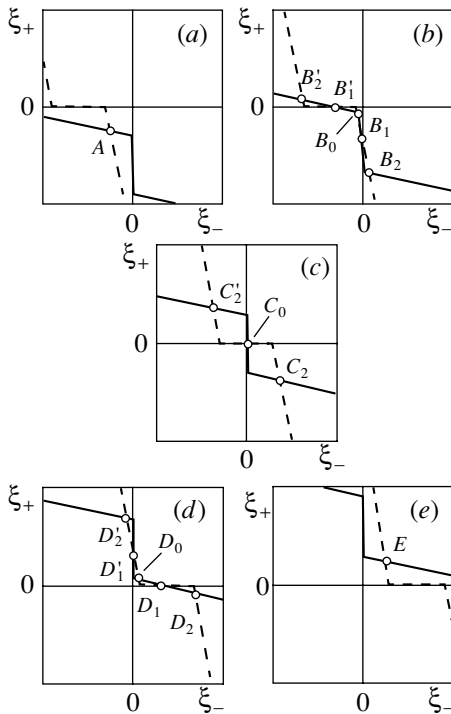


Fig. 8. The same as in Fig. 2 for the case of $|g| > f$.

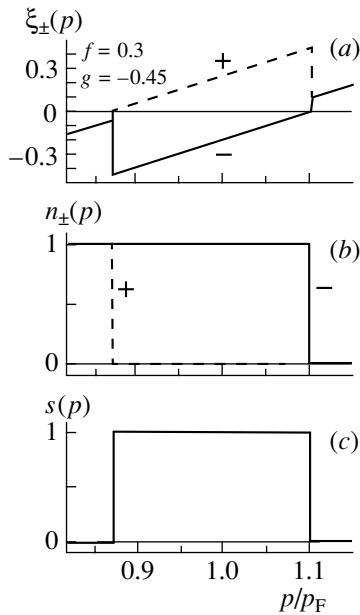


Fig. 10. The same as in Fig. 3 for $f = 0.3, g = -0.45$.

certain value of this variable, depending only on the parameter f , bifurcation emerges, and there appear three intersection points (B_0, B_1 , and B'_1 in Fig. 2*b*). One of them, B_0 , lies at the origin, while the other two, B_1 and B'_1 , lie on the ξ_+ and ξ_- axes, respectively. A similar situation occurs in Figs. 2*c* and 2*d*.

The intersection at the origin persists, while the other two crossing points lie inside the quadrants in Fig. 2*c* (C_1 and C'_1) and on the ξ_- and ξ_+ axes in Fig. 2*d* (D_1 and D'_1). The last figure (Fig. 2*e*) shows the fifth case with one intersection point at positive values of ξ_+ and ξ_- .

The chain $A-B_0-C_0-D_0-E$ is associated with the solution (denoted as Φ_0) for which the sp spectra coincide: $\xi_+(p) = \xi_-(p) = 0$ within the interval $[p_i, p_f]$, the length of which is determined by the pa-

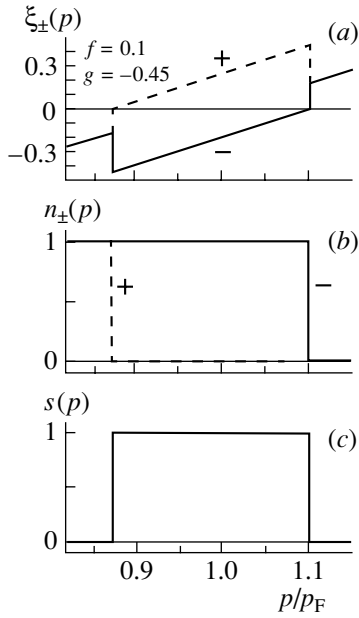


Fig. 11. The same as in Fig. 3 for $f = 0.1, g = -0.45$.

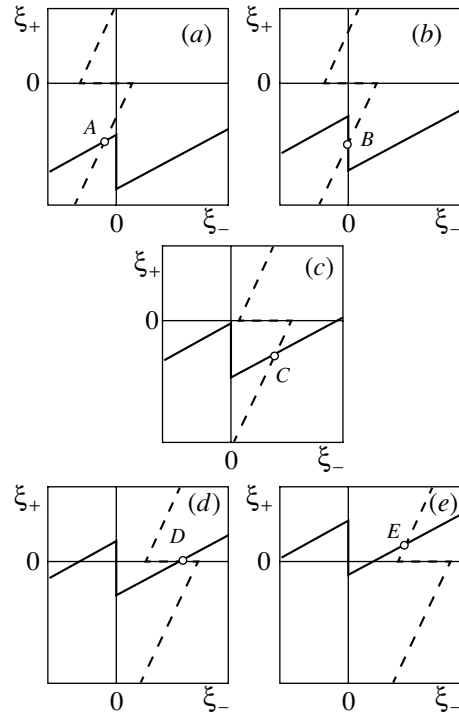


Fig. 13. The same as in Fig. 12 for the case of $\beta H > |g|/2$.

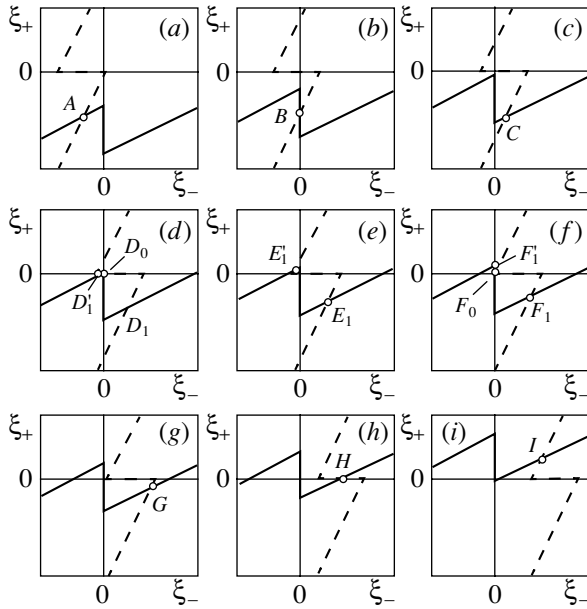


Fig. 12. Graphical illustration of the dynamics of solutions of the set (9) with increasing ξ_p^0 in the case of $|g| < f, \beta H < |g|/2$.

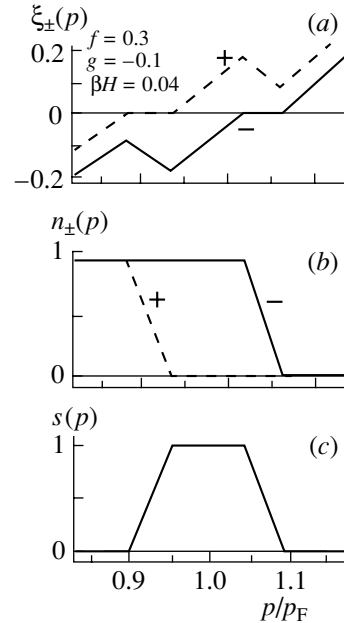


Fig. 14. The same as in Fig. 3 for $f = 0.3, g = -0.1, \beta H = 0.04$.

parameter f only, as if there was no spin–spin interaction at all. The analysis shows that, as long as the constant g remains positive, it is the solution Φ_0 that has the lowest energy compared with the others.

As for solutions related to the chains $A-B_1-C_1-D_1-E$ and $A-B'_1-C'_1-D'_1-E$ (Φ_1 and Φ'_1 , respectively), the situation is different. The solution Φ_1 , corresponding to the first chain, is shown in

Fig. 3. We see that the FC region, the boundaries of which were insensitive to g at any $g > 0$, is destroyed: the spectra $\xi_+(p)$ and $\xi_-(p)$ repel each other. As the momentum p moves from the lower point, where these spectra simultaneously attain the FS, only the

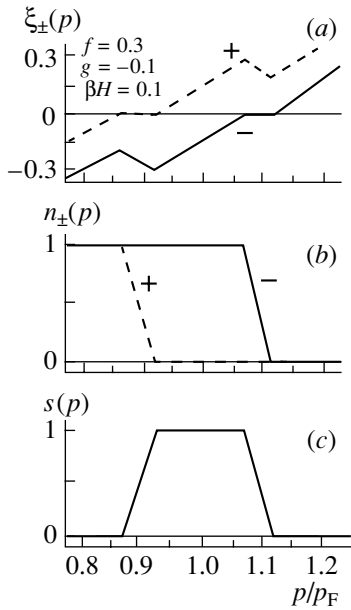


Fig. 15. The same as in Fig. 3 for $f = 0.3$, $g = -0.1$, $\beta H = 0.1$.

FC plateau at the spectrum $\xi_+(p)$ survives, with the energy splitting between the spectra $\xi_+(p)$ and $\xi_-(p)$ growing linearly with the p increase. Attaining the maximum at the point where the plateau at $\xi_+(p)$ vanishes, this splitting ceases to increase and remains constant until the point where a new FC plateau emerges at the spectrum $\xi_-(p)$, and, finally, both spectra once again merge at the point where the FC disappears forever.

The second chain refers to the solution Φ'_1 , symmetric to the previous one, with replacement of \pm by \mp , and, thus, corresponds to the opposite sign of the projection of spontaneous spin S on the fixed axis. Since both directions are equivalent, the two solutions with nonzero S have equal energies. It can be verified that, at any $g < 0$, these solutions provide the minimum of the ground-state energy, while the solution Φ_0 with $S = 0$ gives the maximum. Indeed, calculations yield the gain in energy of the solutions Φ_1 and Φ'_1 , as compared with the energy of the Landau state $E_1/E_L - 1 \simeq -0.027$, while, for the solution Φ_0 , one obtains $E_0/E_L - 1 \simeq -0.019$.

Thus, the reason for these alterations of the FC is the occurrence of the spontaneous spin

$$S = \sum_p s(p) = \sum_p (n_-(p) - n_+(p)) \quad (7)$$

arising at any $g < 0$. For illustration, the spin density $s(p)$ is drawn in Fig. 3c. We infer that the spin density $s(p)$ differs from 0 only in the region $[p_i, p_f]$. Therefore, the total spin S depends primarily on the value

of parameter f . For the parameters f and g given in Fig. 3, one obtains $S/\rho \simeq 0.299$.

For comparison, the results for the other two sets of parameters, $f = 0.3$, $g = -0.01$ and $f = 0.1$, $g = -0.033$, are drawn in Figs. 4 and 5, respectively. The striking feature of these results is that, for the given value $f = 0.3$, the magnitude of the spontaneous spin S for $g = -0.01$, $S/\rho \simeq 0.232$, is of the same order as in the case of $g = -0.1$. The energy gain of the solution with the spontaneous spin, corresponding to f and g for Fig. 4, $E_1/E_L - 1 \simeq -0.019$. Figure 5 shows that multiplication of both parameters f and g by the factor $1/3$ results in the scaling of the spectra, occupation numbers, and spontaneous spin by the same factor.

The situation drastically changes if the magnitude of the spin–spin force becomes comparable to that of the scalar one. This is seen in Figs. 6 and 7, showing the results obtained for the sets $f = 0.3$, $g = -0.3$ and $f = 0.1$, $g = -0.1$, respectively. We see that the FC practically disappears, while the Landau state reappears. Now, the occupation numbers $n_+(p)$ and $n_-(p)$ have the Migdal jump from 0 to 1 at the points p_i and p_f , respectively, and the spontaneous spin attains the maximum value, which is equal to the phase volume of the spherical layer between p_i and p_f ($S/\rho \simeq 0.448$ and $S/\rho \simeq 0.149$ for the parameters of Figs. 6 and 7, respectively). Figure 8 illustrates the evolution of solutions for the set (6) versus $\xi_{\mathbf{p}}^0$ in the case when the absolute value of the spin–spin constant g is larger than the scalar one f . In this case, the set (6) has five solutions: Φ_0 , corresponding to the chain $A-B_0-C_0-D_0-E$; Φ_1 and Φ'_1 , corresponding to the chains $A-B_1-C_0-D_1-E$ and $A-B'_1-C_0-D'_1-E$, respectively; and a new couple of solutions, Φ_2 and Φ'_2 , corresponding to the chains $A-B_2-C_2-D_2-E$ and $A-B'_2-C'_2-D'_2-E$. The calculation of the energies yields the solutions Φ_2 and Φ'_2 , equal in energy, beating Φ_0 , Φ_1 , and Φ'_1 . The solution Φ_2 is drawn in Figs. 9, 10, and 11 for three sets of parameters: $f = 0.1$, $g = -0.15$; $f = 0.3$, $g = -0.45$; and $f = 0.1$, $g = -0.45$, respectively. These figures show that, in this case, the spontaneous spin is defined only by the parameter g , and the parameter f defines the magnitudes of the jumps in the spectra $\xi_+(p)$ and $\xi_-(p)$. It is worth noting that, while the flat portions of the spectra, corresponding to FC, disappear and the Landau state is recovered, the phantom of the FC manifests itself in the emergence of the spontaneous spin.

The above analysis can be generalized to the case of an external magnetic field. In this case, the equations for the sp spectra read

$$\xi_{\pm}(p) = \xi_{\mathbf{p}}^0 + \frac{1}{2}f(n_+(p) + n_-(p)) \quad (8)$$

$$\begin{aligned}
& + \frac{1}{2}g(n_+(p) - n_-(p)) + \beta H, \\
\xi_-(p) & = \xi_{\mathbf{p}}^0 + \frac{1}{2}f(n_+(p) + n_-(p)) \\
& - \frac{1}{2}g(n_+(p) - n_-(p)) - \beta H,
\end{aligned}$$

where H is the effective magnetic field acting on the fermion spin and β is the magnetic moment of the fermion. Upon rewriting Eqs. (8) to a form convenient for graphical analysis, we obtain

$$\begin{aligned}
\xi_+ & = \left(1 - \frac{a}{b}\right) \xi_{\mathbf{p}}^0 + \frac{a}{b} \xi_- + \left(b - \frac{a^2}{b}\right) n_- \quad (9) \\
& + \left(1 + \frac{a}{b}\right) \beta H, \\
\xi_- & = \left(1 - \frac{a}{b}\right) \xi_{\mathbf{p}}^0 + \frac{a}{b} \xi_+ + \left(b - \frac{a^2}{b}\right) n_+ \\
& - \left(1 + \frac{a}{b}\right) \beta H.
\end{aligned}$$

Solutions to Eqs. (9) are represented by broken lines with the same slopes and jumps as in the case of zero magnetic field but shifted by the value $(1 + a/b)\beta H$ along the ξ_+ and ξ_- axes. For $|g| < f$, two cases can be distinguished. In the case where $\beta H < |g|/2$ (βH is in units of $\varepsilon_{\mathbf{F}}^0$), drawn in Fig. 12, two segments, vertical and horizontal, lying on the axes, intersect each other and the situation with three intersection points, discussed above, holds. In the case where $\beta H > |g|/2$, the single intersection point of the two lines remains at any ξ_0 (see Fig. 13). The sp spectra and occupation numbers are shown in Fig. 14 for $f = 0.3$, $g = -0.1$, and $\beta H = 0.04$ and in Fig. 15 for the same values of f and g but at $\beta H = 0.1$. In both cases, the magnetic field promotes splitting of the sp spectra $\xi_+(p)$ and $\xi_-(p)$ but does not influence their flat parts.

In conclusion, in the Nozières-like model of a Fermi system with scalar and spin-dependent long-range forces, it is shown that the fermion condensation, occurring in the vicinity of a phase transition, results in the emergence of weak magnetization which precedes the ferromagnetic transition.

ACKNOWLEDGMENTS

We thank A. Lichtenstein, G. Kotliar, and V. Yakovenko for many valuable discussions.

This research was supported in part by the National Science Foundation (grant nos. PHY99-07949 and PHY-0140316), by the McDonnell Center for the Space Sciences at Washington University, and by the Ministry for Industry and Science (grant no. NS-1885.2003.2) (V.A.K. and M.V.Z.). One of us (V.A.K.) thanks the University of California (Santa Barbara) for its kind hospitality.

REFERENCES

1. S. Doniach and S. Engelsberg, *Phys. Rev. Lett.* **17**, 750 (1966).
2. V. A. Khodel and V. R. Shaginyan, *Pis'ma Zh. Éksp. Teor. Fiz.* **51**, 488 (1990) [*JETP Lett.* **51**, 553 (1990)].
3. L. D. Landau, *Zh. Éksp. Teor. Fiz.* **30**, 1058 (1956); *Zh. Éksp. Teor. Fiz.* **35**, 97 (1958).
4. P. Nozières, *J. Phys. I (France)* **2**, 443 (1992).
5. G. E. Volovik, *Pis'ma Zh. Éksp. Teor. Fiz.* **53**, 208 (1991) [*JETP Lett.* **53**, 222 (1991)].
6. V. A. Khodel, J. W. Clark, and V. R. Shaginyan, *Solid State Commun.* **96**, 353 (1995).
7. J. Dukelsky, V. A. Khodel, P. Schuck, and V. R. Shaginyan, *Z. Phys. B* **102**, 245 (1997).
8. M. V. Zverev and M. Baldo, *Zh. Éksp. Teor. Fiz.* **114**, 2078 (1998) [*JETP* **87**, 1129 (1998)]; *J. Phys.: Condens. Matter* **11**, 2059 (1999).

Extended Random-Phase Approximation and Lipkin–Nogami Method

S. Mishev¹⁾, D. Karadjov¹⁾, and V. V. Voronov*

Joint Institute for Nuclear Research, Dubna, Moscow oblast, 141980 Russia

Received February 18, 2003

Abstract—The Lipkin–Nogami method, which makes it possible to take more accurately into account the law of particle-number conservation, is incorporated in the extended scheme of the random-phase approximation. The effect of ground-state correlations on the transition charge density of the lowest quadrupole state is investigated for the example of the ^{68}Zn nucleus. © 2003 MAIK “Nauka/Interperiodica”.

1. INTRODUCTION

Various properties of vibrational nuclear states were successfully described in the random-phase approximation (RPA), which takes partly into account ground-state correlations. The RPA is the simplest example of boson expansions introduced in the theory of the nucleus in the studies of Belyaev and Zelevinsky [1] and of Marumori, Yamamura, and Tokunaga [2]. It is well known that the RPA violates the Pauli exclusion principle. Since the first attempt at improving the RPA [3], much attention of researchers has been given to this problem [4–16]. In general, the effective nuclear Hamiltonian must include forces in the particle–particle channel for a nonzero angular momentum [17]. A generalization of the extended RPA (ERPA) with allowance for forces in the particle–particle channel was performed in [18]. It is worth mentioning studies that demonstrate the importance of taking into account ground-state correlations beyond the RPA for the charge-exchange branch of excitations [19, 20] treated with allowance for interaction in the particle–particle channel and for nuclei at finite temperatures [21]. An overview of various ERPA versions and their generalizations aimed at taking into account the coupling of one-phonon configurations with more complex ones is given in [22].

In all of the aforementioned studies employing ERPA, monopole pairing [23, 24] was considered in the Bardeen–Cooper–Schrieffer (BCS) approximation, where the law of particle-number conservation is satisfied only on average. The ERPA analysis of the properties of vibrational states in [22] revealed that, by treating ground-state correlations more consistently than in the RPA, one can improve, for example, the

description of transition charge densities of vibrational states within the internal region of spherical nuclei. Nevertheless, disagreement between theoretical results and experimental data remains in some cases, and this may be due, in particular, to the violation of the law of particle-number conservation.

In the present article, we propose improving the description of pairing by combining the ERPA with the well-known Lipkin–Nogami method [25], which is rather simply realized in practice.

2. BASIC EQUATIONS

Since the inclusion of multipole forces in the particle–particle channel has but a slight effect on ground-state correlations [18], we restrict our consideration to the particle–hole channel. We use the Hamiltonian of the quasiparticle–phonon model (QPM) [26]. It includes terms that describe a mean nuclear field in terms of the Woods–Saxon potential, interactions that lead to isoscalar monopole pairing, and the sum of isoscalar and isovector separable multipole–multipole interactions in the particle–hole channel that involve the Bohr–Mottelson radial dependence [27]; that is,

$$H = \sum_{\tau} \left\{ \sum_{jm} (E_j - \lambda_{1\tau}) a_{jm}^+ a_{jm} \quad (1) \right. \\ - \frac{1}{4} G_{\tau}^{(0)} : (R_0^+(\tau) P_0(\tau))^{\tau} \\ : - \frac{1}{2} \sum_{\lambda\mu\sigma=\pm 1} (\kappa_0^{(\lambda)} + \sigma \kappa_1^{(\lambda)}) \\ \left. \times : (M_{\lambda\mu}^+(\tau) M_{\lambda\mu}(\sigma\tau)) : \right\}.$$

Here, τ is the isotopic index, $\tau = \{n, p\}$, where n (p) is a neutron (proton), with the substitution $\tau \leftrightarrow -\tau$

¹⁾Institute for Nuclear Research and Nuclear Energy, Blvd. Tzarigradsko chaussee 72, BG-1784 Sofia, Bulgaria.
* e-mail: voronov@thsun1.jinr.ru

being equivalent to the interchange $p \leftrightarrow n$; E_j are the energies of single-particle states described by the quantum numbers jm (where j stands for the set of the quantum numbers nlj); $\lambda_{1\tau}$ are the chemical potentials determined from the condition requiring that the number of neutrons and protons be conserved on average (isovector monopole pairing is disregarded); $G_\tau^{(0)}$ are the strengths of monopole pairing;

$$P_0^+(\tau) = \sum_{jm}^{\tau} (-1)^{j-m} a_{jm}^+ a_{j-m}^+;$$

$\kappa_0^{(\lambda)}$ and $\kappa_1^{(\lambda)}$ are the isoscalar and isovector strengths of multipole interaction; and

$$M_{\lambda\mu}^+(\tau) = \frac{1}{\sqrt{2\lambda+1}} \times \sum_{\substack{j'm' \\ jm}}^{\tau} (-1)^{j+m} \langle jmj' - m' | \lambda\mu \rangle f_{jj'}^{(\lambda)} a_{jm}^+ a_{j'm'}^+;$$

where $f_{jj'}^{(\lambda)}$ is the single-particle matrix element of multipole interaction. The ensuing analysis is performed in the representation of quasiparticles defined by means of the canonical Bogolyubov transformation

$$a_{jm}^+ = u_j \alpha_{jm}^+ + (-1)^{j-m} v_j \alpha_{j-m}.$$

The Hamiltonian in (1) can be expressed in terms of two-quasiparticle operators as [26]

$$B(jj'; \lambda\mu) = \sum_{mm''} (-1)^{j'+m''} \langle jmj' m'' | \lambda\mu \rangle \alpha_{jm}^+ \alpha_{j'm''}^+;$$

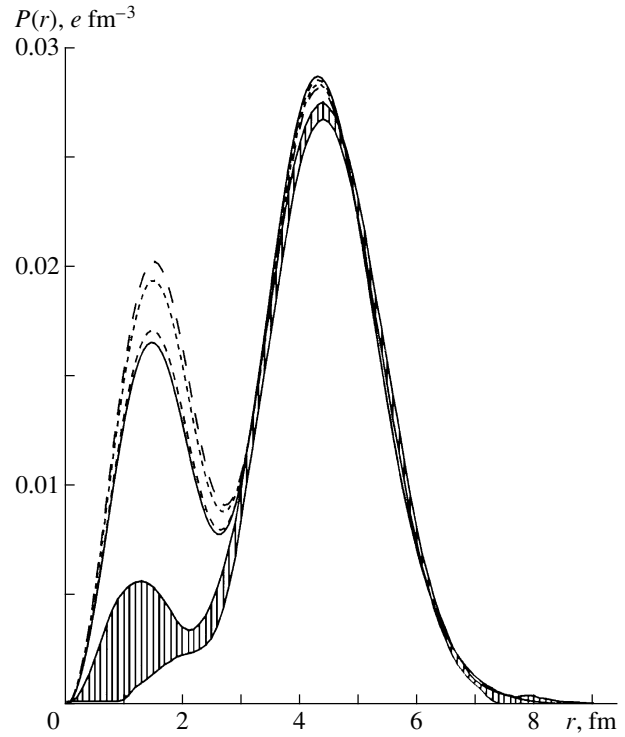
$$A^+(jj'; \lambda\mu) = \sum_{mm'} \langle jmj' m' | \lambda\mu \rangle \alpha_{jm}^+ \alpha_{j'm'}^+.$$

Let us make a linear transformation to go over from the operators $A^+(jj'; \lambda\mu)$ and $A(jj'; \lambda\mu)$ to the phonon creation and annihilation operators:

$$Q_{\lambda\mu,i}^+ = \frac{1}{2} \sum_{jj'} \{ \psi_{jj'}^{\lambda i} A^+(jj'; \lambda\mu) - (-1)^{\lambda-\mu} \varphi_{jj'}^{\lambda i} A(jj'; \lambda-\mu) \}. \quad (2)$$

We now assume that the phonon vacuum $|0\rangle$ ($Q_{\lambda\mu,i}|0\rangle = 0$) is the ground state of an even-even nucleus, so that excited states have the form $Q_{\lambda\mu,i}^+|0\rangle$. Taking into account the orthogonality condition for different excited states and their normalization ($\langle 0|[Q_{\lambda\mu,i}, Q_{\lambda\mu,i'}^+] |0\rangle = \delta_{ii'}$), we obtain

$$\frac{1}{2} \sum_{jj'} (1 - q_{jj'}) \left[\psi_{jj'}^{\lambda i} \psi_{jj'}^{\lambda i'} - \varphi_{jj'}^{\lambda i} \varphi_{jj'}^{\lambda i'} \right] = \delta_{ii'},$$



Transition charge density of the 2_1^+ state in the ^{68}Zn nucleus: (solid curve) results of the ERPA calculation by the Lipkin–Nogami method, [short (long) dashes] results of the ERPA (RPA) calculation, and (dotted curve) results of the calculation by the Lipkin–Nogami method in the RPA. The shaded area represents experimental data from [28].

where $q_{jj'} = q_j + q_{j'}$, $q_j \equiv (2j+1)^{-1/2} \langle 0|B(jj; 00)|0\rangle$ being the quasiparticle distribution in the ground state. In the ERPA [22], the pairing part of the Hamiltonian can be diagonalized with the aid of the variational principle, where the quasiparticle vacuum is replaced by the phonon vacuum. As a result, the quasiparticle energies $\varepsilon_j = \sqrt{\Delta_\tau^2 + (E_j - \lambda_{1\tau})^2}$ and the coefficients u_j and v_j have the same form as in the BCS approximation, while the new quantities for pairing gap $\Delta_\tau = \frac{1}{2} G_\tau^{(0)} \sum_j (1 - 2q_j)(2j+1)u_j v_j$ and for the chemical potential $\lambda_{1\tau}$ can be found from modified BCS equations (see [22]).

In the conventional Lipkin–Nogami method, the equations for the gap and the chemical potential are derived from the variational principle involving BCS trial functions,

$$\delta \langle \text{BCS} | H - \lambda_{2\tau} \hat{N}^2 | \text{BCS} \rangle = 0, \quad (3)$$

where \hat{N} is the particle-number operator given by

$$\hat{N} = \sum_{jm} a_{jm}^+ a_{jm}. \quad (4)$$

Replacing the BCS vacuum by the phonon vacuum and performing the same transformations as in [25], one can derive a set of nonlinear equations for determining the properties of quasiparticles and phonons; that is,

$$\sum_{\tau} \left[\left(\kappa_0^{(\lambda)} + \kappa_1^{(\lambda)} \right) X_{\tau}^{\lambda i} - 2\kappa_0^{(\lambda)} \kappa_1^{(\lambda)} X_{\tau}^{\lambda i} X_{-\tau}^{\lambda i} \right] = 1, \quad (5)$$

$$X_{\tau}^{\lambda i} = \sum_{jj'}_{\tau} \frac{(f_{jj'}^{(\lambda)} u_{jj'}^{(+)})^2 \varepsilon_{jj'} (1 - q_{jj'})}{(\varepsilon_{jj'})^2 - \omega_{\lambda i}^2}, \quad (6)$$

$$\sum_{jj'} (1 - q_{jj'}) [(\psi_{jj'}^{\lambda i})^2 - (\varphi_{jj'}^{\lambda i})^2] - 2 = 0, \quad (7)$$

$$\frac{4\lambda_{2\tau}}{G_{\tau}^{(0)}} = \frac{\sum_j \pi_j^2 u_j^3 v_j (1 - 2q_j) \sum_j \pi_j^2 u_j v_j^3 (1 - 2q_j) - 2 \sum_j \pi_j^2 u_j^4 v_j^4 (1 - 2q_j)}{(\sum_j \pi_j^2 u_j^2 v_j^2 (1 - 2q_j))^2 - 2 \sum_j \pi_j^2 u_j^4 v_j^4 (1 - 2q_j)}, \quad (10)$$

$$\langle 0 | \hat{N}_{\tau} | 0 \rangle = \sum_j \pi_j^2 [q_j + v_j^2 (1 - 2q_j)] = n_{\tau}, \quad (11)$$

where $\varepsilon_{jj'} = \varepsilon_j + \varepsilon_{j'}$, $\varepsilon_j = \sqrt{\Delta_{\tau}^2 + (\varepsilon_j^1 - \lambda^{1q\tau})^2}$, $u_{jj'}^{(+)} = u_j v_{j'} + v_j u_{j'}$, and $\pi_j = \sqrt{2j + 1}$.

For $\lambda_{2\tau} = 0$, we arrive at the well-known set of ERPA equations, while, for $q_j = 0$, we have the RPA and BCS equations.

3. RESULTS OF THE CALCULATIONS

By way of example, we have calculated the transition charge density for 2_1^+ state in the ^{68}Zn nucleus. The results of the calculations performed for this state in [16] exhibited significant deviations from experimental data. In the present calculation, we use the parameters of the quasiparticle–phonon Hamiltonian from [16].

The energies and the occupation numbers calculated for proton states in the BCS approximation and by the Lipkin–Nogami method are quoted in the table. Also given there are single-particle energies for the Woods–Saxon potential. In the BCS approximation, we obtained the value of $\lambda_{1p} = -15.2482$ MeV for the chemical potential and the value of $\Delta_p = 0.99011$ MeV for the gap. Within the Lipkin–Nogami method, we arrived at $\lambda_{1p} = -15.02671$ MeV and $\lambda_{2p} = 0.26321$ MeV for the same value of gap. As can be seen from the table, the largest changes in the single-particle energies and occupation numbers with respect to their counterparts in the BCS approximation are observed for levels far off the Fermi surface. This is manifested in the structure of the 2_1^+ state as well, for which the energies and the reduced probabilities of $E2$ transitions evaluated by the Lipkin–Nogami method are virtually coincident with

$$q_j = \frac{1}{2} \sum_{\lambda i, j'} \frac{2\lambda + 1}{2j + 1} (1 - q_{jj'}) (\varphi_{jj'}^{\lambda i})^2, \quad (8)$$

$$2(\varepsilon_j^1 - \lambda^{1q\tau}) u_j v_j = \Delta_{\tau} (u_j^2 - v_j^2), \quad (9)$$

$$\varepsilon_j^1 = E_j - (4\lambda_{2\tau} - G_{\tau}^{(0)}) v_j^2,$$

$$\lambda^{1q\tau} = \lambda_{1\tau} + 2\lambda_{2\tau} (n_q + 1),$$

$$n_q = \sum_j \pi_j^2 v_j^2 (1 - 2q_j) + \sum_j \pi_j^2 q_j,$$

those calculated in the BCS approximation. This is so both in the RPA and in the ERPA.

For the 2_1^+ state in the ^{68}Zn nucleus, the results of our calculations for the transition charge density are shown in the figure along with experimental data from [28]. It can be seen that, owing to a more correct treatment of the Pauli exclusion principle (see [22]), the inclusion of correlations within the ERPA leads to an approximately 20% suppression of the amplitude of the internal peak of the transition charge density in relation to that in the RPA. These results undergo virtually no changes upon taking more accurately into account the law of particle-number conservation by means of the Lipkin–Nogami method. As was shown in [22], the inclusion of two-phonon configurations leads to an additional 10% suppression of the internal peak, but there still remains a noticeable deviation from experimental data.

4. CONCLUSION

In order to take more accurately into account the law of particle-number conservation, the Lipkin–Nogami method is incorporated in the ERPA scheme. For the example of the ^{68}Zn nucleus, we have studied the effect of ground-state correlations on the transition charge density of the lowest quadrupole state. It has been shown that the law of particle-number conservation has but a slight effect on the properties of vibrational states. It seems that, in order to obtain an eventual solution to the problem of describing transition densities in the internal region of nuclei, it is necessary to introduce, in the ERPA, more realistic effective nuclear forces and self-consistent approaches [29, 30].

Single-quasiparticle energies and occupation numbers evaluated by means of the BCS approximation and the Lipkin–Nogami method

State	E_j , MeV	BCS method			Lipkin–Nogami method		
		ε_j , MeV	v_j	u_j	ε_j , MeV	v_j	u_j
$1s_{1/2}$	−42.7234	26.6626	0.9998	0.0186	27.4571	0.9998	0.0180
$1p_{3/2}$	−35.6506	19.59676	0.9997	0.0253	20.3904	0.9997	0.0243
$1p_{1/2}$	−34.2727	18.2208	0.9996	0.0272	19.0143	0.9997	0.0260
$1d_{5/2}$	−27.7093	11.6737	0.9991	0.0424	12.4645	0.9992	0.0397
$1d_{3/2}$	−24.7378	8.7180	0.9984	0.0569	9.5053	0.9986	0.0522
$2s_{1/2}$	−24.2639	8.2478	0.9982	0.0601	9.0341	0.9985	0.0549
$1f_{7/2}$	−19.1206	3.2224	0.9878	0.01555	3.9621	0.9920	0.1259
$2p_{3/2}$	−14.8392	1.1017	0.5299	0.8481	1.0855	0.5432	0.8396
$1f_{5/2}$	−14.1582	1.4198	0.3763	0.9265	1.4994	0.3529	0.9357
$2p_{1/2}$	−13.0023	2.2997	0.2207	0.9753	2.4874	0.2033	0.9791
$1g_{1/2}$	−10.0485	5.0856	0.0978	0.9952	5.3285	0.0933	0.9956
$2d_{5/2}$	−5.6700	9.4119	0.0527	0.9986	9.6651	0.0513	0.9987
$3s_{1/2}$	−3.7428	11.3292	0.0437	0.9990	11.5838	0.0428	0.9991
$1g_{7/2}$	−2.9084	12.1604	0.0407	0.9992	12.4153	0.0399	0.9992
$2d_{3/2}$	−2.5735	12.4941	0.0397	0.9992	12.7492	0.0389	0.9992
$1h_{11/2}$	−0.6506	14.4114	0.0344	0.9994	14.6671	0.0338	0.9994
$2f_{7/2}$	2.7817	17.8367	0.0278	0.9996	18.0930	0.0274	0.9996
$3p_{3/2}$	3.3317	18.3859	0.0269	0.9996	18.6422	0.0266	0.9996

REFERENCES

- S. T. Belyaev and V. G. Zelevinskiĭ, Zh. Éksp. Teor. Fiz. **42**, 1590 (1962); S. T. Belyaev and V. G. Zelevinskiĭ, Nucl. Phys. **39**, 582 (1962).
- T. Marumori, M. Yamamura, and A. Tokunaga, Prog. Theor. Phys. **31**, 1009 (1964).
- Ken-ji Hara, Prog. Theor. Phys. **32**, 88 (1964).
- K. Ikeda, T. Udagawa, and H. Yamamura, Prog. Theor. Phys. **33**, 22 (1965).
- D. J. Rowe, Rev. Mod. Phys. **40**, 153 (1968).
- J. da Providencia, Nucl. Phys. A **108**, 589 (1968).
- R. V. Jolos and W. Rybarska, Z. Phys. A **296**, 73 (1980).
- V. Navrotska-Rybarska, O. Stoyanova, and Ch. Stoyanov, Yad. Fiz. **33**, 1494 (1981) [Sov. J. Nucl. Phys. **33**, 802 (1981)].
- C. H. Johnson and C. Mahaux, Phys. Rev. C **38**, 2589 (1988).
- H. Lenske and J. Wambach, Phys. Lett. B **249**, 377 (1990).
- A. Klein, N. R. Walet, and G. Do Dang, Nucl. Phys. A **535**, 1 (1991).
- D. Karadjov, V. V. Voronov, and F. Catara, Phys. Lett. B **306**, 197 (1993).
- D. Karadjov, V. V. Voronov, and F. Catara, J. Phys. G **20**, 1431 (1994).
- M. Sambataro and F. Catara, Phys. Rev. C **51**, 3066 (1995).
- J. Dukelsky and P. Schuck, Phys. Lett. B **387**, 233 (1996).
- D. Karadjov *et al.*, Nucl. Phys. A **643**, 259 (1998).
- S. T. Belyaev, Yad. Fiz. **4**, 936 (1966) [Sov. J. Nucl. Phys. **4**, 671 (1966)].
- A. P. Severyukhin, V. V. Voronov, and D. Karadzov, Report of Joint Inst. Nucl. Res. No. 4-99-121 (Dubna, 1999).
- J. Toivanen and J. Suhonen, Phys. Rev. Lett. **75**, 410 (1995).
- F. Krmpotic *et al.*, Nucl. Phys. A **612**, 223 (1997).
- A. N. Storozhenko, D. S. Kosov, and A. I. Vdovin, Yad. Fiz. **62**, 63 (1999) [Phys. At. Nucl. **62**, 58 (1999)].
- V. V. Voronov, D. Karadjov, F. Catara, and A. P. Severyukhin, Phys. Part. Nucl. **31**, 905 (2000).
- V. G. Solov'ev, Zh. Éksp. Teor. Fiz. **35**, 823 (1958).

24. S. T. Belyaev, K. Dan. Vidensk. Selsk. Mat. Fys. Medd. **31** (11)(1959).
25. H. J. Lipkin, Ann. Phys. (N.Y.) **12**, 425 (1960); Y. Nogami, Phys. Rev. **134**, B313 (1964).
26. V. G. Solov'ev, *Theory of Atomic Nuclei* (Énergoizdat, Moscow, 1989; Institute of Physics, Bristol, 1992).
27. A. Bohr and B. R. Mottelson, *Nuclear Structure*, Vol. 2: *Nuclear Deformations* (Benjamin, New York, 1975; Mir, Moscow, 1977).
28. R. Neuhausen, Nucl. Phys. A **282**, 125 (1977).
29. S. A. Fayans, V. A. Khodel, and E. E. Saperstein, Nucl. Phys. A **317**, 424 (1979).
30. A. P. Severyukhin, Ch. Stoyanov, V. V. Voronov, and N. V. Giai, Phys. Rev. C **66**, 034304 (2002).

Translated by S. Slabospitsky

Semimicroscopic Description of Basic Properties of Isoscalar Monopole and Dipole Excitations in Medium-Mass Spherical Nuclei

M. L. Gorelik and M. H. Urin

Moscow Engineering Physics Institute (State University), Kashirskoe sh. 31, Moscow, 115409 Russia

Received February 25, 2003

Abstract—A description of basic properties (strength function, transition density, probabilities of direct nucleonic decays) of isoscalar giant monopole (including an overtone) and dipole resonances in medium-mass spherical nuclei is proposed within a semimicroscopic approach. The approach relies on employing the random-phase approximation and involves taking exactly into account a single-particle continuum and some conditions of partial self-consistency and phenomenologically describing the coupling of states of the particle–hole type to multiquasiparticle configurations. The results of the calculations that were performed for ^{90}Zr , $^{116,124}\text{Sn}$, ^{144}Sm , and ^{208}Pb nuclei are compared with available experimental data.

© 2003 MAIK “Nauka/Interperiodica”.

*With admiration of the long-standing creative
ability of the hero of the celebration ...*

1. INTRODUCTION

In recent years, much attention has been given to experimentally and theoretically studying compression modes of nuclear excitations. Such modes include an isoscalar giant monopole resonance and an isoscalar giant dipole resonance (ISGMR and ISGDR, respectively). Interest in such resonances is motivated to a considerable extent by the hope of extracting, from experimental data, the compressibility of nuclear matter. However, the microscopic structure and detailed properties of giant resonances as collective excitations of an open finite Fermi system are of interest in and of themselves. From the microscopic point of view, giant resonances correspond to collective excitations of the particle–hole type. For example, an isoscalar giant monopole resonance is formed primarily owing to nucleon transitions between shells separated by one shell ($2\hbar\omega$ transitions), while an overtone of such a resonance (ISGMR2) is due primarily to transitions between shells separated by three shells ($4\hbar\omega$ transitions). The main (or upper) component of an isoscalar giant dipole resonance is formed owing to transitions between shells separated by two shells ($3\hbar\omega$ transitions), while its lower component (pygmy resonance or pygmy-ISGDR) is associated with transitions to the neighboring shell ($1\hbar\omega$ transitions.) Being an isoscalar dipole excitation, an ISGDR can be treated as an overtone having zero excitation energy of the unphysical (ghost) 1^- state corresponding to center-of-mass motion.

Systematic experimental data on the properties of isoscalar giant monopole and dipole resonances were obtained from an analysis of the inclusive cross sections for small-angle inelastic scattering of 100- to 400-MeV alpha particles on ^{90}Zr , ^{116}Sn , ^{144}Sm , and ^{208}Pb nuclei [1, 2]. This yielded, among other things, information about the distribution of isoscalar monopole and dipole strengths over a rather wide energy interval and, hence, about such quantities as the energy centroid, the widths of the main maxima, and the fraction of exhaustion of the energy-weighted sum rule. Experimental data on the partial widths with respect to direct neutronic decays of isoscalar giant monopole resonances were obtained from an analysis of cross sections for $(\alpha, \alpha'n)$ reactions [3–7]. A direct nucleonic decay of an isoscalar giant dipole resonance is being presently investigated with the aid of $(\alpha, \alpha'N)$ reactions [8].

In view of space limitations, we will only briefly touch here upon the latest theoretical approaches to describing the properties of isoscalar giant resonances. Within the microscopic approach developed by Colo *et al.* [9], one realizes the random-phase approximation (RPA) in a discrete basis of particle–hole ($1p-1h$) configurations and employs a Hartree–Fock nuclear mean field and particle–hole interaction obtained on the basis of Skyrme forces, taking explicitly into account the coupling of $1p-1h$ and $2p-2h$ configurations. So far, this approach has been applied only to calculating strength functions for giant resonances. In the analogous approach proposed by Shlomo *et al.* [10], the coupling of $1p-1h$ and $2p-2h$ configurations is taken into account phenomenologically in terms of an energy-independent smear-

ing parameter. In addition to strength functions, the quantities that have been calculated within this approach include transition densities for isoscalar giant monopole and dipole resonances, whereupon the cross sections for (α, α') reactions involving the excitation of such resonances are determined on the basis of these densities. The semimicroscopic approach in the development of which the present authors take part also relies on the random-phase approximation, but the realization of this approximation here makes it possible to take exactly into account a single-particle continuum (continuum RPA or CRPA). A phenomenological isoscalar part of the mean field and a phenomenological Landau–Migdal amplitude are used within this approach along with some conditions of self-consistency, the smearing parameter being chosen to be excitation-energy dependent. In addition to strength functions and transition densities, the probabilities of direct nucleonic decays of resonances belonging to the ISGMR, ISGMR2, and ISGDR types were calculated [11, 12] within the semimicroscopic approach in question. The strength functions for isoscalar giant resonances were also calculated within the relativistic version of the random-phase approximation [13] and within the semiclassical approach based on solving Vlasov equations for the distribution function [14]. In all probability, theoretical approaches will be selected on the basis of two criteria: (i) the completeness of description of the properties of giant resonances and (ii) the degree to which the model being considered is self-consistent. In this connection, we note that only within our semimicroscopic approach was it possible to obtain a systematic description of direct nucleonic decays of giant resonances, the consistency of the model being tested not only by the proximity of the calculated energy of the 1^- ghost state to zero but also by an analysis of the degree to which the energy-weighted sum rule corresponding to the radius vector of the center of mass of the nucleus being considered is exhausted by this state. The semimicroscopic approach was also used to describe basic properties of some isovector spinless and spin-flip giant resonances [15, 16].

In this article, we give an overview of the main results that the present authors obtained both in what is concerned with the formulation of the semimicroscopic approach and in what is concerned with its applications to describing basic properties of isoscalar monopole and dipole excitations in medium-mass spherical nuclei. The ensuing exposition is organized as follows. In Section 2, we give underlying relations of the approach that include the model Hamiltonian, CRPA equations, the conditions of partial self-consistency, the description of the coupling of $1p-1h$ configurations to multiquasiparticle configurations, and methods for calculating basic properties

of giant resonances. In Section 3, we present model parameters and the results obtained by calculating the properties of resonances belonging to the ISGMR, ISGDR, and ISGMR2 types. In Section 4, we discuss our results and consider prospects for a further development of the approach.

2. BASIC RELATIONS OF THE SEMIMICROSCOPIC APPROACH

2.1. Model Hamiltonian

The semimicroscopic approach in question is based on the use of the model Hamiltonian corresponding to a phenomenological version of the theory of finite Fermi systems [17]. The Hamiltonian involves a mean field $U(x)$ and interaction in the particle–hole channel, $F(x, x')$ (here, x stands for a set of nucleon coordinates, including spin and isospin variables). In view of a high excitation energy of the giant resonances being considered, the pairing of nucleons in nuclei featuring unfilled shells can be disregarded to an acceptable degree of precision. The mean field contains a phenomenological isoscalar part (which includes a spin–orbit term), as well as an isovector and a Coulomb component, which are calculated self-consistently; that is,

$$U(x) = U_0(x) + U_1(x) + U_C(x), \quad (1)$$

$$U_0(x) = U_0(r) + U_{ol}(x),$$

$$U_1(x) = \frac{1}{2}v(r)\tau^{(3)},$$

$$U_C(x) = \frac{1}{2}(1 - \tau^{(3)})U_C(r).$$

Here, $U_0(r)$ and $U_{ol}(x) = U_{ol}(r)\boldsymbol{\sigma} \cdot \mathbf{1}$ are, respectively, the central and the spin–orbit component of the isoscalar mean field; $v(r)$ is the symmetry potential; and $U_C(r)$ is the mean energy of the Coulomb interaction between protons and the nucleus being considered. The mean field determines the bound-state energies ε_λ [$\lambda = n_r, j, l$; ($\lambda) = j, l$ is the set of single-particle quantum numbers]; radial wave functions $r^{-1}\chi_\lambda(r)$; and the Green's functions $(rr')^{-1}g_{(\lambda)}(r, r', \varepsilon)$ for the radial Schrödinger equation, which are defined for an arbitrary energy and which are expressed in terms of the regular and the nonregular solution to this equation. The densities of neutrons (n) and protons (p),

$$n^\alpha(r) = \frac{1}{4\pi r^2} \sum_\lambda (2j_\lambda + 1) n_\lambda^\alpha (\chi_\lambda^\alpha(r))^2 \quad (2)$$

(n_λ^α are occupation numbers, $\alpha = n, p$), are used below to realize the conditions of partial self-consistency and to calculate the energy-weighted sum rule.

The interaction of quasiparticles in the particle-hole channel was chosen in the form of Landau–Migdal forces [17]. The spinless part of this interaction has the form

$$F(x, x') = (F(r) + F'(r)\boldsymbol{\tau} \cdot \boldsymbol{\tau}')\delta(\mathbf{r} - \mathbf{r}'), \quad (3)$$

where $F(r)$ and $F'(r)$ are phenomenological quantities that specify the strengths of, respectively, the isoscalar and the isovector component of the interaction. The isovector self-consistency condition, which is a corollary of the isospin symmetry of the model Hamiltonian, makes it possible to calculate the symmetry potential self-consistently: $v(r) = 2F'(n^n(r) - n^p(r))$ [18]. The mean Coulomb field of a nucleus is also calculated self-consistently in the Hartree approximation: $U_C(r) = U_C[n^p(r)]$. A partial self-consistency that is associated with an approximate restoration of the translational invariance of the model will be discussed below.

2.2. Equations of the Random-Phase Approximation

The equations of the random-phase approximation are given below in the form that is used in the theory of finite Fermi systems [17]. Suppose that $\hat{V} \exp\{-i\frac{\omega}{\hbar}t\} + \text{h.c.}$ is a periodic (in time) external single-particle field acting on a nucleus ($\hat{V} = \sum_a V(x_a)$). In order to study isoscalar excitations of multipole order L , we represent the expression for the trial operator in the form $V_L(x) = V_L(r)Y_{LM}(\mathbf{r}/r)$. The strength function $S_L(\omega)$ corresponding to the above external field is proportional to the imaginary part of the corresponding polarizability $P_L(\omega)$. Upon the separation of spin–angular and isotopic variables, this strength function assumes the form

$$S_L(\omega) = -\frac{1}{\pi} \text{Im} P_L(\omega), \quad (4)$$

$$P_L(\omega) = \sum_{\alpha=n,p} \int V_L^*(r) A_{L,\alpha}(r, r', \omega) \tilde{V}_{L,\alpha}(r', \omega) dr dr',$$

where $(rr')^{-2}A_{L,\alpha}(r, r', \omega)$ is the radial part of the free response function (particle–hole propagator), ω is the excitation energy, and $\tilde{V}_{L,\alpha}(r', \omega)$ is the radial part of the corresponding effective field. The set of equations for the effective fields has the form

$$\begin{aligned} \tilde{V}_{L,\alpha}(r, \omega) &= V_L(r) \\ &+ \sum_{\beta} \frac{F_{\alpha\beta}(r)}{r^2} \int A_{L,\beta}(r, r', \omega) \tilde{V}_{L,\beta}(r', \omega) dr', \end{aligned} \quad (5)$$

where $F_{\alpha\beta}(r) = [(F(r) + F'(r))\delta_{\alpha\beta} + (F(r) - F'(r))\tau_{\alpha\beta}^{(1)}]$ is the strength matrix of the particle–hole interaction (3) and $\boldsymbol{\tau}(\tau^{(1)}, \tau^{(2)}, \tau^{(3)})$ are the isospin

Pauli matrices. The expression for the propagator $A_{L,\alpha}(r, r', \omega)$ can be represented in a form where the contribution of the single-particle continuum is taken exactly into account; that is,

$$\begin{aligned} A_{L,\alpha} &= \sum_{\mu,(\lambda)} (t_{(\lambda)(\mu)}^L)^2 n_{\mu}^{\alpha} \chi_{\mu}^{\alpha}(r) \chi_{\mu}^{\alpha}(r') \\ &\times \left[g_{(\lambda)}^{\alpha}(r, r', \varepsilon_{\mu} + \omega) + g_{(\lambda)}^{\alpha}(r, r', \varepsilon_{\mu} - \omega) \right], \end{aligned} \quad (6)$$

where, in just the same way as in (2), the occupation numbers $n_{\mu} = N_{\mu}/(2j_{\mu} + 1)$ are expressed in terms of the number N_{μ} of nucleons that occupy the μ level and where $t_{(\lambda)(\mu)}^L = (2L + 1)^{-1/2} \times \langle(\lambda)||Y_L||(\mu)\rangle$ is a kinematical factor.

It should be noted that relations (4)–(6) refer literally to the case of describing isoscalar 0^+ excitations ($L = S = 0$). For excitations characterized by a nonzero value of the total angular momentum J^{π} (π is parity), states in which the orbital angular momenta L or the total spins S (or both) are different may be coupled owing to spin–orbit interaction. Usually, the inclusion of this coupling changes only slightly the calculated features of giant resonances (see, for example, [19]). In accordance with Eqs. (4)–(6), the properties of isoscalar giant dipole resonances are explored below without taking into account the coupling of this resonance to isoscalar spin–dipole 1^- excitations ($L = 1, S = 1$).

For a given energy interval $\delta = \omega_2 - \omega_1$, the relative strength of a giant resonance is characterized by the quantity

$$x_L = \frac{\int_{(\delta)} \omega S_L(\omega) d\omega}{(\text{EWSR})_L} = \int_{(\delta)} y_L(\omega) d\omega, \quad (7)$$

where $y_L(\omega)$ is the reduced strength function and $(\text{EWSR})_L$ is the energy-dependent sum rule, which is weakly dependent on the choice of model and which is given by [20]

$$\begin{aligned} (\text{EWSR})_L &= (\hbar^2/2m) \sum_{\alpha} \int [(dV_L/dr)^2 \\ &+ L(L + 1)(V_L/r)^2] n^{\alpha}(r) r^2 dr. \end{aligned} \quad (8)$$

Here, m is the nucleon mass and $n^{\alpha}(r)$ is the nucleon density (2). The mean giant-resonance energy ω_L and its root-mean-square deviation Δ_L are determined by the strength function $S_L(\omega)$ and by the chosen interval of averaging, δ .

The radial part of the differential (that is, excitation-energy-dependent) transition density of an isoscalar giant resonance, $\rho_L(x, \omega) =$

$r^{-2}\rho_L(r, \omega)Y_{LM}(\mathbf{r}/r)$, is determined from the relation

$$S_L(\omega) = \left(\int V_L(r)\rho_L(r, \omega)dr \right)^2. \quad (9)$$

On the basis of this definition and relations (4) and (5), we obtain the following representation for the radial transition density:

$$\rho_L(r, \omega)/r^2 = -\frac{1}{\pi} \frac{\text{Im} \sum_{\alpha} \tilde{V}_{L,\alpha}(r, \omega)}{2F(r)S_L^{1/2}(\omega)}. \quad (10)$$

In order to compare transition densities associated with different energy intervals, it is convenient to use the differential transition density

$$\mathcal{R}_L(r, \omega) = \rho_L(r, \omega)/S_L^{1/2}(\omega), \quad (11)$$

which is normalized by the condition $\int V_L(r)\mathcal{R}_L(r, \omega)dr = 1$.

From an alternative expression that can be obtained for the strength function on the basis of relations (4)–(6), it follows that the optical theorem is realized for excitation-energy (ω) values in excess of the nucleon binding energy; that is,

$$S_L(\omega) = -\frac{1}{\pi} \text{Im} \sum_{\alpha} \int \tilde{V}_{L,\alpha}^*(r, \omega) \quad (12)$$

$$\times A_{L,\alpha}(r, r', \omega) \tilde{V}_{L,\alpha}(r', \omega) dr dr' = \sum_c |M_{L,c}|^2,$$

$$M_{L,c}(\omega) = (n_{\mu}^{\alpha})^{1/2} t_{(\lambda)(\mu)}^L \int \chi_{\varepsilon(\lambda)}^{\alpha(+)} \tilde{V}_{L,\alpha}(r, \omega) \chi_{\mu}^{\alpha} dr, \quad (13)$$

$$\varepsilon = \varepsilon_{\mu} + \omega,$$

where $r^{-1}\chi_{\varepsilon(\lambda)}^{\alpha(+)}$ is the radial wave function that describes the scattering of nucleons on the potential $U(x)$ and which is normalized to a delta function of energy, $c = \mu, (\lambda)$, and α stands for a set of quantum numbers that characterize the nucleon channel of a reaction induced by the external field $\tilde{V}_L(x)$. The quantity $M_{L,c}(\omega)$ in (13) has the meaning of the amplitude for nucleon emission under the effect of the external field. The relative probability of a process where the direct nucleonic decay of a giant resonance is accompanied by the population of a single-hole state μ^{-1} can be characterized by the quantity

$$b_{\mu,\alpha} = \frac{\sum_{(\lambda)} \int_{(\delta)} |M_{L,c}(\omega)|^2 d\omega}{\int_{(\delta)} S_L(\omega) d\omega}. \quad (14)$$

Within the random-phase approximation, the relation $\sum_{\mu,\alpha} b_{\mu,\alpha} = 1$ naturally holds for any interval δ , as follows from Eqs. (12) and (13).

2.3. Choice of Trial Operators and Ghost State

The choice of radial dependence for the trial operators $V_L(r)$ is dictated by the requirement that the corresponding giant resonance exhaust a major part of the energy-weighted sum rule $(EWSR)_L$ associated with this operator. In describing an isoscalar giant monopole resonance, the operator $V_{L=0}(r) = r^2$ satisfies this condition; for the ghost state, this is $V_{L=1}^{SS}(r) = r$ (the corresponding operator $\tilde{V}_{L=1}^{SS}$ is proportional to the radius vector of the center of mass of the nucleus being considered).

As applied to the approach used in the present study, the term “semimicroscopic” has two facets. The first concerns the phenomenological choice of the isoscalar component of the mean field $U_0(x)$ in (1), while the second refers to a phenomenological description of the coupling of particle–hole configurations to multiquasiparticle configurations (see Subsection 2.4 below). The translational-invariance violation associated with the choice of the field $U_0(x)$ can be partly removed if the strength $F(r)$ of the isoscalar component of the interaction in (3) is chosen on the basis of the condition requiring that the ghost-state energy ω_{SS} be close to zero. The degree to which the broken symmetry is restored depends on the proximity of the quantity x_{SS} to unity. Within the random-phase approximation, this quantity can be calculated with the aid of the polarizability $P_{L=1}^{SS}(\omega)$ corresponding to the trial operator $V_{L=1}^{SS}(r)$, since, in accordance with the spectral expansion (see, for example, [11]), the polarizability in question taken in the limit $\omega \rightarrow \omega_{SS} \rightarrow 0$ can be parametrized in the form

$$P_{L=1}^{SS}(\omega) \rightarrow \frac{2x_{SS}}{\omega^2 - \omega_{SS}^2} (EWSR)_{L=1}^{SS}. \quad (15)$$

In accordance with the above requirement for the description of overtones, the radial dependence of the corresponding trial operators $V_L^{(2)}(r)$ is chosen with allowance for the condition requiring that the fundamental tone not be excited; that is,

$$\int V_L^{(2)}(r)\rho_L(r, \omega_{\max})dr = 0, \quad (16)$$

where $r^{-2}\rho_L(r, \omega_{\max})$ is the radial transition density as calculated for the fundamental tone at the energy value corresponding to the maximum of the relevant giant resonance. In order to describe the properties of giant resonances belonging to the ISGDR and IS-GMR2 types, the radial dependence of trial operators was chosen in the form

$$V_{L=1}(r) = r^3 - \eta_1 r; \quad V_{L=0}^{(2)}(r) = r^4 - \eta_0 r^2, \quad (17)$$

where the parameters η_1 and η_0 are determined by the conditions in (16). If translational invariance is restored completely, the transition density of the ghost state is proportional to dn/dr . In this case, it follows from Eqs. (16) and (17) that $\eta_1 = 5\langle r^2 \rangle / 3$, where averaging is performed over the nucleon density $n(r)$.

2.4. Coupling to Multi-quasiparticle Configurations

As one of its basic elements, the semimicroscopic approach involves phenomenologically taking into account the fragmentation of doorway states of the particle-hole type (this is equivalent to taking into account their coupling to multi-quasiparticle configurations). Depending on the excitation energy (on the strength of coupling of doorway states to the single-particle continuum), we employ various methods for taking fragmentation into account. For fairly high excitation energies, at which doorway resonances overlap with allowance for their total nucleonic widths (strong coupling to the continuum), we calculate energy-averaged quantities by making the substitution $\omega \rightarrow \omega + \frac{i}{2}I(\omega)$ in the CRPA equations. Upon applying this procedure (its implementation in practice is described in Subsection 3.2 below), we find averaged quantities that specify basic properties of giant resonances:

$$\begin{aligned}\bar{S}_L(\omega) &= S_L(\omega + \frac{i}{2}I(\omega)), & (18) \\ \bar{\rho}_L(r, \omega) &= \rho_L(r, \omega + \frac{i}{2}I(\omega)), \\ \bar{M}_{L,c}(\omega) &= M_{L,c}(\omega + \frac{i}{2}I(\omega)).\end{aligned}$$

The parameter $I(\omega)$ can be interpreted as the mean fragmentation width of doorway states; by its physical significance, it is close to the imaginary part of the optical potential for nucleons. We employ the parametrization

$$I(\omega) = \alpha \frac{(\omega - \Delta)^2}{1 + (\omega - \Delta)^2/B^2}, \quad I(\omega < \Delta) = 0, \quad (19)$$

which is applied for the imaginary part of the potential in some versions of the optical model of nucleon-nucleus scattering (see, for example, [21]).

In dealing with nonoverlapping doorway resonances, we restrict our consideration to the case of one isolated doorway state. To an acceptable degree of precision, this case is realized in describing an isoscalar giant monopole resonance. A Breit-Wigner parametrization of a doorway resonance in the energy

Table 1. Calculated and experimental values (in MeV) of the nucleon-separation energy for some nuclei

Nucleus	B_n^{calc}	B_n^{expt}	B_p^{calc}	B_p^{expt}
^{90}Zr	11.64	11.98		
^{116}Sn			9.25	9.28
^{124}Sn			12.58	12.11
^{144}Sm	11.59	10.55		
^{208}Pb	7.24	7.37	7.99	8.01

dependences of the strength function (4), the effective fields (5), and the reaction amplitudes (13),

$$\begin{aligned}S_L(\omega) &= -\frac{1}{\pi} \text{Im} \frac{R_g}{\omega - \omega_g + \frac{i}{2}\Gamma_g}, & (20) \\ \tilde{V}_{L,\alpha}(r, \omega) &= V_L(r) + \frac{R_g^{1/2} v_{g,\alpha}^L(r)}{\omega - \omega_g + \frac{i}{2}\Gamma_g}, \\ |M_{L,c}(\omega)| &= \frac{1}{\sqrt{2\pi}} \left| \frac{R_g^{1/2} (\Gamma_{gc})^{1/2}}{\omega - \omega_g + \frac{i}{2}\Gamma_g} \right|, & (21)\end{aligned}$$

makes it possible to perform a CRPA calculation of the following resonance parameters: the energy ω_g ; the strength R_g ; and the radial components of the transition potential, $v_{g,\alpha}^L(r) = \sum_{\beta} F_{\alpha\beta}(r) \rho_{g,\beta}^L(r)$, and, hence, of the transition density, $\rho_g^L(r) = \sum_{\alpha} \rho_{g,\alpha}^L(r)$. We note that $R_g^{1/2} = \int \rho_g^L(r) V_L(r) dr$ and that the ratio of the transition densities is $\rho_g^L(r, \omega) / \rho_g^L(r) = ((\Gamma_g/2\pi)((\omega - \omega_g)^2 + \Gamma_g^2/4)^{-1})^{1/2}$. The inclusion of doorway-resonance coupling to multi-quasiparticle configurations requires, in addition to making the substitution $\omega \rightarrow \omega + \frac{i}{2}I_g$ in relations (20) and (21), modifying the partial nucleonic widths Γ_{gc} in (21) in order to take into account a significant change in the potential-barrier penetrability $P_{\alpha,(\lambda)}$ at the width $I_g = I(\omega_g)$ ($I_g \gg \Gamma_g$); that is,

$$\Gamma_{gc} \rightarrow \bar{\Gamma}_{gc} = \Gamma_{gc} \bar{P}_{g,\alpha,(\lambda)} / P_{\alpha,(\lambda)}(\varepsilon_{g\mu}), \quad (22)$$

$$\bar{P}_{g,\alpha,(\lambda)} = \frac{1}{\sqrt{2\pi}\sigma_g} \int P_{\alpha,(\lambda)}(\varepsilon) \exp\left(-\frac{(\varepsilon - \varepsilon_{g\mu})^2}{2\sigma_g^2}\right) d\varepsilon,$$

where $\varepsilon_{g\mu} = \omega_g + \varepsilon_{\mu}$ and $\sigma_g = I_g/2.35$.

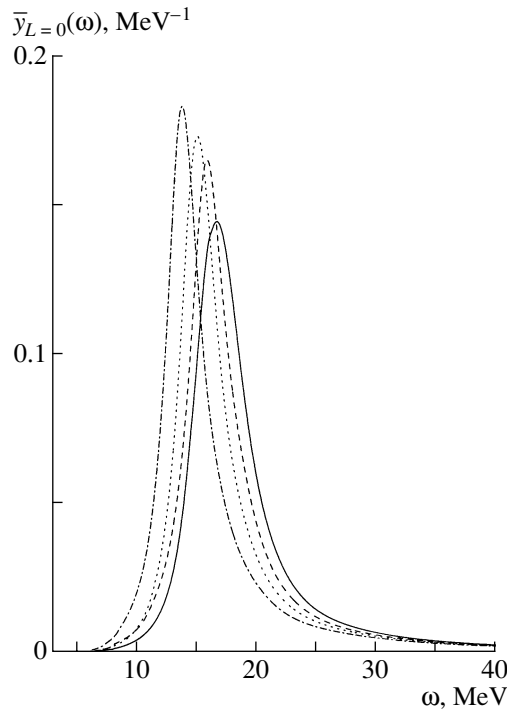


Fig. 1. Reduced strength functions $\bar{y}_L(\omega)$ for giant resonances of the ISGMR type ($L = 0$) in (solid curve) ^{90}Zr , (dashed curve) ^{116}Sn , (dotted curve) ^{144}Sm , and (dash-dotted curve) ^{208}Pb nuclei.

3. CHOICE OF MODEL PARAMETERS AND DETAILS AND RESULTS OF THE CALCULATIONS

3.1. Choice of Model Parameters

The mean field and particle–hole interaction form input information for any approach based on the application of the random-phase approximation. The parametrization and parameters of the isoscalar component of the mean field were chosen to be close to those for the Nemirovsky–Chepurnov potential [22]:

$$U_0(r) = -U_0 f_{\text{WS}}(r, R, a), \quad U_{\text{ol}}(r) = -U_{\text{ol}} \frac{1}{r} \frac{df_{\text{WS}}}{dr}. \quad (23)$$

Here, $f_{\text{WS}}(r, R, a) = \left(1 + \exp\left(\frac{r-R}{a}\right)\right)^{-1}$ is the Woods–Saxon function, where $R = r_0 A^{1/3}$ with $r_0 = 1.24$ fm, $a = 0.63$ fm, $U_0 = 54$ MeV, (24)

$$U_{\text{ol}} = 13.9 \left(1 + 2 \frac{N-Z}{A}\right) \text{ MeV fm}^2.$$

The strengths of the particle-hole interaction (3) are parametrized in the form

$$F(r) = C[f^{\text{ex}} + (f^{\text{in}} - f^{\text{ex}})f_{\text{WS}}(r, R, a)], \quad (25)$$

$$F'(r) = C f',$$

$$C = 300 \text{ MeV fm}^3; \quad f' = 1.0, \quad f^{\text{in}} = 0.0875, \\ f^{\text{ex}} = -(2.7 - 2.9).$$

The symmetry potential $v(r)$ and the mean Coulomb field $U_C(r)$ in (1) were calculated self-consistently by using the densities in (2). The strength parameters U_0 (24) and f' (25) were chosen in such a way as to reproduce satisfactorily the experimental values of the nucleon-separation energy for some filled-shell nuclei from ^{90}Zr to ^{208}Pb (see Table 1). For each nucleus, the parameter f^{ex} was chosen in such a way that the energy of the unphysical state was close to zero (in the practical calculations, $\omega_{SS} < 50$ keV). The values that we found agree with the systematics presented in [17, 23]. These values are quoted in Table 2 along with the calculated fractions x_{SS} of exhaustion of the corresponding energy-weighted sum rule by the ghost state (see Subsection 2.3). The parameter f^{in} (25) was fitted to the experimental energy of the isoscalar giant monopole resonance in the ^{208}Pb nucleus.

In order to calculate the energy-averaged features of the isoscalar giant resonances being considered, we employ the following values of the parameters in expression (19) for the fragmentation width $I(\omega)$:

$$\alpha = 0.085 \text{ MeV}^{-1}, \quad \Delta = 3 \text{ MeV}, \quad B = 7 \text{ MeV}. \quad (26)$$

These values (or those that are close to them) were used in [15, 24] to describe the total widths of some isovector giant resonances. A practical implementation of the “ $\omega + \frac{i}{2}I$ ” method implies, in accordance with (18), the calculation of ω -dependent single-particle quantities [radial Green’s function’s in (6), radial nucleon wave functions in a continuum in (13)] by using a single-particle potential whose imaginary part is $\mp I(\omega)f_{\text{WS}}(r, R^*, a)$ (depending on the sign with which ω appears in single-particle quantities). In the calculations, we used the value $R^* = 1.3R$, since the averaged effective fields and strength functions are weakly dependent on the quantity R^* in the region $R^* > 1.3R$.

In order to calculate the features of overtones (ISGDR, ISGMR2), it is necessary to find the parameters η_1 and η_0 appearing in the definition of the trial operators (17). The parameter η_1 was found for each nucleus from the condition requiring that the ghost state not be excited by the field $V_{L=1}(r)$. This condition is equivalent to that which requires the orthogonality of the trial operator $V_{L=1}(r)$ and the transition density of the ghost state—that is, to condition (16) in which the transition density $\rho_{SS}(r)$

Table 2. ISGMR parameters calculated for various energy intervals (the last row in each block of the table corresponds to $I = 0.05$ MeV); also given in the table are the relative isoscalar strength of the 1^- ghost state and the values used for the parameters of Landau–Migdal forces (the value of $f^{\text{in}} = 0.0875$ was taken for all nuclei)

Nucleus	$-f^{\text{ex}}$	x_{SS} , %	$\omega_1 - \omega_2$, MeV	ω_L , MeV	Δ_L , MeV	x_L , %
^{208}Pb	2.897	91.9	10–20	14.29	2.05	80.2
			3–60	15.22	5.13	99.2
			10–20	13.99	1.10	97.9
^{144}Sm	2.811	93.6	10–20	15.28	2.00	78.0
			3–60	16.53	5.16	98.5
			10–20	15.27	0.96	98.7
^{116}Sn	2.832	93.6	10–20	15.79	2.08	74.7
			3–60	17.18	5.29	98.4
			10–20	15.97	1.24	97.9
^{90}Zr	2.753	94.5	10–25	17.10	2.71	85.4
			3–60	18.05	5.30	98.2
			10–25	16.89	1.35	99.8

is calculated in the single-level approximation. The values found in this way for the parameter η_1 proved to be close to $\eta_1 = 5\langle r^2 \rangle / 3$. This circumstance furnishes an additional piece of evidence that the degree of consistency of the present model is quite acceptable (see Subsection 2.3). The parameter value of $\eta_0 = 75.6 \text{ fm}^2$ in the definition of the trial operator $V_{L=0}^{(2)}(r)$ (17) was calculated according to Eq. (16) for the ^{208}Pb nucleus by using the transition density $\rho_{L=0}(r, \omega_{\text{max}})$ found within the CRPA approach.

3.2. Reduced Strength Functions, Transition Densities, and Relative Probabilities of Direct Nucleonic Decays

Let us now proceed to consider the results obtained by calculating the energy-averaged strength functions $\bar{y}_L(\omega) = y_L \left(\omega + \frac{i}{2}I \right)$ and the energy-averaged transition densities $\bar{\mathcal{R}}_L(\omega) = \mathcal{R}_L \left(\omega + \frac{i}{2}I \right)$ [for definitions, see Eqs. (7), (11), and (18)] for isoscalar giant monopole and dipole resonances. For ^{90}Zr , ^{116}Sn , ^{144}Sm , and ^{208}Pb nuclei, the reduced strength functions $\bar{y}_{L=0}$ and $\bar{y}_{L=1}$ calculated for a rather wide energy interval are displayed in Figs. 1 and 2, respectively. For the selected energy intervals, these strength functions make it possible to calculate the mean energy ω_L ; the root-mean-square deviation of energy, Δ_L ; and the fraction of exhaustion of the corresponding energy-weighted sum rule

$(EWSR)_L$, x_L . The results of these calculations are quoted in Table 2 for giant resonances of the ISGMR type and in Table 3 for giant resonances of the ISGDR type. Also presented in these tables are the data obtained by using a small value of I ($I = 0.05$ MeV), which give an idea of the energy region housing the main part of the strength of isoscalar giant resonances within the CRPA—that is, without taking into account the coupling of doorway states to multiparticle configurations—and which provide an illustration of how this strength is redistributed with allowance for this coupling. In Table 4, the calculated mean energies and their root-mean-square deviations are contrasted against relevant experimental data from [1, 2].

The ISGMR2 strength function in the ^{208}Pb nucleus is displayed in Fig. 3. Also shown in the same figure for the sake of comparison are the strength functions $\bar{y}_{L=0}$ and $\bar{y}_{L=1}$. In order to illustrate the convenience of using the trial operator $V_{L=0}^{(2)}(r)$ (17) in describing the properties of the ISGMR overtone, the relative strength of isoscalar monopole excitations that was calculated for various trial operators (r^2 , r^4 , $r^4 - R^2 r^2$ [25], $r^4 - \eta_0 r^2$) is depicted in Fig. 4 as a function of the upper limit ω .

The normalized differential transition densities of the giant resonances being considered, $\bar{\mathcal{R}}_L(r, \omega)$, were calculated for the ^{208}Pb nucleus. The transition density $\bar{\mathcal{R}}_{L=0}(r, \omega_{\text{max}})$ calculated at the energy of the ISGMR maximum is displayed in Fig. 5, along with the transition density found for this resonance

Table 3. ISGDR parameters calculated for various energy intervals (in each block of the table, the last row corresponds to $I = 0.05$ MeV)

Nucleus	Pygmy-ISGDR				ISGDR			
	$\omega_1 - \omega_2$, MeV	ω_L , MeV	Δ_L , MeV	x_L , %	$\omega_1 - \omega_2$, MeV	ω_L , MeV	Δ_L , MeV	x_L , %
^{208}Pb	8–15	11.10	1.91	13.3	15–24	20.71	2.41	41.3
	5–15	9.87	2.52	16.7	15–30	22.57	3.36	68.6
					15–60	24.03	5.83	81.1
^{144}Sm	5–15	9.67	2.30	18.2	15–30	22.75	2.49	79.7
	5–15	10.74	2.19	12.3	15–35	24.38	4.13	76.4
					15–60	25.43	6.00	84.8
^{116}Sn	5–15	10.64	1.84	13.9	15–35	24.40	3.02	84.9
	11–18	14.02	2.01	10.8	18–32	25.21	3.33	65.5
	5–15	10.36	2.42	13.2	15–35	24.90	4.38	74.7
^{90}Zr					15–60	26.10	6.28	84.3
	5–15	10.31	2.25	15.0	15–35	25.09	3.42	83.3
	11–18	13.89	2.08	9.9	18–32	25.64	3.52	64.5
	5–16	11.42	2.23	11.3	16–40	26.30	4.93	79.7
					16–60	27.13	6.37	85.7
	5–16	11.19	1.70	12.3	16–40	26.10	3.93	87.3

Table 4. Calculated parameters (ω_L and Δ_L in MeV) of giant resonances belonging to the ISGMR and ISGDR types along with experimental data from [1] and [2], respectively

Nucleus	ISGMR				Pygmy-ISGDR				ISGDR			
	ω_L		Δ_L		ω_L		Δ_L		ω_L		Δ_L	
	exp.	calc.	exp.	calc.	exp.	calc.	exp.	calc.	exp.	calc.	exp.	calc.
^{208}Pb	14.7 ± 0.28	14.3	1.93 ± 0.15	2.05	12.2 ± 0.6	11.1	1.9 ± 0.5	1.9	19.9 ± 0.8	20.7	2.5 ± 0.6	2.4
^{116}Sn	16.07 ± 0.12	15.8	2.16 ± 0.08	2.1	14.7 ± 0.5	14.0	1.6 ± 0.5	2.0	23.0 ± 0.6	25.2	3.7 ± 2.5	3.3
^{90}Zn	17.89 ± 0.20	17.1	3.14 ± 0.09	2.7	16.2 ± 0.8	13.9	1.9 ± 0.7	2.1	25.7 ± 0.7	25.6	3.5 ± 0.6	3.5

on the basis of the scaling model [26], $r^{-2}\rho_{L=0}^{\text{tr}} \sim 3n + rdn/dr$, and also normalized by the condition $\int V_{L=0}(r)\rho_{L=0}^{\text{tr}}(r)dr = 1$. For the isoscalar giant dipole resonance in the ^{208}Pb nucleus, the calculation of the transition density $\bar{\mathcal{R}}_L(r, \omega)$ was performed at a few values of ω , including those in the pygmy-ISGDR region (see Fig. 6). In addition to an illustration of the change in the coordinate dependence of the transition density with excitation energy, Fig. 6 also displays the density corresponding to $\rho_{L=1}^{\text{tr}}(r)$ [26]. The normalized differential transition density for resonances of the ISGMR2 type, $\bar{\mathcal{R}}_{L=0}^{(2)}(r, \omega)$, is shown in Fig. 7

for the excitation energies corresponding to the main maximum and two pygmy resonances.

The relative partial probabilities of direct nucleonic decays of highly excited giant resonances belonging to the ISGDR and ISGMR2 types can be calculated by formula (14) with allowance for (18); that is,

$$b_{\mu, \alpha} = \frac{\sum_{(\lambda)} \int_{(\delta)} |\bar{M}_{L,c}(\omega)|^2 d\omega}{\int_{(\delta)} S_L(\omega) d\omega}; \quad b_{\alpha}^{\text{tot}} = \sum_{\mu} b_{\mu, \alpha}. \quad (27)$$

In order to take into account a non-single-hole nature of the product-nucleus state μ^{-1} populated in the

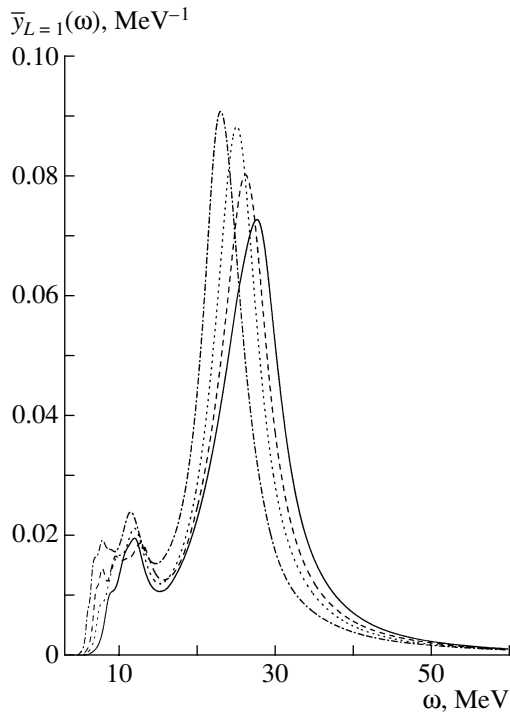


Fig. 2. Reduced strength functions $\bar{y}_L(\omega)$ for giant resonances of the ISGDR type ($L = 1$) in (solid curve) ^{90}Zr , (dashed curve) ^{116}Sn , (dotted curve) ^{144}Sm , and (dash-dotted curve) ^{208}Pb nuclei.

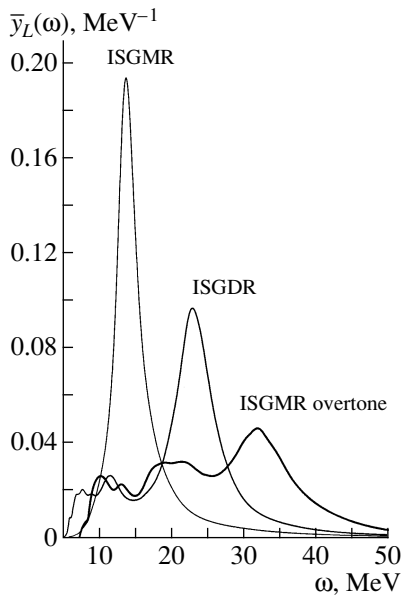


Fig. 3. Reduced strength functions $\bar{y}_L(\omega)$ for some isoscalar giant resonances in the ^{208}Pb nucleus.

nucleonic-decay process (in view of coupling to low-lying collective states, or of nucleon pairing, or of both effects), we replaced, in the expression for $\bar{M}_{L,c}$

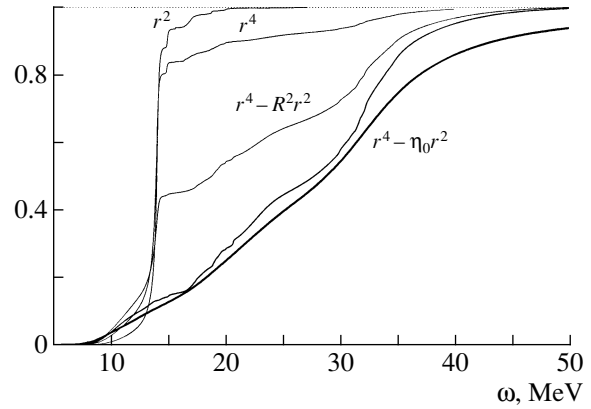


Fig. 4. Relative strength of the overtone of the isoscalar monopole resonance in the ^{208}Pb nucleus as a function of the upper limit of integration for various trial operators. The thick solid curve represents the results of the calculation performed with allowance for the coupling of particle-hole doorway states to multiparticle configurations.

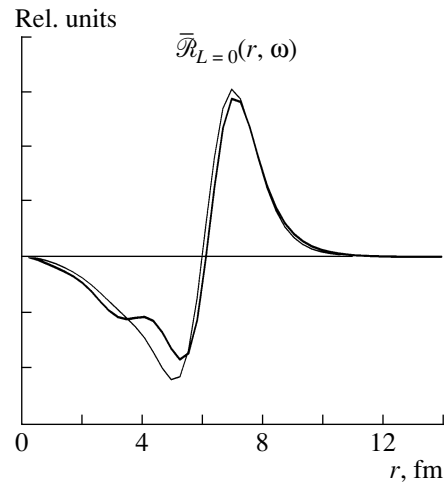


Fig. 5. Normalized differential transition density of the isoscalar giant monopole resonance in the ^{208}Pb nucleus. The thin curve corresponds to the normalized transition density calculated for this resonance on the basis of the scaling model [26].

in (27), the occupation numbers n_μ^α [see Eq. (13)] by the experimental values of the spectroscopic factor s_μ^α . The partial probabilities of the direct neutronic and protonic decays of the main (upper) components of giant resonances belonging to the ISGDR and ISGMR2 types are given in Tables 5 and 6, respectively, according to the calculations by formula (27).

3.3. Partial Widths with Respect to the Direct Neutronic Decays of Isoscalar Giant Resonances

The direct neutronic decay of the main tone of an isoscalar giant monopole resonance treated as a res-

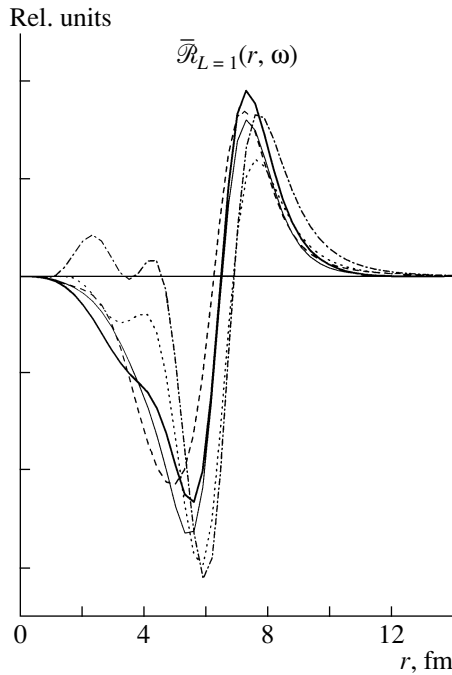


Fig. 6. Normalized differential transition density calculated for the ISGDR in the ^{208}Pb nucleus at the energy values of $\omega =$ (solid curve) 23.06, (dashed curve) 11.26, (dotted curve) 7.76, and (dash-dotted curve) 6.81 MeV. The thin curve corresponds to the normalized transition density calculated for this resonance on the basis of the scaling model [26].

onance weakly coupled to a continuum is described in an alternative way (see Subsection 2.4). In order to calculate the mean partial decay widths $\bar{\Gamma}_{g\mu} = \sum_{(\lambda)} \bar{\Gamma}_{gc}$ according to (13), (21), and (22), we use the following experimental data: the total resonance width $\Gamma_{g,\text{tot}}^{\text{exp}}$ (instead of I_g), the channel energy $\varepsilon_{g\mu}^{\text{exp}} = \varepsilon_{\mu}^{\text{exp}} + \omega_g^{\text{exp}}$ (instead of the calculated energy $\varepsilon_{g\mu}$), and the experimental values of the spectroscopic factors s_{μ} (instead of the occupation numbers n_{μ}).

For the isoscalar giant monopole resonance in the ^{90}Zr nucleus, we used the values of $\omega_g^{\text{exp}} = 16.1 \pm 0.4$ MeV and $\Gamma_{g,\text{tot}}^{\text{exp}} = 3.1 \pm 0.4$ MeV, which were obtained in [4]. The results of the calculation of the partial nucleonic widths are quoted in Table 7. Also given in this table are experimental data obtained either by separating (for the population of the $9/2^+$ state in ^{89}Zr) the contribution of statistical decay or without separating this contribution. The total width $\Gamma_{g,\text{tot}}^{\text{exp}} = 3.8 \pm 0.5$ MeV and the energy $\omega_g^{\text{exp}} = 15.40 \pm 0.35$ MeV of the isoscalar giant monopole resonance in the ^{124}Sn nucleus were borrowed from [5]. The calculated partial widths of this giant resonance are presented in Table 8, along with

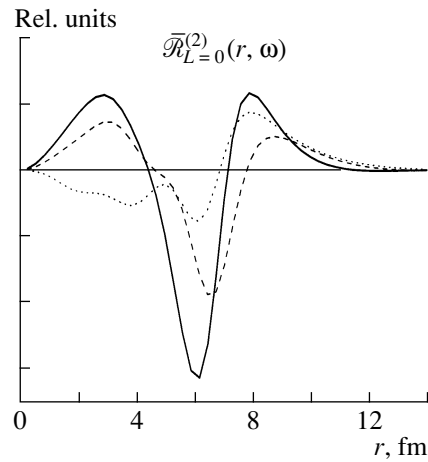


Fig. 7. Normalized differential transition density calculated for the overtone of the isoscalar giant monopole resonance in the ^{208}Pb nucleus at the energy values of (solid curve) 32, (dashed curve) 22, and (dotted curve) 12 MeV.

the spectroscopic factors used and relevant experimental data, including the total width with respect to direct neutronic decay. For partial neutronic widths of the isoscalar giant monopole resonance in the ^{208}Pb nucleus, experimental data were obtained in [3, 6, 7]. Together with the results of the calculations, these data (including partial widths derived without separating the contribution of statistical decay [8]) are given in Table 9.

4. DISCUSSION OF THE RESULTS AND PROSPECTS FOR THE DEVELOPMENT OF THE APPROACH

4.1. Discussion of the Results Obtained

First, we would like to emphasize the relative simplicity, the clarity, and an acceptable degree of self-consistency of our semimicroscopic approach to describing giant resonances. The use of the phenomenological isoscalar component of the mean field, along with a few conditions of partial self-consistency, and of strength ($U_0, U_{\sigma l}, f'$) and geometric (r_0, a) parameters that are universal for medium-mass nuclei makes it possible to describe the nucleon-separation energies in closed-shell nuclei (Table 1) and the low-energy section of the quasiparticle spectrum (see, for example, [11]). The degree to which the translational invariance of the model is restored [$x_{SS} > 91\%$ (see Table 2), $\eta_1 = 5\langle r^2 \rangle / 3$] also seems satisfactory. In relation to other microscopic and semimicroscopic approaches, that which is used here is advantageous in that it enables one describe all basic properties of giant resonances,

Table 5. Partial probabilities of processes in which the direct nucleonic decay of the upper component of the isoscalar giant dipole resonance (15–30 MeV) in the ^{208}Pb nucleus leads to the population of single-hole states of the product nucleus

μ_n^{-1}	$s_\mu^a)$	$b_\mu, \%$	μ_p^{-1}	$s_\mu^b)$	$b_\mu, \%$
(1/2) ⁻	1.0	0.7	(1/2) ⁺	0.55	0.55
(5/2) ⁻	0.91	2.2	(3/2) ⁺	0.57	0.68
(3/2) ⁻	0.98	1.8	(11/2) ⁻	0.58	0.19
(13/2) ⁺	1.0	3.2	(5/2) ⁺	0.54	0.64
(7/2) ⁻	0.7	2.9	(7/2) ⁺	0.26	0.04
(9/2) ⁻	0.61	1.0			
$\sum b_\mu, \%$		11.8	$\sum b_\mu, \%$		2.1
$b^{\text{tot}}, \%$		15.5*	$b^{\text{tot}}, \%$		2.1

^{a)} Data from [27].

^{b)} Data from [28].

* $s_\mu = 0.6$ for all deep neutron-hole states.

including the strength function over a broad energy interval, the differential transition density in the same interval, and partial probabilities of direct nucleonic decays.

Let us now proceed to discuss the results obtained by calculating the basic properties of isoscalar monopole and dipole excitations in some medium-mass nuclei having one or two filled shells. The strength function of an isoscalar giant monopole resonance, $\bar{y}_{L=0}(\omega)$, exhibits one distinct maximum (see Fig. 1). The corresponding monopole strength is exhausted within a rather broad energy interval (3–60 MeV), this interval becoming considerably narrower if one disregards coupling to multiparticle configurations (see Table 2). If the calculation employs the same energy interval as in experiments, then it follows from the results presented in Table 4 that the mean energy $\omega_{L=0}$ and its root-mean-square deviation $\Delta_{L=0}$ found for the isoscalar giant monopole resonance with the aid of the strength function $\bar{y}_{L=0}(\omega)$ are in satisfactory agreement with relevant experimental data. (We recall that the strength constant f^{in} was fitted to the experimental energy of the isoscalar giant monopole resonance in the ^{208}Pb nucleus.) As might have been expected, the transition density at the energy value corresponding to the maximum of the isoscalar giant monopole resonance exhibits one node within the nucleus being considered (see Fig. 5), since, from the definitions in (10) and (18) and from relations (5) and (6), it follows that this density satisfies the condition $\int \bar{\mathcal{R}}_{L=0}(r, \omega) dr = 0$.

Table 6. Partial probabilities of processes in which the direct nucleonic decay of the upper component of the overtone of the isoscalar giant monopole resonance (25–35 MeV) in the ^{208}Pb nucleus leads to the population of single-hole states of the product nucleus

μ_n^{-1}	$s_\mu^a)$	$b_\mu, \%$	μ_p^{-1}	$s_\mu^b)$	$b_\mu, \%$
(1/2) ⁻	1.0	0.2	(1/2) ⁺	0.55	1.3
(5/2) ⁻	0.91	0.6	(3/2) ⁺	0.57	2.2
(3/2) ⁻	0.98	0.6	(11/2) ⁻	0.58	3.0
(13/2) ⁺	1.0	1.0	(5/2) ⁺	0.54	3.4
(7/2) ⁻	0.7	1.2	(7/2) ⁺	0.26	0.7
(9/2) ⁻	0.61	0.51			
$\sum b_\mu, \%$		4.1	$\sum b_\mu, \%$		10.6
$b^{\text{tot}}, \%$		13.3*	$b^{\text{tot}}, \%$		13.8**

^{a)} Data from [27].

^{b)} Data from [28].

* $s_\mu = 0.6$ for all deep neutron-hole states.

** $s_\mu = 0.5$ for all deep proton-hole states.

Experimental data concerning direct nucleonic decays of isoscalar giant resonances have so far been obtained only for the partial nucleonic widths of the isoscalar giant monopole resonances in ^{90}Zr , ^{124}Sn , and ^{208}Pb nuclei (see Tables 7–9). These data were quantitatively described on the basis of the Breit–Wigner parametrization of the corresponding polarizabilities and amplitudes for the external-field-induced reactions involving nucleon emission (see Subsection 2.4). The calculated partial widths agree, at least qualitatively, with the corresponding experimental data (Tables 7–9). Good agreement was attained for the total width with respect to the direct neutronic decay of the isoscalar giant monopole resonances, $\Gamma_g = \sum_\mu \Gamma_{g,\mu}$, in ^{124}Sn and ^{208}Pb nuclei. In this connection, we note that the CRPA calculation of the width Γ_g for ^{208}Pb in [29, 30] yielded considerably exaggerated values. In all probability, the reason behind this discrepancy is that the approaches used in those studies are not quite consistent.

The strength function for the overtone of the isoscalar giant monopole resonance in the ^{208}Pb nucleus, $\bar{y}_{L=0}^{(2)}(\omega)$, exhibits one main maximum at $\omega_{\text{max}} = 32$ MeV and two pygmy resonances at lower energies (Fig. 3). The main maximum exhausts slightly more than 50% of the corresponding energy-weighted sum rule. The remaining strength is distributed among the pygmy resonances in approximately equal shares. As might have been expected,

Table 7. Partial widths with respect to direct nucleonic decays of the isoscalar giant monopole resonance in the ^{90}Zr nucleus

μ^{-1}	E_x, MeV	$\bar{\Gamma}_{\mu}^{\uparrow}, \text{keV}^{(*)}$	$\Gamma_{\mu}^{\uparrow}, \text{keV}^{a)}$
Neutron			
9/2 ⁺	0.00	59	155 ± 31 ^{b)}
1/2 ⁻	0.59	358	~220
Proton			
1/2 ⁻	0.00	221	~175
9/2 ⁺	0.91	9	
3/2 ⁻	1.51	187	~80
5/2 ⁻	1.74	10	

a) Experimental data obtained without separating the contribution of statistical decay [8].

b) Data from [4].

(*) $s_{\mu} = 1$ for all states μ^{-1} .

the radial dependence of the transition density of the ISGMR overtone, $\bar{\mathcal{R}}_{L=0}^{(2)}(r, \omega_{\max})$, exhibits two nodes within the nucleus (see Fig. 7) and is close to the density obtained within the semiclassical approach [31]. The radial dependence $\bar{\mathcal{R}}_{L=0}^{(2)}(r, \omega)$ changes noticeably upon going over to lower energies (Fig. 7). In view of a relatively higher probability of direct protonic decay (see Table 6), it is reasonable to seek an ISGMR2 overtone in a protonic reaction channel featuring the excitation of this resonance—for example, in $(\alpha, \alpha'p)$ reactions. A similar attempt at discovering an isovector spin–monopole resonance in the reaction $^{208}\text{Pb}(^3\text{He}, tp)$ proved to be successful [32].

The reduced strength function for an isoscalar giant dipole resonance, $\bar{y}_{L=1}(\omega)$, reveals, in addition to the main maximum, which exhausts a major part of the corresponding strength, a pygmy resonance at a lower energy (see Fig. 2 and Table 3). The mean energy $\omega_{L=1}$ and its root-mean-square deviation $\Delta_{L=1}$ calculated with this strength function for both components of the isoscalar giant dipole resonance are in satisfactory agreement with relevant experimental data [2] for the identical choice of the averaging interval δ (see Table 4). For a wider interval δ , the calculated values of $\omega_{L=1}$ (and of $\Delta_{L=1}$ as well) increase (see Table 3) and, for the main component of the isoscalar giant dipole resonance, appear to be close to values obtained on the basis of other approaches [9, 10]. In just the same way as in the case of an isoscalar giant monopole resonance, the total strength of the isoscalar giant dipole resonance is

Table 8. Partial widths with respect to direct neutronic decays of the isoscalar giant monopole resonance in the ^{124}Sn nucleus

μ^{-1}	E_x, MeV	$(2j_{\mu} + 1)s_{\mu}^{a)}$	$\bar{\Gamma}_{\mu}^{\uparrow}, \text{keV}$	$\Gamma_{\mu}^{\uparrow}, \text{keV}^{a)}$
11/2 ⁻	0.00	9.3 ± 1.5	29	} 100 ± 40
3/2 ⁺	0.00	2.8 ± 0.5	69	
1/2 ⁺	0.15	1.6 ± 0.2	27	
7/2 ⁺	1.06	1.4 ± 0.2	44	} < 250 ± 60
7/2 ⁺	1.16	9.0 ± 3.1	275	
5/2 ⁺	1.19	2.9 ± 0.5	69	
5/2 ⁺	1.50	2.8 ± 0.2	65	
$\Gamma^{\uparrow}, \text{keV}$			578	570 ± 190

a) Data from [5].

exhausted within a broad (5–60 MeV) energy interval (see Table 3). The radial dependence of the transition density in the ^{208}Pb nucleus changes noticeably with energy, but the distinction between that at the energy value corresponding to the maximum of the main component and that for the pygmy component is moderately small (see Fig. 6). For either component, the calculated strength x_L (see Table 3) proved to be well below its experimental counterpart [2]. A possible overestimation of these quantities may be due to the use of schematic transition densities in the analysis of experimental data. The use of microscopic (energy-dependent) transition densities in such an analysis seems preferable and would be, in future, a severe test of microscopic approaches. Comparing the results obtained by calculating the relative probabilities for the direct nucleonic decays of the giant resonances in the ^{208}Pb nucleus that belong to the ISGDR and ISGMR2 types (see Tables 5, 6), we note the proximity of the total probabilities of the direct neutronic decays of the two resonances in question, despite a large difference in energy (about 10 MeV) between them and, hence, in the penetrability of the potential barrier for neutrons. In contrast to what occurs in the case of protonic decays (see Tables 5, 6), this difference may be compensated owing to the distinction between the numbers of nodes in the radial dependences of the transition densities (see Figs. 6, 7). Despite a low relative probability expected for the direct protonic decays of an isoscalar giant dipole resonance (see Table 5), attempts are made to discover it experimentally in $(\alpha, \alpha'p)$ reactions [8].

In conclusion, we would like to emphasize that, by and large, our semimicroscopic approach provides a satisfactory description of experimental data on the

Table 9. Partial widths with respect to direct neutronic decays of the isoscalar giant monopole resonance in the ^{208}Pb nucleus

μ^{-1}	E_x , MeV	s_μ ^{a)}	$\bar{\Gamma}_\mu^\dagger$, keV	Γ_μ^\dagger , keV ^{b)}	Γ_μ^\dagger , keV ^{c)}
(1/2) ⁻	0.00	1.0	31	Incl. (13/2) + (19 ± 27)	140 ± 35
(13/2) ⁺	1.63	0.91	4	75 ± 35 (73 ± 33)	Incl. (1/2) ⁻
(5/2) ⁻	0.57	0.98	180	<35 (65 ± 43)	70 ± 15
(3/2) ⁻	0.89	1.0	57	75 ± 40 (133 ± 45)	50 ± 10
(7/2) ⁻	2.34	0.7	135	< 140 ± 30 (155 ± 33)	165 ± 40
(9/2) ⁻	3.41	0.61	3	Incl. (5/2) ⁺ (7/2) ⁺	
Γ^\dagger , keV			410	325 ± 105 (445 ± 181)	425 ± 100

Note: Given parenthetically are experimental data where the contribution of static decay is not isolated.

^{a)} Data from [27].

^{b)} Data from [7].

^{c)} Data from [3].

properties of isoscalar monopole and dipole excitations in medium-mass spherical nuclei. It is of course desirable that these data become more comprehensive and accurate and that the approach itself be further developed and refined (see below).

4.2. Prospects for the Development of the Approach

Let us briefly touch upon the possibilities for refining the present semimicroscopic approach.

(i) As soon as the spin-orbit interaction is switched off [$U_{\sigma l} = 0$ in (1) and (23)], the degree to which the translational invariance of the model is restored is considerably improved: $x_{SS} > 99.5\%$ for a hypothetical nucleus whose mass and charge numbers are $A = 208$ and $Z = 82$, respectively. This circumstance indicates that it is necessary to take into account the coupling of isoscalar dipole 1^- spinless and spin-flip excitations that exists because of spin-orbit interaction. This coupling is realized owing, for example, to the nucleon-spin-dependent components of the Landau-Migdal interaction.

(ii) An attempt can be made to describe the effect of fragmentation of giant resonances strongly coupled to a single-particle continuum in terms of the imaginary part of a realistic potential for nucleons (that is, without employing free parameters). An attempt at implementing this possibility in describing the fragmentation width of an isobaric analogous resonance (this width is controlled by the so-called effect of

external Coulomb mixing) proved to be successful in [33].

(iii) The method proposed in Migdal's monograph [17] for self-consistently calculating the isoscalar component $U_0(r)$ of the mean field seems implementable through taking into account the "differential" condition of the translational invariance of the model,

$$\frac{dU_0[n]}{dr} = F[n] \frac{dn}{dr}, \quad (28)$$

where the strength of the isoscalar component of the interaction in (3) is chosen in the form of a functional of the nucleon density (2). Should this method be successfully realized, the number of phenomenological parameters in the model will be reduced considerably.

ACKNOWLEDGMENTS

We are grateful to A.I. Vdovin and E.E. Saperstein for discussions on some aspects of this study.

REFERENCES

1. Y.-W. Lui, D. H. Youngblood, and H. L. Clark, Nucl. Phys. A **649**, 49c (1999); M. N. Harakeh, N. Kalantar-Nayestanaki, U. Garg, *et al.*, Nucl. Phys. A **649**, 57c (1999).
2. H. L. Clark, Y.-W. Lui, and D. H. Youngblood, Phys. Rev. C **63**, 031301 (2001).

3. A. Bracco, J. R. Beene, N. Van Giai, *et al.*, Phys. Rev. Lett. **60**, 2603 (1988).
4. W. T. A. Borghols *et al.*, Nucl. Phys. A **504**, 231 (1989).
5. W. T. A. Borghols *et al.*, Nucl. Phys. A **515**, 173 (1990).
6. S. Brandenburg *et al.*, Nucl. Phys. A **466**, 29 (1987).
7. S. Brandenburg *et al.*, Phys. Rev. C **39**, 2448 (1989).
8. U. Garg, M. Fujiwara, and M. N. Harakeh, private communication.
9. G. Colo, N. Van Giai, P. F. Bortignon, and M. R. Quaglia, Phys. Lett. B **485**, 362 (2000).
10. S. Shlomo and A. I. Sanzhur, Phys. Rev. C **65**, 044310 (2002).
11. M. L. Gorelik, S. Shlomo, and M. H. Urin, Phys. Rev. C **62**, 044301 (2000).
12. M. L. Gorelik and M. H. Urin, Phys. Rev. C **64**, 047301 (2001); Izv. Akad. Nauk, Ser. Fiz. **66**, 374 (2002).
13. D. Vretenar, A. Wandelt, and P. Ring, Phys. Lett. B **487**, 334 (2000).
14. A. Kolomiets, O. Pochivalov, and S. Shlomo, Phys. Rev. C **61**, 034312 (2000).
15. V. A. Rodin and M. H. Urin, Nucl. Phys. A **687**, 276c (2001); Phys. Rev. C **66**, 064608 (2002).
16. M. L. Gorelik and M. H. Urin, Phys. Rev. C **63**, 064312 (2001); Yad. Fiz. **64**, 560 (2001) [Phys. At. Nucl. **64**, 506 (2001)].
17. A. B. Migdal, *Theory of Finite Fermi Systems and Applications to Atomic Nuclei*, 2nd ed. (Nauka, Moscow, 1983; Interscience, New York, 1967).
18. B. L. Birbrair and V. A. Sadovnikova, Yad. Fiz. **20**, 645 (1974) [Sov. J. Nucl. Phys. **20**, 347 (1975)].
19. M. H. Urin and O. N. Vyazankin, Nucl. Phys. A **537**, 534 (1992).
20. A. Bohr and B. R. Mottelson, *Nuclear Structure, Vol. 2: Nuclear Deformations* (Benjamin, New York, 1975; Mir, Moscow, 1977).
21. C. Mahaux and R. Sartor, Nucl. Phys. A **503**, 525 (1989).
22. V. A. Cheprunov, Yad. Fiz. **6**, 955 (1966) [Sov. J. Nucl. Phys. **6**, 696 (1967)].
23. J. Speth, E. Werner, and W. Wild, Phys. Rep. C **33**, 127 (1977).
24. V. A. Rodin and M. H. Urin, Phys. Lett. B **480**, 45 (2000).
25. S. E. Muraviev, I. Rotter, S. Shlomo, and M. H. Urin, Phys. Rev. C **59**, 2040 (1999).
26. S. Stringari, Phys. Lett. B **108B**, 232 (1982).
27. C. A. Whitten, N. Stein, G. E. Holland, and D. A. Bromley, Phys. Rev. **188**, 1941 (1969).
28. I. Bobeldijk *et al.*, Phys. Rev. Lett. **73**, 2684 (1994).
29. G. Colo, P. F. Bortignon, N. Van Giai, *et al.*, Phys. Lett. B **276**, 279 (1992).
30. S. E. Muraviev and M. H. Urin, Phys. Lett. B **280**, 1 (1992); Nucl. Phys. A **572**, 267 (1994).
31. S. Shlomo, A. I. Sanzhur, and V. M. Kolomietz, *Progress in Research, Cyclotron Institute, TAMU, April 1, 2000–March 31, 2001*, p. III-5.
32. R. G. T. Zegers *et al.*, Phys. Rev. Lett. **90**, 202501 (2003).
33. I. V. Safonov and M. H. Urin, Izv. Akad. Nauk, Ser. Fiz. **67**, 45 (2003).

Translated by A. Isaakyan

Potential Barrier in the Problem of the Evolution of a Dinuclear System

R. V. Jolos*

Joint Institute for Nuclear Research, Dubna, Moscow oblast, 141980 Russia

Received January 17, 2003

Abstract—A method for calculating the potential energy of a dinuclear system evolving along the charge-asymmetry coordinate is analyzed. It is shown that the shape of the potential is determined primarily by the dependence of the proton separation energy on the mass and the charge number of nuclei that form the dinuclear system and by the concerted effect of the Coulomb fields of these nuclei on the single-particle motion of constituent nucleons. © 2003 MAIK “Nauka/Interperiodica”.

The article is dedicated to the 80th anniversary of the birth of Academician S.T. Belyaev, who made an outstanding contribution to the development of nuclear physics. His scientific publications are characterized by the presence of a brilliant idea and by the clarity and elegance of the exposition. Many people, including myself, benefited greatly from his studies.

Investigation of the evolution of a massive nuclear system featuring a large number of degrees of freedom is an important and interesting problem, which, at the same time, is very difficult. First, it is necessary to single out the most significant collective variables in terms of which one would describe this evolution process. These variables may be weakly coupled to other degrees of freedom, but, most often, this coupling is rather strong. In the latter case, the choice of collective variables is additionally motivated by the possibility of obtaining experimental information about their variation; at the same time, changes in other characteristics of the system cannot be determined from data. For example, collisions of rather fast nuclei produce a dinuclear system of high excitation energy, at which the level density in this system is so high that it is impossible to pinpoint a specific quantum-mechanical final state.

Upon choosing dynamical variables for describing the evolution of the system, it is necessary to derive equations that would govern the time variation of these variables. Depending on the character of the problem, different approaches can be applied: from solving the Schrödinger equation for the wave function of the system [1] to determining the distribution with respect to the collective variables under consideration in solving a kinetic equation [2]. In all of these cases, we are dealing with the configuration space spanned by these collective variables, the dynamical

equations in question describing the evolution of the system in this space. Changes in the collective variables are due to the changes that a variation of the collective-variable-dependent mean field induces in the character of motion of individual nucleons. Thus, both the potential as a function of collective variables and the tensor of inertia are effective characteristics that reflect complicated variations in the system as it moves from one point of the configuration space of collective variables to another. The positions of the minima, barriers, saddle points, and valleys of the potential surface are the most important features that determine the behavior of a complex multiparticle system. Therefore, it is useful to understand their origin by considering the problem within various approaches. Here, we will consider the problem of determining the potential on the basis of off-diagonal matrix elements of the Hamiltonian [3]. We will analyze the behavior of the system whose formation in the collision of two heavy nuclei is followed by the evolution toward an equilibrium state. In such a system, collective variables are strongly coupled to the internal motion of nucleons. Within a macroscopic description, the averaged effect of this coupling can be expressed in terms of the friction tensor, while fluctuations may be treated, for example, in terms of random forces in the Langevin equation [4].

We will describe the motion of nucleons in interacting nuclei by means of the single-particle time-dependent Hamiltonian [5]

$$\hat{H}(t) = \sum_{i=1}^A \left(-\frac{\hbar^2}{2m} \Delta_i \right) + U_P(\mathbf{r}_i - \mathbf{R}(t)) + U_T(\mathbf{r}_i), \quad (1)$$

where the subscripts P and T refer to the projectile ion and the target nucleus, respectively; $\mathbf{R}(t)$ is

* e-mail: jolos@thsun1.jinr.ru

the time-dependent distance between the centers of mass of the interacting nuclei; and U_P and U_T are the single-particle potentials of the projectile ion and the target nucleus, these potentials including both nuclear and Coulomb fields. In order to write the Hamiltonian in the second-quantization representation, we must fix a single-particle basis. We will construct it from the asymptotic wave functions for the noninteracting nuclei being considered: $|P\rangle$ for the projectile ion and $|T\rangle$ for the target nucleus. This is an asymptotic basis. The corresponding basis vectors are orthogonal to one another only if $\mathbf{R}(t) \rightarrow \infty$. In case of a weak overlap of nuclei, it is convenient to use the basis specified as

$$|\tilde{P}\rangle = |P\rangle - \frac{1}{2} \sum_T |T\rangle \langle T|P\rangle, \quad (2)$$

$$|\tilde{T}\rangle = |T\rangle - \frac{1}{2} \sum_P |P\rangle \langle P|T\rangle. \quad (3)$$

For this basis, the orthogonality condition is satisfied to second-order terms in the overlap integral $|\langle P|T\rangle|$. In the second-quantization representation, the Hamiltonian in (1) assumes the form

$$\hat{H}(t) = \hat{H}_0 + \hat{V}, \quad (4)$$

$$\hat{H}_0 = \sum_P \tilde{\epsilon}_P(\mathbf{R}(t)) a_{P\alpha}^\dagger a_{P\alpha} + \sum_T \tilde{\epsilon}_T(\mathbf{R}(t)) a_{T\alpha}^\dagger a_{T\alpha}, \quad (5)$$

$$\begin{aligned} \hat{V} = & \sum_{P \neq P'} \chi_{PP'}(\mathbf{R}(t)) a_{P\alpha}^\dagger a_{P'\alpha} \\ & + \sum_{T \neq T'} \chi_{TT'}(\mathbf{R}(t)) a_{T\alpha}^\dagger a_{T'\alpha} \\ & + \sum_{P,T} g_{PT}(\mathbf{R}(t)) (a_{P\alpha}^\dagger a_{T\alpha} + a_{T\alpha}^\dagger a_{P\alpha}). \end{aligned} \quad (6)$$

The last term in the expression for \hat{V} is responsible for transitions of nucleons between the two nuclei. The following notation is used in Eqs. (5) and (6):

$$\tilde{\epsilon}_P(\mathbf{R}(t)) = \epsilon_P + \langle P|U_T|P\rangle, \quad (7)$$

$$\tilde{\epsilon}_T(\mathbf{R}(t)) = \epsilon_T + \langle T|U_P|T\rangle, \quad (8)$$

$$\chi_{PP'}(\mathbf{R}(t)) = \langle P|U_T|P'\rangle, \quad (9)$$

$$\chi_{TT'}(\mathbf{R}(t)) = \langle T|U_P|T'\rangle, \quad (10)$$

$$g_{PT}(\mathbf{R}(t)) = \frac{1}{2} \langle P|U_P + U_T|T\rangle. \quad (11)$$

In Eqs. (7) and (8), $\epsilon_{P,T}$ are the single-particle energies of the noninteracting nuclei in question.

It is clear from (2) and (3) that the functions of the single-particle basis are time-dependent. Therefore, the creation and annihilation operators $a_{P(T)}^\dagger$ and $a_{P(T)}$ are also time-dependent, but this dependence affects the results only in the second order in the overlap integral $\langle P|T\rangle$. Hereafter, we disregard second-order effects, as we have already done this in deriving Eqs. (7)–(11).

A state of the dinuclear system formed in the collision of two nuclei can be characterized by the total energy (it is an integral of the motion) and by the charge asymmetry Z , which is a collective variable. We can take the charge of the light nucleus for Z . We also introduce a set of additional quantum numbers n in order to distinguish between states of the dinuclear system that correspond to a fixed value of Z . For n , we can take the numbers of holes and particles in the clusters that form the dinuclear system. Obviously, there are many states in which values of Z and n take the same values, so that these quantum numbers characterize a macroscopic cell in configuration space rather than an individual microscopic state of the system.

Let us assume that the kinetic approach is applicable to describing multinucleon-transfer processes [6] and that the quantity $P_Z(n, t)$ characterizes the probability of finding the system at a time instant t in the macroscopic configuration-space cell characterized by the quantum numbers Z and n . The probability $P_Z(n, t)$ satisfies the equation

$$\begin{aligned} \frac{d}{dt} P_Z(n, t) = & \sum_{Z', n'} \lambda(Z, n|Z', n') \\ & \times (P_{Z'}(n', t) - P_Z(n, t)), \end{aligned} \quad (12)$$

where $\lambda(Z, n|Z', n')$ is the microscopic transition probability [$\lambda(Z, n|Z', n') = \lambda(Z', n'|Z, n)$].

The microscopic transition probabilities are expressed in terms of the Hamiltonian as

$$\begin{aligned} \lambda(Z, n|Z', n') & \quad (13) \\ = & \frac{1}{\Delta t} \left| \langle Z, n | \hat{T} \exp \left(-\frac{i}{\hbar} \int_t^{t+\Delta t} H(t') dt' \right) | Z', n' \rangle \right|^2. \end{aligned}$$

The characteristic time Δt must exceed the relaxation time of the nuclear mean field (about 10^{-22} s). The vector $|Z, n\rangle$ is the wave packet formed by the vectors of states belonging to the same macroscopic cell. We also assume that Δt is significantly less than $2\pi\hbar/\Delta E$, where ΔE is the scatter of the energies of states belonging to the same macroscopic cell. Through this assumption, we introduce one averaged

energy E_n^Z that characterizes a macroscopic cell; that is, we assume that

$$\hat{H}_0|Z, n\rangle = E_n^Z|Z, n\rangle. \quad (14)$$

If \hat{V} is small, we arrive at

$$\lambda(Z, n|Z', n') = |\langle Z, n|V|Z', n'\rangle|^2 \quad (15)$$

$$\times \left(\sin \frac{\Delta t(E_n^Z - E_{n'}^{Z'})}{2\hbar} \right)^2 / \left(\frac{1}{4} \Delta t(E_n^Z - E_{n'}^{Z'})^2 \right).$$

As was mentioned above, the occupation numbers of single-particle states are taken for the quantum numbers n and n' . From the single-particle nature of the interaction \hat{V} , it follows that $\lambda(Z, n|Z', n')$ does not vanish only if the quantum numbers n and n' differ by one particle-hole pair. In this case, the difference of the configuration energies reduces to the difference of the energies of single-particle states coupled by the interaction \hat{V} . In what follows, we will not consider that part of \hat{V} which is responsible for the excitation of nuclei without nucleon transfer, taking it effectively into account by introducing temperature. The relation $Z' = Z \pm 1$ then holds, and we obtain

$$\lambda(Z, n|Z + 1, n') = \frac{2}{\hbar} \sum_{P,T} g_{PT}^2 n_P^{Z+1, n'} \quad (16)$$

$$\times (1 - n_T^{Z+1, n'}) n_T^{Z, n} (1 - n_P^{Z, n})$$

$$\times \left[\sin \frac{\Delta t(\tilde{\epsilon}_T^Z - \tilde{\epsilon}_P^Z)}{2\hbar} \right]^2 / \left(\frac{\Delta t(\tilde{\epsilon}_T^Z - \tilde{\epsilon}_P^Z)^2}{2\hbar} \right),$$

$$\lambda(Z, n|Z - 1, n') = \frac{2}{\hbar} \sum_{P,T} g_{PT}^2 n_T^{Z-1, n'} \quad (17)$$

$$\times (1 - n_P^{Z-1, n'}) n_P^{Z, n} (1 - n_T^{Z, n})$$

$$\times \left[\sin \frac{\Delta t(\tilde{\epsilon}_T^Z - \tilde{\epsilon}_P^Z)}{2\hbar} \right]^2 / \left(\frac{\Delta t(\tilde{\epsilon}_T^Z - \tilde{\epsilon}_P^Z)^2}{2\hbar} \right).$$

In the last two equations, the occupation numbers n_P and n_T are equal to zero or unity, because, for the n and n' configurations, we chose states where the occupation numbers of single-particle states are fixed.

We assume that the equilibrium distribution with respect to n at given Z is established within a time that is significantly shorter than the time within which the charge asymmetry Z changes. Since we are interested only in the time intervals of Z variation, we assume that $P_Z(n, t)$ can be represented in the form

$$P_Z(n, t) = P_Z(t)\Phi_Z(n), \quad (18)$$

where $\sum_n \Phi_Z(n) = 1$. Substituting (18) into (12) and performing summation over n , we obtain

$$\frac{dP_Z(t)}{dt} = \Delta_{Z+1}^{(-)} P_{Z+1}(t) + \Delta_{Z-1}^{(+)} P_{Z-1}(t) \quad (19)$$

$$- \left(\Delta_Z^{(-)} + \Delta_Z^{(+)} \right) P_Z(t),$$

where

$$\Delta_Z^{(-)} = \frac{2}{\hbar} \sum_{P,T} g_{PT}^2 \left(\sum_{n'} \Phi_Z(n') n_P^{Z, n'} (1 - n_T^{Z, n'}) \right) \quad (20)$$

$$\times \left(\sin \frac{\Delta t(\tilde{\epsilon}_T^Z - \tilde{\epsilon}_P^Z)}{2\hbar} \right)^2 / \left(\frac{\Delta t(\tilde{\epsilon}_T^Z - \tilde{\epsilon}_P^Z)^2}{2\hbar} \right),$$

$$\Delta_Z^{(+)} = \frac{2}{\hbar} \sum_{P,T} g_{PT}^2 \left(\sum_{n'} \Phi_Z(n') n_T^{Z, n'} (1 - n_P^{Z, n'}) \right) \quad (21)$$

$$\times \left(\sin \frac{\Delta t(\tilde{\epsilon}_T^Z - \tilde{\epsilon}_P^Z)}{2\hbar} \right)^2 / \left(\frac{\Delta t(\tilde{\epsilon}_T^Z - \tilde{\epsilon}_P^Z)^2}{2\hbar} \right).$$

In the expression

$$\sum_{n'} \Phi_Z(n') n_{T(P)}^{Z, n'} (1 - n_{P(T)}^{Z, n'}), \quad (22)$$

averaging is performed over all shell configurations of given charge asymmetry Z and given excitation energy. It is natural to assume that the sum in (22) can be expressed in terms of the temperature (Fermi) occupation numbers taken at the temperature τ corresponding to the excitation energy of the system; that is,

$$\sum_{n'} \Phi_Z(n') n_{T(P)}^{Z, n'} (1 - n_{P(T)}^{Z, n'}) \quad (23)$$

$$= n_{T(P)}^Z(\tau) (1 - n_{P(T)}^Z(\tau)).$$

Equation (19) has a time-independent solution. Equating the left-hand side of Eq. (19) to zero, we obtain the condition of the existence of a time-independent solution:

$$\Delta_{Z-1}^{(+)} P_{Z-1} = \Delta_Z^{(-)} P_Z, \quad (24)$$

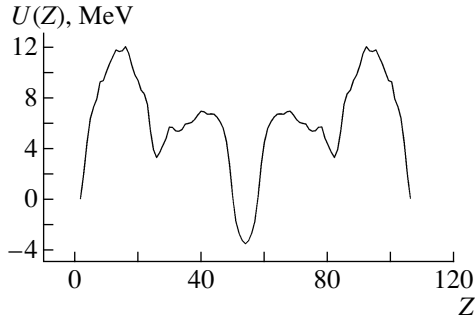
$$\Delta_{Z+1}^{(-)} P_{Z+1} = \Delta_Z^{(+)} P_Z. \quad (25)$$

Both these relations are equivalent to

$$P_{Z+1}/P_Z = \Delta_Z^{(+)} / \Delta_{Z+1}^{(-)}. \quad (26)$$

For $t \rightarrow \infty$, the probability $P_Z(t)$ tends to a time-independent limit that is proportional to $\exp(-U(Z)/\tau)$, where $U(Z)$ is the mean value of the Hamiltonian in a state of charge asymmetry Z . Substituting this result into (26), we obtain

$$\Delta_{Z+1}^{(-)} / \Delta_Z^{(+)} = \exp \left(\frac{U(Z+1) - U(Z)}{\tau} \right). \quad (27)$$



Potential $U(Z)$ calculated according to (28) and (36) for the system characterized by $Z_{\text{total}} = 108$ and $A_{\text{total}} = 272$. The temperature τ is set to 1 MeV.

This expression leads to the following iterative procedure for calculating $U(Z)$:

$$U(Z+1) = U(Z) + \tau \ln \left(\frac{\Delta_{Z+1}^{(-)}}{\Delta_Z^{(+)}} \right). \quad (28)$$

Using relations (20) and (21) and assuming that Δt is small, we arrive at

$$\frac{\Delta_{Z+1}^{(-)}}{\Delta_Z^{(+)}} = \frac{\sum_{P,T} g_{PT}^2 n_P^{Z+1} (1 - n_T^{Z+1})}{\sum_{P,T} g_{PT}^2 n_T^Z (1 - n_P^Z)}. \quad (29)$$

To calculate this relation, we employ, for the matrix elements, the approximation

$$g_{PT} = g_0 \exp \left(-\frac{|\tilde{\epsilon}_P - \tilde{\epsilon}_T|}{\Delta} \right), \quad (30)$$

$\Delta = 8-10 \text{ MeV},$

which proved to be quite successful in calculating the charge distributions of products originating from multinucleon-transfer reactions [5].

Let us consider the sum in the numerator on the right-hand side of (29),

$$\sum_{P,T} g_{PT}^2 n_P^{Z+1} (1 - n_T^{Z+1}). \quad (31)$$

(The sum in the denominator can be calculated in a similar way.) With the aid of (30), expression (31) can be recast into the form

$$\sum_{P,T} g_{PT}^2 n_P^{Z+1} (1 - n_T^{Z+1}) = \int d\epsilon \exp \left(-2\frac{\epsilon}{\Delta} \right) g^{Z+1}(\epsilon), \quad (32)$$

where

$$g^{Z+1}(\epsilon) \equiv \delta(\epsilon - (\tilde{\epsilon}_T - \tilde{\epsilon}_P)) n_P^{Z+1} (1 - n_T^{Z+1}) \quad (33)$$

is the density of particle-hole states. With allowance for the Coulomb interaction of nuclei that form the dinuclear system, we have

$$\tilde{\epsilon}_P - \tilde{\epsilon}_T = \epsilon_P - \epsilon_T + \frac{(Z_T - Z_P)e^2}{R}, \quad (34)$$

where $Z_{T(P)}$ is the target (projectile) charges, $\epsilon_{T(P)}$ stands for the single-particle energies of the non-interacting target (projectile), and R is the distance between the centers of the interacting nuclei. It is clear from (34) that the Coulomb interaction shifts significantly the single-particle energies of the light-nucleus protons upward with respect to those of the heavy-nucleus protons. This shift becomes greater with increasing charge asymmetry in the dinuclear system. We will also see that this has a pronounced effect on the shape of $U(Z)$.

We will use a linear approximation for the density of particle-hole excitations. In this case, we have, for example,

$$g^{Z+1}(\epsilon) = \left(\epsilon + \lambda_P^{Z+1} - \lambda_T^{Z+1} + \frac{(Z_T - Z_P)e^2}{R} \right) g_{0,P}^{Z+1} g_{0,T}^{Z+1}. \quad (35)$$

Here, $\lambda_{P(T)}^{Z+1}$ is the proton separation energy in the nuclei of the dinuclear system having the charge asymmetry $Z+1$, while $g_{0,P}^{Z+1} = A_P^{Z+1}/14 \text{ MeV}^{-1}$ and $g_{0,T}^{Z+1} = A_T^{Z+1}/14 \text{ MeV}^{-1}$, where $A_{P(T)}^{Z+1}$ is the mass number of the projectile (target) at the specific charge asymmetry $Z+1$. The use of a linear approximation for the density of the particle-hole states means that, of all shell effects, we retain only the charge- and the mass-number dependence of the proton separation energy, since a linear approximation follows from the assumption that the single-particle states are located equidistantly. However, the calculations performed in [5] for the charge and mass distributions of the products originating from multinucleon-transfer reactions showed that the effects due to the variations of the nucleon separation energy with Z and A are dominant.

Using (35), we obtain

$$\frac{\Delta_{Z+1}^{(-)}}{\Delta_Z^{(+)}} = \frac{A_P^{Z+1} A_T^{Z+1}}{A_P^Z A_T^Z} \times \frac{\exp \left(-\frac{2}{\Delta} |X_{PT}^{Z+1}| \right) + \frac{4}{\Delta} X_{PT}^{Z+1} \Theta(X_{PT}^{Z+1})}{\exp \left(-\frac{2}{\Delta} |X_{TP}^Z| \right) + \frac{4}{\Delta} X_{TP}^Z \Theta(X_{TP}^Z)}, \quad (36)$$

where

$$X_{PT}^{Z+1} \equiv \lambda_P^{Z+1} - \lambda_T^{Z+1} + \frac{(Z_T - Z_P)e^2}{R}, \quad (37)$$

$$X_{TP}^Z \equiv \lambda_T^Z - \lambda_P^Z - \frac{(Z_T - Z_P)e^2}{R}, \quad (38)$$

and $\Theta(X_{PT}^{Z+1})$ is a Heaviside theta function. Substituting (36) into (28), we arrive at a difference equation for calculating the potential $U(Z)$. It is clear from (36)–(38) that the shape of the potential $U(Z)$ is determined by the proton separation energies in the interacting nuclei and especially by the shift of the single-particle proton levels that is induced by the Coulomb potential of the partner nucleus. In other words, the shape of the potential $U(Z)$ is determined by the Z dependence of the quantity X_{PT}^{Z+1} (37). The present calculations reveal that, at small Z , X_{PT}^{Z+1} is predominantly positive, which leads to the growth of $U(Z)$ with increasing Z . As Z increases further, the role of the Coulomb term in (37) becomes less pronounced, X_{PT}^{Z+1} changes sign, and $U(Z)$ decreases. This is the way in which the potential $U(Z)$ develops a barrier.

The figure displays the results of the calculation for $U(Z)$. It is clear from the figure that the potential has a maximum at $Z = 16$, which is known in the literature as the Businaro–Gallone maximum. Behind this maximum, $U(Z)$ decreases as the charge number increases to $Z = 26$, whereupon it again slightly increases, forming a rather broad maximum followed by an abrupt decrease within the range between $Z = 44$ and 54.

Thus, we have reconstructed the potential for the problem being considered, relying on the probability of the transitions from one point of configuration space (in our case, the one-dimensional space generated by the coordinate Z) to another and calculating this probability on the basis of the microscopic Hamiltonian. At small Z , the strong Coulomb field of the heavy nucleus shifts the single-particle proton levels of the light nucleus upward with respect to the single-particle proton levels of the heavy nucleus.

Therefore, the probabilities of proton transfers from the light to the heavy nucleus exceed the probabilities of inverse transfers at small Z . This behavior of the proton-transfer probabilities is reflected in the growth of $U(Z)$ with increasing Z at small Z . As Z increases further, the effects of the Coulomb potentials of nuclei begin to compensate each other, with the result that the probability of proton transfer from the heavy to the light nucleus becomes greater than the probability of inverse transfer, in which case the potential $U(Z)$ decreases with increasing Z . In this way, the potential $U(Z)$ develops a barrier, which a dinuclear system must overcome in the course of its evolution—for example, from a symmetric initial state to a significantly asymmetric final state.

ACKNOWLEDGMENTS

I am grateful to Yu.V. Gaponov for a discussion that revived my interest in the problem and to G.G. Adamian, N.V. Antonenko, and A.K. Nasirov for stimulating discussions.

REFERENCES

1. D. L. Hill and J. A. Wheeler, Phys. Rev. **89**, 1102 (1953).
2. H. Hofmann, Phys. Rep. **284**, 137 (1997).
3. G. G. Adamian, N. V. Antonenko, R. V. Jolos, and A. K. Nasirov, Nucl. Phys. A **551**, 321 (1993).
4. P. Fröbrich and R. Lipperheide, *Theory of Nuclear Reactions* (Clarendon, Oxford, 1996).
5. N. V. Antonenko, R. V. Jolos, G. G. Adamian, and A. K. Nasirov, Fiz. Élem. Chastits At. Yadra **25**, 1379 (1994) [Phys. Part. Nucl. **25**, 583 (1994)].
6. W. Nörenberg, Phys. Lett. B **53B**, 289 (1974).

Translated by M. Kobrinsky

Self-Consistent Approach to Off-Shell Transport*

Yu. B. Ivanov¹⁾, J. Knoll^{**}, and D. N. Voskresensky²⁾

Gesellschaft für Schwerionenforschung mbH, Darmstadt, Germany

Received March 3, 2003

Abstract—The properties of two forms of the gradient expanded Kadanoff–Baym equations, i.e., the Kadanoff–Baym and Botermans–Malliet forms, suitable for describing the transport dynamics of particles and resonances with broad spectral widths, are discussed in context of conservation laws, the definition of a kinetic entropy, and the possibility of numerical realization. Recent results on exact conservations of charge and energy–momentum within Kadanoff–Baym form of quantum kinetics based on local coupling schemes are extended to two cases relevant in many applications. These concern the interaction via a finite-range potential and, relevant in nuclear and hadron physics, e.g., for the pion–nucleon interaction, the case of derivative coupling. © 2003 MAIK “Nauka/Interperiodica”.

1. INTRODUCTION

Ever since L. Boltzmann suggested his famous kinetic equation, the field of non-equilibrium physics and stochastic processes has grown tremendously, expanding in various directions. The interactions among particles driven by mean fields were included, quasiparticles were introduced in order to include much of the medium effects, the kinematics was extended to the relativistic case, and ultimately theoretical foundations of the transport equation were given from an underlying quantum many-body or field theory. In this line of achievements also stands the work of Budker and Belyaev, who demonstrated the Lorentz invariance of the relativistic distribution function and derived relativistic Fokker–Planck kinetic equation [1]. The work entered into many textbooks and found numerous applications in atomic physics and electron–positron plasma. Presently, the relativistic transport concepts are a conventional tool to analyze the dynamics of dense and highly excited matter produced in relativistic heavy-ion collisions.

Along with semiphenomenological extensions, great progress was achieved in microscopic foundation of the kinetic theory, which is mainly associated with the names of Bogolyubov, Born, Green, Kirkwood, Yvon, and Zubarev. The appropriate framework for describing non-equilibrium processes within

the real-time formalism of quantum-field theory was developed by Schwinger, Kadanoff, Baym, and Keldysh [2–4]. This formalism allows extensions of the kinetic picture beyond conventional approximations (like the quasiparticle one) and has found now numerous applications in many domains of physics.

The interest in transport descriptions of heavy-ion collisions beyond the quasiparticle approximation was initiated by Danielewicz [5], using the gradient expanded Kadanoff–Baym (KB) equations. These attempts have recently been revived [6–13] in order to properly describe the transport properties of broad resonances (like the ρ meson and Δ isobar). In a dense environment, a stable particle also acquires a considerable width because of collisional broadening. A proper dynamical treatment of their widths in a dense nuclear medium within transport theoretical concepts is still a challenging problem. Transport approaches for treating such off-shell dynamics were proposed in [7–13]. They all were based on the KB equations [3, 14], which describe the nonequilibrium quantum evolution at the truncation level of the Schwinger–Dyson equation. Expanded up to the first spacetime gradients, the KB equations provide transport equations for the one-body phase-space distribution functions with a collision term and Poisson bracket terms arising from the first-order gradient terms. Presently, two slightly different forms of the gradient-expanded KB equations are used: the original KB form [3], as follows right after the gradient expansion without any further approximations, and the Botermans–Malliet (BM) one [15], which is derived from the KB form by omitting certain second-order spacetime gradient corrections.

In this paper, we would like to compare these two forms of “quantum” kinetic equations and discuss

*This article was submitted by the authors in English.

¹⁾Russian Research Centre Kurchatov Institute, pl. Kurchatova 1, Moscow, 123182 Russia; e-mail: V.Ivanov@gsi.de

²⁾Moscow Institute for Physics and Engineering, Kashirskoe sh. 31, Moscow, 115409 Russia; e-mail: D.Voskresensky@gsi.de

** e-mail: J.Knoll@gsi.de

their advantages and disadvantages from the point of view of their conserving properties, the possibility of numerical realization, etc. (Section 2). Technical details on the conserving properties are deferred to Appendices B–D, since they illustrate some of the general consideration of [10] together with some extensions to cases particularly relevant in nuclear physics. Appendix C treats nonrelativistic nucleon–nucleon interactions via a potential of finite range. The derivative coupling is considered in Appendix D using the example of P -wave pion–nucleon interaction. In Section 3, we supplement some considerations about the construction of a kinetic entropy within these two transport schemes. To make the paper self-contained, we summarize the time-contour matrix notation in Appendix A and introduce the Φ -functional formalism for derivative coupling in Appendix B. A summary is given in Section 4.

2. OFF-SHELL KADANOFF–BAYM AND BOTERMANS–MALFLIET KINETICS

In this section, we summarize the formulation of the off-shell kinetic equations in two different forms:

$$G_0^{-1}(p) = \begin{cases} p^2 - m^2 & \text{for relativistic bosons} \\ p_0 - \mathbf{p}^2/(2m) & \text{for nonrelativistic fermions or bosons.} \end{cases} \quad (2)$$

For a complete definition, Eq. (1) has to be supplemented with further equations, e.g., for the retarded Green’s function together with the retarded relations (A.6). In addition to these equations, the exact set of KB equations also includes the prototype of the mass-shell equation, which we also discuss below. If a system under consideration is only slightly spatially inhomogeneous and slowly evolving in time, a good approximation is provided by an expansion up to first order in spacetime gradients. Then, the main problem to arrive at a proper kinetic equation consists in accurately disentangling the rather complicated right-hand side of Eq. (1). This problem in the context of conserving approximations will be addressed here.

A. Φ -Derivable Approximations

In actual calculations, one has to use certain approximations or truncation schemes to the exact nonequilibrium theory, which make conserving properties (such as charge and energy–momentum conservations) and thermodynamic consistency of the transport theory not evident. It was shown [8, 16, 17] that there exists a class of self-consistent approximations, called Φ -derivable approximations, which are conserving at the expectation value level

in the KB form, i.e., as follows right after the gradient expansion of the exact KB equations, and in the BM form [15], which differs from the KB form only in the second order of the gradient expansion. We assume that the reader is familiar with the real-time formulation of nonequilibrium many-body theory and use the contour matrix notation, detailed in Appendix A.

The starting point of all considerations is the set of KB equations which express the spacetime changes of the Wigner transformed correlation function $iG^{-+}(X, p)$ in terms of the real-time contour convolution of the self-energy Σ with the Green’s function G . We give the kinetic equation in compact notation [cf. below Eq. (A.4)]:

$$v_\mu \partial_X^\mu iG^{-+}(X, p) = [\Sigma \otimes G - G \otimes \Sigma]_{X,p}^{-+} \quad (1)$$

with $v^\mu = \frac{\partial}{\partial p_\mu} G_0^{-1}(p)$,

where $G_0^{-1}(p)$ is the Fourier transform of the inverse free Green’s function:

and at the same time thermodynamically consistent, i.e., they provide true Noether currents and a conserved energy–momentum tensor. In these schemes, the self-consistent self-energies are generated from a functional $\Phi[G]$ through the following variational procedure [8]:

$$-i\Sigma_{ik}(X, p) = \mp \frac{\delta i\Phi[G]}{\delta iG^{ki}(X, p)} \quad (3)$$

$$\times \begin{cases} 2 & \text{for real fields,} \\ 1 & \text{for complex fields,} \end{cases} \quad i, k \in \{-+\}.$$

The functional $\Phi[G]$ specifies the truncation scheme. It consists of a set of properly chosen closed two-particle irreducible diagrams, where lines denote the self-consistent propagator G , while vertices are bare. The functional variation with respect to G diagrammatically implies an opening of a propagator line of Φ .

Particular examples of Φ -derivable approximations can be found in Appendices C and D, which consider applications of the general formalism to cases important in nuclear physics. The treatment of the pion–nucleon derivative coupling in Appendix D requires the corresponding extension of the Φ -derivable formalism, which has not been done up

to now. Therefore, in Appendix B, we perform such an extension and derive the relevant modifications of the variational rules and the ensuing additional terms in the current and energy–momentum tensor expressions.

The conserving properties of these approximations are exact at the level of KB Eqs. (1), while after the expansion up to the first spacetime gradients they are generally expected to be only approximately fulfilled.

B. Physical Notation

It is helpful to eliminate the imaginary factors inherent in the standard Green’s function formulation and introduce quantities that are real and, in the quasi-homogeneous limit, positive, with clear physical meaning, thereby. Thus, instead of Green’s functions $G^{ij}(X, p)$ and self-energies $\Sigma^{ij}(X, p)$ with $i, j \in \{-+\}$ (see Appendix A) in the Wigner representation, we use the kinetic notation of [8]. We define³⁾

$$F(X, p) = A(X, p)f(X, p) = (\mp) iG^{-+}(X, p), \quad (4)$$

$$\tilde{F}(X, p) = A(X, p)[1 \mp f(X, p)] = iG^{+-}(X, p)$$

for the generalized Wigner functions F and \tilde{F} and the corresponding *four*-phase-space distribution functions $f(X, p)$ and Fermi/Bose factors $[1 \mp f(X, p)]$. Here,

$$A(X, p) \equiv -2\text{Im}G^R(X, p) = \tilde{F} \pm F \quad (5)$$

is the spectral function, and G^R is the retarded propagator. The spectral function satisfies the sum rule

$$\int_0^\infty \frac{dp_0}{2\pi} A(X, p) = 1 \text{ for nonrelativistic particles,} \quad (6)$$

$$\int_{-\infty}^\infty \frac{dp_0}{2\pi} p_0 A(X, p) = 1 \text{ for relativistic bosons,} \quad (7)$$

which follows from the canonical equal-time (anti)commutation relations for (fermionic) bosonic field operators. Likewise, the gain and loss rates of the collision integral are defined as

$$\Gamma^{\text{in}}(X, p) = \mp i\Sigma^{-+}(X, p), \quad (8)$$

$$\Gamma^{\text{out}}(X, p) = i\Sigma^{+-}(X, p)$$

with the damping width

$$\Gamma(X, p) \equiv -2\text{Im}\Sigma^R(X, p) = \Gamma^{\text{out}}(X, p) \pm \Gamma^{\text{in}}(X, p), \quad (9)$$

where Σ^R is the retarded self-energy.

³⁾Here and below, the upper sign corresponds to fermions, while the lower sign corresponds to bosons.

In terms of the above kinetic notation, the gradient-expanded KB equations are reduced to equations for four real quantities: two equations for the real and imaginary parts of the retarded Green’s function, while there are two equations for the phase-space occupation F : the KB kinetic equation and the prototype “mass-shell equation.” The latter doubling of equations reflects the well-known redundancy of the KB equations. Before the gradient expansion, both equations are completely identical. However, after the gradient expansion, their interrelation is no longer obvious and deserves special care (see below).

The equations for the retarded propagator in first-order gradient approximation can be immediately solved with the result [3, 15]

$$G^R = \frac{1}{M(X, p) + i\Gamma(X, p)/2} \quad (10)$$

$$\rightarrow \begin{cases} A(X, p) = \frac{\Gamma(X, p)}{M^2(X, p) + \Gamma^2(X, p)/4} \\ \text{Re}G^R(X, p) = \frac{M(X, p)}{M^2(X, p) + \Gamma^2(X, p)/4}, \end{cases}$$

with the “mass” function

$$M(X, p) = G_0^{-1}(p) - \text{Re}\Sigma^R(X, p). \quad (11)$$

Although solution (10) is simply algebraic, it is valid up to first-order gradients.

C. Kadanoff–Baym Form

In terms of the above notation, the KB kinetic equation for F in the first-order gradient approximation takes the form

$$\mathcal{D}F(X, p) - \{\Gamma^{\text{in}}, \text{Re}G^R\} = C(X, p). \quad (12)$$

We denote this as the *quantum transport equation in the KB choice*.⁴⁾ Here, the differential drift operator is defined as

$$\mathcal{D} = \left(v_\mu - \frac{\partial \text{Re}\Sigma^R}{\partial p^\mu} \right) \partial_X^\mu + \frac{\partial \text{Re}\Sigma^R}{\partial X^\mu} \frac{\partial}{\partial p_\mu}, \quad (13)$$

and $\{\dots, \dots\}$ denotes the four-dimensional Poisson bracket,

$$\{f(X, p), \varphi(X, p)\} = \frac{\partial f}{\partial p^\mu} \frac{\partial \varphi}{\partial X_\mu} - \frac{\partial f}{\partial X^\mu} \frac{\partial \varphi}{\partial p_\mu} \quad (14)$$

in covariant notation. Please note that, now, after the gradient approximation, all quantities on the left-hand side are to be taken in the local approximation, i.e., void of any further gradient terms. Thus, the occurring self-energies are obtained from evaluating

⁴⁾If the system consists of several different particle species, there is a set of coupled kinetic equations corresponding to each species (e.g., see Appendix D).

the diagrams as in the momentum representation with the coordinates X of all Green's functions kept identical. The right-hand side specifies the collision term⁵⁾

$$C(X, p) = \Gamma^{\text{in}}(X, p)\tilde{F}(X, p) - \Gamma^{\text{out}}(X, p)F(X, p). \quad (15)$$

If the diagrams for the self-energy contain internal vertices, which give rise to memory or nonlocal effects, the gain and loss rates contain additional gradient terms, which have to be constructed, e.g., according to the rules given in [10]. The resulting local part of the collision term is charge (e.g., the baryonic number) and energy–momentum conserving by itself:

$$\text{tr} \int \frac{d^4p}{(2\pi)^4} \begin{pmatrix} e \\ p^\mu \end{pmatrix} C^{\text{loc}} = 0. \quad (16)$$

Here and below, e denotes the elementary charge, while tr implies the sum over all possible internal degrees of freedom, like spin, and over possible particle species. We do not explicitly introduce the particle-species label to avoid overcomplication of equations. In terms of a local functional Φ^{loc} , the explicit form of the local collision term is

$$C^{\text{loc}}(X, p) = \frac{\delta i\Phi^{\text{loc}}}{\delta \tilde{F}(X, p)} \tilde{F}(X, p) - \frac{\delta i\Phi^{\text{loc}}}{\delta F(X, p)} F(X, p) \quad (17)$$

[cf. Eq. (3)]. In this paper, we limit the considerations to cases void of memory effects in this collision term. The latter effects were studied in [8].

Relation (16) permits us to derive the current

$$j_{\text{KB-eff}}^\mu(X) = \text{etr} \int \frac{d^4p}{(2\pi)^4} \left[v^\mu F(X, p) + \text{Re}\Sigma^R \frac{\partial F}{\partial p_\mu} - \text{Re}G^R \frac{\partial \Gamma^{\text{in}}}{\partial p_\mu} \right] \quad (18)$$

of a charge e (e.g., the baryonic one) from the KB kinetic equation (12), which is conserved:

$$\partial_\mu j_{\text{KB-eff}}^\mu(X) = 0. \quad (19)$$

Note that this current formally differs from the true Noether current

$$j^\mu(X) = \text{etr} \int \frac{d^4p}{(2\pi)^4} v^\mu F(X, p) + j_{(\text{der})}^\mu(X), \quad (20)$$

which follows right from the operator expression for this quantity (cf. [8] and Appendix B). The additional term $j_{(\text{der})}^\mu$ appears only in the case of derivative coupling [see Eq. (B.19)]. In view of the gradient approximation employed, one could generally expect

both currents to differ beyond the validity range of the gradient approximation. However, as demonstrated in detail in [10], these two currents are exactly equal for Φ -derivable approximations if a consistent gradient expansion is performed also in the gain and loss rates (8) of the collision term (15). In this case, the exact conservation of the Noether current results from the corresponding invariance of the Φ functional {Eq. (6.9) in [17]}, which survives the gradient expansion:

$$\text{etr} \int \frac{d^4p}{(2\pi)^4} [\{\text{Re}\Sigma^R, F\} - \{\text{Re}G^R, \Gamma^{\text{in}}\} + C] = \partial_\mu j_{(\text{der})}^\mu. \quad (21)$$

The latter relation is written for the general case of memory or nonlocal effects included in C . If such effects in C are absent, the collision term drops out of Eq. (21) according to Eq. (16).

Within Φ -derivable approximations, also the conservation of energy–momentum can be established for local (pointlike) couplings providing a local energy–momentum tensor. The p^ν -weighted 4-momentum integral of the KB kinetic equation leads to the following consistency relation [8]⁶⁾:

$$\partial^\nu (\mathcal{E}^{\text{pot}} - \mathcal{E}^{\text{int}}) - \partial_\mu \mathcal{E}_{(\text{der})}^{\mu\nu} = \text{tr} \left(\frac{1}{2} \right)_{\text{n.b.}} \times \int \frac{p^\nu d^4p}{(2\pi)^4} [\{\text{Re}\Sigma^R, F\} - \{\text{Re}G^R, \Gamma^{\text{in}}\} + C], \quad (22)$$

which is again *exact* after the gradient expansion, as shown in [10] (see also Appendices C and D). It implies that the Noether energy–momentum tensor

$$\Theta^{\mu\nu}(X) = \text{tr} \left(\frac{1}{2} \right)_{\text{n.b.}} \int \frac{d^4p}{(2\pi)^4} v^\mu p^\nu F(X, p) + g^{\mu\nu} (\mathcal{E}^{\text{int}} - \mathcal{E}^{\text{pot}}) + \mathcal{E}_{(\text{der})}^{\mu\nu} \quad (23)$$

is exactly conserved by the kinetic equation (12)

$$\partial_\mu \Theta^{\mu\nu}(X) = 0. \quad (24)$$

Here, potential energy density $\mathcal{E}^{\text{pot}}(X)$, which a probe particle with Wigner density $F(X, p)$ would experience due to the interaction with all other particles in the system, is

$$\mathcal{E}^{\text{pot}}(X) = \text{tr} \left(\frac{1}{2} \right)_{\text{n.b.}} \int \frac{d^4p}{(2\pi)^4} [\text{Re}\Sigma^R F + \text{Re}G^R \Gamma^{\text{in}}]. \quad (25)$$

⁶⁾Here, in compliance with Eq. (3), we define the factor

$$\frac{1}{2_{\text{n.b.}}} = \begin{cases} 1/2 & \text{for neutral bosons (real fields)} \\ 1 & \text{else.} \end{cases}$$

⁵⁾See an example in Eq. (C.3).

The interaction energy density $\mathcal{E}^{\text{int}}(X)$ specifies that part of the total energy density which is due to interactions. In simple cases, it relates to \mathcal{E}^{pot} by a simple counting factor, namely, if all the interaction vertices of a theory have the same number n_l of lines attached to them

$$\mathcal{E}^{\text{int}}(X) = \frac{2}{n_l} \mathcal{E}^{\text{pot}}(X). \quad (26)$$

In particular, for two-body interactions, one has $n_l = 4$ and thus $\mathcal{E}^{\text{int}} = \frac{1}{2} \mathcal{E}^{\text{pot}}$, while for the fermion–boson interaction $n_l = 3$, which results in $\mathcal{E}^{\text{int}} = \frac{2}{3} \mathcal{E}^{\text{pot}}$. In Appendices C and D, we discuss cases of this type. The additional term $\mathcal{E}_{(\text{der})}^{\mu\nu}$ appears in Eq. (23) only in the case of derivative coupling [cf. Eq. (B.18)].

The considerations given above summarize the results of [10], which are quite general. However, they are restricted to local (pointlike) interactions and are void of derivative couplings. This excludes two important cases relevant to many areas in physics, nuclear physics in particular. These are the cases of interaction mediated by finite-range nonrelativistic potentials and of derivative couplings like the P -wave pion–nucleon interaction. Since the considerations are rather technical, they are exemplified in Appendices C and D. There, the results of [10] are generalized, proving that, also in these cases, conserved currents and expressions for a conserved total energy and total momentum can be constructed. These two appendices also provide further illustrations of the discussion given in the present section.

The conserving feature is especially important for devising numerical simulation codes based on this kinetic equation. Indeed, if a test-particle method is used, one should be sure that the number of test particles is conserved exactly rather than approximately. For a direct application of this method, however, there is a particular problem with the KB kinetic equation. In the test-particle method, the distribution functions are represented by an ensemble of test particles as follows:

$$F(X, p) \sim \sum_i \delta^{(3)}(\mathbf{X} - \mathbf{X}_i(T)) \delta^{(4)}(p - p_i(T)), \quad (27)$$

where the i sum runs over test particles. Then, the $\mathcal{D}F$ term in Eq. (12) just corresponds to the classical motion of these test particles subjected to forces inferred from $\text{Re}\Sigma^R$, while the collision term C gives a stochastic change of test-particles' momenta, when their trajectories “cross.” The additional term, i.e., the Poisson bracket term $\{\Gamma^{\text{in}}, \text{Re}G^R\}$, spoils this simplistic picture, since derivatives acting on the distribution function F appear here only indirectly. Namely,

they are encoded through derivatives of Γ^{in} . This term is responsible for backflow effects, which restore the Noether current to be the conserved one. However, such backflow phenomena are difficult to absorb into test particles, since they describe the response of the medium to the motion of the charges. In order to conserve the number of test particles between subsequent collisions, one would have to unite the additional term $\{\Gamma^{\text{in}}, \text{Re}G^R\}$ with the drift term $\mathcal{D}F$ even in the simplest case, when the collision term is charge conserving by itself [see Eq. (16)] and derivative currents vanish, $j_{(\text{der})}^\mu = 0$. However, the interpretation of the additional term $\{\Gamma^{\text{in}}, \text{Re}G^R\}$ causes problems within this picture, since it is not just proportional to the same δ functions as in Eq. (27) and thus cannot be included in the collisionless propagation of test particles. This problem, of course, does not prevent a direct solution of the kinetic equation. For example, one can apply well-developed lattice methods, which are, however, much more complicated and time-consuming as compared to the test-particle approach.

Within the same approximation level, the set of Dyson equations for Green's functions $G^{ij}(X, p)$ provides us with an alternative equation for F ,

$$MF - \text{Re}G^R \Gamma^{\text{in}} = \frac{1}{4} (\{\Gamma, F\} - \{\Gamma^{\text{in}}, A\}), \quad (28)$$

which is called the mass-shell equation, since in the quasiparticle limit it provides the mass condition $M = 0$. This equation coincides with the kinetic one (12) only within the first-order gradient approximation [8, 11, 12, 15], while both equations are exactly identical before the gradient expansion. In view of this still remaining difference, the practical recipe is to forget about the mass-shell equation (28), since the retarded Eq. (10) determines the spectral distribution, and to treat Eq. (12) as a proper quantum kinetic equation. Still, this is an ambiguous recipe, which historically was one of the motivations to proceed to the Botermans–Malfliet form of the quantum kinetic equation.

D. Botermans–Malfliet Form

As can be seen from the mass-shell Eq. (28) and Eq. (12) [8, 11, 12, 15], the gain rate Γ^{in} departs from $F\Gamma/A$ only by corrections of first order in the gradients:

$$\Gamma^{\text{in}} = \Gamma F/A + O(\partial_X) \quad (29)$$

(in equilibrium, both equate to each another). This fact permits one to substitute the right-hand side estimate for Γ^{in} in any of the gradient terms, i.e., in the Poisson-bracketed terms of Eqs. (12) and (28), and neglect the correction $O(\partial_X)$, as it already

leads to terms of second order in the gradients. Upon this substitution, first proposed by Botermans and Malfliet [15], one arrives at the following form of the kinetic and mass-shell equations:

$$\mathcal{D}F(X, p) - \left\{ \Gamma \frac{F}{A}, \text{Re}G^R \right\} = C(X, p), \quad (30)$$

$$MF - \text{Re}G^R \Gamma^{\text{in}} = \frac{1}{4} \left(\{\Gamma, F\} - \left\{ \frac{\Gamma F}{A}, A \right\} \right), \quad (31)$$

which are already exactly identical, as they were before the gradient expansion, and still equivalent to those in the KB form within the first-order gradient approximation. The so-obtained Eq. (30) will be called the *quantum kinetic equation in BM choice*. This equation exactly conserves the following effective current:

$$j_{\text{BM-eff}}^\mu(X) = \text{etr} \int \frac{d^4 p}{(2\pi)^4} \left[v^\mu F(X, p) + \text{Re}\Sigma^R \frac{\partial F}{\partial p_\mu} - \text{Re}G^R \frac{\partial(\Gamma F/A)}{\partial p_\mu} \right], \quad (32)$$

which differs from the Noether current j^μ in terms of the order of $O(\partial_X)$, provided a Φ -derivable approximation is used for self-energies. All the properties of the KB-choice kinetic equation within a Φ -derivable approximation also transcribe to Eq. (30) in the BM choice through the substitution $\Gamma^{\text{in}} = \Gamma F/A$ in Eqs. (21), (22), and (25). This substitution, however, touches the accuracy of those relations. For instance, the conservation laws of the Noether currents (20) and the energy–momentum tensor (23) are then only approximately fulfilled together with the corresponding consistency relations (21) and (22), which now appear as

$$\text{etr} \int \frac{d^4 p}{(2\pi)^4} \left[\{\text{Re}\Sigma^R, F\} - \{\text{Re}G^R, \Gamma F/A\} + C \right] \simeq \partial_\mu j_{(\text{der})}^\mu, \quad (33)$$

$$\partial^\nu (\mathcal{E}^{\text{pot}} - \mathcal{E}^{\text{int}}) - \partial_\mu \mathcal{E}_{(\text{der})}^{\mu\nu} \simeq \text{tr} \left(\frac{1}{2} \right)_{\text{n.b.}} \times \int \frac{p^\nu d^4 p}{(2\pi)^4} \left[\{\text{Re}\Sigma^R, F\} - \left\{ \text{Re}G^R, \frac{\Gamma F}{A} \right\} + C \right], \quad (34)$$

respectively, and hold only up to first-order gradients.

The effective BM current (32) was used by Leupold [12] as a basis for the construction of a test-particle ansatz for the nonrelativistic case. In this case, the additional term $\{\Gamma F/A, \text{Re}G^R\}$ in the BM kinetic equation (30) is expressed in terms of the same distribution function as the drift term $\mathcal{D}F$. Therefore, one can unify these terms to construct equations of

motion for test particles, which provide exact conservation of $j_{\text{BM-eff}}^\mu$. To automatically fulfill this effective-current conservation, the test-particle ansatz is introduced for the combination

$$\frac{1}{2} \Gamma A \left(1 - \frac{\partial \text{Re}\Sigma^R}{\partial p_0} - \frac{M}{\Gamma} \frac{\partial \Gamma}{\partial p_0} \right) F(X, p) \sim \sum_i \delta^{(3)}(\mathbf{X} - \mathbf{X}_i(T)) \delta^{(4)}(p - p_i(T)), \quad (35)$$

rather than for the distribution function itself. Note that the energy $p_i^0(T)$ of the test particle is a free coordinate, not restricted by a mass-shell condition. Cassing and Juchem [11] extended this test-particle ansatz to the relativistic case. The equations of motion for the test particle, which follow from this ansatz, in particular, give the time evolution of the off-shellness of a test particle [11, 12]

$$\frac{dM}{dT} = \frac{M}{\Gamma} \frac{d\Gamma}{dT}, \quad (36)$$

the origin of which can be traced back to the additional term $\{\Gamma F/A, \text{Re}G^R\}$ in the BM kinetic Eq. (30). Here, M is the mass of the test particle relative to its on-shell value [see Eq. (11)], and this equation of motion implies that, once the width drops in time, the particles are driven towards the on-shell mass $M = 0$. This clarifies the meaning of the additional term $\{\Gamma F/A, \text{Re}G^R\}$ in the off-shell BM transport: it provides the time evolution of the off-shellness.

3. ENTROPY

Another important feature of the kinetic description is the approach to thermal equilibrium during evolution of a closed system. In terms of transport theory, the sufficient (while not necessary!) condition of it is the existence of an H theorem. Leaving aside all complications associated with nonlocal effects in the collision term and possible lack of positive definiteness of the transition rates, discussed in [8], we confine our consideration to simple approximations [cf. (C.1)]. As demonstrated in [8], in the BM approximation to the quantum kinetic Eq. (30), the H theorem can indeed be formulated:

$$\partial_\mu s_{\text{BM}}^\mu(X) = \text{tr} \int \frac{d^4 p}{(2\pi)^4} \ln \frac{\tilde{F}}{F} C^{\text{loc}}(X, p) \geq 0, \quad (37)$$

where the quantity

$$s_{\text{BM}}^\mu = \text{tr} \int \frac{d^4 p}{(2\pi)^4} \left[\left(v^\mu - \frac{\partial \text{Re}\Sigma^R}{\partial p_\mu} \right) \times \left(\mp \tilde{F} \ln \frac{\tilde{F}}{A} - F \ln \frac{F}{A} \right) - \text{Re}G^R \right] \quad (38)$$

$$\times \left(\mp \ln \frac{\tilde{F}}{A} \frac{\partial}{\partial p_\mu} \left(\Gamma \frac{\tilde{F}}{A} \right) - \ln \frac{F}{A} \frac{\partial}{\partial p_\mu} \left(\Gamma \frac{F}{A} \right) \right) \Bigg]$$

obtained from the left-hand side of the BM kinetic Eq. (30) is interpreted as an entropy flow for the BM choice. For the Φ -derivable approximation (C.1), the right-hand side of relation (37) takes the following form:

$$\begin{aligned} & \text{tr} \int \frac{d^4 p}{(2\pi)^4} \ln \frac{\tilde{F}}{F} C^{\text{loc}}(X, p) \quad (39) \\ &= \text{tr} \frac{1}{4} \int \frac{d^4 p_1}{(2\pi)^4} \frac{d^4 p_2}{(2\pi)^4} \frac{d^4 p_3}{(2\pi)^4} \frac{d^4 p_4}{(2\pi)^4} \\ & \times R^{\text{loc}} (2\pi)^4 \delta^4(p_1 + p_2 - p_3 - p_4) \\ & \times \left(F_1 F_2 \tilde{F}_3 \tilde{F}_4 - \tilde{F}_1 \tilde{F}_2 F_3 F_4 \right) \ln \frac{F_1 F_2 \tilde{F}_3 \tilde{F}_4}{\tilde{F}_1 \tilde{F}_2 F_3 F_4}, \end{aligned}$$

where R^{loc} is the transition rate determined by Eq. (C.4). This expression is indeed non-negative, since $(x - y) \ln(x/y) \geq 0$ for any positive x and y , and is of the second order in deviation from equilibrium ($F - F_{\text{eq}}$), as both $(F_1 F_2 \tilde{F}_3 \tilde{F}_4 - \tilde{F}_1 \tilde{F}_2 F_3 F_4)$ and $\ln(F_1 F_2 \tilde{F}_3 \tilde{F}_4 / \tilde{F}_1 \tilde{F}_2 F_3 F_4)$ approach zero at equilibrium. From the kinetic equation, it follows that the deviation from equilibrium is of the first order in time gradients: $(F - F_{\text{eq}}) \propto O(\partial_T F)$. This implies that the right-hand side of relation (37) is of the second order in time gradients, which is, strictly speaking, beyond our first-order gradient approximation. However, from the point of view of practical use, this feature is highly welcome as it guarantees equilibration. A further advantage of the kinetic entropy flux (38) is that, in equilibrium, its zero component merges the thermodynamic expression for the entropy deduced from the thermodynamic potential in the Φ -derivable scheme [8, 18, 19].

In the case of the KB choice (12), the situation is more controversial. Performing all the same manipulations with the KB kinetic Eq. (12) as those in [8], we arrive at the following relation:

$$\partial_\mu s_{\text{KB}}^\mu(X) = \text{tr} \int \frac{d^4 p}{(2\pi)^4} \ln \frac{\tilde{F}}{F} C^{\text{loc}} - \delta H_{\text{KB}}, \quad (40)$$

where

$$\begin{aligned} s_{\text{KB}}^\mu &= \text{tr} \int \frac{d^4 p}{(2\pi)^4} \left[\left(v^\mu - \frac{\partial \text{Re} \Sigma^R}{\partial p_\mu} \right) \right. \\ & \times \left(\mp \tilde{F} \ln \frac{\tilde{F}}{A} - F \ln \frac{F}{A} \right) \\ & \left. - \text{Re} G^R \left(\mp \ln \frac{\tilde{F}}{A} \frac{\partial \Gamma^{\text{out}}}{\partial p_\mu} - \ln \frac{F}{A} \frac{\partial \Gamma^{\text{in}}}{\partial p_\mu} \right) \right], \quad (41) \end{aligned}$$

$$\delta H_{\text{KB}} = - \int \frac{d^4 p}{(2\pi)^4} \text{Re} G^R \left\{ \ln \frac{\tilde{F}}{F}, \frac{C^{\text{loc}}}{A} \right\}. \quad (42)$$

The KB entropy flow s_{KB}^μ is identical to the BM one s_{BM}^μ up to zeroth-order gradients, while they differ in the first-order gradient corrections. One can easily obtain s_{BM}^μ from the KB entropy flow by doing replacement (29) in Γ^{in} and a similar replacement in Γ^{out} .

The additional term δH_{KB} on the right-hand side of relation (40) is of the second order in gradients, due to the Poisson bracket and $C^{\text{loc}} \propto O(\partial_T F)$. Therefore, the right-hand side of (40) consists of two terms, which are of the same order of magnitude, and one of them (δH_{KB}) is sign indefinite. This prevents us from concluding the positive definiteness of the right-hand side of Eq. (40). Alternatively, we were not able to cast this term into a full divergence as to be included into the definition of the KB entropy flow. This fact by itself does not imply that the system does not approach equilibrium or even the absence of an H theorem for the KB kinetic equation, but suggests that equilibration should be tested in actual calculations. The local H theorem we are looking for is a very stringent condition, providing a monotonic approach to equilibrium. In fact, equilibration may well be nonmonotonic in time.

Still, for the KB kinetic equation, we are able to prove the H theorem in a limiting case, i.e., close to local thermal equilibrium or for a quasi-stationary state, which slowly evolves in space and time. To be definite, let us talk about the local thermal equilibrium. In terms of the distribution function

$$F(X, p) = F_{\text{loc.eq}}(X, p) + \delta F(X, p), \quad (43)$$

the above assumption implies that $|\delta F| \ll F_{\text{loc.eq}}$ and $|\partial_X F_{\text{loc.eq}}| \lesssim |\partial_X \delta F|$. Then, we can write

$$\begin{aligned} \delta H_{\text{KB}} &= \partial_\mu \delta s_{\text{KB}}^\mu(X) \quad (44) \\ &+ \int \frac{d^4 p}{(2\pi)^4} \frac{C^{\text{loc}}}{A} \left\{ \ln \frac{\tilde{F}}{F}, \text{Re} G^R \right\}, \end{aligned}$$

where

$$\begin{aligned} \delta s_{\text{KB}}^\mu(X) &= - \text{tr} \int \frac{d^4 p}{(2\pi)^4} \frac{\text{Re} G^R}{A} \\ & \times \frac{\partial \ln(\tilde{F}/F)}{\partial p_\mu} C^{\text{loc}}(X, p). \quad (45) \end{aligned}$$

Here, the remaining term

$$\begin{aligned} & \int \frac{d^4 p}{(2\pi)^4} \frac{C^{\text{loc}}}{A} \left\{ \ln \frac{\tilde{F}}{F}, \text{Re} G^R \right\} \propto O(\delta F \partial_X \delta F) \quad (46) \\ & + O(\delta F \partial_X F_{\text{loc.eq}}) \end{aligned}$$

can be neglected, as it has additional gradient smallness as compared to the first term on the right-hand side of Eq. (40). Here, we have taken into account that $C^{\text{loc}} \propto \delta F$ and $\left\{ \ln(\tilde{F}/F), \text{Re}G^R \right\} \propto \partial_X(F_{\text{loc.eq}} + \delta F)$. Thus, from Eq. (40), we conclude that

$$\partial_\mu \left(s_{\text{KB}}^\mu + \delta s_{\text{KB}}^\mu \right) \geq 0 \quad \text{near local equilibrium, (47)}$$

which is the H theorem for this case with the total entropy flow $s_{\text{KB}}^\mu + \delta s_{\text{KB}}^\mu$. Note that δs_{KB}^μ is proportional to the collision term and hence equals zero in equilibrium. The applicability range of this result is the same as that for the memory entropy derived in [8] for the BM choice.

4. SUMMARY AND PERSPECTIVES

In conclusion, we would like to summarize the present status of the two considered approaches to off-shell transport.

From a consistency point of view, the BM choice looks more appealing, since it preserves the exact identity between the kinetic and mass-shell equation, a property inherent in the original KB equations [8]. For the KB choice, this identity between the kinetic and mass-shell equations is only *approximately* preserved, namely, within the validity range of the first-order gradient approximation. However, this disadvantage is not of great practical use, since, in any case, only one of these two equations, namely, the kinetic one, should be used in actual calculations.

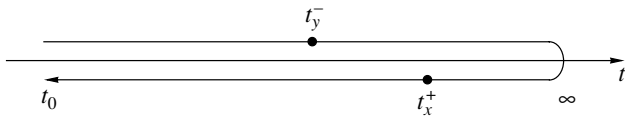
For the construction of conservation laws related to global symmetries or energy and momentum, the *local* collision term entirely drops out of the balance. Thus, the conservation laws solely depend on the properties of the first-order gradient terms in the kinetic equation. In this respect, the KB kinetic equation has a conceptual advantage as it leads to *exact* [10] rather than approximate conservation laws, provided the scheme is based on Φ -derivable approximations. Thereby, the expectation values of the original operator expressions of conserved quantities (e.g., Noether currents) are exactly conserved. The reason is that the KB kinetic equation preserves certain contour symmetries among the various gradient terms, while they are violated for the BM choice. Of course, within their range of applicability, these two approaches are equivalent, because the BM kinetic equation conserves the charge and energy–momentum within the theoretical accuracy of the gradient approximation. Still, the fact that the KB choice possesses exact conservation laws puts this version at the level of a generic equation, much like the Boltzmann or hydrodynamic equations, to be used as phenomenological dynamical equations for

practical applications. Such conserving dynamical schemes may be useful even though the applicability condition of the approximation might be violated at some stages of evolution. For instance, such a situation happens at the initial stage of heavy-ion collisions. As the conservations are exact, we can still use the gradient approximation, relying on a minor role of this rather short initial stage in the total evolution of a system. Moreover, exact conservation laws allow us to keep control of numerical codes.

Although the KB kinetic equations possess exactly conserved Noether currents, a practical numerical approach (e.g., by a test-particle method) to its solution has not yet been established. The obstacle is the special Poisson bracket term in the KB kinetic Eq. (12) which lacks proper interpretation since the phase-space occupation function $F(X, p)$ enters only indirectly through the gain-rate gradient terms. What is known is that this term encodes the backflow component, which ensures that the Noether currents are conserved. However, such backflow features are difficult to implement in a test-particle scheme. This problem, of course, does not exclude solution of the KB kinetic equation, e.g., within well-adapted lattice methods, which are, however, much more complicated and time consuming as compared to the test-particle approach. For the BM kinetic equation, on the other hand, an efficient test-particle method is already available [11, 12], for the price that it deals with an alternative current rather than the Noether current.

As a novel part, we showed (cf. Appendices) that the exact conservation laws in the KB kinetic equations, originally derived for local interaction terms, which lead to a local energy–momentum tensor, also do hold for derivative couplings and for interactions of finite range, like a nonrelativistic potential. For the latter case, of course, only global conservation of energy and momentum can be achieved. In order to deal with the derivative coupling, we extended the Φ -derivable approach to this case.

An important feature of kinetic descriptions is the approach to thermal equilibrium during evolution of a closed system. A sufficient (while not necessary!) condition is provided by an H theorem. As was demonstrated in [8], at least within simplest Φ -derivable approximations for the kinetic equation in BM choice, an H theorem indeed can be proven. In equilibrium, the so-derived kinetic entropy merges the corresponding equilibrium expression, which in the context of Φ -derivable approximations results from the thermodynamic potential (cf. [8, 18, 19]). For the KB kinetic equation, the result is by far weaker. Here, we were able to prove the H theorem only within simplest Φ -derivable approximations and for a system very close to an almost spatially homogeneous



Closed real-time contour with two external points x, y on the contour.

thermal local equilibrium or stationary state. These results, in general, do not imply that the system does not approach equilibrium but suggest that equilibration should be tested in actual calculations. Furthermore, the local H theorem with a local entropy current that we considered for the BM case may be far too restrictive, providing a monotonic approach to equilibrium. In fact, for kinetic equations with memory or nonlocal effects, equilibration may well be nonmonotonic in time.

Though the discussion in this paper is confined to problems of Φ -derivable off-shell transport based on the first-order gradient expansion, significant progress has recently been achieved also in solving KB equations directly without any gradient expansion for selected examples. These concern nonequilibrium processes in scalar and spinor–scalar models on one- and three-space dimensions (see, e.g., [20–22] and references therein). It was found [20, 21] that, after a comparably short but violent nonequilibrium evolution, the time dependence of the Wigner-transformed spectral function becomes rather weak even for moderate coupling constants. During this slow evolution, the system is still far away from equilibrium. This fact provides a necessary condition for a successful gradient expansion and hence indicates a wide range of applicability of the approaches discussed in this paper. Even though the rapid far-from-equilibrium dynamics is formally beyond the scope of applicability of the gradient-expanded quantum kinetics, nevertheless, the KB choice includes all the ingredients required for such a treatment, i.e., the proper mean-field dynamics, together with the off-shell transport of particles, thereby satisfying exact rather than approximate conservation laws even far away from equilibrium.

Further progress in understanding the properties of Φ -derivable approximations to finite-temperature quantum field theory was reported concerning the question of renormalizability. The new results are equally applicable to quantum kinetic equations, both in KB and in BM choices. In [23], it was shown that truncated nonperturbative self-consistent Dyson resummation schemes can be renormalized with local counterterms defined at the vacuum level. The requirements are that the underlying theory is renormalizable and that the self-consistent scheme follows Baym's Φ -derivable concept. This result proves that

there is no arbitrariness in studying the in-medium modifications of model parameters, like the mass and the coupling constants, within this class of approximation schemes. It is sufficient to adjust them in the vacuum, for instance, by fitting them to scattering data, in order to predict their changes in the medium without ambiguity. This result also guarantees the standard Φ -derivable properties, like thermodynamic consistency and exact conservation laws, for the renormalized approximation schemes to hold. In [24], the theoretical concepts for the renormalization devised in [23] were applied to the ϕ^4 model, demonstrating the practicability of the method.

In general, the symmetries of the classical action that lead to Ward–Takahashi identities for the proper vertex functions are violated for Φ -derivable approximations for functions beyond the one-point level, i.e., on the correlator level. This causes problems concerning the Nambu–Goldstone modes [25] in the broken symmetry case or concerning local symmetries (gauge symmetries) [26] on a level where the gauge fields are treated beyond the classical field approximation, i.e., on the propagator level. In [26], it was shown that, on top of any solution of a Φ -derivable approximation, which is constructed from a symmetric Lagrangian, there exists a non-perturbative effective action which generates proper vertex functions in the same sense as the 1PI effective action. These external vertex functions fulfill the Ward–Takahashi identities of the underlying symmetry. However, in general, they coincide with the self-consistent ones only up to one-point order. Thus, usually, the so-generated external self-energy and higher vertex functions are different from the Φ -derivable expressions. Therefore, the pleasant property of the Φ -derivable approximations, namely, the conserving one, proves to be lost. The derivation of approximation schemes that satisfy all symmetry properties of the underlying classical action and at the same time are fully self-consistent and conserving still remains as an open task.

As has been already mentioned, the gauge invariance may be lost in Φ -derivable approximations too. In particular, this problem prevents applications of Φ -derivable approximations (including kinetic ones) to description of quark–gluon plasma based on QCD. This occurs because, in general, solutions for dressed propagators and vertices do not satisfy Ward–Takahashi identities. This pathology shows up as an explicit dependence of results on the choice of the gauge condition. In [27], it was demonstrated, in fact, that Φ -derivable approximations have a controlled gauge dependence, i.e., the gauge-dependent terms appear at orders higher than the truncation order. Furthermore, using the stationary point obtained for the approximation to evaluate the complete

2PI effective action boosts the order at which the gauge-dependent terms appear, to twice the order of truncation. This is still not a solution of the gauge problem in the rigorous sense but certain progress to its better control and understanding.

ACKNOWLEDGMENTS

We are grateful to G. Baym, J. Berges, P. Danielewicz, H. Feldmeier, B. Friman, H. van Hees, C. Greiner, E.E. Kolomeitsev, and S. Leupold for fruitful discussions on various aspects of this research.

This work was supported in part by the Deutsche Forschungsgemeinschaft (DFG project 436 RUS 113/558/0-2), the Russian Foundation for Basic Research (project no. 03-02-04008), the Ministry for Industry and Science of the Russian Federation (grant no. NS-1885.2003.2), and the German BMBF (contract RUS-01/690).

APPENDIX A

Matrix Notation

In calculations that apply to the Wigner transformations, it is necessary to decompose the full contour into its two branches—the *time-ordered* and *antitime-ordered* branches. One then has to distinguish between the physical spacetime coordinates x and the corresponding contour coordinates x^C , which for a given $x = (t, \mathbf{x})$ take two values $x^- = (t^-, \mathbf{x})$ and $x^+ = (t^+, \mathbf{x})$ on the two branches of the contour (see figure).

Closed real-time contour integrations can then be decomposed as

$$\int_C dx \dots = \int_{t_0}^{\infty} dx \dots + \int_{\infty}^{t_0} dx \dots \tag{A.1}$$

$$= \int_{t_0}^{\infty} dx \dots - \int_{t_0}^{\infty} dx \dots,$$

where only the time limits are explicitly given. The extra minus sign of the antitime-ordered branch can conveniently be formulated by a $\{-+\}$ “metric” with the metric tensor in $\{-+\}$ indices

$$(\sigma^{ij}) = (\sigma_{ij}) = \begin{pmatrix} 1 & 0 \\ 0 & -1 \end{pmatrix}, \tag{A.2}$$

which provides a proper matrix algebra for multipoint functions on the contour with “co”- and “contra”-contour values. Thus, for any two-point function F , the contour values are defined as

$$F^{ij}(x, y) := F(x^i, y^j), \quad i, j \in \{-, +\}, \tag{A.3}$$

with

$$F_i^j(x, y) := \sigma_{ik} F^{kj}(x, y),$$

$$F_j^i(x, y) := F^{ik}(x, y) \sigma_{kj},$$

$$F_{ij}(x, y) := \sigma_{ik} \sigma_{jl} F^{kl}(x, y)$$

on the different branches of the contour. Here summation over repeated indices is implied. Then, contour folding of contour two-point functions, e.g., in Dyson equations, simply becomes

$$H(x^i, y^k) = H^{ik}(x, y) = [F \otimes G]^{ik} \tag{A.4}$$

$$\equiv \int_C dz F(x^i, z) G(z, y^k) = \int dz F_j^i(x, z) G^{jk}(z, y)$$

in the matrix notation.

For any multipoint function, the external point x_{\max} , which has the largest physical time, can be placed on either branch of the contour without changing the value, since the contour-time evolution from x_{\max}^- to x_{\max}^+ provides unity. Therefore, one-point functions have the same value on both sides on the contour.

Due to the change of operator ordering, genuine multipoint functions are, in general, discontinuous whenever two contour coordinates become identical. In particular, two-point functions like $iF(x, y) = \langle \mathcal{T}_C \hat{A}(x) \hat{B}(y) \rangle$ become⁷⁾

$$iF(x, y) = \begin{pmatrix} iF^{--}(x, y) & iF^{-+}(x, y) \\ iF^{+-}(x, y) & iF^{++}(x, y) \end{pmatrix} \tag{A.5}$$

$$= \begin{pmatrix} \langle \mathcal{T} \hat{A}(x) \hat{B}(y) \rangle & \mp \langle \hat{B}(y) \hat{A}(x) \rangle \\ \langle \hat{A}(x) \hat{B}(y) \rangle & \langle \mathcal{T}^{-1} \hat{A}(x) \hat{B}(y) \rangle \end{pmatrix},$$

where \mathcal{T} and \mathcal{T}^{-1} are the usual time- and antitime-ordering operators. Since there are altogether only two possible orderings of the two operators, in fact given by the Wightman functions F^{-+} and F^{+-} , which are both continuous, not all four components of F are independent. Equation (A.5) implies the following relations between nonequilibrium and usual retarded and advanced functions:

$$F^R(x, y) = F^{--}(x, y) - F^{-+}(x, y) \tag{A.6}$$

$$= F^{+-}(x, y) - F^{++}(x, y)$$

$$:= \Theta(x_0 - y_0)$$

$$\times (F^{+-}(x, y) - F^{-+}(x, y)),$$

$$F^A(x, y) = F^{--}(x, y) - F^{+-}(x, y)$$

$$= F^{-+}(x, y) - F^{++}(x, y)$$

⁷⁾Frequently used alternative notation is $F^< = F^{-+}$ and $F^> = F^{+-}$.

$$:= -\Theta(y_0 - x_0) \\ \times (F^{+-}(x, y) - F^{-+}(x, y)),$$

where $\Theta(x_0 - y_0)$ is the step function of the time difference. The rules for the co-contour functions F^{--} , etc., follow from Eq. (A.3).

For such two-point functions, complex conjugation implies

$$(iF^{-+}(x, y))^* = iF^{-+}(y, x) \rightarrow iF^{-+}(X, p) = \text{real}, \quad (\text{A.7})$$

$$(iF^{+-}(x, y))^* = iF^{+-}(y, x) \rightarrow iF^{+-}(X, p) = \text{real},$$

$$(iF^{--}(x, y))^* = iF^{++}(y, x) \rightarrow (iF^{--}(X, p))^* \\ = iF^{++}(X, p),$$

$$(F^R(x, y))^* = F^A(y, x) \rightarrow (F^R(X, p))^* \\ = F^A(X, p),$$

where the right parts specify the corresponding properties in the Wigner representation. Diagrammatically, these rules imply the simultaneous swapping of all “+” vertices into “-” vertices and vice versa together with reversing of the line arrow sense of all propagator lines in the diagram.

Contrary to the common case (A.5), the symmetrized contour convolution

$$E(x) = \int_c dz [F(x, z)G(z, x) + G(x, z)F(z, x)] \quad (\text{A.8})$$

is continuous when two contour coordinates become identical. This can be easily checked, proceeding from relations (A.6) for F and G functions. Moreover, for this symmetrized convolution with two coincident points, we obtain a very simple expression in the Wigner representation if all gradient corrections to the convolution are neglected (so-called local approximation),

$$E^{\text{loc}}(X) = \int \frac{d^4p}{(2\pi)^4} [F^{--}(X, p)G^{--}(X, p) \\ - F^{++}(X, p)G^{++}(X, p)]. \quad (\text{A.9})$$

In particular, this form is applicable to the potential (25) and derivative (D.4) energy densities.

APPENDIX B

Derivative Coupling

To be specific, we consider a multicomponent system with different constituents a described by non-relativistic fermionic and relativistic scalar bosonic field operators, summarized as $\hat{\phi} = \{\hat{\phi}_a(x)\}$. The free Lagrangians of these fields are

$$\hat{\mathcal{L}}L_a^0 = \begin{cases} \frac{1}{2} \left(i\hat{\phi}_a^\dagger \partial_t \hat{\phi}_a - i\partial_t \hat{\phi}_a^\dagger \hat{\phi}_a - \frac{1}{m_a} \nabla \hat{\phi}_a^\dagger \nabla \hat{\phi}_a \right) & \text{for nonrelativistic fermions} \\ \frac{1}{2} \frac{1}{m_a} \left(\partial_\mu \hat{\phi}_a \partial^\mu \hat{\phi}_a - m_a^2 \hat{\phi}_a^2 \right) & \text{for neutral relativistic bosons} \\ \frac{1}{m_a} \partial_\mu \hat{\phi}_a^\dagger \partial^\mu \hat{\phi}_a - m_a^2 \hat{\phi}_a^\dagger \hat{\phi}_a & \text{for charged relativistic bosons.} \end{cases} \quad (\text{B.1})$$

We assume that these fields interact via linear derivative coupling, such that the interaction Lagrangian depends not only on these fields but also on their derivatives: $\hat{\mathcal{L}}^{\text{int}} = \hat{\mathcal{L}}^{\text{int}}\{\hat{\phi}_a, \hat{\phi}_a^\dagger, \partial^\mu \hat{\phi}_a, \partial^\mu \hat{\phi}_a^\dagger\}$. The variational principle of stationary action determines Euler–Lagrange equations of motion for the field operators

$$\partial_\mu \frac{\partial \hat{\mathcal{L}}L^0}{\partial(\partial_\mu \hat{\phi}_a^\dagger)} - \frac{\partial \hat{\mathcal{L}}L^0}{\partial(\hat{\phi}_a^\dagger)} = \frac{\partial \hat{\mathcal{L}}L^{\text{int}}}{\partial(\hat{\phi}_a^\dagger)} \quad (\text{B.2}) \\ - \partial_\mu \frac{\partial \hat{\mathcal{L}}L^{\text{int}}}{\partial(\partial_\mu \hat{\phi}_a^\dagger)} =: \frac{\delta \hat{\mathcal{L}}L^{\text{int}}}{\delta \hat{\phi}_a^\dagger(x)}$$

and the corresponding adjoint equation, where the “variational” δ derivative is defined as

$$\frac{\delta}{\delta f(x)} \cdots := \frac{\partial}{\partial f(x)} \cdots - \partial_\mu \left(\frac{\partial}{\partial(\partial_\mu f(x))} \cdots \right). \quad (\text{B.3})$$

This is the key definition, which allows us to recast the local-coupling formulas to the derivative coupling case. In fact, the “variational” δ derivative specifies the *full* derivative over $f(x)$, implying that all derivatives acting on $f(x)$ in the action should be redirected to other terms by means of partial integration before taking variational derivatives of $f(x)$.

The equations of motion can also be written in the differential form,

$$G_0^{-1}(x)\hat{\phi}_a(x) = -\hat{J}_a(x) \equiv -\frac{\delta\hat{\mathcal{L}}^{\text{int}}}{\delta\hat{\phi}_a^\dagger(x)} \quad (\text{B.4})$$

and similarly for the corresponding adjoint equation. The $\hat{J}_a(x)$ operator is the local source current of field a with mass m_a , and $G_0^{-1}(x)$ is the free evolution operator⁸⁾

$$G_0^{-1}(x) = \begin{cases} -\partial_\mu\partial^\mu - m_a^2 & \text{for relativistic bosons} \\ i\partial_t + \frac{1}{2m_a}\partial_x^2 & \text{for nonrelativistic particles} \end{cases} \quad (\text{B.5})$$

with free propagator $G_0(y, x)$ as resolvent [cf. Eq. (2)].

Invariances of the Lagrangian provide a set of conservation laws, the most prominent of which are those for the energy–momentum and certain currents. In addition to the standard canonical energy–momentum tensor [28], different representations of this tensor have been considered [29, 30]. Using the Euler–Lagrange equations of motion and the definition of the source current (B.4), one can show that the following form also defines a conserving energy–momentum tensor:

$$\hat{\Theta}^{\mu\nu}(x) = -\frac{1}{2}\left[\sum_a\left(\frac{1}{2}\right)_{\text{n.b.}}(\partial_x^\nu - \partial_y^\nu) \times \left(\frac{\partial\hat{\mathcal{L}}^0(x)}{\partial(\partial_\mu\hat{\phi}_a)}\hat{\phi}_a(y) - \hat{\phi}_a^\dagger(x)\frac{\partial\hat{\mathcal{L}}^0(y)}{\partial(\partial_\mu\hat{\phi}_a^\dagger)}\right)\right]_{x=y} + g^{\mu\nu}(\hat{\mathcal{E}}^{\text{int}}(x) - \hat{\mathcal{E}}^{\text{pot}}(x)) + \hat{\mathcal{E}}_{(\text{der})}^{\mu\nu}(x). \quad (\text{B.6})$$

Here we have introduced the operators of the interaction-energy density $\hat{\mathcal{E}}^{\text{int}}$ and the potential-energy density $\hat{\mathcal{E}}^{\text{pot}}$:

$$\hat{\mathcal{E}}^{\text{int}}(x) = -\hat{\mathcal{L}}^{\text{int}}(x), \quad (\text{B.7})$$

$$\hat{\mathcal{E}}^{\text{pot}}(x) = -\frac{1}{2}\sum_a\left(\frac{1}{2}\right)_{\text{n.b.}} \times \left(\hat{J}_a^\dagger(x)\hat{\phi}_a(x) + \hat{\phi}_a^\dagger(x)\hat{J}_a(x)\right). \quad (\text{B.8})$$

Furthermore, we have singled out the contribution

$$\hat{\mathcal{E}}_{(\text{der})}^{\mu\nu}(x) = \sum_a\left(\frac{1}{2}\right)_{\text{n.b.}} \quad (\text{B.9})$$

⁸⁾Note that the first line in (B.5) is not the nonrelativistic limit of the second one. We have already divided the second line by $2m_a$, to take into account different normalizations of relativistic and nonrelativistic wave functions.

$$\times \left(\frac{\partial\hat{\mathcal{L}}^{\text{int}}}{\partial(\partial_\mu\hat{\phi}_a)}\partial^\nu\hat{\phi}_a + \partial^\nu\hat{\phi}_a^\dagger\frac{\partial\hat{\mathcal{L}}^{\text{int}}}{\partial(\partial_\mu\hat{\phi}_a^\dagger)}\right)$$

arising in the case of derivative coupling. Here and below, the case of neutral bosons results from equating $\hat{\phi}_a = \hat{\phi}_a^\dagger$ in all the formulas. Proper counting is assured by the extra $\left(\frac{1}{2}\right)_{\text{n.b.}}$ factor which takes the value 1/2 for neutral boson (real fields) and 1 for complex fields.

If the Lagrangian is invariant under some global transformation of charged fields (with the charges e_a), e.g.,

$$\hat{\phi}_a(x) \rightarrow e^{-ie_a\Lambda}\hat{\phi}_a(x); \quad \hat{\phi}_a^\dagger(x) \rightarrow e^{ie_a\Lambda}\hat{\phi}_a^\dagger(x), \quad (\text{B.10})$$

there exists a Noether current defined as [28]

$$\hat{j}^\mu = -i\sum_a e_a \left(\frac{\partial\hat{\mathcal{L}}}{\partial(\partial_\mu\hat{\phi}_a)}\hat{\phi}_a - \hat{\phi}_a^\dagger\frac{\partial\hat{\mathcal{L}}}{\partial(\partial_\mu\hat{\phi}_a^\dagger)}\right) = \hat{j}_{(\text{conv})}^\mu + \hat{j}_{(\text{der})}^\mu, \quad (\text{B.11})$$

which is conserved, i.e., $\partial_\mu\hat{j}^\mu = 0$. Here we have decomposed it into two terms: the conventional one

$$\hat{j}_{(\text{conv})}^\mu = -i\sum_a e_a \left(\frac{\partial\hat{\mathcal{L}}^0}{\partial(\partial_\mu\hat{\phi}_a)}\hat{\phi}_a - \hat{\phi}_a^\dagger\frac{\partial\hat{\mathcal{L}}^0}{\partial(\partial_\mu\hat{\phi}_a^\dagger)}\right), \quad (\text{B.12})$$

which is associated with the free Lagrangian, and the derivative term

$$\hat{j}_{(\text{der})}^\mu = -i\sum_a e_a \left(\frac{\partial\hat{\mathcal{L}}^{\text{int}}}{\partial(\partial_\mu\hat{\phi}_a)}\hat{\phi}_a - \hat{\phi}_a^\dagger\frac{\partial\hat{\mathcal{L}}^{\text{int}}}{\partial(\partial_\mu\hat{\phi}_a^\dagger)}\right), \quad (\text{B.13})$$

which is nonzero only for derivative coupling.

To define the Φ functional for the case under consideration, all the steps described in [17] should be repeated. Then, we arrive at the Φ functional that depends also on the gradients of mean fields ($\partial_\mu\phi_a$ and $\partial_\mu\phi_a^*$) and Green's functions ($\partial_x^\mu G(x, y)$ and $\partial_y^\mu G(x, y)$), rather than on their values only. The variational rules of this functional formally look similar to those in [17],

$$iJ_a(x) = \frac{\delta i\Phi}{\delta\phi_a^*(x)}, \quad (\text{B.14})$$

$$-i\Sigma_a(x, y) = (\mp)\frac{\delta i\Phi}{\delta iG_a(y, x)} \quad (\text{B.15})$$

$$\times \begin{cases} 2 & \text{for real fields} \\ 1 & \text{for complex fields,} \end{cases}$$

$$-\mathcal{E}^{\text{int}}(x) = \frac{\delta i\Phi}{\delta i\lambda(x)}, \quad (\text{B.16})$$

but should be understood in terms of the variational δ derivative of Eq. (B.3) for one-point functions (like $\phi_a(x)$ and $\lambda(x)$) and its generalization

$$\begin{aligned} \frac{\delta i\Phi}{\delta iG(y,x)} &:= \frac{\delta_0 i\Phi}{\delta_0 iG(y,x)} \\ -\partial_x^\mu \left(\frac{\delta_0 i\Phi}{\delta_0 (\partial_x^\mu iG(y,x))} \right) &- \partial_y^\mu \left(\frac{\delta_0 i\Phi}{\delta_0 (\partial_y^\mu iG(y,x))} \right) \\ + \partial_x^\mu \partial_y^\nu \left(\frac{\delta_0 i\Phi}{\delta_0 (\partial_x^\mu \partial_y^\nu iG(y,x))} \right) \end{aligned} \quad (\text{B.17})$$

to two-point functions. Here, $\delta_0/\delta_0 iG(y,x)$ means the conventional variation over $G(y,x)$, which does not touch $\partial_x^\mu iG$, $\partial_y^\mu iG$, and $\partial_x^\mu \partial_y^\nu iG$ terms in $i\Phi$. Similar to the variational δ derivative of Eq. (B.3), the δ variation of Eq. (B.17) means the *full* variation over $G(y,x)$, implying that all derivatives acting on $G(y,x)$ in the Φ functional should be redirected to other terms by means of partial integration before taking variation over $G(y,x)$. The factor $\lambda(x)$ appearing in Eq. (B.16) is an auxiliary scaling parameter of the coupling constant. In terms of the Φ functional, the additional derivative contributions to mean values of the energy–momentum tensor (B.9) and current (B.13) take the form

$$\mathcal{E}_{(\text{der})}^{\mu\nu} =: \langle \hat{\mathcal{E}}_{(\text{der})}^{\mu\nu} \rangle \quad (\text{B.18})$$

$$\begin{aligned} = \sum_a \left(\left(\frac{1}{2} \right)_{\text{n.b.}} \left[\frac{\delta\Phi}{\delta(\partial_\mu \phi_a(x))} \partial^\nu \phi_a(x) \right. \right. \\ \left. \left. + \frac{\delta\Phi}{\delta(\partial_\mu \phi_a^*(x))} \partial^\nu \phi_a^*(x) \right] \right. \\ \left. + \int_c dz \left[\frac{\delta\Phi}{\delta(\partial_\mu^x iG_a(z,x))} \partial_x^\nu iG_a(z,x) \right. \right. \\ \left. \left. + \partial_x^\nu iG_a(x,z) \frac{\delta\Phi}{\delta(\partial_\mu^x iG_a(x,z))} \right] \right), \end{aligned}$$

$$j_{(\text{der})}^\mu =: \langle \hat{j}_{(\text{der})}^\mu \rangle = -i \sum_a e_a \quad (\text{B.19})$$

$$\begin{aligned} \times \left(\left[\frac{\delta\Phi}{\delta(\partial_\mu \phi_a(x))} \phi_a(x) - \frac{\delta\Phi}{\delta(\partial_\mu \phi_a^*(x))} \phi_a^*(x) \right] \right. \\ \left. + \int_c dz \left[iG_a(x,z) \frac{\delta\Phi}{\delta(\partial_\mu^x iG_a(x,z))} \right. \right. \\ \left. \left. - \frac{\delta\Phi}{\delta(\partial_\mu^x iG_a(z,x))} iG_a(z,x) \right] \right), \end{aligned}$$

while the remaining terms of $\Theta^{\mu\nu}$ and j^μ retain the same form as that for local coupling (cf. [17]). Here, the variation is also understood in terms of Eq. (B.17) to take account of the $\partial_x^\mu \partial_y^\nu iG_a(y,x)$ dependence of the Φ functional.

The next step to the kinetic description consists in gradient expansion of KB equations and all the related quantities. Expansion of the equations of motion up to the first order in gradients implies that the conserving quantities and self-energies, except for possible memory terms in the collision integral, are required only up to zero order in gradients. These zero-order quantities are determined by the local Φ functional, where all gradient corrections are neglected. Since in the local approximation $\partial_x^\mu iG$, $\partial_y^\nu iG$, and $\partial_x^\mu \partial_y^\nu iG$ transform into $-iq^\mu iG(X,q)$, $iq^\nu iG(X,q)$, and $-iq^\mu iq^\nu iG(X,q)$, respectively, no partial integrations are needed for the variations of Eqs. (B.15), (B.16). This means that conventional variation rules of Eq. (3) still hold in this case. At the same time, derivative contributions to the conserving quantities, Eqs. (B.18) and (B.19), involve only variations over derivatives of the Green's functions and, hence, should be carefully defined within the local approximation for the particular application considered.

APPENDIX C

Nonrelativistic Nuclear Matter

Currently, calculations of ground-state and low-temperature properties of nuclear matter are performed within the G - or T -matrix approximations to the self-energy [31–33]. Based on realistic non-relativistic nucleon–nucleon potentials, they quantitatively reproduce phenomenological properties of nuclear matter. However, already for the ground state, the resulting chemical potential, i.e., the single-particle separation energy, deviates from the binding energy per particle, violating the Hugenholtz–van Hove theorem. This is a manifestation of problems with the thermodynamic consistency in these approximations, which gets even worse at nonzero temperatures. This problem was discussed in [31, 34, 35]. A consistent way to overcome this problem consists in using a self-consistent T -matrix approximation [31] based on the Φ -derivable approximation.

Dynamic simulations of nuclear matter are even more demanding to the choice of approximation to the self-energy, because the requirement of charge and energy–momentum conservations should be met except for that of the thermodynamic consistency. Again, all these requirements are met provided the approximation is Φ -derivable. Since dynamic simulations are much more complicated as compared to

static ones, up to now they have been performed in a simpler approximation to the self-energy, i.e., the direct Born approximation [5, 7], which provides a qualitative description of the dynamics. These simulations were based on the KB equations without any gradient expansion. Here, we would like to call attention to the fact that the use of the gradient expansion in the KB form (see Section 2C) would simplify these dynamic simulations and, at the same time, preserve the pleasant features of exact conservations and thermodynamic consistency.

In view of a reasonable level of complexity feasible for current computing, we confine our consideration to the full Born approximation to the Φ functional

$$i\Phi^{\text{HFB}} = \underbrace{\frac{1}{2} \text{diagram}_1 + \frac{1}{2} \text{diagram}_2}_{\Phi^{\text{HF}}} + \underbrace{\frac{1}{4} \text{diagram}_3 + \frac{1}{4} \text{diagram}_4}_{\Phi^{\text{Born}}} \quad (\text{C.1})$$

which includes the Hartree–Fock contribution Φ^{HF} [the first two diagrams in Eq. (C.1)] and the true Born contribution Φ^{Born} (the last two diagrams). Here, the wavy line symbolizes a nonlocal nucleon–nucleon potential $V(|\mathbf{x}_1 - \mathbf{x}_2|)$, or $V(|\mathbf{q}|)$ in the momentum representation. For simplicity, below we denote the latter as $V(q)$, keeping in mind that, in fact, it does not depend on either q_0 or direction of \mathbf{q} .

Note that the Φ^{Born} part gives rise to the self-energy containing internal vertices. This implies that the corresponding collision term involves nonlocal effects (see discussion in [8]). However, only “spatial nonlocality” appears in the collision term, while the memory in time is absent since $V(|\mathbf{x}_1 - \mathbf{x}_2|)\delta(t_1 - t_2)$ is time-local. According to the general consideration of [10], exact conservations in the gradient approximation take place if all the nonlocal terms are consistently taken into account up to first-order gradients. Below, we show that, in the particular case of the Φ^{HFB} functional, the exact conservations hold true even if we neglect the spatial nonlocality generated by Φ^{HFB} . These exact conservations imply global rather than local conservation of the energy–momentum, which is in fact natural for the case of instant interaction of finite range considered here.

Neglecting the gradient terms induced by the finite range of V , we consider the Φ^{Born} functional in the local approximation, where all Green’s functions in the Wigner representation are taken at the same centroid coordinate X . Alongside some variational expressions, we use an X -dependent local Φ functional,

$\Phi(X)$, where the last spatial integration is omitted, i.e.,

$$\Phi = \int dX \Phi(X). \quad (\text{C.2})$$

The Φ^{HFB} of Eq. (C.1) gives rise to the following local collision term:

$$C^{\text{HFB-loc}} = \int \frac{d^4 p_2}{(2\pi)^4} \frac{d^4 p_3}{(2\pi)^4} \frac{d^4 p_4}{(2\pi)^4} R^{\text{HFB}} \quad (\text{C.3})$$

$$\times \left(\tilde{F}_1 \tilde{F}_2 F_3 F_4 - F_1 F_2 \tilde{F}_3 \tilde{F}_4 \right) \delta^4(p_1 + p_2 - p_3 - p_4),$$

$$R^{\text{HFB}} = \frac{(2\pi)^4}{2} [V(p_1 - p_3) + V(p_1 - p_4)]^2, \quad (\text{C.4})$$

where $F_1 = F(X, p_1)$, etc. [cf. Eq. (17)].

1. Charge Conservation

In Φ^{HFB} , the G^{--} and G^{++} Green’s functions are encountered only in different $\pm\pm$ Φ diagrams, and hence we can vary G^{--} and G^{++} independently. Therefore, Φ^{HFB} is invariant under the following transformation:

$$G^{--}(X, p) \rightarrow G^{--}(X, p + \xi(X)), \quad (\text{C.5})$$

$$G^{++}(X, p) \rightarrow G^{++}(X, p - \xi(X)),$$

with F , \tilde{F} , and V kept unchanged. Here, $\xi(X)$ is an arbitrary function. If $|\xi(X)| \ll 1$, transformation (C.5) reads

$$\delta G^{--} = \xi_\mu(X) \frac{\partial G^{--}}{\partial p_\mu}, \quad (\text{C.6})$$

$$\delta G^{++} = -\xi_\mu(X) \frac{\partial G^{++}}{\partial p_\mu}.$$

Performing variation of Φ^{Born} under the transformation (C.6) within the canonical variation rules (3), we arrive at

$$i\delta\Phi^{\text{loc}} = \int dX \xi_\mu(X) \text{Tr} \int \frac{d^4 p}{(2\pi)^4} \quad (\text{C.7})$$

$$\times \left(i\Sigma_{--} \frac{\partial iG^{--}}{\partial p_\mu} - i\Sigma_{++} \frac{\partial iG^{++}}{\partial p_\mu} \right)$$

$$= 2i \int dX \xi_\mu(X) \text{Tr} \int \frac{d^4 p}{(2\pi)^4}$$

$$\times \left(\Gamma^{\text{in}} \frac{\partial \text{Re}G^R}{\partial p_\mu} + \text{Re}\Sigma^R \frac{\partial F}{\partial p_\mu} \right) = 0.$$

Here, we have used the fact that the integral

$$\text{tr} \int \frac{d^4 p}{(2\pi)^4} \left(\Gamma \frac{\partial \text{Re}G^R}{\partial p_\mu} + \text{Re}\Sigma^R \frac{\partial A}{\partial p_\mu} \right) \quad (\text{C.8})$$

$$= -\frac{1}{2} \text{Im tr} \int \frac{d^4 p}{(2\pi)^4} \Sigma^R \frac{\partial G^R}{\partial p_\mu} = 0$$

equals zero due to analyticity of G^R and Σ^R . Thus, we obtain the relation

$$\text{tr} \int \frac{d^4 p}{(2\pi)^4} \left(\Gamma^{\text{in}} \frac{\partial \text{Re} G^R}{\partial p_\mu} + \text{Re} \Sigma^R \frac{\partial F}{\partial p_\mu} \right) = 0, \quad (\text{C.9})$$

which guarantees the Noether current conservation [cf. Eq. (21)] with $j_{(\text{der})}^\mu = 0$.

2. Energy–Momentum Conservation

In order to construct the conservation laws related to spacetime homogeneity, we perform the following transformation:

$$G^{--}(X, p) \rightarrow G^{--}(X + \xi(X), p), \quad (\text{C.10})$$

$$G^{++}(X, p) \rightarrow G^{++}(X - \xi(X), p),$$

with F , \tilde{F} , and V kept unchanged. This transformation only acts on $\Phi^{\text{HFB}-}$ and $\Phi^{\text{HFB}+}$, i.e., those involving only “–” or “+” vertices, respectively,

$$\delta \Phi^{\text{HFB}} \quad (\text{C.11})$$

$$\begin{aligned} i\delta \Phi^{\text{HFB}} &= \int dX \xi_\mu(X) \text{tr} \int \frac{d^4 p}{(2\pi)^4} \left(i\Sigma^{--} \frac{\partial iG^{--}}{\partial X_\mu} - i\Sigma^{++} \frac{\partial iG^{++}}{\partial X_\mu} \right) = 2i \int dX \xi_\mu(X) \text{tr} \int \frac{d^4 p}{(2\pi)^4} \quad (\text{C.13}) \\ &\times \left(\Gamma^{\text{in}} \frac{\partial \text{Re} G^R}{\partial X_\mu} + \text{Re} \Sigma^R \frac{\partial F}{\partial X_\mu} \right) - i \underbrace{\int dX \xi_\mu(X) \text{tr} \int \frac{d^4 p}{(2\pi)^4} \left(\Gamma \frac{\partial \text{Re} G^R}{\partial X_\mu} + \text{Re} \Sigma^R \frac{\partial A}{\partial X_\mu} \right)}_{=0}, \end{aligned}$$

where the last integral is again zero due to analyticity. Therefore, we arrive at the important identity

$$\begin{aligned} \text{tr} \int \frac{d^4 p}{(2\pi)^4} \left(\Gamma^{\text{in}} \frac{\partial \text{Re} G^R}{\partial X_\mu} + \text{Re} \Sigma^R \frac{\partial F}{\partial X_\mu} \right) \quad (\text{C.14}) \\ = \partial^\mu \text{tr} \int \frac{d^4 p}{(2\pi)^4} \left[\frac{1}{2} \Sigma^{\text{HF}} F \right. \\ \left. + \frac{1}{4} \left(\Gamma^{\text{in}} \text{Re} G^R + (\text{Re} \Sigma^R - \Sigma^{\text{HF}}) F \right) \right]. \end{aligned}$$

Next, we investigate the transformation

$$G^{--}(X, p) \rightarrow G^{--}(X, \Lambda_{\mu\nu}(X) p^\nu), \quad (\text{C.15})$$

$$G^{++}(X, p) \rightarrow G^{++}(X, \Lambda_{\mu\nu}^{-1}(X) p^\nu),$$

$$V^-(q) \rightarrow V^-(\Lambda_{\mu\nu}(X) q^\nu), \quad (\text{C.16})$$

$$V^+(q) \rightarrow V^+(\Lambda_{\mu\nu}^{-1}(X) q^\nu)$$

for the entire Φ^{HFB} , while F and \tilde{F} are kept unchanged. For the Hartree–Fock part Φ^{HF} , one finds

$$\tilde{p}_\mu = \Lambda_{\mu\nu} p^\nu, \quad (\text{C.17})$$

$$= \int dX \xi_\mu(X) \partial^\mu \left(\Phi^{\text{HFB}}(X^-) - \Phi^{\text{HFB}}(X^+) \right),$$

where $\Phi^{\text{HFB}}(X^i)$ are understood in the sense of (C.2). Note that

$$\begin{aligned} &i \left(\Phi^{\text{HFB}}(X^-) - \Phi^{\text{HFB}}(X^+) \right) \quad (\text{C.12}) \\ &= i \text{tr} \int \frac{d^4 p}{(2\pi)^4} \Sigma^{\text{HF}} F + \frac{1}{2} i \text{Tr} \int \frac{d^4 p}{(2\pi)^4} \\ &\quad \times \left(\Gamma^{\text{in}} \text{Re} G^R + (\text{Re} \Sigma^R - \Sigma^{\text{HF}}) F \right) \\ &\quad - \underbrace{\text{tr} \int \frac{d^4 p}{(2\pi)^4} \left(\Gamma \text{Re} G^R + (\text{Re} \Sigma^R - \Sigma^{\text{HF}}) A \right)}_{=0}, \end{aligned}$$

where the last integral is again zero due to analyticity, similar to (C.8). Here, the first term on the right-hand side results from the first two (Hartree–Fock) diagrams in Eq. (C.1), while the last two integrals follow from the last two (Born) diagrams. Alternatively, we can perform variation of Φ^{Born} applying the canonical variation rules (3):

$$\tilde{p}'_\mu = \Lambda_{\mu\nu} p'^\nu \rightarrow d^4 p d^4 p' = (\det \Lambda)^{-2} d^4 \tilde{p} d^4 \tilde{p}',$$

$$\delta \Phi^{\text{HF}-} = \int dX [(\det \Lambda)^{-2} - 1] \Phi^{\text{HF}}(X^-), \quad (\text{C.18})$$

$$\delta \Phi^{\text{HF}+} = \int dX [(\det \Lambda)^2 - 1] \Phi^{\text{HF}}(X^+), \quad (\text{C.19})$$

where again $\Phi^{\text{HF}-}$ and $\Phi^{\text{HF}+}$ are the Φ^{HF} diagrams involving only “–” or “+” vertices, respectively. In general, an arbitrary diagram $\Phi^{n_G, n_\lambda(-)}$, consisting of n_G Green’s functions, n_λ of “–” interactions, and no “+” interactions, transforms as

$$\delta \Phi^{n_G, n_\lambda(-)} \quad (\text{C.20})$$

$$= \int dX \left[(\det \Lambda)^{-(n_G - n_\lambda + 1)} - 1 \right] \Phi^{n_G, n_\lambda(-)}(X),$$

since the change of each momentum integration gives $(\det \Lambda)^{-1}$ [cf. Eq. (C.17)], while the transformation of the $\delta(p)$ function at each vertex (apart from one vertex due to global momentum conservation of the

diagram) produces $\det \Lambda$:

$$\delta^4(p + p' - q) = \det \Lambda \delta^4(\tilde{p} + \tilde{p}' - \tilde{q}). \quad (\text{C.21})$$

Similarly,

$$\delta \Phi^{n_G, n_\lambda(+)} \quad (\text{C.22})$$

$$= \int dX [(\det \Lambda)^{n_G - n_\lambda + 1} - 1] \Phi^{n_G, n_\lambda(+)}(X).$$

According to these rules the “-” and “+” diagrams of the second order in the interaction, $\Phi^{\text{Born-}}$ and $\Phi^{\text{Born+}}$, are transformed as follows:

$$\delta \Phi^{\text{Born-}} = \int dX [(\det \Lambda)^{-3} - 1] \Phi^{\text{Born-}}(X), \quad (\text{C.23})$$

$$\delta \Phi^{\text{Born+}} = \int dX [(\det \Lambda)^3 - 1] \Phi^{\text{Born+}}(X). \quad (\text{C.24})$$

If the Λ transformation is infinitesimal, $\Lambda_{\mu\nu}(X) = 1 + \omega_{\mu\nu}(X)$ with $|\omega_{\mu\nu}| \ll 1$ and $\det \Lambda = 1 + \text{Tr}\omega$, $\det(\Lambda^{-1}) = 1 - \text{tr}\omega$, we obtain

$$\begin{aligned} & \delta \left(\Phi^{\text{HFB-}} + \Phi^{\text{HFB+}} \right) \quad (\text{C.25}) \\ &= - \int dX 2\text{tr}\omega \left(\Phi^{\text{HF-}}(X) - \Phi^{\text{HF+}}(X) \right) \\ & - \int dX 3\text{tr}\omega \left(\Phi^{\text{Born-}}(X) - \Phi^{\text{Born+}}(X) \right) \end{aligned}$$

[cf. Eq. (C.12)]. The $\Phi^{\text{Born-+}}$ and $\Phi^{\text{Born+-}}$ components, i.e., those containing both “-” and “+” vertices, are modified by only the V transformation. Moreover, this transformation leaves them invariant,

$$\begin{aligned} & i\delta \Phi^{\text{Born-+}} \quad (\text{C.26}) \\ &= \int dX \omega_{\mu\nu} \text{tr} \int \frac{d^4 p}{(2\pi)^4} p^\nu \left(\frac{\delta i \Phi^{\text{Born-+}}(X)}{\delta i V^-} \frac{\partial i V^-}{\partial p_\mu} \right. \\ & \quad \left. - \frac{\delta i \Phi^{\text{Born-+}}(X)}{\delta i V^+} \frac{\partial i V^+}{\partial p_\mu} \right) \\ &= \int dX \omega_{\mu\nu} \text{tr} \int \frac{d^4 p}{(2\pi)^4} p^\nu \left(\frac{\delta i \Phi^{\text{Born-+}}(X)}{\delta V^-} V^- \right. \\ & \quad \left. - \frac{\delta i \Phi^{\text{Born-+}}(X)}{\delta V^+} V^+ \right) \frac{1}{V} \frac{\partial V}{\partial p_\mu} = 0, \end{aligned}$$

since $\Phi^{\text{Born-+}}$ is symmetric with respect to V^- and V^+ . Thus,

$$\begin{aligned} & i\delta \Phi^{\text{HFB}} = - \int dX (\text{tr}\omega) i \text{tr} \int \frac{d^4 p}{(2\pi)^4} \quad (\text{C.27}) \\ & \times \left[2\Sigma^{\text{HF}} F - \frac{3}{2} \left(\Gamma^{\text{in}} \text{Re} G^R + (\text{Re} \Sigma^R - \Sigma^{\text{HF}}) F \right) \right]. \end{aligned}$$

Alternatively, we can perform variation of Φ^{HFB} applying the canonical variation rules (3):

$$\begin{aligned} & i\delta \Phi^{\text{HFB}} = \int dX \omega_{\mu\nu} \left[\text{tr} \int \frac{d^4 p}{(2\pi)^4} p^\nu \left(i\Sigma_{--} \frac{\partial i G^{--}}{\partial p_\mu} - i\Sigma_{++} \frac{\partial i G^{++}}{\partial p_\mu} \right) + 2i Q^{\mu\nu}(X) \right] \quad (\text{C.28}) \\ &= 2i \int dX \omega_{\mu\nu} \left[\text{tr} \int \frac{d^4 p}{(2\pi)^4} p^\nu \left(\Gamma^{\text{in}} \frac{\partial \text{Re} G^R}{\partial p_\mu} + \text{Re} \Sigma^R \frac{\partial F}{\partial p_\mu} \right) + Q^{\mu\nu}(X) \right] \\ & \quad - i \underbrace{\int dX \omega_{\mu\nu} \text{tr} \int \frac{d^4 p}{(2\pi)^4} p^\nu \left(\Gamma \frac{\partial \text{Re} G^R}{\partial p_\mu} + \text{Re} \Sigma^R \frac{\partial A}{\partial p_\mu} \right)}_{= 0}, \end{aligned}$$

where the last integral again equals zero due to analyticity. Here, we have introduced the quantity

$$\begin{aligned} & 2i Q^{\mu\nu}(X) = \text{tr} \int \frac{d^4 p}{(2\pi)^4} p^\nu \quad (\text{C.29}) \\ & \times \left(\frac{\delta i \Phi^{\text{HFB-}}(X)}{\delta i V^-} \frac{\partial i V^-}{\partial p_\mu} - \frac{\delta i \Phi^{\text{HFB+}}(X)}{\delta i V^+} \frac{\partial i V^+}{\partial p_\mu} \right) \end{aligned}$$

arising from variation over V . All we have to know about this quantity is that $Q^{\mu\nu} = 0$ when $\mu = 0$ and/or $\nu = 0$. This property results from p_0 indepen-

dence of $V(|\mathbf{p}|)$. In particular, this property yields

$$\int d^3 X \partial_\mu Q^{\mu\nu}(X) = 0, \quad (\text{C.30})$$

where the X integration runs only over space.

Hence, comparing Eq. (C.28) to Eq. (C.27), we arrive at another important identity:

$$\begin{aligned} & \text{tr} \int \frac{d^4 p}{(2\pi)^4} p^\nu \left(\Gamma^{\text{in}} \frac{\partial \text{Re} G^R}{\partial p_\mu} + \text{Re} \Sigma^R \frac{\partial F}{\partial p_\mu} \right) \quad (\text{C.31}) \\ & + Q^{\mu\nu}(X) = -g^{\mu\nu} \text{tr} \int \frac{d^4 p}{(2\pi)^4} \Sigma^{\text{HF}} F \end{aligned}$$

$$-g^{\mu\nu} \frac{3}{4} \text{tr} \int \frac{d^4 p}{(2\pi)^4} \left(\Gamma^{\text{in}} \text{Re} G^R + (\text{Re} \Sigma^R - \Sigma^{\text{HF}}) F \right).$$

We turn now to the right-hand side of the consistency relation for energy–momentum conservation (22)

$$K^\nu = \text{tr} \int d^3 X \frac{p^\nu d^4 p}{(2\pi)^4} [\{ \text{Re} \Sigma^R, F \} - \{ \text{Re} G^R, \Gamma^{\text{in}} \}] \quad (\text{C.32})$$

integrated over space, which is suitable for the global conservation. In this expression, the local collision term (C.3) drops out according to Eq. (16). It can be transformed by means of the identity

$$\int \frac{d^4 p}{(2\pi)^4} p^\nu \{ \varphi, f \} = \int \frac{d^4 p}{(2\pi)^4} \left[\partial^\mu \left(p^\nu f \frac{\partial \varphi}{\partial p^\mu} \right) + f \partial^\nu \varphi \right], \quad (\text{C.33})$$

where φ and f are arbitrary functions, with the result

$$K^\nu = -\text{tr} \int d^3 X \partial^\mu \int \frac{d^4 p}{(2\pi)^4} p^\nu \times \left(\text{Re} \Sigma^R \frac{\partial F}{\partial p^\mu} + \Gamma^{\text{in}} \frac{\partial \text{Re} G^R}{\partial p^\mu} \right) - \text{tr} \int d^3 X \frac{d^4 p}{(2\pi)^4} (\text{Re} \Sigma^R \partial^\nu F + \Gamma^{\text{in}} \partial^\nu \text{Re} G^R).$$

Now, applying identities (C.14), (C.30), and (C.31) to the right-hand side of Eq. (C.34), we obtain

$$K^\nu = \int d^3 X \partial_\mu g^{\mu\nu} \text{tr} \int \frac{d^4 p}{(2\pi)^4} \frac{1}{2} \times (\Gamma^{\text{in}} \text{Re} G^R + \text{Re} \Sigma^R F), \quad (\text{C.35})$$

which is precisely needed for the global conservation of the Noether energy–momentum

$$\frac{\partial}{\partial T} \int d^3 X \Theta^{0\nu}(X) = 0, \quad (\text{C.36})$$

since, for the case under consideration, $\mathcal{E}^{\text{int}} = \frac{1}{2} \mathcal{E}^{\text{pot}}$ [cf. Eq. (26)].

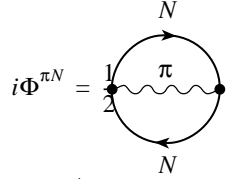
APPENDIX D

Nucleon–Pion System

For the discussion of the physical aspects of the nucleon–pion problem, we refer to [9]. Here, we would like to clarify some technical details. We choose the nonrelativistic form of pion–nucleon interaction [36]

$$\hat{\mathcal{L}}^{\text{int}} = g \hat{\psi}^\dagger [(\boldsymbol{\sigma} \cdot \nabla)(\boldsymbol{\tau} \cdot \hat{\phi})] \hat{\psi}, \quad (\text{D.1})$$

where $\hat{\psi}$ and $\hat{\phi}$ are nonrelativistic nucleon and Klein–Gordon pion field operators, respectively. Below, subscripts N or π correspondingly attribute a quantity to either nucleon or pion subsystems, respectively. We accept a simple approximation defined by the following Φ functional:

$$i\Phi^{\pi N} = \frac{1}{2} \text{tr} \int dX \frac{d^4 p_1}{(2\pi)^4} \frac{d^4 p_2}{(2\pi)^4} \frac{d^4 q}{(2\pi)^4} \times \delta^4(p_1 - p_2 + q) iG^{ij}(X, p_1) (-ig) (-i\mathbf{q} \cdot \boldsymbol{\sigma}) \tau \times i\Delta_{ij}(X, q) (-ig) (i\mathbf{q} \cdot \boldsymbol{\sigma}) \tau iG^{ji}(X, p_2), \quad (\text{D.2})$$


where G and Δ are the nucleon and pion Green's functions, respectively, and tr runs over spin and isospin indices. Here, we have assumed an isotopically symmetric system, where the pion Green's functions of all isotopic charges coincide. Though this approximation is evidently oversimplified to produce quantitative results (cf. [9]), it is able to reproduce qualitative features of the dynamics. Moreover, this approximation is at the edge of present computing abilities. The formal basics of the Φ -functional formalism are given in Appendix B.

The charge current, defined by Eqs. (20) and (B.11), relates to the baryon number conservation and hence is trivial from the point of view of the pion–nucleon interaction. Indeed, to prove the baryon number conservation, we should perform transformation (C.5) with F_N , \tilde{F}_N , and Δ^{ij} kept unchanged. The pion Green's functions Δ_{ij} are not subjected to this transformation, since pions are neutral from the point of view of baryonic charge. All the subsequent considerations are completely identical to that of the Fock diagram [the second term in Eq. (C.1)] and lead to the same final result (C.9), i.e., to the exact Noether current conservation.

The energy–momentum conservation is more instructive in this respect. Before proceeding to the conservation laws themselves, we should define the derivative contribution to the energy–momentum tensor (B.18). In our case of vanishing mean fields, the pion Green's function enters the Φ functional only doubly differentiated. Therefore, expression (B.18) takes the form

$$\mathcal{E}_{(\text{der})}^{\mu\nu} = \frac{1}{2} \int dz \left(\frac{\delta_0 \Phi}{\delta_0 (\partial_\lambda^\alpha \partial_\mu^\beta i\Delta(z, x))} \partial_\lambda^z \partial_x^\nu i\Delta(z, x) + \partial_\nu^x \partial_z^\lambda i\Delta(x, z) \frac{\delta_0 \Phi}{\delta_0 (\partial_\mu^\alpha \partial_\lambda^\beta i\Delta(x, z))} \right), \quad (\text{D.3})$$

where δ_0 is already the conventional variation. In the Wigner representation with due regard for Eq. (A.9), it transforms into

$$\begin{aligned} & \mathcal{E}_{(\text{der})}^{\mu\nu}(X) \tag{D.4} \\ &= -\text{tr} \int \frac{d^4 p_1}{(2\pi)^4} \frac{d^4 p_2}{(2\pi)^4} \frac{d^4 q}{(2\pi)^4} \delta^4(p_1 - p_2 + q) g^2 \\ & \quad \times [iG^{--}(X, p_1)(-q^\nu \sigma^\mu) \boldsymbol{\tau} i\Delta^{--}(X, q) \\ & \quad \times (i\mathbf{q} \cdot \boldsymbol{\sigma}) \boldsymbol{\tau} iG^{--}(X, p_2) - iG^{++}(X, p_1) \\ & \quad \times (-q^\nu \sigma^\mu) \boldsymbol{\tau} i\Delta^{++}(X, q)(i\mathbf{q} \cdot \boldsymbol{\sigma}) \boldsymbol{\tau} iG^{++}(X, p_2)]. \end{aligned}$$

Contrary to usual convention, here we use Greek indices μ and ν for the components of 3-vectors in order to distinguish them from the “+ -” summation indices. The potential energy density is still determined by the standard expression (25) but in terms of the sum over nucleons and pions. Within the approximation of Eq. (D.2), \mathcal{E}^{pot} can be alternatively expressed as

$$\mathcal{E}^{\text{pot}}(X) = \mathcal{E}_N^{\text{pot}} + \mathcal{E}_\pi^{\text{pot}} = \frac{3}{2}[\Phi^{\pi N-}(X) - \Phi^{\pi N+}(X)], \tag{D.5}$$

where $\Phi^{\pi N-}$ ($\Phi^{\pi N+}$) refers to the $\Phi^{\pi N}$ functional with removed integration over dX and all vertices being of “-” (“+”) type. In view of relation (26),

$$\mathcal{E}^{\text{int}}(X) - \mathcal{E}^{\text{pot}}(X) = -\frac{1}{2}[\Phi^{\pi N-}(X) - \Phi^{\pi N+}(X)]. \tag{D.6}$$

Energy–Momentum Conservation

We briefly repeat the steps proving the exact energy–momentum conservation for nonrelativistic nuclear matter (Appendix C) with the emphasis on the specifics of the derivative coupling.

First, the transformation of Eq. (C.10) for the nucleon Green’s functions together with the corresponding transformation of the pion Green’s functions

$$\begin{aligned} \Delta^{--}(X, p) &\rightarrow \Delta^{--}(X + \xi(X), p), \tag{D.7} \\ \Delta^{++}(X, p) &\rightarrow \Delta^{++}(X - \xi(X), p), \end{aligned}$$

with F_π and \tilde{F}_π being kept unchanged, has to be performed. This transformation is unaffected by the derivative coupling, and in a similar way as before, we arrive at the identity

$$\begin{aligned} & \text{tr} \int \frac{d^4 p}{(2\pi)^4} \left[\left(\Gamma_N^{\text{in}} \frac{\partial \text{Re}G^R}{\partial X_\mu} + \text{Re}\Sigma^R \frac{\partial F_N}{\partial X_\mu} \right) \tag{D.8} \right. \\ & \quad \left. + \frac{1}{2} \left(\Gamma_\pi^{\text{in}} \frac{\partial \text{Re}\Delta^R}{\partial X_\mu} + \text{Re}\Pi^R \frac{\partial F_\pi}{\partial X_\mu} \right) \right] \end{aligned}$$

$$= -\partial^\mu (\mathcal{E}^{\text{int}} - \mathcal{E}^{\text{pot}}).$$

Here, Σ and Π refer to nucleon and pion self-energies, respectively, and subscripts N or π correspondingly attribute a quantity to either nucleon or pion subsystems. The right-hand side of this identity is written with due regards to Eq. (D.6).

Let us now perform the transformation (C.15) for both nucleon and pion Green’s functions, as well as q factors encountered in vertices of $\Phi^{\pi N}$. Then, the variation of $\Phi^{\pi N}$ gives

$$\delta\Phi^{\pi N} = \int dX \omega_{\mu\nu} \tag{D.9}$$

$$\begin{aligned} & \times \left[-2g^{\mu\nu} (\Phi^{\pi N-}(X) - \Phi^{\pi N+}(X)) + 2\mathcal{E}_{(\text{der})}^{\mu\nu} \right] \\ &= \int dX \omega_{\mu\nu} \left[4g^{\mu\nu} (\mathcal{E}^{\text{int}} - \mathcal{E}^{\text{pot}}) + 2\mathcal{E}_{(\text{der})}^{\mu\nu} \right], \end{aligned}$$

where the $\mathcal{E}_{(\text{der})}^{\mu\nu}$ results from the variation of q factors in vertices of $\Phi^{\pi N}$. Alternatively, performing variation of $\Phi^{\pi N}$ according to the canonical variation rules (3) and equating the result to expression (D.9), we arrive at another identity,

$$\begin{aligned} & \text{tr} \int \frac{d^4 p}{(2\pi)^4} \left[\left(\Gamma_N^{\text{in}} \frac{\partial \text{Re}G^R}{\partial p_\mu} + \text{Re}\Sigma^R \frac{\partial F_N}{\partial p_\mu} \right) \tag{D.10} \right. \\ & \quad \left. + \frac{1}{2} \left(\Gamma_\pi^{\text{in}} \frac{\partial \text{Re}\Delta^R}{\partial p_\mu} + \text{Re}\Pi^R \frac{\partial F_\pi}{\partial p_\mu} \right) \right] \\ &= 2g^{\mu\nu} (\mathcal{E}^{\text{int}} - \mathcal{E}^{\text{pot}}) + \mathcal{E}_{(\text{der})}^{\mu\nu}. \end{aligned}$$

The right-hand side of the consistency relation for energy–momentum conservation (22) now reads

$$\begin{aligned} K^\nu &= \text{tr} \int \frac{p^\nu d^4 p}{(2\pi)^4} \left[(\{\text{Re}\Sigma^R, F_N\} \tag{D.11} \right. \\ & \quad \left. - \{\text{Re}G^R, \Gamma_N^{\text{in}}\}) + \frac{1}{2} (\{\text{Re}\Pi^R, F_\pi\} - \{\text{Re}\Delta^R, \Gamma_\pi^{\text{in}}\}) \right]. \end{aligned}$$

By means of identity (C.33), it is transformed to the form

$$\begin{aligned} K^\nu &= -\partial^\mu \text{tr} \int \frac{d^4 p}{(2\pi)^4} p^\nu \left[\left(\text{Re}\Sigma^R \frac{\partial F_N}{\partial p^\mu} \tag{D.12} \right. \right. \\ & \quad \left. \left. + \Gamma_N^{\text{in}} \frac{\partial \text{Re}G^R}{\partial p^\mu} \right) + \frac{1}{2} \left(\text{Re}\Pi^R \frac{\partial F_\pi}{\partial p^\mu} + \Gamma_\pi^{\text{in}} \frac{\partial \text{Re}\Delta^R}{\partial p^\mu} \right) \right] \\ & \quad - \text{tr} \int \frac{d^4 p}{(2\pi)^4} \left[(\text{Re}\Sigma^R \partial^\nu F_N + \Gamma_N^{\text{in}} \partial^\nu \text{Re}G^R) \right. \\ & \quad \left. + \frac{1}{2} (\text{Re}\Pi^R \partial^\nu F_\pi + \Gamma_\pi^{\text{in}} \partial^\nu \text{Re}\Delta^R) \right]. \end{aligned}$$

Now, applying identities (D.8) and (D.10) to the right-hand side of Eq. (D.12), we obtain

$$K^\nu = \partial^\nu (\mathcal{E}^{\text{pot}} - \mathcal{E}^{\text{int}}) - \partial_\mu \mathcal{E}_{(\text{der})}^{\mu\nu}, \tag{D.13}$$

which is precisely needed for the local conservation of the Noether energy–momentum.

REFERENCES

1. S. T. Belyaev and G. I. Budker, Dokl. Akad. Nauk SSSR **107**, 807 (1965).
2. J. Schwinger, J. Math. Phys. (N.Y.) **2**, 407 (1961).
3. L. P. Kadanoff and G. Baym, *Quantum Statistical Mechanics* (Benjamin, New York, 1962).
4. L. P. Keldysh, Zh. Éksp. Teor. Fiz. **47**, 1515 (1964) [Sov. Phys. JETP **20**, 1018 (1965)].
5. P. Danielewicz, Ann. Phys. (N.Y.) **152**, 305 (1984).
6. J. Knoll and D. N. Voskresensky, Phys. Lett. B **351**, 43 (1995); Ann. Phys. (N. Y.) **249**, 532 (1996).
7. P. Bozek, Phys. Rev. C **56**, 1452 (1997).
8. Yu. B. Ivanov, J. Knoll, and D. N. Voskresensky, Nucl. Phys. A **672**, 313 (2000).
9. Yu. B. Ivanov, J. Knoll, H. van Hees, and D. N. Voskresensky, Yad. Fiz. **64**, 711 (2001) [Phys. At. Nucl. **64**, 652 (2001)].
10. J. Knoll, Yu. B. Ivanov, and D. N. Voskresensky, Ann. Phys. (N.Y.) **293**, 126 (2001).
11. W. Cassing and S. Juchem, Nucl. Phys. A **665**, 377 (2000); Nucl. Phys. A **672**, 417 (2000).
12. S. Leupold, Nucl. Phys. A **672**, 475 (2000).
13. M. Effenberger and U. Mosel, Phys. Rev. C **60**, 51901 (1999).
14. P. Danielewicz, Ann. Phys. (N.Y.) **152**, 239 (1984).
15. W. Botermans and R. Malfliet, Phys. Rep. **198**, 115 (1990).
16. G. Baym, Phys. Rev. **127**, 1391 (1962).
17. Yu. B. Ivanov, J. Knoll, and D. N. Voskresensky, Nucl. Phys. A **657**, 413 (1999).
18. R. E. Norton and J. M. Cornwall, Ann. Phys. (N.Y.) **91**, 106 (1975).
19. G. M. Carneiro and C. J. Pethick, Phys. Rev. B **11**, 1106 (1975).
20. G. Aarts and J. Berges, Phys. Rev. D **64**, 105 010 (2001).
21. J. Berges, S. Borsanyi, and J. Serreau, hep-ph/0212404.
22. J. Berges and J. Serreau, hep-ph/0208070.
23. H. van Hees and J. Knoll, Phys. Rev. D **65**, 025 010 (2002).
24. H. van Hees and J. Knoll, Phys. Rev. D **65**, 105 005 (2002).
25. G. Baym and G. Grinstein, Phys. Rev. D **15**, 2897 (1977).
26. H. van Hees and J. Knoll, Phys. Rev. D **66**, 025 028 (2002).
27. A. Arrizabalaga and J. Smit, Phys. Rev. D **66**, 065 014 (2002).
28. C. Itzykson and J.-B. Zuber, *Quantum Field Theory* (McGraw-Hill, New York, 1980).
29. J. Belinfante, Physica **6**, 887 (1939).
30. C. G. Callan, S. Coleman, and R. Jackiw, Ann. Phys. (N.Y.) **59**, 42 (1970).
31. P. Bożek and P. Czerski, Eur. Phys. J. A **11**, 271 (2001); P. Bożek, Phys. Rev. C **59**, 2619 (1999); Nucl. Phys. A **657**, 187 (1999).
32. W. H. Dickhoff, Phys. Rev. C **58**, 2807 (1998); W. H. Dickhoff *et al.*, Phys. Rev. C **60**, 064 319 (1999).
33. Y. Dewulf, D. Van Neck, and M. Waroquier, Phys. Lett. B **510**, 89 (2001).
34. M. Baldo *et al.*, Phys. Rev. C **41**, 1748 (1990).
35. F. de Jong and R. Malfliet, Phys. Rev. C **44**, 998 (1991).
36. T. Ericson and W. Weise, *Pions and Nuclei* (Clarendon Press, Oxford, 1988); A. B. Migdal, E. E. Saperstein, M. A. Troitsky, and D. N. Voskresensky, Phys. Rep. **192**, 179 (1990).

Noncompact $u_q(2, 1)$ Quantum Algebra: Discrete Series of Highest Weight Irreducible Representations

Yu. F. Smirnov, Yu. I. Kharitonov^{†1)}, and R. M. Asherova²⁾

*Institute of Nuclear Physics,
Moscow State University, Vorob'evy gory, Moscow, 119899 Russia*

Received February 5, 2003

Abstract—The structure of unitary irreducible representations of the noncompact $u_q(2, 1)$ quantum algebra that are related to a negative discrete series is examined. With the aid of projection operators for the $su_q(2)$ subalgebra, a q analog of the Gelfand–Graev formulas is derived in the basis corresponding to the reduction $u_q(2, 1) \rightarrow su_q(2) \times u(1)$. Projection operators for the $su_q(1, 1)$ subalgebra are employed to study the same representations for the reduction $u_q(2, 1) \rightarrow u(1) \times su_q(1, 1)$. The matrix elements of the generators of the $u_q(2, 1)$ algebra are computed in this new basis. A general analytic expression for an element of the transformation brackets $\langle U|T \rangle_q$ between the bases associated with the above two reductions (the elements of this matrix are referred to as q Weyl coefficients) is obtained for a general case where the deformation parameter q is not equal to a root of unity. It is shown explicitly that, apart from a phase, the q Weyl coefficients coincide with the q Racah coefficients for the $su_q(2)$ quantum algebra.

© 2003 MAIK “Nauka/Interperiodica”.

1. INTRODUCTION

It is well known that group-theory methods are widely used in the theory of the nucleus. They form the basis of nuclear spectroscopy and of various nuclear models, including the shell model, models dealing with collective degrees of freedom, and the interacting-boson model. Since group-theory and algebraic models usually admit an analytic solution, they are employed to study various properties of nuclear systems—in particular, some of their asymptotic properties. For example, the popular Elliott model, based on $SU(3)$ symmetry, was successfully employed by Belyaev and his colleagues [1] to analyze the asymptotic properties of the generalized density matrix.

The discovery of quantum algebras and quantum groups that was made more than 20 years ago by mathematical physicists of the Leningrad school [2–4] gave new impetus to the development of algebraic methods in theoretical physics—in particular, to searches for applications of the representations of quantum groups and algebras in physics. For example, the construction of q analogs of various

nuclear models became a new field of research in theoretical nuclear physics. The point is that quantum algebras involve an additional variable parameter, the deformation parameter q . This renders models based on quantum algebras more adaptable and extends their potential in describing physical systems (see, for example, the study of Raychev *et al.* [5] and the review article of Bonatsos and Daskaloyannis [6], which is devoted to applications of quantum algebras in theoretical nuclear physics).

However, searches for physical applications of quantum algebras must be preceded by a detailed investigation of their irreducible representations. In this connection, the structure of unitary irreducible representations of the compact $u_q(3)$ quantum algebra was examined in detail in [7–16]. In our opinion, it is important to extend these results to the noncompact $u_q(2, 1)$ quantum algebra. The classical algebra $u(2, 1)$ describes the dynamical symmetry of a two-dimensional harmonic oscillator and of some other physical systems. In view of this, a comprehensive analysis of unitary irreducible representations of its quantum analog may be helpful in constructing respective physical models. In the present study, we restrict our consideration to the unitary irreducible representations associated with a negative discrete series.

Unitary irreducible representations of conventional (nondeformed) $u(n, m)$ algebras were studied by Gelfand and Graev [17] (see also [18]), who

[†]Deceased.

¹⁾Petersburg Nuclear Physics Institute, Russian Academy of Sciences, Gatchina, 188350 Russia.

²⁾Institute of Physics and Power Engineering, pl. Bondarenko 1, Obninsk, Kaluga oblast, 249020 Russia.

showed, among other things, that the unitary irreducible representations of the $u(2, 1)$ algebra can be divided into three discrete series. The series of highest weight unitary irreducible representations or a negative discrete series consists of representations such that each includes a highest weight vector $|H\rangle$ —that is, a vector annihilated by any raising generator of the algebra. A positive discrete series is the series of representations such that each includes a lowest weight vector $|L\rangle$ —that is, a vector annihilated by any lowering generator. There is yet another series, that which is referred to as an intermediate one and which is formed by unitary irreducible representations having neither a highest weight vector $|H\rangle$ nor a lowest weight vector $|L\rangle$. For this reason, this series deserves a dedicated consideration. Gelfand and Graev [17] presented the explicit expressions for the matrix elements associated with the above representations—that is, the matrix elements of the generators A_{ik} of the $u(n, m)$ algebra in the basis corresponding to the following reduction of this algebra to a chain of subalgebras:

$$u(n, m) \rightarrow u(n, m - 1) \rightarrow \dots \rightarrow u(n) \quad (1) \\ \rightarrow \dots \rightarrow u(2) \rightarrow u(1), n \geq m.$$

However, those authors did not give a regular procedure for deriving the expressions that they quoted in [17]. For the $u(n, 1)$ algebras, these formulas were derived in [19–21], but there is still no derivation of such formulas for the general case of the $u(n, m)$ algebras.

In this study, we extend, to the case of the $u_q(2, 1)$ quantum algebra, the approach proposed by Vilenkin in [22] for the case of the $u(2, 1)$ classical algebra and examine the structure of its unitary irreducible representations associated with the negative series. The results obtained in this way are readily generalized to the case of the positive discrete series. The intermediate discrete series of unitary irreducible representations will be considered in a separate publication. As in [7–16], we assume that the deformation parameter q is specified by an arbitrary positive number and define q numbers and q factorials as follows:

$$[n] = \frac{q^n - q^{-n}}{q - q^{-1}}, \quad (2)$$

$$[n]! = [n][n - 1] \dots [2][1], \quad [0]! = 1. \quad (3)$$

Below, we employ brackets to denote q numbers, enclose the signatures of unitary irreducible representations in Dirac brackets, and reserve parentheses for the weight of a vector—for example, the symbol $|\langle f_1 f_2 f_3 \rangle(m_1 m_2 m_3)\rangle$ stands for a basis vector of weight $(m_1 m_2 m_3)$ in the unitary irreducible representation $D^{\langle f_1 f_2 f_3 \rangle} = D^{\langle f \rangle}$.

2. DISCRETE SERIES OF HIGHEST WEIGHT UNITARY IRREDUCIBLE REPRESENTATIONS

The $u(2, 1)$ algebra is known to involve nine generators A_{ik} ($i, k = 1, 2, 3$) satisfying the same commutation relations as the corresponding generators of the compact $u(3)$ classical Lie algebra. However, properties of the $u(2, 1)$ generators under Hermitian conjugation differ from those of the $u(3)$ generators. The “compact” generators A_{11} , A_{22} , A_{33} , A_{12} , and A_{21} of the $u(2, 1)$ algebra have the same Hermitian properties as the $u(3)$ generators,

$$A_{ik}^+ = A_{ki}, \quad (4)$$

whereas the “noncompact” generators A_{13} , A_{23} , A_{31} , and A_{32} satisfy the relations

$$A_{13}^+ = -A_{31}, \quad (5)$$

$$A_{23}^+ = -A_{32}. \quad (6)$$

The minus sign in formulas (5) and (6) generates a fundamental distinction between the structure of any unitary irreducible representation of the $u(2, 1)$ algebra and the structure of the corresponding unitary irreducible representation of the $u(3)$ algebra: all unitary irreducible representations of the compact $u(3)$ algebra are finite-dimensional, whereas all unitary irreducible representations of the noncompact $u(2, 1)$ algebra (with the exception of the trivial identity representation) are infinite-dimensional.

The noncompact $u_q(2, 1)$ quantum algebra is also specified by nine generators A_{ik} ($i, k = 1, 2, 3$) satisfying the same commutation relations as the generators of the $u_q(3)$ compact quantum algebra. The explicit expressions for these generators can be found in [7]. As to their properties with respect to Hermitian conjugation, those in (4) and (6) remain valid, whereas, in view of the relations

$$A_{13}^+ = \tilde{A}_{31} = A_{32}A_{21} - qA_{21}A_{32} \neq A_{31}, \quad (7)$$

$$A_{31}^+ = \tilde{A}_{13} = A_{12}A_{23} - q^{-1}A_{23}A_{12} \neq A_{13} \quad (8)$$

for the $u_q(3)$ algebra, that in (5) must be replaced by

$$A_{13}^+ = -\tilde{A}_{31}. \quad (9)$$

With the aid of (7) and (8), this relation can be recast into either of the following two equivalent forms:

$$A_{13}^+ = -A_{31} + (q - q^{-1})A_{21}A_{12} \quad (10)$$

or

$$A_{13}^+ = -q^2 A_{31} - (1 - q^2)A_{32}A_{21}. \quad (11)$$

For the $u_q(2, 1)$ algebra, we will consider the unitary irreducible representation $D^{\langle f \rangle}$ of highest weight

$(f) = (f_1 f_2 f_3)$; that is, we assume that, in the space of this representation, there is a highest weight vector $|H\rangle$ that satisfies the relations

$$A_{ii}|H\rangle = f_i|H\rangle \quad (i = 1, 2, 3); \quad (12)$$

which annihilated by any raising operator A_{ik} ,

$$A_{ik}|H\rangle = 0 \quad (i < k); \quad (13)$$

and which is normalized to unity,

$$\langle H|H\rangle = 1. \quad (14)$$

All other basis vectors $|X\rangle$ of this unitary irreducible representation can be derived by applying the lowering operators A_{21} , A_{31} , and A_{32} to $|H\rangle$,

$$|X\rangle = A_{21}^g A_{31}^k A_{32}^\ell |H\rangle. \quad (15)$$

In order to construct a basis of any unitary irreducible representation of the $u_q(2, 1)$ algebra, it is necessary to specify a chain of subalgebras, and this can be done, as is well known, in three ways. The first way is to use the U -spin subalgebra involving the generators A_{11} , A_{12} , A_{21} , and A_{22} , in which case the respective reduction is

$$u_q(2, 1) \rightarrow u_q(2) \rightarrow u_q(1). \quad (16)$$

One can also use the generators A_{22} , A_{23} , A_{32} , and A_{33} forming the basis of the T -spin subalgebra or the generators A_{11} , A_{13} , A_{31} , and A_{33} generating the V -spin subalgebra. Either of these two subalgebras corresponds to the reduction

$$u_q(2, 1) \rightarrow u_q(1, 1) \rightarrow u_q(1). \quad (17)$$

In this study, we restrict our consideration to the case of U - and T -spin bases.

3. BASIS VECTORS AND THE MATRIX ELEMENTS OF THE GENERATORS IN THE BASIS ASSOCIATED WITH U -SPIN REDUCTION

First, we consider that the generators A_{11} , A_{12} , A_{21} , and A_{22} form a basis of the U -spin algebra, which is a compact subalgebra of the noncompact $u_q(2, 1)$ algebra, the generators

$$U_+ = A_{12}, \quad U_- = A_{21}, \quad U_0 = \frac{1}{2}(A_{11} - A_{22}) \quad (18)$$

generating the compact simple $su_q(2)$ subalgebra.

In the case of U -spin reduction, the basis of an unitary irreducible representation of the $u_q(2, 1)$ algebra can be derived in the same way as the basis of the $u_q(3)$ algebra [11]; that is,

$$|\langle f \rangle m_3 U M_U \rangle_q = \frac{1}{N(k\ell)N(U M_U)} A_{21}^{U-M_U} \quad (19)$$

$$\times P^U A_{31}^k A_{32}^\ell |H\rangle,$$

where

$$m_3 = f_3 + k + \ell; \quad (20)$$

$$U = \frac{1}{2}(f_1 - f_2 - k + \ell); \quad (21)$$

$$M_U = \frac{1}{2}(m_1 - m_2), \quad -U \leq M_U \leq U; \quad (22)$$

$$P^U = \sum_{r=0}^{\infty} (-1)^r \frac{[2U+1]!}{[r]![2U+r+1]!} A_{21}^r A_{12} \quad (23)$$

is the projection operator for the $su_q(2)$ algebra [23];

$$N(U M_U) = \sqrt{\frac{[2U]![U-M_U]!}{[U+M_U]!}}; \quad (24)$$

$N(k\ell)$ are normalization factors; and

$$|H\rangle = |\langle f \rangle f_3 U_H U_H \rangle, \quad U_H = \frac{1}{2}(f_1 - f_2) \quad (25)$$

is a highest weight vector. The main distinction between the $u_q(2, 1)$ and $u_q(3)$ algebras lies in the normalization factor $N(k\ell)$. In the Appendix, it is shown that, in the latter case, the square of the normalization factor has the form

$$N^2(k\ell) = \frac{[k]![\ell]![f_3 - f_1 + k - 2]!}{[f_3 - f_2 - 1]![f_3 - f_1 - 2]!} \times \frac{[f_3 - f_2 + \ell - 1]![f_1 - f_2]![f_1 - f_2 - k + \ell + 1]!}{[f_1 - f_2 - k]![f_1 - f_2 + \ell + 1]!}. \quad (26)$$

Here, we impose the conventional requirement that the arguments of all q factorials be nonnegative integers. This requirement ensures that the square of the norm of a basis vector is positive. It also follows that a nonzero vector exists only under the conditions

$$f_1 \geq f_2, \quad (27)$$

$$f_3 - f_1 - 2 \geq 0,$$

$$0 \leq k \leq f_1 - f_2.$$

At the same time, no condition is imposed on the exponent ℓ ($\ell = 0, 1, 2, \dots$), with the result that, in the case of a U basis, a unitary irreducible representation of the $u_q(2, 1)$ algebra is infinite-dimensional.

In [17], each basis vector of a highest weight unitary irreducible representation was characterized by the scheme

$$\left| \begin{array}{ccc} m_{13} & m_{23} & m_{33} \\ & m_{12} & m_{22} \\ & & m_{11} \end{array} \right\rangle, \quad (28)$$

where the integers m_{ij} satisfy the conditions

$$m_{13} \geq m_{23} \geq m_{33} \geq 0, \quad (29)$$

$$m_{23} - 1 \geq m_{12} \geq m_{33} - 1, \quad (30)$$

$$m_{22} \leq m_{33} - 1. \quad (31)$$

The numbers in the first row in (28) specify unitary irreducible representations of the $u_q(2, 1)$ algebra. They are related to the components of the highest weight vector by the equations

$$f_1 = m_{23} - 1, \quad (32)$$

$$f_2 = m_{33} - 1, \quad (33)$$

$$f_3 = m_{13} + 2. \quad (34)$$

The numbers in the second row in (28) represent the signature of a unitary irreducible representation of the $u_q(2)$ subalgebra. In our notation,

$$m_{12} = f_1 - k, \quad (35)$$

$$m_{22} = f_2 - \ell. \quad (36)$$

The number in the third row is

$$m_{11} = U + M_U + m_{22}. \quad (37)$$

From the condition $f_1 \geq f_2$, it follows that

$$m_{23} \geq m_{33}. \quad (38)$$

The condition $f_3 - f_1 - 2 \geq 0$ means that

$$m_{13} \geq m_{23} - 1. \quad (39)$$

Combining these conditions, we obtain

$$m_{13} + 1 \geq m_{23} \geq m_{33}. \quad (40)$$

At the same time, the condition $0 \leq k \leq f_1 - f_2$ is equivalent to the constraints

$$m_{23} - 1 \geq m_{12} \geq m_{33} - 1. \quad (41)$$

With regard for the allowed values of the exponent ℓ , $\ell = 0, 1, 2, \dots$, we derive

$$m_{22} \leq m_{33} - 1. \quad (42)$$

The condition $-U \leq M_U \leq U$ leads to the constraints

$$m_{12} \geq m_{11} \geq m_{22}. \quad (43)$$

A comparison of formulas (39)–(42) with (29)–(31) demonstrates that our constraints on the structure of the basis vectors are identical to the constraints on the values of m_{ij} in the Gelfand–Graev scheme, with the only exception that, in our case, there exists a unitary irreducible representation for which $m_{13} = m_{23} - 1$. This means that there are unitary irreducible representations corresponding to the Gelfand–Graev signature,

$$\{m_{13}m_{23}m_{33}\} = \{m_{23} - 1, m_{23}m_{33}\}, \quad (44)$$

which are beyond the standard constraints (29). The existence of such nonstandard discrete series of unitary irreducible representations of the $u(2, 1)$ algebra was indicated in [20, 21]. The $u_q(2, 1)$ quantum algebra has analogous special series of unitary irreducible representations.

Further, it should be noted that, at $f_1 = f_2$, in which case $k = 0$, the condition that the norm $N^2(0\ell)$ is positive requires fulfillment of the inequality

$$f_3 - f_2 - 1 + \ell > 0 \quad (45)$$

for all values of ℓ , including $\ell = 0$ and $\ell = 1$. As a consequence, the highest weights corresponding to $f_3 - f_2 > 0$ and $f_3 - f_2 > 1$ are allowed at $f_1 = f_2$ (that is, at $m_{23} = m_{33}$). Therefore, there are two more nonstandard series of highest weight unitary irreducible representations such that condition (29) is violated for them. These are those that are characterized by the Gelfand–Graev signatures $\{m_{23} - 1, m_{23}m_{23}\}$ and $\{m_{23} - 2, m_{23}m_{23}\}$. The former can be treated as a particular case of the series in (44), whereas the series whose signature is

$$\{m_{23} - 2, m_{23}m_{23}\} \quad (46)$$

provides yet another nonstandard discrete series of highest weight unitary irreducible representations of the $u_q(2, 1)$ algebra.

Let us now consider the matrix elements of the generators in the U basis. In the basis specified by (19), the weight generators A_{ii} ($i = 1, 2, 3$) naturally have a diagonal form, their matrix elements being given by

$$m_1 = f_1 - k - (U - M_U), \quad (47)$$

$$m_2 = f_2 - \ell + (U - M_U), \quad (48)$$

$$m_3 = f_3 + k + \ell, \quad (49)$$

where

$$m_1 + m_2 + m_3 = f_1 + f_2 + f_3. \quad (50)$$

The action of the generators $A_{12} = U_+$ and $A_{21} = U_-$ is well known from the theory of angular momenta:

$$U_{\pm}|\langle f \rangle m_3 U M_U \rangle_q = \sqrt{[U \mp M_U][U \pm M_U + 1]}|\langle f \rangle m_3 U M_U \pm 1 \rangle_q. \quad (51)$$

The matrix elements of the remaining four nondiagonal generators are presented in Table 1; their derivation is given in [24].

Table 1. Matrix elements of the generators of the noncompact $u_q(2, 1)$ quantum algebra for the unitary irreducible representation $D^{\{f\}-}$ associated with the negative discrete series (U basis used here was derived from the highest weight vector $|H\rangle$)

$a_{13} \left(m_3 - 1, U + \frac{1}{2}, M_U + \frac{1}{2} \right)$	$= -q^{-U+M_U} \left[\frac{[k][f_3 - f_1 + k - 2][2U - \ell + 1][U + M_U + 1]}{[2U + 1][2U + 2]} \right]^{1/2}$
$a_{23} \left(m_3 - 1, U + \frac{1}{2}, M_U - \frac{1}{2} \right)$	$= - \left[\frac{[k][f_3 - f_1 + k - 2][2U - \ell + 1][U - M_U + 1]}{[2U + 1][2U + 2]} \right]^{1/2}$
$a_{13} \left(m_3 - 1, U - \frac{1}{2}, M_U + \frac{1}{2} \right)$	$= q^{U+M_U+1} \left[\frac{[\ell][f_3 - f_2 + \ell - 1][2U + k + 1][U - M_U]}{[2U][2U + 1]} \right]^{1/2}$
$a_{23} \left(m_3 - 1, U - \frac{1}{2}, M_U - \frac{1}{2} \right)$	$= - \left[\frac{[\ell][f_3 - f_2 + \ell - 1][2U + k + 1][U + M_U]}{[2U][2U + 1]} \right]^{1/2}$
$a_{31} \left(m_3 + 1, U - \frac{1}{2}, M_U - \frac{1}{2} \right)$	$= q^{U-M_U} \left[\frac{[k + 1][f_3 - f_1 + k - 1][2U - \ell][U + M_U]}{[2U][2U + 1]} \right]^{1/2}$
$a_{32} \left(m_3 + 1, U - \frac{1}{2}, M_U + \frac{1}{2} \right)$	$= \left[\frac{[k + 1][f_3 - f_1 + k - 1][2U - \ell][U - M_U]}{[2U][2U + 1]} \right]^{1/2}$
$a_{31} \left(m_3 + 1, U + \frac{1}{2}, M_U - \frac{1}{2} \right)$	$= -q^{-U-M_U-1} \left[\frac{[\ell + 1][f_3 - f_2 + \ell][2U + k + 2][U - M_U + 1]}{[2U + 1][2U + 2]} \right]^{1/2}$
$a_{32} \left(m_3 + 1, U + \frac{1}{2}, M_U + \frac{1}{2} \right)$	$= \left[\frac{[\ell + 1][f_3 - f_2 + \ell][2U + k + 2][U + M_U + 1]}{[2U + 1][2U + 2]} \right]^{1/2}$

4. BASIS VECTORS AND MATRIX ELEMENTS OF THE GENERATORS IN THE BASIS ASSOCIATED WITH T -SPIN REDUCTION

Let us consider the structure of the unitary irreducible representation $D^{(f)}$ of highest weight $(f_1 f_2 f_3)$ in the case of the reduction

$$u_q(2, 1) \rightarrow u_q(1, 1) \tag{52}$$

of the $u_q(2, 1)$ algebra to the $u_q(1, 1)$ subalgebra specified by the generators $A_{22}, A_{23}, A_{32},$ and A_{33} or to the $su_q(2)$ subalgebra of a noncompact T spin, the generators in the latter case being

$$T_+ = A_{23}, \quad T_- = A_{32}, \quad T_0 = \frac{1}{2}(A_{22} - A_{33}). \tag{53}$$

We note that condition (1) imposed in [17] on a chain of subalgebras is not satisfied in formulas (52). For this reason, the results obtained in [17] are not valid in the case of the T -spin basis even for the classical $u(2, 1)$ algebra, not to mention its deformation $u_q(2, 1)$.

Before proceeding to discuss the $u_q(2, 1)$ algebra as a whole, it is reasonable to recall general information about the $su_q(1, 1)$ subalgebra and its unitary irreducible representations. The generators of the $su_q(1, 1)$ subalgebra satisfy the well-known commutation relations

$$[T_0, T_+] = T_+, \tag{54}$$

$$[T_0, T_-] = -T_-, \tag{55}$$

$$[T_+, T_-] = [2T_0]. \tag{56}$$

Under Hermitian conjugation, they transform as follows:

$$T_0^+ = T_0, \tag{57}$$

$$T_+^+ = -T_-. \tag{58}$$

The unitary irreducible representations D^T of the negative discrete series are infinite-dimensional; the respective T -spin basis is given by

$$T = -\frac{1}{2}, 0, \frac{1}{2}, 1, \frac{3}{2}, 2, \dots \tag{59}$$

The T -spin projection M (or the weight of a vector), which is an eigenvalue of the operator of the T -spin projection T_0 , takes the negative values

$$M = -T - 1, -T - 2, \dots, \tag{60}$$

the highest weight being $-T - 1$. We assume that the highest weight vector

$$|H\rangle = |T, -T - 1\rangle \tag{61}$$

is known and that it satisfies the requirements

$$T_+|H\rangle = 0, \tag{62}$$

$$T_0|H\rangle = (-T - 1)|H\rangle, \tag{63}$$

and the normalization condition $\langle H|H\rangle = 1$.

The basis vectors of a lower weight can be obtained from the highest weight vector by the formula

$$|TM\rangle = \frac{1}{N(TM)} T_-^{-T-M-1} |H\rangle. \tag{64}$$

The square of the norm of a vector that is derived in this way has the form ($x = -T - M - 1$)

$$\begin{aligned} N^2(TM) &= (-1)^x \langle H | A_{23}^x A_{32}^x | H \rangle \tag{65} \\ &= [x][2T + x + 1] N^2(T, M + 1) \\ &= \frac{[-T - M - 1][T - M]!}{[2T + 1]!}. \end{aligned}$$

It can be seen that the condition $N^2(TM) > 0$ imposes no constraints on $x = 0, 1, 2, \dots$; therefore, this unitary irreducible representation is infinite-dimensional. Nonzero matrix elements of the generators in the basis specified by (64) are given by

$$\langle TM | T_0 | TM \rangle = M, \tag{66}$$

$$\begin{aligned} \langle TM + 1 | T_+ | TM \rangle \tag{67} \\ = -\{[-T - M - 1][T - M]\}^{1/2}, \end{aligned}$$

$$\langle TM - 1 | T_- | TM \rangle = \{[-T - M][T - M + 1]\}^{1/2}. \tag{68}$$

The Casimir operator for the $su_q(1, 1)$ algebra has the same form as for the $su_q(2)$ algebra:

$$C_2(su_q(1, 1)) = T_- T_+ + [T_0 + 1/2]^2. \tag{69}$$

All vectors in (64) are the eigenvectors of this operator and correspond to the same eigenvalue:

$$C_2(su_q(1, 1)) | TM \rangle = [T + 1/2]^2 | TM \rangle. \tag{70}$$

We also need the extremal projection operator $P^T = P_{-T-1, -T-1}^T$ for the discrete series of the highest weight unitary irreducible representation. As in the case of the $su_q(2)$ algebra, we will seek the expression for the extremal projection operator in the form of a series:

$$P^T = \sum_{r=0} C_r T_-^r T_+^r. \tag{71}$$

In what follows, we apply this projection operator only to those vectors $|-T - 1\rangle$ that have a specific weight $(-T - 1)$, but which, in general, do not have a specific value of the T spin—that is, to vectors that are represented by linear combinations of the form

$$|-T - 1\rangle = \sum_{T'} |T', -T - 1\rangle. \tag{72}$$

In contrast to the case of $su_q(2)$ algebra, however, the sum over T' is finite in the case under study, because the inequality $T' \leq |M'| - 1$ must hold for the basis

vectors $|T'M'\rangle$ of the negative discrete series. In the case of (72), this means that $T' \leq T$. Hence, the variable T' in the sum in (72) runs through the values from $T_{\min} = -1/2$ or 0 to T , depending on whether T is an integer or a half-integer. By applying the operator in (71) to the vectors in (72), one can show that only a finite number of terms in (71) make a nonvanishing contribution—namely, those that satisfy the inequality $-T - 1 + r \leq -1$ or $-1/2$ (that is, $r \leq T$ or $T + 1/2$). Hence, the terms in (71) that involve higher powers of r can be disregarded.

The projection operator P^T satisfies the equations

$$T_+ P^T = 0, \tag{73}$$

$$P^T |T, -T - 1\rangle = |T, -T - 1\rangle. \tag{74}$$

From (73), it follows that the coefficients C_r satisfy the recursion relation

$$C_{r-1} + [r][-2T + r - 1]C_r = 0. \tag{75}$$

From this relation, we obtain

$$C_r = C_0 \frac{[2T - r]!}{[r]![2T]!}, \quad r \leq 2T. \tag{76}$$

From the condition (74), it follows that

$$C_0 = 1. \tag{77}$$

At $r = 2T + 1$, relation (75) is meaningless, but we have shown above that we do not need the coefficients C_r for $r > T$ or $T + 1/2$. Thus, it is sufficient, for our purposes, to use the simple projection operator

$$P^T = \sum_{r=0}^{r=2T} \frac{[2T - r]!}{[r]![2T]!} T_-^r T_+^r. \tag{78}$$

A projection operator of a more general form can be represented as

$$P_{MM'}^T = \frac{(-1)^{-T-M'-1}}{N(TM)N(TM')} T_-^{-T-M-1} P^T T_+^{-T-M'-1}. \tag{79}$$

As a matter of fact, Vilenkin [22] used similar projection operators (of course, only for $q = 1$) long ago to derive the harmonic projections of polynomials depending on n Cartesian variables.

Let us present yet another relation helpful for subsequent computations:

$$\begin{aligned} &P_{-T-1, M}^T P_{M, -T-1}^T \tag{80} \\ &= \frac{(-1)^{-T-M-1}}{N^2(TM)} P^T T_+^{-T-M-1} T_-^{-T-M-1} P^T = P^T. \end{aligned}$$

From this equation, it follows that

$$P^T T_+^{-T-M-1} T_-^{-T-M-1} P^T \tag{81}$$

Table 2. Matrix elements of the generators of the noncompact $u_q(2, 1)$ quantum algebra for the unitary irreducible representation $D^{\{f\}}$ of the negative discrete series (T -spin basis used was constructed with the aid of the highest weight vector $|H\rangle$)

$a_{12} \left(m_1 + 1, T + \frac{1}{2}, M - \frac{1}{2} \right)$	$= \left[\frac{[p][f_1 - f_2 - p + 1][2T - s + 1][T - M + 1]}{[2T + 1][2T + 2]} \right]^{1/2}$
$a_{13} \left(m_1 + 1, T + \frac{1}{2}, M + \frac{1}{2} \right)$	$= q^{T-M+1} \left[\frac{[p][f_1 - f_2 - p + 1][2T - s + 1][-T - M - 1]}{[2T + 1][2T + 2]} \right]^{1/2}$
$a_{12} \left(m_1 + 1, T - \frac{1}{2}, M - \frac{1}{2} \right)$	$= - \left[\frac{[s][f_3 - f_1 + s - 2][2T + p + 1][-T - M]}{[2T][2T + 1]} \right]^{1/2}$
$a_{13} \left(m_1 + 1, T - \frac{1}{2}, M + \frac{1}{2} \right)$	$= -q^{-T-M} \left[\frac{[s][f_3 - f_2 + s - 2][2T + p + 1][T - M]}{[2T][2T + 1]} \right]^{1/2}$
$a_{21} \left(m_1 - 1, T - \frac{1}{2}, M + \frac{1}{2} \right)$	$= \left[\frac{[p + 1][f_1 - f_2 - p][2T - s][T - M]}{[2T][2T + 1]} \right]^{1/2}$
$a_{31} \left(m_1 - 1, T - \frac{1}{2}, M - \frac{1}{2} \right)$	$= q^{-T+M-1} \left[\frac{[p + 1][f_1 - f_2 - p][2T - s][-T - M]}{[2T][2T + 1]} \right]^{1/2}$
$a_{21} \left(m_1 - 1, T + \frac{1}{2}, M + \frac{1}{2} \right)$	$= - \left[\frac{[s + 1][f_3 - f_1 + s - 1][2T + p + 2][-T - M - 1]}{[2T + 1][2T + 2]} \right]^{1/2}$
$a_{31} \left(m_1 - 1, T + \frac{1}{2}, M - \frac{1}{2} \right)$	$= q^{T+M} \left[\frac{[s + 1][f_3 - f_1 + s - 1][2T + p + 2][T - M + 1]}{[2T + 1][2T + 2]} \right]^{1/2}$

$$= (-1)^{-T-M-1} N^2(TM) P^T.$$

We now return to a consideration of the highest weight unitary irreducible representations of the $u_q(2, 1)$ algebra. As in the case of the $u_q(3)$ algebra, the basis vectors of the unitary irreducible representation $D^{\{f\}}$ of the $u_q(2, 1)$ algebra that correspond to the highest weight $(f) = (f_1 f_2 f_3)$ will be represented in the form

$$|\{f\} m_1 T M_T \rangle_q \tag{82}$$

$$= \frac{1}{N(sp)N(TM_T)} A_{32}^{-T-M_T-1} P^T A_{31}^s A_{21}^p |H\rangle,$$

where

$$T = \frac{1}{2}(f_3 - f_2 - p + s - 2), \tag{83}$$

$$-T - 1 = \frac{1}{2}(f_2 - f_3 + p - s). \tag{84}$$

The normalization factor $N(TM_T)$ is determined by formula (65), while the projection operator P^T is given by (78). The normalization factor $N(sp)$ for the vectors of the T -spin basis is calculated by a method similar to that used for the norm of the vectors of the U -spin basis and described in the Appendix (see also [24]). The square of this norm is

$$N^2(sp) = \frac{1}{q^{2s}} \frac{[s]![p]![f_1 - f_2]![f_3 - f_1 + s - 2]!}{[f_1 - f_2 - p]![f_3 - f_1 - 2]!} \tag{85}$$

$$\times \frac{[f_3 - f_2 + s - 1]![f_3 - f_2 - p - 2]!}{[f_3 - f_2 - 1]![f_3 - f_2 - p + s - 2]!}.$$

From the analysis of the norm of the basis vectors, we derive the conditions

$$f_1 \geq f_2, \tag{86}$$

$$f_3 - f_1 - 2 \geq 0, \tag{87}$$

$$0 \leq p \leq f_1 - f_2. \tag{88}$$

There are no constraints on the exponent s ; that is, $s = 0, 1, 2, \dots$. Since the number of values of the projection M_T is infinite, this means that the representations under study are infinite-dimensional. The constraints in (86) and (87) on the signature of unitary irreducible representations are identical to those obtained for the U -spin basis. For this reason, the classification of the standard and nonstandard discrete series for the T -spin basis remains unchanged, as might have been expected.

Let us now proceed to discuss the matrix elements of the generators. For the weight generators A_{ii} in the T -spin basis, only diagonal matrix elements do not vanish. They are given by

$$m_1 = f_1 - p - s, \tag{89}$$

$$m_2 = f_2 + p + (T + M_T + 1), \tag{90}$$

$$m_3 = f_3 + s - (T + M_T + 1). \tag{91}$$

The matrix elements of the generators $A_{23} = T_+$ and $A_{32} = T_-$ can be determined by formulas (67) and (68).

The matrix elements of the remaining four non-diagonal generators are presented in Table 2 (the derivation of these expressions is given in [24]).

5. WEYL COEFFICIENT $\langle U|T \rangle_q$
FOR THE NEGATIVE DISCRETE SERIES
OF UNITARY IRREDUCIBLE
REPRESENTATIONS OF THE $u_q(2, 1)$
QUANTUM ALGEBRA

By definition, the Weyl coefficient $\langle U|T \rangle_q$ for an irreducible representation $\{f\}$ of the $u_q(2, 1)$ quantum algebra has the form

$$\langle U|T \rangle_q = {}_q \langle \{f\} m_3 U M_U | \{f\} m_1 T M_T \rangle_q \quad (92)$$

$$= \frac{(-1)^{k+\ell}}{N(k\ell)N(UM_U)N(sp)N(TM_T)}$$

$$\times {}_q \langle H | A_{23}^\ell A_{13}^k P^U A_{12}^a A_{32}^b P^T A_{31}^s A_{21}^p | H \rangle_q,$$

where $|H\rangle$ is the highest weight vector of the irreducible representation $\{f\}$;

$$a = U - M_U; \quad b = -T - M_T - 1; \quad (93)$$

and the normalization factors $N(k\ell)$, $N(UM_U)$, $N(sp)$, and $N(TM_T)$ and the projection operators P^U and P^T were defined in the foregoing. Since the weight on the left-hand side of Eq. (92) for the matrix element is equal to the weight on the right-hand side, we conclude that the parameters k and ℓ are related to s and p by the equations

$$U - M_U = p + s - k, \quad (94)$$

$$-T - M_T - 1 = \ell + k - s. \quad (95)$$

The computation of the above matrix element is performed by making use of the commutation relations

between the generators raised to a power. The scheme of the computations is identical to that in the case of the $u_q(3)$ algebra [25]. Taking into account the explicit form of the projection operator P^U , we arrive at

$$B \equiv {}_q \langle H | A_{23}^\ell A_{13}^k P^U A_{12}^a A_{32}^b P^T A_{31}^s A_{21}^p | H \rangle_q \quad (96)$$

$$= \sum_r (-1)^r \frac{[2U + 1]!}{[r]![2U + r + 1]!}$$

$$\times {}_q \langle H | A_{23}^\ell A_{13}^k A_{21}^r A_{12}^{r+a} A_{32}^b P^T A_{31}^s A_{21}^p | H \rangle_q.$$

With the aid of the commutation relations, we transfer the operator A_{21}^r in the matrix element to the left until it appears immediately after the vector $\langle H|$ and consider that $\langle H|A_{21} = 0$. The expression for B then takes the form

$$B = \sum_r \frac{[2U + 1]![k]!}{[r]![2U + r + 1]![k - r]!} q^{r(2U+1+r)} B_1, \quad (97)$$

where

$$B_1 = {}_q \langle H | A_{23}^{\ell+r} A_{13}^{k-r} A_{12}^{r+a} A_{32}^b P^T A_{31}^s A_{21}^p | H \rangle_q. \quad (98)$$

To compute the matrix element B_1 , the generators A_{23} must be transferred to the right until they appear immediately before the projection operator P^T , whereupon the equation $A_{23}P^T = 0$ is taken into account. The commutation of these generators with A_{12}^{r+a} yields an additional summation. As a result, the matrix element B_1 reduces to a single sum over x ; that is,

$$B_1 = \sum_x (-1)^x \frac{[\ell + r]![r + a]![b]!}{[x]![r + a - x]![\ell + r - x]![b - \ell - r + x]!} q^{(k-r)(r+a-x)-x-(\ell+r-x)(r+a-x)}$$

$$\times \prod_z [f_2 - f_3 + p - s + \ell + r - x - b - z] B_2,$$

where

$$B_2 = {}_q \langle H | A_{12}^{r+a-x} A_{13}^{k-r+x} A_{32}^{b-\ell-r+x} P^T A_{31}^s A_{21}^p | H \rangle_q. \quad (99)$$

Considering that, in the case of T -spin basis,

$$2T = f_3 - f_2 - p + s - 2 \quad (100)$$

and that all factors in the product \prod_z are negative, we recast this product into the form

$$\prod_z [f_2 - f_3 + p - s + \ell + r - x - b - z] \quad (101)$$

$$= (-1)^{\ell+r-x} \prod_z [f_3 - f_2 - p + s - \ell - r$$

$$+ x + b + z] = (-1)^{\ell+r-x} \frac{[T - M_T]!}{[T - M_T - \ell - r + x]!}.$$

Further, we transfer the remaining generators A_{32} in the expression for the matrix element B_2 to the left until they appear immediately after the vector $\langle H|$, which annihilates them, and consider that the definition of the square of the norm entails the relation

$${}_q \langle H | A_{12}^p A_{13}^s P^T A_{31}^s A_{21}^p | H \rangle_q = (-1)^s q^{2s} N^2(sp). \quad (102)$$

Combining the above results, we reduce the expression for the Weyl coefficient $\langle U|T \rangle_q$ to the form

$$\langle U|T \rangle_q = (-1)^{k+s} q^{2s} \frac{N(sp)[2U + 1]![-T - 1 - M_T]![T - M_T]![k]!}{N(k\ell)N(UM_U)N(TM_T)[s]!} Q, \quad (103)$$

where

$$Q = \sum_{r,x} (-1)^r q^\phi \frac{[U - M_U + r]![\ell + r]![k - r + x]!}{[r]![2U + r + 1]![k - r]![x]![U - M_U + r - x]![\ell + r - x]!} \quad (104)$$

$$\times \frac{1}{[-T - 1 - M_T - \ell - r + x]![T - M_T - \ell - r + x]!}$$

Here, the exponent of the q factor (q^ϕ) is given by

$$\begin{aligned} \phi &= r(2U + r + 1) + (k - r)(\ell + r) - x \quad (105) \\ &- (\ell + r - x)(U - M_U + r - x) + (k - r) \\ &\times (U - M_U + r - x) - (-T - 1 - M_T \\ &- \ell - r + x)(-T - 1 + M_T + \ell + r - x). \end{aligned}$$

Let us now prove that, in just the same way as for the $u_q(3)$ algebra, the q Weyl coefficient for the $u_q(2, 1)$ algebra can be expressed in terms of the q Racah coefficient for the $su_q(2)$ algebra. For this purpose, the technique developed in [25] for a resummation of finite sums of q factorials on the basis of the summation formulas presented there is employed to reduce the sum over two variables Q to a sum over one variable. Introducing the variable $y = -T - 1 - M_T - \ell - r + x$ and taking Eqs. (94) and (95) into account, we recast the double sum Q into the form

$$Q = q^{k\ell - s + k - p(\ell - s)} \sum_y q^{y(2T + 1 + p + \ell - s)} \quad (106)$$

$$\times \frac{[s + y]! Q_1}{[y]![p - y]![\ell - s + k - y]![2T + 1 + y]!},$$

where

$$Q_1 = \sum_r (-1)^r \quad (107)$$

$$\times \frac{[U - M_U + r]![\ell + r]! q^{r(U + M_U - \ell + s + y)}}{[r]![2U + r + 1]![k - r]![s - k + r + y]!}.$$

Further, it is helpful to use the Kronecker symbol $\delta(r, v)$ in order to introduce additional summations in Q_1 :

$$\sum_z (-1)^{r-z} \frac{q^{-z(r-v-1)-r}}{[r-z]![z-v]!} = \delta(r, v). \quad (108)$$

In this way, the sum over r is represented as a triple sum over the indices r, z , and v . After that, we replace the variable r by $r' = r - z$ and perform summation over r' by formula (A.13) from [25]:

$$\begin{aligned} &\sum_{r'} (-1)^{r'} \frac{[\ell + z + r']! q^{-r'(\ell - s + z - y + 1)}}{[r']![k - z - r']![s - k + y + z + r']!} \quad (109) \\ &= \frac{(-1)^{k-z} [\ell - s + k - y]! q^{-(k-z)(\ell + z + 1)}}{[k - z]![s + y]![\ell - s - y + z]!}. \end{aligned}$$

Using formula (A.12) from [25] to compute the sum over v in the expression for Q_1 , we arrive at

$$\begin{aligned} &\sum_v (-1)^v \frac{[U - M_U + v]! q^{v(U + M_U + z)}}{[z]![2U + v + 1]![z - v]!} \quad (110) \\ &= \frac{[U - M_U]![U + M_U + z]! q^{-z(U - M_U + 1)}}{[z]![2U + z + 1]![U + M_U]!}. \end{aligned}$$

Upon summation over the indices r' and v , the expression for Q_1 takes the form

$$Q_1 = \sum_z (-1)^{k-z} q^{-z(\ell - s - y + z + U - M_U + 1) - (k-z)(\ell + z + 1)} \quad (111)$$

$$\times \frac{[U - M_U]![U + M_U + z]![\ell - s + k - y]![\ell + z]!}{[z]![2U + z + 1]![U + M_U]![k - z]![\ell - s + z - y]![s + y]!}.$$

while the expression for Q becomes

$$Q = q^{k\ell - s + k - p(\ell - s)} \frac{[U - M_U]!}{[U + M_U]!} \sum_z (-1)^{k-z} \quad (112)$$

$$\times \frac{[U + M_U + z]![\ell + z]!}{[z]![2U + z + 1]![k - z]!} q^{-z(p - k + 1) - k(\ell + z + 1)} Q_2,$$

where we have singled out explicitly summation over the index y ,

$$Q_2 = \sum_y q^{y(2T + 1 + p + \ell - s + z)} \quad (113)$$

$$\times \frac{1}{[y]![p - y]![\ell - s + z - y]![2T + 1 + y]!}.$$

The final step in our resummation procedure consists in performing summation over y by formula (A.9) from [25]. As a result, the expression for Q reduces to a sum over one index,

$$Q = (-1)^k q^{-s} \frac{[U - M_U]!}{[U + M_U]![p]![2T + 1 + p]!} \sum_z \frac{(-1)^z [U + M_U + z]![\ell + z]![2T + 1 + p + \ell - s + z]!}{[z]![2U + z + 1]![k - z]![\ell - s + z]![2T + 1 + \ell - s + z]!}. \tag{114}$$

Thus, the Weyl coefficient for the $u_q(2, 1)$ algebra is given by

$$\begin{aligned} \langle U|T \rangle_q &= (-1)^s \left[\frac{[2U + 1][2T + 1][U - M_U]![-T - 1 - M_T]![T - M_T]!}{[U + M_U]![2T + p + 1]!} \right. \\ &\times \frac{[k]![f_1 - f_2 - k]![f_1 - f_2 + \ell + 1]!}{[s]![\ell]![p]![f_3 - f_1 + k - 2]!} \left. \frac{[f_3 - f_1 + s - 2]![f_3 - f_2 - p - 2]!}{[f_3 - f_2 + \ell - 1]![f_1 - f_2 - p]!} \right]^{1/2} \\ &\times \sum_z (-1)^z \frac{[U + M_U + z]![\ell + z]![2T + 1 + p + \ell - s + z]!}{[z]![2U + z + 1]![k - z]![\ell - s + z]![2T + 1 + \ell - s + z]!}. \end{aligned} \tag{115}$$

This formula makes it possible to relate the q Weyl coefficient for the $u_q(2, 1)$ quantum algebra to the q Racah coefficients for the $su_q(2)$ quantum algebra.

6. RELATION BETWEEN THE q WEYL COEFFICIENTS FOR THE $u_q(2, 1)$ QUANTUM ALGEBRA AND THE q RACAH COEFFICIENTS FOR THE $su_q(2)$ QUANTUM ALGEBRA

The explicit expression for the q Weyl coefficient for the $u_q(3)$ algebra was obtained in [25], and its relation to the Racah coefficient for the $su_q(2)$ quantum algebra was established there.

Here, we show that expression (115) for the q Weyl coefficient for the $u_q(2, 1)$ quantum algebra can also be related to the q Racah coefficient for the $su_q(2)$ quantum algebra. Our consideration is based on transforming one of five general formulas in [25] for the q Racah coefficient for the $su_q(2)$ quantum algebra {namely, formula (5.29) in [25]}. Replacing the summation index n by $z = a - b + c - n$, we arrive at

$$\begin{aligned} \left\{ \begin{matrix} abc \\ def \end{matrix} \right\}_q &= (-1)^{a+c+d+f} \frac{\Delta(abc)_q \Delta(bdf)_q}{\Delta(aef)_q \Delta(cde)_q} \tag{116} \\ &\times \sum_z \frac{(-1)^{a-b+c-z} [-c + d + e + z]!}{[z]![a - b + c - z]![a - c + d + f + z]!} \\ &\times \frac{[-a + e + f + z]![-b + d + f + 1 + z]!}{[b - c + e + f + 1 + z]![a + b + d + e + 1 + z]!}, \end{aligned}$$

where

$$\Delta(abc)_q = \sqrt{\frac{[a + b - c]![a - b + c]![-a + b + c]!}{[a + b + c + 1]!}}.$$

A comparison of expression (116) with formula (115) for the q Weyl coefficient for the negative discrete series of the representations of $u_q(2, 1)$ reveals that the summands in the two formulas coincide, provided that

$$\begin{aligned} a &= \frac{1}{2}(f_3 - f_1 + k + s - 2), \tag{117} \\ b &= \frac{1}{2}(f_3 - f_2 - k + s - 2), \\ d &= \frac{1}{2}(p + l), \quad e = \frac{1}{2}(f_1 - f_2 - p + l), \\ c &= \frac{1}{2}(f_1 - f_2), \\ f &= \frac{1}{2}(f_3 - f_2 - p - s + k + l - 2). \end{aligned}$$

Using the Regge symmetry property {see formula (5.24) in [25]}, we recast the q -6j symbol (116) into the form

$$\left\{ \begin{matrix} abc \\ def \end{matrix} \right\}_q = \left\{ \begin{matrix} s_3 - e & f & s_3 - a \\ s_3 - b & c & s_3 - d \end{matrix} \right\}_q, \tag{118}$$

where $s_3 = (a + b + d + e)/2$. Further, the substitution of the values of the parameters a, b, c, d, e , and f from formula (117) gives the relation between the q Weyl coefficient (115) for the $u_q(2, 1)$ quantum algebra and the q Racah coefficient [or the q -6j symbol (118)] for the $su_q(2)$ quantum algebra,

$$\begin{aligned} \langle U|T \rangle_q &= (-1)^{2d^- + e^- + f^- - b^- - c^-} \tag{119} \\ &\times U(a^- b^- e^- d^-; c^- f^-)_q \\ &= (-1)^{a^- + 2e^- + 3d^- + f^- - c^-} \sqrt{[2T + 1][2U + 1]} \end{aligned}$$

$$\times \left\{ \begin{matrix} a^- & b^- & c^- \\ d^- & e^- & f^- \end{matrix} \right\}_q,$$

where

$$a^- = s_3 - e = \frac{1}{2}(f_3 - f_1 + p + s - 2), \quad (120)$$

$$b^- = f = \frac{1}{2}(f_3 - f_2 - p - s + k + l - 2),$$

$$d^- = s_3 - b = \frac{1}{2}(k + l), \quad e^- = c = \frac{1}{2}(f_1 - f_2),$$

$$c^- = s_3 - a = U, \quad f^- = s_3 - d = T.$$

7. CONCLUSION

In this study, the projection operators for the $su_q(2)$ subalgebra have been used to explore the negative discrete series of unitary irreducible representations of the noncompact $u_q(2, 1)$ quantum algebra. The q analog of the Gelfand–Graev formulas has been derived in the basis associated with the reduction $u_q(2, 1) \rightarrow su_q(2)u(1)$. It seems that the reduction $u_q(2, 1) \rightarrow u(1)su_q(1, 1)$ for the discrete series of highest weight representations has been considered for the first time in the present study. With the aid of the projection operator for the $su_q(1, 1)$ subalgebra, we have constructed the basis of the representation for this reduction and calculated the matrix elements of the generators. We have obtained analytic expressions for the elements of the transformation brackets $\langle U|T \rangle_q$ relating the U -spin and T -spin bases of highest weight irreducible representations. By the analogy with the q Weyl coefficients for the $u_q(3)$ algebra [25], they can be called the q Weyl coefficients for the noncompact $u_q(2, 1)$ algebra. It has been explicitly shown that these q Weyl coefficients are equivalent (apart from a phase) to specific q Racah coefficient for the $u_q(2)$ algebra or are proportional to the q -6j symbol for the $u_q(2)$ algebra. The series of lowest weight representations can be studied in a similar way. The intermediate discrete series requires a dedicated investigation, and this will be done in our further studies.

ACKNOWLEDGMENTS

This work was supported by the Russian Foundation for Basic Research (project no. 02-01-00668).

APPENDIX

Normalization of the U -Spin Basis Vectors of the $u_q(2, 1)$ Algebra (Negative Discrete Series)

The structure of the U -spin basis vectors is specified by formulas (19)–(26).

Here, we use the transformation properties of the “noncompact” generators under Hermitian conjugation and the properties of the projection operator P^U :

$$(P^U)^+ = P^U, \quad (A.1)$$

$$(P^U)^2 = P^U, \quad (A.2)$$

$$A_{12}^{U-M} A_{21}^{U-M} P^U = N^2(UM)P^U. \quad (A.3)$$

With allowance for these formulas, the square of the norm $N^2(k\ell)$ takes the form

$$N^2(k\ell) = (-1)^{k+\ell} \langle H|A_{23}^\ell \tilde{A}_{13}^k P^U A_{31}^k A_{32}^\ell |H \rangle, \quad (A.4)$$

where

$$\tilde{A}_{13} = A_{12}A_{23} - q^{-1}A_{23}A_{12}. \quad (A.5)$$

Since, by definition, the relation

$$A_{13} = A_{12}A_{23} - qA_{23}A_{12} \quad (A.6)$$

holds, we can represent the generator \tilde{A}_{13} in the form

$$\tilde{A}_{13} = A_{13} + (q - q^{-1})A_{23}A_{12}. \quad (A.7)$$

From the relations

$$A_{12}P^U = U_+P^U = 0 \quad (A.8)$$

it follows that

$$N^2(k\ell) = (-1)^{k+\ell} \langle H|A_{23}^\ell A_{13}^k P^U A_{31}^k A_{32}^\ell |H \rangle. \quad (A.9)$$

A straightforward computation of $N^2(k\ell)$ by transferring the raising generators to the highest weight vector $|H\rangle$ is rather cumbersome. In view of this, we will try to construct a recursion relation between the expressions for $N^2(k\ell)$ for various values of k and ℓ , bearing in mind that

$$\langle H|P^U|H \rangle = \langle H|H \rangle = 1. \quad (A.10)$$

We begin by establishing a relation between $N^2(k\ell)$ and $N^2(k-1, \ell)$. In the expression for $N^2(k\ell)$, we replace, for this purpose, A_{13}^k by $A_{13}^{k-1}P^{U+1/2}A_{13}$. This is legitimate because, in (A.9), the projection operator $P^{U+1/2}$ taken in this combination is equivalent to the identity operator. Indeed, we have

$$P^{U+1/2}A_{13}P^U = \sum_r (-1)^r \frac{[2U+2]!}{[r]![2U+r+2]!} A_{21}^r \quad (A.11)$$

$$\times A_{12}^r A_{13}P^U = A_{13}P^U,$$

since the generators A_{12}^r and A_{13} commute (apart from the factor q^{-r} , which is immaterial in the case under study), and since $A_{12}^r P^U = \delta_{r,0}P^U$. We now

consider applying the generator A_{13} to the projection operator P^U :

$$\begin{aligned} A_{13}P^U &= \sum_r (-1)^r \frac{[2U+1]!}{[r]![2U+r+1]!} A_{13}A_{21}^r A_{12}^r \\ &= \sum_r (-1)^r \frac{[2U+1]!}{[r]![2U+r+1]!} \\ &\quad \times (A_{21}^r A_{13} - [r]A_{21}^{r-1} A_{23}q^{A_{11}-A_{22}-r+1}) A_{12}^r. \end{aligned} \quad (\text{A.12})$$

From here on, we use the commutation relations from [7, 24, 25] for the generators raised to a power. In view of the relation $P^{U+1/2}A_{21} = (A_{12}P^{U+1/2})^+ = 0$, the application of this operator on the projection operator $P^{U+1/2}$ from the left yields

$$\begin{aligned} P^{U+1/2}A_{13}P^U & \quad (\text{A.13}) \\ &= P^{U+1/2} \left(A_{13} + \frac{A_{23}}{[2U+2]} q^{A_{11}-A_{22}} A_{12} \right), \end{aligned}$$

where

$$[2U+2] = [f_1 - f_2 - k + \ell + 2]; \quad (\text{A.14})$$

as a result, the square of the norm becomes

$$N^2(k\ell) = (-1)^{k+\ell} \langle H | A_{23} A_{13}^{k-1} P^{U+1/2} | H \rangle \quad (\text{A.15})$$

$$\begin{aligned} P^{U+1/2} \left(A_{13} + \frac{A_{23}}{[f_1 - f_2 - k + \ell + 2]} q^{A_{11}-A_{22}} A_{12} \right) A_{31}^k A_{32}^\ell | H \rangle &= [k] \left([f_1 - f_3 - k - \ell + 1] \right. \\ &\quad \left. - \frac{[\ell + 1][f_2 - f_3 - \ell]}{[f_1 - f_2 - k + \ell + 2]} \right) P^{U+1/2} A_{31}^{k-1} A_{32}^\ell | H \rangle = [k] \frac{[f_1 - f_3 - k + 2][f_1 - f_2 - k + 1]}{[f_1 - f_2 - k + \ell + 2]} P^{U+1/2} A_{31}^{k-1} A_{32}^\ell | H \rangle. \end{aligned} \quad (\text{A.20})$$

Thus, the square of the norm, $N^2(k\ell)$, takes the form

$$\begin{aligned} N^2(k\ell) &= (-1)^{k+\ell-1} \quad (\text{A.21}) \\ &\times \frac{[k][f_3 - f_1 + k - 2][f_1 - f_2 - k + 1]}{[f_1 - f_2 - k + \ell + 2]} \\ &\times \langle H | A_{23} A_{13}^{k-1} P^{U+1/2} A_{31}^{k-1} A_{32}^\ell | H \rangle. \end{aligned}$$

In other words, we have derived a recursion relation between $N^2(k\ell)$ and $N^2(k-1, \ell)$,

$$\begin{aligned} N^2(k\ell) & \quad (\text{A.22}) \\ &= \frac{[k][f_3 - f_1 + k - 2][f_1 - f_2 - k + 1]}{[f_1 - f_2 - k + \ell + 2]} \end{aligned}$$

$$N^2(k\ell) = [k]! [\ell]! [f_3 - f_1 + k - 2]! \frac{[f_3 - f_2 + \ell - 1]! [f_1 - f_2]! [f_1 - f_2 - k + \ell + 1]!}{[f_3 - f_2 - 1]! [f_3 - f_1 - 2]! [f_1 - f_2 - k]! [f_1 - f_2 + \ell + 1]!}. \quad (\text{A.24})$$

REFERENCES

1. S. T. Belyaev, I. M. Pavlichenkov, and Yu. F. Smirnov, Nucl. Phys. A **444**, 36 (1985).

$$\times \left(A_{13} + \frac{A_{23}q^{A_{11}-A_{22}}}{[f_1 - f_2 - k + \ell + 2]} A_{12} \right) A_{31}^k A_{32}^\ell | H \rangle.$$

Commuting the generators A_{13} and A_{31}^k , we arrive at

$$A_{13}A_{31}^k A_{32}^\ell | H \rangle \quad (\text{A.16})$$

$$= [k][f_1 - f_3 - k - \ell + 1] A_{31}^{k-1} A_{32}^\ell | H \rangle$$

and

$$A_{23}q^{A_{11}-A_{22}} A_{12} A_{31}^k A_{32}^\ell | H \rangle \quad (\text{A.17})$$

$$= q^{(f_1-f_2-k+\ell+2)} A_{23} A_{12} A_{31}^k A_{32}^\ell | H \rangle.$$

The commutation of the generators A_{12} and A_{31}^k makes it possible to derive the relation

$$A_{23}q^{A_{11}-A_{22}} A_{12} A_{31}^k A_{32}^\ell | H \rangle \quad (\text{A.18})$$

$$= -[k] A_{23} A_{31}^{k-1} A_{32}^{\ell+1} | H \rangle.$$

Transferring the generator A_{23} to the right until it appears immediately in front of the highest weight vector $|H\rangle$, which annihilates it, we obtain

$$A_{23}q^{A_{11}-A_{22}} A_{12} A_{31}^k A_{32}^\ell | H \rangle \quad (\text{A.19})$$

$$= -[k][\ell + 1][f_2 - f_3 - \ell] A_{31}^{k-1} A_{32}^\ell | H \rangle;$$

therefore, we have

$$\times N^2(k-1, \ell).$$

The recursion relation

$$N^2(0\ell) = (-1)^\ell \langle H | A_{23} P^U A_{32}^\ell | H \rangle \quad (\text{A.23})$$

$$= [\ell][f_3 - f_2 + \ell - 1] N^2(0, \ell - 1)$$

can be obtained in a similar way. Using these recursion relations, we arrive at an ultimate expression for the square of the norm in (A.21):

2. P. P. Kulish and N. Yu. Reshetikhin, Zap. Nauchn. Semin. LOMI **101**, 101 (1981).

3. E. K. Sklyanin, *Funktsion. Analiz Pril.* **16** (4), 27 (1982).
4. L. D. Faddeev and L. A. Takhtajan, *Lect. Notes Phys.* **246**, 183 (1986).
5. P. P. Raychev, R. P. Roussev, and Yu. F. Smirnov, *J. Phys. G* **16**, L137 (1990).
6. D. Bonatsos and C. Daskaloyannis, *Prog. Part. Nucl. Phys.* **43**, 537 (1999).
7. Yu. F. Smirnov, V. N. Tolstoĭ, and Yu. I. Kharitonov, *Yad. Fiz.* **54**, 721 (1991) [*Sov. J. Nucl. Phys.* **54**, 437 (1991)].
8. Yu. F. Smirnov, V. N. Tolstoĭ, and Yu. I. Kharitonov, *Yad. Fiz.* **56** (5), 223 (1993) [*Phys. At. Nucl.* **56**, 1143 (1993)].
9. A. A. Malashin, Yu. F. Smirnov, and Yu. I. Kharitonov, *Yad. Fiz.* **58**, 665 (1995) [*Phys. At. Nucl.* **58**, 595 (1995)].
10. Yu. F. Smirnov and Yu. I. Kharitonov, *Yad. Fiz.* **58**, 749 (1995) [*Phys. At. Nucl.* **58**, 690 (1995)].
11. A. A. Malashin, Yu. F. Smirnov, and Yu. I. Kharitonov, *Yad. Fiz.* **58**, 1105 (1995) [*Phys. At. Nucl.* **58**, 1031 (1995)].
12. Yu. F. Smirnov and Yu. I. Kharitonov, *Yad. Fiz.* **59**, 379 (1996) [*Phys. At. Nucl.* **59**, 360 (1996)].
13. Yu. F. Smirnov and Yu. I. Kharitonov, Preprint No. 2140 (Petersburg Nucl. Phys. Inst., St. Petersburg, 1996).
14. Yu. F. Smirnov and Yu. I. Kharitonov, Preprint No. 2251 (Petersburg Nucl. Phys. Inst., St. Petersburg, 1998).
15. Yu. F. Smirnov and Yu. I. Kharitonov, Preprint No. 2301 (Petersburg Nucl. Phys. Inst., St. Petersburg, 1999).
16. Yu. F. Smirnov and Yu. I. Kharitonov, Preprint No. 2345 (Petersburg Nucl. Phys. Inst., St. Petersburg, 2000).
17. I. M. Gel'fand and M. I. Graev, *Izv. Akad. Nauk SSSR, Ser. Mat.* **29**, 1329 (1965).
18. A. O. Barut and R. Raczka, *Theory of Group Representations and Application*, 2nd ed. (World Sci., Singapore, 1986; Mir, Moscow, 1980).
19. U. Ottoson, *Commun. Math. Phys.* **10**, 114 (1968).
20. Yu. F. Smirnov, V. N. Tolstoy, V. A. Knyr, and L. Ya. Stotland, *Proceedings of the III Seminar "Group Theory Methods in Physics," Yurmala, 1985* (Nauka, Moscow, 1986), Vol. 2, p. 77.
21. I. T. Todorov, Preprint IC/66/71, ICTP (Triest, 1966).
22. N. Ya. Vilenkin, *Special Functions and the Theory of Group Representations* (Nauka, Moscow, 1965; Am. Math. Soc., Providence, R.I., 1968).
23. Yu. F. Smirnov, V. N. Tolstoĭ, and Yu. I. Kharitonov, *Yad. Fiz.* **53**, 959 (1991) [*Sov. J. Nucl. Phys.* **53**, 593 (1991)].
24. Yu. F. Smirnov and Yu. I. Kharitonov, Preprint No. 2394 (Petersburg Nucl. Phys. Inst., St. Petersburg, 2000).
25. R. M. Asherova, Yu. F. Smirnov, and V. N. Tolstoy, *Yad. Fiz.* **59**, 1859 (1996) [*Phys. At. Nucl.* **59**, 1795 (1996)].

Translated by R. Rogalyov

ELEMENTARY PARTICLES AND FIELDS
Experiment

**The Kr2Det Project: Search for Mass-3 State Contribution $|U_{e3}|^2$
to the Electron Neutrino Using a One-Reactor–Two-Detector Oscillation
Experiment at the Krasnoyarsk Underground Site***

V. P. Martemyanov , L. A. Mikaelyan*** , V. V. Sinev**** ,
V. I. Kopeikin***** , and Yu. V. Kozlov*******

Russian Research Centre Kurchatov Institute, pl. Kurchatova 1, Moscow, 123182 Russia

Received January 23, 2003

Abstract—The main physical goal of the project is to search with reactor antineutrinos for small mixing angle oscillations in the mass parameter region around $\Delta m_{\text{atm}}^2 \sim 2.5 \times 10^{-3} \text{ eV}^2$ in order to find the element U_{e3} of the neutrino mixing matrix or to set a new more stringent constraint. To achieve this, we propose a “one-reactor–two-detector” experiment with two identical antineutrino spectrometers located ~ 100 and ~ 1000 m from the Krasnoyarsk underground reactor (~ 600 m w.e.). In the no-oscillation case, the ratio of measured positron spectra of the $\bar{\nu}_e + p \rightarrow e^+ + n$ reaction is energy independent. Deviation from a constant value of this ratio is the oscillation signature. In this scheme, results do not depend on the exact knowledge of the reactor power, ν_e spectra, burnup effects, and target volumes, and an important point that the backgrounds can periodically be measured during reactor off periods. We give a schematic description of the detectors, calculate the neutrino detection rates, and estimate the backgrounds. We also outline the detector monitoring and calibration procedures. We hope that systematic uncertainties will not exceed 0.5% and that the sensitivity of $|U_{e3}|^2 \approx 4 \times 10^{-3}$ (at $\Delta m^2 = 2.5 \times 10^{-3} \text{ eV}^2$) can be achieved.

© 2003 MAIK “Nauka/Interperiodica”.

1. INTRODUCTION

The Super-Kamiokande studies of atmospheric neutrinos [1] found intensive ($\sin^2 2\theta_{\text{atm}} > 0.9$) $\nu_\mu \rightarrow \nu_x$ oscillations and have confined the mass parameter to the interval $1.4 \times 10^{-3} < \Delta m_{\text{atm}}^2 < 4.2 \times 10^{-3} \text{ eV}^2$ with $\Delta m_{\text{atm}}^2 = 2.5 \times 10^{-3} \text{ eV}^2$ as the most probable value. The $\nu_\mu \rightarrow \nu_\tau$ has been found to be the dominant channel of the atmospheric neutrino oscillations, while much room is left also for the $\nu_e \rightarrow \nu_{\mu,\tau}$ transitions.

The ~ 1 -km baseline reactor experiment CHOOZ [2] searched for electron antineutrino disappearance in the atmospheric mass parameter region. No oscillations have been found (Fig. 1, curve “CHOOZ”):

$$\sin^2 2\theta_{\text{CHOOZ}} \leq 0.14 \quad (1)$$

$$(90\% \text{ C.L. at } \Delta m^2 = 2.5 \times 10^{-3} \text{ eV}^2),$$

$$\sin^2 2\theta_{\text{CHOOZ}} \leq 0.19 \text{ (at } \Delta m^2 = 2.0 \times 10^{-3} \text{ eV}^2).$$

The reactor neutrino mixing parameter $\sin^2 2\theta$ in the atmospheric mass parameter region plays an important role in neutrino oscillation physics. In three active neutrino mixing schemes with normal neutrino mass hierarchy, it is expressed through the contribution of the mass-3 eigenstate to the electron neutrino flavor state $U_{e3} = \sin \theta_{13}$:

$$\sin^2 2\theta_{\text{CHOOZ}} = \sin^2 2\theta_{13} = 4|U_{e3}|^2(1 - |U_{e3}|^2). \quad (2)$$

We also mention that, with a nonzero value of U_{e3} in the lepton sector, CP -violation effects can exist.

The negative results of the CHOOZ experiment impose an important constraint:

$$\sin^2 2\theta_{13} \leq 0.14, \quad (3)$$

$$|U_{e3}|^2 \leq 3.6 \times 10^{-2} \text{ (at } \Delta m^2 = 2.5 \times 10^{-3} \text{ eV}^2).$$

The quantity $\sin^2 2\theta_{13}$ can be hundreds and thousands of times smaller than the present CHOOZ limits. In this case, the necessary sensitivity can, in the distant future and in several steps, be achieved at neutrino factories in experiments using hundred- and thousand-kiloton detectors located a few thousand kilometers from the accelerator neutrino source (for review, see [3]).

*This article was submitted by the authors in English.

**e-mail: vpmar@dnuc.polyn.kiae.su

***e-mail: lmikael@polyn.kiae.su

****e-mail: sinev@polyn.kiae.su

*****e-mail: kopeykin@polyn.kiae.su

*****e-mail: kozlov@dnuc.polyn.kiae.su

The first step can, however, be done sooner (and cheaper) at reactors as has been discussed since 1999 [4, 5]. Recently, an idea to search for U_{e3} at reactors in Japan was published [6]. Doing this first step is still more important because no physical reason is known why $\sin^2 2\theta_{13}$ should be very small. It may quite happen that this quantity is only several times smaller than the present upper limits (1).

The main physical goals of the reactor experiment considered here are

- (i) to obtain new information on the electron neutrino mass composition (U_{e3});
- (ii) to provide normalization for future experiments at accelerators;
- (iii) to achieve better understanding of the role that ν_e can have in the atmospheric neutrino phenomena.

The main practical goal is to decrease, relative to CHOOZ, statistical and systematic uncertainties as much as possible.

Analysis of all available solar neutrino data [7] confirms the large-mixing-angle MSW as the most probable solution with the best-fit value of the solar neutrino mass parameter $\Delta m_{\text{sol}}^2 \approx 6 \times 10^{-5} \text{ eV}^2$. We assume therefore that

$$\Delta m_{\text{sol}}^2 \ll \Delta m_{\text{atm}}^2 = m_3^2 - m_2^2 \approx m_3^2 - m_1^2 \quad (4)$$

and use in this paper a two-mode expression for the reactor antineutrino survival probability $P(\bar{\nu}_e \rightarrow \bar{\nu}_e)$:

$$P(\bar{\nu}_e \rightarrow \bar{\nu}_e) = 1 - \sin^2 2\theta \sin^2(1.27\Delta m^2 L/E), \quad (5)$$

where L (in m) is the reactor–detector distance and E (in MeV) is the antineutrino energy. There is, however, some probability that Δm_{sol}^2 is not so small as assumed above. In this case, $\Delta m_{\text{sol}}^2/\Delta m_{\text{atm}}^2$ cannot be neglected and somewhat more complicated expressions for $P(\bar{\nu}_e \rightarrow \bar{\nu}_e)$ should be used as discussed in [6, 8].

Reactor antineutrinos have a continuous energy spectrum and are detected via the inverse beta-decay reaction

$$\bar{\nu}_e + p \rightarrow e^+ + n. \quad (6)$$

The visible positron energy E_e is related to the $\bar{\nu}_e$ energy as

$$E_e = E - 1.80 + E_{\text{annih}} \approx E - 0.8. \quad (7)$$

A typical positron energy spectrum is shown in Fig. 2.

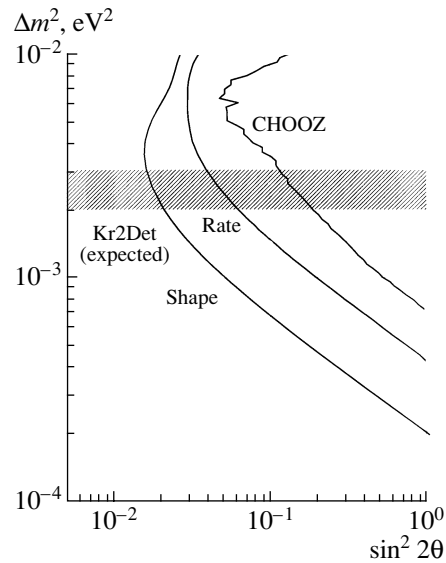


Fig. 1. Reactor antineutrino oscillation plots. Curves “CHOOZ” and “Kr2Det” (expected) “Shape” and “Rate” are 90% C.L. ν_e disappearance limits. The Kr2Det limits are obtained assuming 40 000 detected antineutrinos, 10 : 1 effect to background ratio, and systematic uncertainties $\sigma_{\text{shape}} = 0.5\%$ and $\sigma_{\text{rate}} = 0.8\%$. The shaded area represents the most probable atmospheric neutrino mass parameter region.

2. ONE-REACTOR–TWO-DETECTOR SCHEME

Two identical liquid scintillation spectrometers are stationed at distances $L_{\text{far}} \approx 1000 \text{ m}$ (far position) and $L_{\text{near}} \approx 115 \text{ m}$ from the underground Krasnoyarsk reactor (Fig. 3). The overburden at Krasnoyarsk is $\sim 600 \text{ m w.e.}$, which is twice as much as in the CHOOZ experiment. (At short distances from the reactor, the one-reactor–two-detector approach was first probed at Rovno [9] and later successfully used at Bugey [10].)

Two types of analysis can be used.

Analysis I is based on comparison of the shapes of positron spectra $S(E_e)_{\text{far}}$ and $S(E_e)_{\text{near}}$ measured simultaneously in two detectors. In the no-oscillation case, the ratio $S(E_e)_{\text{far}}/S(E_e)_{\text{near}}$ is energy independent. Small deviations from the constant value of this ratio

$$X_{\text{shape}} = S(E_e)_{\text{far}}/S(E_e)_{\text{near}} \quad (8)$$

$$= C(1 - \sin^2 2\theta \sin^2(1.27\Delta m^2 L_{\text{far}}/E))/(1 - \sin^2 2\theta \sin^2(1.27\Delta m^2 L_{\text{near}}/E))$$

are sought for oscillation parameters.

In the one-reactor–two-detector scheme,

(i) results of analysis I do not depend on the exact knowledge of the reactor power, absolute ν_e flux and energy spectrum, burnup effects, absolute values of

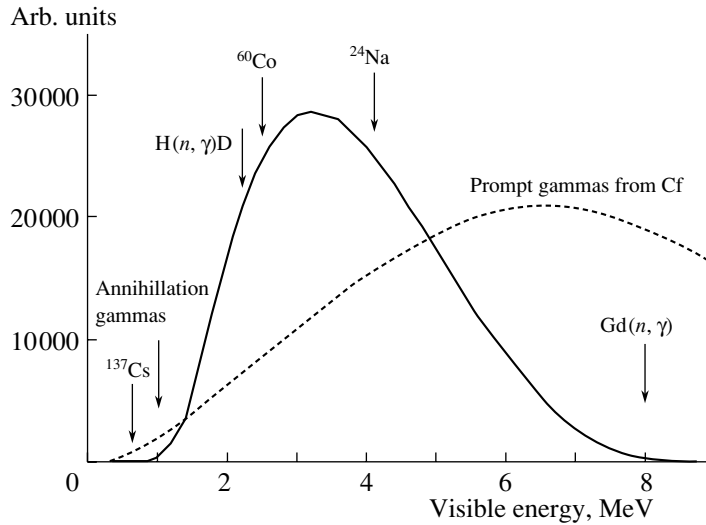


Fig. 2. Positron visible energy spectrum.

hydrogen atom concentrations, detection efficiencies, target volumes, and reactor–detector distances;

(ii) at Krasnoyarsk, the detector backgrounds can be measured during reactor off periods, which periodically follow 50-day-long reactor on periods.

Calculated ratios $S(E_e)_{\text{far}}/S(E_e)_{\text{near}}$ for a set of oscillation parameters are shown in Fig. 4.

Analysis II is based on the ratio of the total number of neutrinos N_{far} and N_{near} detected at two distances:

$$X_{\text{rate}}(\sin^2 2\theta, \Delta m^2) = (L_{\text{far}}/L_{\text{near}})^2 \quad (8')$$

$$\times (V_{\text{near}}/V_{\text{far}})(\varepsilon_{\text{near}}/\varepsilon_{\text{far}})N_{\text{far}}/N_{\text{near}}.$$

Here, V_{near} , V_{far} and ε , ε_{far} are the target volumes and neutrino detection efficiencies. In the no oscillation case, $X_{\text{rate}} = 1$.

Analysis II is also independent of the exact knowledge of the reactor neutrino flux and energy spectrum. The absolute values of detection efficiencies are practically canceled; only their small difference is to be considered here, while the ratios $(L_{\text{far}}/L_{\text{near}})^2$ and $(V_{\text{near}}/V_{\text{far}})$ should be known accurately.

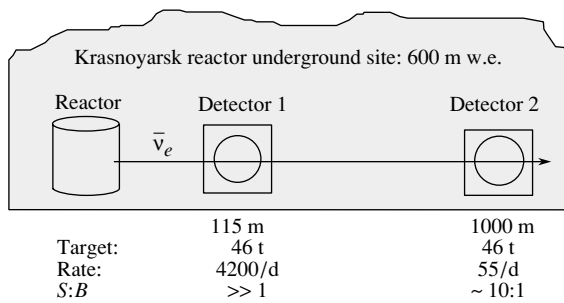


Fig. 3. Scheme of the Kr2Det experiment.

3. DETECTORS

A miniature version of the KamLAND [11] and BOREXINO [12] and a scaled-up version of the CHOOZ three-concentric-zone-detector scheme is chosen for the design of the spectrometers (Fig. 5).

At this stage, we consider a 4.7-m-diameter liquid

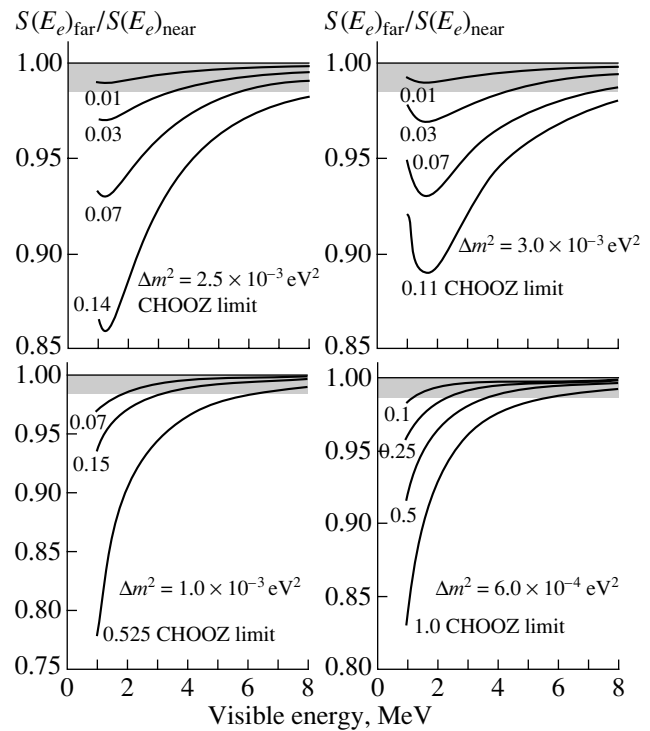


Fig. 4. Calculated ratio of positron spectra $S(E_e)_{\text{far}}/S(E_e)_{\text{near}}$ for some oscillation parameters ($L_{\text{far}} = 1000$ m, $L_{\text{near}} = 115$ m, $N_{\text{far}} = 16 \times 10^3$ yr).

scintillator target, enclosed in a transparent spherical balloon. The target is viewed by ~ 800 8-in EMI-9350 (9350–9356) photomultipliers through an ~ 90 -cm layer of mineral oil of zone 2 of the detector. PMTs of this type have successfully been used in the CHOOZ experiment and are used now in the BOREXINO and SNO detectors [13]. A 20% light collection and 150–200 photoelectron signal is expected for 1-MeV positron energy deposition. The PMTs are mounted on a stainless steel screen, which separates external zone 3 from the central zones of the detector. The ~ 75 -cm-thick zone 3 is filled with mineral oil (or liquid scintillator) and serves as active (muon) and passive shielding from the external radioactivity.

There are two underground rooms to install the detectors at the Krasnoyarsk reactor site. One of them, located ~ 115 m from the reactor, is a 10-m-high 15×15 m square room. The other is a 125-m-long, 11.5-m-high, and 15-m-wide corridor ~ 1000 m from the reactor.

The final choice of the scintillator has not been made thus far. We hope for progress in manufacturing Gd (~ 0.9 g/l) loaded scintillators to improve the response to neutrons and suppress accidentals, which originate from U/Th gammas coming from the surrounding rock. The Palo Verde Gd scintillator showed better stability than the scintillator used in CHOOZ. The LENS project considers scintillators with rare-earth concentrations as high as ~ 50 g/l.

Currently, we consider a no-Gd scintillator based on the mixture of paraffin and pseudocumene ($\sim 20\%$) with ~ 2 g/l PPO as primary fluore. This scintillator has a C/H ratio of 1.85, density of 0.85 kg/l, and 0.785×10^{29} H atom/t.

4. DETECTOR CALIBRATIONS AND MONITORING; SYSTEMATIC UNCERTAINTIES

The ratio of measured positron spectra $S(E_e)_{\text{far}}/S(E_e)_{\text{near}}$ (8) can be slightly distorted because of the relative difference in response functions of the two “identical” spectrometers.

The goal of calibration procedures that we consider is to measure this difference and introduce necessary corrections. This can be done by a combination of different methods. First, we consider periodic control of the energy scales at many points using γ sources shown by arrows in Fig. 2. A useful continuous monitoring of the scales at 2.23 MeV can provide neutrons produced by through-going muons and captured by the target protons during the veto time.

The second method uses small ^{252}Cf or ^{238}U spontaneous fission sources periodically placed in

PMT type EMI-9350, diameter—8 in., coverage—20%, PMT number—842

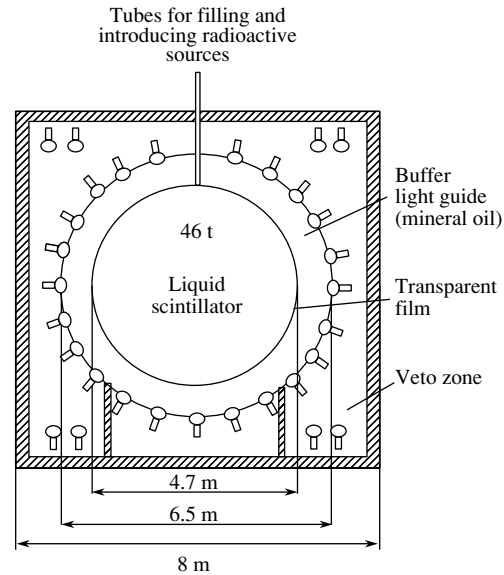


Fig. 5. The Kr2Det ν_e spectrometer (schematic).

the detectors. These sources generate a continuous energy spectrum due to prompt fission gammas and neutron recoils (the dashed curve in Fig. 2). The deviation from unity of the measured spectra can be used to calculate relevant corrections.

We hope that systematic uncertainty due to the detector spectrometric difference essential for Analysis I can be controlled down to 0.5%.

In Analysis II, the systematic uncertainty in the quantity $(L_{\text{far}}/L_{\text{near}})^2 (V_{\text{near}}/V_{\text{far}}) (\epsilon_{\text{near}}/\epsilon_{\text{far}})$ in Eq. (8') can hopefully be kept within 0.8%.

5. NEUTRINO DETECTION RATES AND BACKGROUNDS

The neutrino events satisfy the following requirements: (i) a time window on the delay between e^+ and neutron signals of 2–600 μs ; (ii) an energy window of 1.7–3.1 MeV for the neutron candidate and of 1.2–8.0 MeV for e^+ ; (iii) distance between e^+ and neutron less than 120 cm. At this stage, no pulse shape analysis to reject proton recoils is planned.

Under these assumptions, a neutrino detection efficiency of 75% has been found and neutrino detection rate $N(e^+, n) = 55/\text{d}$ calculated for the far detector.

The time-correlated background of 0.1/d per one target ton was found by extrapolation of the value 0.25/d per target ton measured at CHOOZ:

$$\begin{aligned} \text{CHOOZ (300 m w.e.), } & 0.25/(\text{d t}) \\ \rightarrow \text{Kr2Det (600 m w.e.), } & 0.1/(\text{d t}). \end{aligned} \quad (9)$$

Detector parameters

	Distance, m	Target mass, t	$N(e^+, n)$, d	$N(e^+, n)$, yr*	Background, d ⁻¹	
					correlated	accidental**
Far detector	1000	46	55	16.5×10^3	5	~0.3
Near detector	115	46	4200	12.5×10^5	5	~0.3

* 300 d/yr of full power.

** Only due to radioactivity of the detector internal materials.

The accidental coincidences come from the internal radioactivity of detector materials and U and Th contained in the surrounding rock. The internal component of the background was estimated to be less than 0.3/d, which is an order of magnitude smaller than the rate of the correlated background (see Kozlov *et al.* [5]). In contrast to the KamLAND and Borexino experiments, three-order higher concentrations of U, Th, K, and Rn can be tolerated in the liquids used in the Kr2Det case.

First estimates of accidentals coming from the radioactivity of the rock showed, however, that external passive shielding of the detector should be increased when a scintillator without Gd is used as the neutrino target.

Calculated neutrino detection rates $N(e^+, n)$ and backgrounds for the scintillator with no Gd are summarized in the table.

6. EXPECTED RESULTS AND CONCLUSIONS

Expected 90% C.L. constraints on the oscillation parameters (Fig. 1, curves Kr2Det) are obtained for 40 000 detected ν_e in the far detector (750 d of full power). The systematic uncertainties $\sigma_{\text{shape}} = 0.5\%$ in Analysis I and $\sigma_{\text{rate}} = 0.8\%$ in Analysis II have been assumed. The “shape” analysis is somewhat more sensitive and can shift (at $\Delta m^2 = 2.5 \times 10^{-3} \text{ eV}^2$) the $\sin^2 2\theta$ upper limit from 0.14 (CHOOZ) to 0.017.

The one-reactor–two-detector approach fully eliminates uncertainties associated with the reactor neutrino source inherent to the absolute method used at CHOOZ.

The small relative difference in conceptually identical detector properties can be minimized through calibration and monitoring procedures.

The detector backgrounds can be measured during reactor off periods, which periodically follow 50-d-long reactor on periods.

A good signal to background ratio can be achieved due to the sufficiently deep underground position of the detectors.

High statistics can be accumulated in a reasonably short time period using detectors with ~45-t targets, which are relatively small if compared to modern neutrino detectors.

The neutrino community has accumulated positive experience in building and running 3-concentric-zone detectors similar to the Kr2Det detectors.

We conclude that proposed study is feasible and that new important information on the electron neutrino internal structure ($\sin^2 2\theta_{13}$) can be obtained.

The KamLAND experiment in Japan has observed a large neutrino deficit ~180 km from the reactors and continues to study neutrino oscillations in the solar mass parameter region [14]. Laboratory experiments at reactors, KamLAND and Kr2Det, can provide full information on the electron neutrino mixing, at least in the 3-neutrino mixing scheme.

ACKNOWLEDGMENTS

We are grateful to F.V. Feilitzsch, K.T. Knoepfle, Yu. Kamyshev, T. Lasserre, L. Oberauer, A. Piepke, S. Schoenert, and F. Suekane for fruitful discussions. We thank S.T. Belyaev and W. Hofmann for attention and support.

This work was supported by the Russian Foundation for Basic Research (project nos. 03-02-16055 and NSH-1246.2003.2).

REFERENCES

1. S. Fukida *et al.* (Super-Kamiokande Collab.), Phys. Rev. Lett. **85**, 3999 (2000); hep-ex/0009001.
2. M. Apollonio *et al.* (CHOOZ Collab.), Phys. Lett. B **466**, 415 (1999).
3. S. Geer, Comments Mod. Phys. **2** (6), 284 (2002); hep-ph/0210113.
4. L. A. Mikaelyan and V. V. Sinev, Phys. At. Nucl. **63**, 1002 (2000); hep-ex/9908047.

5. L. A. Mikaelyan, Nucl. Phys. B (Proc. Suppl.) **87**, 284 (2000); L. A. Mikaelyan, hep-ex/9910042; L. Mikaelyan, Nucl. Phys. B (Proc. Suppl.) **91**, 120 (2001); hep-ex/0008046; Yu. Kozlov, L. Mikaelyan, and V. Sinev, hep-ph/0109277.
6. H. Minakata *et al.*, hep-ph/0211111.
7. A. Yu. Smirnov, hep-ph/0209131.
8. S. Schoenert, T. Lasserre, and L. Oberauer, hep-ex/0203013.
9. S. Ketov *et al.*, Pis'ma Zh. Éksp. Teor. Fiz. **55**, 544 (1992)[JETP Lett. **55**, 564 (1992)].
10. B. Achkar *et al.*, Nucl. Phys. B **434**, 503 (1995).
11. A. Piepke (KamLAND Collab.), Nucl. Phys. B (Proc. Suppl.) **91**, 99 (2001).
12. G. Alimonti *et al.* (BOREXINO Collab.), Astropart. Phys. **16**, 205 (2002).
13. A. Baldini, C. Bemporad, *et al.*, Nucl. Instrum. Methods Phys. Res. A **372**, 207 (1996).
14. KamLAND Collab., hep-ex/0212021.

ELEMENTARY PARTICLES AND FIELDS

Theory

P- and T-Violating Schiff Moment of the Mercury Nucleus*

V. F. Dmitriev** and R. A. Sen'kov

*Budker Institute of Nuclear Physics, Siberian Division, Russian Academy of Sciences, pr. Akademika
Lavrent'eva 11, Novosibirsk, 630090 Russia
Novosibirsk State University, ul. Pirogova 2, Novosibirsk, 630090 Russia*

Received March 11, 2003

Abstract—The Schiff moment of the ^{199}Hg nucleus was calculated using finite-range P - and T -violating weak nucleon–nucleon interaction. Effects of the core polarization were considered in the framework of RPA with effective residual forces. © 2003 MAIK “Nauka/Interperiodica”.

To My Teacher ...

1. INTRODUCTION

The most precise limit on parity- and time-invariance-violating nucleon–nucleon interaction has been obtained from the measurement of the atomic electric dipole moment of ^{199}Hg [1]. The hadronic part of the atomic dipole moment associated with the electric dipole moment of the ^{199}Hg nucleus manifests itself through the Schiff moment, which is the first nonzero term in the expansion of the nuclear electromagnetic potential after including the screening of the atomic electrons [2–4].

The operator for the Schiff moment is [5]

$$S_\mu = \frac{1}{10} \sqrt{\frac{4\pi}{3}} \sum_i^A e_i \left(r_i^3 - \frac{5}{3} \langle r^2 \rangle_{\text{ch}} r_i \right) Y_{1\mu}(\hat{\mathbf{r}}_i), \quad (1)$$

where e_i is e for a proton and zero for a neutron. The Schiff moment generates a T - and P -odd electrostatic potential in the form

$$\phi(\mathbf{r}) = 4\pi \mathbf{S} \cdot \nabla \delta(\mathbf{r}). \quad (2)$$

Interaction of atomic electrons with the potential given by Eq. (2) produces an atomic dipole moment

$$d_{\text{atom}} = \sum_n \frac{\langle 0 | -e \sum_i^Z \phi(\mathbf{r}_i) | n \rangle \langle n | -e \sum_i^Z z_i | 0 \rangle}{E_n - E_0} + \text{h.c.} \quad (3)$$

Due to contact origin of the potential, the electrons in s - and p -atomic orbitals only contribute to the dipole moment given by Eq. (3).

The nuclear Schiff moment has been calculated thus far in a simplified model [5, 6] without considering many-body nuclear-structure effects. These effects have to be understood properly if we intend to extract the parameters of P - and T -violating nuclear interaction from the value of the Schiff moment. For light nuclei, the properties of the Schiff moment strength obtained in modern shell-model calculations were discussed in [7]. The study of the polarization effects associated with the coupling to the isoscalar dipole compression mode was performed in [8]. In our paper, we calculate the Schiff moment of the ^{199}Hg nucleus within the RPA framework with effective residual strong forces using finite range P - and T -odd weak nuclear interaction.

2. BASIC INGREDIENTS OF THE THEORY

2.1. Nucleon–Nucleon P- and T-Odd Interaction

We use the interaction generated by P - and T -violating pion exchange [9, 11]

$$W(\mathbf{r}_1 - \mathbf{r}_2) = -\frac{g}{8\pi m_p} [(g_0 \boldsymbol{\tau}_1 \cdot \boldsymbol{\tau}_2 + g_2(\boldsymbol{\tau}_1 \cdot \boldsymbol{\tau}_2 - 3\tau_1^3 \tau_2^3))(\boldsymbol{\sigma}_1 - \boldsymbol{\sigma}_2) + g_1(\tau_1^3 \boldsymbol{\sigma}_1 - \tau_2^3 \boldsymbol{\sigma}_2)] \nabla_1 \frac{e^{-m_\pi r_{12}}}{r_{12}}, \quad (4)$$

where g is the usual strong pion–nucleon pseudoscalar coupling constant; g_0 , g_1 , and g_2 correspond to isoscalar, isovector, and isotensor P - and T -odd couplings; and m_p is the proton mass. In contrast to P -odd and T -even interaction, in Eq. (4) the exchange of π^0 is allowed. This term produces the direct contribution to the P - and the T -odd part of the nuclear mean field, while the other terms produce the exchange contribution only. Since the direct contribution dominates for finite-range potentials, we

*This article was submitted by the authors in English.

**e-mail: dmitriev@inp.nsk.su

can expect that the interaction (4) is the leading one and the exchange of heavier mesons can be omitted.

In previous calculations, the phenomenological contact interaction has often been used instead of finite-range interaction given by Eq. (4). It has the form [12]

$$W_c(\mathbf{r}_a - \mathbf{r}_b) = \frac{G}{\sqrt{2}} \frac{1}{2m_p} ((\eta_{ab}\boldsymbol{\sigma}_a - \eta_{ba}\boldsymbol{\sigma}_b) \quad (5)$$

$$\times \nabla_a \delta(\mathbf{r}_a - \mathbf{r}_b) + \eta'_{ab}[\boldsymbol{\sigma}_a \cdot \boldsymbol{\sigma}_b]$$

$$\times \{(\mathbf{p}_a - \mathbf{p}_b), \delta(\mathbf{r}_a - \mathbf{r}_b)\},$$

where G is the Fermi constant. In the limit $m_\pi \rightarrow \infty$, the interaction (4) transforms into Eq. (5) after the substitution $gg_i \rightarrow Gm_\pi^2\eta/\sqrt{2}$. We shall use this factor when comparing our results with those obtained using the contact interaction given by Eq. (5).

2.2. Nuclear Mean Field and Correction from the Weak Forces

In our calculations, we used the full single-particle spectrum including continuum. The single-particle basis was obtained using the partially self-consistent mean-field potential of [13]. The potential includes four terms. The isoscalar term is the standard Woods–Saxon potential

$$U_0(r) = -\frac{V}{1 + \exp(r - R)/a}, \quad (6)$$

with the parameters being $V = 52.03$ MeV, $R = 1.2709A^{1/3}$ fm, and $a = 0.742$ fm. Two other terms $U_{ls}(r)$ and $U_\tau(r)$ were calculated self-consistently using two-body Migdal-type interaction [14] for the spin–orbit and isovector parts of the potential. The last term is the Coulomb potential calculated for a uniformly charged sphere with $R_C = 1.18A^{1/3}$ fm. The mean-field potential obtained in this way produces a good fit for single-particle energies and rms radii for nuclei in the lead region.

The correction to the mean field (6) from the weak interaction (4) consists of direct and exchange terms. The direct term has the form

$$\delta U_{\text{dir}}(\mathbf{r}) = \frac{gm_\pi^2}{\pi m_p} (\boldsymbol{\sigma} \cdot \mathbf{n}) \tau^3 \int_0^\infty r'^2 dr' b_{10}(r, r') \quad (7)$$

$$\times [(g_0 - 2g_2)(\rho_p(r) - \rho_n(r)) + g_1(\rho_p(r) + \rho_n(r))],$$

where the function $b_{10}(r_1, r_2)$ is a combination of spherical Bessel functions of imaginary argument

$$b_{l_1 l_2}(r_1, r_2) = i_{l_1}(m_\pi r_1) k_{l_2}(m_\pi r_2) \theta(r_2 - r_1) \quad (8)$$

$$- i_{l_2}(m_\pi r_2) k_{l_1}(m_\pi r_1) \theta(r_1 - r_2).$$

Note that the potential given by Eq. (7) is a pure isovector. The contribution of the isovector interaction component dominates in Eq. (7), the isoscalar

and isotensor components of the interaction being suppressed by the factor $(N - Z)/A$. For zero-range interaction, the potential would be proportional to $\nabla\rho(r)$. The gradient makes this potential very sensitive to the details of the nuclear surface. Our potential given by Eq. (7) is less sensitive to the surface due to additional integration over a region of the order of the pion Compton wavelength.

The exchange term is more complicated. The matrix element of it taken over angular variable is a nonlocal operator in radial coordinates:

$$\langle \tilde{\nu} | \delta U_{\text{exch}}(\mathbf{r}, \mathbf{r}') | \nu \rangle = W_\nu(r, r'),$$

where $|\tilde{\nu}\rangle = -(\boldsymbol{\sigma} \cdot \mathbf{n})|\nu\rangle$ and

$$W_\nu(r, r') = \frac{1}{2j_\nu + 1} \frac{gm_\pi^2}{\pi m_p} \quad (9)$$

$$\times \text{tr}_2 \left\{ \sum_{\kappa l_1 l_2} \left(\frac{g_0}{2} (3 - \tau_1^3 \tau_2^3) - 2g_2 \tau_1^3 \tau_2^3 \right. \right.$$

$$+ \left. \frac{g_1}{2} (\tau_1^3 + \tau_2^3) \right) n_\kappa \begin{pmatrix} l_1 & l_2 & 1 \\ 0 & 0 & 0 \end{pmatrix} b_{l_1 l_2}(r, r') R_\kappa(r)$$

$$\times R_\kappa(r') \left[(-)^{l_1} [l_1] (\kappa || T_{l_2}^{l_1} || \tilde{\nu})^* (\kappa || Y_{l_2} || \nu) \right.$$

$$\left. \left. - (-1)^{l_2} [l_2] (\tilde{\nu} || Y_{l_1} || \kappa) (\nu || T_{l_1}^{l_2} || \kappa)^* \right] \right\}.$$

The trace is assumed over isospin variable of the second particle, n_κ is the occupation number of the single-particle state $|\kappa\rangle$, $[l] = \sqrt{2l + 1}$, and the tensor operator $T_{JM}^L(\mathbf{n}) = \{\boldsymbol{\sigma} \otimes Y_L(\mathbf{n})\}_{JM}$.

The correction to the single-particle wave function $\psi_\nu(\mathbf{r})$ can be represented as

$$\delta\psi_\nu(\mathbf{r}) = (\boldsymbol{\sigma} \cdot \mathbf{n}) \Omega_\nu(\mathbf{n}) \delta R_\nu(r),$$

where $\Omega_\nu(\mathbf{n})$ is the angular part of the wave function. The radial correction $\delta R_\nu(r)$ is the sum of the direct and the exchange terms $\delta R_\nu(r) = \delta R_{\nu\text{dir}}(r) + \delta R_{\nu\text{exch}}(r)$, where

$$\delta R_{\nu\text{dir}}(r) = \int_0^\infty G_{j_\nu \tilde{l}_\nu}(r, r' | \epsilon_\nu) \delta U_{\text{dir}}(r') R_\nu(r') r'^2 dr', \quad (10)$$

$$\delta R_{\nu\text{exch}}(r) = \int_0^\infty G_{j_\nu \tilde{l}_\nu}(r, r' | \epsilon_\nu) W_\nu(r', r'')$$

$$\times R_\nu(r'') r'^2 r''^2 dr' dr''.$$

Here, $G_{j_\nu \tilde{l}_\nu}(r, r' | \epsilon_\nu)$ is the Green's function of the radial Schrödinger equation for the total angular momentum j_ν and the orbital angular momentum $\tilde{l}_\nu = 2j_\nu - l_\nu$, and ϵ_ν is the single particle energy.

3. CORE POLARIZATION

The effects of the core polarization for a one-particle operator can be treated through introduction of a renormalized operator $\tilde{\mathbf{S}}$ satisfying the equation

$$\begin{aligned} \tilde{\mathbf{S}}_{\nu'\nu} &= \mathbf{S}_{\nu'\nu}^0 & (11) \\ + \sum_{\mu'\mu} \tilde{\mathbf{S}}_{\mu\mu'} \frac{n_\mu - n_{\mu'}}{\epsilon_\mu - \epsilon_{\mu'} + \omega} \langle \nu'\mu' | F + W | \mu\nu \rangle, \end{aligned}$$

where \mathbf{S}^0 is the bare Schiff moment operator given by Eq. (1), and n_μ and ϵ_μ are the single-particle occupation numbers and energies. For static moments, the external frequency $\omega \rightarrow 0$. The interaction in Eq. (11) includes both the strong residual interaction F and the weak one. The latter we take in the form given by Eq. (4). Strictly speaking, the interaction of two nucleons in nuclear matter differs from the interaction in the vacuum. We do not discuss this effect here but keep the weak interaction in the form (4). The single-particle wave functions in Eq. (11) are the eigenstates of the mean field, which is the sum of the strong field and the weak corrections given by Eqs. (7) and (9). Since the weak forces are really small compared to the strong interaction, it is natural to treat them perturbatively. The simplest way to do it is to represent $\langle \mathbf{r} | \nu \rangle = \psi_\nu(\mathbf{r}) + \delta\psi_\nu(\mathbf{r})$ and to gather the terms linear in $\delta\psi$ and $W(\mathbf{r}_1 - \mathbf{r}_2)$. It is convenient to represent the matrix element of the Schiff moment as a sum of three terms

$$\tilde{\mathbf{S}}_{\nu\nu} = \langle \delta\psi_\nu | \mathbf{S} | \psi_\nu \rangle + \langle \psi_\nu | \mathbf{S} | \delta\psi_\nu \rangle + \langle \psi_\nu | \delta\mathbf{S} | \psi_\nu \rangle. \quad (12)$$

The operator \mathbf{S} in the first two terms satisfies the same Eq. (11), where only the strong interaction is included. The corrections from the weak forces for these terms are in the wave functions of an odd nucleon only. The third term represents an induced contribution [15] arising from the P - and T -violating corrections to the intermediate states $|\mu\rangle$ and $|\mu'\rangle$. The equation for $\delta\mathbf{S}$ is

$$\begin{aligned} (\delta\mathbf{S} - \delta\mathbf{S}_{\text{nl}})_{\nu'\nu} &= (\delta\mathbf{S}_0)_{\nu'\nu} & (13) \\ + \sum_{\mu'\mu} (\delta\mathbf{S} - \delta\mathbf{S}_{\text{nl}})_{\mu\mu'} \frac{n_\mu - n_{\mu'}}{\epsilon_\mu - \epsilon_{\mu'}} \langle \nu'\mu' | F | \mu\nu \rangle, \end{aligned}$$

where $\delta\mathbf{S}_{\text{nl}}$ is the nonlocal part of $\delta\mathbf{S}$ produced by the exchange matrix elements of weak interaction W :

$$(\delta\mathbf{S}_{\text{nl}})_{\nu'\nu} = \sum_{\mu\mu'} (\mathbf{S})_{\mu\mu'} \frac{n_\mu - n_{\mu'}}{\epsilon_\mu - \epsilon_{\mu'}} \langle \nu'\mu' | W_{\text{exch}} | \mu\nu \rangle. \quad (14)$$

The equation for $\delta\mathbf{S}_0$ is

$$(\delta\mathbf{S}_0)_{\nu'\nu} = \sum_{\mu\mu'} \frac{n_\mu - n_{\mu'}}{\epsilon_\mu - \epsilon_{\mu'}} (\langle \mu | \mathbf{S} | \mu' \rangle \langle \nu'\mu' | W_{\text{dir}} | \mu\nu \rangle) \quad (15)$$

$$\begin{aligned} + \langle \mu | \delta\mathbf{S}_{\text{nl}} | \mu' \rangle \langle \nu'\mu' | F | \mu\nu \rangle &+ \langle \delta\psi_\mu | \mathbf{S} | \mu' \rangle \langle \nu'\mu' | F | \mu\nu \rangle \\ + \langle \mu | \mathbf{S} | \delta\psi_{\mu'} \rangle \langle \nu'\mu' | F | \mu\nu \rangle &+ \langle \mu | \mathbf{S} | \mu' \rangle \langle \nu' \delta\psi_{\mu'} | F | \mu\nu \rangle \\ + \langle \mu | \mathbf{S} | \mu' \rangle \langle \nu'\mu' | F | \delta\psi_{\mu\nu} \rangle. \end{aligned}$$

Note that, in the absence of the core polarization, only the first term in Eq. (15) contributes to $\delta\mathbf{S}_0$. And this is the only term that produces the Schiff moment of the nucleus with an odd neutron, like ^{199}Hg . The residual interaction F has the form

$$\begin{aligned} F &= C (f(r) + f'(\boldsymbol{\tau}_1 \cdot \boldsymbol{\tau}_2) + g_s(\boldsymbol{\sigma}_1 \cdot \boldsymbol{\sigma}_2) & (16) \\ &+ g'_s(\boldsymbol{\sigma}_1 \cdot \boldsymbol{\sigma}_2)(\boldsymbol{\tau}_1 \cdot \boldsymbol{\tau}_2)) \delta(\mathbf{r}_1 - \mathbf{r}_2), \end{aligned}$$

where $C = 300 \text{ MeV fm}^3$ and $f(r) = f_{\text{ex}} + (f_{\text{in}} - f_{\text{ex}})\rho(r)/\rho(0)$. Note that the angular dependence of the operators \mathbf{S} and $\delta\mathbf{S}$ is completely different. While $S_\mu \sim Y_{1\mu}(\mathbf{n})$, the induced part δS_μ is a superposition of spin-dependent operators σ_μ and $\{\sigma \otimes Y_2(\mathbf{n})\}_{1\mu}$. For this reason, different parts of the interaction (16) contribute to renormalization of \mathbf{S} and $\delta\mathbf{S}$.

For a spherical nucleus, we can separate the angular variables and solve the obtained equations in coordinate space. The equations are

$$S^a(r) = S_0^a(r) + \int_0^\infty A^{ab}(r, r') S^b(r') dr', \quad (17)$$

where $a = p, n$, and $S_0^p(r)$ is the radial part of the Schiff moment operator Eq. (1) multiplied by r . The particle-hole propagator $A(r, r')$ was calculated by means of the Green's functions of radial Schrödinger equation:

$$\begin{aligned} A(r, r') &= \frac{C}{3} \text{Tr}_2 \{ (f(r) + f'(\boldsymbol{\tau}_1 \cdot \boldsymbol{\tau}_2)) & (18) \\ &\times \sum_{\kappa j l} n_\kappa |\langle j l || Y_1 || \kappa \rangle|^2 r R_\kappa(r) r' R_\kappa(r') \\ &\times (G_{j l}(r, r' | \epsilon_\kappa + \omega) + G_{j l}(r, r' | \epsilon_\kappa - \omega)) \}. \end{aligned}$$

Similar equations can be written for $\delta S(r)$ —the local part of the induced moment. They differ from Eq. (18) in type of tensor operators and in residual interaction.

3.1. Separation of the Spurious Component

The integral Eq. (17) must have a zero eigenmode related to the center-of-mass motion. However, in our case, the isoscalar part of the mean field Eq. (6) is not consistent with the interaction Eq. (16) and, in general, we do not have zero energy for the center-of-mass motion. The situation can be improved using some freedom in the value of the interaction constant f_{in} in Eq. (16). We can fix the value by the condition $\omega_0 = 0$ for the lowest isoscalar dipole mode. Since this procedure is numerical, the

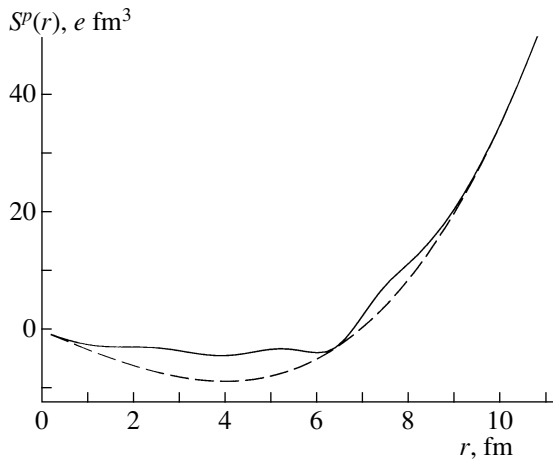


Fig. 1. The proton component of the Schiff moment. Solid curve is the renormalized operator after subtraction of the spurious component; dashed curve is the bare operator Eq. (1).

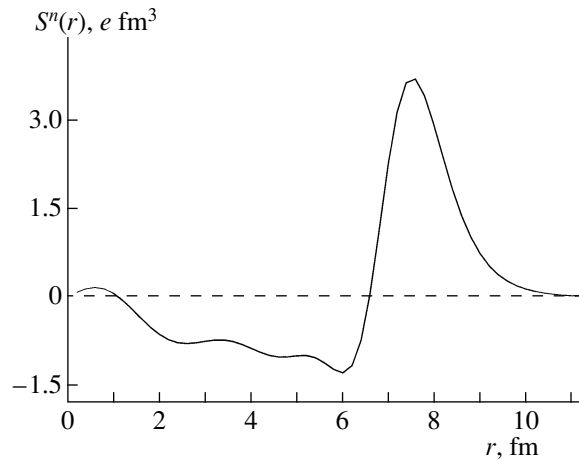


Fig. 2. The neutron component of the renormalized Schiff moment.

condition $\omega_0 = 0$ cannot be fulfilled exactly but with finite accuracy. For ^{199}Hg , we found that the set $f_{\text{in}} = 0.3935$, $f_{\text{ex}} = -2.6$, and $f' = 1.07$ gives for ω_0 the value $\omega_0 = 0.1$ keV, which is really small compared to the energy of dipole transitions.

The finite accuracy in determination of the spurious mode brings another problem for solutions to Eq. (17). The bare operator $S_0(r)$ becomes nonorthogonal to the spurious mode transition density. This results in admixture of the spurious component to all solutions of Eq. (17). The spurious component should be subtracted since it can change the solution considerably. The subtraction can be performed using analytical properties of the solution as a function of ω . The solution of the inhomogeneous linear integral Eq. (17) as a function of ω has the first-order poles at $\omega = \pm E_{\text{ex}}$, where E_{ex} are the excitation energies of the RPA modes. Thus, at small ω , the solution can be represented as

$$S(r|\omega) = \frac{a(r)}{\omega^2 - \omega_0^2} + b(r|\omega = 0) + O\left(\frac{\omega^2}{E_{\text{ex}}^2}\right). \quad (19)$$

The first term in Eq. (19) is the spurious component contribution. Let us define the following set of integrals in a complex ω plane along a circle with the radius satisfying the conditions $\omega_0 \ll |\omega| \ll E_{\text{ex}}$:

$$J_n(r) = \oint \omega^n S(r|\omega) \frac{d\omega}{2\pi i}. \quad (20)$$

Using Eq. (19), we can perform the integration analytically. As a result, we obtain

$$b(r|\omega = 0) = J_{-1}(r), \quad (21)$$

$$\omega_0^2 = J_3(r)/J_1(r).$$

The numerical integration in Eq. (20) has been performed using a 32-point Gauss formula. The integration radius was $|\omega| = 0.1$ MeV. The obtained field $b(r|\omega = 0)$ was practically insensitive to the integration radius. The value of ω_0^2 was independent of r in first five or six digits. The loss of accuracy was noticeable only at $|\omega| \sim \omega_0$.

Figure 1 shows the result for renormalized $S(r) = b(r|\omega = 0)$ with the spurious component subtracted. It is shown by the solid curve. The dashed curve shows the unrenormalized component $S_0(r)$. The effects of the core polarization are not large. We found that, for ^{209}Bi , they change the valence proton contribution by $\sim 15\%$, which is in fair agreement with the estimates of [8]. The proton component does not contribute to the Schiff moment of ^{199}Hg since the valence nucleon is a neutron. However, due to neutron-proton residual strong interaction, some neutron component is produced by the core polarization. This component is shown in Fig. 2. Qualitatively, the behavior of the neutron component inside a nucleus resembles the behavior of the bare operator in Fig. 1. However, the magnitude of the neutron component is smaller and the behavior outside of the nucleus is completely different.

4. RESULTS FOR ^{199}Hg

In Table 1, we show the contributions of the neutron component discussed above to the Schiff moment of ^{199}Hg . The three columns correspond to three isospin channels. The first row is the contribution from δR_{dir} produced by δU_{dir} given by Eq. (7). The second row is the contribution from δR_{exch} produced by δU_{exch} given by Eq. (9), and the third row is the sum of them.

Table 1. Contributions of the neutron component to the Schiff moment of ^{199}Hg (in $e \text{ fm}^3$)

	gg_0	gg_1	gg_2
Direct	0.0038	-0.024	-0.0076
Exchange	0.0032	-0.002	-0.0015
Total	0.0070	-0.026	-0.0091

In the direct contributions, the isospin channel $T = 1$ dominates, as was mentioned above. The exchange contributions are small, in general. For the isospin channels $T = 0, 2$, they are comparable to the direct contributions just because the latter are suppressed by the factor $(N - Z)/A$.

The contributions from $\delta\mathbf{S}$ are more significant. In Table 2, we list the contributions from the direct and the exchange parts of the weak interaction W . In the first two rows, the unrenormalized contributions $\delta\mathbf{S}_0$ are shown. Again, the exchange contributions are considerably smaller than the direct ones. The contributions from the channels $T = 1$ and 2 are comparable here, although the $T = 1$ contribution is still larger. The next two rows show the renormalized contributions $\delta\mathbf{S}$. The effect of the core polarization is significant here. The induced moment $\delta\mathbf{S}$ includes spin-dependent operators. Therefore, the spin-spin part of the residual interaction Eq. (16) is responsible for their renormalization. The spin-spin interaction is repulsive with the constants $g_s = 0.63$ and $g'_s = 1.01$. The repulsion results in a decrease in the absolute values of the renormalized contributions. Finally, in the last row, we show the contribution of the nonlocal term $\delta\mathbf{S}_{\text{nl}}$ [Eq. (14)]. It has the exchange origin as well, and its contribution is really insignificant. All the contributions (total from Table 1 and $\delta\mathbf{S}$ direct, exchange, and nonlocal from Table 2) can be summarized as follows:

$$S = -0.0004gg_0 - 0.055gg_1 + 0.009gg_2 [e \text{ fm}^3]. \quad (22)$$

The obtained value for the Schiff moment in Eq. (22) cannot be compared directly with previous calculations performed using the contact interaction Eq. (5). The reason is in the different definition of the dimensionless constants gg_i in Eq. (4) and η_{ab} in Eq. (5). To perform the comparison, we redefine the constants g_i ,

$$g_i = \frac{Gm_\pi^2}{\sqrt{2}} \tilde{g}_i. \quad (23)$$

With this factor, the integration over space of the Yukawa function gives 1, exactly as the integration of $\delta(\mathbf{r})$. Introducing this factor, we obtain

$$S = (-0.01g\tilde{g}_0 - 0.86g\tilde{g}_1 + 0.14g\tilde{g}_2) \times 10^{-8} [e \text{ fm}^3]. \quad (24)$$

Table 2. Induced contributions to the Schiff moment of ^{199}Hg (in $e \text{ fm}^3$)

	gg_0	gg_1	gg_2
Direct $\delta\mathbf{S}_0$	-0.0302	-0.0631	0.0604
Exchange $\delta\mathbf{S}_0$	-0.0007	-0.0012	-0.0007
Direct $\delta\mathbf{S}$	-0.0086	-0.0285	0.0172
Exchange $\delta\mathbf{S}$	-0.0002	-0.0008	-0.0003
Non-local $\delta\mathbf{S}_{\text{nl}}$	0.0014	-0.00004	0.0013

This value should be compared with $S = -1.4 \times 10^{-8} \eta_{np}$ from [16] and $S \approx -1.6 \times 10^{-8} \eta_{np}$ from [6]. Remembering that $\eta_{np} \sim g(\tilde{g}_0 + \tilde{g}_1 - 2\tilde{g}_2)$, we conclude that the difference between our result and previous calculations is significant for the $T = 0$ and 2 channels. Our values are smaller in absolute value. In order to trace the origin of this difference, we repeated our calculations using the contact interaction and omitting the core polarization. The contact interaction was obtained by replacing the Yukawa function in Eq. (4) by the δ function. The result is

$$S = -0.96 \times 10^{-8} g(\tilde{g}_0 + \tilde{g}_1 - 2\tilde{g}_2) [e \text{ fm}^3]. \quad (25)$$

If we omit completely the effect of the core polarization in calculations with the finite-range interaction Eq. (4), then the contribution in the first row of Table 2, used for comparison with previous calculations, becomes

$$S = -0.086g(g_0 + g_1 - 2g_2) [e \text{ fm}^3],$$

which corresponds to

$$S = -1.35 \times 10^{-8} g(\tilde{g}_0 + \tilde{g}_1 - 2\tilde{g}_2) [e \text{ fm}^3]. \quad (26)$$

Comparing Eqs. (25) and (26), we conclude that the effect of a finite weak-interaction range is not very significant. The main effect bringing the value of the Schiff moment from that in Eq. (26) to the value in Eq. (24) comes from the core polarization.

The last remark concerns the pairing effects. The nucleus ^{199}Hg has seven neutron holes in the unfilled shell. One of them is fixed in the $p_{1/2}$ state and six others should be distributed among the other states in the shell. From mass differences, we found $\Delta_n = 0.69 \text{ MeV}$. This value of the pairing gap is typical for the developed pairing. For dipole transitions, the transition energy is large compared to Δ and the pairing effects are small. They were omitted in Eq. (17). For the induced moment, the situation is different. There, the transitions with $\Delta J = 0, 1$ and $\Delta L = 0, 2$ are responsible for the core polarization. Such transitions exist inside the last unfilled neutron shell and, due to Pauli blocking, they are sensitive to

the details of the shell occupation. For a T -odd operator, the effects of pairing in the core polarization can be considered in the way used in [15]. We found that the main effect of pairing is in fixing the occupation numbers in the upper unfilled neutron shell. As soon as we keep the occupation numbers fixed, the results for $\delta\mathbf{S}$ are changed within a few percent when we set $\Delta_n = 0$.

In summary, we calculated the Schiff moment of ^{199}Hg nucleus using finite-range weak interaction and considering the core polarization effects. The effects of the finite interaction range are not very significant for the mercury nucleus. They do not change the order of magnitude of the Schiff-moment calculated with the contact interaction. The effects of the core polarization are twofold. First, the proton–neutron residual interaction renormalizes the Schiff moment operator, producing a small neutron component. Second, the induced Schiff moment is produced due to P - and T -violating components in the intermediate single-particle states. The induced moment is proportional to both the strong residual and the weak interactions. The effects of the core polarization for the mercury nucleus are large and they have to be taken into account in calculations of P - and T -violating effects in the mercury nucleus.

ACKNOWLEDGMENTS

We appreciate discussions with I.B. Kriplovich during this work.

REFERENCES

1. M. V. Romalis, W. C. Griffith, J. P. Jacobs, and E. N. Fortson, Phys. Rev. Lett. **86**, 2505 (2001).
2. E. M. Purcell and N. F. Ramsey, Phys. Rev. **78**, 807 (1950).
3. L. I. Schiff, Phys. Rev. **132**, 2194 (1963).
4. P. G. H. Sandars, Phys. Rev. Lett. **19**, 1396 (1967).
5. V. V. Flambaum, I. B. Khriplovich, and O. P. Sushkov, Zh. Éksp. Teor. Fiz. **87**, 1521 (1984) [Sov. Phys. JETP **60**, 873 (1984)].
6. V. V. Flambaum and J. S. M. Ginges, Phys. Rev. A **65**, 032113 (2002).
7. J. Engel, J. L. Friar, and A. C. Hayes, Phys. Rev. C **61**, 035502 (2000).
8. I. Hamamoto and B. A. Brown, Phys. Rev. C **62**, 024318 (2000).
9. W. C. Haxton and E. M. Henley, Phys. Rev. Lett. **51**, 1937 (1983).
10. P. Herczeg, Hyperfine Interact. **43**, 77 (1988).
11. I. B. Khriplovich and R. V. Korokin, Nucl. Phys. A **665**, 365 (2000).
12. I. B. Khriplovich, *Parity Nonconservation in Atomic Phenomena* (Gordon and Breach, Philadelphia, 1991).
13. B. L. Birbrair and V. A. Sadovnikova, Yad. Fiz. **20**, 645 (1975) [Sov. J. Nucl. Phys. **20**, 347 (1975)].
14. A. B. Migdal, *Theory of Finite Fermi System* (Wiley, New York, 1967).
15. V. F. Dmitriev and V. B. Telitsin, Nucl. Phys. A **613**, 237 (1997); **674**, 168 (2000).
16. V. V. Flambaum, I. B. Khriplovich, and O. P. Sushkov, Nucl. Phys. A **449**, 750 (1986).

ELEMENTARY PARTICLES AND FIELDS Theory

Angular Asymmetries in the Reactions $\vec{p}p \rightarrow d\pi^+\eta$ and $\vec{p}n \rightarrow d\pi^0\eta$ and a_0-f_0 Mixing*

A. E. Kudryavtsev¹⁾, V. E. Tarasov^{1)**}, J. Haidenbauer²⁾, C. Hanhart²⁾, and J. Speth²⁾

Received March 4, 2003

Abstract—The reactions $pp \rightarrow d\pi^+\eta$ and $pn \rightarrow d\pi^0\eta$ are of special interest for investigating the $a_0(980)$ ($J^P = 0^+$) resonance in the process $NN \rightarrow da_0 \rightarrow d\pi\eta$. We study some aspects of those reactions within a general formalism and also in a concrete phenomenological model. In particular, it is shown that the presence of nonresonant (i.e., without excitation of the a_0 resonance) contributions to these reactions yields nonvanishing values for specific polarization observables, i.e., to effects like those generated by $a_0^0-f_0$ mixing. An experimental determination of these observables for the reaction $\vec{p}p \rightarrow d\pi^+\eta$ would provide concrete information on the magnitude of those nonresonant contributions to $\pi\eta$ production. We also discuss the possibility of extracting information about $a_0^0-f_0$ mixing from the reaction $\vec{p}n \rightarrow d\pi^0\eta$ with a polarized proton beam. © 2003 MAIK “Nauka/Interperiodica”.

1. INTRODUCTION

The reactions $pp \rightarrow dK^+\bar{K}^0$ and $pp \rightarrow d\pi^+\eta$ are presently the subject of experimental investigations by the ANKE collaboration at the COSY accelerator in Jülich [1–3]. The main issue of this study is to obtain further information about the scalar $a_0^+(980)$ resonance, which decays predominantly into the $K^+\bar{K}^0$ and $\pi^+\eta$ channels [4]. Also, a measurement of the production of the neutral a_0^0 meson in the reaction $pn \rightarrow da_0^0$ with the ANKE spectrometer is planned [5–7]. The a_0^0 production is closely related to the problem of $a_0^0-f_0$ mixing [8]. A nonzero value for the transition amplitude $a_0^0 \leftrightarrow f_0$ provides a forward–backward asymmetry for the reaction $pn \rightarrow da_0^0$. As was shown in [9], near the threshold this forward–backward asymmetry is large, on the order of 10–15%. Thus, it is evident that the study of this asymmetry can provide useful information on the process of a_0-f_0 mixing.

In a recent paper [10], some aspects of the reaction $\vec{p}n \rightarrow da_0^0$ were discussed for the case of a perpendicular polarized proton beam. Specifically, it was shown that, for energies close to threshold, the

angular-asymmetry parameter defined by

$$A(\theta, \varphi) = \frac{\sigma(\theta, \varphi) - \sigma(\pi - \theta, \varphi + \pi)}{\sigma(\theta, \varphi) + \sigma(\pi - \theta, \varphi + \pi)}, \quad (1)$$

with

$$\sigma(\theta, \varphi) \equiv \frac{d\sigma}{d\Omega}(\theta, \varphi) \quad (2)$$

[θ and φ are the polar and azimuthal angles of the outgoing $\pi\eta$ system in the center-of-mass system (CMS) of the reaction], is proportional to the $a_0^0-f_0$ mixing amplitude, i.e.,

$$A(\theta, \varphi) \sim \xi k, \quad (3)$$

where k is the relative momentum of the a_0^0 meson with respect to the deuteron and ξ is the $a_0^0-f_0$ mixing parameter. This result is valid in the lowest order with respect to the momentum k , i.e., keeping only contributions that are at most linear in k . It was shown in [10] that corrections to $A(\theta, \varphi)$ from isospin-conserving terms are of order of k^3 and, therefore, they are of relevance at higher energies only. Thus, the study of the angular asymmetry [Eq. (1)] near the a_0^0 threshold in the reaction $\vec{p}n \rightarrow da_0^0$ gives information on various invariant amplitudes for this reaction [10] but, in particular, on the $a_0^0-f_0$ mixing parameter ξ .

The present paper focuses on the reaction $NN \rightarrow d\pi\eta$. We take into consideration that the $\pi\eta$ system can be produced not only via the formation of the $a_0(980)$ resonance, i.e., in an S -wave state, but also via other reaction mechanisms and then can be in a P wave or in even higher partial waves. For brevity,

*This article was submitted by the authors in English.

¹⁾Institute of Theoretical and Experimental Physics, Bol'shaya Cheremushkinskaya ul. 25, Moscow, 117259 Russia.

²⁾Institut für Kernphysik, Forschungszentrum Jülich, Germany.

** e-mail: tarasov@heron.itep.ru

in the following, we will refer to the latter contributions as nonresonant or as background of the $NN \rightarrow da_0 \rightarrow d\pi\eta$ amplitude. (Note that there can also be a background in the S -wave state, as discussed in [11, 12]—but this is not the issue we are concerned with here.) Consequences of this nonresonant background contribution for polarization observables of the reactions $\bar{p}p \rightarrow d\pi^+\eta$ and $\bar{p}n \rightarrow d\pi^0\eta$ will be discussed. Specifically, it will be shown that, because of the presence of the nonresonant background, in these reactions the angular-asymmetry parameter $A(\theta, \varphi)$ becomes nonzero even without isospin violation. Indeed, like the effect induced by the $a_0^0-f_0$ mixing discussed above, the contribution of the nonresonant background is also linear in k and therefore is difficult to separate from effects of the $a_0^0-f_0$ mixing in the reaction $\bar{p}n \rightarrow d\pi^0\eta$. However, a measurement of this asymmetry in the reaction $\bar{p}p \rightarrow d\pi^+\eta$ can provide us with information on the contribution of the nonresonant background to the reaction $pp \rightarrow da_0^+ \rightarrow d\pi^+\eta$.

Recently, the reactions $pp \rightarrow dK^+\bar{K}^0$ and $pp \rightarrow d\pi^+\eta$ were studied theoretically in a chiral unitary approach taking into account the coupling between the $K^+\bar{K}^0$ and $\pi^+\eta$ channels [13]. The elementary $\pi\eta$ production amplitude was assumed to be given by the diagram shown in Fig. 1a, where the π and η mesons emerge from different nucleons and rescatter with each other before being emitted. Since chiral dynamics suppressed the coupling of the $\pi\eta$ system to P waves [14], it follows within this approach that the $\pi^+\eta$ system is preferably produced in S waves and that P waves, i.e., the nonresonant background discussed above, should be practically negligible.³⁾ Their result motivated us to consider in the present paper a different production mechanism that does not involve the $\pi\eta$ amplitude directly and therefore is not constrained by chiral symmetry. We assume that the reaction $pp \rightarrow d\pi\eta$ proceeds via pion exchange between the nucleons followed by the excitation of the $\Delta(1232)$ and the $N^*(1535)$ resonances [12], which then produce the π and η mesons in their respective decay (cf. Fig. 1b). Such a reaction mechanism is certainly suppressed at energies near the $\pi\eta$ threshold, where chiral dynamics should be dominating. However, in the region of the a_0 resonance, the excess energy for the $\pi\eta$ system is already around 300 MeV. Therefore, this mechanism could already be of relevance and, specifically, it will introduce P -wave contributions. We will present the corresponding results for the angular symmetry $A(\theta, \varphi)$ and also for differential cross sections. Clearly, in this context, an experimental

³⁾Note, however, that P waves arise naturally in the effective Lagrangian approach of Achasov *et al.* [15] based on the anomalous Wess–Zumino action.

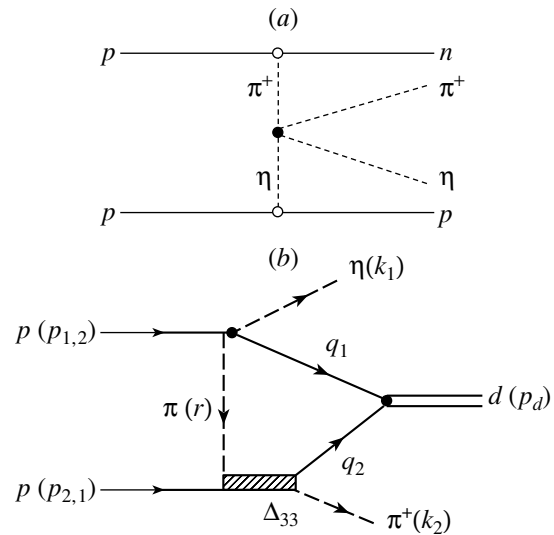


Fig. 1. Nonresonant mechanisms for the reaction $pp \rightarrow d\pi^+\eta$: (a) $\pi\eta$ rescattering; (b) one-pion-exchange diagram involving the $\pi N \rightarrow \Delta \rightarrow \pi N$ and $\pi N \rightarrow \eta N$ reaction amplitudes.

study of this asymmetry parameter is very interesting because it may shed light on the validity of the chiral unitary approach [13] for the calculation of amplitudes for the reactions $pp \rightarrow dK^+\bar{K}^0$ and $pp \rightarrow d\pi^+\eta$ near the a_0 threshold.

Finally, we will show that a systematic study of the angular-asymmetry parameters for both reactions, $\bar{p}p \rightarrow d\pi^+\eta$ and $\bar{p}n \rightarrow d\pi^0\eta$, may allow us to obtain quantitative information on the $a_0^0-f_0$ mixing parameter.

The paper is organized as follows. In Section 2, we provide the general form of the reaction amplitude for the process $NN \rightarrow d\pi\eta$ near threshold, where we allow the $\pi\eta$ system to be in an S or P wave. Furthermore, we derive expressions for the corresponding differential cross sections. In Section 3, we consider a phenomenological model for the nonresonant (P -wave) contributions to the reaction $pp \rightarrow d\pi^+\eta$ and present concrete estimations for the angular symmetry $A(\theta, \varphi)$ and also for differential cross sections. Implications of a possibly nonzero background contribution to the reaction $NN \rightarrow d\pi\eta$ on the issue of $a_0^0-f_0$ are discussed in Section 4. The paper ends with a short summary.

2. GENERAL FORM OF REACTION AMPLITUDE

Let us consider first the reaction $pp \rightarrow d\pi^+\eta$. If the $\pi^+\eta$ system is produced by the decay of the a_0^+ meson, it is in an S wave. However, if we produce the $\pi^+\eta$ state with an invariant mass of $m \approx m_{a_0} \approx$

980 MeV/ c^2 but not via the a_0^+ resonance, then the orbital angular momentum of the $\pi\eta$ system may be large because, as mentioned, the energy available in the $\pi\eta$ system is already around 300 MeV.

We start with the most general form of the amplitude \mathcal{M} for the reaction $NN \rightarrow d\pi\eta$. It is given by

$$\mathcal{M} = \phi_1^T \sigma_y [F + \mathbf{G} \cdot \boldsymbol{\sigma}] \phi_2, \quad (4)$$

where ϕ_1^T and ϕ_2 are the spinors of the nucleons (T indicates the transposed state vector). The amplitude in Eq. (4) involves two terms, F and $\mathbf{G} \cdot \boldsymbol{\sigma}$, corresponding to the initial total spin of the nucleons of $S_{NN} = 0$ and $S_{NN} = 1$, respectively.

Note that both functions F and \mathbf{G} are to be linear functions of the polarization vector $\boldsymbol{\epsilon}^*$ of the outgoing deuteron. In the following, we limit ourselves to the consideration of S - and P -wave states for the produced $\pi\eta$ system and, accordingly, we write both functions F and \mathbf{G} as $F = F_S + F_P$ and $\mathbf{G} = \mathbf{G}_S + \mathbf{G}_P$. Taking into account the Pauli principle together with parity and angular momentum conservation and considering only terms that are at most linear in k , we get

$$\begin{aligned} F_S &= 0, \\ \mathbf{G}_S &= a_S \mathbf{p}(\mathbf{k} \cdot \boldsymbol{\epsilon}^*) + b_S \boldsymbol{\epsilon}^*(\mathbf{k} \cdot \mathbf{p}) \\ &+ c_S \mathbf{k}(\mathbf{p} \cdot \boldsymbol{\epsilon}^*) + d_S \mathbf{p}(\mathbf{p} \cdot \boldsymbol{\epsilon}^*)(\mathbf{k} \cdot \mathbf{p}) \end{aligned} \quad (5)$$

for the case of the $\pi\eta$ system being in an S wave (e.g., production via the a_0 resonance) and

$$\begin{aligned} F_P &= a_0(\boldsymbol{\epsilon}^* \cdot [\mathbf{k} \times \mathbf{q}]) + b_0(\boldsymbol{\epsilon}^* \cdot [\mathbf{p} \times \mathbf{q}])(\mathbf{p} \cdot \mathbf{k}) \\ &+ c_0(\boldsymbol{\epsilon}^* \cdot [\mathbf{p} \times \mathbf{k}])(\mathbf{p} \cdot \mathbf{q}), \end{aligned} \quad (6)$$

$$\begin{aligned} \mathbf{G}_P &= a_1 \boldsymbol{\epsilon}^*(\mathbf{p} \cdot \mathbf{q}) + b_1 \mathbf{p}(\boldsymbol{\epsilon}^* \cdot \mathbf{q}) + c_1 \mathbf{q}(\boldsymbol{\epsilon}^* \cdot \mathbf{p}) \\ &+ d_1 \mathbf{p}(\boldsymbol{\epsilon}^* \cdot \mathbf{p})(\mathbf{p} \cdot \mathbf{q}) \end{aligned} \quad (7)$$

for the case of the $\pi\eta$ system being produced in a P wave. Here, $a_S, a_0, a_1, b_S, b_0, b_1, c_S, c_0, c_1, d_S$, and d_1 are independent scalar amplitudes, which may be considered as being basically constants for the near-threshold production (k is small) of the $\pi\eta$ system with an invariant mass $m = m_{a_0}$ of the a_0 meson. In Eqs. (5)–(7), we used the following notation:

\mathbf{p} is the initial relative momentum in the CMS of the reaction.

\mathbf{k} is the final relative momentum of the deuteron with respect to the $\pi\eta$ system in the CMS of the reaction.

\mathbf{q} is the relative momentum between the pion and the η in the $\pi\eta$ CM frame.

The matrix element \mathcal{M} [Eq. (4)] squared and averaged over the polarizations of the initial neutron is given by

$$\overline{|\mathcal{M}|^2} = \frac{1}{2} [|F|^2 + 2\text{Re}(F^* \mathbf{G} \cdot \boldsymbol{\zeta}) + (\mathbf{G}^* \cdot \mathbf{G}) \quad (8)$$

$$+ i(\boldsymbol{\zeta} \cdot [\mathbf{G} \times \mathbf{G}^*])],$$

where $\boldsymbol{\zeta}$ is the polarization vector of the initial proton, i.e., $\boldsymbol{\zeta} = \phi_1^+ \boldsymbol{\sigma} \phi_1$. In what follows, we shall consider the vector \mathbf{p} to be aligned in the direction of the z axis and the vector $\boldsymbol{\zeta}$ to be aligned in x direction, so that $\boldsymbol{\zeta} \perp \mathbf{p}$.

Since we are interested in the behavior of the differential cross section $d^2\sigma/dm d\Omega_{\mathbf{k}}$ and in the angular-asymmetry parameter $A(\theta, \varphi)$, we integrate expression (8) over the direction of the momentum \mathbf{q} :

$$\frac{d^2\sigma}{dm d\Omega_{\mathbf{k}}} = N \int \frac{d\Omega_{\mathbf{q}}}{4\pi} \overline{|\mathcal{M}|^2} := \sigma(m; \theta, \varphi). \quad (9)$$

Here, m is the invariant mass of the $\pi\eta$ system, $N = kq/(4\pi)^4 ps$, and s is the square of the total energy in the CMS of the reaction. After the integration over $d\Omega_{\mathbf{q}}$, the S – P interference term in $\sigma(m; \theta, \varphi)$ disappears. The contribution of the S -wave part of \mathcal{M} (4) to $\sigma(m; \theta, \varphi)$ can be obtained from Eqs. (22) and (23) of [10] and reads

$$\begin{aligned} \left(\frac{d^2\sigma}{dm d\Omega_{\mathbf{k}}} \right)_S &= N \left\{ p^2 k^2 \left[\frac{1}{2} (|a_S|^2 + |b_S|^2) \right. \right. \\ &+ \left[|b_S|^2 + \frac{1}{2} |b_S + p^2 d_S|^2 + \text{Re}(a_S^* c_S \right. \\ &+ (a_S + c_S)^*(b_S + p^2 d_S)) \left. \right] \cos^2 \theta \left. \right\} \\ &+ \zeta p k \text{Im}(a_S^* b_S + a_S^* c_S + b_S^* c_S \\ &+ p^2 d_S^* c_S) \sin \theta \cos \theta \sin \varphi \left. \right\}. \end{aligned} \quad (10)$$

The contribution from the P -wave part can be deduced from Eqs. (6)–(9) and amounts to

$$\begin{aligned} \left(\frac{d^2\sigma}{dm d\Omega_{\mathbf{k}}} \right)_P &= N \left\{ \frac{k^2 q^2}{6} \left[2|a_0|^2 + 2|b_0|^2 p^4 \cos^2 \theta \right. \right. \\ &+ |c_0|^2 p^4 \sin^2 \theta + 4\text{Re}(a_0^* b_0) p^2 \cos^2 \theta \\ &- 2\text{Re}(a_0^* c_0) p^2 \sin^2 \theta \left. \right] + \frac{q^2}{3} \text{Re}(a_0^* a_1 - a_0^* c_1 \\ &- c_0^* a_1 p^2)(\boldsymbol{\zeta} \cdot [\mathbf{k} \times \mathbf{p}]) + \frac{p^2 q^2}{6} \left[(3|a_1|^2 + |b_1|^2 \right. \\ &+ |c_1|^2) + p^4 |d_1|^2 + 2\text{Re}(a_1^*(b_1 + c_1 + p^2 d_1) \\ &+ b_1^* c_1 + (b_1^* + c_1^*) p^2 d_1) \left. \right] \left. \right\}. \end{aligned} \quad (11)$$

It can be easily seen from Eq. (11) that the only contribution to the angular-asymmetry parameter $A(\theta, \varphi)$, defined in Eq. (1), comes from the term proportional to $\boldsymbol{\zeta} \cdot [\mathbf{k} \times \mathbf{p}] = \zeta p k \sin \theta \sin \varphi$, where θ and φ are the polar and azimuthal angles of the

outgoing $\pi\eta$ system in the CMS of the reaction. Hence, because of the P -wave (nonresonant background) contribution, we get a nonvanishing angular asymmetry and this asymmetry is linear in k . Note that $A(\theta, \varphi) = 0$ in the case where the $\pi\eta$ system is produced in an S wave, as follows from Eq. (10).

Therefore, it is clear that the angular asymmetry $A(\theta, \varphi)$ in the reaction $\bar{p}p \rightarrow d\pi^+\eta$ can provide information on the magnitude of contributions from partial waves with $l \geq 1$ in the $\pi\eta$ system.

3. ESTIMATION OF THE ANGULAR ASYMMETRY FOR NONRESONANT $\pi^+\eta$ PRODUCTION

Let us now come to a concrete estimation for the angular-asymmetry parameter. For that purpose, we consider a simple model for the reaction $pp \rightarrow d\pi^+\eta$ in which the $\pi^+\eta$ system can be produced with nonzero internal angular momentum ($l \geq 1$). Specifically, we adopt the one-pion-exchange diagram in Fig. 1b. We assume that the dominant contribution arises from the intermediate $\Delta(1232)$ state in the subprocess $\pi N \rightarrow \pi N$ and from the S -wave amplitude of the subprocess $\pi N \rightarrow \eta N$. The latter is basically given by the contribution of the $N^*(1535)$ -resonance state. This diagram with the same subprocesses was already used in [12] in the context of the a_0 production process in $pN \rightarrow da_0 \rightarrow d(\pi\eta)$. However, in that work, the authors were primarily interested in the S -wave part of the one-pion-exchange $\pi\eta$ production amplitude. Therefore, the angular distribution of the outgoing pion was not calculated in [12].

The evaluation of this diagram, treating the intermediate nucleons and the final deuteron nonrelativistically, leads to the following expression for the corresponding $\pi\eta$ -production amplitude \mathcal{M} :

$$\begin{aligned} \mathcal{M} &= \mathcal{M}_1 + \mathcal{M}_2, & (12) \\ \mathcal{M}_{1,2} &= \pm A_{1,2} \phi_{1,2}^T \sigma_y (\boldsymbol{\epsilon}^* \cdot \boldsymbol{\sigma}) \\ &\times (2\mathbf{n}'_{1,2} \cdot \mathbf{n}_2 + i\boldsymbol{\sigma} \cdot [\mathbf{n}'_{1,2} \times \mathbf{n}_2]) \phi_{2,1}. \end{aligned}$$

Note that the amplitude \mathcal{M} is antisymmetric with respect to the initial nucleons, i.e., $\mathcal{M}_1 \leftrightarrow -\mathcal{M}_2$ when the nucleons are interchanged. The quantities $A_{1,2}$ are given by

$$\begin{aligned} A_{1,2} &= T \frac{E + m_N}{2m_N \sqrt{2}m_N} M_{\pi^0 N \rightarrow \eta N} M_{\pi N \rightarrow \pi N} & (13) \\ &\times \int \frac{d\mathbf{q}}{(2\pi)^3} u(\mathbf{q}) G_\pi(t_{1,2}). \end{aligned}$$

Further, $2\mathbf{n}'_{1,2} \cdot \mathbf{n}_2 + i\boldsymbol{\sigma} \cdot [\mathbf{n}'_{1,2} \times \mathbf{n}_2]$ is the spin operator of the Δ state in the πN -scattering amplitude, and $\mathbf{n}'_{1,2} = \mathbf{r}_{1,2}/r_{1,2}$ and $\mathbf{n}_2 = \mathbf{k}_2/k_2$ are unit vectors. The corresponding momenta, $\mathbf{r}_{1,2} = \mathbf{k}_2 + \mathbf{q}_2 -$

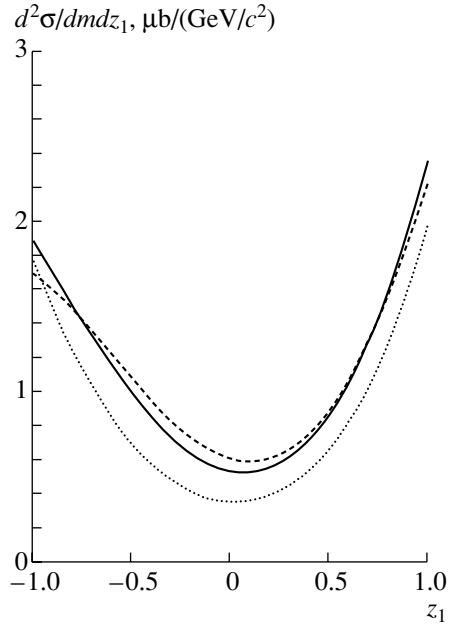


Fig. 2. Angular distributions of the outgoing π^+ meson in the $\pi^+\eta$ rest frame for several values m of the $\pi^+\eta$ invariant mass in the a_0 -mass region. The dashed, solid, and dotted curves correspond to $m = 950$, 980 , and 1020 MeV/c^2 , respectively. The calculations are performed at $T_{\text{lab}} = 2.65$ GeV and for a cutoff parameter (16) $\Lambda = 1$ GeV/c .

$\mathbf{p}_{2,1}$ and \mathbf{k}_2 , are the 3-momenta of the intermediate (virtual) and final pion in the CMS of the reaction, in the notation used in Fig. 1b. The quantity $T = 4\sqrt{2}/3$ is an isospin factor, and m_N and E are the mass and total CMS energy of the initial proton. The S -wave amplitude for $\pi^0 N \rightarrow \eta N$ is obtained from the relation (see also [16])

$$\begin{aligned} |M_{\pi^0 N \rightarrow \eta N}(s_1)|^2 &= 8\pi s_1 \frac{p_{\text{CM}}^\pi}{p_{\text{CM}}^\eta} \sigma_{\pi^0 p \rightarrow \eta N} & (14) \\ &(s_1 = m_{\eta N}^2), \end{aligned}$$

where the cross section (in μb) $\sigma_{\pi^0 p \rightarrow \eta N} = (21.2 \pm 1.8) p_{\text{CM}}^\eta (p_{\text{CM}}^\eta \text{ in } \text{MeV}/c)$ is taken from the experiment [17]. The scalar amplitude for $\pi N \rightarrow \pi N$ resulting from the Δ resonance reads

$$\begin{aligned} M_{\pi N \rightarrow \pi N}(m_{\pi N}) &= \frac{g_{\pi N \Delta}^2 k_{\text{CM}}(\pi') k_{\text{CM}}(\pi)}{m_{\pi N} - M_\Delta + i\Gamma_\Delta/2}, & (15) \\ g_{\pi N \Delta}^2 &= \frac{4\pi M_\Delta \Gamma_{\Delta \rightarrow \pi N}}{k_R^3}, \end{aligned}$$

where $k_{\text{CM}}(\pi')$ and $k_{\text{CM}}(\pi)$ are the relative momenta at the $\Delta N \pi$ vertices with the virtual and final pion, respectively, and k_R is the relative momentum in the decay $\Delta \rightarrow N \pi$ at the nominal mass $m_{\pi N} = M_\Delta$.

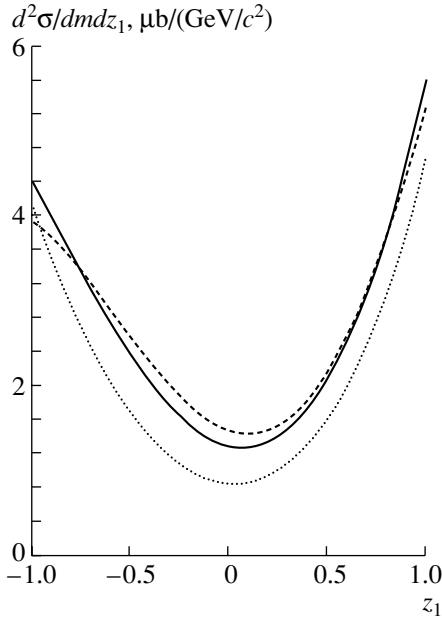


Fig. 3. The same distributions as in Fig. 2, but for $\Lambda = 1.3 \text{ GeV}/c$.

In the following, all the values taken out of the loop integral (13) are calculated at fixed values $\mathbf{q}_1 = \mathbf{q}_2 = \mathbf{p}_d/2$ of the intermediate on-mass-shell nucleons, where \mathbf{p}_d is the momentum of the final deuteron in the reaction CM. The loop integral in Eq. (13) contains only the wave function $u(q)$ of the deuteron and the pion propagator $G_\pi(t)$. We use the S -wave part of the deuteron wave function of the full Bonn potential [18]. The propagator of the virtual pion, including a form factor $F_\pi(t)$ of monopole type for each $\Delta N\pi$ vertex, reads

$$G_\pi(t) = \frac{F_\pi^2(t)}{t - \mu^2 + i0}, \quad F_\pi(t) = \frac{\mu^2 - \Lambda^2}{t - \Lambda^2}, \quad (16)$$

where μ is the pion mass. For the cutoff parameter Λ , we consider the values $\Lambda = 1-1.3 \text{ GeV}$ [12]. The 4-momentum transfer squared t for nonrelativistic intermediate nucleons is given by the relations [$t = t_{1,2}$ for the corresponding part $\mathcal{M}_{1,2}$ of the total anti-symmetric amplitude \mathcal{M} according to Eq. (12)]

$$t_{1,2} - \mu^2 + i0 = -x [(\mathbf{q} - \Delta_{1,2})^2 - a_{1,2}^2 - i0], \quad x = (E - \omega_2)/m, \quad (17)$$

$$a_{1,2}^2 = \frac{1}{x} \left[(T_N - \omega_2)^2 + (\mathbf{p}_{2,1} - \mathbf{k}_2)^2 \right] \times \left(\frac{1}{x} - 1 \right) - \mu^2, \quad \Delta_{1,2} = \frac{\mathbf{p}_{2,1} - \mathbf{k}_2}{x} - \frac{\mathbf{p}_d}{2},$$

where $T_N = E - m_N$ and ω_2 is the total energy of the final pion in the CMS of the reaction.

Let us rewrite the total amplitude \mathcal{M} [Eq. (12)] in the form of Eq. (4). Then, we get

$$\mathcal{M} = \mathcal{M}_1 + \mathcal{M}_2 = \phi_1^T \sigma_y [F + \mathbf{G} \cdot \boldsymbol{\sigma}] \phi_2, \quad (18)$$

$$\mathcal{M}_{1,2} = \pm A_{1,2} \phi_{1,2}^T \sigma_y [F_{1,2} + \mathbf{G}_{1,2} \cdot \boldsymbol{\sigma}] \phi_{2,1},$$

where

$$F = A_1 F_1 + A_2 F_2, \quad \mathbf{G} = A_1 \mathbf{G}_1 - A_2 \mathbf{G}_2, \quad (19)$$

$$F_{1,2} = i(\boldsymbol{\epsilon} \cdot [\mathbf{n}'_{1,2} \times \mathbf{n}_2]),$$

$$\mathbf{G}_{1,2} = 2(\mathbf{n}'_{1,2} \cdot \mathbf{n}_2)\boldsymbol{\epsilon} + (\mathbf{n}'_{1,2} \cdot \boldsymbol{\epsilon})\mathbf{n}_2 - (\mathbf{n}_2 \cdot \boldsymbol{\epsilon})\mathbf{n}'_{1,2}.$$

Using Eqs. (8), (9), and (12)–(19), we evaluated the angular asymmetry $A(\theta, \varphi)$, defined in Eq. (1), at the angle $\theta = 90^\circ$, where the term $2\text{Re}(F^* \times \mathbf{G} \cdot \boldsymbol{\zeta}) \sim \boldsymbol{\zeta} \cdot [\mathbf{k} \times \mathbf{p}] = \zeta p k \sin \theta \sin \varphi$ should produce the maximal effect. The calculations were performed at $m = 980 \text{ MeV}$ (i.e., in the a_0 -meson region). It turned out that the resulting angular-asymmetry parameter $A(\theta, \varphi)$ is very small, i.e., $A(90^\circ, \varphi) \leq 1\%$. In order to understand this, we need to go back to the equations above. Indeed, one can immediately see that, in the case of zero relative phase between the quantities A_1 and A_2 given by Eq. (13), one should obtain exactly $A(\theta, \varphi) = 0$. This is due to the relative phase of 90° between the functions F and \mathbf{G} in the term $2\text{Re}(F^* \mathbf{G} \cdot \boldsymbol{\zeta})$ of Eq. (8) because of the factor i in F [see Eq. (19) for F_1]. The latter results from the spin structure of the πN -scattering amplitude, which in our case is given by the excitation of the Δ resonance alone, and is connected with the Hermitian form of the interaction [cf. the factor i in front of the $\boldsymbol{\sigma}$ matrix in Eq. (12)]. In fact, the loop integral in Eq. (13) generates an imaginary part from the on-mass-shell contribution of the exchanged pion. Therefore, due to permutation of the initial protons, the quantities A_1 and A_2 acquire some nonzero relative phase. But still there is only a small effect on the angular asymmetry.

In this context, let us mention that the interaction in the initial NN system, which is neglected in the simple model calculation presented here, should also introduce a relative phase between those two amplitudes and therefore might lead to an enhancement in the predictions for the angular-asymmetry parameter.

In any case, the smallness of this asymmetry effect does not mean that the P -wave fraction in the $\pi\eta$ system is also small. To illustrate this, we present here some results for the reaction with an unpolarized proton beam, namely, the distribution $d^2\sigma/dm dz_1$ at selected values of the invariant mass m of the $\pi\eta$ system around the a_0 mass and for two values of the cutoff parameter Λ ($\Lambda = 1$ and $1.3 \text{ GeV}/c$). Here, $z_1 = \cos \theta_1$, where θ_1 is the polar angle of the outgoing π^+ meson with respect to the direction of the proton-beam momentum in the $\pi^+\eta$ rest frame.

The calculations were done at the proton beam energy $T_{\text{lab}} = 2.65$ GeV. The resulting angular spectra are shown in Figs. 2 and 3. Evidently, they are not isotropic but exhibit a strong angular dependence and, therefore, demonstrate that there are significant contributions from higher partial waves ($l \geq 1$). Thus, a measurement of the angular distribution for the produced $\pi^+\eta$ system would be rather instructive. In particular, it should allow one to examine the validity of the chiral unitary approach used in [13], which implies a completely isotropic angular distribution, in the energy region of the $a_0(980)$ resonance.

4. THE REACTION $\vec{p}n \rightarrow d\pi^0\eta$ AND THE a_0-f_0 MIXING AMPLITUDE

Let us now consider the reaction $pn \rightarrow d\pi^0\eta$. As discussed in [10], if the $\pi^0\eta$ system is produced in an S wave, then the only nonzero contribution to the angular-asymmetry parameter comes from the $a_0^0-f_0$ mixing amplitude. Indeed, we have shown there that—in lowest order in k —the isospin-violating contribution to $A(\theta, \varphi)$ is proportional to ξk . Thus, an extraction of the $a_0^0-f_0$ mixing parameter ξ would, in principle, be feasible from experimental information on the angular asymmetry.

However, as should be clear after the discussion in Section 2, there could also be contributions to $A(\theta, \varphi)$ from isospin-conserving terms because of the possible presence of P waves in the $\pi\eta$ system. Such contributions arise from the term in the differential cross section proportional to $\boldsymbol{\zeta} \cdot [\mathbf{k} \times \mathbf{p}]$. This term is maximal at $\theta = 90^\circ$ and vanishes at $\theta = 0^\circ$. As a consequence, a separation of both contributions to $A(\theta, \varphi)$ is rather complicated.

Still, there is a possibility to separate the contribution from the isospin-violating part, namely, by carrying out a combined study of the polarized differential cross sections for both reactions $\vec{p}p \rightarrow d\pi^+\eta$ and $\vec{p}n \rightarrow d\pi^0\eta$. In order to illustrate how this can be achieved, let us first remind the reader that the amplitudes of those reactions are related by

$$\mathcal{M}(pn \rightarrow d\pi^0\eta) = \frac{1}{\sqrt{2}}\mathcal{M}(pp \rightarrow d\pi^+\eta), \quad (20)$$

if isospin is conserved. This relation suggests that one should consider a “subtracted” differential cross section,

$$\sigma_\Delta(m; \theta, \varphi) := \frac{d^2\sigma_0}{dm d\Omega_{\mathbf{k}}} - \frac{1}{2} \frac{d^2\sigma_+}{dm d\Omega_{\mathbf{k}}}, \quad (21)$$

where σ_0 and σ_+ are the cross sections of the processes $\vec{p}n \rightarrow d\pi^0\eta$ and $\vec{p}p \rightarrow d\pi^+\eta$, respectively. Evidently, the angular asymmetry $A(\theta, \varphi)$ evaluated according to Eq. (1) for this “subtracted” differential

cross section $\sigma_\Delta(m; \theta, \varphi)$ does not contain terms induced by isospin-conserving processes and hence provides only information on isospin-violating effects. Note that, in the simple model considered in Section 3, the angular asymmetry in the reaction $\vec{p}p \rightarrow d\pi^+\eta$ is small in any case and, therefore, one might expect that any effects seen in the experiment should come mainly from isospin-violating $a_0^0-f_0$ mixing.

5. SUMMARY

We presented a discussion on effects of background contributions to differential cross sections and the angular asymmetry $A(\theta, \varphi)$ for the reactions $\vec{p}p \rightarrow d\pi^+\eta$ and $\vec{p}n \rightarrow d\pi^0\eta$. Specifically, we pointed out that, already in lowest order in the relative momentum between the deuteron and the $\pi\eta$ system, the angular asymmetry $A(\theta, \varphi)$ can be nonzero—even without isospin mixing effects—because of the presence of higher partial waves in the $\pi\eta$ system. As a consequence, a measurement of the angular asymmetry $A(\theta, \varphi)$ with polarized proton beams for the reaction $\vec{p}p \rightarrow d\pi^+\eta$ should provide useful information on the role of higher partial waves in this reaction. It would also allow one to examine the validity of model calculations of the reaction $pp \rightarrow d\pi^+\eta$ based on chiral constraints [13] for energies around the a_0 threshold.

We also argued that a combined analysis of differential cross sections for both reactions, $\vec{p}p \rightarrow d\pi^+\eta$ and $\vec{p}n \rightarrow d\pi^0\eta$, may facilitate the extraction of isospin-violating effects induced by $a_0^0-f_0$ mixing and allow one to shed light on the nature of these scalar mesons.

ACKNOWLEDGMENTS

We are grateful to V.V. Baru and M. Büscher for useful discussions.

This work was partly supported by DFG-RFBI, grant no. 02-02-04001 (436 RUS 113/652/1-1), and by the Russian Foundation for Basic Research, project no. 00-15-96562.

REFERENCES

1. *Proceedings of the Workshop on $a_0(980)$ Physics with ANKE*, Ed. by M. Büscher and V. Kleber (Berichte des Forschungszentrums Jülich, Jül-3801, 2000), p. 3.
2. M. Büscher, F. P. Sassen, N. N. Achasov, and L. Kondratyuk, hep-ph/0301126.
3. P. Fedorets and V. Kleber, in *Proceedings of the Conference on Quarks and Nuclear Physics, QNP 2002* (Jülich, Germany, 2002), Eur. Phys. J. A (in press).
4. C. Caso *et al.* (Review of Particle Physics), Eur. Phys. J. C **3**, 1 (1998).

5. M. Büscher *et al.*, <http://www.fz-juelich.de/ikp/anke/doc/anke/proposal/a0-f0.ps.gz>.
6. V. E. Tarasov and A. E. Kudryavtsev, *Proceedings of the Workshop on $a_0(980)$ Physics with ANKE*, Ed. by M. Büscher and V. Kleber (Berichte des Forschungszentrums Jülich, Jül-3801, 2000), p. 151.
7. *Proceedings of the 2nd ANKE Workshop "Strangeness Production in pp and pA Interactions at ANKE,"* Ed. by M. Büscher, V. Kleber, P. Kulessa, and M. Nekipelov (Berichte des Forschungszentrums Jülich, Jül-3922, 2001), p. 209.
8. N. N. Achasov, S. A. Devyanin, and G. N. Shestakov, *Phys. Lett. B* **88B**, 367 (1979); *Yad. Fiz.* **33**, 1337 (1981) [*Sov. J. Nucl. Phys.* **33**, 715 (1981)].
9. A. E. Kudryavtsev and V. E. Tarasov, *Pis'ma Zh. Éksp. Teor. Fiz.* **72**, 589 (2000) [*JETP Lett.* **72**, 410 (2000)]; *nucl-th/0102053*.
10. A. E. Kudryavtsev, V. E. Tarasov, J. Haidenbauer, *et al.*, *Phys. Rev. C* **66**, 015207 (2002).
11. H. Müller, *Eur. Phys. J. A* **11**, 113 (2001).
12. L. A. Kondratyuk, E. L. Bratkovskaya, V. Yu. Grishina, *et al.*, *nucl-th/0207033*; *Yad. Fiz.* **66**, 155 (2003) [*Phys. At. Nucl.* **66**, 152 (2003)].
13. E. Oset, J. A. Oller, and Ulf-G. Meißner, *Eur. Phys. J. A* **12**, 435 (2001).
14. V. Bernard, N. Kaiser, and Ulf-G. Meißner, *Phys. Rev. D* **44**, 3698 (1991).
15. N. N. Achasov and G. N. Shestakov, *Phys. Rev. D* **63**, 014017 (2001); *Yad. Fiz.* **65**, 579 (2002) [*Phys. At. Nucl.* **65**, 552 (2002)].
16. V. Yu. Grishina *et al.*, *Phys. Lett. B* **475**, 9 (2000).
17. D. M. Binnie *et al.*, *Phys. Rev. D* **8**, 2789 (1973).
18. R. Machleidt, K. Holinde, and Ch. Elster, *Phys. Rep.* **149**, 1 (1987).